

**ISSN 1916-9698 (Print)**  
**ISSN 1916-9701 (Online)**

# **INTERNATIONAL JOURNAL OF CHEMISTRY**

**Vol. 2, No. 2**  
**August 2010**



**Canadian Center of Science and Education®**

# Editorial Board

Adel F. Shoukry	Kuwait University, Kuwait
Ahmad Sazali Hamzah	Universiti Teknologi MARA, Malaysia
Anne Brown	Canadian Center of Science and Education, Canada
Barbaros Akkurt	Istanbul Technical University, Turkey
Charoenkwan Kraiya	Chulalongkorn University, Thailand
Dilip Venkatrao Jarikote	University College Dublin, Ireland
Dong Ma	CNH Technologies, Inc., USA
Guy L. Plourde	University of Northern British Columbia, Canada
Haidong Huang	New Jersey Institute of Technology, USA
Ismail Ab Rahman	Universiti Sains Malaysia, Malaysia
Jiantao Guo	The Scripps Research Institute, USA
Jignasu P Mehta	Bhavnagar University, India
Kan Wang	University of Pittsburgh, USA
Konstantinos Kasiotis	Benaki Phytopathological Institute, Greece
Linus Okoro	American University of Nigeria, Nigeria
Manoj B. Gawande	Quinta da Torre, Portugal
Mohamed Abass	Ain Shams University, Egypt
Monira Nessem Michael	National institute of standards (NIS), Egypt
Mu.Naushad	SRM University, India
Oleg Larionov	Harvard University, USA
Pankaj Das	Dibrugarh University, India
Patrick Marcel Schaeffer	James Cook University, Australia
Prathapan Sreedharan	Cochin University of Science and Technology, India
R. K. Dey	Birla Institute of Technology, India
Rasha Mohamed El Nashar	The German University In Cairo, Egypt
Sagar Pal	Birla Institute of Technology, India
Shyamal Kumar Chattopadhyay	Bengal Engineering and Science University, India
Sie-Tiong Ha	Universiti Tunku Abdul Rahman, Malaysia
Sirshendu De	Indian Institute of Technology, India
Sushil Kumar Kansal	Punjab University, India
Waseem Hassan	Universidade Federal de Santa Maria, Brazil
Yogeswaran Umasankar	National Taipei University of Technology, Taiwan
Yuanmin Wang	Bowling Green State University, USA

## Contents

Cyclic Voltammetric Studies of Electropolymerized Films Based on Ruthenium(II/III) Bis(1,10 phenanthroline) (4-methyl-4'-vinyl-2,2'-bipyridine)	3
<i>Kenneth L. Brown &amp; Seth B. Gray</i>	
Photocatalytic Degradation of Phenol Using Fe-TiO <sub>2</sub> by Different Illumination Sources	10
<i>Reyad Awwad Shawabkeh, Omar A. Khashman &amp; Gasan I. Bisharat</i>	
Computational Models of Thermal Cycling in Chemical Systems	19
<i>Carl Barratt, Dante M. Lepore, Matthew J. Cherubini &amp; Pauline M. Schwartz</i>	
The Effect of Both UV/Ozone and Chitosan on Natural Fabrics	28
<i>Eman Mohamed Osman, Monira Nesim Michael &amp; Hoda Gohar</i>	
Studies in the Chemistry of Some New 1,2,4-thiadiazolidine by Oxidative Cyclisation	40
<i>Dipak T. Tayade, Rahul A. Bhagwatkar &amp; Radheshyam C. Panpalia</i>	
Poly(Furfural-Acetone) as New Adsorbent for Removal of Cu(II) from Aqueous Solution: Thermodynamic and Kinetic Studies	44
<i>Tariq S. Najim, Suhad A. Yassin &amp; Ali J. Majli</i>	
Corrosion and Corrosion Inhibition of Mild Steel in H <sub>2</sub> SO <sub>4</sub> Solutions by Zizyphus Spina-Christi as Green Inhibitor	54
<i>Aisha M. Al- Turkustani, Sanaa T. Arab &amp; Areej A. Al- Reheli</i>	
Kinetic Studies on Lipase-catalyzed Transesterification of Phosphatidylcholine with $\alpha$ -linolenic Acid Ethyl Ester	77
<i>Junmin Du, Dong Wu, Xianglin Hou &amp; Cuiping Feng</i>	
Spectrophotometric Determination of Lead in Environment Samples by Benzoic Acid Azo PhenylCalix[4]arene (BAPC)	86
<i>Le Van Tan &amp; Nguyen Thi Ngoc Le</i>	
Retention Profile of Selenium (IV) from Aqueous Media Containing Bromide Ions Employing Polyurethane Foams	91
<i>A. S. Bashammakh</i>	
One-pot Preparation of $\beta$ -amino Carbonyl Compounds by Mannich Reaction Using MgO/ZrO <sub>2</sub> as Effective and Reusable Catalyst	98
<i>Nagrik D.M., Ambhore D.M. &amp; Gawande M.B.</i>	
The Effect of Gel and Pressure Induced Flow (PIF) Processing Conditions on the Dispersion and Intercalation of MMT Nanoclay in UHMWPE/ Montmorillonite (MMT) Clay based Nanocomposite Sheets	102
<i>Musa E. Babiker, Zhang Sen, Tang Yi Fei, Guangcheng Wang &amp; Yu Muhuo</i>	
Synthesis, Characterization and Antimicrobial Study of Some New Cyclohexenone Derivatives	114
<i>Anil N. Mayekar, Hongqi Li, H. S. Yathirajan, B. Narayana &amp; N. Suchetha Kumari</i>	
Analysis of the Characteristics of Nickel-Plating Baths	124
<i>Ahmet Ozan GEZERMAN &amp; Burcu Didem CORBACIOGLU</i>	
Corrosion Inhibition of Carbon Steel in Open Recirculating Cooling Water System of Petroleum Refinery by Thiourea and Imidazole in Presence of Zinc (II) Sulphate	138
<i>P.K. Gogoi &amp; B. Barhai</i>	

# Contents

Preparation and Characterization of Disulfide Functionalized Multi-Walled Carbon Nanotubes for Biomedical Applications	144
<i>Ke Long Huang, Ling Hu &amp; Su Qin Liu</i>	
Synthesis and Antibacterial Activity of Novel Organoselenium Compounds	149
<i>P. M. Radhakrishna, K. C. Sharadamma, H. M. Vagdevi, P. M. Abhilekha, S. Rubeena Mubeen &amp; K. Nischal</i>	
Extraction Equilibrium and Simple Extractive Spectrophotometric Determination of Gold (I& III) in Water Using the Ion - Pairing Amiloride Hydrochloride	155
<i>A.S. Bashammakh &amp; M.S. El-Shahawi</i>	
Molecular Interactions in Binary Mixture of Polymethylmethacrylate with Acetic Acid	164
<i>Richa Saxena &amp; S.C. Bhatt</i>	
A Novel Approach for Preparing Red Phosphorus Microcapsule by Hydrothermal Method	173
<i>Yajuan Zhao, Xing Huang, Yulei Tai &amp; Daofa He</i>	
Application of a New pH-metric Method to the Kinetic Study of Copolymerization of Polysaccharides Fucan N1 with PMMA in Presence of Cerium Ce <sup>+4</sup>	179
<i>El B. Sakri</i>	
Kinetics and Mechanism of Oxidation of Nicotine by Permanganate Ion in Acid Perchlorate Solutions	193
<i>Ishaq A. Zaaferany</i>	
Water Quality in Some Primary Schools in Shala e Bajgorës	201
<i>Lavdim Zeqiri, Malësore Pllana, Sadije Kadriu, Kadri Berisha &amp; Shukri Maxhuni</i>	
Synthesis of Novel Multifluorinated Pyrazolone-5-one Derivatives via Conventional and Non-conventional Methods	206
<i>Amol Gadakh, Chetan Pandit, Sahebrao S. Rindhe &amp; Bhausaheb Karale</i>	
Quaternized Chitosan as an Efficient Catalyst for Synthesis of N-alkylthio-phthalimides	213
<i>Zhang Hu &amp; Sidong Li</i>	
Dimensional Stability, Thermal Degradation and Termite Resistant Studies of Chemically Treated Wood	218
<i>Juthika Sonowal &amp; P.K. Gogoi</i>	
Kinetics and Mechanism of Oxidation of 2-amino-1-Butanol and 3-Amino-1-propanol by Potassium Ferrate	226
<i>Jinhuan Shan, Jiying Zhang, Haixia Shen &amp; Xiaoqian Wang</i>	
Instrumental Neutron Activation Analysis of Total Halogen and Extractable Organohalogen in Fish Samples from the Densu Basin	234
<i>Alfred Kwablah Anim, Samuel Afful &amp; Yaw Serfor-Armah</i>	
Performance Characteristics of Cells Containing Two Potentiometric Sensors: Application to a Cell Containing Hydralazinium and Chloride Electrodes	243
<i>Laila A. Al-Shatti, Hayat Marafie &amp; Adel F. Shoukry</i>	
Densities, Viscosities and Refractive Indices of n- Butanol + Allyl Chloride Mixture at 298K	250
<i>Aruna P. Maharolkar, Y. Sudke, S. Kamble, A. Tidar, A. G. Murugkar, S.S. Patil, P. W. Khirade &amp; S. C. Mehrotra</i>	
DNA Chemical Damage and Its Detected	261
<i>Shao Jun</i>	



# Cyclic Voltammetric Studies of Electropolymerized Films Based on Ruthenium(II/III) Bis(1,10 phenanthroline) (4-methyl-4'-vinyl-2,2'-bipyridine)

Kenneth L. Brown (Corresponding author) & Seth B. Gray

Department of Chemistry, Hope College

35 East 12<sup>th</sup> Street, Holland, Michigan 49424, USA

Tel: 1-616-395-7173 E-mail: brownk@hope.edu

## Abstract

A ruthenium complex of bis(1,10-phenanthroline)(4-methyl-4'-vinyl-2,2'-bipyridine) was used to modify glassy carbon electrodes during cyclic voltammetry. The modification procedure is rapid and produces a polymer film on the glassy carbon electrode. Characterization cyclic voltammograms of the ruthenium-based polymer films in supporting electrolyte solutions are very similar to the electropolymerization cyclic voltammograms. The polymer thin films derived from the ruthenium complex exhibit Nernstian electron transfer with respect to the applied potential at low scan rates. This is shown by the small peak separation between the cathodic and anodic peaks during characterization. At scan rates greater than 1.00 V/sec, the films model the Randles-Sevcik equation for diffusion-controlled mass transfer processes. Surface coverage ranges from  $9.42 \times 10^{-11}$  mol/cm<sup>2</sup> to  $4.76 \times 10^{-10}$  mol/cm<sup>2</sup> and was calculated by integrating the area under the anodic peak of the characterization cyclic voltammograms.

**Keywords:** Electropolymerization, Cyclic voltammetry, Thin films

## 1. Introduction

Chemically modified electrodes (CMEs) over the past several decades have sparked considerable interest in analytical chemistry with respect to catalysis, electrochemical and chromo-electrochemical detection of organic compounds, and chemical sensor development. Since the pioneering work by Lane and Hubbard, over 20 years ago, involving chemisorbed metals on platinum electrode surfaces, numerous methods have been developed to immobilize compounds on electrode surfaces (Lane 1973). Several modification techniques of electrode surfaces include covalent attachment, spin coating, and electropolymerization. This research focuses on polymer films on glassy carbon electrode derived from electropolymerization.

Deliberate chemical alteration of the electrode surface may result in a more favorable interaction between an analyte and electrode surface by changing the thermodynamic and kinetic behavior of reactants, products, or intermediates involved in the redox transformation. These new electrodes possess properties which may be exploited to lay a foundation for new and interesting applications and devices such as electrochromic displays and sensors (Green et. al 1983, Hurrell et. al 1989, Li et. al 1991, Wang 1996, Allen et. al 1994, Bobacka et. al 1994). Electropolymerization offers a unique strategy of reproducibly immobilizing metal complexes with various degrees of electrochemical activity onto electrode surfaces (Brown et. al 1998, Brown et. al 2002). Research in the development of chemically modified electrodes by electrochemical polymerization using Ru(II) and Fe(II) vinylbipyridine complexes was performed by Calvert (Calvert et al. 1983). Others such as Guarr et al. have investigated the mechanism of electropolymerization for ruthenium bis(1,10-phenanthroline)(4-methyl-4'-vinyl-2,2'-bipyridine), Ru(II)-(phen)<sub>2</sub>vbpy (where vbpy=vinyl bipyridine), complexes onto glassy carbon electrode surfaces (Guarr et. al 1987). The electrodes presented herein require approximately 30 minutes to modify depending upon the scan rate used for electropolymerization.

More recently, we investigated the use of electrodes chemically modified with Ru(II)-5-amino-1,10-phenanthroline-bis(bipyridine) complexes towards the electrochemical oxidation detection of hydrazine at significantly lowered overpotentials (Pinter et. al 2007). These films were based on the oxidation of the amine group of the organic moiety. Planning the incorporation of immobilized ruthenium complexes for the design of amperometric sensors for hydrazine, we have revisited the electropolymerization of a ruthenium compound containing mixed ligands of vinylbipyridine and phenanthroline. The films derived from these mixed ligands were electrochemically characterized using cyclic voltammetry. The characterization data would provide

useful information related to the design of sensors for hydrazine. This paper reports on some of the electrochemical characteristics of the ruthenium-based films on glassy carbon electrode surfaces.

## 2. Experimental

### 2.1 Reagents and Solutions

The ruthenium complex, Ru(II)-(phen)<sub>2</sub>vbpy, was provided by Guarr and co-workers. Propylene carbonate and tetraethylammonium perchlorate (TEAP), used as solvent and supporting electrolyte for electropolymerization of the monomer and characterization of the films were obtained from Sigma-Aldrich (St. Louis, MO). The TEAP was dried under vacuum prior to use. The concentration of monomer and TEAP were  $1.00 \times 10^{-3}$  M and 0.100 M respectively.

### 2.2 Instrumentation

Electropolymerizations and other cyclic voltammetric measurements were performed with a 601A Electrochemical Analyzer (CHInstruments, Inc., Austin, TX). The three-electrode electrochemical cell used in this work consisted of a glassy carbon working electrode (diameter = 3 mm), a Ag/AgCl, 3 M NaCl reference electrode, and a platinum wire auxiliary electrode, all from CHInstruments.

### 2.3 Electropolymerization and Characterization of Thin Films

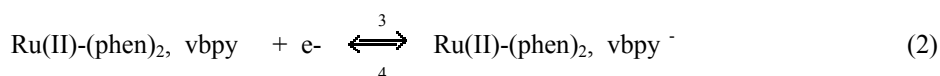
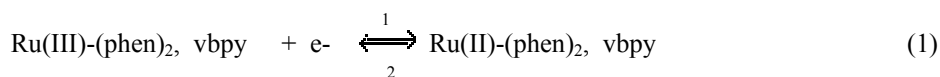
Before commencing with the electrode modification with the ruthenium complex, the glassy carbon working electrode was polished by placing several drops of polishing alumina suspension (0.05  $\mu$ m particle size from Bioanalytical Systems) on a wetted polishing pad and moving the electrode in a circular motion across the surface of the polishing pad. Prior to all electropolymerizations, the solutions containing the ruthenium complex and the supporting electrolyte were deoxygenated with nitrogen gas for five minutes and a nitrogen blanket was maintained over the solutions for the duration of the experiments. The electropolymerization was accomplished by cycling the potential of the glassy carbon electrode between +1.600 V and -1.600 V. The dependence of peak current on the scan rate of electropolymerization was made using scan rates from 0.100 V/sec to 1.000 V/sec. The maximum number of electropolymerization cycles was 90.

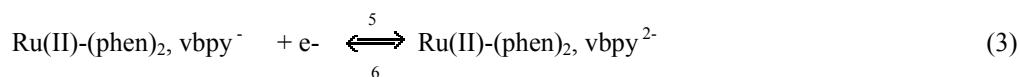
The films were characterized between +1.600 V and -1.600 V or -0.400 V vs. Ag/AgCl in the supporting electrolyte solution of propylene carbonate with TEAP. Scan rates for characterization ranged from 0.10 V/sec to 10 V/sec.

## 3. Results and Discussion

### 3.1 Electropolymerization of Ru(II)-(phen)<sub>2</sub>vbpy on Glassy Carbon Electrodes

The deposition of the ruthenium complex onto glassy carbon electrodes by initiating reductive electrochemical polymerizations of the ruthenium complex was accomplished by cycling the potential applied to the glassy carbon electrode from 1.600 V to -1.600 V. This is an efficient way of producing a multi-layered polymer film and hence produce a three-dimensional network of ruthenium redox centers. Several researchers have reported values of 24-1560 monolayers based upon the packing density of the polymer films formed from Bis(vinylterpyridine)cobalt(II). These films were used in the electrochemical reduction of carbon dioxide and oxygen (Abruna et.al 1981, Hurrell et. al 1988). After completing 90 cycles of electropolymerization, three redox couples showing electrochemical reversibility persisted as shown in Figure 1. The first redox couple (Peaks 1 and 2) has a formal reduction potential,  $E^{0'} = (E_{pa} + E_{pc})/2$ , of 1.215 V and is related the electrochemical activity of Ru(III/II). Two other key redox couples with  $E^{0'}$  values of -1.255 V (Peaks 3 and 4) and -1.413 V (Peaks 5 and 6) were identified. These peaks correspond to the electrochemical activity of the ligand, vinylbipyridine (Meyer et. al 2005, Guarr et. al 1987, Calvert et.al 1983). Several research groups also identified two ligand-based redox processes of the ruthenium vinylbipyridine complexes based upon potential scanning methods. Cathodic peak 7 (ca. -1.150 V) and anodic peak 8 (ca. 1.250 V) did not appear until cycle 5, and are associated with the processes of charge trapping as the polymeric thin film forms (Guarr et. al 1987). Equations 1-3 summarize the electrochemical reactions corresponding to the reversible electrochemical processes shown in Figure 1.





Diffusion controlled conditions dominate the mass transfer mechanism of the monomer to the electrode surface during electropolymerization as evidenced by linear diagnostic plots of the peak current versus the square root of the scan rate (Figure 2) provided during the third cycle of the electropolymerization (Brown et. al 2002). Peak separation for the Ru(III/II) redox couple ranges from 0.071 V-0.118 V using scan rates of 0.100 V/sec–1.00 V/sec, and follows the trend for electrochemical systems transitioning from reversible to quasireversible electrochemistry.

The semi-conducting film containing Ru(III/II) redox centers acts as a mediator at the film-solution interface to facilitate the electropolymerization process. Increases in the peak currents per cyclic voltammetric scan for electropolymerization indicates the formation and growth of the polymeric thin film on the glassy carbon electrode. After 90 cycles of electropolymerization, the peak currents approach a steady-state value. This is partly due to a reduced electrode surface area available for deposition as the number of electropolymerization cycles approaches 90, and a thicker film which causes a reduction in charge migration rate within the film. Furthermore, plots of the peak current versus the voltammetric cycle of electropolymerization are linear with a non-zero intercept which signifies a fast initial electropolymerization process that begins diffusion of the monomer to the electrode surface (Calvert et. al 1983). The mechanism for the electropolymerization of this complex and similar complexes with vinyl groups have been reported in detail and involves the formation of radical anions which react at the electrode surface and subsequent chemical reactions (Guarr et. al 1987).

### 3.2 Electrochemical Behavior of Ru(II)-(phen)<sub>2</sub>, vbpy Polymer Films

After electrochemical deposition of the ruthenium complex, the glassy carbon electrode revealed a slight orange color. Figure 3 shows the subsequent electrochemical characterization of the electrode surface in 0.10 M TEAP in propylene carbonate at a scan rate of 0.100 V/sec which produced the same redox couples as shown in Figure 1. The peaks related to the charge trapping process were also observed when characterizing the thin films in the same supporting electrolyte solution. Observation of the peaks in the same proximity as the peaks in the solution phase electrochemistry provides further evidence for successful immobilization of the ruthenium complex onto the glassy carbon electrode. The electrochemical observations reflect charge transfer within the polymer film between neighboring redox centers through a proposed “electron-hopping” mechanism and are related to Equations 1-3.

Characterizing the film in the supporting electrolyte solution of 0.10 M TEAP in propylene carbonate with a circumscribed potential window from 1.600 V to 0.400 V (Figure 4) restricts the electrochemistry to involve the Ru(III/II) redox couple, corresponding to Equation 1. At scan rates higher than 1.000 V/sec, the voltammograms resemble solution phase diffusion mass transfer conditions. The  $\Delta E_p$  values range from 0.0210 V to 0.485 V using scan rates between 0.100 V/sec to 10.0 V/sec. The increase in peak separation with higher scan rates is attributed to kinetic limitations of charge transfer between redox sites within the polymer film. Scan rates lower than 0.020 V sec<sup>-1</sup> produced  $\Delta E_p \sim 0$  V. This peak separation indicates facile charge transfer within the film and Nernstian equilibrium conditions of charge transfer with the applied potential. The peak width at half-height is greater than 90.6 mV which indicates non-equivalent redox centers and/or repulsive or attractive forces within the film [Brown et. al 2002]. Worth mentioning is that when the film is in a fully reduced state, the film has a negative charge which must be compensated by a counterion entering the film, (i.e., N(CH<sub>3</sub>CH<sub>2</sub>)<sub>4</sub><sup>+</sup>), in order to maintain charge electroneutrality. Due to solvent-ion interactions, the entering counterion is accompanied by solvent sphere(s). This may result in possible polymeric film swelling. Diagnostic plots of the anodic and cathodic peak current versus the scan rate from 1.600 V to 0.400 V for the thin films were linear for scan rates < 1 V/sec. Using scan rates < 1 V/sec allowed for finite diffusion boundary conditions to dominate the electrochemical charge transfer process. However, plots of the peak current versus the square root of the scan rate were linear for scan rates > 1 V/sec, indicating semi-infinite diffusion conditions. Under the latter conditions, it is possible that not all the redox sites are reduced and oxidized during the voltammetric scan. In this case, the charge transfer models the Randles-Sevcik equation:

$$I_p = (2.69 \times 10^5) n^{3/2} A D^{1/2} \nu^{1/2} C$$

where  $D$  represents the apparent charge transfer coefficient and  $C$  represents the concentration of oxidized or reduced ruthenium sites within the film. The other symbols have their normal electrochemical convention. In addition, at higher scan rates, the depletion layer above the surface of the electrode is thinner than the film thickness, and hence the system resembles semi-infinite diffusional boundary conditions (Collins 1996).

### 3.2.1 Surface Coverage

Surface coverage of the electrode was determined using the equation:  $\Gamma = Q/nFA$ , where  $\Gamma$  is the surface coverage in mol/cm<sup>2</sup>,  $Q$  is the charge in coulombs,  $A$  is the area of the electrode surface in cm<sup>2</sup>, and  $n$  is the number of electrons transferred during redox transformation. The value of  $Q$  was determined by integrating the area under the cathodic peak or anodic peak during the characterization of the electrode in the supporting electrolyte solution. The surface coverage was determined using anodic peak, corresponding to the  $\text{Ru}^{2+} \rightarrow \text{Ru}^{3+} + e^-$  process. Figure 5 shows the surface coverage with respect to the number of cycles of electropolymerization. Surface coverage ranges from  $9.42 \times 10^{-11}$  mol/cm<sup>2</sup> to  $4.76 \times 10^{-10}$  mol/cm<sup>2</sup>, corresponding to 30-90 cycles of electropolymerization. In addition, Figure 5 shows a leveling-effect corresponding to approximately 90 cycles of electropolymerization, correlating with the time needed to reach a steady-state peak current during the electropolymerization process.

## 4. Conclusion

Compared to other electrode modification procedures, the preparation of these films by electropolymerization using cyclic voltammetry is relatively simple in design, and is a one-step process. Building into the monomer an organic moiety such as a vinyl substituent allows for successful electropolymerization reactions to occur. The thin films exhibit facile electron transfer properties in propylene carbonate/TEAP supporting electrolyte solutions. For example, characterization scan rates near 1.000 V/sec produced peak separations under 0.100 V. At low scan rates, the peak separations are practically 0 mV. However, metal-based modified electrodes have peak separations of approximately 0.700 V at 1.000 V/sec (Razmi-Zerbin et. al 2002). The films presented herein require about 30 minutes to prepare and are now being investigated for long-term stability for potential use in flow injection analysis in the determination of hydrazine.

## References

- Abruna, H.D., Denisevich, P., Umana, M., Meyer, T.J., and Murray, R.W. (1981). Rectifying interfaces using two-layer films of electrochemically polymerized vinylpyridine and vinylbipyridine complexes of ruthenium and iron on electrodes. *J. Am. Chem. Soc.*, 103, 1-5.
- Allen, J.R., Florido, A., Young, S.D., Daunert, S., and Bachus, L.G. (1995). Nitrite-selective electrode based on an electropolymerized cobalt phthalocyanine. *Electroanalysis*, 7, 710-713.
- Bobacka, J., Gao, Z., Ivaska, A., and Lewenstam, A. (1994). Mechanism of ionic and redox sensitivity of p-type conducting polymers: Part 2. *Experimental study of polypyrrole*, 368, 33-41.
- Brown, K. and Mottola, H. (1998). Voltammetric, chronocoulometric and spectroelectrochemical studies of electropolymerized films based on Cu(II/I)-4,9,16,23-tetraaminophthalocyanine. *Langmuir*, 14, 3411-3417.
- Brown, K., Shaw, J., Ambrose, M., and Mottola, H. (2002). Voltammetric, chronocoulometric and spectroelectrochemical studies of electropolymerized films based on Co(III/II)- and Zn(II) 4,9,16,23-tetraaminophthalocyanine: effect of high pH. *Microchemical Journal*, 72, 285-298.
- Calvert, J.M., Schemehl, R.H., Sullivan, B.P., Facci, J.S., T.J. Meyer, and R.W.Murray, (1983). Synthetic and mechanistic investigations of the reductive electrochemical polymerization of vinyl-containing complexes of iron(II), ruthenium(II), and osmium(II). *Inorg. Chem.*, 22, 2151-2162.
- Collins, Greg. E. (1996). Gas-Phase chemical sensing using electrochemiluminescence. *Sensors and Actuators B*, 35-36, 202-206.
- Green, M.J., Faulkner, L.R. (1983). Reversible Oxidation and Rereduction of Entire Films of Transition-Metal Phthalocyanines. *J. Am. Chem. Soc.*, 105, 2950-2955.
- Guarr, T.F. and Anson F.C. (1987). Electropolymerization of Bis(1,10-phenanthroline) (4-methyl-4'-vinyl-2,2'-bipyridine) complexes through direct attack on the ligand ring system. *J. Phys. Chem.*, 91: 4037-4043.
- Hurrell, H.C., Mogstad, A.L., Usifer, D.A., Potts, K.T., and Abruna, H.D. (1989). Electrocatalytic activity of electropolymerized films of Bis(vinylterpyridine)cobalt(2+) for the reduction of carbon dioxide and oxygen. *Inorganic Chemistry*, 28, 1080-1084.
- Kang, T.F., Xie, Z.-Y., Tang, H., Shen, G.-L., and Yu, R.-Q. (1997). Potentiometric pH sensors based on chemically modified electrodes with electropolymerized metal-tetraaminophthalocyanine. *Talanta*, 47, 291-296.
- Lane, R.F., and Hubbard, A.T. (1973). Electrochemistry of Chemisorbed Molecules. I. Reactants Connected to Electrodes through Olefinic Substituents. *J. Phys. Chem.*, 77, 11, 1401-1410.

Li, H., and Guarr, T.F. (1991). Electrocatalytic oxidation of oxalic acid at electrodes coated with polymeric metallophthalocyanines. *J. Electroanal. Chem.*, 371, 189-202.

Pinter, J.S., Brown, K.L., DeYoung, P.A., and Peaslee, G.F. (2007). Amperometric detection of hydrazine by cyclic voltammetry and flow injection analysis using ruthenium modified glassy carbon electrodes. *Talanta*, 71, 1219-1225.

Razmi-Nerbin, H. and Rournaghi-Azar, M.H. (2002). Nickel pentacyanonitrosylferrate film modified aluminum electrode for electrocatalytic oxidation of hydrazine. *J. Solid State Electrochem*, 6, 126-133.

Wang, J. (1996). Electrocatalytic reduction and flow injection analysis of organic peroxides at polymeric tetra-amino iron phthalocyanine modified electrode. *Analytical Letters*, 29(9), 1575-1587.

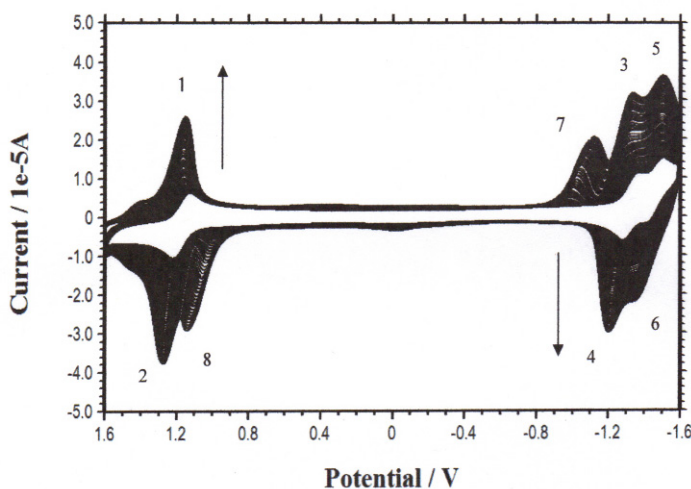


Figure 1. Electropolymerization of  $1.00 \times 10^{-3}$  M Ru(II)-(phen)<sub>2</sub>vbp. Supporting electrolyte is 0.100 M TEAP and solvent is propylene carbonate. Scan Rate = 0.100 V/sec. Seventy cycles of electropolymerization from 1.600 V to -1.600 V vs. Ag/AgCl

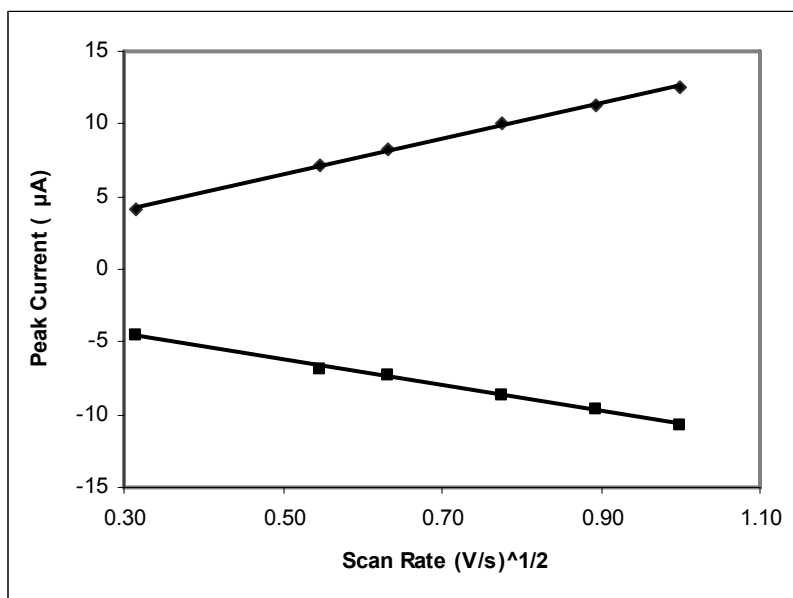


Figure 2. Plots of cathodic and anodic peak currents at various scan rates during electropolymerization of the ruthenium complex ( $1.00 \times 10^{-3}$  M Ru(II)-(phen)<sub>2</sub>vbpy in 0.10 M TEAP in propylene carbonate). Scan rates: 0.100 V/sec -1.00 V/sec. Peak currents taken during the third cycle of electropolymerization corresponding to the Ru(III/II) redox couple

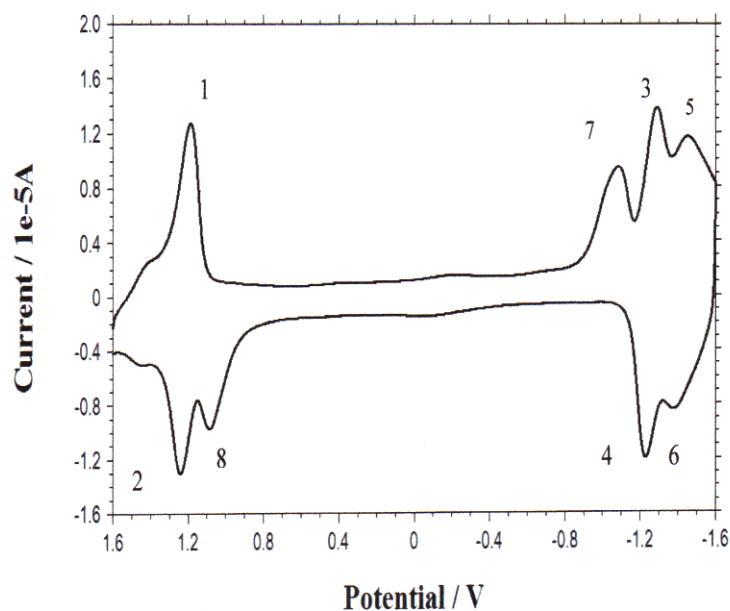


Figure 3. Characterization of ruthenium film in 0.100 M TEAP in propylene carbonate at 0.100 V/sec from 1.600 V to -1.600 V vs. Ag/AgCl

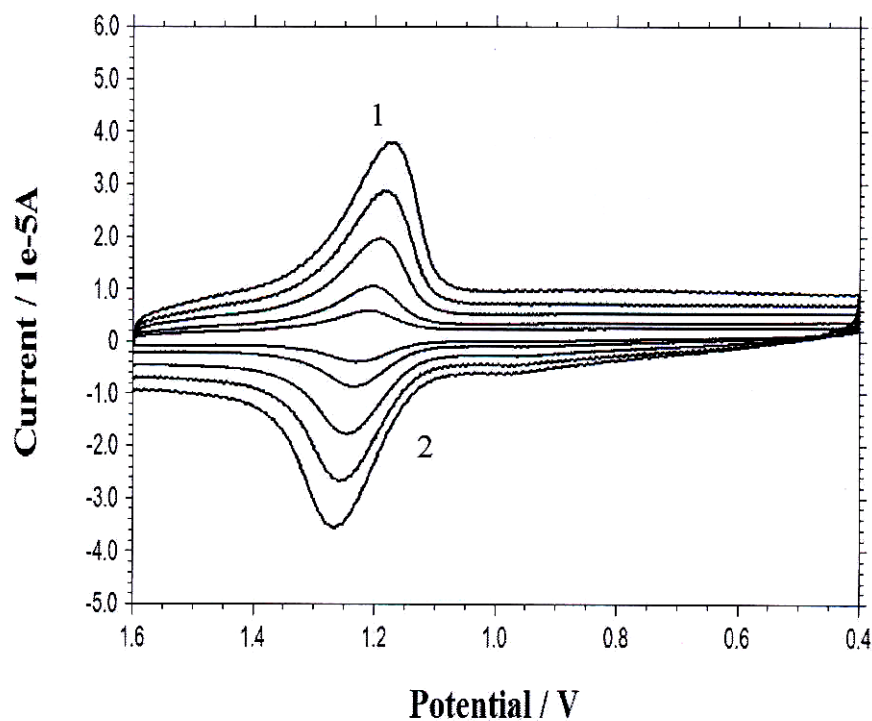


Figure 4. Characterization of ruthenium film in 0.100 M TEAP in propylene carbonate at 0.100 V/sec– 1.00 V/sec from 1.600 V to 0.400 V based on the Ru(III/II) redox couple

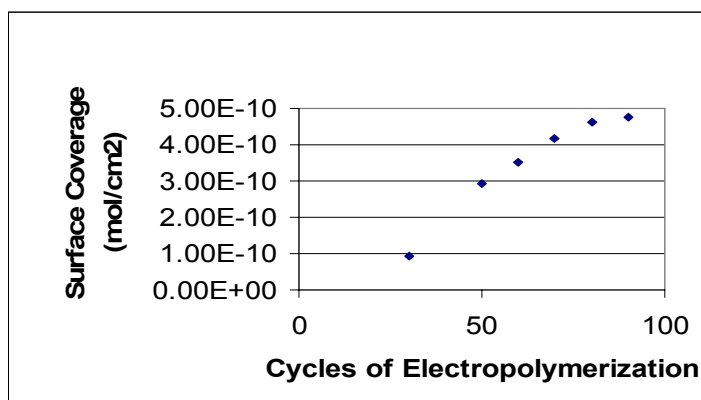


Figure 5. Profile of surface coverage with the number of electropolymerization cycles. Data taken from the characterization of the film corresponding to  $\text{Ru}^{2+} \rightarrow \text{Ru}^{3+} + \text{e}^-$  anodic peak in 0.10 M TEAP in propylene carbonate

# Photocatalytic Degradation of Phenol using Fe-TiO<sub>2</sub> by Different Illumination Sources

Reyad Awwad Shawabkeh (Corresponding author)

Department of Chemical Engineering, King Fahd University of Petroleum & Minerals

Dhahran, 31261, Saudi Arabia

E-mail: rshawabk@kfupm.edu.sa

Omar A. Khashman

Department of Environmental Engineering, Al-Hussein Bin Talal University

Maan, Jordan

Gasan I. Bisharat

Department of Chemical Engineering, Mutah University

Karak, 61710, Jordan

## Abstract

A Fe-doped titanium dioxide (Fe-TiO<sub>2</sub>) was prepared using hydrothermal method and used for degradation of phenol from aqueous solution. The samples were characterized by X-ray diffraction (XRD) and showed a presence of both TiO<sub>2</sub> and Fe<sub>2</sub>O<sub>3</sub> peaks. The photocatalytic activity of Fe-TiO<sub>2</sub> catalyst was evaluated for oxidation of phenol in aqueous solution using different illumination sources. Visible light irradiation from sun, UV light sources with 190 and 390 nm, fluorescence and dark environment were used and found that the degradation of phenol was in the order of 7.8%, 12%, 7.5%, 6.8% and 5% obtained after 24 h, respectively. It was found that the increase in exposure time to UV, the increase in solution temperature and pH have increased the rate of phenol degradation in solution. This rate was best fitted using first order kinetic model with reaction constant of  $6.268 \times 10^{-3}$ .

**Keywords:** Titanium dioxide, Iron oxides, Adsorption, XRD, Phenol

## 1. Introduction

Phenolic compounds are considered one of the major hazardous materials that have a perilous impact on environment. These materials were listed by The Agency for Toxic Substances and Disease Registry-USA (ATSDR) as one of the year 2007 priority contaminants that have significant potential threat to human health. Exposure to these compounds can cause liver damage, hemolytic anemia, paralysis and severe injury to the internal organs in human body (ATSDR, 2007). The maximum allowable limit for phenol concentration in water as set by Environmental Protection Agency (EPA) is 4 mg/L (EPA, 2007). As the concentration of phenols in the downstream gets much higher than this value, it becomes an urgent need for preventing such pollutants from entering water resources. Different technological treatment method could be employed for minimizing the concentration of phenols in aqueous solutions. These methods include chlorination (Ge, Zhu, & Wang, 2008; Sharma, et al., 2009), solvent extraction (Egorov, Smirnova, & Pletnev, 2008; Juang, Huang, & Hsu, 2008), adsorption (Shawabkeh & Abu-Nameh, 2007) and membrane process (Lee, Huang, Lee, Pan, & Chang, 2008; Mortaheb, Amini, Sadeghian, Mokhtarani, & Daneshyar, 2008; Wu & Li, 2008). These processes are either costly or have the inherent drawbacks due to the tendency of the formation of secondary toxic materials (Busca, Berardinelli, Resini, & Arrighi, 2008; Patra & Munichandraiah, 2008). Alternatively, photocatalytic degradation method can be employed to organics to produce harmless and low-molecular-weight compounds, particularly CO<sub>2</sub> and H<sub>2</sub>O.

Photo-oxidation of phenols can be attained by contacting these mixtures with semiconductors, particularly TiO<sub>2</sub>, and exposure to a UV illumination source that has energy higher than the band gap of these semiconductors. When illumination occurs on the surface of the semiconductors, the conduction band electrons and valence band



holes were generated at the interface of the solid-solution leading to oxidizing the phenolic compound to less harmful ones. The efficiency of this process depends on the type of the semiconductor, the intensity and wave length of the light, the solution characteristics and the exposure time.

Titanium dioxide is one of the well know semiconductor that is used in photocatalytic reactions. It can generate highly reactive oxygen species such as  $O_2^{\cdot-}$ ,  $HO_2^{\cdot}$  and  $HO^{\cdot}$  leading to the oxidation of a wide variety of aliphatic and aromatic hydrocarbons (Granados O, Paez M, Martinez O, & Paez-Mozo, 2005). Unlikely,  $TiO_2$  is less active in the visible region and only anatase crystalline form of  $TiO_2$  could be photoactive. Therefore, several attempts were performed to enhance the photocatalytic activity of  $TiO_2$ . These include doping of transition metals into the surface of  $TiO_2$  (Nahar, Hasegawa, Kagaya, & Kuroda, 2007; Wang, Ye, Wu, & Hu, 2008), acid pre-treatment of the anatase surface (Colon, Sanchez-Espana, Hidalgo, & Navio, 2006), impregnation with different dyestuff and complexes (Escobar, et al., 2008; Kawamura, Okuto, Taruta, Takusagawa, & Kitajima, 1996; Moon, Yun, Chung, Kang, & Yi, 2003), modification with other semiconductors (Ma, Brown, Howe, Overbury, & Dai, 2008) or supporting on surface of activated carbon, aluminosilicates and zeolite (Gan, Liu, Zhang, & Chen, 2008; Jayasankar, Ananthakumar, Mukundan, Wunderlich, & Warriar, 2008; Mahalakshmi, Vishnu Priya, Arabindoo, Palanichamy, & Murugesan, 2008; Razavi, Rahimpour, & Kaboli, 2008; Yang, Liu, Yang, & Yu, 2008).

Iron oxides are widely used in water treatments as adsorbents and amphoteric ion exchangers because they readily undergo reduction or oxidation, depending upon the surrounding conditions (Nganai, Lomnicki, & Dellinger, 2009). The photocatalytic of iron doped  $TiO_2$  is used to extend the photocatalyst's response into the visible region and hence improve the oxidation of several organic compounds such as chloroform, toluene, benzene, alcohols and ethers (Gan, et al., 2008).

This work aims at doping iron oxides into  $TiO_2$  surface and utilizes the produced catalyst for degradation of phenol from aqueous solution.

## 2. Materials and methods

### 2.1 Materials

Titanium dioxide (Degussa P25; composed of 80% anatase and 20% rutile) was purchased from Degussa Chemicals (Hanau, Germany) and used without further treatment. Nitric acid, ferric nitrate and high purity phenol were supplied by Sigma-Aldrich Chemical Company. All solutions were prepared using deionized water from a Milli Q system (Millipore, France). All glassware were Pyrex washed with soap, rinsed with nitric acid the washed with deionized water.

### 2.2 Catalyst preparation and characterization

Two hundred grams of  $TiO_2$  were mixed with 100 ml of concentrated nitric acid and kept under vigorous stirring for 30 minutes. After mixing, the acid treated  $TiO_2$  is filtrated, washed with deionized water, dried at 105 °C and stored in a closed container. Five grams of the acid treated titania was added to 200 ml of 6.2 mM  $Fe(NO_3)_3 \cdot 9H_2O$  and mixed for 30 minutes. Then, the mixture was transferred into 1 L Teflon-lined autoclave and placed in an oven at 180 °C for 24 h. The sample is then calcinated in a muffle furnace at  $500 \pm 25$  °C for 7 hours. The produced material was washed with deionized water, dried at 105 °C and stored in a cool dry place for further usage.

Samples of the doped  $TiO_2$  were characterized using an X-Ray diffraction (XRD) using PAN analytical X-Ray, Philips analytical. The dried sample was tested at 40 kV and 40 mA; the spectra were analyzed using PC-ADP diffraction software. Caption microscope images were performed using MIC-D digital microscope (Olympus-Japan) where 0.1g sample was scanned at 10µm grids.

### 2.3 Photo-oxidation experiments

In order to test the effect of light source and catalyst activity on oxidation of phenol, ten samples of 116 mg/L phenol each were treated with 0.2 g either  $TiO_2$  or Fe- $TiO_2$  in 100 ml and exposed to different light source environments such as UV 190-250 nm, UV 390 nm, sun light, fluorescence light (405 nm) and dark place. Blank samples were also treated in same manner for the purpose of comparison. After 24 h of shaking at isothermal

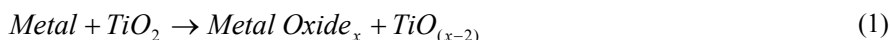
temperature ( $25 \pm 1$  °C), the samples were analyzed using Thermoelectron Heλiosα UV-Vis Spectrophotometer operated at a wavelength of 267 nm.

Isotherm study of phenol degradation was carried out in a set of 9 (100 ml) Erlenmeyer flasks. Samples of 0.1 g each of the Fe-TiO<sub>2</sub> was added to 50 ml phenol solutions (25-200 mg/L) and shaken isothermally ( $25 \pm 1$  °C) for 30 h under UV 190 nm. The solution was maintained at pH 10.55 by adding few drops of sodium hydroxide solution. Then at the end of the isotherm experiments the solution was settled down for 1 h, centrifuged at 4000 rpm and analyzed using the UV-Vis spectrophotometer. The difference between the initial and final concentration of phenol was measured. Similar procedures were carried out to obtain the effect of variation of temperature and solution pH.

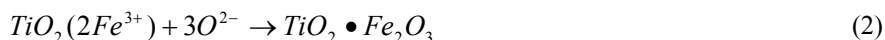
Kinetic experiments were conducted by mixing 1000 ml of 116 mg/L phenol solution with 2.0g Fe-TiO<sub>2</sub> in a baffled glass beaker (2000 ml) fitted with a triple-blade electrical stirrer. The mixture was illuminated with UV 190 nm for 30 minute. The pH was controlled at  $10.55 \pm 0.01$  and the temperature was maintained constant at ( $25 \pm 1$  °C. Aliquots were syringed out periodically during irradiation time using fritted glass filter, centrifuged at 4000 rpm for 5 minutes and then analyzed by using UV-Vis Spectrophotometer.

### 3. Results and discussion

The commercial titanium dioxide was treated with nitric acid followed by doping of iron oxide onto the surface. The formation of iron oxide on the surface of TiO<sub>2</sub> occurred because the process is thermodynamically favorable. Persuod and Madey (Bahnmann, Bockelmann, Goslich, Hilgendorff, & Weichgrebe, 1993) showed that if a metal is deposited on surface of TiO<sub>2</sub>, this metal should reduce the TiO<sub>2</sub> to Ti<sub>2</sub>O<sub>3</sub> or TiO, and itself become oxidized according:



In the presence of oxygen and calcinations at 500 °C, the adsorbed iron will produce iron oxide film doped on the surface of TiO<sub>2</sub> as (Bahnmann, et al., 1993; Grey & Ward, 1973; Sposite, 1989) :



XRD analysis of the produced sample (Figure 1) was examined using Cu-K radiation which shows two major peaks in the region 25-60 2θ. The peak at 29.49 2θ is due to the presence of TiO<sub>2</sub> while the one at 34.29 is due to the formation of Fe<sub>2</sub>O<sub>3</sub>.

Microscopic image for the doped samples is shown in Figure 2. It is shown a highly porous material with agglomerated TiO<sub>2</sub> placed on iron oxide surface occurred. An irregular and porous surface is observed where the dark area represents the iron oxides surrounded by the TiO<sub>2</sub>. The external diameter of the macrospores is ranging from 1-10 μm.

The doped TiO<sub>2</sub> was further tested for its oxidation potential against phenol and compared with that of TiO<sub>2</sub>. Figure 3 illustrates the effect of light sources on the degradation of phenol. It is cleared that the maximum removal of phenol is attained using UV 190 nm, followed by sun light, UV 390 and fluorescence lights. The experiments that conducted in the dark place were considered as blank samples and the percent reduction in phenol concentration attained by this sample could be explained by an adsorption process took place at the surface of Fe-TiO<sub>2</sub>. The highest degradation efficiency of phenol at 190 nm is attributed to the high energy associated with this wavelength. The difference between final concentrations of phenol obtained by the samples treated at different light sources and those of blank represent the percent of phenol reduction. Therefore, this light source was further used for studying the kinetics of phenol degradation.

This degradation mechanism of phenol over the surface of Fe-TiO<sub>2</sub> may explained by the oxidation of phenol using hydroxyl radical generated in solution. The phenol molecules are adsorbed by the surface of iron oxides coated on TiO<sub>2</sub> particles as a result of decreasing the surface tension of solution. When UV light illuminates at energy higher than the band gap of TiO<sub>2</sub> it generates conduction band electrons and valence band holes. The valence band hole can either be trapped at the surface of the TiO<sub>2</sub> or react with surface hydroxyl ions in water to form hydroxyl radical which oxidize phenol in both cases according (Lifongo, Bowden, & Brimblecombe, 2004):



On the other hand, the conduction band electrons either reduce  $H^+$  in solution to form  $H_{2(g)}$  or reacts with oxygen to form super-oxide radical,  $O_2^{\bullet-}$  according



Then the  $OH^{\bullet}$  radical react with phenol ( $C_6H_6O$ ) to produce carbon dioxide and water as (Gondal & Seddigi, 2006)



### 3.1 Effect of degradation parameters

The photocatalytic degradation of phenol was studied over a wide range of initial concentration from 25 to 200 mg/L (Figure 4). At low concentration (25-75 mg/L) a maximum degradation was achieved to reach a value of 18.5%, while a decrease in this capacity is occurred with further increasing in phenol concentration. This is due to the absorption of major illuminated light by phenol molecules which reduced the photocatalytic activity of the  $TiO_2$  (Das, Parida, & De, 2005). Therefore, less phenol molecules will be degraded per a unit dose of  $TiO_2$ .

On the other hand, fixed phenol solutions were irradiated at different pH values and found that the increase in solution pH will increase the percent degradation (Figure 5). The maximum removal value was 20.86% obtained at pH 10 while this value decreased to 4.2% at pH 2. The decrease in phenol degradation with decreasing pH may be attributed to the decrease in hydroxyl ions that are needed to react with valence band hole to form hydroxyl radicals as shown in Equation 7 (Colon, et al., 2006). In contrast, the adsorption of organics from aqueous solutions is increased with decreasing the pH as a result of neutralization of the surface of adsorbent with the excessive hydrogen ions in the solution which gives a controversially contradiction conclusion. However, this is not the case here because the hydrogen ions are consumed by reaction with conduction band electrons to liberate hydrogen gas.

Effect of temperature on the degradation of phenol is illustrated in Figure 6. As the solution temperature increases the percent degradation of phenol is increased. This increase could be explained by the enhancement of the reaction rate took place between the phenol molecules and the hydroxyl radicals (Daneshvar, Rabbani, Modirshahla, & Behnajady, 2004). Moreover, the enhancement of the degradation is probably due to the increasing collision frequency of phenol molecules (Evgenidou, Fytianos, & Poullos, 2005).

The rate of decrease of phenol concentration in solution is assumed to follow a first order reaction as

$$\frac{-dC_{ph}}{dt} = kC_{ph} \quad (10)$$

Where  $C_{ph}$  is the concentration of phenol in solution at a given time,  $t$ , and  $k$  is the reaction rate constant,

The integration to the above equation yield an exponential concentration profile with time according

$$C_{ph} = C_{o,ph} e^{-kt} \quad (11)$$

Where  $C_{o,ph}$  is the initial phenol concentration in solution. The experimental data in Figure 7 were fitted to the above equation and the value of the reaction constant,  $k$ , was found to be  $6.268 \times 10^{-3}$  with regression coefficient of 0.973 and  $\sum (error)^2 = 26.6$ .

## 4. Conclusion

It has been experimentally demonstrated that titanium dioxide doped with iron oxides could be used to photo-degrade phenol. This degradation is best attained at low solution acidity (pH ~ 10) and high temperature value using UV 254 nm irradiation source. The higher initial concentration of phenol will decrease the efficiency

of degradation process. The presence of iron oxides increased the adsorption of phenol and hence the rate of degradation. This catalyst can be employed commercially as a wastewater treatment filter, which has a low cost, non toxic, and has a good potential for selective removal of target solutes form solution.

## References

- ATSDR. (2007). CERCLA Priority List of Hazardous Substances, from Department of Health and Human Services, USA. [Online] Available: <http://www.atsdr.cdc.gov/cercla/05list.html>:
- Bahnmann, D., Bockelmann, D., Goslich, R., Hilgendorff, M., & Weichgrebe, D. (1993). In D. O. a. H. Al-Ekabi (Ed.), *Photocatalytic Purification and Treatment of Water and Air* (pp. 301-320). Amsterdam, The Netherlands: Elsevier Science.
- Busca, G., Berardinelli, S., Resini, C., & Arrighi, L. (2008). Technologies for the removal of phenol from fluid streams: A short review of recent developments. *Journal of Hazardous Materials*, 160(2-3), 265.
- Colon, G., Sanchez-Espana, J. M., Hidalgo, M. C., & Navio, J. A. (2006). Effect of TiO<sub>2</sub> acidic pre-treatment on the photocatalytic properties for phenol degradation. *Journal of Photochemistry and Photobiology A: Chemistry*, 179(1-2), 20.
- Daneshvar, N., Rabbani, M., Modirshahla, N., & Behnajady, M. A. (2004). Kinetic modeling of photocatalytic degradation of Acid Red 27 in UV/TiO<sub>2</sub> process. *Journal of Photochemistry and Photobiology A: Chemistry*, 168(1-2), 39.
- Das, D. P., Parida, K., & De, B. R. (2005). Photo-oxidation of phenol over titania pillared zirconium phosphate and titanium phosphate. *Journal of Molecular Catalysis A: Chemical*, 240(1-2), 1.
- Egorov, V. M., Smirnova, S. V., & Pletnev, I. V. (2008). Highly efficient extraction of phenols and aromatic amines into novel ionic liquids incorporating quaternary ammonium cation. *Separation and Purification Technology*, 63(3), 710.
- EPA. (2007). *EPA National Library Network*. [Online] Available: <http://www.epa.gov/natlbra/ols.htm>.
- Escobar, J., Barrera, M. C., de los Reyes, J. A., Toledo, J. A., Santes, V., & Coli'n, J. A. (2008). Effect of chelating ligands on Ni-Mo impregnation over wide-pore ZrO<sub>2</sub>-TiO<sub>2</sub>. *Journal of Molecular Catalysis A: Chemical*, 287(1-2), 33.
- Evgenidou, E., Fytianos, K., & Poullos, I. (2005). Photocatalytic oxidation of dimethoate in aqueous solutions. *Journal of Photochemistry and Photobiology A: Chemistry*, 175(1), 29.
- Gan, L., Liu, M., Zhang, X., & Chen, L. (2008). Synthesis and photocatalytic activity of Fe-doped TiO<sub>2</sub>-activated carbon composite materials response to visible light. *Tongji Daxue Xuebao/Journal of Tongji University*, 36(4), 538.
- Ge, F., Zhu, L., & Wang, J. (2008). Distribution of chlorination products of phenols under various pHs in water disinfection. *Desalination*, 225(1-3), 156.
- Gondal, M. A., & Seddigi, Z. (2006). Laser-induced photo-catalytic removal of phenol using n-type WO<sub>3</sub> semiconductor catalyst. *Chemical Physics Letters*, 417(1-3), 124.
- Granados O, G., Paez M, C. A., Martinez O, F., & Paez-Mozo, E. A. (2005). Photocatalytic degradation of phenol on TiO<sub>2</sub> and TiO<sub>2</sub>/Pt sensitized with metallophthalocyanines. *Catalysis Today*, 107-108, 589.
- Grey, I. E., & Ward, J. (1973). An X-ray and Mo'ssbauer study of the FeTi<sub>2</sub>O<sub>5</sub>Ti<sub>3</sub>O<sub>5</sub> system. *Journal of Solid State Chemistry*, 7(3), 300.
- Jayasankar, M., Ananthakumar, S., Mukundan, P., Wunderlich, W., & Warriar, K. G. K. (2008). Al<sub>2</sub>O<sub>3</sub> @ TiO<sub>2</sub>-A simple sol-gel strategy to the synthesis of low temperature sintered alumina-aluminium titanate composites through a core-shell approach. *Journal of Solid State Chemistry*, 181(10), 2748.
- Juang, R. S., Huang, W. C., & Hsu, Y. H. (2008). Treatment of phenol in synthetic saline wastewater by solvent extraction and two-phase membrane biodegradation. *Journal of Hazardous Materials*.
- Kawamura, H., Okuto, S., Taruta, S., Takusagawa, N., & Kitajima, K. (1996). Inhomogeneous distribution of TiO<sub>2</sub> in porous glass specimen anchored by impregnation method using aqueous solutions. *Nippon Seramikkusu Kyokai Gakujutsu Ronbunshi/Journal of the Ceramic Society of Japan*, 104(12), 1160.
- Lee, M. S., Huang, C., Lee, K. R., Pan, J. R., & Chang, W. K. (2008). Factors affecting phenol transfer through polydimethylsiloxane composite membrane. *Desalination*, 234(1-3), 416.

- Lifongo, L. L., Bowden, D. J., & Brimblecombe, P. (2004). Photodegradation of haloacetic acids in water. *Chemosphere*, 55(3), 467.
- Ma, Z., Brown, S., Howe, J. Y., Overbury, S. H., & Dai, S. (2008). Surface modification of Au/TiO<sub>2</sub> catalysts by SiO<sub>2</sub> via atomic layer deposition. *Journal of Physical Chemistry C*, 112(25), 9448.
- Mahalakshmi, M., Vishnu Priya, S., Arabindoo, B., Palanichamy, M., & Murugesan, V. (2008). Photocatalytic degradation of aqueous propoxur solution using TiO<sub>2</sub> and H<sup>+</sup> zeolite-supported TiO<sub>2</sub>. *Journal of Hazardous Materials*.
- Moon, J., Yun, C. Y., Chung, K.-W., Kang, M.-S., & Yi, J. (2003). Photocatalytic activation of TiO<sub>2</sub> under visible light using Acid Red 44. *Catalysis Today*, 87(1-4), 77.
- Mortaheb, H. R., Amini, M. H., Sadeghian, F., Mokhtarani, B., & Daneshyar, H. (2008). Study on a new surfactant for removal of phenol from wastewater by emulsion liquid membrane. *Journal of Hazardous Materials*, 160(2-3), 582.
- Nahar, M. S., Hasegawa, K., Kagaya, S., & Kuroda, S. (2007). Comparative assessment of the efficiency of Fe-doped TiO<sub>2</sub> prepared by two doping methods and photocatalytic degradation of phenol in domestic water suspensions. *Science and Technology of Advanced Materials*, 8(4), 286.
- Nganai, S., Lomnicki, S., & Dellinger, B. (2009). Ferric oxide mediated formation of PCDD/Fs from 2-monochlorophenol. *Environmental Science and Technology*, 43(2), 368.
- Patra, S., & Munichandraiah, N. (2008). Electro-oxidation of phenol on polyethylenedioxythiophene conductive-polymer-deposited stainless steel substrate. *Journal of the Electrochemical Society*, 155(3), F23.
- Razavi, M., Rahimpour, M. R., & Kaboli, R. (2008). Synthesis of TiC nanocomposite powder from impure TiO<sub>2</sub> and carbon black by mechanically activated sintering. *Journal of Alloys and Compounds*, 460(1-2), 694.
- Sharma, V. K., Anquandah, G. A. K., Yngard, R. A., Kim, H., Fekete, J., Bouzek, K., et al. (2009). Nonylphenol, octylphenol, and bisphenol-A in the aquatic environment: A review on occurrence, fate, and treatment. *Journal of Environmental Science and Health - Part A Toxic/Hazardous Substances and Environmental Engineering*, 44(5), 423.
- Shawabkeh, R. A., & Abu-Nameh, E. S. M. (2007). Absorption of phenol and methylene blue by activated carbon from pecan shells. *Colloid Journal*, 69(3), 355.
- Sposite, G. (1989). *The Chemistry of soil*. Oxford: University Press.
- Wang, Y. L., Ye, J. Y., Wu, H. S., & Hu, Y. H. (2008). Study on photocatalytic degradation of phenol by Ag-doped ZnO thin films. *Rengong Jingti Xuebao/Journal of Synthetic Crystals*, 37(4), 1033.
- Wu, H. S., & Li, C. C. (2008). Kinetic study of phenol recovery using phase-transfer catalysis in horizontal membrane reactor. *Chemical Engineering Journal*, 144(3), 502.
- Yang, H. N., Liu, L. F., Yang, F. L., & Yu, J. C. (2008). Fibrous TiO<sub>2</sub> prepared by chemical vapor deposition using activated carbon fibers as template via adsorption, hydrolysis and calcinations. *Journal of Zhejiang University: Science A*, 9(7), 981.

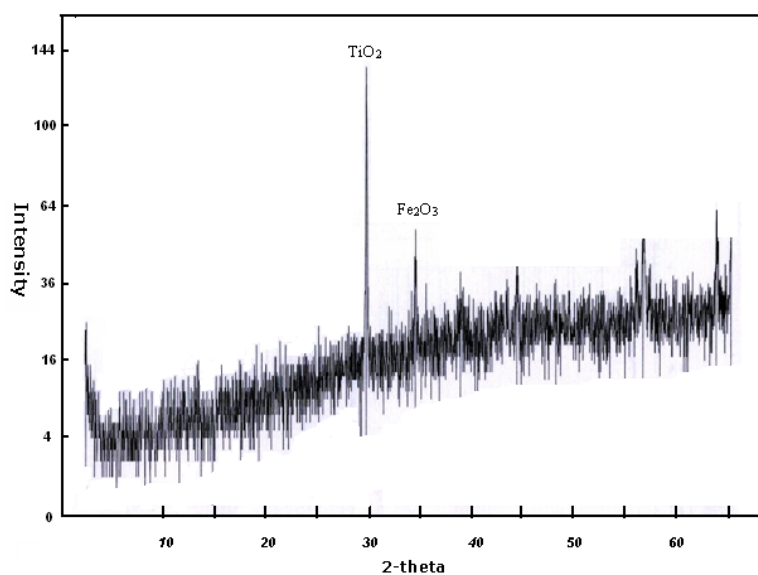


Figure 1. XRD pattern for the doped titanium dioxide



Figure 2. Microscopic image of the doped TiO<sub>2</sub>

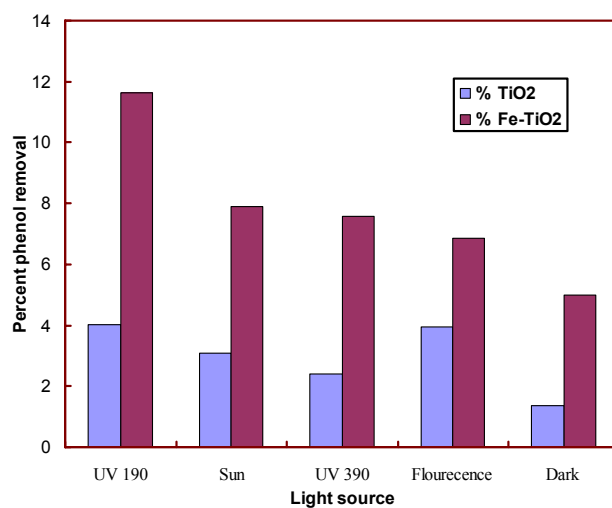


Figure 3. Effect of different light source on the degradation of phenol

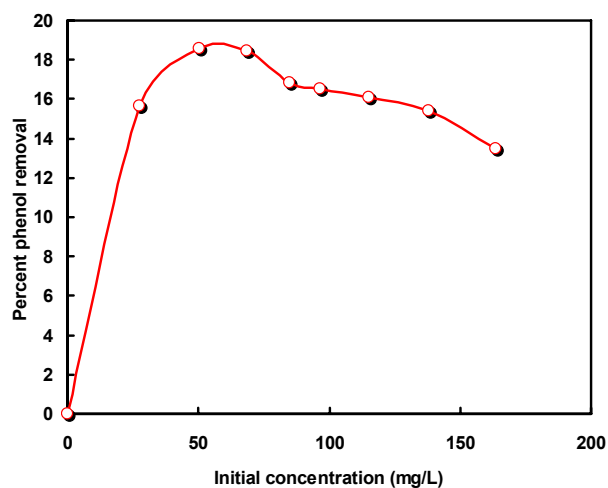


Figure 4. Effect of initial concentration on phenol degradation

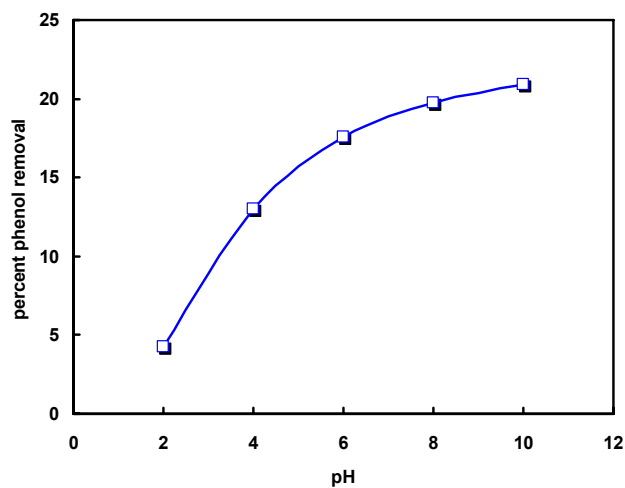


Figure 5. Effect pH on photo-degradation of phenol from aqueous solution

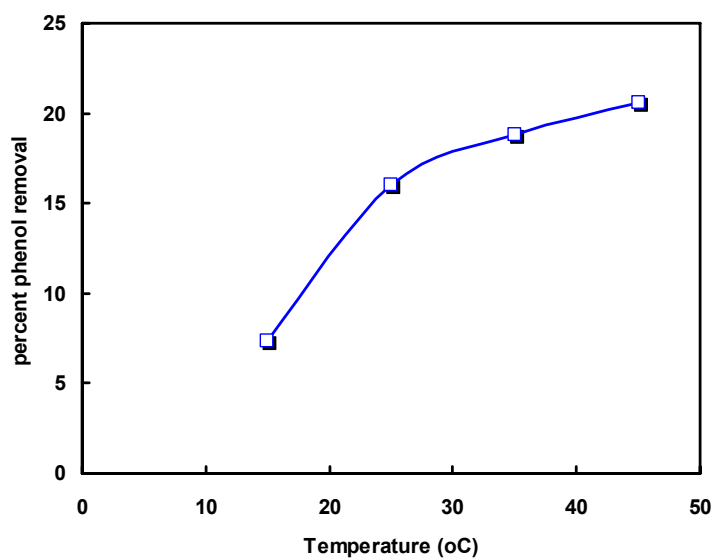


Figure 6. Effect of temperature on phenol photocatalytic degradation

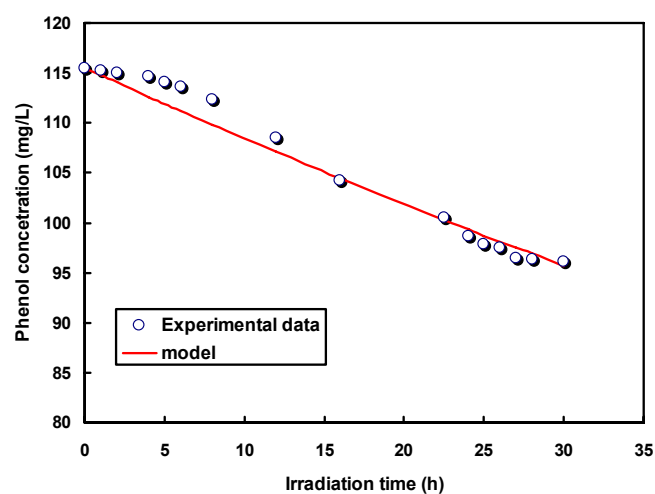


Figure 7. Rate of kinetic of phenol removal from aqueous solution



# Computational Models of Thermal Cycling in Chemical Systems

Carl Barratt

Department of Mechanical, Civil and Environmental Engineering  
Tagliatela College of Engineering, University of New Haven, West Haven, CT, 06516, USA

Dante M. Lepore, Matthew J. Cherubini & Pauline M. Schwartz (Corresponding author)

Department of Chemistry and Chemical Engineering, Tagliatela College of Engineering  
University of New Haven, West Haven, CT, 06516, USA

Tel: 1-203-932-7170 E-mail: pschwartz@newhaven.edu

## Abstract

Computational models of chemical systems provide clues to counterintuitive interactions and insights for new applications. We have been investigating models of chemical reaction systems under forced, thermal cycling conditions and have found that some hypothetical processes generate higher yields under thermal cycling than under single, fixed temperature conditions. A simple kinetic model of an actual process, the two-temperature polymerase chain reaction that replicates DNA, is used to simulate the important features of a chemical system operating under thermal cycling. This model provides insights into the design of other chemical systems that may have important applications in chemistry, biochemistry and chemical engineering.

**Keywords:** Polymerase chain reaction, Thermal cycling

## 1. Introduction

Computational models of chemical systems provide insight into new reaction processes and mechanisms. The models described here were inspired by a mathematical concept from game theory, known as Parrondo's paradox, whereby two losing games can produce a winning outcome if appropriately alternated (Abbott D. 2010; Harmer G. P. & Abbott D. 1999; Martin H. & von Baeyer H. C. 2004; The University of Adelaide, School of Electrical Engineering, Parrondo's Paradox Official Website). To mimic alternating game strategies, we have been investigating the effect of thermal cycling on chemical reaction systems, and have indeed discovered that certain chemical processes can generate significantly higher yields of product under thermal cycling than under single, fixed-temperature conditions (Osipovitch D. C., Barratt C. & Schwartz P. M. 2009). While there are few actual chemical processes that are carried out under thermal cycling, there are several examples of reactions carried out in microreactors that have been found empirically to occur more rapidly under fast, forced thermal cycling (Brandner J. J., Emig G., Liauw MA & Schubert K. 2004; Hansen H. A., Olsen J. L., Jensen S., Hansen O. & Quaade U. J. 2006; Jensen S., Thorsteinsson S., Hansen O. & Quaade J. J. 2008; Luther M., Brandner J. J., Schubert K., Renken A. & Kiwi-Minsker L. 2008; Luther M., Brandner J. J., Kiwi-Minsker L., Renken A. & Schubert K. 2008; Silveston P. L. & Hudgins R. R. 2004). To motivate a more general investigation of the utility of thermal cycling, we developed a simple kinetic model of the two-temperature polymerase chain reaction (2T-PCR) as an actual chemical system that replicates DNA.

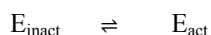
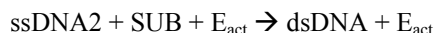
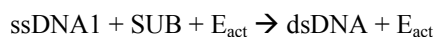
The polymerase chain reaction is a fundamental tool in molecular biology, which permits amplification of double stranded DNA (dsDNA) in a thermal cycling process (Kramer M. F. & Coen D. M. 2001; Lo Y. M. D. & Chan K. C. A. 2006). Traditional PCR involves three temperature steps: denaturation of dsDNA at a high temperature to two complementary, single-stranded DNA (ssDNA) templates (a 5'-3' ssDNA and a 3'-5' ssDNA); annealing of specific primers to the ssDNA templates at an intermediate temperature; and extension and replication of DNA at a lower temperature catalyzed by a DNA polymerase in the presence of deoxyribonucleotide substrates (dATP, dGTP, dCTP and TTP). Under appropriate conditions, the traditional three-temperature protocol for PCR can be replaced by a two-temperature cycle (Cha R. S. & Thilly W. G. 1993; Horton J. H., Hagen M. D. & Ko K. S. 1994; Neuzil P., Zhang C., Pippert J., Oh S. & Zhuo L. 2006). With two-temperature PCR, there is a cyclic process between a short period at high temperature (90-95°C) to denature dsDNA into two ssDNA templates and then a longer period at 60-75°C in which both annealing and extension of complementary primers occur. Every cycle of the PCR reaction theoretically doubles the amount of dsDNA, i.e.

is 100% efficient so that with  $n$  temperature cycles,  $2^n$  copies of the original dsDNA are generated,  $n$  being determined by how much substrate is present: doubling falls off as substrates (primers and/or deoxyribonucleotides) are depleted.

The goal of creating chemical systems that operate like PCR has eluded investigators. PCR as a chemical system is driven by forced thermal cycling and is unlike spontaneously oscillating reactions (such as the BZ reaction or Turing systems). Like PCR, some very interesting self-replicating, autocatalytic systems have been devised (Beutel K. M. & Peacock-Lopez E. 2007; Kamioka S., Ajami D. & Rebek J. 2010; Patzke V. & von Kiedrowski G. 2007; Rebek J. 1992; Robertson A., Sinclair A. J. & Philp D. 2000; Sievers D. & von Kiedrowski G. 1998; Vidonne A. & Philp D. 2009; Wang B. & Sutherland I. O. 1997; Wintner E. A., Conn M. M. & Rebek J. 1994), but these reactions have not been investigated under thermal cycling conditions. Yoon and Mirkin recently reported a PCR-like cascade reaction using a rhodium coordination complex (Yoon H. J. & Mirkin C. A. 2008); however, as pointed out by D. Blackmon, "the sigmoidal profiles observed in that case may be attributed to an in situ catalyst activation process .... and is not related either to self-replication or to PCR-type amplification" (Blackmond D. G. 2009). We suggest that computational modeling of the kinetic features of two-temperature PCR may provide essential clues to creating actual chemical processes that, when carried out under thermal cycling, would possess the advantages of a self-replicating chemical system.

## 2. The Chemical System under Investigation – 2T-PCR

A simplified PCR system that we are investigating is represented by the following reaction equations:



in which ssDNA1 and ssDNA2 designates the two complementary ssDNA templates of dsDNA;

SUB represents the substrates, both the deoxyribonucleotides and primers;  $E_{\text{act}}$  represents the active enzyme that functions at the lower temperature and  $E_{\text{inact}}$  is the inactive form of the enzyme at the higher temperature.

### 2.1 Parameter selection and assumptions

For the model systems, we chose parameters that reflect typical conditions for real-time, two temperature PCR (Cha R. S. & Thilly W. G. 1993; Horton J. H., Hagen M. D. & Ko K. S. 1994; Neuzil P., Zhang C., Pipper J., Oh S. & Zhuo L. 2006). A time course for the thermal cycling was chosen in which the PCR commenced at a high temperature (370K, 97°C) to denature the initial dsDNA. Then, cycles were chosen such that a period of 75 sec. at a low temperature (330K, 57°C) was followed by a short time, 15 sec., at the higher temperature. The temperature protocol is typical for 2T-PCR. The simulations were analyzed for 25 cycles. SUB starts at a high concentration and becomes limiting for synthesis of dsDNA. In the initial models, the concentration of dsDNA is taken as  $1 \times 10^{-5}$  M. The models make several assumptions including no loss in enzyme activity over time and no side reactions (such as primer-dimer interactions). This allowed us to focus on the core reactions of PCR as a chemical system.

## 3. Kinetic Description and Theoretical Analysis of the Chemical System

Kinetic parameters,  $A$  (the Arrhenius constant) and  $E_a$  (the activation energy), which yielded a working model, are shown in Table 1. Rate constants,  $k_1$  through  $k_6$  at 330K and 370K, were obtained in the usual way using the Arrhenius equation. The initial concentrations are set to be:  $[\text{dsDNA}]_0 = 1.0 \times 10^{-5}$  M,  $[\text{ssDNA}]_0 = 0.0$  M,  $[\text{SUB}]_0 = 0.5$  M,  $[E_{\text{inact}}]_0 = 0.0$  M,  $[E_{\text{act}}]_0 = 1.0 \times 10^{-3}$  M.

The governing differential equations for the simplified PCR reactions shown above are:

$$\begin{aligned}
\frac{d}{dt}[E_{inact}] &= -k_1[E_{inact}] + k_2[E_{act}] \\
\frac{d}{dt}[SUB] &= -(k_5[ssDNA1] + k_6[ssDNA2])[SUB][E_{act}] \\
\frac{d}{dt}[E_{act}] &= k_1[E_{inact}] - k_2[E_{act}] \\
\frac{d}{dt}[dsDNA] &= -k_3[dsDNA] + k_4[ssDNA1][ssDNA2] \\
&\quad + (k_5[ssDNA1] + k_6[ssDNA2])[SUB][E_{act}] \\
\frac{d}{dt}[ssDNA1] &= k_3[dsDNA] - k_4[ssDNA1][ssDNA2] - k_5[ssDNA1][SUB][E_{act}] \\
\frac{d}{dt}[ssDNA2] &= k_3[dsDNA] - k_4[ssDNA1][ssDNA2] - k_6[ssDNA1][SUB][E_{act}]
\end{aligned}$$

To simplify the notation, we define variables X, Y, A, B, C, representing the concentrations at time t of the various chemicals:

$$X = [E_{inact}], \quad Y = [E_{act}] \text{ and } k_5 = k_6$$

$$A = [SUB] \quad (\text{not to be confused with the Arrhenius constant } A)$$

$$B1 = [ssDNA1], \quad B2 = [ssDNA2], \quad B = [ssDNA] \text{ and } B1 = B2 = B$$

$$C = [dsDNA]$$

Then the governing equations for X, Y, A, C and B now read:

$$dX/dt = -k_1X + k_2Y \quad (1)$$

$$dY/dt = k_1X - k_2Y \quad (2)$$

$$dA/dt = -2k_5AYB \quad (3)$$

$$dC/dt = -k_3C + k_4B^2 + 2k_5AYB \quad (4)$$

$$dB/dt = k_3C - k_4B^2 - k_5AYB, \quad (5)$$

Eqs.(1) and (2), governing the enzyme concentrations  $E_{inact}$  and  $E_{act}$  are easy to solve to give

$$\begin{aligned}
(1+k_2/k_1)X &= \{k_2/k_1 + \exp(-(k_1+k_2)t)\} X_0 + k_2/k_1 \{1 - \exp(-(k_1+k_2)t)\} Y_0, \\
(1+k_2/k_1)Y &= \{1 - \exp(-(k_1+k_2)t)\} X_0 + \{1+(k_2/k_1)\exp(-(k_1+k_2)t)\} Y_0.
\end{aligned}$$

For the  $k_1$  and  $k_2$  used in the present investigation, Y fairly quickly (within a few seconds) flatlines after a change in temperature from 330K to 370K or vice versa, to the “constant” value of  $Y = (X_0 + Y_0)/(1+k_2/k_1)$ .

Eqs.(3),(4) and (5) are coupled and nonlinear and thus difficult to solve in general. However, they do yield to analysis in three distinct regions, viz:

a) Constant temperature,  $T=330K$  or  $T=370K$ , for  $A \sim \text{constant}$ .

b) The “doubling” region, in which temperature oscillates between 330K and 370K and also  $A \sim \text{constant}$ . This consists of the first  $\sim 10$  cycles, i.e.  $0 < t < 900$  secs. The cycle period is taken to be 90s, of which the first 15s is at  $T_1 = 370\text{K}$ , the remaining 75s at  $T_2 = 330\text{K}$ .

c) The “plateau” region which begins after  $\sim 15$  cycles, by which time the substrate has depleted to  $A \sim 0$ .

### 3.1 Constant temperature region (a)

Numerical solution reveals that throughout the integration region,  $A \sim 1$ , so that  $K = k_5 AY$  is essentially constant. Also, we find that  $KB \gg k_4 B^2$ . Thus the equations for  $C$  and  $B$  are to very good approximation linear and easily solved, yielding, for  $B_0 = 0$

$$C + \alpha_+ B = e^{k_3(\alpha_+ - 1)t} C_0, \quad C + \alpha_- B = e^{k_3(\alpha_- - 1)t} C_0$$

in which  $2\alpha_{\pm} = 1 - \eta \pm \sqrt{((1 - \eta)^2 + 8\eta)}$  with  $\eta = K/k_3$ . For constant  $T = 330\text{K}$  the parameters used in the

present paper lead to  $C \sim e^{4.8 \times 10^{-5} t} C_0$ . Thus, over the period of interest,  $0 < t < 2340\text{s}$  (26 cycles),  $C$  increases steadily from the initial value  $C_0 = 10^{-5}$  to  $1.12 \times 10^{-5}$ .

For constant  $T = 370\text{K}$ , we obtain  $C \sim (e^{-2.96t} + 2 \times 10^{-3} e^{0.00296t}) C_0$ . In this case, the fast exponential causes  $C$  to drop precipitously from the initial  $C_0 = 10^{-5}$  to a value  $C \sim 2 \times 10^{-8}$  in the initial few seconds. Thereafter, the slow exponential dominates the solution and  $C$  increases steadily with time constant  $(1/3) \times 10^3\text{s}$  to a value  $C \sim 2 \times 10^{-5}$  at  $t = 2340\text{s}$ . In fact, this is a slight overestimate because, as indicated by numerical solution of the equations, at  $T = 370\text{K}$ ,  $A$  has depleted from  $A = 0.5$  to  $A = 0.487$  at  $t = 2340$  secs, and  $C$  is actually  $\sim 1.73 \times 10^{-5}$ . Either way, an important point, as will be confirmed below, is that under constant temperature conditions the production rate for  $C$  is significantly lower than that obtained when the temperatures are cycled.

### 3.2 The “doubling” region, $0 < t < 900$ secs (b)

For the first 10 cycles or so, the concentration,  $A$ , of substrate, remains almost fixed at  $A = 0.5$ . Also, as in a) we find numerically that  $KB \gg k_4 B^2$  and because of the quick flatlining of  $Y$  at each temperature,  $K = k_5 AY$  is also constant throughout each partial cycle. The general solution of the kinetic equations is:

$$C + \alpha_+ B = e^{k_3(\alpha_+ - 1)t} (C_0 + \alpha_+ B_0), \quad C + \alpha_- B = e^{k_3(\alpha_- - 1)t} (C_0 + \alpha_- B_0) \quad (6)$$

where, again,  $2\alpha_{\pm} = 1 - \eta \pm \sqrt{(1 - \eta)^2 + 8\eta}$  with  $\eta = K/k_3$ .

We here note that  $C_0, B_0$  represent the values of the concentrations  $C$  and  $B$  at the beginning of each  $T = \text{constant}$  partial cycle; they are the values of  $C$  and  $B$  acquired in the previous partial cycle.

At  $370\text{K}$ ,  $Y \sim 6.7 \times 10^{-5}$ , to give  $\eta = k_5 AY/k_3 \sim 1.02 \times 10^{-3}$ . Because  $\eta \ll 1$ ,  $\alpha_{\pm}$  can be approximated by,  $\alpha_+ \sim 1 + \eta$ ,  $\alpha_- \sim -2\eta$ . Then Eq. 6 yields, at  $t = 15\text{s}$ ,  $C \sim 2\eta(C_0 + B_0)$ ,  $B \sim (C_0 + B_0)$ . These values of  $C$  and  $B$  become the initial concentrations  $C_0$  and  $B_0$  for the  $330\text{K}$  segment of the cycle. At  $330\text{K}$ ,  $Y \sim 0.001$ ,  $\eta \sim 833 \gg 1$ , so that  $\alpha_+ \sim 2$ ,  $\alpha_- \sim -\eta$ . Then Eq. 6 leads to  $C \sim 2(C_0 + B_0) \sim 2C_0$ . Such concentration doubling per cycle persists for at least the first 10  $370\text{K}$ - $330\text{K}$  cycles, until the concentration,  $A$ , of substrate begins to fall off.

### 3.3 The “plateau” region ( $> 20$ cycles) (c)

The Eqs 3-5 yields:

$$C + B + A/2 = \text{constant} = C_0 + B_0 + A_0/2$$

so that when the system enters the “plateau” region defined by  $A \sim 0$ , which occurs (for the parameters used in this paper) after  $\sim 20$  cycles, we have thereafter

$$C + B = \sigma, \text{ where the constant } \sigma = C_0 + B_0 + A_0/2 = 10^{-5} + 0 + 0.25.$$

Using this constraint between  $C$  and  $B$ , the  $dC/dt$  equation now simplifies (recall  $A \sim 0$ ) to

$$\frac{dC}{dt} = -k_3 C + k_4 (\sigma - C)^2$$

which, although nonlinear, is easily solved to yield

$$C - \beta = \alpha \left[ \frac{(C_1 - \beta) - \alpha \tanh(\alpha k_4 t)}{\alpha - (C_1 - \beta) \tanh(\alpha k_4 t)} \right]$$

where

$$\beta = \sigma + \frac{k_3}{2k_4}, \quad \sigma = C_0 + A_0 / 2, \quad \alpha^2 = \beta^2 - \sigma^2.$$

It should be noted that when using the above solution,  $t$  is again reset to  $t = 0$  at the beginning of each “partial cycle”, i.e. when  $k_3$  and  $k_4$  change values, and  $C_1$  is the value of  $C$  at the beginning of the next partial cycle. For the parameters used in our model, we obtain, for  $T = 330\text{K}$ ,  $\beta \sim 0.25$ ,  $\alpha \sim 0.00675$  and for  $T = 370\text{K}$ ,  $\beta \sim 4.25$ ,  $\alpha \sim 4.2426$ . Notice that, for  $T=370\text{K}$ , the large value of  $\alpha k_4$  means that within just a few seconds,  $C$  flatlines to  $C = \beta - \alpha \sim 0.00736$ , the value  $C_1$  at the beginning of the  $T=330\text{K}$  partial cycle, at the end of which (75s later)  $C$  has the value of 0.208, the maximum value that it achieves.

It is found that the above solutions a) b) c) reproduce accurately the behavior of the system, as revealed by a Runge-Kutta solution of the governing equations and/or by use of computational methods (see below). By way of summarizing the above analysis, we have been able to solve the nonlinear governing kinetic equations in the special cases a)  $T = \text{constant} = 330\text{K}$  or  $370\text{K}$ , b) the “doubling” period,  $0 < t < 900$  secs, during which period the concentration of dsDNA approximately doubles in each 370-330 cycle, and c) the “plateau” region the onset of which occurs when the substrate  $A$  has depleted ( $A=0$ ) and in which region the concentration of dsDNA oscillates between 0.00736 M and 0.208 M. What is clear though, whether from the numerical or analytic solutions, is that cycling the temperatures between two values leads to substantially higher production of dsDNA than maintaining the temperature fixed at either temperature.

#### 4. Computational analysis of the chemical systems

##### 4.1 Deterministic methods

Kintecus (version 3.953) was developed by James Ianni as a powerful simulation program for chemical dynamics (Ianni J. C. 2009); it is free for academic use. As a deterministic, Arrhenius-based program the inputs include: the reaction steps, energies of activation ( $E_a$ ) and Arrhenius constant,  $A$ . The program assumes elementary reaction steps and numerically solves the differential equations for the related rate laws. The concentrations of participating species are calculated and displayed over time at either a fixed temperature or under varying temperature conditions.

##### 4.2 Deterministic model of 2T-PCR

A model of two-temperature PCR was developed using Kintecus, a computational package based on deterministic kinetic equations. A model was designed with kinetic parameters, initial concentrations of reactants, a temperature-sensitive catalyst and an appropriate protocol for the temperature cycles (Table 1 and Fig. 1a.).  $E_{\text{act}}$  represents the active enzyme that functions at 330K;  $E_{\text{inact}}$  is the inactive form of the enzyme at the higher temperature (370K). SUB represents the substrates, both the deoxyribonucleotides and primers; SUB starts at a high concentration and becomes limiting for synthesis of dsDNA. The two ssDNA templates are designated as ssDNA1 and ssDNA2. The output from the model describes a pattern of replication of dsDNA that is typical for experimental results obtained using real-time, two-temperature PCR (Fig. 1b.); there is replication of DNA during the low temperature part of the cycle, denaturation of dsDNA during the high temperature phase, an exponential phase in which there is doubling of dsDNA during each cycle and a plateau phase in which replication is approached as availability of substrates becomes limiting.

We used the deterministic model to simulate the generation of standard curves. The initial concentration of dsDNA was varied from  $1 \times 10^{-5}\text{M}$  to  $1 \times 10^{-8}\text{M}$  (Fig. 2.). The x-axis is time but can be re-calculated as cycle number. The plot shows the peak DNA concentration at the each cycle. The amplification efficiency is related to the slope of the curve in the log-linear exponential phase; theoretically, the efficiency of PCR is 100%, i.e. the concentration of dsDNA is doubled at each thermal cycle. In the models (Fig.1b and Fig.2) the calculated efficiency is 100%.

##### 4.3 Stochastic methods

CKS (Chemical Kinetics Simulation) is a program provided by IBM for developing stochastically based models (Hinsberg W. & Houle F. Chemical kinetics simulator 1.01). Inputs include the reaction steps, kinetic constants

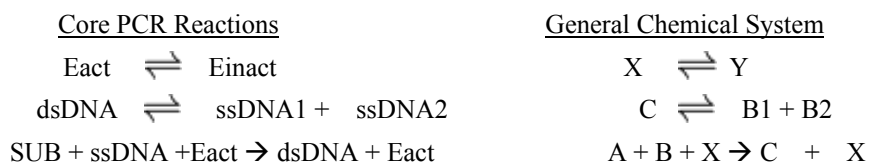
for the temperature dependent reactions, the initial concentrations of reactants and time course for the thermal cycling; stochastic parameters including the random number seed, the time course for the simulation and the number of “molecules” in the model.

#### 4.4 Stochastic model of 2T-PCR

A kinetic model of 2T-PCR using a stochastic chemical kinetics simulation program, CKS (Hinsberg W. & Houle F. Chemical Kinetics Simulator 1.01), is shown in Figure 3. The input parameters for this model were those used from the deterministic model described above (Table 1 and Fig. 1). The stochastic model of 2T-PCR is equivalent to the above deterministic model for 2T-PCR.

### 5. Discussion

Systems chemistry is a new and exciting area that explores the interaction of molecules in multi-reaction systems often displaying behavior not expected from individual components. The models of 2T-PCR recapitulate the real behavior of this system; from the numerical or computational methods, cycling the temperatures between two values leads to substantially higher production of dsDNA (target product) than maintaining the temperature fixed at either temperature. Viewing 2T-PCR as a chemical system provides insight into features of more general chemical processes that might use thermal cycling advantageously. The model highlights two catalytic events, an enzyme catalyzed reaction and an autocatalytic process in which DNA acts as a template for its replication. The interaction of these components is an essential feature of the non-linear behavior of this chemical system under thermal cycling. To extend this to a more general pattern, we suggest the following analogy:



where X and Y are active and inactive catalytic forms, C is a complementary polymer of two templates, B1 and B2 and A is substrates.

Our simple kinetic model of thermal cycling is likely to suggest many possible applications where thermal cycling would be advantageous for product formation in a chemical system. One possible application of our model is the replication of RNA in a prebiotic environment (Ferris J. P., Joshi P. C., Wang K-J., Miyakawa S. & Huang W. 2004; Ferris J. P. 2006; Ferris J. P. & Delano J. W. 2008; Joshi P. C., Aldersley M. F., Delano J. W. & Ferris J. P. 2009; Lincoln T. A. & Joyce G. F. 2009). Our models suggest that catalytic surfaces and substrates might interact with complementary RNA templates under thermal cycling conditions to replicate RNA. deRoss has proposed the hypothesis that an PCR-like process might have replicated dsRNA in a non-enzymatic fashion as an early chapter in the RNA World hypothesis (de Roos D. G. 2007). Kinetic models of chemical systems operating under thermal cycling may provide clues to creating innovative applications in chemistry and chemical engineering.

### Acknowledgements

We gratefully acknowledge funding through the University of New Haven Faculty Research Support to CB and PMS. We thank the University for supporting undergraduate summer fellowships for DML and MJC. We thank our students – Devon McCarthy, Matt Porto, Thomas Gordon, Caitlin Engle and Przemyslaw J. Chorzepa – for their work on this project.

### References

- Abbott D. (2010). Asymmetry and Disorder: A Decade of Parrondo's Paradox. *Fluctuation and Noise Letters*, in press. (see DOI: 10.1142/S0219477510000010)
- Beutel K. M. & Peacock-Lopez E. (2007). Complex dynamics on a cross-catalytic self-replication mechanism. *J. Chem. Physics*, 126, 125104.
- Blackmond D. G. (2009). An Examination of the Role of Autocatalytic Cycles in the Chemistry of Proposed Primordial Reactions. *Angew. Chem. Int. Ed.*, 48, 386–390.
- Brandner J. J., Emig G., Liauw MA & Schubert K. (2004). Fast temperature cycling in microstructure devices. *Chemical Engineering Journal*, 101, 217-224.
- Cha R. S. & Thilly W. G. (1993). Specificity, efficiency, and fidelity of PCR. *Genome Res.*, 3, S18-S29.

- de Roos D. G. (2007). Modeling evolution on design-by-contract: Predicts an origin of life through an abiotic double-stranded RNA World. *Biology Direct*, 2, 12 (see doi:10.1186/1745-6150-2-12).
- Ferris J. P., Joshi P. C., Wang K.-J., Miyakawa S. & Huang W. (2004). Catalysis in prebiotic chemistry: application to the synthesis of RNA oligomers. *Advances in Space Research*, 33, 100–105.
- Ferris J. P. (2006). Montmorillonite-catalysed formation of RNA oligomers: The possible role of catalysis in the origins of life. *Phil. Trans. R. Soc. B*, 361, 1777–1786.
- Ferris J. P. & Delano J. W. (2008). The RNA World Scenario for the Origin of Life,” in *Chemical Evolution across Space and Time: From the Big Bang to Prebiotic Chemistry* (ACS Symposium Series), eds. L. Zaikowski and J. Friedrich (Oxford University Press).
- Hansen H. A., Olsen J. L., Jensen S., Hansen O. & Quaade U. J. (2006). Rate enhancement in microfabricated chemical reactors under fast forced temperature oscillations. *Catalysis Communications*, 7, 272–275.
- Harmer G. P. & Abbott D. (1999). Game Theory - Losing Strategies Can Win by Parrondo's Paradox. *Nature*, 402, 864.
- Hinsberg W. & Houle F. Chemical kinetics simulator (CKS) 1.01, IBM's Almaden Research Centre. [Online] Available: <http://www.almaden.ibm.com/st/msim/ckspage.html>
- Horton J. H., Hagen M. D. & Ko K. S. (1994). Optimized conditions for cycle sequencing of PCR products. *PCR Methods Appl.*, 3, 359–360.
- Ianni J. C. (2009). Kintecus. (2009). [Online] Available: [www.kintecus.com](http://www.kintecus.com). and Kintecus Manual, [Online] available: [www.kintecus.com/Kintecus\\_V39.pdf](http://www.kintecus.com/Kintecus_V39.pdf).
- Jensen S., Thorsteinsson S., Hansen O. & Quaade J. J. (2008). Parametric investigation of rate enhancement during fast temperature cycling of CO oxidation in microreactors. *Chemical Engineering Journal*, 135S: S237–S241.
- Joshi P. C., Aldersley M. F., Delano J. W. & Ferris J. P. (2009). Mechanism of montmorillonite catalysis in the formation of RNA oligomers. *J. Am. Chem. Soc.*, 131, 13369–13374.
- Kamioka S., Ajami D. & Rebek J. (2010). Autocatalysis and organocatalysis with synthetic structures. *Proc. Nat'l. Acad. Sci., U.S.A.*, 107, 541–544.
- Kramer M. F. & Coen D. M. (2001). Enzymatic amplification of DNA by PCR: Standard procedures and optimization. *Current Protocols in Molecular Biology*, 15.1.1–15.1.14.
- Lincoln T. A. & Joyce G. F. (2009). Self-sustained replication of an RNA enzyme. *Science*, 323, 1229–1232.
- Lo Y. M. D. & Chan K. C. A. (2006). Introduction to the polymerase chain reaction. *Methods Mol. Biol.*, 336, 1–10.
- Luther M., Brandner J. J., Schubert K., Renken A. & Kiwi-Minsker L. (2008). Novel design of a microstructured reactor allowing fast temperature oscillations. *Chemical Engineering Journal*, 135S, S254–S258.
- Luther M., Brandner J. J., Kiwi-Minsker L., Renken A. & Schubert K. (2008). Forced periodic temperature cycling of chemical reactions in microstructure devices. *Chemical Engineering Science*, 63, 4955 – 4961.
- Martin H. & von Baeyer H. C. (2004). Simple games to illustrate Parrondo's paradox. *American Journal of Physics*, 72, 710–714.
- Neuzil P., Zhang C., Pipper J., Oh S. & Zhuo L. (2006). Ultra fast miniaturized real-time PCR: 40 cycles in less than six minutes. *Nucleic Acids Research*, 34, e77.
- Osipovitch D. C., Barratt C. & Schwartz P. M. (2009). Systems chemistry and Parrondo's paradox: Computational models of thermal cycling. *New J. Chem.*, 33, 2022–2027.
- Patzke V. & von Kiedrowski G. (2007). Self replicating systems. *ARKIVOC*, 293–310, Part 5.
- Rebek J. (1992). Molecular recognition and self-replication. *Journal of Molecular Recognition*, 5, 83 – 88.
- Robertson A., Sinclair A. J. & Philp D. (2000). Minimal self-replicating systems. *Chem. Soc. Rev.*, 29, 141–152.
- Sievers D. & von Kiedrowski G. (1998). Self-replication of hexadeoxynucleotide analogues: Autocatalysis versus cross-catalysis. *Chemistry-A European Journal*, 4, 629–641.
- Silveston P. L. & Hudgins R. R. (2004). Periodic temperature forcing of catalytic reactions. *Chemical Engineering Science*, 59, 4043–4053.

The University of Adelaide, School of Electrical Engineering, Parrondo's Paradox Official Website. [Online] Available: <http://www.eleceng.adelaide.edu.au/Groups/parrondo/>.

Vidonne A. & Philp D. (2009). Making molecules make themselves - The chemistry of artificial replicators. *European Journal of Organic Chemistry*, 5, 593-610.

Wang B. & Sutherland I. O. (1997). Self-replication in a Diels–Alder reaction. *Chem. Commun.*, 1997, 1495-6.

Wintner E. A., Conn M. M. & Rebek J. (1994). Self-replicating molecules: A second generation. *J. Am. Chem. Soc.*, 116, 8817-8884.

Yoon H. J. & Mirkin C. A. (2008). PCR-like Cascade Reactions in the Context of an Allosteric Enzyme Mimic. *J. Am. Chem. Soc.*, 130, 11590–11591.

Table 1. Description of kinetic parameters for model of 2T-PCR

A	E <sub>a</sub>	Reaction	Rate Constant	k@330	k@370	Increase k@370/k@330	k[forward]/k[reverse] @ 330	k[forward]/k[reverse] @ 370
3.00E+00	6	E <sub>inact</sub> ⇒E <sub>act</sub>	k <sub>1</sub>	3.37E-01	4.27E-01	1.27E+02	3.51E+03	7.19E-02
2.00E+40	280	E <sub>act</sub> ⇒E <sub>inact</sub>	k <sub>2</sub>	9.59E-05	5.93E+00	6.18E+06		
1.00E+40	280	dsDNA⇒ssDNA1 + ssDNA2	k <sub>3</sub>	4.79E-05	2.97E+00	6.18E+06	1.82E-04	7.90E+00
7.00E+00	9	ssDNA1 + ssDNA2 ⇒ dsDNA	k <sub>4</sub>	2.63E-01	3.75E-01	1.43E+02		
1.15E+02	1	SUB + ssDNA1 + E <sub>act</sub> ⇒ dsDNA + E <sub>act</sub>	k <sub>5</sub>	7.99E+01	8.31E+01	1.04E+02		
1.15E+02	1	SUB + ssDNA2 + E <sub>act</sub> ⇒ dsDNA + E <sub>act</sub>	k <sub>6</sub>	7.99E+01	8.31E+01	1.04E+02		

E<sub>act</sub> and E<sub>inact</sub> represent the concentrations of the catalyst, i.e. DNA polymerase, dsDNA the target molecule, and ssDNA1 and ssDNA2 the templates. SUB represents the four deoxynucleotides and primers for PCR. The kinetic parameters (A and E<sub>a</sub>) are used by the Arrhenius equation ( $k = A e^{(-E_a/RT)}$ ) using R = 0.008315 kJ/mol) to calculate rates and determine concentrations of components over time. The initial concentrations are: [dsDNA]<sub>0</sub> = 1.0×10<sup>-5</sup> M, [ssDNA]<sub>0</sub> = 0.0 M, [SUB]<sub>0</sub> = 0.5 M, [E<sub>inact</sub>]<sub>0</sub> = 0.0 M, [E<sub>act</sub>]<sub>0</sub> = 1.0×10<sup>-3</sup> M.

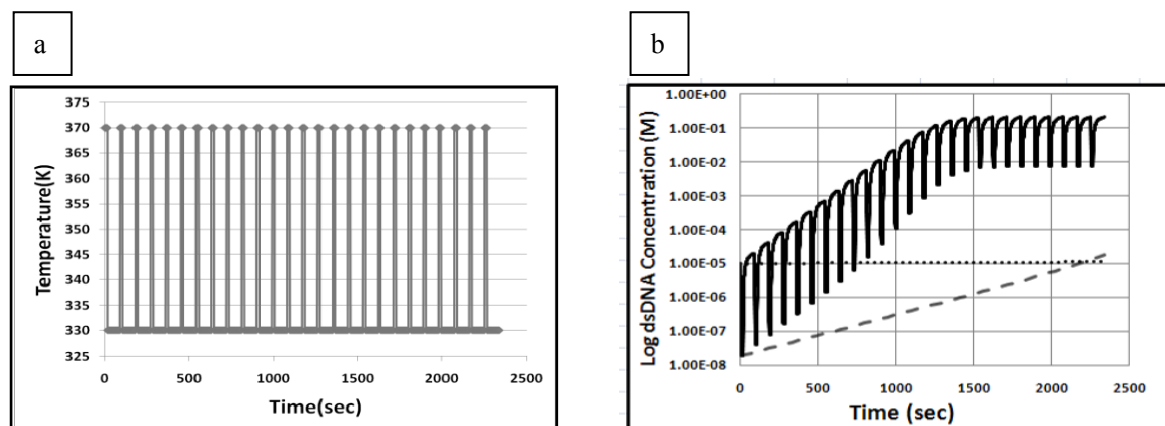


Figure 1. Deterministic, Two-temperature PCR Model. (a) The temperature versus time profile. The temperature profile is typical of PCR, starting at the higher temperature, 370K, and then cycling between 330K (75sec) and 370K (15sec) for 25 cycles. (b) Formation of dsDNA (log scale) versus time at (.....) for 330K and (---) for 370K and (—) for thermal cycling as in Fig 1a. Initial dsDNA is 1 x 10<sup>-5</sup> M



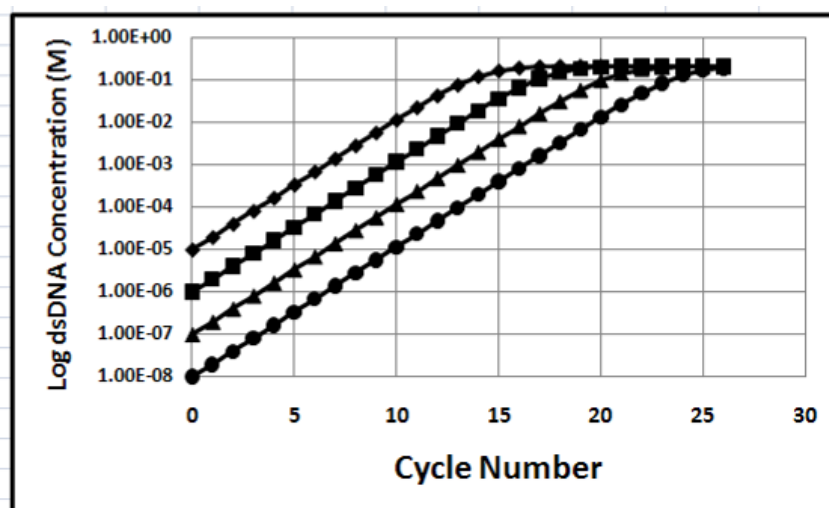


Figure 2. dsDNA Standard Curves. The standard curves were generated from the model described in Table 1 and Fig. 1. The curves correspond with initial concentration of dsDNA:  $\diamond$   $1 \times 10^{-5} \text{M}$ ,  $\blacksquare$   $1 \times 10^{-6} \text{M}$ ,  $\blacktriangle$   $1 \times 10^{-7} \text{M}$ ,  $\bullet$   $1 \times 10^{-8} \text{M}$

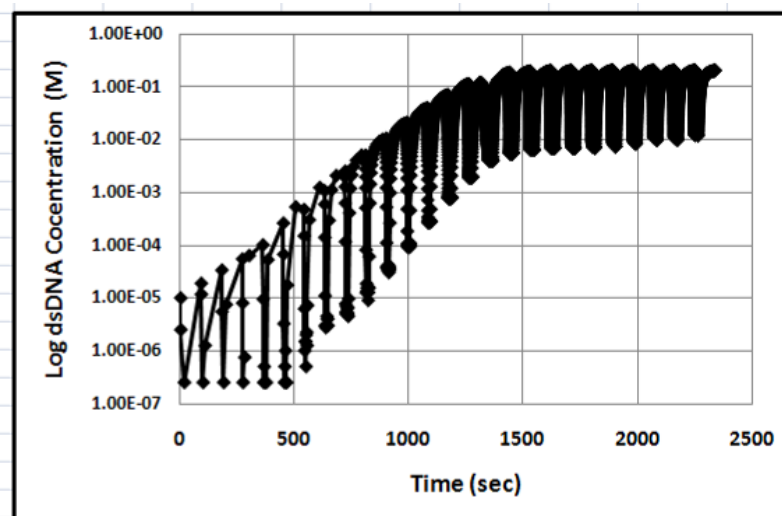


Figure 3. Output from the Stochastic 2T PCR Model. Simulation conditions includes: total number of events =  $9 \times 10^8$ ; total number of particles =  $2 \times 10^6$ ; equilibrium enabled with recording intervals of 200 events. Note: early points are unreliable due to low initial concentrations of dsDNA, which is typical of a stochastic model

# The Effect of Both UV\Ozone and Chitosan on Natural Fabrics

Eman Mohamed Osman (Corresponding author)

National Institute for Standards, Chemistry Metrology Division

Textile Metrology Lab., Tersa st. El Haram, Giza, Egypt

P.O. Box: 136 Giza, Code: 12211

Tel: 202-3740-1116 E-mail: eman\_osman21@yahoo.com

Monira Nesim Michael

Head of the Electricity Division

National Institute for Standards, Chemistry Metrology Division

Textile Metrology Lab., Tersa st. El Haram, Giza, Egypt

Hoda Gohar

National Institute for Standards, Chemistry Metrology Division

Textile Metrology Lab., Tersa st. El Haram, Giza, Egypt

## Abstract

This work has focused on developing eco-friendly treatments for modifying the fabric surface. Thus; we studied in details the effect of individual and combined uv\ozone and chitosan on wool and silk fabric samples. All the treated samples are characterized and evaluated by: i) Fourier transform infrared spectra with attenuated total reflection analysis (FTIR-ATR), ii) Performance properties, iii) Mechanical measurements, and iv) Dyeing characteristics using two different dye classes namely, reactive dye (C.I. Reactive Orange 69) and direct dye (C.I. Direct Yellow 11) applied on both wool and silk samples modified with the above mentioned three techniques.

**Keywords:** Uv\ozone, Chitosan, Young's Modulus, FTIR-ATR, Performance, Mechanical, Dyeing

## 1. Introduction

In recent years a great attention has been evoted to biopolymers because of their biocompatibility and biological functions and consequently, potential application in the biomedical and pharmaceutical fields. Chitosan is an examples of these biopolymers having B- 1,4 linked glucose amine residues, the second most abundant polysaccharide found on earth next to cellulose. Chitosan has a great potential for a wide range of uses due to its biodegradability, biocompatibility, antimicrobial activity, non-toxicity and ability to improve wound healing (Eagle, 2003).

In the textile industry, chitosan is used as print- paste thickener and is also used to improve the antimicrobial property of textile. Textile fibers that having poor affinity for dyes can be blended or surface coated with chitosan which makes them more receptive to dyeing with many dyes (Bahmani et al, 2006). Chitosan can also be used in the dye bath to improve the dyeability of textiles. This might be due to the improved electrostatic attraction between the protonated amino group in chitosan and the anionic dye leading to extremely high affinity for many classes of dyes (Wyeth et al, 2004).

The surface of the fiber has an important effect on overall processing properties of the fabrics. For wool fabrics, modification of the outer epicuticle and exocuticle imparts beneficial improvement to wool dyeability, printability, wettability .... The outermost surface of the wool fiber is thought to have a covalently bound lipid layer, which is responsible for the hydrophobic nature of the epicuticle. The main component of the surface lipid is a C<sub>21</sub>- fatty acids which are thought to be bound to the epicuticle mainly by thioester linkages to cystine residues. Notably, aqueous chlorination treatments have been used to modify the wool surface (Michael & El-Zaher, 2004).

Exposure of silk to sunlight produces an obvious photo- yellowing followed by photo- tendering. Silk yellowing is due to the photo- oxidation of tyrosine and tryptophane residues, resulting in the formation of yellow chromophores. Tyrosine is considered the most important source of silk yellowing due to its greater abundance. Silk photo- tendering is caused by the breakage of peptide bonds occurring initially at the weaker C-N bond (Phattananarudee & Kiatkanjornwong, 2008).

Recently, with the present national and international awareness of environment, ecology and environmental legislation, this work is focused on using individual and combined uv\ozone and chitosan treatments both can be described as dry and biopolymer treatment respectively to achieve the same processing benefits as aqueous processing.

## 2. Experimental Work

### 2.1 Materials

#### 2.1.1 Fabrics

- Silk fabric, weight is 69.83 g/m<sup>2</sup> and thickness is 0.21 mm, it is supplied by El-Khateeb Factory, Akhmeem, Egypt, purified in laboratory by scouring with a solution containing 5 g/l of detergent using liquor ratio 1:50 at temperature 40°C for 15 minutes (Osman, 2001).
- Wool fabric, weight is 176.71 g/m<sup>2</sup> and thickness is 0.528 mm, it is supplied by Golden Tex Company, Egypt, and purified in laboratory by scouring with a solution containing 2 g/l of non- ionic detergent using liquor ratio 1:50 at temperature 60°C for 15 minutes.

Finally, all the samples are thoroughly washed with tap water and dried at ambient conditions.

#### 2.1.2 Chemicals

- Chitosan

Highly viscous chitosan (poly (1,4)- 2- amino- 2 deoxy- B- D- glucose) (Gohar, 2006), supplied by Fulka Chemie GmbH- 9471 Buchs, Sigma- Aldrich.

- Dyes

Direct dye: Drimarin yellow (C.I. Direct Yellow 11) and

Reactive dye: Difloro-chloro prymidine (C.I. Reactive Orange 69).

These two dyes are supplied by Clariant Company.

## 3. Modification Methods

### 3.1 UV\Ozone Treatment (Treatment I)

The samples under test – either wool or silk- in the form of strips are firstly exposed to UV source in a medium of ozone for 20 minute. A high intensity, low pressure mercury lamp without outer envelope- LRF- 02971, 200 watt, 220 volts, made in Poland- is placed in a cubic box with side length 60 cm, and the samples were put around the source at distance 20 cm. Molecular oxygen is subjected to the 184.9 nm radiation and when ozone is irradiated at 253.7 nm, the radiation is absorbed by most hydrocarbons and also by ozone (Michael & El-zaher, 2004). The products of this excitation react with atomic oxygen to form simpler, volatile molecules, which desorbed from the surfaces. Therefore, when both wavelengths are present atomic oxygen is continuously generated and ozone is continually formed and then destroyed (Ibrahim, 2003). This is confirmed by measuring the produced O<sub>3</sub>, using 49 c O<sub>3</sub> Analyzer Thermo Environmental Inst. Inc. USA.

### 3.2 Chitosan Treatment (Treatment II)

Different concentrations of chitosan (0.5%, 1%, 1.5%, and 2%) are freshly prepared by gradual dissolution a known weight of the powder in acidified water (1% acetic acid) at room temperature. Trintol (1 g/l) is added to the treatment bath just before padding. The samples under test are separately padded and then dried at 80°C for 5 minutes followed by thermo-fixation at 140°C for 3 minutes, finally washed with warm water (Eagle, 2003).

### 3.3 Combined UV\ Ozone and Chitosan (Treatment III)

Another treatment is carried out using combined uv\ozone and chitosan. Thus, wool and silk samples firstly exposed to UV source for 20 minutes under the above mentioned conditions (treatment I) followed by treatment with different chitosan concentrations as mentioned above (treatment II).

## 4. Testing and Analysis

### 4.1 Fourier Transform Infra Red Spectroscopy with Attenuation Total Reflection (FTIR-ATR)

FTIR-ATR spectra of the above mentioned samples were recorded by means of Nicolet 380 Spectrometer using a zinc selenid crystal, in the wavelength range 650- 4000  $\text{cm}^{-1}$ . To ensure reproducible contact between the crystal face and the fabric, a pressure of about 18 Kpa (Barbara, 2005) is applied to the crystal holder. The FTIR absorbance frequencies for the treated samples are recorded with an average of 128 scans using a resolution of 4  $\text{cm}^{-1}$ .

### 4.2 Mechanical Measurements

Tensile strength and percentage elongation at break for all the samples under test were measured and evaluated using Shimadzu Universal Tester of type S-500 Japan. The measurements are carried out according to ASTM-Standard Method 2000, D 3822-96.

Young's modulus (Y-values) of the measured samples which is inversely proportional to elasticity can be obtained from the ratio between tensile strength and elongation at break by applying the following equation (Keony, 1993).

$$\text{Young's modulus} = \frac{\text{Force}}{\text{Unit area}} \times \frac{\text{applied}}{\text{Increase}} \times \frac{\text{Initial length}}{\text{In length}}$$

### 4.3 Wetting time

It is time of complete immersion of a sample (5 cm x 5 cm) dropped flat onto the surface of distilled water from a height of about 3 cm (AATCC, 79-1995). The wetting time is determined for all the above mentioned samples under test.

### 4.4. Yellowness Index Determination:

The yellowness index for all the different examined samples are measured and evaluated according to ASTM D 1925 using Color Eye 3100 Spectrophotometer SDL, England. The mean value of three measurements is recorded for each sample.

## 5. Dyeing Testing and Analysis

### 5.1 Dyeing Method

All the treated samples under test are separately dyed by each of the above mentioned dyes in a laboratory dyeing apparatus using the conventional exhaustion dyeing method without any addition of chemicals to the dyeing bath, where a fixed dye concentration of 2 g/l is used (Eagle, 2003). All dyeings are carried out at temperature 80°C for 60 minutes with a liquor ratio of 1:50. The dyed samples are thoroughly washed and finally dried at ambient conditions.

### 5.2 Color Strength (K/S) Determination

The color strength (K/S) values of the different examined samples are measured at the wavelength characteristic to each color (Christie et al, 2000). The measurements are carried out using Color Eye 3100 Spectrophotometer SDL, England.

### 5.3 Light Exposure, Light Fastness Evaluation and Color Difference ( $\Delta E$ )

The different examined dyed samples are exposed to artificial daylight using Xenon Tester (weathering) (AATCC, 169-RA 64, 1995) at temperature  $25 \pm 2^\circ\text{C}$  and relative humidity  $65 \pm 5\%$  alongside with a Standard Blue Scale. The fastness grades are assessed visually according to ASTM standard method (ASTM, G23, 1990) and the results are evaluated more precise from color difference measurements ( $\Delta E$ ) (Christie et al, 2000).

## 6. Results and Discussion

Wool polymer contains some important chemical groups that able to form inter-polymer forces of attraction. These groups are: the polar peptide groups (i.e. -CO-NH-) and the carbonyl groups (-CO-), which will form hydrogen bonds with the slightly positively charged hydrogen of the imino groups (-NH-) of another peptide groups. Besides, some wool polymers have carboxylate groups (-COO-), and amino groups (-NH<sub>3</sub><sup>+</sup>) as side groups, between these two groups salt linkages or ionic bonds will form. Also, cystine linkages, the sulphur-containing amino acid (i.e. disulphide bonds) are very strong since they form covalent bonds. Finally, the existence of the above mentioned inter-polymer forces tends to make the van der Waals' forces rather significant (Tamada, 2004),.

Silk polymer is composed of sixteen different amino acids compared with the twenty amino acids of wool polymer. Three of these sixteen amino acids namely, alanine, glycine and serine, make up about four-fifth of the

silk polymers' composition. Also, silk polymers are not composed of any amino acid containing sulphur. So, silk may be considered to have the same composition as that of wool except that the silk polymer system hasn't disulphide bonds. The important chemical groupings of the silk polymer are the peptide groups which give rise to hydrogen bonds, and the carboxyl and amine groups which give rise to the salt linkages (Jun & Chen, 2006). Table (1) shows the percentage ratio of some amino acids present in both wool and silk fabrics. The amino acids found in silk fabric are joined by sericin gum. Glycin, serine and alanine are found in the crystalline portion, where the bulky side chains are found in the amorphous region.

#### 6.1 Fourier Transform Infrared Spectra (FTIR-ATR) Analysis

FTIR-ATR (Barbara, 2005) has been employed to study the effect of the three treatment techniques on the behavior of the different function groups as well as the different amino acids present in both wool and silk fabric samples, the results are shown in tables (2 & 3) respectively.

The absorption band at  $3566\text{ cm}^{-1}$  assigned to O-H asymmetric stretching in wool samples, it is a sharp and strong band, and the change in its intensity is directly proportional to the dipole-dipole moment of the molecule (Phattananarudee & Kiatkanjornwong, 2008).

The absorption band at  $\approx 3275\text{ cm}^{-1}$  assigned to N-H stretching of the serine amino acid in both wool and silk samples, and its presence ratio is 8.97% and 12.49% respectively (Yuen et al, 2007).

The band at  $\approx 2920\text{ cm}^{-1}$  assigned to C-H stretching is observed at the spectra of both two fabrics wool and silk.

The signal at  $1645\text{ cm}^{-1}$  assigned to C=O stretching of aspartic acid is observed only in wool spectra, its presence ratio is  $\approx 6.19\%$

The band at  $1610\text{ cm}^{-1}$  assigned to N-H bending of lysine amino acid present in both spectra of wool (3.34%) and silk (0.66%) samples.

The band  $\approx 1515\text{ cm}^{-1}$  assigned to C=O asymmetric of glutamic acid, is found in both spectra of wool (13.11%) and silk (2.08%).

The signal at  $\nu = 1443\text{ cm}^{-1}$  assigned to C-C stretching in ring of tyrosine, is found only in silk spectrum, its presence ratio is  $\approx 10.63\%$ .

The band  $\approx 1231\text{ cm}^{-1}$  assigned to C-N stretching is only found in silk samples spectrum.

The signal at  $\nu = 1070\text{ cm}^{-1}$  assigned to cystine oxides (monoxide and dioxide) is only found in wool spectrum.

In general, there is an increase in the peak intensity values of all the characteristic bands for both fabric samples under test after their treatment with uv\ozone for 20 minutes. Also, when the blank samples are treated with 0.5% chitosan, the peak intensity of all the characteristic bands for both fabrics increases followed by a gradual increase in the intensity values with increasing chitosan concentration (from 0.5% to 2%) except the band at  $3566\text{ cm}^{-1}$  of O-H asymmetric stretching and the band at  $1070\text{ cm}^{-1}$  of cystine for wool samples and band at  $1619\text{ cm}^{-1}$  of N-H bending of lysine amino acid for silk samples. The decrease in cystine oxides band intensity may be due to the conversion of cystine oxide to cystine amino acid (Phattananarudee & Kiatkanjornwong, 2008).

On treating blank samples with uv\ozone followed by different chitosan concentrations, most of the function groups belonging to wool samples show increase in the intensity values with increasing chitosan concentrations, while the function groups characteristic to silk samples depict decrease in the intensity values with increasing chitosan concentration

#### 6.2 Effect of the Different Treatment Methods on the Performance properties of Wool and Silk samples

##### 6.2.1 Whiteness (W) and Yellowness (Y) Indices

The change in yellowness and whiteness indices can be considered as a sensitive indication of surface modification for the natural fabrics under test during the different treatments. Table (4) shows the effect of the three different treatment techniques on yellowness and whiteness indices.

For treatment I, there is enormous increase in yellowness values of silk samples compared to that obtained in wool which shows a slight increase in yellowing and the reverse of these results holds true for whiteness trend. These can be attributed to: i) The presence of disulphide covalent bonds in wool polymer and its increasing after treatment I as mentioned in table (2) resisting the yellowing, ii) presence and higher content% of the amino acids tyrosine and serine respectively -which are the most important source of yellowing and it's increase with uv\ozone exposure (tables 2 & 3), whereas the increment in silk is higher than that in wool. Besides, the amino acids may be photo-oxidized via exposure to uv\ozone resulting in the formation of yellow chromophores (Jun & Chen, 2006).

For treatment II, the yellowness values of silk samples were higher than that of wool samples and tend to increase with increasing chitosan concentrations while for wool a decrease in yellowness is observed. The observed decrease in yellowness values of wool samples can be attributed to its structure characteristics where the type and the content of the different amino acids increase with increasing chitosan concentration as indicated from FTIR (table 2). Such chitosan layer has been reported to adhere tightly to wool through thermosetting process and ionic interaction between the carboxyl groups in wool and the free amino groups in chitosan, besides hydrogen bonding between hydroxyl groups of chitosan and the amino groups of wool (Michael & El-Zaher, 2004)

For treatment III, the yellowness values of silk samples show a significant increase at the lowest chitosan concentrations followed by decrease with increasing chitosan concentration. While for wool samples, there is a very slight gradual increase in yellowness values with increasing chitosan concentrations. The observed yellowness increase at lower chitosan concentrations can be attributed to the predominant effect of uv\ozone as mentioned in treatment I. For treated silk samples, on increasing chitosan concentrations, both the coating layer thickness and ionic interaction increase leading to a decrease in the yellowness of the surface. For wool samples, the photo-yellowing on the surface is due to the increase in the intensity of amino acids with uv\ozone that responsible for producing colored products is predominate over the coating layer formed by chitosan. In general, the natural coloration of chitosan that appears yellowish to some extent increase yellowness with increasing the thickness of the coating layer, especially in case of treatment with uv\ozone (Bahamani et al, 2006; Yuen et al, 2007)

In short, the results indicate that, the ranking order of the yellowness index follow the order: For wool: treatment III (at the highest chitosan concentration) > treatment I > treatment II (at the highest chitosan concentration)

For silk: treatment II (at the highest chitosan concentration > treatment I > treatment III (at the highest chitosan concentration)

#### 6.2.2 Wettability

It is well known that wool is more hydrophobic than silk, this agrees with the obtained results) where the wetting time of blank wool samples is much higher than that of silk in (table 5). On exposing wool and silk samples to uv\ozone for 20 minutes, the wetting time of both fabrics are decreased by about 56% and 50% respectively. This can be interpreted on the results obtained from FTIR spectra (tables 2& 3) where there is an increase in the intensity of the different function groups and amino acids that responsible for increasing the surface polarity of samples under test, i.e. become more hydrophilic leading to improving the wettability (Gohar, 2006) consequently decreasing the wetting time.

For both treatments II& III, there is an enormous decrease in the wetting time with increasing chitosan concentrations for the two fabrics under test, i.e. the wettability of wool is greatly improved compared to silk, especially at the highest chitosan concentrations. This result can be explained on the light of the increment intensity of different function groups and amino acids for both fabrics (tables 2& 3), taking into consideration that the increment in wool is much higher than that of silk. Moreover, the characteristic nature of silk yarns which are more compacted than wool, so when the yarns are coated with viscous chitosan it can pack and glue yarn together reducing the voids of inter-fiber spaces. As a result, the solution can not further penetrate into the yarns because the decreased inter fiber spaces can not accommodate a large amount of water remaining on the surface (Phattananudee & Kiatkanjornwong, 2008), each relative to its blank sample.

Generally, the improvement of the wettability (i.e. less wetting time) follows the order:

For both wool and silk: treatment III (at the highest chitosan concentration) > treatment II (at the highest chitosan concentration) > treatment I.

#### 6.3 Mechanical Properties of the Treated Wool and Silk Samples

The change in the mechanical properties of the treated wool and silk samples using the three different treatment techniques reflect not only the changes in the chemical structure of the polymer system but also its morphology (Wyeth et al, 2004)

The data in table (6) clarify the effect of the different techniques on the mechanical properties of both wool and silk samples under test. For treatment I, there is a decrease in %elongation for both fabrics under test and a slight change is observed in case of tensile strength and young's modulus (that is inversely related to elasticity).

For treatment II, there is no detectable change in tensile strength values observed with increasing chitosan concentrations in case of wool samples; while in case of silk samples an increase is observed at higher chitosan

concentrations. Regarding to the %elongation, a gradual decrease is observed for both fabrics under test. The observed change in young's modulus shows a gradual increase in wool and a gradual decrease in silk samples.

For treatment III, there is no detectable change is observed in the tensile strength values for wool samples while for silk samples increase with increasing chitosan concentrations. Moreover, %elongation and young's modulus of wool samples increase and that of silk samples decrease with chitosan concentrations compared to the blank ones.

Many scientists have correlated the resulting alteration in mechanical properties of the treated protein samples with chemical changes in keratin structure and amino groups. The main reason for losing fiber strength was assumed to be the cleavage of the cystine bridges or of the main chain bonds between carbon atom and amide N-atom of the wool proteins (Wilson et al, 2000)

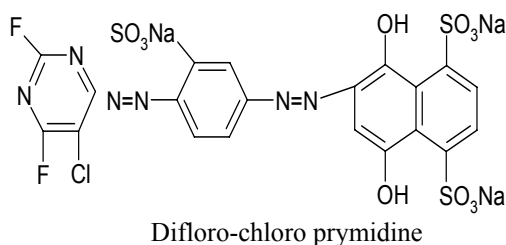
On this basis, the change in the mechanical properties can be correlated with the change in chemical groups and amino acids with the treatment techniques as detected from FTIR-ATR spectra (tables 1&2). Where the observed change in the mechanical properties can be related to the change in both amino acids and carboxyl groups content, these are the basis for salt-links between adjacent keratin chains.

In general, it is found that, the mechanical properties of wool samples are improved while for silk, the tensile strength is improved and both %elongation and young's modulus are decreased.

#### 6.4 Effect of the Three Different Treating Techniques on the Dyeing Properties

The dyeing properties of the treated dyed fabrics are examined throughout studying two main parameters; dyeability expressed as color strength (K/S) and fastness to light which is assessed visually using the Standard Blue Scale and evaluated instrumentally by measuring the color difference parameter ( $\Delta E$ ) to give more accurate and precise value for the actual amount of faded dye (Christie et al, 2000). On this basis, the dyeings are carried out using two different dye classes namely, reactive difluoro-chloro pyrimidine (C.I. Reactive Orange 69) and direct drimarin yellow (C.I. Direct Yellow 11).

Table (7) and figure (1) clarify the effect of the different treatment techniques on the dyeing properties of wool and silk samples using difluoro-chloro pyrimidine (C.I. reactive orange 69) with general formula (Korchagin & Matetsk, 1973):



Generally, the structure of this dye contains a large number of polar constituents ( $-\text{OH}^-$ ,  $\text{SO}_3^-$ ) which are very active to react with the reactive side groups of the fabric samples through covalent bond formation and the chance of this reaction increases by increasing the active side groups on treated samples (Korchagin & Matetsk, 1973).

It is clear from the results that, the dyeing properties of blank wool samples are higher than that of silk ones; this can be related to their natures. In wool keratin, there are a variety of functional groups with which reactive dyes may react. These groups include the amino ( $-\text{NH}_2$ ), hydroxyl ( $-\text{OH}$ ), thiol ( $-\text{SH}$ ) and carboxyl ( $\text{COO}^-$ ) which can react with the dye forming hydrogen bonding and covalent bonds. While in silk, the link to the dye is carried out through ( $-\text{NH}$ ) group (Tamada, 2004).

For treatment I, it is obvious that, there is an improvement in the dyeing properties for both fabrics as (K/S) and (L.F.) values increase and ( $\Delta E$ ) decrease and the improvement in wool is greater than that in silk. This can be attributed to the effect of uv/ozone exposure, where the intensity of the above mentioned function groups increase (tables 2& 3).

Treatment II shows a gradual increase in dyeability of both fabrics with increasing chitosan concentrations. Also, the increment in wool is greater than that in silk samples; this can be related to the increasing intensity of the amino groups with increasing chitosan concentrations. These groups have been reported to act as a built-in

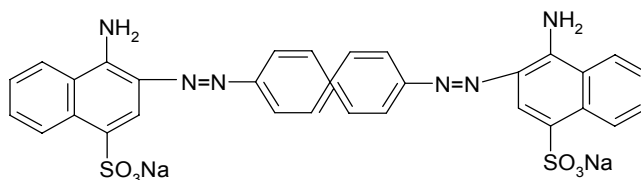
catalyst on the treated samples and to imparting a cationic surface which attracts the oppositely charged dye anions leading to enhancement the dyeability and the light fastness (Jocic et al, 2005)

It has been reported that dyeing properties depend mainly on the dye concentration and nitrogen content of chitosan pretreatment within the surface of the fabrics (Phattanasuddee & Kiatkanjornwong, 2008). This has been explained by interaction between the protonated amino groups of chitosan and anionic dyes via ionic interaction through an ion exchange process, and hence the color difference ( $\Delta E$ ) values decrease.

The greater improvement of wool dyeing properties with chitosan concentrations is related to (NH) group which is responsible for the basicity of wool. Although wool itself contain amino groups, further introduction of amino groups on the wool fabric surface as a result of modifications leading to induction of new dye site on the fibers, enhancing the absorption-ability of wool (Gohar, 2006), thus causing the wool fiber to become more hydrophilic and this increase the dye-uptake.

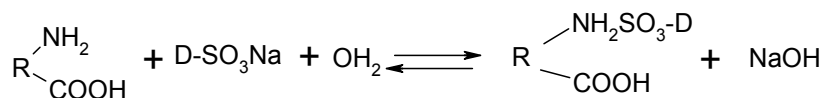
For treatment III, there is an increase in (K/S) values with increasing chitosan concentrations. The highest (K/S) values obtained after treatment III compared to treatments I & II which can be related to either higher chitosan adsorption occurs on both samples pretreated with uv/ozone or the treatment with uv/ozone activate some functional groups followed by chitosan which activate another functional groups, the net result is increasing the number and intensity of the activated function groups. So, highest (K/S) values are obtained alongside with (L.F) values.

Table (8) and figure (2) represent the dyeing properties data of wool and silk samples dyed with direct drimarin yellow (C.I. Direct Yellow 11) with the formula (Korchagin & Matetsky, 1973):



Drimarin yellow

Generally, direct dyes interact with wool according to the following:



From the chemical structure of this dye (Korchagin, & Matetsky 1973), there is an amino group in Para position to the azo group; this makes the dye in a clear coplanar structure having long chain and this interns increase the chance for interaction with the fiber via hydrogen bond. Besides, promoting the formation of aggregated particles easily exhausted and diffused inside the fiber pores and since wool having higher porosity than silk so K/S values of blank wool samples are greater than that of silk as indicated from table (8).

For treatment I, it is found that, both color strength (K/S) and light fastness (L.F) increase with uv/ozone exposure for both fabrics and the color difference values ( $\Delta E$ ) decrease.

For both treatments II and III, the results show that the dyeability characteristics of wool (K/S and L.F) are higher than that of silk and tend to increase with increasing chitosan concentrations. This can be related to the nature of wool which has a variety of function groups (OH, NH, SH and COO) that can react with the dye forming hydrogen and covalent bond while silk can react only through the NH groups (Tamada, 2004)

In short, the results clarify that the improvement in the dyeing properties (K/S and L.F) of both reactive and direct dyes applied on both fabrics wool and silk take the order: treatment III (at the highest chitosan concentration) > treatment II (at the highest chitosan concentration) > treatment I. While the corresponding color difference values ( $\Delta E$ ) follow the reverse trend.

## 7. Conclusion

This work studies in detail the effect of three different treatment techniques individual and combined uv/ozone and different chitosan concentrations on wool and silk protein fabrics. Treatment I: exposure to uv/ozone for 20 minutes, treatment II: different chitosan concentrations and treatment III: combined the above two techniques (I & II). The evaluation of these three techniques is carried out through studying FTIR-ATR spectra which indicate that there is an improvement in the different function groups characterizes each fabric and this give an indication



for the improvement in the performance properties and dyeing characteristics. On this basis, the performance properties of the pretreated fabrics are studied that include whiteness and yellowness indices (W & Y) and the wettability (sec.). The results of yellowness index indicate that, the yellowness values of treated silk samples are higher than that of wool and take the following order for both fabrics: treatment III (at the highest chitosan concentration) > treatment II (at the highest chitosan concentration) > treatment I

As it is known, wool is more hydrophobic than silk and the results of wettability show that, the wetting time of treated wool samples are greatly improved (i.e. become more hydrophilic) after each treatment. So, the improving in wettability of both fabrics takes the order: Treatment III (at the highest chitosan concentration) > treatment II (at the highest chitosan concentration) > treatment I compared to the corresponding blank samples.

In regarding to the mechanical properties of the tested samples it is found that, the mechanical properties of wool are improved while for silk, only the tensile strength is improved where both %elongation and young's modulus are not.

When studying the dyeing properties of the wool and silk samples dyed with either reactive or direct dye, it is found that, there is increase in K/S and L.F. values (i.e. improving the dyeability) of the treated samples for both dyes compared with the untreated dyed ones due to increasing the hydrophilicity of the treated fibers.

## References

- AATCC. (1995). Test Method 79.
- AATCC. (1995). Xenon Lamp Exposure, 169- RA 64.
- ASTM, G 23. (1990).
- Bahmani, S.A., East, G.C., & Holme, I. (2006). JSDC, 116, 94-99.
- Barbara, H. (2005). *Infrared Spectroscopy: Fundamentals and Application*, John Wiley & Sons, Ltd., Southern Gate, Chichester, England.
- Christie, R.M., Mather, R.R., & Wardmum, R.H. (2000). The chemistry of Color Application, *Blackwell Science*, London.
- Eagle, W.Y.G., (2003). *The Effect of Chitosan and its Derivatives on the Dyeability of Silk*, Ph.D. Thesis, Hong Kong Polytechnic University.
- Gohar, H.H. (2006). Evaluation and Characterization of the Physicochemical Properties of Wool Fabric Exposed to UV/Ozone and Treated with Natural Biopolymer, MSc. Thesis, Faculty of applied Arts, Helwan University, Egypt.
- Ibrahim, S.F. (2003). Investigation into the Effect of UV/Ozone treatments on Physical Properties and Dyeing Kinetics of Some Polymeric Fabrics, Ph.D. Thesis, Faculty of science, Cairo university, Egypt.
- Jocic, D., Vilchez, S., Topalovic, T., et al, (2005). *Carbohydrate Polymers*, 60, 51-59.
- Jun, Z., & Chen, G.Q., (2006). The study of the Structures of Silk Fibers Grafted with Hexafluorobutyl Methacrylate, International Forum of textile and Engineering for Doctoral candidates, China.
- Keony, F.P. (1993). The Proceeding of the 16<sup>th</sup> Roc. *Polymer Symposium*, vol. IX, 1, p. 373
- Korchagin, F. M., & Matetsky, A. (1973). *Chemical Technology of Fibrous Materials*, MIR publishers, Moscow.
- Michael, M.N., & El-Zaher, N.A. (2004). *Egypt. J. Chem.*, 47, 1, 93-100.
- Osman, E.M. (2001). Applying Natural Dyed on Natural Fabrics and Studying Their Diffusion Kinetics and Photo Fading Characteristics, Ph.D. Thesis, Faculty of science, Helwan University, Egypt
- Phattanasudee, S. K., & Kiatkanjornwong, S. (2008). Pretreatment of Silk Fabric Surface with Amino Compounds for Ink Jet Printing, *Progress in Organic Coatings*.
- Tamada, Y. (2004). Sulfation of silk fibroin by Chlorosulfonic Acid and the Anticoagulant Activity, *Biomaterials*, 25, 3, 377-383.
- Wilson, D., Valluzzi, D., & Kaplan, D. (2000). *Biophysical Journals*, 78, 2690-2701.
- Wyeth, p., Greiff, s., Kutzke, H. S., & Riekel, C. (2004). Surveying Silk Fiber Degradation by Crystallinity Determination: a Study on the Tang-Dynasty Silk Treasure from Famen Temple, China. [Online] Available: <http://eprints.soton.ac.uk/17245>
- Yuen, C.W.M., Ku, S.K.A., Kan, C.W., & Choi, P.S.R. (2007). *Coloration technology*, 123, 267-270.

Table 1. The percent ratio of amino acids in both wool and silk

Amino acids	The content percent in <i>wool</i>	The content percent in <i>silk</i>
Serine	8.97	12.49
Lysine	3.34	0.66
Glutamic	13.11	2.08
Aspartic	6.19	-----
Tyrosine	-----	10.63
cystine	11.3	-----

Table 2. Effect of the three treatment techniques on the behavior of the different function groups present in wool samples

Function groups & amino acids	Blank	Different Treatment Techniques								
		UV\Ozone(20 min) (Treatment I)	Chitosan conc. (Treatment II)				Combined UV and chitosan (Treatment III)			
			0.5%	1%	1.5%	2%	0.5%	1%	1.5%	2%
3566 cm <sup>-1</sup> O-H Assym. stretch	8.24	9.86	9.00	8.44	8.08	8.04	9.69	10.73	11.53	11.10
3275 cm <sup>-1</sup> N-H stretch ( <i>Serine</i> )	20.1	21.3	20.5	21.9	23.0	23.7	24.8	25.9	25.7	26.8
2925cm <sup>-1</sup> C-H stretch	13.2	18.2	14.4	15.2	16.6	17.0	17.0	18.8	19.9	20.7
1645 cm <sup>-1</sup> C=O stretch ( <i>Aspartic</i> )	80.0	84.0	84.2	84.8	84.8	84.9	81.6	81.7	82.4	83.2
1610 cm <sup>-1</sup> N-H bending ( <i>Lysine</i> )	75.1	76.8	82.9	83.4	84.8	88.3	75.15	76.19	74.8	77.9
1520 cm <sup>-1</sup> COO <sup>-</sup> carboxylation ( <i>Glutamic</i> )	77.7	81.8	83.3	84.3	85.4	94.2	82.5	84.5	86.5	88.2
1070 cm <sup>-1</sup> Cystine monoxide	43.7	49.5	46.9	46.4	42.6	40.0	45.4	47.4	47.5	48.7

Table 3. Effect of the three treatment techniques on the behavior of the different function groups present in silk samples

Function group	Blank	Different Treatment Techniques								
		UV\Ozone(20 min) (Treatment I)	Chitosan conc. (Treatment II)				Combined UV and chitosan (Treatment III)			
			0.5%	1%	1.5%	2%	0.5%	1%	1.5%	2%
3280 cm <sup>-1</sup> N-H stretch ( <i>Serine</i> )	31.3	33.4	34.5	33.4	33.8	34.7	34.8	33.2	32.4	30.6
2920 cm <sup>-1</sup> C-H stretch	14.6	15.7	16.8	17.0	18.2	19.7	19.3	16.0	15.5	15.2
1619 cm <sup>-1</sup> N-H bending ( <i>Lysine</i> )	97.1	98.9	100.02	99.7	92.4	81.9	99.8	97.2	97.6	95.7
1515 cm <sup>-1</sup> C=O assym. Stretch ( <i>Glutamic</i> )	81.1	84.2	81.6	82.5	83.4	84.4	85.9	84.0	82.1	79.9
1443 cm <sup>-1</sup> C-C stretch in ring ( <i>Tyrosine</i> )	49.9	55.0	51.9	53.0	53.4	54.6	63.5	58.9	53.1	49.0
1231 cm <sup>-1</sup> C-N stretch	50.4	54.7	51.6	52.7	53.2	56.6	59.0	56.1	57.0	55.7

Table 4. The change in whiteness (W) and yellowness (Y) parameters of wool and silk fabrics modified with the three different techniques

Fabric	Blank		UV\Ozone(20 min) (Treatment I)		Chitosan conc. (Treatment II)			Combined UV and chitosan (Treatment III)		
	W	Y	W	Y	Conc.	W	Y	Conc.	W	Y
wool	10.53	18.52	6.87	20.52	0.5%	11.34	17.98	0.5%	4.32	21.3
					1%	13.29	17.25	1%	-2.81	22.09
					1.5%	13.84	16.19	1.5%	-4.89	22.41
					2%	14.23	15.22	2%	-7.25	22.65
silk	25.48	17.06	12.36	22.35	0.5%	20.78	19.18	0.5%	-7.26	27.90
					1%	16.25	20.35	1%	1.56	24.27
					1.5%	10.33	27.15	1.5%	7.34	21.88
					2%	-17.62	33.95	2%	15.12	20.14

Table 5. Wettability (sec.) of wool and silk fabrics modified with either chitosan or uv\ozone or both combined together

Fabric	Blank (Wetting time sec.)	UV\Ozone(20 min) (Wetting time sec.) (Treatment I)	Chitosan conc. (Treatment II)		Combined UV and chitosan (Treatment III)	
			Conc.	Wetting time sec.	Conc.	Wetting time sec.
wool	1238	705	0.5%	707	0.5%	790
			1%	431	1%	555
			1.5%	307	1.5%	120
			2%	110	2%	101
silk	720	360	0.5%	300	0.5%	330
			1%	220	1%	280
			1.5%	190	1.5%	190
			2%	135	2%	110

Table 6. Mechanical properties of wool and silk fabrics modified with either uv\ozone or chitosan or both together

Fabric	Mechanical properties	Blank	UV\Ozone(20 min) (Treatment I)	Chitosan conc. (Treatment II)				Combined UV and chitosan (Treatment III)			
				0.5%	1%	1.5%	2%	0.5%	1%	1.5%	2%
Wool	Tensile strength	7.15	7.89	7.69	7.99	7.45	7.49	8.08	8.66	8.63	8.74
	%elongation	13.03	11.23	13.7	12.56	11.04	10.88	11.91	12.82	13.11	14.90
	E- Modulus	32.04	34.91	32.55	33.67	36.82	38.20	33.70	35.31	34.9	36.50
Silk	Tensile strength	6.28	7.18	5.80	6.43	7.36	8.75	6.82	7.60	8.07	9.93
	%elongation	9.37	4.23	9.30	8.74	7.21	7.04	6.14	5.97	5.44	5.02
	E- Modulus	15.39	15.77	10.71	10.54	10.02	9.93	11.25	10.63	10.28	10.00

Table 7. Effect of the three different techniques on dyeing properties of wool and silk samples dyed with reactive dye

Fabric	Blank			UV\Ozone(20 min) (Treatment I)			Chitosan conc. (Treatment II)				Combined UV and chitosan (Treatment III)			
	K\S	$\Delta E$	L.F.	K\S	$\Delta E$	L.F.	Conc.	K\S	$\Delta E$	L.F.	Conc.	K\S	$\Delta E$	L.F.
Wool	2.45	2.12	5	4.84	1.05	5/6	0.5%	4.87	2.31	5/6	0.5%	8.45	1.83	5/6
							1%	4.55	1.93	5/6	1%	9.06	1.50	5/6
							1.5%	5.95	1.30	6	1.5%	9.06	1.08	6
							2%	6.25	0.87	6	2%	10.95	1.03	6/7
Silk	1.84	3.76	4	3.12	2.51	4/5	0.5%	3.12	2.20	5	0.5%	3.67	2.42	5
							1%	3.64	1.64	5/6	1%	3.73	1.60	5
							1.5%	3.89	1.05	5/6	1.5%	4.02	1.00	5/6
							2%	4.19	0.98	6	2%	4.87	0.71	5/6

Table 8. Effect of the three different techniques on dyeing properties of wool and silk samples dyed with direct dye

fabric	Blank			UV\Ozone(20 min) (Treatment I)			Chitosan conc. (Treatment II)				Combined UV and chitosan (Treatment III)			
	K\S	$\Delta E$	L.F.	K\S	$\Delta E$	L.F.	Conc.	K\S	$\Delta E$	L.F.	Conc.	K\S	$\Delta E$	L.F.
Wool	2.81	3.13	4/5	3.10	1.08	5	0.5%	3.53	2.35	5/6	0.5%	4.59	1.09	5/6
							1%	4.16	1.32	5/6	1%	4.74	1.01	6
							1.5%	5.63	1.14	6	1.5%	5.01	0.80	6/7
							2%	6.01	1.01	6	2%	6.72	0.60	6/7
Silk	1.79	3.01	4/5	2.06	2.84	5	0.5%	3.20	3.09	5/6	0.5%	3.55	3.98	5/6
							1%	4.24	2.39	5/6	1%	4.27	2.88	5/6
							1.5%	5.06	2.06	6	1.5%	5.99	2.61	6
							2%	5.91	1.22	6	2%	6.45	2.11	6

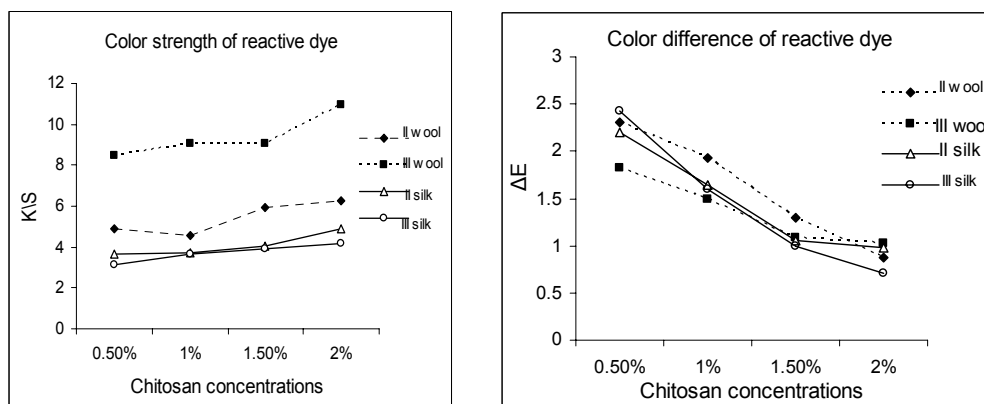


Figure 1. Dyeing properties of reactive dye applied on treated wool and silk samples

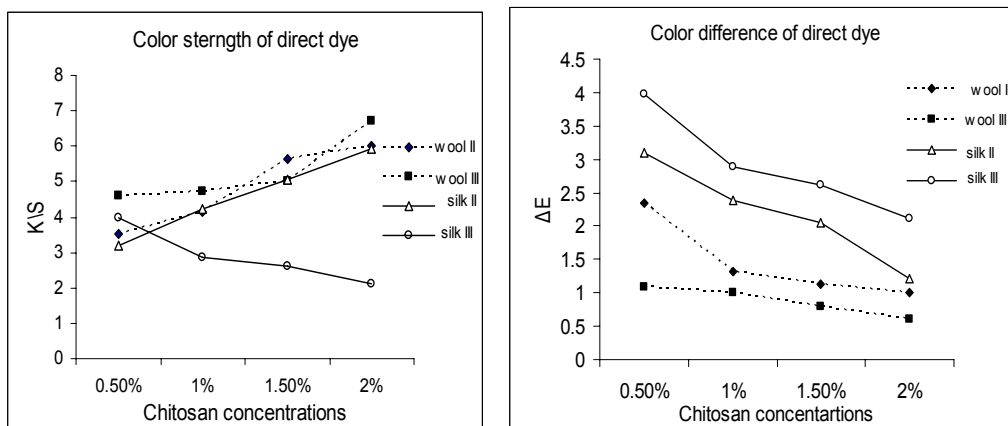


Figure 2. Dyeing properties of direct dye applied on treated wool and silk samples

# Studies in the Chemistry of Some New 1,2,4-thiadiazolidine by Oxidative Cyclisation

Dipak T. Tayade, Rahul A. Bhagwatkar (Corresponding author) & Radheshyam C. Panpalia

Department of Chemistry, S.R.R.L. Science College, MORSHI

Maharashtra, INDIA-444905

Tel: 91-997-016-5107 E-mail: bhagwatkar83@gmail.com

## Abstract

Recently in this laboratory a novel series of Hector's bases (1, 2, 4-thiadiazolidine) had been synthesised. 1-substituted-3-formamidinothiocarbamides (1a-f) and 1,3-bis(N-substituted-thioamido)guanidines (1g-l) were oxidatively cyclised by using aqueous bromine as oxidizing agent in chloroform medium to synthesised yet new series of Hector's bases, viz; 3-imino-5-substituted imino-1,2,4-thiadiazolidine (2a-f) and 3-substituted thioamidoimino-5-substitutedimino-1,2,4-thiadiazolidine (2g-l), respectively. The oxidative cyclisation of (1a-l) was also carried out by making use of  $H_2O_2$  in concentrated HCl as the oxidizing agent. The Hector's bases isolated in these reactions were characterised on the basis of conventional elemental analysis, chemical characteristics and IR and  $^1H$ -NMR spectral analysis.

**Keywords:** Hector's base, Oxidative cyclisation, 1-substituted-3-formamidino-thiocarbamide, 1, 3-bis(N-substituted thioamido)guanidines

## 1. Introduction

The first Hector's base was synthesised by Hector (1889, 1892). After Hector Hofmann and Garbail (1992), Hegershoff (1901), Kurzer (1956), Dost (1906) and Lal (1939) synthesise various series of Hector's bases and all synthesised compounds were termed and justified as Hector's bases by them. However, Sahasrabudhey (1942), Suresh (1960), Joshua (1961) investigated that all the Hector's bases which are synthesised by them are not necessarily be true Hector's bases and some were thiadiazoles and thiadiazolidines. The justification of this statement was done on the basis of gasometric studies, chemical characteristics and spectroscopic evidences (Suresh, K. S., 1959). It means that some thiadiazoles as well as thiadiazolidines are Hector's bases, but not all (For Hector's bases they must obey some typical properties (Hector D. S., 1892; Steanly, G. M., 1950; Tiwari, S. S., 1970)). The literature survey also reveals that the heterocyclic compounds having Hector's base nucleus enhance pharmaceutical, medicinal, agricultural and industrial applications. (Planka, M., 1968; Ahluwalia, U. K., 1968; Metzger, C., 1988; Zhang Ziyi, 1969) Hence medicine containing Hector's base nucleus are now used extensively in medicinal, agricultural, pharmaceutical and biotechnological faculties. These drugs were shown to possess a diverse range of physiological activities, (Budianu, C. H., 1987; McGuinness, 1988) plant growth promoting activity, antitumour, (Fernandes, 1986) herbical, (Farooq Saleem, 1987) antibacterial, (Farooq Saleem, 1989; Andotra, C. S., 1988) amoebicidal and antidiabetic (Rollas, S., 1984) properties. Very few work has been caring out on the synthesis of Hector's bases and their applications. As a part of research work being undertaken in the synthesis of nitrogen and sulphur containing heteroacycles and heterocycles having various application in drug chemistry, pharmaceutical, medicinal, agricultural, industrial and biotechnological sciences. Therefore, it was thought to investigate the reactions of cyanoguanidine with various isothiocyanates and also the reinvestigation of cyanoguanidine with substituted thiourea in hydrochloric acid to synthesise cyanoamidino-substituted-thiocarbamides (1a-f) and 1,3-diformamidino-thiocarbamide (2a)/N-substituted-formamidino(formamidino)thiocarbamide (2b-e) respectively further more the oxidative cyclisation of cyanoamidino-substituted thiocarbamides and 1,3-diformamidino-thiocarbamide (2a)/N-substituted-formamidino(formamidino)thiocarbamide with aqueous bromine in chloroform and also with  $H_2O_2$  in concentrated hydrochloric acid gave a novel series of Hector's bases (3a-f and 4a-e) which are hitherto unknown. The present work describes suitable and somewhat direct method for the synthesis of Hector's bases. When the oxidation was carried out with  $H_2O_2$ , the yield was comparatively poor and the greater time span required for the completion of reaction.

## 2. Materials and Methods

### 2.1 1-phenyl-3-formamidinothiocarbamide (1a)

A mixture of guanidine (0.01 M) and phenylisothiocyanate (0.01 M) and carbon tetrachloride (50 mL) was refluxed on a water bath for 2 hours. During boiling, the reaction mixture containing the suspended guanidine went into solution and after 1 hour yellowish, needle-shaped crystals gradually separated out. The reaction mixture was then again refluxed for 1 hour then filtered while hot. The new product was dried at room temperature and recrystallized from aqueous ethanol and identified as 1-phenyl-3-formamidinothiocarbamide (1a), yield 74%, m.p. 130°C. The reaction scheme was shown in Scheme-I. Similarly, other compounds (1b–f) were synthesised by above mentioned method and enlisted in Table-I.

### 2.2 1,3-Bis (N-phenylthioamido)guanidine (1g)

A similar procedure outlined in section 1.1 was used with some minor modifications, such as phenylisothiocyanate (0.01 M) was replaced with phenylisothiocyanate (0.02 M) Reaction yielded 67 %, m.p. was 149°C. The reaction scheme was shown in Scheme-II. Similarly, other compounds (1h–l) were synthesised by above mentioned method and enlisted in Table-II.

### 2.3 3-Imino-5-phenylimino-1,2,4-thiadiazolidines (2a)

In china dish the paste of 1-phenyl-3-formamidino thiocarbamide, (0.5 M) was prepared in chloroform. To this aqueous bromine in chloroform (10%) was added with constant stirring. Initially the colour of bromine disappeared, the addition was continued till the colour of bromine persisted. The reaction mixture was allowed to stand for 4 hours at room conditions. A pale ivory powder separated out, which on crystallisation from ethanol, gave (2a), yield 83%, m.p. 130°C. The reaction scheme was shown in Scheme-III. Similarly, other compounds (2b–f) were synthesised by above-mentioned method and enlisted in Table – III.

### 2.4 3-Phenylthiocarbamido-5-phenylimino-1,2,4-thiadiazolidines (2g)

A similar procedure outlined in section 1.3 was used with some minor modifications, such as 1-phenyl-3-formamidino thiocarbamide was replaced with 1,3-bis-(N-phenylthioamido)guanidine Reaction yielded 79% , m.p. was 195°C. The reaction scheme was shown in Scheme-IV. Similarly, other compounds (2h–l) were synthesised by above-mentioned method and enlisted in Table – IV.

## 3. Instrumentation

All the chemicals used were of AnalaR grade (India make) alkyl/arylisothiocyanates were prepared according to literature method (Vogel, A. Z., 1954), melting points of all synthesised compounds were determined in open capillary and uncorrected. IR-spectra were recorded on Perkin-Elmer spectrophotometer in the range 4000-400  $\text{cm}^{-1}$  in KBr pellets.  $^1\text{H-NMR}$  spectrums were recorded with TMS as internal standard using  $\text{CDCl}_3$  and  $\text{DMSO-d}_6$ . The purity of the compounds was checked on silica gel-G plates by TLC.

## References

- Ahaluwalla, U. K., Dutta, U., Sharma, H. R. (1968). *Ind. J. Chem.*, 26B, 88.
- Andotra, C. S., Sharma, S. K. (1988). *Pract. Nati. Acad. Sci., Ind. Sect.*, A 58(2), 215.
- Budianu, C. H., Rusu, G., Nistor, B. (1987). *Rev. Med. Chir.*
- Dost, K. (1906). *Chem. Ber.*, 39, 863.
- Farooq Saleem. (1987). *Eur. Patent CHAPPL* 87/1, 360009.
- Farooq Saleem. (1989). *Chem. Abstr.*, 110, 114893.
- Fernandes, P. S., Sonar, T. M. (1986). *J. Ind. Chem. Soc.*, 53(4), 427.
- Gabriel, S., Hoffmann, A. W. (1992). *Chem. Ber.*, 25 1578.
- Hector D. S. (1889). *Chem. Ber.*, 22, 1176.
- Hector D. S. (1892). *Chem. Ber.*, 25, 779.
- Hector D. S. (1892). *Oefvers Kong Vet. Akad.*, 89.
- Hugershoff, A. (1901). *Chem. Ber.*, 34, 3130.
- Joshua, C. P. (1961). *Tetrahedron Lett.* 19, 663.
- Kurzer, F. (1956). *J. Chem. Soc.*, 2345.
- Lal, R. B., Krall, H. (1939). *J. Ind. Chem. Soc.*, 16, 31.

Mcguinness, J. A., Minaffeli, J. A., Bell, A. R. (1988). US Patent 4775, C171-90, 408.

Metzger, C., Ludwing, E., Zeng Fuli. (1988). *Gaodeng Xuexia Huazue Xuebao* 9 (3), 239.

Planka, M. (1968). *J. Sci. Food Agr.*, 19, 502.

Rollas, S. (1982). Istanbul Univ. Eczacilic Fak., Mecn., 18, 3.

Rollas, S. (1984). *Chem. Abstr.*, 101, 908429.

Sahsrabudhey, R. H., Krall, H. (1942). *ibid.*, 19, 25.

Steanly, G. M. (1950). US Pat., 8, 252479, *Chem. Abstr.*, 44, 59191.

Suresh, K. S. (1959). *J. Sci. Res.*, (B.H.U.) IX (2), 94.

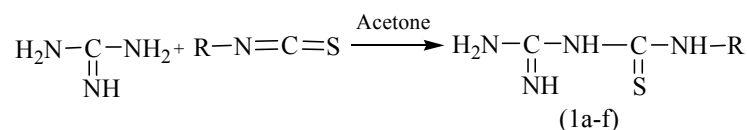
Suresh, K. S. (1960). *J. Ind. Chem. Soc.*, 35, 25c.

Tiwari, S. S., Sengupta, A. K., Kumar. (1970). *J. Ind. Pharma.*, 32, 91.

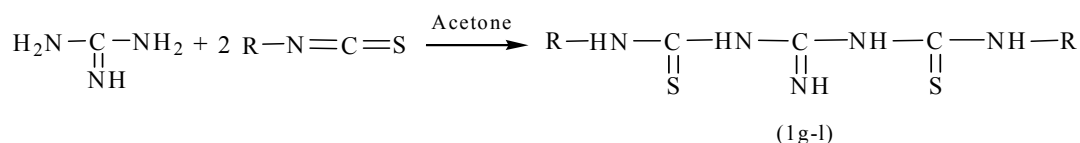
Vogel, A. Z. (1954). Text book of Practical Organic Chemistry including Qualitative Organic analysis, ELBS Landon Greek and Co., Ltd, ISBN 0 582 44245 1, 615.

Zhang Ziyi, Yan Kexin, Helmath, H. (1969-70). S. Afr. Patent, 6805647, *Chem. Abstr.*, 72, 7905n.

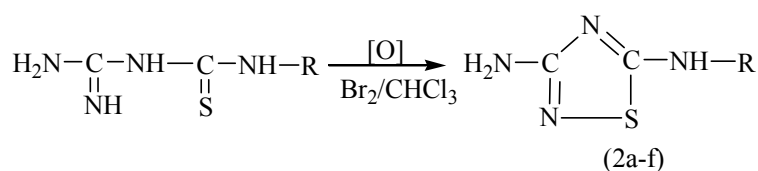
## Reaction Schemes



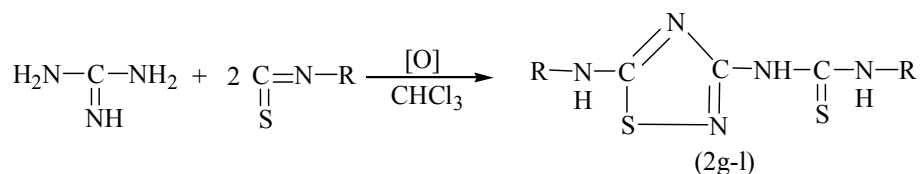
Scheme-I



Scheme-II



Scheme-III



Scheme-IV



**Physical data for synthesised compounds****Table-I**

Compound No.	1-substituted-3-formamidinothiocarbamide	Yield (%)	m. p. ( $^{\circ}\text{C}$ )
1b	-p-Cl-phenyl-	84	142
1c	-p-tolyl-	64	204
1d	-methyl-	72	189
1e	-ethyl-	59	115
1f	-t-butyl-	67	149

**Table-II**

Compound No.	1,3-Bis(N-substituted thioamido)guanidine	Yield %	m.p. ( $^{\circ}\text{C}$ )
1h	-(N-p-Cl-phenyl thioamido)-	82	194
1i	-(N-p-tolyl thioamido)-	72	189
1j	-(N-methyl thioamido)-	82	160
1k	-(N-ethyl thioamido)-	68	172
1l	-(N-t-butyl thioamido)-	62	169

**Table – III**

Compound No.	N-substituted-formamidino(formamidino)thiocarbamide	Yield %	m.p. ( $^{\circ}\text{C}$ )
2b	-(p-Cl-phenyl)-	79	147
2c	- (p-tolyl)-	68	120
2d	- (methyl)-	78	157
2e	- (ethyl)-	80	142
2f	- (t-butyl)-	63	110

**Table-IV**

Compound No.	N-substituted-formamidino(formamidino)thiocarbamide	Yield %	m.p. ( $^{\circ}\text{C}$ )
2h	- (p-Cl-phenyl)-	80	200
2i	- (p-tolyl)-	83	182
2j	- (methyl)-	69	110
2k	- (ethyl)-	72	95
2l	- (t-butyl)-	54	124

**Table-V** IR spectra of synthesised compounds in ( $\text{cm}^{-1}$ )

Compound	$\nu$ (N-H)	$\nu$ (C=N)	$\nu$ (>C=NH)	$\nu$ (>C-N)	$\nu$ (>C=S)	$\nu$ (>C-S)
(1a)	3393	1661	---	---	1101	517
(1g)	3387	1666	1575	1395	1178	---
(2a)	3308	1660	---	1332	1154	---
(2g)	3383	---	1566	---	1173	882

**Table-V** NMR spectra of synthesised compounds in (ppm)

Compound	Ar-NH	Ar-H	N-H
(1a)	$\delta$ 7.41-8.54	$\delta$ 6.85	$\delta$ 3.97
(1g)	$\delta$ 7.99-8.00	$\delta$ 6.90	$\delta$ 3.25-3.27
(2a)	---	$\delta$ 7.26	$\delta$ 4.02 and 4.00
(2g)	$\delta$ 7.26-7.79	$\delta$ 6.43-6.79	$\delta$ 4.02

# Poly(Furfural-Acetone) as New Adsorbent for Removal of Cu(II) from Aqueous Solution: Thermodynamic and Kinetic Studies

Tariq S.Najim (Corresponding author)

Chemistry Department, College of Science, Mustansiriya University Baghdad, Iraq

E-mail: tariq\_pru@yahoo.com

Suhad A.Yassin

Chemistry Department, College of Science, Duhok University, Duhok, Iraq

E-mail: suhad1000@yahoo.com

Ali J.Majli

Chemistry Department, College of Science, Mustansiriya University Baghdad, Iraq

E-mail: ali\_master2004@yahoo.com

## Abstract

Poly(furfural-acetone) was prepared and used for the removal of Cu(II) from aqueous solution. The optimum pH for the removal was found to be 6. The adsorption kinetic of Cu(II) was studied, and the rates of sorption were found to conform to Pseudo-Second-order kinetic with a correlation coefficient ( $R^2=1$ ), results indicate that the pH 6 of the system supported the adsorption of Cu(II) on PFA, which involve higher negative value of  $\Delta G^\circ$ . On the other hand, the degree of spontaneity of the reaction increases with increasing temperature for all concentrations of Cu(II). The positive values of  $\Delta H^\circ$  reveals, the endothermic nature of the process and its value lie in the range of physisorption. It was also observed that the randomness increases at the solid-solution interface from the positive values of  $\Delta S^\circ$ . Estimation of sticking probability  $S^*$  values reveal that the process is favorable due to low value of  $S^*(S^*<1)$ . Activation energy  $E_a$  values were consistent with values of  $\Delta H^\circ$  both are positive and their values lie in the range of physisorption.

**Keywords:** Poly(furfural-acetone), Adsorption, Copper, Thermodynamic Parameters, Sticking Probability

## 1. Introduction

Pollution from heavy metals is a major concern in developing countries. The discharge of heavy metals into water-courses is a serious pollution problem which may affect the quality of water supply. Increasing concentrations of these metals in the water constitute a severe health hazard mainly due to their non-degradability and toxicity. Numerous metals such as chromium Cr(III) and Cr(VI), Copper (Cu), Lead (pb), Manganese (Mn), Mercury (Hg), Cadmium (Cd), etc. are known to be significantly toxic (Nordberg, 2007). Copper, the metal considered in this project, is a widely used material. Copper metal contamination exists in aqueous waste streams from many industries such as electronic and electrical, metal plating, mining, manufacture of complex heat sinks, Cu plumbing, as a component in ceramic glazing and glass coloring. Unfortunately, Cu is a persistent, bioaccumulative and toxic chemical that does not readily break down in the environment and is not easily metabolized (Ireland, 1991; Vernet, 1992). It may accumulate in the human or ecological food chain through consumption or uptake and may be hazardous to human health or the environment. Drinking water that contains higher than normal levels of Cu may cause vomiting, diarrhea, stomach cramp and nausea. The chronic effects of consumption of high levels of copper are liver and kidney damage (Najua, 2008). The safe level of Cu in drinking water for human is between 1.5 to 2.0 mg/L. hence, removal of copper from water and waste water assumes important (Najua, 2008). Chelating resin provide a dramatic improvement in ion selectivity relative to traditional ion exchange resin but still suffer from two distinct drawbacks: slow metal uptake kinetics and limited operating pH range (Rivas, 2001; Rivas, 1995), on the otherhand, chelating polymer resins are found to be more selective by nature (Rivas, 2001; Rivas, 1995) as compared to other conventional techniques in the removal of metal ion (Huang, 1971; Wing, 1975; Netzer, 1974; Sundersen, 1978; Patterson,

1977; Lindstdt, 1971; Shukla, 1994). In the light of the above, poly (furfural-acetone) was prepared and the kinetic models and thermodynamic parameter of the adsorption of Cu on the polymer were investigated.

## 2. Experimental

### 2.1 Preparation of poly (furfural-acetone)

The poly(furfural-acetone), PFA was prepared by direct polymerization of furfural and acetone in the presence of aqueous alkali solution according to literature (Patel, 1983) the FTIR spectrum of PFA was done using FTIR spectrophotometer Type Shimadzu 8000.

### 2.2 Preparation of Copper(II) solutions and analysis

A stock solution of  $\text{Cu}(\text{NO}_3)_2 \cdot 3\text{H}_2\text{O}$ , 500 mg/L was obtained by dissolving 1.9005g Of  $\text{Cu}(\text{NO}_3)_2$  in 1L of deionized water, this solution was used for further experimental solution preparation. The pH values were adjusted with 0.1M  $\text{HNO}_3$  or 0.1M  $\text{NaOH}$ . Analytical grade reagents were used throughout this study. The pH values of Cu(II) solutions were measured by pH meter Type HANA,301 instruments. The residual Cu(II) in the sorption solutions was determined by atomic absorption spectrophotometer Type AAnalyst 200 Perkin Elmer.

### 2.3 Effect of pH

The pH effect on adsorption were done using batch process. The initial pH values were adjusted to 4.0, 5.0, 6.0, 7.0 and 8.0 with 0.1M  $\text{HNO}_3$  and 0.1M  $\text{NaOH}$ . The effect of pH on the adsorption of Cu(II) onto poly( furfural-acetone ) were determined using 0.1g of PFA in 50 ml of Cu(II) solution of 10 ppm at 20 °C, shaking was carried out using horizontal thermostat shaker model LSB-015S, at 140 rpm, for 100 minutes time. In all batch experiments and after completion of adsorption time, samples were collected from duplicate flasks, filtered by whattman filter paper no.40, the filtrate was analyzed for residual copper concentration. The amount of Cu(II) adsorbed onto the polymer,  $q_e$  mg/g, was calculated using the following equation:

$$q_e = (C_i - C_e)V/M \quad (1)$$

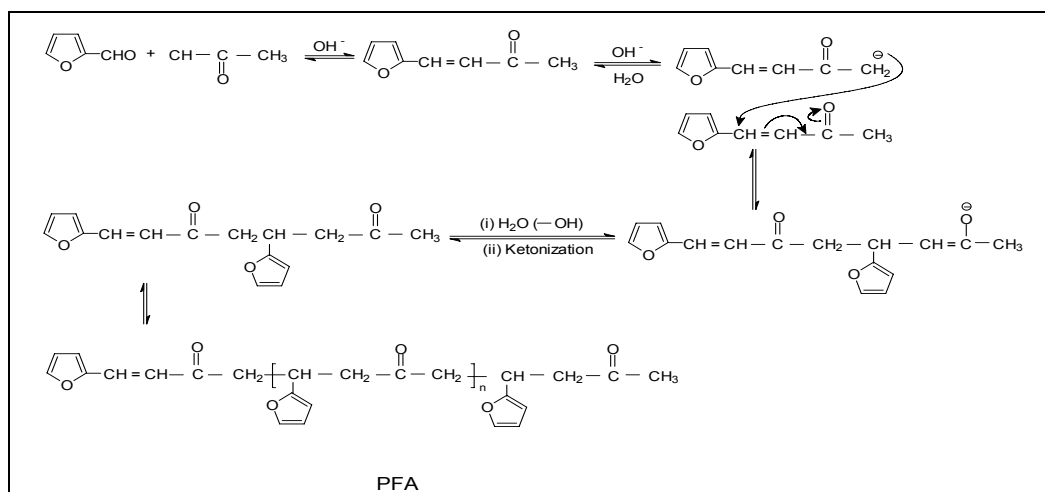
Where  $C_i$  and  $C_e$  are the initial and equilibrium liquid phase concentration of Cu(II) respectively, V is the volume of the solution (L) and M is the weight of the polymer used (g). the copper percent removal (R%) was calculated using the following equation:

$$R\% = (C_i - C_e / C_i) 100 \quad (2)$$

## 3. Results and Discussion

### 3.1 Characterization of PFA

Poly(furfural-acetone) was prepared according to literature (Patel, 1983). The final Structure of the polymer is formed through the following mechanism (Patel, 1983):



PFA was a yellow powder, soluble in acetone, dioxane and ethyl methyl ketone, softening point 160-173°C. The intrinsic viscosity of PFA in acetone was  $3.6 \times 10^{-2} \text{ dl.g}^{-1}$ . The number average molecular weight was determined by conductometric titration in nonaqueous medium and was 1500. Figure1 represent the FTIR spectrum of PFA, The characteristic bands observed at 3116 and 3125  $\text{cm}^{-1}$  are attributed to C-H stretching vibration of furan ring.

The band of  $2923.88\text{ cm}^{-1}$  are attributed to C-H stretching vibration of  $\text{CH}_3$  and/or- $\text{CH}_2$ -. There are two types of carbonyl groups in the proposed structured of PFA, one is conjugated which has lower vibration, observed at  $1666.38\text{ cm}^{-1}$  and normal C=O band at  $1712.67\text{ cm}^{-1}$ . The ethylenic linkage is observed at  $1604.66\text{ cm}^{-1}$ , while the  $\alpha$ -olefinic carbon of substituted furan are observed at  $1504.37$  and  $1357.79\text{ cm}^{-1}$ . Thus the observed spectral characteristics are explicable on the basis of the structure proposed by PFA.

### 3.2 Effect of pH

The effect of pH (4.0 to 8.0) on removal of Cu(II) was studied. It was observed that maximum percentage of Cu(II) removal was at pH 6 by using 2 g/L of PFA and 10 ppm of Cu(II) concentration at  $20^\circ\text{C}$ , the maximum removal efficiency was 96%. Figure 2 represent the effect of pH of the solution on the adsorption of Cu(II) onto PFA. The electrostatic attraction between positive charges of Cu(II) and lone pair of electrons on the oxygen atoms of carbonyl groups and furan rings could be the main attribution for such process at neutral solution.

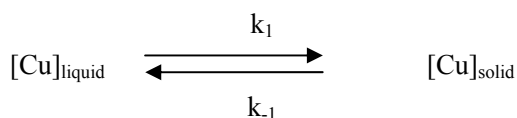
### 3.3 Adsorption kinetic study

Four kinetics models have been used to investigate the mechanism of sorption and potential rate controlling steps, which is helpful for selecting optimum operating conditions for the full-scale batch process. Table 1 shows the final kinetic equations used in this study. Where,  $q_e$  and  $q_t$  refer to the amount of Cu adsorbed ( $\text{mg.g}^{-1}$ ) at equilibrium and at any time,  $t(\text{min})$ , respectively,  $k_1$ , and  $k_2$  are the first and second order equilibrium rate constants respectively,  $h$  is initial adsorption rate in the pseudo-second order kinetic,  $\alpha$  is the initial adsorption rate ( $\text{mg.g}^{-1}$ ) in the Elovich kinetic model, and  $\beta$  is the desorption constant ( $\text{g.mg}^{-1}$ ) related to the extent of surface coverage and activation energy for chemisorption,  $K_{\text{diff}}$  ( $\text{mg.g}^{-1}\text{ min}^{-1}$ ) is the intraparticle diffusion rate constant and  $B_L$  is related to the thickness of the boundary layer, the layer separate between the liquid phase and the solid phase (adsorbent). From application of the **first-order** kinetic equation for the adsorption of Cu(II) onto PFA, a straight line was obtained, with correlation coefficient of 0.9951, nevertheless, the rate of removal of copper onto PFA does not follow the pseudo-first order equation due to the big difference between experimental  $q_e$  ( $q_{\text{exp}}$ ) and calculated  $q_e$  ( $q_{\text{cal}}$ ), Table 2.

When the experimental data were applied to the **pseudo-second-order** rate equation, a straight line was obtained with correlation coefficient of 1.00 figure 3, and the value of  $q_e(\text{cal})$  in well agreement with the  $q_e(\text{exp})$  table 2, indicating that the rate of removal of copper onto PFA follow the pseudo-second-order equation. The high value of the initial adsorption rate,  $h=14.168\text{ mg.g}^{-1}\text{ min}^{-1}$  table 2 indicate that the most of Cu(II) adsorbed at the beginning of the process, where more than 94% adsorbed at the first 5 minutes. When, the **Elovich** kinetic model was applied to the experimental data, where, the  $q_t$  was plot versus  $\ln(t)$  a straight line was obtained with correlation coefficient of 0.97971, fig.4, confirms that the Elovich model also applicable, the kinetic parameter are listed in table 2. The **intraparticle** diffusion is another kinetic model to study the rate-determining step for Cu(II) removal by PFA. If intraparticle diffusion occurs, then plot of  $q_t$  vs.  $t^{1/2}$  will be linear and the line will pass through the origin, if the intra-particle diffusion was the only rate limiting parameter controlling the process. Otherwise, some other mechanism is also involved. Fig.5 present intraparticle plot for Cu(II) removal by PFA the correlation coefficient was, 0.9475, indicates the applicable of intraparticle diffusion, but the large value of  $B_L$  4.688 indicates a large thickness of boundary layer, which mean, a decrease in the chance of external mass transfer and the chance of internal mass transfer, this attribution is confirmed by low value of  $K_{\text{diff}}$ ,  $0.022\text{ mg.g}^{-1}\text{ min}^{-1/2}$ . So, the second order kinetic mainly controls the sorption rate.

## 4. Adsorption thermodynamics

The change in Gibbs free energy ( $\Delta G^\circ$ ), enthalpy ( $\Delta H^\circ$ ), and entropy ( $\Delta S^\circ$ ) for the adsorption process was obtained using the following equation (Arivoli, 2008; Edwin, 2008; Arivoli, 2008; Edwin, 2008; El Nemr, 2007):



$$K_o = \frac{[Cu]_{solid}}{[Cu]_{liquid}} \quad (3)$$

$$\Delta G^o = -RT \ln K_o \quad (4)$$

$$\text{Log} K_o = \frac{\Delta S^o}{2.303R} - \frac{\Delta H^o}{2.303RT} \quad (5)$$

Where  $K_o$  is the equilibrium constant,  $[Cu]_{solid}$  is the concentration of Cu, ppm, at the solid phase at equilibrium,  $[Cu]_{liquid}$  is the liquid phase concentration of copper, ppm, T is the temperature(K) and R is the ideal gas constant ( $8.314 \text{ J mol}^{-1} \text{ K}^{-1}$ ). The enthalpy change ( $\Delta H^o$ ) and the entropy change ( $\Delta S^o$ ) are calculated from plot of  $\log K_o$  versus  $1/T$  Fig. 6. The results of these thermodynamic calculation are shown in Table 3.

The Gibbs free energy indicate the spontaneity of the adsorption process, where higher negative values a more energetically favorable adsorption process. The calculation of  $\Delta G^o$  values at different pH, Table 4 gave an indication that at pH 6, the adsorption of Cu(II) onto PFA is more preferable due to the highest negative value of  $\Delta G^o$ . The positive  $\Delta G^o$  value obtained at pH 4, table 4, indicate a decrease in adsorption process at pH 4. The study confirm that as the pH of the system increase, the adsorption of Cu(II) increases and reach the optimum at pH 6, which involve higher negative value of  $\Delta G^o$ . The negative values of the Gibbs free energy show the removal process of copper by PFA is spontaneous and that the degree of spontaneity of the reaction increases with increasing temperature for all concentrations of Cu(II)table3. The overall process seems to be endothermic ( $\Delta H^o = 12.48, 2.425, 4.6$  and  $2.27 \text{ KJ mol}^{-1}$ ), moreover, the  $\Delta H^o$  values lie in the range of physisorption process, table 3. Table 3 also shows that the  $\Delta S^o$  values were positive (i.e that entropy increases as a result of the removal process of copper). This occurs as a result of redistribution of energy between the adsorbate and the adsorbent. Before adsorption occurs, the heavy metal ions near the surface of the adsorbent will be more ordered than in the subsequent adsorbed state. As a result, the distribution of rotational and translational energy among a small number of molecules will increase with increasing adsorption by producing a positive value of  $\Delta S^o$  and randomness will increase at the solid-solution interface during the process of adsorption (Argun, 2007). Adsorption is thus likely to occur spontaneously at normal and high temperatures because  $\Delta H > 0$  and  $\Delta S > 0$ .

The other parameters which can be estimated from the experimental data are, the activation energy  $E_a$  and sticking probability  $S^*$ , which they can give further support for the assertion of physical adsorption in the studied case. They were calculated using modified Arrhenius type equation related to surface coverage ( $\theta$ ) as follows (Amin, 2009; Najim, 2009).

$$\theta = \left[ 1 - \frac{C_e}{C_i} \right] \quad \text{or} \quad \frac{C_e}{C_i} = 1 - \theta \quad \text{.....(6)}$$

$$S^* = (1 - \theta) e^{\frac{-E_a}{RT}} \quad \text{.....(7)}$$

$$\ln S^* = \ln(1 - \theta) - \frac{E_a}{RT} \quad \text{.....(8)}$$

$$\ln(1 - \theta) = \ln S^* + \frac{E_a}{RT} \quad \text{.....(9)}$$

The sticking probability  $S^*$ , is a function of the adsorbate/adsorbent system under investigation, its value lies in the range  $0 < S^* < 1$  for preferable process, and is dependent on the temperature of the system (Amin, 2009; Najim, 2009). The values of  $E_a$  and  $S^*$  can be calculated from slope and intercept of the plot of  $\ln(1 - \theta)$  versus  $1/T$  respectively, figure 7 and table 5. The values of  $E_a$ , table5, found to be 10.796, 1.7, 2.694 and 1.193  $\text{KJ mol}^{-1}$  were consistent with the values of  $\Delta H^o$ , table3, both are positive, indicate the endothermic nature of the adsorption process and the values lie in the range of physical adsorption.  $E_a$  values almost decreases with increasing temperature, that indicate the preferable process at higher temperature, which is in agreement with the values of  $\Delta G^o$  Table3. The values of sticking probability are less than one, table 5, which indicate that the probability of Cu(II) ions to stick on surface of PFA is high as  $S^* < 1$  these values confirm that, the sorption process is physisorption.

## 5. Conclusion

The present study indicates that the new adsorbent is effective for the removal of copper from aqueous solution. The lone pair of electrons on the oxygen atoms of carbonyl groups and furan rings may be the main chelating positions for removal of copper from aqueous solution. The adsorption process is highly dependent on pH, the maximum removal of copper was obtained at pH 6. The experimental data fit well with the second-order kinetic. The values of  $\Delta H^\circ$  and  $E_a$  were both positive and lie in the range of physisorption.

## References

- Amin, N.K. (2009). Removal of direct blue-106 dye from aqueous solution using new activated carbons developed from pomegranate peel: Adsorption equilibrium and kinetics. *J. Hazard. Materials*, 165(1-3): 52-62.
- Argun, M.E., Dursun, S., Ozdemir, C., and Karatas, M. (2007). Heavy metal adsorption by modified Oak sawdust: Thermodynamics and kinetics. *J. Hazard. Materials*, 141, 77-85.
- Arivoli, S., and Thenkuzhali, M. (2008). Kinetic, Mechanistic, Thermodynamic and Equilibrium studies on the Adsorption of Rhodamine B by acid activated low cost carbon. *E-J. of chemistry*, 5(2), 187-200.
- Arivoli, S., Hema, M., Karuppaiah, M., and Saravanan, S. (2008). Adsorption of Chromium ion by acid activated low cost carbon : Kinetic, Mechanistic, Thermodynamic and Equilibrium studies. *E-J. of chemistry*, 5(4): 820-831.
- Chien, S.H., and Clayton, W.R. (1980). Application of Elovich equation to the kinetics of phosphate release and sorption on soils. *Soil Sci. Am. J.*, 44, 265-268.
- Edwin, A.V. (2008). Removal of Phenol and o-Cresol by Adsorption onto activated carbon. *E-J. of chemistry*, 5(2), 224-232.
- Edwin, A.V. (2008). Studies on the removal of Rhodamine B and Malachite from aqueous solutions by activated carbon. *E-J. of chemistry*, 5(4), 844-852.
- El Nemr, A., Elsikaily, A., Khaled, A., and Abdulwaahab, O. (2007). Removal of toxic Cr(VI) from aqueous solution by activated carbon developed from Casuarina Equisetifolia. *Chemistry and Ecology*, 23(2), 119-129.
- Huang, C.P. and Bstarz, F.B. (1971). *J. Environ. Eng.*, 104, 863.
- Ireland, M.P. (1991). *Biological Monitoring of Heavy metals*. Wiley, New York.
- Lagergren, S. (1898). Zur theorie der sogenannten adsorption gelöster stoffe, Kungliga Svenska Vetenskademien. *Handlingar*, 24, 1-39.
- Lindstedt, K.K., Hanch, C.P., and Connor, J.J. (1971). *J. Water Pollution Control Fed.*, 43, 1507.
- Mckay, G., and Ho, Y.S. (1999). Pseudo-Second order model for sorption process. *Process Biochem.*, 34, 451-465.
- Najim, T.S., and Yassin, S.A. (2009). Removal of Cr(VI) from aqueous solution using modified pomegranate peel: Mechanistic and Thermodynamic studies. *E-J. of Chemistry*, 6(S1): S153-S158.
- Najim, T.S., and Yassin, S.A. (2009). Removal of Cr(VI) from aqueous solution using modified Pomegranate peel: Equilibrium and Kinetic studies. *E-J. of Chemistry*, 6(S1): S129-S142.
- Najua, D.T., Chuah, A.L., Zawani, Z., and Abdul Rashid, S. (2008). Adsorption of copper from aqueous solution by elais guineensis kernel activated carbon. *J. of Engineering science and Technology*, 3(2), 180-189.
- Netzer, A., Wilkinson, P. and Beszedits, S. (1974). *Water Res.*, 8(12), 813-817.
- Nordberg, G.F., Flower, B.A., Nordberg, M., and Friberg, L. (2007). *Handbook on the Toxicology of Metals*. 3<sup>rd</sup> edition, Academic Press Inc. New York.
- Patel, A.A., and Patel, S.R. (1983). Synthesis and Characterization of Furfural-Acetone polymers. *Eur. Polym. J.*, 19(3): 231-234.
- Patterson, J.W., Allen, H.F. and Scala, J.J. (1977). *J. Water pollution Control Fed.*, 49, 2397.
- Rivas, B.L., Pooley, S.A., Maturana, H.A. and Villegas, S. (2001). Metal ion uptake properties of Acrylamide Derivative Resins. *Macromolecular chemistry and physics*, 202(3), 443-447.
- Rivas, B.L., Maturana, H.A., Ocampo, X. and peric, I.M. (1995). Adsorption behaviour of Cu(II) and UO<sub>2</sub>(II) ions on crosslinked poly[2,2-bis(acrylamido) acetic acid]. *J. Applied polymer Sci.*, 58(12), 2201-2205.
- Shukla, M., and Pandeya, G.S. (1994). *Indian J. chem.. Technol.*, 1, 308.

Sundersen, B.B., Bulusis, K.R. and Kulkarni, D.M. (1978). *Indian J. Environ. Health*, 20, 413.

Vernet, J.P. (1992). *Impact of Heavy metals on the Environment*. Elsevier, New York.

Weber, W.J., and Morris, J.C. (1963). Kinetics of adsorption on carbon from solution. *J. Santi. Eng. Div. ASCE*, 89, (SA2), 31-59.

Wing, R.E., Doone, W.H. and Russel, C.R. (1975). Insoluble starch xanthate: Use in heavy metal removal. *J. Applied Polymer Sci.*, 19(3), 847-854.

Table 1. Kinetic equations used in this study

Kinetic models	Kinetic equation	Reference
Pseudo first- order	$\text{Log}(q_e - q_t) = \text{Log} q_e - \frac{k_1}{2.303}(t)$	(Lagergren, 1898)
Pseudo-second- order	$\frac{t}{q_t} = \frac{1}{k_2 q_e^2} + \frac{1}{q_e}(t)$ $h = k_2 q_e^2$	(Mckay, 1999)
Elovich kinetic model	$q_t = \frac{1}{\beta} \ln(\alpha\beta) + \frac{1}{\beta} \ln(t)$	(Chien, 1980)
Intra.Particle diffusion	$q_t = K_{dif} t^{\frac{1}{2}} + B_L$	(Weber, 1963)

Table 2. Parameter obtained from Pseudo-first-order, Pseudo-second-order, Elovich and Intraparticle diffusion kinetic models for the adsorption of Cu(II) onto PFA, 2g/L at pH 6 and 20°C

Pseudo-first-order				Pseudo-second-order				Elovich		
k <sub>1</sub>	q <sub>(exp)</sub>	q <sub>(cal)</sub>	R <sup>2</sup>	k <sub>2</sub>	q <sub>e(cal)</sub>	h	R <sup>2</sup>	α	β	R <sup>2</sup>
0.034	4.888	0.1842	0.9951	0.592	4.892	14.168	1.00	1.003	17.54	0.9797
Intraparticle diffusion										
K <sub>diff</sub>	B <sub>L</sub>	R <sup>2</sup>								
0.022	4.688	0.9475								

Table 3. Thermodynamic parameter for the removal of Cu(II) by PFA, 2g /L

Cu(II) Conc ppm	$\Delta H^\circ$ KJ mol <sup>-1</sup>	$\Delta S^\circ$ Jmol <sup>-1</sup> K <sup>-1</sup>	$\Delta G^\circ$ KJ mol <sup>-1</sup>				R <sup>2</sup>
			15 °C	25 °C	35 °C	45 °C	
20	12.48	56.51	-3.729	-4.145	-4.382	-5.679	0.9963
30	2.425	14.96	-2.398	-2.178	-1.931	-2.013	0.9165
40	4.6	18.07	-0.551	-0.823	-0.988	-1.208	0.9952
50	2.27	8.38	-0.123	-0.306	-0.349	-0.421	0.9982

Table 4. Thermodynamic parameter for the adsorption of Cu(II),10 ppm, by PFA 2g/L temperature 20 °C, at different pH

pH	Ce	Ca	Ca/Ce	Ln K <sub>o</sub>	$\Delta G^\circ$ KJmol <sup>-1</sup>
4	5.135	4.865	0.9474	-0.054	0.1315
5	3.292	6.708	2.0377	0.7118	-1.734
6	0.382	9.618	25.178	3.226	-7.858
7	0.402	9.598	23.876	3.173	-7.729
8	0.462	9.538	20.775	3.034	-7.391

Table 5. Sticking probability and activation energy for the adsorption of Cu(II) onto PFA

Cu(II) conc.ppm	Ea KJ mol <sup>-1</sup>	S*	R <sup>2</sup>
20	10.796	0.0019	0.996
30	1.700	0.154	0.9138
40	2.694	0.143	0.9936
50	1.193	0.295	0.9988



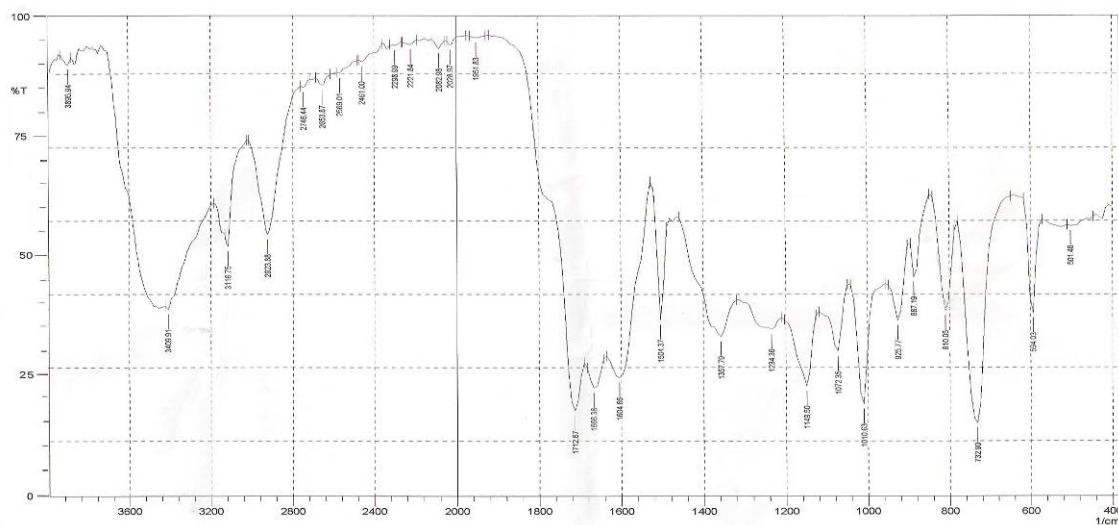


Figure 1. FTIR spectrum of PFA

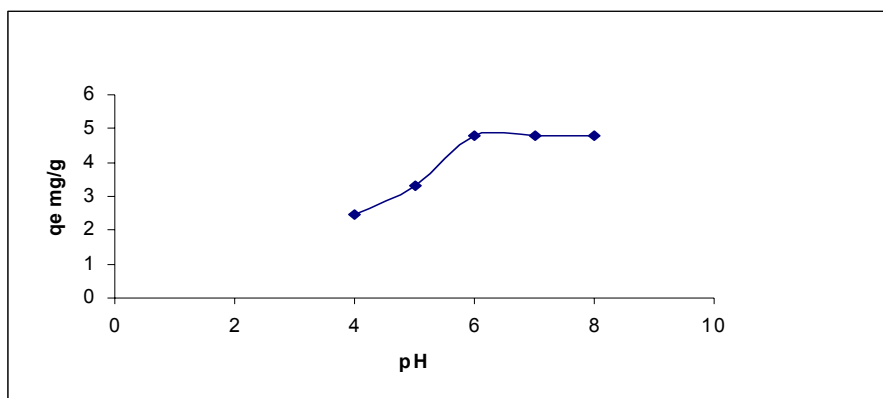


Figure 2. Effect of pH on the adsorption of Cu(II) on to PFA

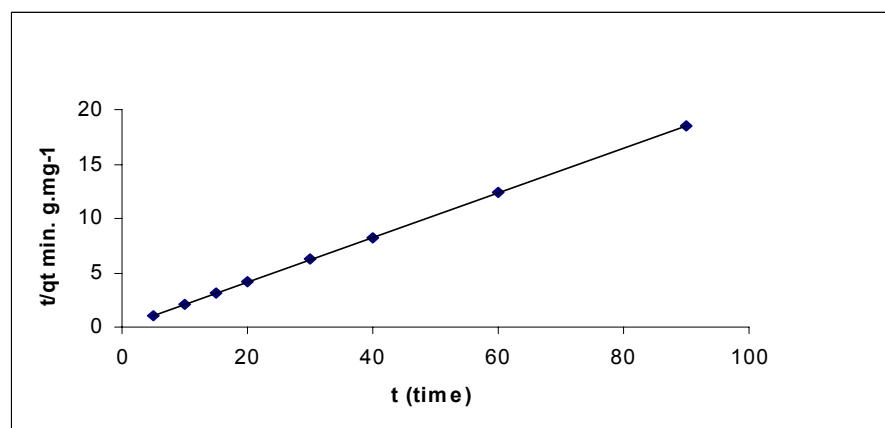


Figure 3. Pseudo-Second-order kinetic for removal of Cu(II) onto PFA at 20 °C

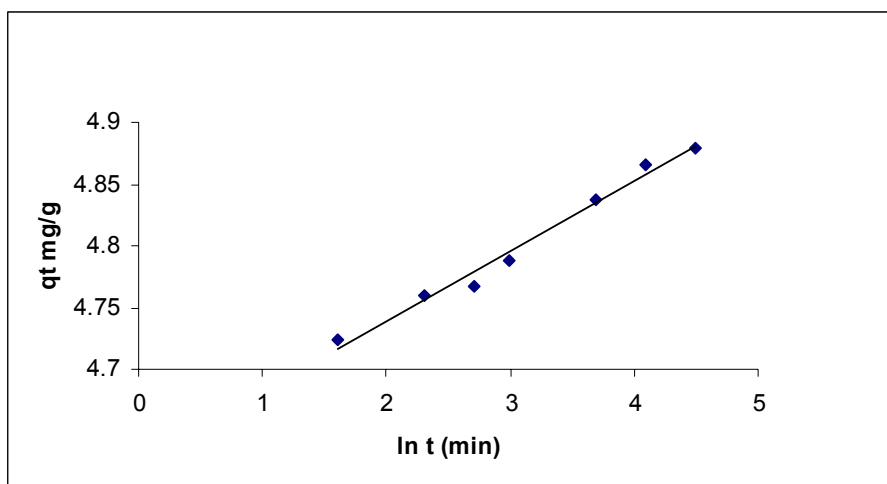


Figure 4. Elovich model plot for removal of Cu(II) onto PFA at 20 °C

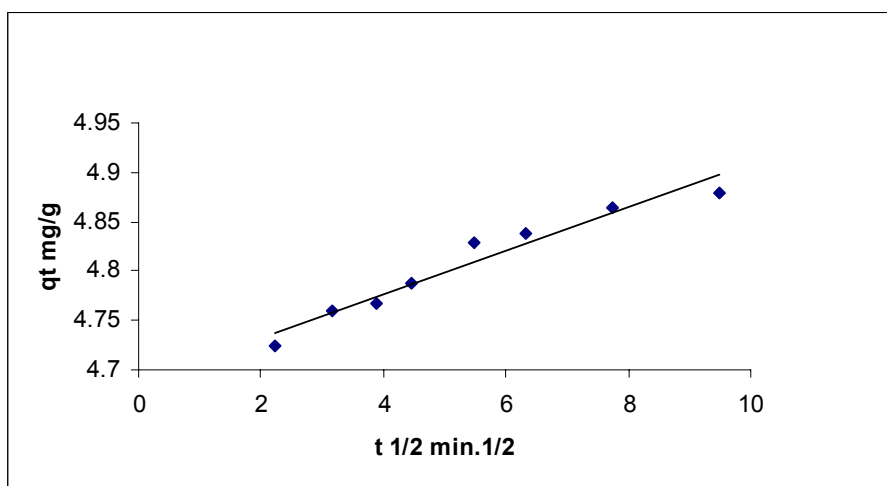


Figure 5. Intraparticle diffusion plot for the removal of Cu(II), 10 ppm, at 20 °C, pH 6.0 by PFA 2 g/L

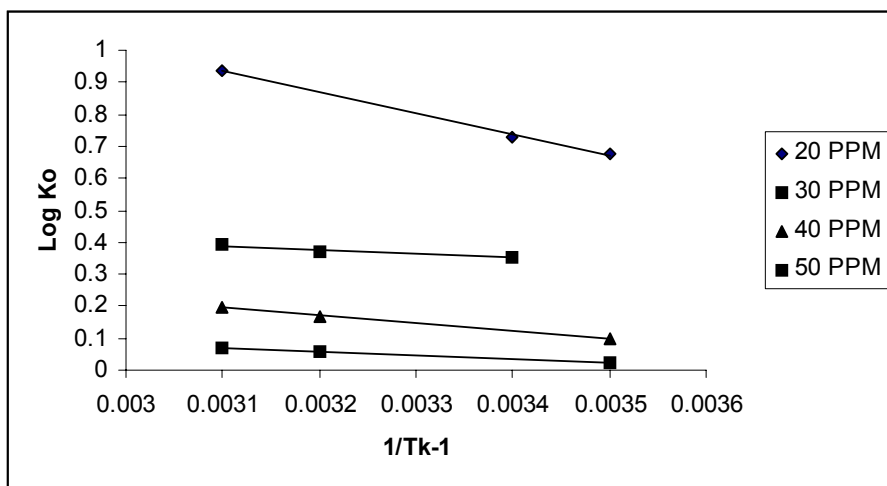


Figure 6. Plot of  $\log K_o$  vs  $1/T$  for the removal of Cu(II) by PFA, 2g/L

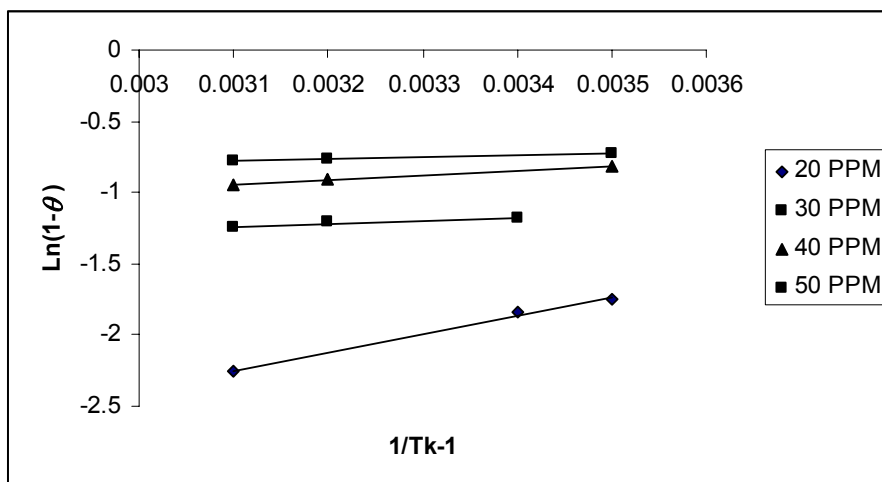


Figure 7. Plot of  $\ln(1-\theta)$  vs. reciprocal of temperature for the adsorption of Cu (II) onto PFA

# Corrosion and Corrosion Inhibition of Mild Steel in $\text{H}_2\text{SO}_4$ Solutions by *Zizyphus Spina-Christi* as Green Inhibitor

Aisha M. Al- Turkustani

King Abdulaziz University, Girls College of Education

Chemistry Department, Jeddah KSA

E-mail: A.M.Turkustani@hotmail.com

Sanaa T. Arab

King Abdulaziz University, Girls College of Education

Chemistry Department, Jeddah KSA

E-mail: Prof.S.T.arab@hotmail.com

Areej A. Al- Reheli

Tabook University, Chemistry Department, Tabook KSA

E-mail: skoon\_n-alil@hotmail.com

## Abstract

The corrosion and corrosion inhibition of mild steel in 1.0 M  $\text{H}_2\text{SO}_4$  containing 10% ethyl alcohol(EtOH) by *Zizyphus Spina-Christi* (**ZSC**) extracts (aqueous extract and alcoholic extract) has been studied using chemical techniques( hydrogen evolution(HE) and mass loss(ML)) and electrochemical techniques(electrochemical impedance spectroscopy(EIS) and potentiodynamic polarization(PDP)). The effect of acid concentration on the corrosion rate of mild steel increases with acid concentration (0.25-1.5) M showing first order corrosion reaction without changing the reaction mechanism, and the results showed that when the concentration of **ZSC** extracts (aqueous extract and alcoholic extract) increased the rate of steel corrosion is decreased, which indicates that the inhibition of the corrosion process is produced. Electrochemical impedance spectroscopy results showed that the corrosion and corrosion inhibition of steel occurred mainly by charge transfer. The electrochemical results of polarization also showed that the extracts of **ZSC** plant act as mixed type inhibitors, they retarded both cathodic and anodic reaction. The experimental results from chemical and electrochemical studies were fit Langmuir isotherm. Values of equilibrium constant of adsorption  $K_{ads}$  and the standard free energy of adsorption  $\Delta G_{ads}^\circ$ , for the extracts are calculated.

**Keywords:** Corrosion, Inhibition, Mild steel, *Zizyphus Spina-Charisti*, Acids, Sulphuric acid

## 1. Introduction

Acid solutions are generally used for the removal of rust and scale in several industrial processes. Sulphuric acid is often used as a pickling acid for steel and its alloys (Bentiss et. al., 1999). Mild steel is employed widely in most industries due to its low cost and availability in ease for the fabrication of various reaction vessels such as cooling tower tanks, pipelines, etc.( Ramesh et. al., 2003). inhibitors are (Vasanth, 2009): substance which retards substances which retard the cathodic processes and / or the anodic processes, that inhibitors function in one or more ways to control corrosion: by adsorption of a thin film onto the surface of a corroding material, by inducing the formation of a thick corrosion product, or by changing the characteristic of the environment resulting in reduced aggressiveness. Inhibitors are generally used in these processes to control the metal dissolution. Acid inhibitors are essentially used in metal finishing industries, acidizing of oil wells, cleaning of boilers and heat exchangers (Khaled, 2003).

Corrosion of metals is a serious environmental problem that has been given adequate attention in the oil and gas industries because, during industrial processes such as acid cleaning and etching, metal surfaces are often made to come in contact with acidic medium, indicating that the use of inhibitors is necessary (Abdallah, 2005; Ananda et.al., 2005; Ashassi-Sorkhabi et.al., 2006). Although there are numerous options for controlling the corrosion of metals, the use of inhibitors is one of the best methods for protecting metals against corrosion. An

inhibitor can be chosen from compounds that have hetero atoms in their aromatic ring system or synthesized from cheap raw materials (Chetounani et.al., 2004; Bouyanzer and Hammouti, 2004; Ebenso et.al., 2004; Bendahou et.al., 2006; Eddy, 2008). However, the problem of finding an inhibitor that has little or no impact on the environment has attracted numerous researches in recent times (Eddy, 2008). Green or safe corrosion inhibitors are biodegradable and do not contain heavy metals or other toxic compounds (Eddy, 2009). Most green corrosion inhibitors are obtained from ethanol, aqueous, acid, methanol, or formaldehyde extract of plant materials (Odiongenyi et.al., 2009). The successful use of naturally occurring substances to inhibit the corrosion of metals in acidic and alkaline environments has been reported by some research groups (El-Etre, 2003; Chetounani et.al., 2004; El-Etre et.al., 2005; Bendahou et.al., 2006; El-Etre, 2006; Ebenso et.al., 2008; \*Eddy et.al., 2008; \*\*Eddy et.al., 2008; \*\*\*Eddy et.al., 2008; Odoemela and \*\*\*\*Eddy, 2008; Ebenso et.al., 2009).

However, the use of aqueous extract and alcoholic extract of *Zizyphus Spina-Christi* (ZSC) plant as a green inhibitor has not been reported elsewhere.

Therefore the objective of the present study is aimed at investigating inhibitive and adsorption properties of aqueous and alcoholic extracts of *Zizyphus Spina-Christi* leaves for the corrosion of mild steel in  $H_2SO_4$ .

*Zizyphus Spina-Christi* plant belongs to the Rhamnaceae subfamily (Fig. (1)), this plant have been successfully used for numerous medicinal applications including internal use (Adzu et.al., 2001). Also, in Saudi Arabia it use to treat ulcers, wounds, eye diseases and bronchitis, which is a diuretic and the reduce of fever (Dweek, 2005).

*Zizyphus Spina-Christi*(ZSC) leaves contains on the sugars and several organic compounds such as glucose, fructose, Ramnoz, Sabonin and Glicosed (Mahran et.al., 1996), and main components of the plant installers alpha Trbinol and contains alkaloids and also it have a high percentage of flavonoids (0.66%), Table (1) illustrate the chemical composition of some of the most important components of *Zizyphus Spina-Christi*(ZSC) plant.

## 2. Experimental

### 2.1 Materials preparation

Mild steel of the composition (wt%) as: Mn(0.275), Ni(0.015), Pb(0.004), Al(0.077) and Fe(99.629) was used for the study. The sample was polished using a series of emery paper up to 1200 grade. It washed thoroughly with deionized water and dried with acetone and with a stream of air. All reagents used ( $H_2SO_4$  and KCl) for the study were analar grade and deionized water was used for their preparation.

### Preparation of *Zizyphas Spina-Christi* (ZSC) Extracts (Inhibitor)

The leaves of ZSC plant was collected from trees in Jeddah city KSA, it has been purified from the impurities and then washed with deionized water and left to dry in the air for two days.

The aqueous extract and alcoholic extract of the plant were prepared as follows:

1. Weight a certain amount (about 500 grams) of dried leaves of the plant and was crushed in an electric mixer, then add to it the appropriate solvent (deionized water or ethyl alcohol) and heat until boiling, the mixture is cooled for 24 hours and then be feltrated.
2. Extraction is repeated several times from the same pool, so extract collect and dried in the air to be concentrated and deposited to the least possible amount of solvent used.
3. The extract was collect after concentrated it and placed in a standard flask 250 ml capacity and complete to the mark with the appropriate solvent and therefore is a solution study.

### 2.2 Corrosion Measurements

Two kinds of measurements were used these are:

#### 2.2.1 Chemical measurement

Hydrogen evolution (HE) and weight loss (ML) were carried out as described elsewhere (Mylius and Niethen, 1957).

#### 2.2.2 Electrochemical measurement

Impedance and polarization measurements have been performed with an ACM Gill AC instruments using a platinum foil as the auxiliary electrode. The electrode potential was measured against a saturated calomel electrode (SCE). Details of the experimental procedure, electrolytic cell and electric circuits have been fully described (Ateya et.al., 1981; Zaafarany; 2009).

The percentage inhibition efficiencies (Inh.%) were calculated using the following equations from chemical methods (HE and ML), respectively:

$$Inh_{HE} \% = (1 - R / R_o) 100 \quad (1)$$

$$Inh_{ML} \% = (1 - R' / R'_o) 100 \quad (2)$$

Where  $R_o$ ,  $R'_o$ ,  $R$  and  $R'$  are the corrosion rates without and with inhibitor, respectively. Also, inhibition efficiencies from electrochemical methods (EIS and PDP), are respectively:

$$Inh_{R_{ct}} \% = (1 - R_{ct}^{-1} / R_{ct_o}^{-1}) 100 \quad (3)$$

$$Inh_p \% = (1 - i_{corr.} / i_{corr.}^o) 100 \quad (4)$$

Where  $R_{ct_o}^{-1}$ ,  $i_{corr.}^o$ ,  $R_{ct}^{-1}$  and  $i_{corr.}$  are charge transfer and corrosion current without and with inhibitor, respectively.

### 3. Results and Discussion

#### 3.1 Effect of Sulfuric Acid Concentration Containing 10% EtOH on Mild Steel Corrosion at 30°C.

##### 3.1.1 Chemical Study

The influence of  $H_2SO_4$ +10%EtOH concentrations (0.25M, 0.5M, 1.0M and 1.5M) on mild steel corrosion at 30°C is shown in Figure (2). It is clear that as the concentration of the  $H_2SO_4$  solution increases, the slope of the straight lines also increases, indicating an increase in the dissolution of mild steel, e.g. increases of corrosion rate. The ideality of the straight lines in Figure (2) indicates the absence of any insoluble formed layer on the surface of the metal through the process of corrosion. The presence of induction period in the beginning of the interaction indicates the dissolution of the oxide layer formed on the surface of mild steel. The decrease of induction period in the beginning of the interaction with increasing acid concentration is detected. The rates of corrosion from HE and ML methods ( $R$  &  $R'$ ) are recorded in Table (2), it is found that the rates of corrosion increases with increasing acid concentration, this indicates that steel corrosion in  $H_2SO_4$  is concentration dependent.

The relation between corrosion rate and acid concentration can be illustrate by the kinetic equation as:

$$\log R = \log A + n \log C \quad (5)$$

Where  $A$  represents corrosion rate constant which represents the rate of metal dissolution (corrosion),  $n$  reaction order and  $C$  molar concentration of  $H_2SO_4$  acid. The relationship  $\log R$  and / or  $\log R'$  Vs.  $\log C$  gave a straight lines as in Figure (3). The slopes of these lines represent the reaction order ( $n$ ) and the intercept is  $\log A$ . It was found that the value of  $n$  is equal to unity indicating that corrosion of mild steel in  $H_2SO_4$  solution is the first order reaction depends on the concentration of  $H_2SO_4$  acid.

##### 3.1.2 Electrochemical Study

###### 3.1.2.1 Electrochemical impedance spectroscopy measurements (EIS)

Figure (4) shows electrochemical impedance spectra (Nyquist plots) at open circuit potential for mild steel corrosion in different concentrations of  $H_2SO_4$  containing 10% EtOH at 30°C. It gives one capacitive loop at high and med frequencies with the presence an inductive loop at low frequencies. This study allow the separation of charge transfer and diffusion process and describe the processes at the surface and also, calculate the charge transfer resistance and adsorption process (Kendig et.al., 1986; Mcdonald, 1987).

As shown from Figure (5a) a good agreement between the theoretically calculated values of impedance and recorded laboratory values with a relatively low error. Also, Figure (5b) shows the equivalent electrical circuit of the system under study, which consists of [ $R_s$  ( $C_{dl}$   $R_{ct}$  ( $QR$ )] using the Setup - ZSimDemo-322 program. The electrochemical impedance parameters, solution resistance ( $R_{sol.}$ ), double layer capacitance ( $C_{dl.}$ ) and constant phase element ( $Q$ ) were calculated and recorded in Table(3). The resistance element with constant phase is given from equation:

$$Z_{CPE} = [Q(J\omega)^n]^{-1} \quad (6)$$

Where  $Z_{CPE}$  electrode resistance,  $Q$  the combination properties of items associated with each surface, electrically active, and does not depend on the frequency,  $n$  is constant value in the range  $-1 \leq n \leq 1$ . It should be noted that when  $n$  is greater value, the more complete and closed of capacitive circuits and the surface is homogeneous, if  $n$  value is small this means that the capacitive circuit unclosed this will lead to a diffusion control and the surface is not homogeneous,  $J$  is imaginary number = -1 and  $\omega$  is the angular frequency value of the imaginary part at the highest of the impedance is equal to  $= 2\pi f$  (Hosseini et.al., 2003). It is clear from Table (3) that:

- The decrease of the relative capacitive circuit from their axes attributed to frequency disturbance as a result of the

heterogeneity of the surface of steel sample under study (Metikos- Hukovic et.al., 1994).

- The presence of capacitive loops show that the process of corrosion is under charge transfer control, i.e., under activation control (Muralidharan, 1993; Ashassi- Sorkhabi, and Seifzadeh, 2006), where it is noted that by increasing acid concentration the radii of the circuit decrease ( $R_{ct}$  decrease) while increasing the value of  $C_{dl}$  due to the increase in the concentration of active species such as  $H^+$  at the electrode surface with increasing acid concentration, which lead to increase the charge transfer process at the electrical double layer.
- The value of  $n$  at all concentrations close to unity and diffraction of the unit due to the dispersion in the frequency of a fixed timetable which is a result to the heterogeneity in the electrical items that presence on the metal surface.

### 3.1.2.2 Potentiodynamic polarization measurements (PDP)

Figure (6) shows the effect of  $H_2SO_4$  concentration containing 10% EtOH on the cathodic and anodic polarization behavior of mild steel at  $30^\circ C$ . It is clear that the increasing in acid concentration lead to displacement both cathodic and anodic curves to high current densities with the shift in corrosion potential to more positive values (noble potentials). Table (4) gives the values of corrosion potential ( $E_{corr.}$ ), corrosion current ( $I_{corr.}$ ), cathodic ( $\beta_c$ ) and anodic ( $\beta_a$ ) Tafel slopes for mild steel corrosion at the different concentrations of  $H_2SO_4$ . The results will be interpreted as:

- A regular increase in corrosion current density  $I_{corr.}$  (acceleration of corrosion) with increase acid concentration, as illustrated in Figure (7a) the dependence of  $I_{corr.}$  on the concentration of the acid according to the following equation (Murthy and Dwarakadasa, 1995):

$$I_{corr.} = a + b \log C_{H_2SO_4} \quad (7)$$

Where  $a$  and  $b$  are constants depend on the characteristics and properties of sample surface.

- The displacement in  $E_{corr.}$  to more positive (less negative) values as increase of acid concentration indicate on the contribution of each of the cathodic and anodic process in the process of corrosion, where the increase in  $E_{corr.}$  values indicate that the corrosion of mild steel in  $H_2SO_4$  solutions containing 10% EtOH is under the anodic control (Uhlig, 1971).

Figure (7b) gives the relationship between the  $E_{corr.}$  and  $\log C$  according to the following equation (Beccaria and Poggi, 1986):

$$E_{corr.} = E_{corr.}^{\circ} + (2.303 RT / nF) \log C \quad (8)$$

where  $E_{corr.}^{\circ}$  represents corrosion potential when the concentration of acid equal to unity,  $R$  universal gas constant,  $T$  temperature in Kelvin,  $n$  the number of electrons,  $F$  Faraday constant = 96500 coulomb and  $C$  concentration, it has been found that the value of  $n = 9.1338 \times 10^{-2}$ .

The plots of  $I_{corr.}$  and/or  $E_{corr.}$  Vs.  $\log C$  of acid give a straight lines with correlation coefficient equal to 92.27 and 96.91, respectively and the line indicates to the corrosion of mild steel depend on acid concentration.

## 3.2 Effect of *Zizyphus Spina-Christi* (ZSC) on mild steel corrosion in 1.0 M $H_2SO_4$ containing 10% EtOH at $30^\circ C$

### 3.2.1 Chemical Study

Dissolution of iron (mild steel) metal which occurs at the anode is spontaneous process, while, the cathodic process under these conditions, in presence of sulfuric acid, is represented by the reduction reaction is hydrogen gas evolution as in the equation:



Where  $H_{ads}$  is hydrogen ions adsorbed on metal surface which catalyze to react with another hydrogen ions to contain covert hydrogen gas in bubble form on cathode surface. The amount of hydrogen gas evolved in presence of inhibitor depends on its ability to prevent this reaction and protected the metal from corrosion (Oguzie, 2005).

Figures (8 and 9) show the variation of hydrogen volume evolved as a function of time when immersion of mild steel sample in 1.0 M  $H_2SO_4$  containing 10% EtOH in presence of aqueous extract (Fig.(8)) and alcoholic extract (Fig.(9)) of *ZSC* plant at  $30^\circ C$ , respectively. A straight lines in all figures were obtained. The presence of an induction period which it is necessary to begin the metal dissolution and the evolution of hydrogen gas is found. It is clear that the induction period increased with concentration of aqueous extract and /or alcoholic extract increase, i.e., reduction in the corrosion rate, but in the case of alcoholic extract after concentration 5%v/v, the induction period become less, this means that is increased in corrosion rate of mild steel sample. Also mass loss measurements give a similar behavior to the measurements of hydrogen gas, this behavior indicates to the high

ability of the extracts to inhibit the corrosion of mild steel under study and the efficiency of inhibition depends on the concentration of aqueous extract and alcoholic extract of **ZSC** plant.

Tables (5 and 6) give corrosion rates ( $R_{\text{corr}}$ ) and inhibition efficiency (Inh.%) calculated from HE and ML methods. It is clear from the Tables that there are a decrease in the corrosion rate (increase in Inh.%) by increase the concentration of aqueous extract and alcoholic extract of **ZSC** leaves and made a more effective equal 91.24 from MLM and 92.62 from HEM, respectively at the concentration 20.0%v/v of the aqueous extract, whereas alcoholic extract (Table(6)) gives corrosion rates which decrease as increase in concentration of the extract until it reaches to 5.0%v/v, after that an increase in the rate of corrosion will occur by increase the concentration of the extract lead to more less but the inhibition efficiency still high (around 90 % ) .

The increase in the Inh.% by increase concentration of the extract may attributed to a dissolved complexes as a result of the interaction of components of the aqueous extract and / or alcoholic extract of the **ZSC** plant with mild steel surface and adsorbed on the surface of the sample, leading to increase the inhibition efficiency as concentration of the extract increased, where the adsorption of these complexes lead to block most of the active centers on the surface of the mild steel sample and thereby increasing the surface coverage (Orubite and Oforka, 2004; El-Etre, 2006; Arab, 2008). But at high concentrations of alcoholic extract of **ZSC** plant, the complexes formed on mild steel surface become soluble complexes in solution, leading to less coverage of the surface of mild steel sample and to less inhibition efficiency.

### 3.2.2 Electrochemical Study

#### 3.2.2.1 Electrochemical impedance spectroscopy measurements (EIS)

Figures (10 and 11) show electrochemical impedance spectra of mild steel under study at the open circuit potential in 1.0 M  $\text{H}_2\text{SO}_4$  solution containing 10% EtOH at 30°C in the presence of different concentrations of aqueous extract and alcoholic extract of the **ZSC** plant, respectively. It is clear from the figures that the presence of a capacitive loops at the low frequencies accompanied by the spread of diffusion tail at the high concentrations of the extracts especially in aqueous extract. Table (7) gives the electrochemical impedance parameters,  $R_{\text{ct}}$ ,  $n$ ,  $C_{\text{dl}}$  and Inh.% of mild steel sample in 1.0 M  $\text{H}_2\text{SO}_4$  containing 10% EtOH in the absence and the presence of different concentrations of aqueous extract and alcoholic extract of **ZSC** plant, and the results interpreted as:

- The presence of organized capacitive circles in the absence and presence of different concentrations of aqueous and alcoholic extracts of **ZSC** plant indicates that the mechanism of corrosion of mild steel sample is under charge transfer control and the presence of the two extracts of **ZSC** plant did not change the mechanical of corrosion (Metikoš- Hukovi and Babic, 1998; Larabi et.al., 2004; Bentiss et.al., 2005).
- The radii of the capacitive circles increased by increasing the concentration of the two extracts, which means that the increase in charge transfer resistance ( $R_{\text{ct}}$ ), indicating that a thin layer of extract molecules formed and adsorbed on the metal surface, so the increase of the corrosion inhibition for mild steel sample under study will occurred. The increase the electrical double layer capacity ( $C_{\text{dl}}$ ) with increase the concentration of the extracts by adsorption the components of **ZSC** plant on the surface of mild steel sample, which leads to reduced thickness of the charged double layer on the surface of mild steel (Aramaki et.al., 1987) is suggested. It is found that in the case of alcoholic extract, by increasing the concentration increase the value of charge transfer resistance ( $R_{\text{ct}}$ ), until it reaches to 7.0% v/v after this, the increase in the concentration of alcoholic extract lead to decrease in  $R_{\text{ct}}$  value, where this concentration called the *critical concentration*.
- The appearance of diffusion tail in the presence of high concentrations of aqueous extract indicates, the formation of a porous layer from extract components (Chen et. al., 2000) with a degree of protection depends on the porosity of this layer. The pores control in the spread of ions to and from the metal surface, this is expected to be less porosity with increasing concentration of the extract. Figure (12) represents schematic diagram of the porosity layer of inhibitor which cover up the surface of the metal.

To simulate the electrochemical processes that occur at the interface metal / inhibitor layer / electrolyte solution, impedance data processing by software simulation results, where it is found that the type of the proposed circuit depends on the concentration of the extract as follows:

1 - Figure (13a) illustrates a good match between the theoretically calculated values of impedance and recorded laboratory with a relatively low error. Figure (13b) shows equivalent electrical circuit of the system under study, which consists of [ $R_s$  ( $C_{\text{dl}}$   $R_{\text{ct}}$  (QR))] where:

- (A) at concentrations [0.2-10.0]%v/v of the aqueous extracts.
- (B) at all concentrations under study of the alcoholic extract.



2 - Figures (14a) and (14b) show the equivalent electrical circuit, which consists of  $R_s [Q (R_{ct} (C_{dl} R))]$  for the corrosion inhibiting systems at high concentrations [16.0-20.0] %v/v of aqueous extract of **ZSC** plant, where it can be seen from Figure (17b) that the presence of a cell composed of (R and  $C_{dl}$ ) are responsible for the corrosion process called cell corrosion.

### 3.2.2.2 Potentiodynamic polarization measurements (PDP)

Figures (15 and 16) show the cathodic and anodic polarization curves for mild steel corrosion in 1.0 M  $H_2SO_4$  containing 10% EtOH in the absence and the presence of different concentrations of aqueous extract and alcoholic extract of **ZSC** plant at 30°C, respectively. It is noted that the addition of increasing concentrations of the extract accompanied by a parallel shift for each of cathodic and anodic polarization curves towards the areas with low current densities. As shown in Table (8), the values of corrosion potential ( $E_{corr}$ ), corrosion current ( $I_{corr}$ ) and Tafel slopes ( $\beta_c$  and  $\beta_a$ ) for mild steel in absence and presence of different concentrations of the two extracts of **ZSC** plant, the results are interpreted as follows:

- $E_{corr}$  shifted to more negative values and / or less negative in irregular way, this shift in cathodic and anodic curves show that the extracts under study acts as mixed inhibitors to control both the cathodic and anodic reactions.
- The inhibition efficiency (Inh.%) increases (lower rates of corrosion) in the case of aqueous extract of **ZSC** plant with increasing the concentration, it gives the highest percentage of inhibition equal to 64.06% at a concentration 20%v/v, whereas in the case of alcoholic extract the inhibition efficiency increase with increasing the concentration up to 5.0%v/v (critical concentration), where the percentage of inhibition is equal to 87.11% after that the decrease inhibition efficiency occurs with increasing the concentration of alcoholic extract, this means, an increase in corrosion rates, i.e., the inhibition efficiency increase with increasing concentration of the extract to reach the critical concentration and then decreased with the increase of concentration. The decrease in the corrosion rate can explain to the inhibition efficiency of aqueous extract and alcoholic extract of **ZSC** plant on the cathodic part of polarization curves through the reduction of hydrogen ions  $H^+$  and also its effectiveness on the anodic part due to adsorption of the extract components on the surface of mild steel sample which contain a barrier hinders the process of hydrogen gas evolution and metal dissolution (Arab and Emran, 2008).
- Table (8) shows that, Tafel slopes  $\beta_c$  and  $\beta_a$  have values which is almost constant in both extracts (aqueous and alcoholic) do not differ from those observed in uninhibited solution and can be explained by the fact that the component particles of the extracts are adsorbed on the active centers on mild steel surface by simple mechanical block (Abdel-Gaber et.al., 2006). No change in the corrosion mechanism by adding different concentrations of the inhibitor is suggested, this has been found in a previous study (S. Rengamani, 1993).

Tables (9 and 10) illustrate the inhibition efficiencies (Inh.%) for mild steel corrosion in 1.0 M  $H_2SO_4$  containing 10% EtOH in absence and presence of different concentrations of the extracts of **ZSC** plant at 30°C from different techniques. It is clear that simple differences between Inh.% calculated from the chemical and electrochemical methods due to that the chemical measurements give an intermediate average corrosion rates while the electrochemical measurements give an instantaneous corrosion rates (Rengamani et.al., 1993; Arab et. al., 2005). As shown from Table (10) that the highest percentage of inhibition were recorded at a concentration of 5.0%v/v of the alcoholic extract from chemical measurements (HE and ML) and from polarization measurements (PDP) and at concentration 7.0%v/v from impedance measurements (EIS) due to the different methods of measurement.

### 3.3 Adsorption Isotherm

The inhibition process in an acid environment occurs by appropriate adsorption of inhibitor molecules or components of the extract under study at the interface metal / solution and the adsorption process occurs as a result of the existence of electrostatic attraction between:

1. Metal-charged and the particles of charged inhibitor.
2. The polar interaction between uncharged inhibitor molecules with the metal.
3. Interaction of the type  $\pi$  with the metal.
4. All of the above (Schweinsberg et.al., 1988).

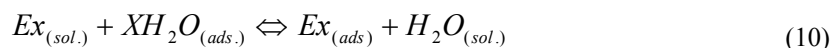
The adsorption process depends on the electronic structure of the inhibitor (molecules of extract), the nature of metal surface, reaction temperature and the number of active centers on the surface (Abdel-Gaber et. al., 2006).

The decrease in corrosion rate of mild steel under study by adding the studied extracts of **ZSC** plant due to the adsorption of components of the extract on the metal surface or to form a protective barrier layer which separate

the surface of the mild steel sample and the center of corrosion (Rengamni et.al., 1994; Muralidharan et. al., 1995). The adsorption process can be described by two main types of interactions: physical adsorption and chemical adsorption, or both, the type of adsorption depends on the nature and charge of the metal, structure of the extract and the type of electrolyte solution (Bentiss et.al., 1999). Figure (17) illustrates the relationship between  $\text{Inh.}\%$  deduced from different methods and the logarithm of the concentration of the studied extracts. The figure shows an adsorption curves with S-shape adsorption isotherm, which indicates that the interaction takes place in one step attributed to the formation of a single layer of extract molecules adsorbed on mild steel surface in the case of aqueous extract. But in the case of alcoholic extract the curve indicated that the adsorption will occur in two steps, because the alcoholic extract contains a large number of active substances are extracted from **ZSC** plant with alcohol that are more than that in the case of aqueous extract, since it is possible that adsorb some small molecules on mild steel surface followed by adsorption of flavonoid compounds and alkaloids of large size. In the case of aqueous extract the waxes, and sugars found in **ZSC** plant will be extracted and these materials would reduce the inhibition effectiveness.

The decrease of inhibition efficiency in the case of alcoholic extract after critical concentration due to the presence of organic compounds in alcoholic extract, which form a fixed complexes and/ or less stable have an oxidative property (Donahue and Nobe, 1967), and it is clear that at low concentrations of the alcoholic extract the inhibition efficiency increase with increasing the concentration of extract which is proposed to be an insoluble complex adsorbed on mild steel surface, leading to more inhibition efficiency with increasing the concentration of the extract under study, this complex lead to block most of the active centers on mild steel surface, thereby increasing the surface coverage. In contrast, at high concentrations of alcoholic extract, the complex formed becomes dissolved in the solution as a result of the accumulation of a large number of molecules, leading to less surface coverage, and reduced the inhibition efficiency (Frignani, 1965).

The assumption that the process of adsorption is the process of replacing between extract molecules and water molecules on the electrode surface is as follows (Bockris, J.O'M. and Swinkels, 1964; Bastidas, 2000):



Where  $Ex_{(sol.)}$  and  $Ex_{(ads.)}$  refer to the extract molecules in solution and extract molecules adsorbed on the metal surface, respectively,  $H_2O_{(ads.)}$  water molecule adsorb on the metal surface and  $X$  is the number of water molecules which replaced by one molecule of the extract. For more information on the electrochemical mechanical interaction is essential to select an appropriate adsorption isotherm. The application of the results obtained it give a straight line as shown in figures (18) and (19) and by applying the following relation (Langmuir) (Tsure et.al., 1978; . Oguzie et.al., 2004):

$$\Theta = KC_{inh} / (1 + KC_{inh.}) \quad (11)$$

$$C_{inh.} \Theta^{-1} = \frac{1}{K_{ads}} + C_{inh.} \quad (12)$$

where  $C$  represents the concentration of extract,  $\Theta$  degree of surface coverage and  $K_{ads}$  equilibrium constant of adsorption which related to free energy of adsorption by the following equation (Rengamni et.al., 1994; Muralidharan et.al., 1995; Bockris and Swinkels, 1994; Bastidas, 2000):

$$K_{ads.} = \frac{1}{C_{H_2O}} \exp(-\Delta G_{ads.} / RT) \quad (13)$$

Where  $C_{H_2O}$  is the molar concentration of water molecules at the interface between the electrode surface and the solution and the energy in this case known as the standard free energy  $\Delta G_{ads.}^\circ$ ,  $R$  universal gas constant is equal to  $8.314 \text{ J.mol}^{-1}$  and  $T$  temperature in Kelvin.

Tables (11 and 12) represent the results derived from the application of Langmuir relationship  $C_{inh} \Theta^{-1}$  Vs.  $C_{inh.}$

where the adsorption parameters are recorded for the studied extracts of **ZSC** plant from different techniques. The results applied give linear correlation coefficients close to one which confirms that the adsorption of the

extracts components on the surface of mild steel sample under study is the basic step in the process of inhibition, the negative value of  $\Delta G_{ads}^{\circ}$  indicates that the adsorption process of inhibitor molecules on mild steel surface is spontaneous.

By examining the chemical composition of *Zizyphus Spina-Charisti* plant, Table (1) shows that the extracts of this plant (aqueous and / or alcoholic) contain both alpha - Trbinol, alkaloids, flavonoids, Bepta alkaloid and glycosides. In view of these components it is clear that the majority of organic compounds containing oxygen or nitrogen atoms and all have pairs of free electrons, so these compounds will be able to adsorb on mild steel surface through the free electrons on the oxygen atom and / or nitrogen atom. The occurrence of the adsorption of the compounds in the extracts on mild steel surface constitutes the barrier for mass and charge transfer, leading to reduced interaction between the sample with central corrosion and thus decrease the corrosion rate, moreover, these compounds may be form complexes with ions of iron (mild steel), causing the covering (lock) of anodic sites (microanodes) and/or cathodic sites (micocathodes) generated on the mild steel surface under conditions of corrosion and lead to disability soluble of iron.

#### 4. Conclusion

The following main conclusions are drawn from the present study:

- The corrosion rate of mild steel increases with increasing  $H_2SO_4$  acid concentration (0.25-1.5)M showing first order corrosion reaction without changing the reaction mechanism.
- The concentration of extract increased the rate of steel corrosion is decreased, which indicates that the inhibition of the corrosion process is produced.
- Electrochemical impedance spectroscopy results showed that the corrosion and corrosion inhibition of steel occurred mainly by charge transfer.
- The electrochemical results of polarization also showed that the extracts of *zizyphus Spina-Christi* act as mixed type inhibitors, they retarded both cathodic and anodic reaction.
- The experimental results from chemical and electrochemical studies were fit Langmuir adsorption isotherm.
- Value of the standard free energy of adsorption  $\Delta G_{ads}^{\circ}$ , for the extracts have negative sign which indicates that the adsorption process of inhibitor molecules on mild steel surface is spontaneous.

#### References

- Abdallah, M. (2004). *Portug. Electrochimica Acta*, 22, 161.
- Abdel-Gaber, A.M., Abd-El-Nabey, B.A., Sidahmed, I. M., El-Zayady, A. M. and Saadawy. (2006). *Corros. Sci.*, 48, 2765-2779.
- Adzu, B., Amos, S., Wambebe, C. and Gamaniel, K. (2001). *Fitoterapia.*, 4, 344-350.
- Anaouda, L., Sathiyathan, R.A., Maruthamuthu, S.B., Selvanayagam, M.C., Mohanan, S.B. and Palaniswamy, N.B. (2005). *Indian J. Chem. Tech.*, 12, 356.
- Arab, S. T., Al-Turkustani, A. M. and Al-Nami, S. Y. (2005). *Mater. Sci. Res. Ind.*, 3, 99-110.
- Arab, S.T., Al-Turkustani, A. M. and Al- Dhahiri, R. H. (2008). *J. Kore. Chem. Soc.*, 52, 281-294.
- Arab, S. T. and Emran, K. M. (2008). *Mater. Lett.*, 62, 1022- 1032.
- Aramaki K., Hagiwara M. and Nishihara, H. (1987). *Corros. Sci.*, 27, 487-497.
- Ashassi- Sorkhabi, H. and Seifzadeh, D. (2006). *Int. J. Electrochem. Sci.*, 1, 92-98.
- Ashassi-Sorkhabi, H., Shaabani, B., Aligholipour, B. and Seifzadeh, D. (2006). *Appl. Surf. Sci.*, 252, 4039.
- Ateya, B.G., Anadouli, B.E. and El-Nizamy, F.M. (1981). *Bull. Chem. Soc.*, Japan, 54, 3157.
- Bastidas, J. J. Polo, E. Cano and G. Torres, (2000). *J. Mater. Sci.*, 35, 2637- 2642.
- Beccaria, A. M. and Poggi, G. (1986). *J. Br. Corros.*, 42, 470.
- Bendahou, M.A., Benadallah, M.B.E. and Hammouti, B.B. (2006). *Pigment and Resin Technol*, 35, 95.
- Bentiss, F., Lagrenee, M., Traisnel, M., J.C. Hornez. (1999). *Corrosion Science*, 41, 789.
- Bentiss, F., Lagrenee, M., Traisnel, M., Mernari, B. and Elattari, H. (1999). *J. App. Electrochem.*, 29,

1073-1078.

Bentiss, F., Lebrini, M. and Lagrene, M. (2005). *Corros. Sci.*, 47, 2915- 2931.

Bockris, J.O'M. and Swinkels, J.O'M. (1964). *J.Electrochem. Soc.*, 111, 736-743.

Bouyanzer, A. and Hammouti, B. (2004). *Pigment and Resin Technol*, 33, 287.

Bouyanzer, A. and Hammouti, B. (2004). *Pigment and Resin Tech*, 33, 287.

Chen Y., Hong T., Gopal, M. and Jepson, W. P. (2000). *Corros. Sci.*, 42, 979- 990.

Chetounani, A. , Hammouti, B. and Benkaddour, M. (2004). *Pigment and Resin Technol*, 33, 26.

Donahue, M. F. and Nobe, K. (1967). *J. Electrochem. Soc.*, 114, 1012.

Dweek, A. C. (2005). *FLS FRESC FRESH*- Technical Editor.

Ebenso, E.E., Ibok, U.J., Ekpe, U.J., Umoren, S., Ekerete, J., Abiola, O.K., Oforka, N.C. and Martinez,S. (2004). *Trans. SAEST*, 39, 117.

Ebenso, E.E., Eddy, N.O. and Odiongenyi, A.O. (2008). *Afri. J. Pure and Appl. Chem.*, 2, 107.

Ebenso, E.E., Eddy, N.O. and Odiongenyi, A.O. (2009). *Portug. Electrochimica Acta*, 27(1), 13.

\*Eddy, N.O., Ekwumemgbo, P. and Odoemelam, S.A. (2008). *Inter. Journal Physical Sciences*, 3, 1.

\*\*Eddy N.O., Odoemelam, S.A. and Akpanudoh, N.W. (2008). *J. Chem. Technol.*, 4, 1.

\*\*\*Eddy, N.O., Odoemelam, S.A. and Odiongenyi, A.O. (2008). *J. Appl. Electrochem*, DOI 10.1007/s10800-008-9731.

\*\*\*\*Eddy, N.O. (2008). *Inhibition of corrosion of mild steel by some antibiotics*, Ph.D. Thesis, University of Calabar.

Eddy, N.O. and Ebenso, African, E.E. (2008). *J. Pure Appl. Chem.*, 2(6), 1.

Eddy, N.O. and Odoemelam, S.A. (2009). *Pigment and Resin Technol*, 38(2), 111.

El-Etre, A.Y. (2003). *Corros. Sci.*, 45, 2485.

El-Etre, A.Y., Abdallah, M. and El-Tantawy, Z.E. (2005). *Corros. Sci.*, 47, 385.

El-Etre, A. Y. (2006). *Appl. Surf. Sci.*, 252, 8521-8525.

Frignani, A., Trabaneli, G., Zucchi, F. and Zucchini, M. (1975). *Proceeding of the 4<sup>th</sup> Eur. Sym. on Corros. Inh.* Univ. Ferrara, Italy, 3, 652.

Hosseini, M., Mertens, S. F. L. and Arshadi, M. R. (2003). *Corros. Sci.*, 45, 1473- 1489.

Kendig M. W., Allen, A. T., Jeanjaquet, S. and Mansfeld, F. (1986). *In Electrochemical Techniques for Corrosion Engineering*, Ed. R. Badoian, NACE.

Khaled, K.F. (2003). *Electrochimica Acta*, 48, 2493.

Larabi, L. and Harek, Portug, Y. (2004). *Electrochiem. Acta*, 22, 227-247.

Mahran, G.E.D.H., Glombitza, K.W., Mirhom, Harmann, Y.W., R. and Michel, C.G. (1996). *Plant Medica.*, 62 163- 165.

Mcdonald, J. R. (1987). *Impedance Spectroscopy*, John Wiley & Sons, New York. 37.

Metikos- Hukovic, M., Babic, R., Grubac, Z. and Brinic, S. (1994). *J.Appl. Electrochem.*, 24, 772- 778.

Metikoš- Hukovi, M., and Babic, R. (1998). *J. Appl. Electrochem.*, 28, 433- 439.

Muralidharan, S., Quraishi, M. A. and Iyer, S. V. K. (1993). *J. Portug. Electrochem. Acta.*, 11, 255.

Muralidharan, S., Phani, K. L.N., Pitchumani, S., Ravichandran, S. and Iyer, S.V. K. (1995). *J. Electrochem. Soc.*, 142 1478- 1483.

Murthy, K. S. and Dwarakadasa, E. S. (1995). *J.Br. Corros.*, 30, 111-115.

Mylius, F. and Niethen, S. (1957). *J. Amer. Chem. Soc.*, 79, 1966.

Odiongenyi, A. O., Odoemelam, S. A. and Eddy, N. O. (2009). *Portug.Electrochimica Acta*, 27 (1), 33.

Odoemelam, S.A. and Eddy, N.O. (2008). *J. Surface Sci. Technol*, 24, 1.

- Oguzie, E. E., Okolue, B.N., Ebenso, E.E., Onuoha, G.N. and Onuchukwu, A. I. (2004). *Mater. Chem. Phys.*, 87, 394-401.
- Oguzie, E. E. (2005). *Pigment & Resin Technology*, 34, 321-326.
- Orubite, K. O. and Oforka, N. C. (2004). *Mater.Lett.*, 58, 1768-1772.
- Ramesh, S., Rajeswari, S. and Maruthamuthu, S. (2003). *Materials Letters*, 57, 4547.
- Rengamani, S., Vasudevan, T. and Iyer, J. (1993). *Indian, J. Technol.*, 31, 519.
- Rengamni, S., Muralidharan, S.K., Ulandainalhan, M. and Iyer, S. V. K. (1994). *J. Appl. Electrochem.*, 24, 355-360.
- Schweinsberg, D., George, G., Nanayakkawa, A. and Steinert, D. (1988). *Corros. Sci.*, 28, 33- 42.
- Tsure, T., Haruyama, S. and Gijutsu, B. J. (1978). *Japan, Soc. Corros. Eng.*, 27, 573.
- Uhlig, H. H. (1971). *Corrosion and Corrosion Control*, 2<sup>nd</sup> Edn., John Wiley and Sons Inc.
- Vasanth, K.L. NACE. *National Association of Corrosion Engineers*, Paper# 233, Corrosion 96.
- Zaafarany, I. (2009). *Por. Electrochemica Acta*, 27(5), 631-643.

Table 1. The chemical composition of some of the most important components of *Zizyphus Spina-Christi* (**ZSP**) plant

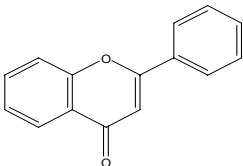
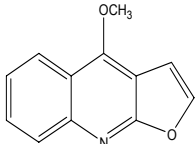
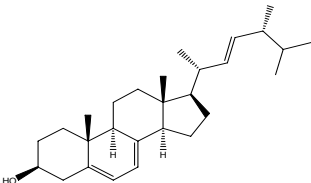
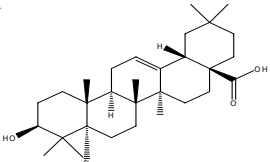
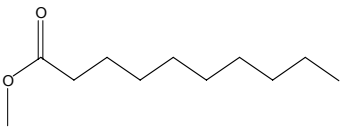
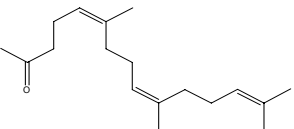
flavonoids 	alkaloids 
styrol 	olenwic acid 
Methyl palmetat 	pharnecylacetone C 

Table 2. Corrosion rates of mild steel (R, R') in different concentrations of H<sub>2</sub>SO<sub>4</sub>+10% EtOH at 30° C

$C_{H_2SO_4}$ (M)	0.25	0.5	1.0	1.5
$R \times 10^2$ (ml.cm <sup>-2</sup> .min. <sup>-1</sup> )	0.9596	2.3743	3.7037	5.1886
$R' \times 10^5$ (g.cm <sup>-2</sup> .min. <sup>-1</sup> )	1.9865	4.5607	7.2565	11.112

Table 3. Electrochemical parameters obtained from impedance measurements for mild steel corrosion in different concentrations of  $H_2SO_4$  +10% EtOH at 30° C

$C_{H_2SO_4}$ (M)	$R_{sol.}$ ( $\Omega.cm.^{-2}$ )	$C_{dl}$ ( $\mu F.cm.^{-2}$ )	$R_{ct}$ ( $\Omega.cm.^{-2}$ )	$Q$ ( $\Omega.^{-1}cm.^{-2} s.^n$ )	$n$
0.25	2.955	73.08	10.69	$6.796 \times 10^{-4}$	0.659
0.50	3.084	132.7	6.190	$7.228 \times 10^{-3}$	0.720
1.00	1.007	163.6	4.521	$2.358 \times 10^{-3}$	0.948
1.50	1.296	231.4	2.729	$4.542 \times 10^{-4}$	0.863

Table 4. Polarization parameters for mild steel corrosion in different concentrations of  $H_2SO_4$ \_10% EtOH at 30° C

$C_{H_2SO_4}$ (M)	$-E_{corr}$ (V)	$I_{corr.}$ (mA.cm. <sup>-2</sup> )	$\theta_a$ (mV.dec. <sup>-1</sup> )	$-\theta_c$ (mV.dec. <sup>-1</sup> )
0.25	0.512	3.629	54.63	69.20
0.50	0.489	5.369	73.55	109.9
1.00	0.450	15.17	40.10	86.80
1.50	0.446	17.21	71.43	146.8

Table 5. Corrosion rates and inhibition efficiency for mild steel sample in 1.0 M  $H_2SO_4$ + 10% EtOH in the presence of different concentrations of aqueous extract ZSC plant at 30° C

$C_{Ex}$ (V/V%)	Corrosion Rate		Inhibition Efficiency	
	$R_{HEM} \times 10^2$ (ml. cm. <sup>-2</sup> min. <sup>-1</sup> )	$R'_{MLM} \times 10^5$ (g. cm. <sup>-2</sup> min. <sup>-1</sup> )	Inh. <sub>HEM</sub> %	Inh. <sub>MLM</sub> %
0.0	3.704	7.256	-	-
0.2	2.783	5.633	24.85	22.36
0.5	2.337	4.709	36.90	35.10
1.0	1.759	3.656	52.51	50.86
2.0	1.342	2.664	63.76	63.28
5.0	1.318	2.445	64.40	66.29
10.0	0.574	1.304	84.49	82.02
16.0	0.457	0.766	87.64	89.44
20.0	0.273	0.635	92.62	91.24

Table 6. Corrosion rates and inhibition efficiency for mild steel sample 1.0 M H<sub>2</sub>SO<sub>4</sub> + 10% EtOH in the presence of different concentrations of alcoholic extract of ZSC plant at 30° C

$C_{Ex}$ (V/V%)	Corrosion Rate		Inhibition Efficiency	
	$R_{HEM} \times 10^2$ (ml. cm. <sup>-2</sup> min. <sup>-1</sup> )	$R'_{MLM} \times 10^5$ (g. cm. <sup>-2</sup> min. <sup>-1</sup> )	Inh. <sub>HEM</sub> %	Inh. <sub>MLM</sub> %
0.0	3.704	7.256	-	-
0.2	1.706	3.438	53.94	52.62
0.5	0.855	1.700	76.90	76.56
1.0	0.692	1.235	81.29	82.99
2.0	0.517	0.902	86.03	87.55
5.0	0.267	0.357	92.78	95.07
7.0	0.308	0.606	91.67	91.46
10.0	0.360	0.712	90.25	90.18

Table 7. Electrochemical impedance parameters for the corrosion of mild steel sample in of 1.0 M H<sub>2</sub>SO<sub>4</sub> +10% EtOH in the absence and presence of different concentrations of aqueous extract (A) and alcoholic extract (B) of ZSC plant at 30° C

Extract (A)	$C_{Ex}$ (V/V%)	$R_{sol.}$ ( $\Omega$ .cm. <sup>-2</sup> )	$C_{dl}$ ( $\mu$ F.cm. <sup>-2</sup> )	$R_{ct}$ ( $\Omega$ .cm <sup>2</sup> )	$Q$ ( $\Omega^{-1}$ cm. <sup>-2</sup> s <sup>n</sup> )	$n$	Inh. % ( $R_{ct}^{-1}$ )
	0.0	1.007	163.6	4.521	$2.358 \times 10^{-3}$	0.948	-
	0.2	1.460	102.5	6.555	$2.287 \times 10^{-3}$	0.875	31.02
	0.5	1.232	96.26	8.566	$1.444 \times 10^{-5}$	0.948	47.22
	1.0	1.274	89.80	9.743	$1.228 \times 10^{-4}$	1.000	53.59
	2.0	1.311	85.43	10.37	$8.168 \times 10^{-4}$	0.974	56.40
	5.0	1.680	75.24	11.68	$2.114 \times 10^{-3}$	0.820	61.29
	10.0	1.542	60.27	14.71	$1.145 \times 10^{-4}$	0.821	69.26
	16.0	0.442	47.87	19.25	$4.179 \times 10^{-3}$	0.221	76.51
	20.0	0.824	46.68	23.20	$7.472 \times 10^{-3}$	0.800	80.51
Extract (B)	0.2	1.826	109.8	11.07	$4.096 \times 10^{-4}$	0.798	59.15
	0.5	1.611	52.04	18.83	$1.910 \times 10^{-4}$	0.835	75.99
	1.0	1.944	48.66	27.78	$1.911 \times 10^{-3}$	0.800	83.72
	2.0	2.207	43.67	32.39	$2.263 \times 10^{-5}$	0.790	86.04
	5.0	2.495	40.11	35.31	$2.840 \times 10^{-5}$	0.738	87.19
	7.0	2.833	32.64	59.79	$3.008 \times 10^{-4}$	0.665	92.43
	10.0	2.294	36.68	48.64	$1.852 \times 10^{-4}$	0.804	90.70

Table 8. Potentiodynamic polarization parameters for the corrosion of mild steel sample in of 1.0 M H<sub>2</sub>SO<sub>4</sub> +10% EtOH in the absence and presence of different concentrations of aqueous extract (A) and alcoholic extract (B) of **ZSC** plant at 30° C

Extract (A)	$C_{Ex}$ (V/V%)	$-E_{corr.}$ (v)	$I_{corr.}$ (mA.cm. <sup>-2</sup> )	$\beta_a$ (mV.dec. <sup>-1</sup> )	$-\beta_c$ (mV.dec. <sup>-1</sup> )	Inh. %
	0.0	0.450	15.17	40.10	86.80	-
	0.2	0.455	10.90	47.36	84.40	28.17
	0.5	0.451	9.40	41.82	84.60	38.05
	1.0	0.444	8.39	49.43	89.34	44.71
	2.0	0.443	7.87	44.73	97.74	48.13
	5.0	0.450	6.96	45.19	96.68	54.13
	10.0	0.447	6.90	40.05	80.49	54.53
	16.0	0.453	5.52	48.26	89.88	63.57
	20.0	0.457	5.45	41.57	80.05	64.06
Extract (B)	0.2	0.450	7.095	50.75	87.06	53.24
	0.5	0.459	6.980	43.14	81.53	54.00
	1.0	0.461	4.881	44.73	80.99	67.83
	2.0	0.456	3.622	46.64	88.63	76.14
	5.0	0.455	1.955	50.62	80.95	87.11
	7.0	0.463	3.041	49.18	80.65	79.96
	10.0	0.452	3.236	45.27	92.35	78.67

Table 9. The inhibition efficiencies for mild steel corrosion in 1.0 M H<sub>2</sub>SO<sub>4</sub> +10%EtOH in presence of different concentrations of aqueous extract of **ZSC** plant from different measurements at 30° C

$C_{Ex}$ (V/V%)	Inhibition Efficiency			
	HEM	MLM	EIS	PDP
0.0	-	-	-	-
0.2	24.85	22.36	31.02	28.17
0.5	36.90	35.10	47.22	38.05
1.0	52.51	50.86	53.59	44.71
2.0	63.76	63.28	56.40	48.13
5.0	64.40	66.29	61.29	54.13
10.0	84.49	82.02	69.26	54.53
16.0	87.64	89.44	76.51	63.57
20.0	92.62	91.24	80.51	64.06



Table 10. The inhibition efficiencies for mild steel corrosion in 1.0 M  $\text{H}_2\text{SO}_4$  +10%EtOH in presence of different concentrations of alcoholic extract of **ZSC** plant from different measurements at 30°C

$C_{Ex}$ (V/V%)	Inhibition Efficiency			
	HEM	MLM	EIS	PDP
0.0	-	-	-	-
0.2	24.85	22.36	31.02	28.17
0.5	36.90	35.10	47.22	38.05
1.0	52.51	50.86	53.59	44.71
2.0	63.76	63.28	56.40	48.13
5.0	64.40	66.29	61.29	54.13
10.0	84.49	82.02	69.26	54.53
16.0	87.64	89.44	76.51	63.57
20.0	92.62	91.24	80.51	64.06

Table 11. Linear correlation coefficients and adsorption parameters for Langmuir relationship for aqueous extract of **ZSC** plant on mild steel in 1.0 M  $\text{H}_2\text{SO}_4$  + 10% EtOH at 30°C

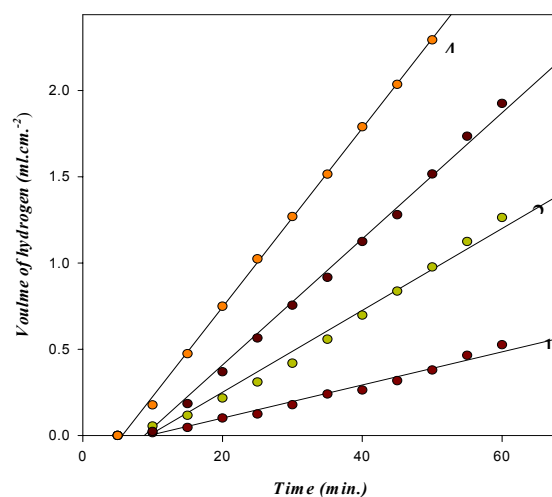
Techniques	Slope	Correlation Coefficient	$K_{ads}$ ( $M^{-1}$ )	$-AG_{ads}^{\circ}$ ( $kJ\ mol^{-1}$ )
HEM	1.06	0.992	1.099	10.37
MLM	1.07	0.994	1.074	10.29
EIS	1.25	0.993	1.275	10.37
PDP	1.55	0.994	1.246	10.67

Table 12. Linear correlation coefficients and adsorption parameters for Langmuir relationship for alcoholic extract of **ZSC** plant on mild steel in 1.0 M  $\text{H}_2\text{SO}_4$  + 10% EtOH at 30°C

Techniques	Slope	Correlation Coefficient	$K_{ads}$ ( $M^{-1}$ )	$-AG_{ads}^{\circ}$ ( $kJ\ mol^{-1}$ )
HEM	1.08	0.999	8.936	15.63
MLM	1.08	0.999	11.26	16.22
EIS	1.08	0.999	7.530	15.20
PDP	1.23	0.996	7.412	15.16



Figure 1. *Zizyphus Spina-Christi* (**ZSP**) plant



(1) 0.25M, (2) 0.5M, (3) 1.0M, (4) 1.5M

Figure 2. Variation of hydrogen/ time curves for mild steel corrosion in different concentrations of  $\text{H}_2\text{SO}_4$  +10%EtOH at  $30^\circ\text{C}$

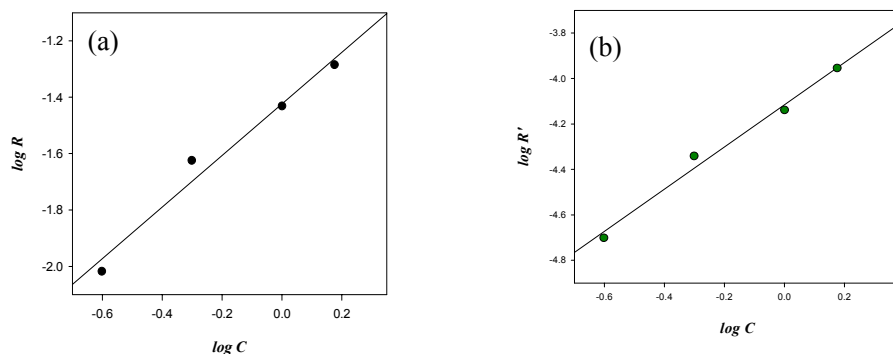
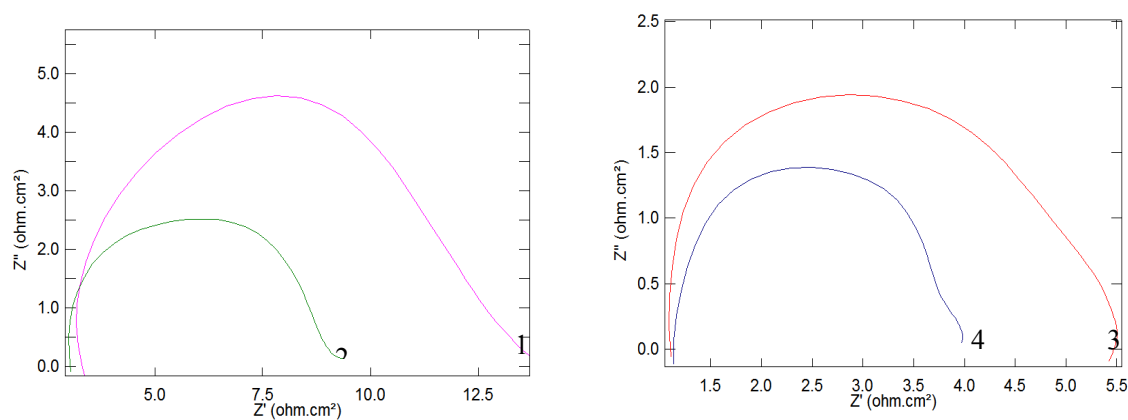


Figure 3. The relation between (a)  $\log R$  and/ or (b)  $\log R'$  for mild steel and  $\log C$  of  $\text{H}_2\text{SO}_4$  + 10% EtOH at  $30^\circ\text{C}$



(1) 0.25M, (2) 0.5M, (3) 1.0M, (4) 1.5M

Figure 4. Nyquist plots for mild steel corrosion in different concentrations of  $\text{H}_2\text{SO}_4$  +10% EtOH at  $30^\circ\text{C}$

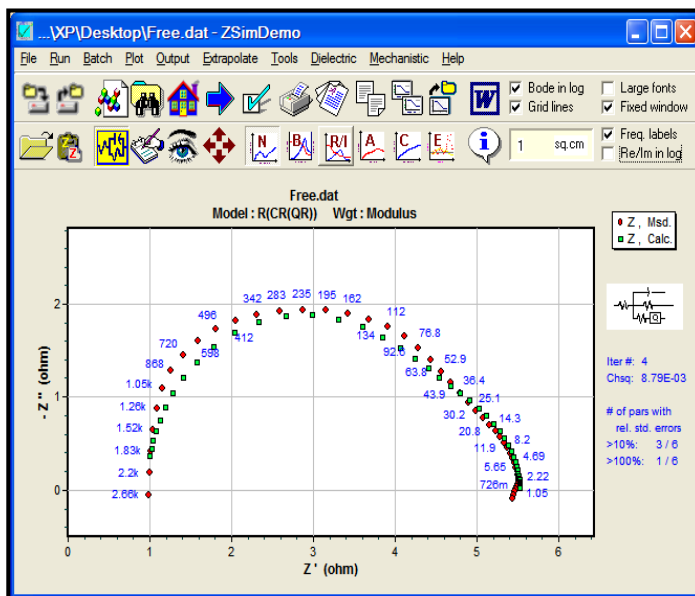


Figure 5a. Simulation of the suggested circuit of EIS for mild steel corrosion in different concentrations of  $\text{H}_2\text{SO}_4$  + 10% EtOH at  $30^\circ\text{C}$

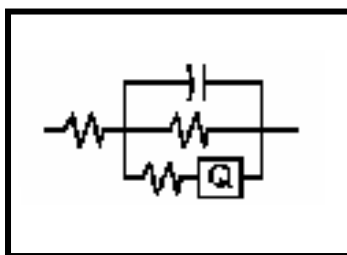
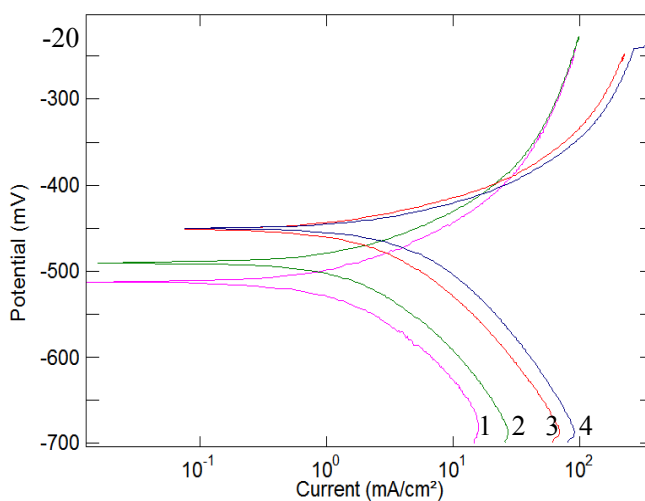


Figure 5b. The equivalent circuit for mild steel corrosion in different Concentrations of  $\text{H}_2\text{SO}_4$ +10%EtOH at  $30^\circ\text{C}$



(1) 0.25M, (2) 0.5M, (3) 1.0M, (4) 1.5M

Figure 6. Polarization curves for mild steel corrosion in different Concentrations of  $\text{H}_2\text{SO}_4$ +10%EtOH at  $30^\circ\text{C}$

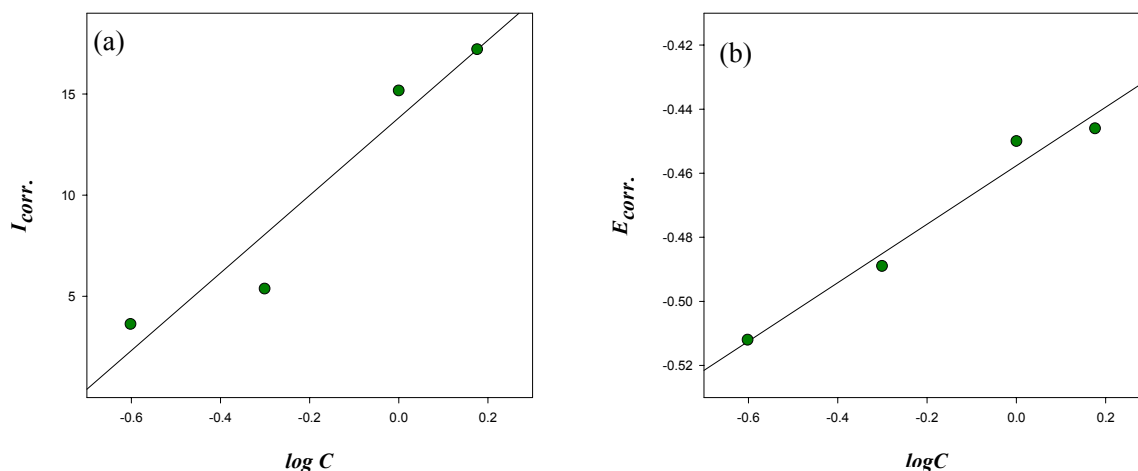
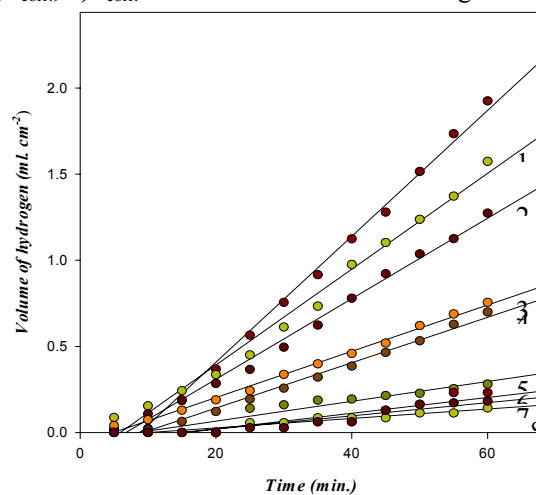
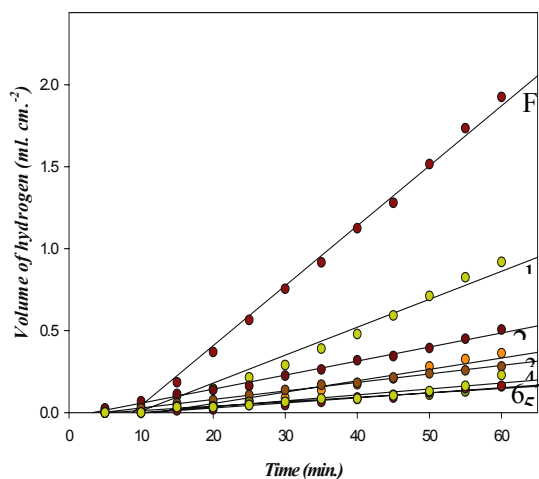


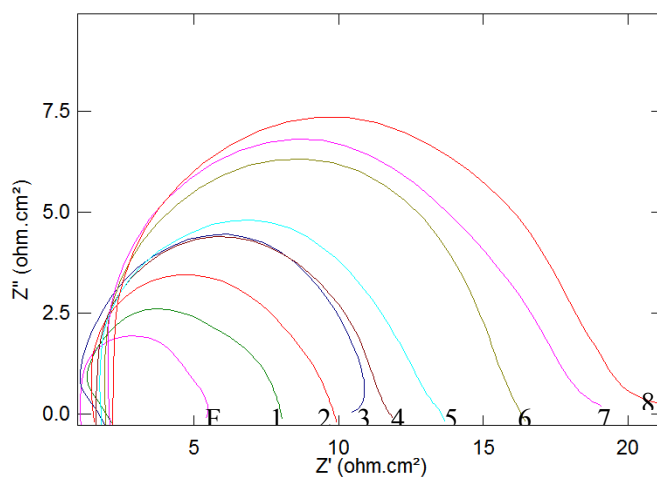
Figure 7. The relation a)  $I_{corr.}$ , b)  $E_{corr.}$  for mild steel corrosion Vs.  $\log C$  of  $H_2SO_4 + 10\% EtOH$  at  $30^\circ C$



[(F) Free, (1) 0.2, (2) 0.5, (3) 1.0, (4) 2.0, (5) 5.0, (6) 10.0, (7) 16.0, and (8) 20.0] % v/v  
Figure 8. Variation of hydrogen/ time curves for mild steel corrosion in different concentrations of  $H_2SO_4 + 10\% EtOH$  in presence of aqueous extract of **ZSC** plant at  $30^\circ C$

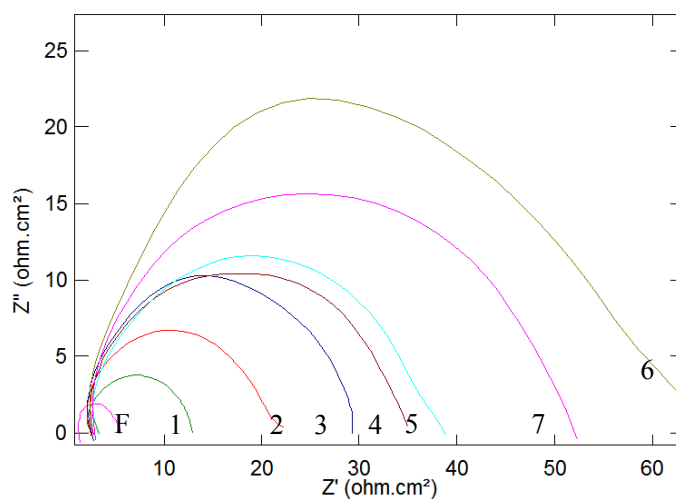


[(F) Free, (1) 0.2, (2) 0.5, (3) 1.0, (4) 2.0, (5) 5.0, (6) 7.0 and (7) 10.0] % v/v  
Figure 9. Variation of hydrogen/ time curves for mild steel corrosion in different concentrations of  $H_2SO_4 + 10\% EtOH$  in presence of alcoholic extract of **ZSC** plant at  $30^\circ C$



[(F) Free, (1)0.2, (2) 0.5, (3) 1.0, (4)2.0, (5)5.0, (6)10.0, (7)16.0 and (8) 20.0]% v/v

Figure 10. Nyquist plots of the corrosion of mild steel sample 1.0 M  $\text{H}_2\text{SO}_4$  10% EtOH in the presence of different concentrations of aqueous extract of **ZSC** plant at 30° C



[(F) Free, (1)0.2, (2)0.5, (3) 1.0, (4)2.0, (5)5.0, (6) 7.0 and (7) 10.0]% v/v

Figure 11. Nyquist plots of the corrosion of mild steel sample 1.0 M  $\text{H}_2\text{SO}_4$ +10% EtOH in the presence of different concentrations of alcoholic extract of **ZSC** plant at 30° C

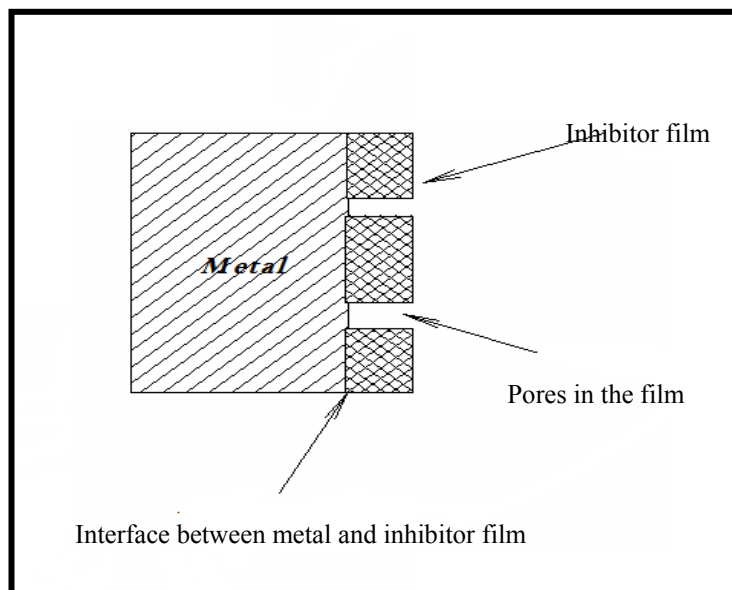


Figure 12. Graphic shows the components of the inhibitor porous layer formed on the surface of the metal.

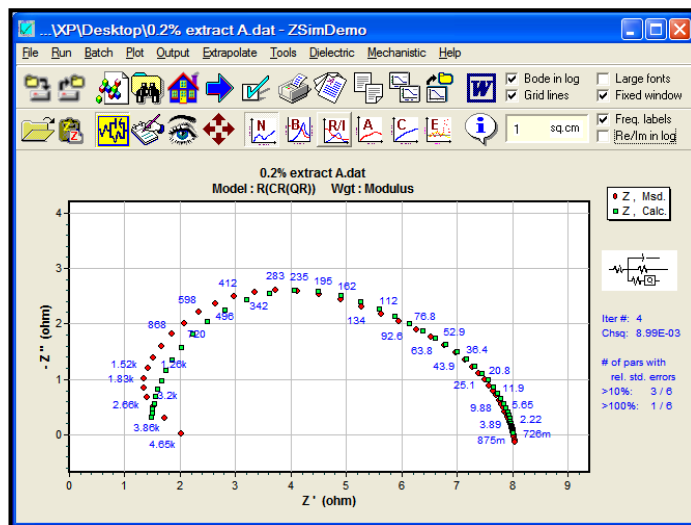


Figure 13a. Simulation of the suggested circuit for EIS for mild steel corrosion in 1.0 M  $\text{H}_2\text{SO}_4$  +10%EtOH in presence of different concentrations in the range [0.2-10.0]%v/v of aqueous extract and at all concentrations of alcoholic extract of ZSC plant at 30°C

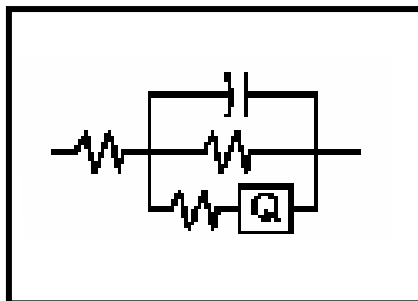


Figure 13b. The equivalent circuit for mild steel corrosion in 1.0M  $\text{H}_2\text{SO}_4$  +10%EtOH in presence of different concentrations in the range [0.2-10.0]%v/v of aqueous extract and at all concentrations of alcoholic extract of ZSC plant at 30°C

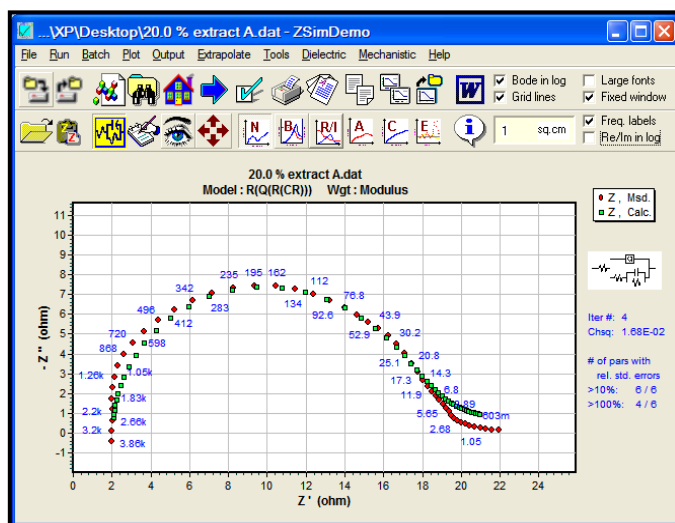


Figure 14a. Simulation of the suggested circuit for EIS for mild steel corrosion in 1.0M  $\text{H}_2\text{SO}_4$  +10%EtOH in presence of high concentrations in the range [16.0-20.0]%v/v of aqueous extract of **ZSC** plant at 30°C

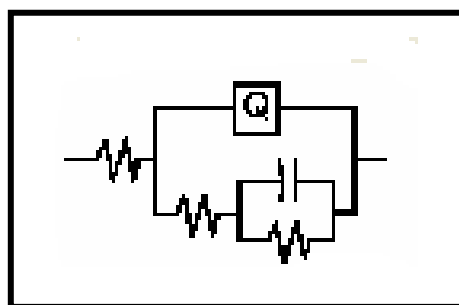
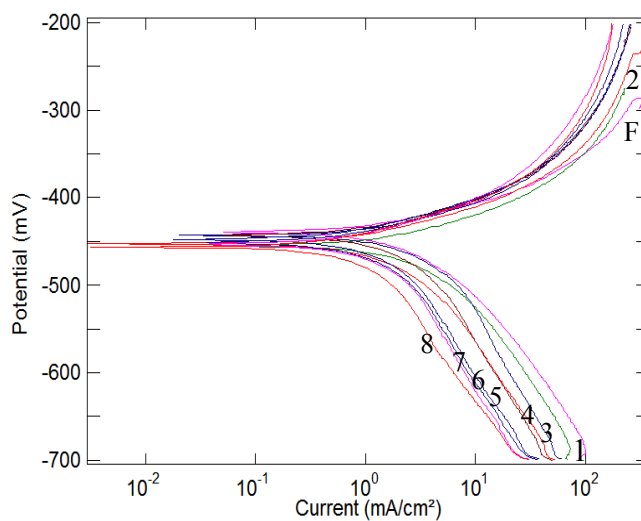
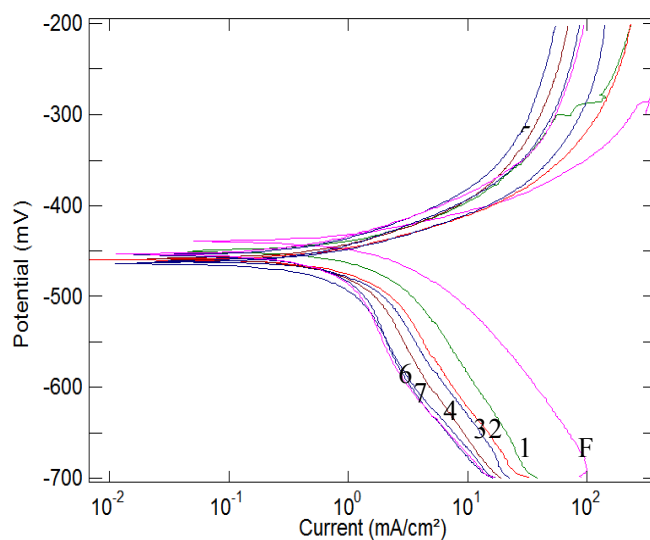


Figure 14b. The equivalent circuit for mild steel corrosion in 1.0 M  $\text{H}_2\text{SO}_4$  +10%EtOH in presence of high concentrations in the range [16.0-20.0]%v/v of aqueous extract of **ZSC** plant at 30°C



[(F) Free, (1)0.2, (2)0.5, (3)1.0, (4)2.0, (5)5.0, (6)10.0, (7)16.0 and (8)20.0]% v/v

Figure 15. Polarization curves for mild steel corrosion in 1.0 M  $\text{H}_2\text{SO}_4$  + 10%EtOH in presence of different concentrations of aqueous extract of **ZSC** plant at 30°C



[(F) Free, (1)0.2, (2)0.5, (3) 1.0, (4)2.0, (5)5.0, (6)7.0 and (7)10.0]% v/v

Figure 16. Polarization curves for mild steel corrosion in 1.0 M  $\text{H}_2\text{SO}_4$  + 10%EtOH in presence of different concentrations of alcoholic extract of **ZSC** plant at 30°C

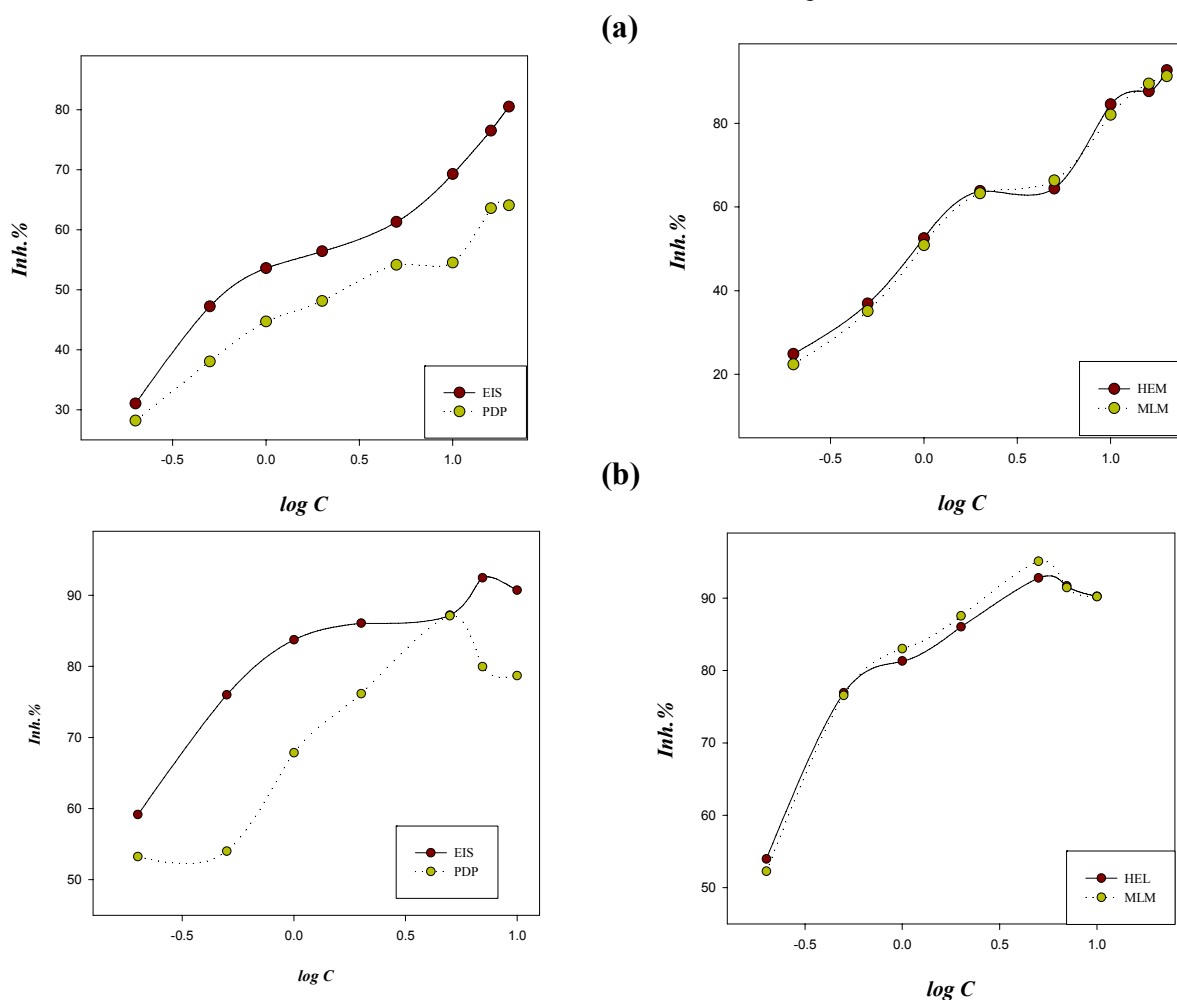


Figure 17. The relation between Inh.% from different methods and log C for mild steel corrosion in 1.0M  $\text{H}_2\text{SO}_4$  + 10%EtOH in presence different concentrations of (a) aqueous extract and (b) alcoholic extract of **ZSC** plant at 30°C



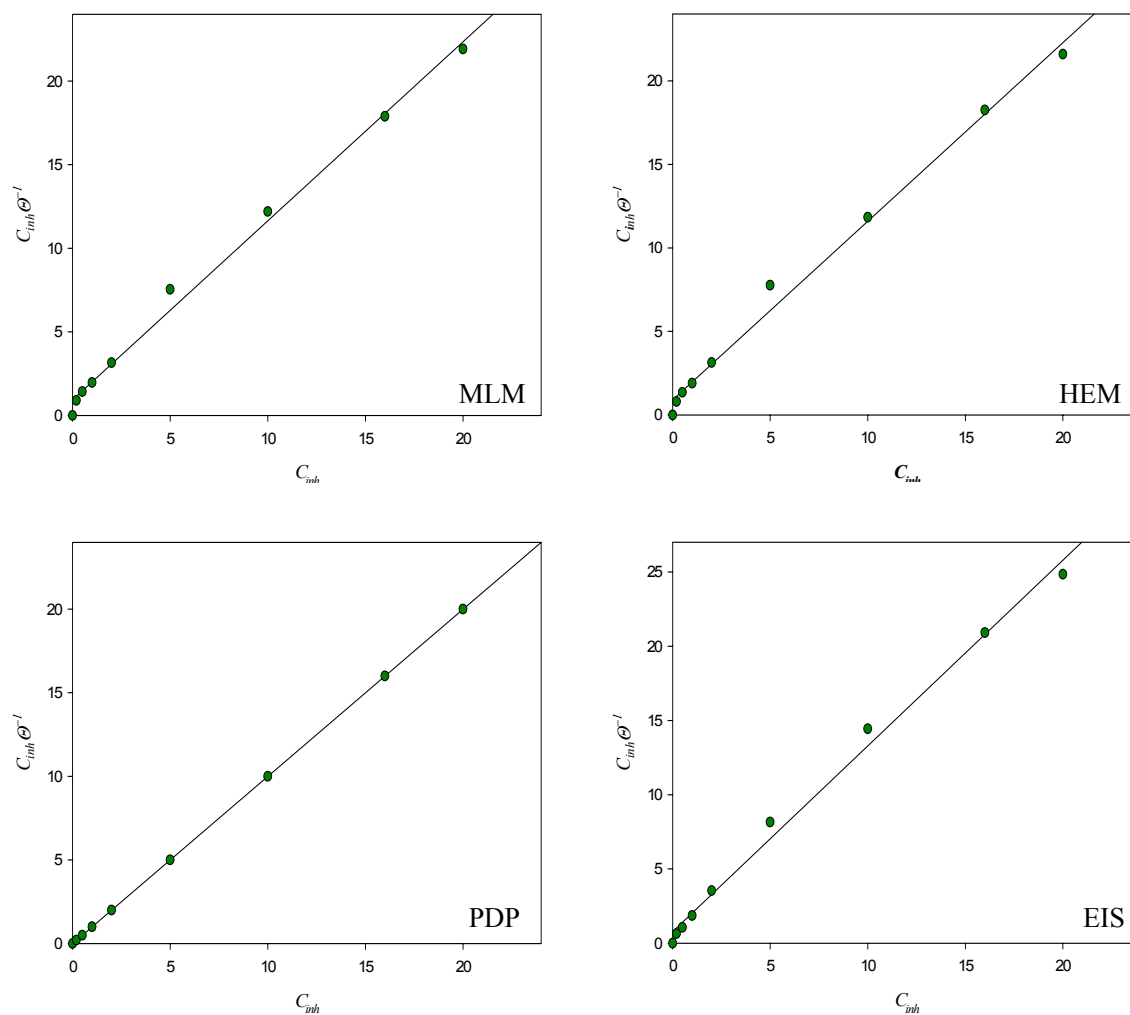


Figure 18. Langmuir relationship for the adsorption of aqueous extract components of **ZSC** on mild steel surface in 1.0 M  $H_2SO_4$  +10%EtOH at 30°C from different methods

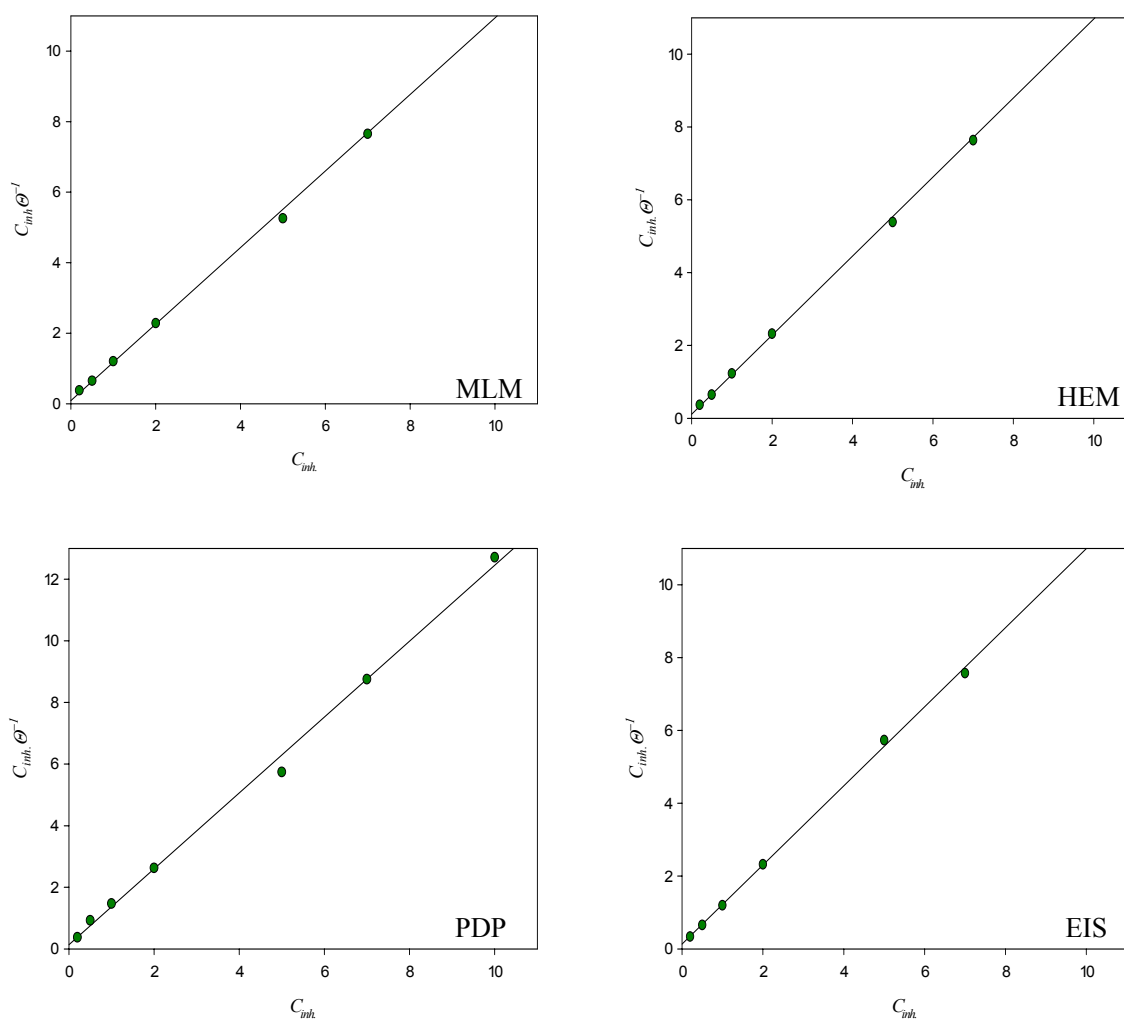


Figure 19. Langmuir relationship for the adsorption of alcoholic extract components of **ZSC** on mild steel surface in 1.0 M  $H_2SO_4$  +10%EtOH at 30°C from different methods

# Kinetic Studies on Lipase-catalyzed Transesterification of Phosphatidylcholine with $\alpha$ -linolenic Acid Ethyl Ester

Junmin Du (Corresponding author)

State Key Laboratory of Coal Conversion

Institute of Coal Chemistry Chinese Academy Sciences, Taiyuan, China

&

Graduate University of the Chinese Academy of Sciences, Beijing, China

Tel: 83-351-408-4708 E-mail: dujm@sxicc.ac.cn

Dong Wu & Xianglin Hou

Institute of Coal Chemistry Chinese Academy Sciences, Taiyuan, China

Cuiping Feng

College of Food Science and Technology, Shanxi Agricultural University, Taigu, China

*The research is financed by the Chinese Academy of Sciences. No. 06SC7413B1 (Sponsoring information)*

## Abstract

The kinetics of the transesterification of phosphatidylcholine (PC) with  $\alpha$ -linolenic acid ethyl ester (ALAE) catalyzed by immobilized lipase in hexane was studied. The reaction proceeded via a Ping-Pong Bi-Bi mechanism without inhibition by both the substrates at various concentrations tested. A reaction kinetic model was proposed with the experimental data. The kinetic constants of the model were determined at 45 °C, which were  $1.2 \times 10^{-2} \mu\text{mol} \cdot \text{min}^{-1} \cdot \text{mg}^{-1}$ , 64.1 mM and 282.8 mM for  $V_{\text{max}}$ ,  $K_{\text{mALA}}$  and  $K_{\text{mPC}}$ , respectively.

**Keywords:** Phosphatidylcholine, A-linolenic acid, Kinetic study, Ping-Pong Bi-Bi mechanism

## 1. Introduction

The phospholipids (PL) form of n-3 polyunsaturated fatty acids (n-3 PUFA) is considered to be nutritionally more favorable than other fatty acid derivatives, such as methyl or ethyl esters even triglycerides (TG). It is because that phospholipids form not only provides high digestion of fatty acid to cell (Dominique et al., 1999), but also has considerable special functions. For example, DHA-containing PL can promote cell differentiation in leukemia (Hosokawa et al., 1999), enhance survivals of tumor-bearing mice (Jenski et al., 1995), and prevent cerebral apoplexy (Eibl et al., 1988). After hydrolysis, phospholipids with PUFA can be decomposed into PUFA and PL, which can act on cell in concurrence and show an increased double effect on human body.

A-linolenic acid (ALA) belongs to n-3 polyunsaturated fatty acids (PUFA). It is the precursor of EPA and DHA and also shows the similar high bioactivity in vivo. Compared with PL including EPA and DHA, an advantage of the synthesis of type- ALA phospholipids with PUFA is no residue of cholesterol in the PL productions. Since PUFA donor ALA is from plant oil (linseed oil) whereas EPA and DHA are from fish oil which has a lot of worries of cholesterol from animal. Therefore, the synthesis of PL of ALA type is very significant to new PL with PUFA.

The simplest and most direct route for the synthesis of ALA type PL is the transesterification between PL and ALA catalyzed with a lipase. Lipases offer high catalytic efficiency, specificity and selectivity by incorporation of the required acyl group into a specific position of the native PL. Some studies (Chojnacka et al., 2009; Junmin et al., 2009) have focused on the reaction conditions including temperature, time, water content, and substrate concentration rate. However, little information has been reported on the kinetics of the lipase-catalyzed transesterification between PL and ALA and the rate equations for the reaction mechanism involving magnitude of constants, especially on using ALAE as acyl donor by gas chromatography, were thus absent. Kinetic studies are the basis for elucidating the transesterification mechanism and designing a bioreactor (Garcia et al., 1999).

The synthesis of type-ALA phospholipids with PUFA by lipase-catalyzed transesterification in hexane can provide more information about these 2 aims. We studied the kinetics on lipase-catalyzed transesterification of phosphatidylcholine (PC) from egg with  $\alpha$ -linolenic acid ethyl ester (ALAE) by gas chromatography.

## 2. Experimental

### 2.1 Materials

Egg-yolk PC (purity 98.5%, average molecular weight 779 g/mol) was self-made by supercritical CO<sub>2</sub> extraction and purification with column chromatography.  $\alpha$ -Linolenic acid methyl ester (C18:3, purity 98.5%) was purchased from Sigma-Aldrich (Shanghai, China). Immobilized lipase Lipozyme TL IM, an sn-1, 3 specific lipase from *Thermomyces lanuginosa*, was donated by Novoyes (Shenyang, China). Solvents used and all other chemicals were of analytical grade and obtained commercially.

### 2.2 Enzyme reactions

A typical experiment was run at 45 °C in a 5 ml container with magnetic stirring at 100 rpm. 100 mg of immobilized enzyme was added to a total of 4 ml hexane reaction solution containing PC and ALAE. After reactions, the samples were centrifuged and the supernatants were collected. All samples were stored at -20 °C prior to analysis of GC. The initial reaction rate was determined after 60 min reaction and it was represented as the amount of ALAE decreased per unit time within the limits of less than 5% of transesterification (for considering no product inhibition).

### 2.3 Water content control

Prior to reaction, the PC and ALAE in the hexane were dehydrated over 4A molecular sievers over 4h and filtrated out. The immobilized enzyme was dehydrated under vacuum until the weight constant. 0.0, 2.5, 5.0, 7.5, 10, 12.5, 15, 17.5 and 20 % water content (by the enzyme weight) was obtained with addition of a known quantity of distilled water to the dried enzyme. The wet enzymes were stored at 4 °C for one week. Water content in the media was analyzed on a 684 KF Coulometer.

### 2.4 Analysis of fatty acids by gas chromatography

Fatty acid ethyl or methyl esters were analyzed on a Shimadzu gas chromatograph GC-14B with flame-ionization detector (Shimadzu, Kyoto, Japan). The glass column packed with 20% DEGS on celite (3mm i.d.×2 m length) was employed; the column temperature was 190 °C and the detector temperature was 250 °C. The n-eicosane was added in reaction solution prior to reaction as internal standard to calculate the amount of various fatty acid esters in the reaction system.

## 3. Results and Discussion

The transesterification of PC and ALAE for ALA containing PC production was shown in Scheme 1(Fig.1). After reaction, the ALAE content would decrease while the content of palmitic acid and stearic acid ethyl esters (PAEE and STEE, abbreviated respectively and can be lumped as a single constituent for comparison) formed would increase in the solution.

### 3.1 Effect of rotation speed and enzyme concentration

In this study, a 100 rpm of stirring speed was adopted and the mass transfer limitations could be neglected after investigation of rotating speed (60-300 rpm). When increasing the enzyme concentration, the initial reaction rate was also increased as shown in Fig.2. It was verified that the reaction was controlled by kinetics.

### 3.2 Effect of water content

Magnus Harrod et al. (1995) observed that there was no reaction at low water activity for synthesis of PC. Similar results were observed in our test. But when water content of enzyme increased, the initial rate began to increase (Fig.3), indicating that water is essential for maintaining lipase activity. Vikbjerg et al. (2007) considered that water addition was the most significant factor on the PLA2 catalyzed acidolysis reactions in terms of incorporation and recovery. One reason was that water enhanced the molecular flexibility favorable to reaction in hexane. Another reason was that the reaction intermediates must be hydrolyzed first through the nucleophilic attack by water. Miller et al. (1991) and Reyes et al. (1994) have probed that water was needed to rupture the native ester bonds by the first step of hydrolysis reaction in the transesterification of triglycerides. In the case of PC and ALAE, Dry lipase indicated that no water was available for rupturing the substrate ester bonds and reaction did not proceed although both PC and ALAE can be used as nucleophile directly for transesterification. When the water content of enzyme was varied from 0.0 to 7.5 % (by weight), the initial rate of consumption of ALAE increased fast and after that it increased continuously but slowly. This seems be

explained that this lipase tends to favor the more water content to the transesterification reaction. However, the lumped values of PAEE and STEE were not in good agreement with the concentration of ALAEE decreased under higher water content (more than 7.5%) with further investigation of product ethyl esters (Fig.3). The discrepancies between them became larger and larger as the initial water content increased in the enzyme. The lower hydrolysis rate of PC compared to ALAEE may be one of the main reasons, suggesting that the hydrolysis of PC for intermediate LPC can be rate-limiting step to the overall transesterification. Low water activity (making it possible to keep competing hydrolysis low) is needed in the lipase-catalysed transesterification (Lin et al. 2002). When the water content of enzyme reached at 5.0%, the discrepancy resulting from hydrolysis became the smallest and the hydrolysis side reaction can be negligible. The hydrolysis of ALAEE was suppressed to match that of PC effectively and the one-step transesterification of PC can proceed truly.

### 3.3 Effect of reaction time

In the most appropriate water content of 5.0%, there was a slow increase in the initial rate of ALAEE in the first minutes of reaction due to the absence of intermediates, indicating that the reaction needs a long time to react (Fig.4). However, after a long time of incubation, the reaction proceeds fast. It should be the accumulated intermediates that resulted in the fast reaction velocity. After about 3 h, the reaction reached to equilibrium. No significant decrease in the initial rate during the later period of reaction, indicating that no product inhibition occurred. In the initial reaction time, there was a decrease in the water content in the first hours of reaction, indicating that water was consumed for hydrolysis (Fig.4). The consumed water was also released by the re-esterification followed product. It neither increased nor decreased in the overall reaction process. To obtain precise reaction rate, 60 min of reaction time was suggested good for determining of initial rate taking into consideration that the substrates was converted less than 5% as well as LPC present at low concentrations.

### 3.4 Effect of substrate concentration

We investigated the effect of substrate concentration on the initial reaction in appropriate water content of 5.0% and reaction time of 60 min. The results are shown in Fig.5. It is obvious that when one of the substrate concentrations is kept constant, the initial reaction rate increased with increasing concentration of another substrate. Also, no evidence for the phenomenon of substrate inhibition can be seen. Alcohol always results in inhibition as alcohol substrate molecule can act as a dead-end inhibitor in the esterification reaction (Chulalaksanukul et al., 1990; Janssen et al., 1999), but alcohol in ALAEE has been esterified with long chain fatty acid, which contributes to certain non-polar effect on protecting enzyme structure from losing water in the present reaction. Appropriate water content (5.0 % based on enzyme) has a key effect on the reaction (Reyes et al., 1994). Water increases enzyme molecular flexibility avoiding exceeding hydrolysis of esters and improves the reaction rate and provides good condition for the transesterification without inhibition of substrates and products.

### 3.5 Kinetic model based on initial rates

Experimental data in Fig.5 was converted into double-reciprocal plot of initial rate of transesterification at varying contents. The plot of  $1/V$  for  $1/ALA$  presents a group of parallel model seen in Fig.6. This indicated that the reaction was in good agreement with Ping-Pong mechanism, which is characterized by parallel lines in the Lineweaver-Burk (double reciprocal) representation at concentrations in which there is no inhibition, as it happens in the present system.

Transesterification of PC with ALA ethyl ester is a two substrate reaction involving two steps. The scheme of the reaction steps was followed as Fig.7. In the first step, the acyl of either PC or ALA ethyl ester binds the free enzyme (E) forming a noncovalent enzyme-ester complex which is transformed to an enzyme-acyl-alcohol intermediate, which is further hydrolyzed as new enzyme-alcohol intermediate (F) with the concomitant release of the first product, either sn-1 positional fatty acids of PC or ALA. In the second step, the new enzyme-alcohol intermediate is esterified with another fatty acid, as new enzyme alcohol-acid would be first formed and then a molecule of water is released and esterification is performed. After that the enzyme-ester intermediate is formed and further isomerized to the original enzyme and the release of the second product, either new PC or new ethyl ester.

According to the mechanism above, the rate equation for the mechanism (Segel, 1975) is given by:

$$V = \frac{V_{\max}[C_{PC}][C_{ALAEE}]}{K_{mALA}[C_{PC}] + K_{mPC}[C_{ALAEE}] + [C_{PC}][C_{ALAEE}]} \quad (1)$$

Where  $V$  is the initial reaction rate;  $[C_{PC}]$  and  $[C_{ALAE}]$  are the concentrations of PC and ALA ethyl ester, respectively;  $V_{max}$  is the maximum velocity or limiting rate;  $K_{mPC}$  and  $K_{mALAE}$  are the Michaelis constants for PC and ALA ethyl ester, respectively.

Intercepts of straight lines in the primary plots in Fig.6 were plotted for the reciprocal of contents (Fig.8.). From Fig.6 and Fig.8, the kinetic constants were obtained. That is:  $V_{max} = 1.2 \times 10^{-2} \mu\text{mol} \cdot \text{min}^{-1} \cdot \text{mg}^{-1}$ ;  $K_{mALAE} = 64.1 \mu\text{mol/mL}$ ;  $K_{mPC} = 282.8 \mu\text{mol/mL}$ . The equation follows as below:

$$V = \frac{1.2 \times 10^{-2} [C_{PC}] [C_{ALAE}]}{64.1 [C_{PC}] + 282.8 [C_{ALAE}] + [C_{PC}] [C_{ALAE}]} \quad (2)$$

### 3.6 Validating of model

With the kinetic rate expression available, it is also possible to model the initial reaction rates using the equation (2) and to compare these with the experimentally observed values. A plot of the experimental rate values versus the calculated rate values give a straight-line which almost passes through the experimental points (Fig.9), showing that the experimental rate data match the values calculated by the model well.

As can be seen from Fig.9 for the lipase, PC has a lower affinity than ALAE as  $K_{PC}$  is higher than ALAE's. The higher  $k_{PC}$  value may be caused from its bulky and polar molecular characterization and this can lead to the time-consuming and low efficiency in the modification of PC. From an applied point of view, a lipase bearing similar  $K$  value for the two substrates will enhance reaction rate efficiently since the transesterification is run synchronously. If some of new measures for reaction, for example, new lipases, can be taken, the transesterification will be enhanced rapidly and greatly. Nevertheless, the result obtained was consistent with the effect of higher water content above where the hydrolysis of PC for intermediate LPC can be rate-limiting step to the overall transesterification. Perhaps, other reaction details such as the re-esterification LPC needs further investigation, however, this model is able to account for the effects of the concentration of the chemical species participating in transesterification throughout the entire reaction and it also provides an easy model of study for the lipase-catalyzed synthesis of ALA type phospholipids with PUFA.

### 4. In conclusion

The kinetics of the transesterification of phosphatidylcholine with  $\alpha$ -linolenic acid ethyl ester catalyzed by immobilized lipase in hexane was studied. Under the appropriate conditions (5.0% water content of enzyme and 60 min of reaction time), the reaction follows Michaelis-Menton equation and a Ping-Pong Bi-Bi mechanism without inhibition by the both substrates at all initial concentrations tested. Water has a key effect on enzyme activity and the hydrolysis of PC for intermediate LPC can be rate-limiting step to the overall transesterification, suggesting that new methods or lipases are needed for improving reaction rate. A simple kinetic model of reaction was proposed and fitted well with the experimental data. The kinetic constants of the model were  $1.2 \times 10^{-2} \mu\text{mol} \cdot \text{min}^{-1} \cdot \text{mg}^{-1}$ , 64.1mM and 282.8 mM for  $V_{max}$ ,  $K_{mALAE}$  and  $K_{mPC}$ , respectively.

### Acknowledgments

Financial support from the Knowledge Innovation Programs of the Chinese Academy of Sciences (06SC7413B1) is gratefully acknowledged.

### References

- Chojnacka A., Gladkowski W., Kielbowicz G., Wawrzenczyk C. (2009). Enzymatic enrichment of egg-yolk phosphatidylcholine with  $\alpha$ -linolenic acid. *Biotechnol. Lett.*, 31:705–709.
- Chulalaksanakul W., Condoret J.S., Delorme P. and Willemot R.M. (1990). Kinetic study of esterification by immobilized lipase in n-hexane. *FEBS.Lett.*, 276 (12)181-184.
- Dominique L D, Christlane P, Martinel L, et al. (1999). Blood compartmental metabolism of docosahexaenoic acid (DHA) in humans after ingestion of a single dose of  $[^{13}\text{C}]$  DHA in phosphatidylcholine. *J. Lipid Res.*, 40: 1867–1874.
- Eibl H, Unger C. (1988). Phospholipids-selective drugs in cancer therapy. *Proc. Soc. Exp. Biol. Med.*, 29:358.
- Garcia, T., Sanchez, N., Martinez, J., Aracil, J. (1999). Enzymatic synthesis of fatty acid esters. Part I. Kinetic approach. *Enzyme Microbiol. Technol.*, 25, 584–590.
- Hosokawa M, Minami K, Kohno H, Tanaka Y, Hibino H. (1999). Differentiation- and apoptosis-inducing activities of phospholipids containing docosahexaenoic acid for mouse myeloid leukemia M1cells. *Fisheries Sci.*, 65(5): 798–799.

Janssen AEM, Sjursnes BJ, Vakurov AV, Halling P. (1999). Kinetics of lipase-catalyzed esterification in organic media: correct model and solvent effects on parameters. *Enzyme Microb Technol.*, 24: 463–70.

Jenski LJ, Zerouga M, Stillwell W. (1995). O-mega3 fatty acids in cancer therapies. *Proc. Soc. Exp. Biol. Med.*, 210: 227–233.

Junmin Du, Dong Wu, Cuiping Feng, Xianglin Hou. (2009). Enzymatical synthesis (a -LNA) of phosphatidylcholine containing polyunsaturated fatty Acids. *J.Mol.Catal. (China)*, 23(4):372-376.

Lin Ma, Mattias Persson, Patrick Adlercreutz. (2002). Water activity dependence of lipase catalysis in organic media explains successful transesterification reactions. *Enzyme Microbiol. Technol.*, 31:1024–1029.

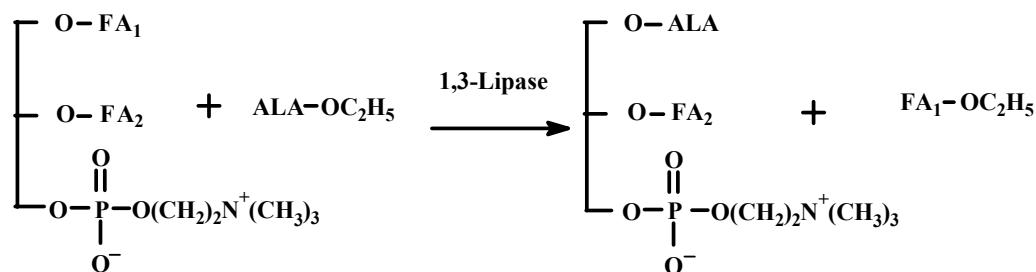
Magnus Harrod and Inger Elfman. (1995). Enzymatic synthesis of phosphatidylcholine with fatty acids, isooctane, carbon dioxide, and propane as solvents *J. Am. Oil Chem. Soc.*, 72:641-646.

Miller Douglas A., Prausnitz John M. and Blanch. Harvey W. (1991). Kinetics of lipase-catalysed interesterification of triglycerides in cyclohexane. *Enzyme Micro. Technol.*, 13(2):98-103.

Reyes Hector R., Hill Charles G., Jr. (1994). Kinetic modeling of interesterification reactions catalyzed by immobilized lipase. *Biotechnol. Bioeng.*, 43: 171-182.

Segel, IH. (1975). *Enzyme Kinetics: Behaviour and analysis of rapid equilibrium and steady-state enzyme systems*. New York. John Wiley and Sons, pp: 606-612.

Vikbjerg A. F., Mu H., Xu X. (2007). Synthesis of structured phospholipids by immobilized phospholipase A2 catalyzed acidolysis. *J. Biotechnol.*, 128: 545–554.



FA=Fatty acid residual, ALA=A-linolenic acid residual

Figure 1. The scheme of the reaction catalyzed by a lipase

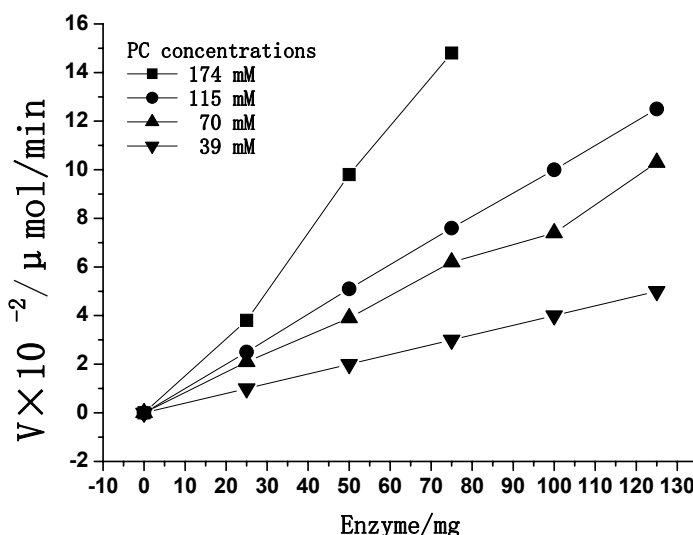


Figure 2. Effect of enzyme content on the initial reaction rate

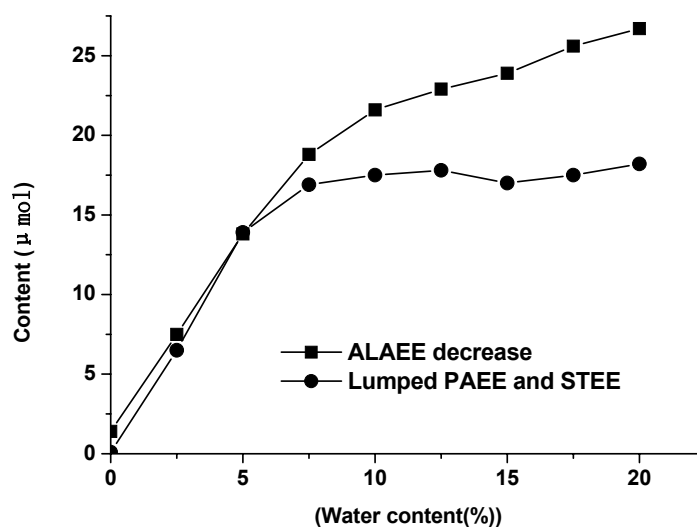


Figure 3. Contents of the constituents in the solution as a function of water content. Reaction condition: PC (90.5 mg), ALAEE (120.0 mg), reaction time (60 min), lipase (100 mg)

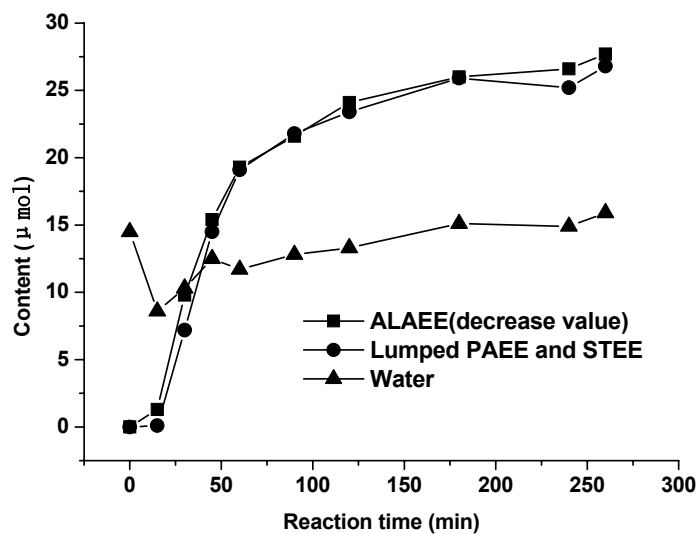


Figure 4. Contents of the constituents in the solution as a function of reaction time. Reaction condition: PC (100.1 mg), ALAEE (140.0 mg), lipase (100 mg), water content (5.0%)



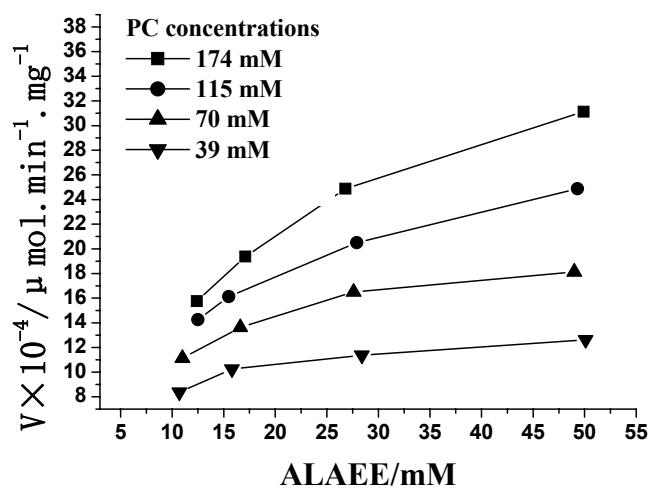


Figure 5. Effect of substrate concentration on the initial reaction

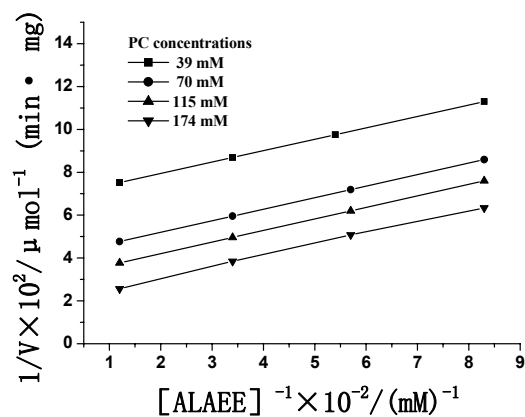
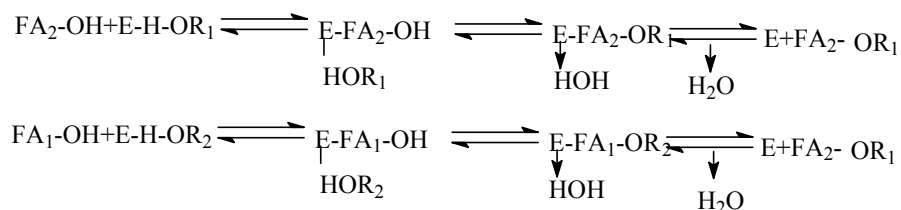
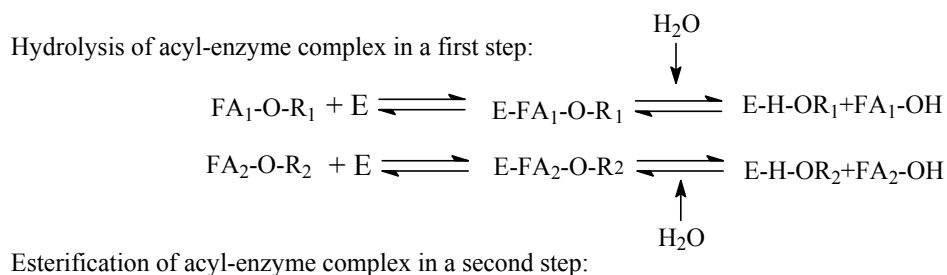


Figure 6. The plot of reciprocal initial velocity of the reaction versus reciprocal ALA ethyl ester concentration



Mechanism of Ping-Pong Bi-Bi for the two-step transesterification:

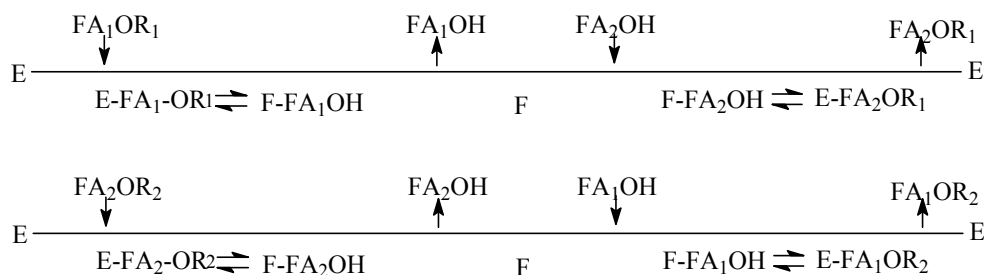


Figure 7. The scheme of the reaction steps ( $\text{R}_1$  and  $\text{R}_2$  represent phospholipid glycerol, and ethanol, respectively)

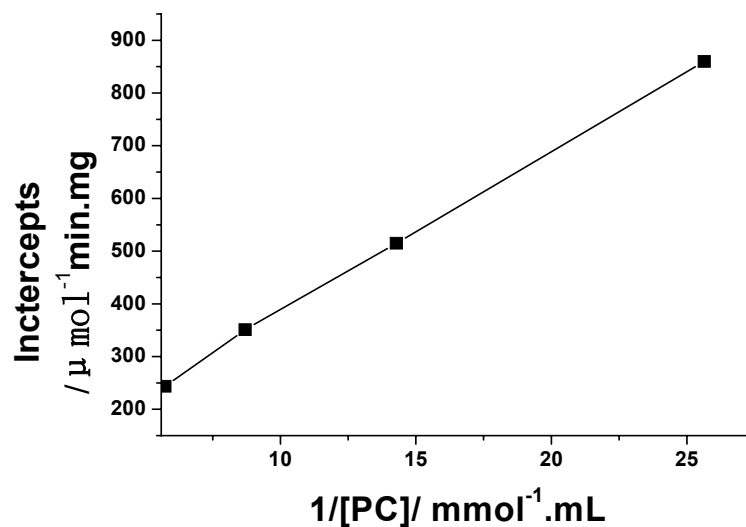


Figure 8. Intercepts of the straight lines in the primary plot in Fig.3 versus the reciprocal PC concentrations

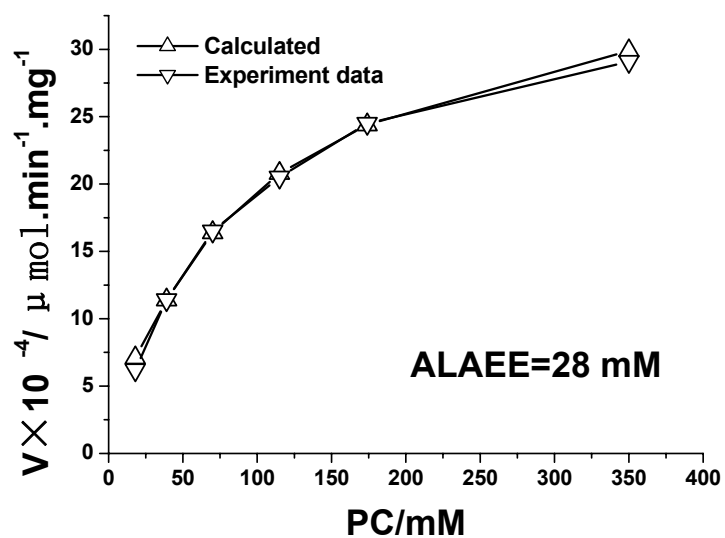


Figure 9. Comparison of experimental rate data and the rate data calculated by the kinetic model

# Spectrophotometric Determination of Lead in Environment Samples by Benzoic Acid Azo PhenylCalix[4]arene (BAPC)

Le Van Tan (Corresponding author)

Ho Chi Minh City University of Industry, Ho Chi Minh City, Viet Nam  
12 Nguyen Van Bao, Ward 4, Go Vap Disc., Ho Chi Minh city, Viet Nam  
Tel: 84-8-38940390 E-mail: tanhuaf@yahoo.com

Nguyen Thi Ngoc Le

Kon Tum of Pedagogical College, Kontum Province, Viet Nam  
Tel: 84-905171134 E-mail: ngocle\_cdsp\_kt@yahoo.com.vn

*The research is financed by DAAD (Germany)*

## Abstract

A new and selective spectrophotometric method for the determination of trace amounts of Pb(II) in aqueous environmental samples is reported. The interaction in solution between Pb(II) and Benzoic acid Azo Phenyl Calix[4]arene (BAPC, **1**) was studied. Upon reaction of PABC and Pb(II) a stable complex is formed. Under the conditions reported here the method furnishes reproducible results with basic media. The calixarene derivative shows strong binding ability to Pb<sup>2+</sup> ion with formation of a 1:1 complex. Beer's law is obeyed in the range of  $2.0 \times 10^{-6}$  –  $2.4 \times 10^{-5}$  mol L<sup>-1</sup> of Pb<sup>2+</sup>. The apparent molar absorptivity ( $\epsilon$ ) of **1**-Pb<sup>2+</sup> complex was  $1.89 \times 10^4$  L mol<sup>-1</sup> cm<sup>-1</sup> at 440 nm, and the detection limit is  $1.4 \times 10^{-6}$  mol L<sup>-1</sup>. The calixarene **1** showed high sensitivity and selectivity for Pb<sup>2+</sup>. The method was used to determine the content of Pb(II) in synthetic and natural samples.

**Keywords:** Spectrometry, Determination of lead traces, Water, Vegetable, Vetiver-grass, Azo-calixarene

## 1. Introduction

Lead is a cumulative poison that enters the body from lead water pipes, lead-based paints and leaded petrol (Renner, R. 1995). Presence of even traces of Pb(II) in environmental samples leads to environmental pollution and many fatal diseases including dysfunction of renal blood and neurological systems. Pb(II) easily deposits in blood, kidney, reproductive system, nervous system and brain, and acute lead poisoning can result in colic shock, severe anemia and irreversible brain damage. Lead compounds as antiknocking agents in automobile fuels cause air pollution.

The determination of trace amounts of lead is very important in the context of environmental monitoring. Atomic absorption and atomic emission spectrometry are used for routine trace analysis of lead, however a large number of spectrometric methods for determination of lead are reported to face interference due to the presence of several metal ions (Table 1) (Du, B. et. al 2002, Farguission, J.1990, Ferreira, S. L. C. et.al 1991, Dutta, S. & Das, A. K. 2007, Kiehei, U. et. al 2000, Mondal, B. C., Das, A. K. 2002, Dutta, S. & Das, A. K. 2007). For this reason there is an ongoing search for new organic reagents for direct and rapid spectrophotometric determination of trace amounts of lead, especially in aqueous solutions.

The structure elucidation of Benzoic acid Azo Phenyl Calix[4]arene (BAPC) was reported in our previous papers (Kim, T. H. et. al 2007, Kim, T. H. et. al 2008). Based on these findings, this paper reports a spectrophotometric method with a new reagent for a simple, fast, and sensitive determination of Pb(II) traces without preconcentration. The formula of the BAPC reagent is shown in Fig. 1.

## 2. Experimental

### 2.1 Reagents

All chemicals were analytical reagent grade. Water was purified and distilled. A stock solution of **1** ( $1.0 \times 10^{-3}$  mol L<sup>-1</sup>) was prepared in MeCN. Lead perchlorate stock solution ( $2.0 \times 10^{-2}$  mol L<sup>-1</sup>) was prepared in water. The Pb<sup>2+</sup> solution was diluted 10 and 100 times to give  $2 \times 10^{-3}$  mol L<sup>-1</sup> and  $2 \times 10^{-4}$  mol L<sup>-1</sup> solutions. A working standard solution of Pb<sup>2+</sup> ( $2.0 \times 10^{-5}$  mol L<sup>-1</sup>) was prepared from this stock solution by dilution with distilled water.

KCl-NaOH buffer solution (pH = 12.5) was used. Aqueous solutions with 0.010 mol.L<sup>-1</sup> concentrations of different cations were obtained by dissolving the appropriate substance in distilled water.

## 2.2 Apparatus

Absorption spectra were measured with a Varian-5000 UV-visible spectrophotometer (USA).

## 2.3 Procedure

The solutions to be studied were prepared in 10 mL volumetric flasks. Measured volumes of Pb(II) and organic reagent solutions were introduced in the flasks and they were filled up to the mark with KCl-NaOH buffer solution (pH = 12.5). Absorbance of each solution was measured against a corresponding blank reagent similarly prepared.

## 2.4 Collection of water, Vetiver grass and soil samples

Soil, water and vetiver grass samples were collected from points in Kontum province (Vietnam). Vetiver grass (scientific name *Vetiveria zizanioides* L.), a robust and easily propagating species capable of adapting to a wide range of climate and soil conditions, requires little care. Vetiver grass grows as bushes. The slabs are relatively hard and most leaves are at the base. With its dense roots Vetiver grass is able to absorb toxic minerals such as N, P, Al, Mg, Hg, Cd and Pb (Troung, P.N.V., Baker, D. 1998) from fertilizers and pesticides thus preventing pollution of soil and water. In addition, Vetiver grass also helps to increase the soil fertility by means of a natural moisturizing effect. The grass roots and its dense body will retain soil and mud on the surface. Stems, leaves and grass roots when buried in soil will break down to organic material, make the ground more soft and airy, thus improving the mechanical properties of soil (Ilker, A., & Metin, T. & Quirine, M. K. & Avni, C. 2008).

Vetiver grass samples were collected carefully using a hand shovel to dig out the soil around the grass. The plants were pulled out carefully, ensuring that no part of the root was lost. The different grass samples were kept individually in properly labelled polyethylene bags. Soil samples were collected from the same point where the grass samples were uprooted. The soil samples were collected to a depth of 15 cm using a soil auger. The soil samples were kept in labelled polyethylene bags. One litter of water was collected for lead determination in water. Polypropylene bottles used for the water samples were previously rinsed with deionized water and 30% HNO<sub>3</sub>. The samples were brought to the laboratory and kept in the fridge prior to analysis for lead.

## 2.5 Sample preparation

Each grass sample was separated into leaves, roots, and stems and dried in an oven at 50 °C for 8 hours. The dried plant samples were milled using a laboratory blender and kept for digestion. Unwanted materials such as stones, leaves and debris were removed from the soil samples by handpicking. The soil sample was further broken down into finer particles using a laboratory mortar and pestle. The soil samples were dried in an oven for 8 hours at 80 °C (Douglas, C. B., Wolfgang, F. 1995).

## 2.6 Sample digestion

### Plant sample digestion

Grass samples were digested following the method of Allen et al. 3g of the milled plant sample were weighed into a conical flask using a digital weighing balance. 3 ml of 60% hydrochloric acid and 10 ml of 70% nitric acid were added to the weighed milled plant sample. The conical flask was then placed on a laboratory hot plate for digestion until the white fume evolving from the conical flask turned brown. The mixture was allowed to cool and then filtered through a Whitman's filter paper, leaving a whitish residue. The filtrate was then filled up to 25 ml with distilled water and stored for analysis.

### Soil sample digestion

The same procedure for the digestion of plant sample was used according to the method of Allen et al.

## 3. Results and Discussion

### 3.1 Absorbance spectra

The spectrum recorded for a solution containing Pb(II) and organic reagent are presented in Fig.2(a). A chemical interaction between Pb(II) and organic reagent has occurred. The maximum absorption of the complex is located at 440 nm.

### 3.2 Influence of the pH

The effect of pH on the absorption efficiency is shown in Fig.2 (b), which indicates that high deposition efficiency was achieved at pH 12-13. The maximum and constant absorbance of the complex is obtained in the pH range of 12.3–12.7, and a pH of 12.5 may thus be chosen for the following experiments. At pH = 12.5, the effects of four

kinds of buffers on the absorbance were also examined. KCl–NaOH buffer solution was chosen.

### 3.3 Stoichiometry of the complex

The effect of reagent concentration was examined by measuring the absorbance of the solution containing a known concentration of Pb(II) and different amounts of organic reagent. The spectrophotometric titration using a constant amount of organic reagent and variable concentration of Pb(II) as well as Job's method were also employed in order to establish the stoichiometry of the complex. The results indicate formation of a complex Pb(II) : PABC = 1 : 1.

### 3.4 The stability constant

The apparent stability constant of the complex was calculated from the data obtained using the mole ratio method. The value of the stability constant is:  $6.2 \times 10^4 \text{ mol}^{-1} \text{ L}$  for PBC. The value of stability constant obtained at  $25 \pm 2^\circ\text{C}$  show a very stable complex for the corresponding stoichiometry. The absorbance of 1-Pb<sup>2+</sup> complex can reach maximum in 10 min and remain unchanged for at least 3 h.

### 3.5 Calibration curve

Beer Lambert law is followed for Pb(II) concentration in the  $2.0 \times 10^{-6} - 2.4 \times 10^{-5} \text{ mol L}^{-1}$  ( $r = 0.9997$ ) of Pb<sup>2+</sup>. Absorbance ( $A$ ) =  $0.025 \times C$  ( $10^{-6} \text{ mol L}^{-1}$  of Pb<sup>2+</sup>) + 0.021 ( $n = 8$ ,  $r = 0.99$ ). The molar absorptivity coefficient ( $\epsilon$ ) is  $1.89 \times 10^4 \text{ L mol}^{-1} \text{ cm}^{-1}$ .

### 3.6 Interferences

The influence of other metal ions such as alkali, alkaline earth, or transition metal ions on the absorption was studied repeatedly with very high concentrations. Results showed that metal ions do not affect the spectrum of the complex. Cu(II), Ca(II), Fe(II), Cr(III), Co(II), Ni(II) have been found to interfere only if their concentration exceeds the lead concentration by a factor or 280-500.

### 3.7 Determination of Pb(II) in natural samples

The spectrophotometric method was applied to the determination of Pb(II) in water, soil and vetiver grass in Kontum province, VietNam. The comparison of results presented in Table 2 shows good agreements between the values determined by the proposed method and other methods.

## 4. Conclusion

The calixarene derivative BAPC forms a 1:1 complex with Pb<sup>2+</sup> suitable for spectrophotometric determination of lead traces in aqueous solution. The optimum conditions for complex formation have been elucidated. The new reagent has been used to analyze samples of water, soil and Vetiver grass in Kontum province. The results showed that this method offers sensitivity comparable to that of the traditional reagents. Advantages of the proposed method are simplicity, rapidity and sensitivity without interference from other metal ions and without sample preconcentration.

## References

- Douglas, C. B., Wolfgang, F. (1995). Speciation of lead in environmental and biological samples. *Pure & Appl. Chem.*, Vol. 67, No. 4, pp. 615-648.
- Du, B., Yang, J., Wei, Q. & Chang, G. (2002). Spectrophotometric determination of trace amounts of lead in environmental water samples in the presence of mixed microemulsion. *Anal Lett*, 35 895-908.
- Dutta, S. & Das, A. K. (2007). Synthesis, characterization and application of a new chelating resin functionalized with ithiooxamide. *J Appl Polym Sc*, 103 2281-2285.
- Fargussion, J. (1990). *The Heavy Elements: Chemistry, Environmental Impact and Health Effect* (Pergamon, Oxford)
- Ferreira, S. L. C., Andrade, M. G. M., Lobo, I. & Costa, A. C. S. (1991). 2-(2-Thiazolylazo)-p-cresol (TAC) as a reagent for the spectrophotometric determination of lead (II). *Anal Lett*, 24, 1675-1682
- Guo, Y., Din, B., Liu, Y., Chang, X. & Meng, S. (2004). Determination of lead using a new chromogenic reagent 2-(2-sulfo-4- acetylphenylazo)- 7-(2,4,6-trichlorophenylazo)- 1,8-dihydroxynaphthalene-3, 6-disulfonic acid, *Microchim. Acta*, 144 257-261.
- Ilker, A., & Metin, T. & Quirine, M. K. & Avni, C. (2008). Humic Acid Addition Enhances B and Pb Phytoextraction by Vetiver Grass (*Vetiveria zizanioides* (L.) Nash). *Water Air Soil Pollut*, 188:335–343
- Kiehei, U., Toshiaki, I., Cheng K.L. (2000). *Handbook of Analytical Reagents*. CRC Press, pp.189-196

Mondal, B. C., Das, A. K. (2002). Microwave-assisted synthesis of a new chelating resin containing 2-aminothiophenyl S-acetic acid and its application to the determination of lead, *React Funct Polym*, 53, 45-52.

Renner, R. (1995). *Environ. Sci. Technol*, 29, 256.

Kim, T. H., Kim, S. H., Tan, L. V., Seo, Y. J., Park, S. Y., Kim, H., Kim, J. S. (2007). Transition metal ion selective ortho-ester diazophenylcalix[4]arene. *Talanta*, 7, 1294 -1297.

Kim, T. H., Kim, S. H., Tan, L. V., Dong Y., Kim, H., Kim, J. S. (2008). Diazo-coupled calix[4]arenes for qualitative analytical screening of metal ions. *Talanta*, 74 1654–1658.

Troung, P.N.V., Baker, D. (1998). Vetiver grass for stabilization of acid sulfate soil, p.196-198. *In Proceedings of Second National Conference on Acid Sulfate Soils*, Coffs Harbour, Sydney.

Table 1. Comparison of Analytical Parameters for the Spectrophotometric Determination of Lead

Reagent	$\lambda$ (nm)	$\epsilon_{\lambda} \times 10^{-4}$ (L.mol <sup>-1</sup> cm <sup>-1</sup> )	Remark
1-(2-Thiazoylazo)-2-naphthol	575	3,6	Light-sensitive, Co, Zn, Fe, Mn EDTA interfere
Porphyrin compounds	479	2,2	Cu, Ni, Mn, Cd, Ca, Mg, Zn Fe interfere
Diphenylthiocarbazone	520	2,5	Light-sensitive
Phenylazoformic acid	525	7,2	
2- phenylhydrazide			
Xylenol orange	580	2,3	Light-sensitive, Hg Zn, Al, Bi, Ni, Re interfere
2-(2-Thiazoylazo)-p-cresol	650	2,1	Ni, Co, Zn, Fe, Cd, Cu interfere
4-(2-Pyridylazo)- resorcinol	520	4,3	Cd, Ni, Cu, Co, Ag, Hg, Zn, Fe interfere
Arsenazo-TB	620	1,8	Light-sensitive, Ti, Th seriously interfere
Diethyl dithiocarbamat acid, Diethylammonium salt	435	1,3	Cu, Hg, Zn, Fe interfere
Arsenazo.III	660	3,0	Al, Cu, Th Ti, U Fe interfere
1 ( This work)	440	1.2	Cu, Ca, Fe, Cr, Co, Ni interfere

Table 2. Determination of Lead in environment samples (mg/kg) n=5

<i>Samples</i>	<i>Found by proposed method ( mg/kg)</i>	<i>Found by other method (mg/kg)</i>
W35	2.32 ±0.09	2.21 - EPA-method 200.7
W39	1.85 ±0.04	1.98 - EPA-method 200.7
W41	2.12 ±0.10	2.03 - EPA-method 200.7
W42	1.89 ±0.05	2.04 - EPA-method 200.7
W52	4.03 ±0.08	3.90 - EPA-method 200.7
S2	-	- - AAS-Tome II
S160	2.14 ±0.12	2.08 - AAS-Tome II
S68	2.52 ±0.08	2.40 - AAS-Tome II
S10	1.32 ±0.10	1.22 - AAS-Tome II
VG 21	0.75 ± 0.07	0.68 - AOAC 985.01
VG36	1.25 ± 0.06	1.12 - AOAC 985.01
VG47	1.18 ± 0.07	1.15 - AOAC 985.01
VG53	0.98 ± 0.05	0.94 - AOAC 985.01

\* W: water, VG: Vetiver grass, S: soil, Number is place

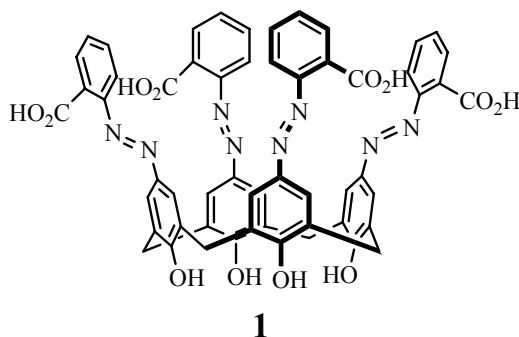
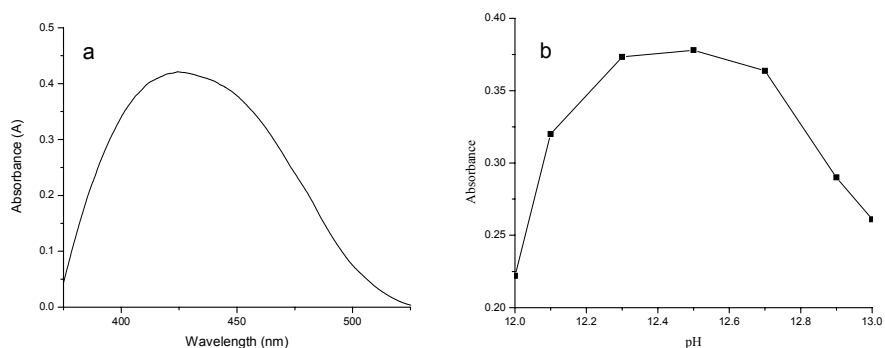


Figure 1. Structure of Benzoic acid Azo Phenyl Calix[4]arene (BAPC)

Figure 2. Absorption spectra of **2** and its  $\text{Pb}^{2+}$  complex at pH 12.5 (a) Effect of pH (b)



# Retention Profile of Selenium (IV) from Aqueous Media Containing Bromide Ions Employing Polyurethane Foams

A. S. Bashammakh

Department of Chemistry, Faculty of Science, King Abdulaziz, University

P.O. Box 80203, Jeddah, Kingdom of Saudi Arabia

E-mail: abashammakh@kau.edu.sa

## Abstract

A simple and accurate method for the quantitative retention of traces of selenium (IV) from aqueous media was developed employing polyurethane foams (PUFs). The dependences of selenium (IV) uptake by the unloaded and tributyl phosphate (TBP) plasticized PUFs on pH, salt effect, nature and concentration of surfactant, etc. was critically studied. The sorption data have followed Langmuir, and Dubinin - Radushkevich (D-R) type sorption isotherms. Thus, "a dual-mode" sorption mechanism involving both absorption related to "solvent extraction" and an added component for "surface adsorption" may be simultaneously present. The sorption and recovery percentage of selenium (IV) from fresh and natural water by the proposed loaded and unloaded foam columns were quantitatively achieved. The method was applied for the retention and recovery of selenium (IV) species spiked to fresh water employing PUFs packed columns.

**Keywords:** Selenium (IV), Polyurethane foam, Isotherms and Chromatographic separation

## 1. Introduction

Selenium is a naturally occurring trace element recognized for its unique intermediate properties between metals and non-metals (Iyengar, 1978, PP. 55 – 82; WHO, 1987). Selenium is distributed in nature in a relatively small concentration in rocks, coal and other fossil fuels. Volcanic eruption, smelting ceramics, and metallurgical operations, manufacture of pesticides, glass and electronic goods are also major sources of selenium in the environment (Shpira, 1971). Selenium enters into natural waters through seepage from seleniferous soils and industrial waste and liberated into soil through complex biogeochemical reaction forming organo selenium compounds (Sitting, 1976). Such class of compounds is more toxic than inorganic selenium compounds and absorbed by plants such as cabbage and mustard (Adriano, 1992). However, trace amounts of selenium have been found to be essential to maintain normal body metabolism (Sitting, 1976), since it takes part in the glutathione peroxidase enzyme etc., (Mertz, 1986). Selenium can also enhance our ability to protect against certain cancer and heart diseases (Holum, 1995).

The analytical applications of tri-n-butyl phosphate (TBP) immobilized PUFs in batch and column operation modes for the preconcentration and separation of trace metal ions have been initiated (Braun, 1985). Since then, several separations and preconcentration of inorganic species in aqueous media have been examined by the foams supported solvent extractants (El-Wakil, 1990, PP. 703 - 716; Palagyi and Braun, 1992; El-Shahawi, 1995, PP. 185 - 190; El-Shahawi, 1997, PP. 483 – 489). A series of organic reagents e.g., TBP, methyl isobutyl ketone, diethyl ether, isopropyl ether and ethyl acetate have been impregnated onto polyurethane foam membranes (Palagyi and Braun, 1992). The produced reagent foams have been used successfully for various analytical purposes (Oleschuk and Chow, 1996, PP. 1545 - 1554; Rzeszutek and Chow, 2001, PP. 265 - 271).

Recent years have seen an upsurge of interest in the application of liquid-solid separation technique for the chemical preconcentration and speciation, removal and subsequent determination of some toxic trace metal species in environmental samples (Ofomaja, 2010; Hosseini, 2009, PP. 807 - 812; Sanchez-Moreno, 2010, 716 - 723). Thus, the present paper describes convenient and low cost liquid-solid extraction procedures for the chemicals separation and subsequent determination of selenium (IV) in water samples employing unloaded and TBP loaded foams from aqueous bromide media. The script also discusses the extraction mechanism, the most probable equilibria and thermodynamic stability of the produced ion-associates on/in the solid sorbent.

## 2. Experimental

### 2.1 Reagents and materials

All chemicals used were of analytical reagent grade quality and were used without further purification. Doubly de-ionized distilled water was used throughout the work. Stock solutions (2 % v/v) of TBP were prepared by

dissolving the exact volume of each reagent separately in chloroform. Stock solution ( $1.00 \text{ mg mL}^{-1}$ ) of selenium (IV) was prepared by dissolving the appropriate weight of selenium oxide ( $\text{SeO}_2$ ) in de-ionized water acidified with few drops of nitric acid ( $1.0 \text{ mol L}^{-1}$ ). Freshly diluted of selenium (IV) solutions were prepared by diluting the stock solution with water. Stock solutions (2 % v/v in benzene) of dioctyl phthalate (DOP) and tri-n-butyl phosphate (TBP) were used.

## 2.2 Apparatus

A Perkin Elmer (Lambda EZ – 210) double beam UV-VIS (190 – 1100 nm) spectrophotometer with 1 cm (path width) quartz cell was used for recording the electronic spectra and the absorbance of the test selenium (IV) complex. The absorbance of the organic extract of selenium (Marczenko, 1986) was measured with a single beam Digital Spectro UV-VIS RS Labomed, Inc spectrophotometer with glass cells (10 mm). An Orion pH-meter (model 9418) with glass and saturated Calomel electrode was used for the pH measurements. Glass columns (18 cm x 15 mm ID) were used in dynamic mode of extraction. A Lab-line Orbital mechanical shaker SO1 (UK) and a Soxhlet extractor were also used in batch experiments and for the foam purifications.

## 2.3 Reagent foam and PUFs packed column preparation:

The reagent foam cubes were prepared by mixing the dried foam cubes with chloroform containing TBP or DOP (2 % v/v) ( $10 \text{ mL g}^{-1}$  dry foam) with efficient stirring for 30 min. The plasticized TBP or DOP reagent foam cubes were then squeezed and dried between two filter papers to remove the excess solution as reported (El-Shahawi and Nassef, 2003, PP. 29 - 39). The unloaded and reagent TBP or DOP loaded PUFs were packed in the glass columns by applying the vacuum method of foam packing as described earlier (Braun, 1985).

## 2.4 Determination of selenium (IV)

Selenium (IV) was determined by iodometry and/or spectrophotometry at wavelength 358 nm as follows: a 10 mL of aqueous solution containing selenium (IV) at concentration level  $20 \text{ } \mu\text{g mL}^{-1}$  was adjusted to pH zero with few drops of HCl (2 M) and  $\sim 0.2 \text{ g}$  of potassium iodide was then added. The solution was then swirled well and the released iodine was determined spectrophotometrically by 3, 3- diaminobenzidine method [Marczenko, 1986].

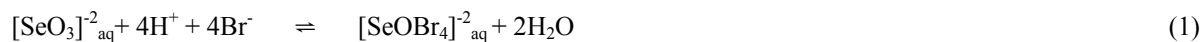
# 3. Results and Discussion

## 3.1 Retention profile of selenium (IV) onto PUFs

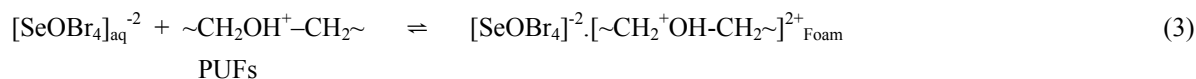
Preliminary investigation on the retention of selenium (IV) ions from the aqueous solution by the unloaded and the reagent TBP immobilized foams was found to depend on the aqueous solution pH. Thus, the sorption profiles of selenium (IV) ions at  $10 \text{ } \mu\text{g mL}^{-1}$  concentration level from the aqueous solutions (50 mL) at different pH and acidity by the unloaded or TBP-immobilized PUFs ( $0.2 \pm 0.01 \text{ g}$ ) were critically investigated. After shaking the test solutions for 1 h, the concentration of selenium (IV) retained on the aqueous solution was then measured [Marczenko, 1986]. The data revealed that, the sorption profile of selenium (IV) by the unloaded and the foam immobilized with TBP foams decreased on increasing the solution pH and shows the highest sorption percentage at pH  $\sim$  zero. The decrease in the selenium (IV) uptake by the loaded foams at higher pH is most likely due to the instability or the hydrolysis of the produced complex species formed between selenium (IV) and the reagent immobilized foam.

The sorption profile of selenium (IV) ions by the unloaded was found less than that obtained with the TBP immobilized PUFs. The influence of HCl concentration on the uptake of selenium (IV) from the aqueous solution containing saturated KBr onto unloaded and TBP loaded foams was carried out. A sharp increase in the extraction of selenium (IV) sorption onto PUFs was achieved on increasing the HCl concentration up to 4.0 M. At acidity higher than 4.0 M, the extraction percentage of selenium decreased due to the degradation of the foam and the possible reduction of selenium (IV) to the elemental selenium which has no ability to form complex with the tested reagents. These results are in a good agreement with data reported elsewhere (El-Shahawi, 2005, PP. 806 - 815). Therefore, in the subsequent experiments, a solution of HCl (4.0 M) was used as an excellent extraction media for selenium (IV) sorption.

Moreover, the effect of KBr concentrations on the extraction of selenium (IV) on the unloaded and the immobilized TBP foam was investigated. The sorption of selenium (IV) increased as the concentration of KBr increased up to (2 M) and remained constant (Fig. 1). Thus, in the subsequent work KBr concentration (2.0 M) level was used in the extraction media. The retention of selenium (IV) onto PUFs cubes most likely proceeds as follow:

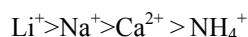


or



The influence of shaking time on the uptake of selenium (IV) from the aqueous media containing HCl (4 M) and KBr (2 M) was carried out employing the unloaded and the reagent TBP loaded PUFs. The sorption of selenium (IV) ions was slow at the initial stage and maximum equilibrium has reached constant values after 80 min shaking time. Maximum sorption was obtained from the extraction media containing HCl (4 M) and KBr (2 M) solution at shaking time  $\geq 80$  min. Thus, the actual sorption of  $(\text{SeOBr}_4)^{-2}$  on the interior surface sites was found slow, and inter particle transport are the main predominating factors controlling the sorption rate (Frag, 2007, PP. 218 - 229). Consequently, 80 min shaking time were adopted in subsequent experiments.

The influence of various concentrations (0.01-0.05 % w/v) and cation size of the of alkali metal ( $\text{Li}^+$ ,  $\text{Na}^+$ ,  $\text{Ca}^{2+}$  and  $\text{NH}_4^+$ ) chlorides on the uptake of selenium (IV) ions from the aqueous media containing HCl (4 M) and KBr (2 M) onto unloaded and TBP immobilized PUFs was studied. The results revealed no significance effect of cation concentration ( $\text{Li}^+$ ,  $\text{Na}^+$ ,  $\text{Ca}^{2+}$  and  $\text{NH}_4^+$ ) as chloride salts on the equilibrium sorption of the tested selenium (IV) ions onto PUFs. The sorption profile of selenium (IV) more or less slightly increased in the following order:



This behavior is characteristics of "solvent extraction" mechanism with the salt acting as salting out. Thus, in the subsequent work the sorption procedures were carried out without salt addition. Similar trends were also obtained in solvent extraction of gold (I, III) ions by PUFs (Frag, 2007, PP. 218 - 229). On the other hand, the effect of some surfactants individually e.g. diallyl phthalate, sodium lauryl sulphate and Triton X-100 on the sorption of selenium (IV) onto unloaded and TBP loaded foam was carried out. A significant increase on the uptake of selenium (IV) onto unloaded and TBP loaded was noticed on the use of diallyl phthalate.

### 3.2 Sorption isotherms of selenium (IV) onto PUFs

The amount of selenium (IV) uptake from the bulk aqueous solution onto the unloaded and TBP immobilized foam was found to depend on its initial concentration and can be expressed in the form of its diffusion and thermodynamic behavior (Fig. 2). Therefore, the uptake of selenium (IV) from the aqueous solution onto the PUFs was subjected to Langmuir and Dubinin-Radushkevich (Somorjai, 1994) isotherms models. The Langmuir sorption isotherm based on the kinetic consideration is expressed in the following linear form (Somorjai, 1994):

$$C_e/C_{\text{ads}} = 1/Qb + C_e/Q \quad (4)$$

where,  $C_e$  is the equilibrium concentration (M) of selenium (IV) in solution,  $C_{\text{ads}}$  is the adsorbed selenium (IV) concentration onto the unloaded and TBP loaded foam, respectively per unit mass of sorbent at equilibrium ( $\text{mmol g}^{-1}$ ), and  $Q$  and  $b$  are constants related to the maximum sorption capacity and the binding energy of solute sorption that is independent of temperature. Plots of  $C_e/C_{\text{ads}}$  versus  $C_e$ , are linear throughout the entire concentration range of selenium (IV). The sorption parameters  $Q$  and  $b$  for the adsorption process evaluated from the slopes and intercepts were found equal  $0.06914 \pm 0.002$ ,  $0.0792 \pm 0.0029 \text{ mol g}^{-1}$  and  $34.223$ ,  $38.73 \text{ dm}^3 \text{ mol}^{-1}$  for selenium (IV) sorption onto unloaded and TBP immobilized foam, respectively. The values of  $Q$  and  $b$  indicating good retention of selenium (IV) onto unloaded and TBP immobilized foam.

The sorption data were also subjected to Dubinin - Radushkevich (D-R) isotherm model (Somorjai, 1994) is postulated within the adsorption space close to the adsorbent surface. The D-R isotherm can be linearized as follows:

$$\ln C_{\text{ads}} = \ln K_{\text{DR}} - \beta \epsilon^2 \quad (5)$$

where,  $C_{\text{ads}}$  is the amount of selenium (IV) retained per unit mass of PUFs,  $K_{\text{DR}}$  is the maximum amount of selenium (IV) retained,  $\beta$  is a constant related to the energy of transfer of the solute from the bulk solution to the solid sorbent and  $\epsilon$  is Polanyi potential which is given by :

$$\epsilon = RT \ln (1+1/C_e) \quad (6)$$

where,  $R$  is gas constant in  $\text{KJ mol}^{-1} \text{K}^{-1}$  and  $T$  is the absolute temperature in Kelvin. The plots of  $\ln C_{\text{ads}}$  versus  $C^2$  were found linear for unloaded and TBP loaded foam. The plots indicate that, the D-R isotherm model is obeyed for selenium (IV) sorption onto the unloaded and TBP loaded foam over the entire concentration range. The values of  $\beta$  and  $K_{\text{DR}}$  calculated from the slopes and intercept were found 0.0013, 0.0011  $\text{mmol}^2 \text{KJ}^2$  and 93.19, 93.042  $\mu\text{mol g}^{-1}$  for unloaded and TBP loaded foam, respectively. The mean free energy ( $E$ ) of the transfers of one mole of solute from infinity to the surface of PUF was determined employing the equation:

$$E = \frac{1}{\sqrt{-2\beta}} \quad (7)$$

The value of  $E$  was found in range of -17.8, -19.3  $\text{KJ mol}^{-1}$  for unloaded and TBP loaded foam, respectively confirming the chemisorption onto the solid PUFs sorbent.

### 3.3 Chromatographic separation of selenium (IV)

The sorption of selenium (IV) from aqueous solutions onto unloaded and TBP loaded PUFs in batch experiments suggested the use of PUFs in column mode for complete extraction and recovery of selenium (IV) from aqueous solution. Columns (10 cm height and 12 mm ID) were packed with ( $3 \pm 0.1$  g) unloaded and TBP loaded foam and were successfully employed for the enrichment of selenium (IV). In these experiments, an aqueous solution (2 L) of doubly distilled water containing selenium (IV) at 5 and 10  $\mu\text{g mL}^{-1}$  level for unloaded and TBP loaded foam respectively, (4.0 M HCl and 2.0 M KBr) was percolated through the foam packed column at 5  $\text{mL min}^{-1}$  flow rate. A separate blank experiment was also carried out by passing an aqueous solution (100 mL) free from selenium (IV) ions under the same experimental conditions through the unloaded and TBP loaded foam columns. Spectrophotometric determination of selenium (IV) in the effluent solution of loaded foam column against reagent blank indicated complete sorption of selenium (IV). The sample and blank columns were washed with an aqueous solution (100.0 mL) of HCl (4.0 M) - KBr (2.0 M). The sorbed chelate of selenium (IV) on/in the foam membrane was then recovered with chloroform (10 mL) at 2  $\text{mL min}^{-1}$  flow rate. Satisfactory recovery ( $\geq 96\%$ ) of the tested selenium (IV) ions was obtained by the proposed unloaded and TBP loaded foam columns.

The height equivalents to a theoretical plate (HETP) and the number of theoretical plate ( $N$ ) were calculated from the breakthrough capacity curve (Braun, 1985). Representative results are shown in Fig. 3. The HETP and  $N$  values for selenium (IV) uptake onto unloaded and TBP loaded foams calculated from breakthrough curve were found equal 0.92, 13.03 and 0.763, 15.72, for unloaded and TBP loaded foam, respectively.

### 3.4 Performance of the PUFs packed column

The performance of the unloaded and TBP loaded foam column was also determined from the critical capacity and breakthrough capacity. The critical capacity was defined as the amount of selenium (IV) that could be retained on the unloaded and TBP loaded foam column at rate 2  $\text{mL min}^{-1}$  until the selenium (IV) was first detected in the effluent solution. Practically, this value was found equal to the actual volume of the effluent solution collected just before first appearance of selenium (IV) in the effluent minus the free column volume. The S-shaped curve is shown in Fig. 3 represent i- the breakthrough volume and ii- the volume needed to reach bed saturation of selenium (IV). The critical capacities of selenium (IV) ions onto unloaded and TBP loaded foam column were found equal to 0.3 and 0.4  $\text{mg g}^{-1}$ , respectively at 1.5 and 2  $\text{mL min}^{-1}$  flow rate. The values of the breakthrough capacity (BC) of selenium (IV) uptake was calculated as reported (Ma, 2000, 191 - 196). The values of BC were found equal to 0.65, 0.78  $\text{mg g}^{-1}$  for selenium (IV) sorption onto unloaded and TBP loaded foam respectively at 2.0  $\text{mL min}^{-1}$ .

The applicability of the proposed method for quantitative collection and recovery of selenium (IV) from natural water was investigated on different samples. The tested sample was spiked with various selenium (IV) concentrations (5-10  $\mu\text{g mL}^{-1}$ ). A one liter water sample spiked with selenium (IV) was percolated through the PUF column at 1.5 and 2  $\text{mL min}^{-1}$  flow rate at optimum conditions of selenium (IV) uptake. The retained selenium (IV) species on the foam column were then recovered by percolating a 20 mL of chloroform at 2-3  $\text{mL min}^{-1}$  flow rate. The selenium (IV) content before and after extraction and also after recovery in elute was determined spectrophotometry.

## 4. Conclusion

The developed extraction procedures provide low cost and precise approach for selenium (IV) preconcentration in various water samples. It compares favorably with many preconcentration methods of selenium (IV) species. The sensitivity of the method could be improved to pico-molar level of selenium (IV) determination by on-line

prior preconcentration from large sample volumes onto TBP immobilized PUFs packed column followed by elution with suitable eluting agent. Work is still continuing on i. studying the on-line preconcentration of selenium (IV) and selenium (VI) after reduction of the latter to the tetra valence in natural water.

## References

- Adriano, D. C. (1992). *Biogeochemistry of Trace Metals*, Lewis, London.
- Braun, T., Navratil, J. D. and Farag, A. B. (1985). *Polyurethane foam sorbents in separation science*, CRC Press, Inc, FL, Boca Raton, FL, USA.
- El-Shahawi, M. S. and Almehdi, M. A. (1995). Qualitative, semi-quantitative and spectrophotometric determination of ruthenium (III) by solid-phase extraction with 3-hydroxy-2-methyl-1,4-naphthoquinone-4-oxime-loaded polyurethane foam columns. *J.Chromatoge. A*, 697, 185-190.
- El-Shahawi, M. S. and Al-Mehrezi, R. S. (1997). Detection and semiquantitative determination of bismuth (III) in water on immobilized and plasticized polyurethane foams with some chromogenic reagents. *Talanta*, 44, 483-489.
- El-Shahawi, M. S. and Nassef, H. A. (2003). Retention and thermodynamic characteristics of mercury (II) complexes onto polyurethane foams. *Anal. Chim. Acta*, 481, 29-39.
- El-Shahawi, M. S. and El-Sonbati, M. A. (2005). Retention profile, kinetics and sequential determination of selenium (IV) and (VI) employing 4,4'-dichlorodithizone immobilized-polyurethane foams. *Talanta*, 67, 806-815.
- El-Wakil, A. M., El-Shahawi, M. S., and Farag, A. B. (1990). Trace analysis by the direct spectrophotometric measurement on polyurethane foam, determination of chromium (VI) as a blue perchromic acid with unloaded and tri-n-butyl phosphate loaded foam. *Anal. Lett.*, 23, 703-716.
- Farag, A. B., Soliman, M. H., Abdel-Rasoul, O. S. and El-Shahawi, M. S. (2007). Sorption characteristics and chromatographic separation of gold (I & III) from silver and base metal ions using polyurethane foams. *Anal. Chim. Acta*, 601, 218-229.
- Holum, R. H. (1995). *Elements of General, Organic and Biological Chemistry*. 9th edn, John Wiley and Sons.
- Hosseini, M. S. and Asadi, M. (2009). Speciation determination of chromium using 1, 4- diaminoanthraquinone with spectrophotometric and spectrofluorometric methods. *Anal.Sci.*, 25, 807- 812.
- Iyengar, G. V., Kollmer, W. E. and Bowen, H. J. M. (1978). *The Elemental Composition of Human Tissues and Body Fluids*. New York, *Verlag Chemie*, Weinheim. 55-82.
- Ma, W. X., Liu, F., Li, K. A., Chen, W. and Tong, S. Y. (2000). Preconcentration, separation and determination of trace Hg (II) in environmental samples with aminopropylbenzoylazo -2-mercaptobenzothiazole bonded to silica gel. *Anal.Chim.Acta*, 416, 191-196.
- Marczenko, Z. (1986). *Spectrophotometric Determination of Elements*, 3rd ed., Ellis Horwood Chichester, UK, and references cited in chapter 46.
- Mertz, W. (1986). *Trace Elements in Human and Animal Nutrition*. Academic Press, London, UK.
- Ofomaja, A. E., Naidoo, E. B. and Modise, S. J. (2010). Removal of copper (II) from aqueous solution by Pine and base modified pine cone powder as sorbent. *J. Environ. Management*, in press.
- Oleschuk, R. D. and Chow, A. (1996). The Separation and isolation of gold by selective extraction and transport through polyurethane ether-type membrane. *Talanta*, 43, 1545-1554.
- Palagyi, S. and Braun, T. (1992). Separation and preconcentration of trace elements and inorganic species on solid polyurethane foam sorbents in: Alfassi, Z. B. and Wai, C. M. (edn) *Preconcentration techniques for trace elements* CRC Press, Boca Raton, FL, USA.
- Rzesutek, K. and Chow, A. (2001). Extractive of metal-dye ion association complexes by thin ether-type polyurethane membranes. *J. Membrane Sci.*, 181, 265-271.
- Sanchez-Moreno, R. A., Gismera, M. J., Sevilla, M. T. and Procopio, J. R. (2010). Evaluation of solid-state platforms for chromium (VI) potentiometric sensor development. *Sensors and Actuators B*, 143, 716-723.
- Shpira, J. R., Klayman, D. L. and Gunter, W. H. (1971). *Organic Selenium Compounds, Their Chemistry and Biology*, New York, John Wiley & Sons Inc.

Sitting, M. I. (1976). Toxic metals, pollution control and worker protection, Noyes Data Corporation, Park Ridge, USA.

Somorjai, G. A. (1994). *Introduction to Surface Chemistry and Catalysis*, John Wiley & Sons INC.

WHO. (1987). *Environmental Health Criteria* 58, Selenium, Geneva.

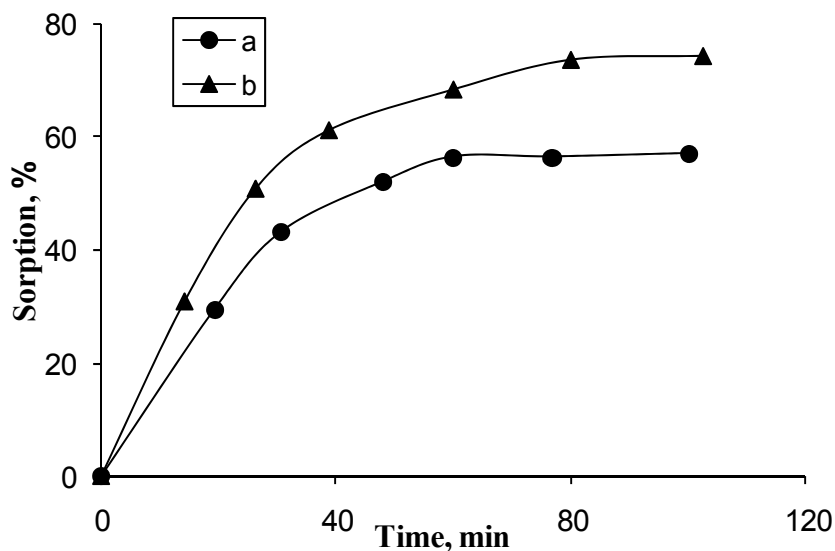


Figure 1. Influence of shaking time on the sorption of selenium (IV) from the aqueous solution onto the unloaded (a) and the TBP immobilized (b) PUFs from aqueous solutions containing HCl (4.0 M) and KBr (2.0 M)

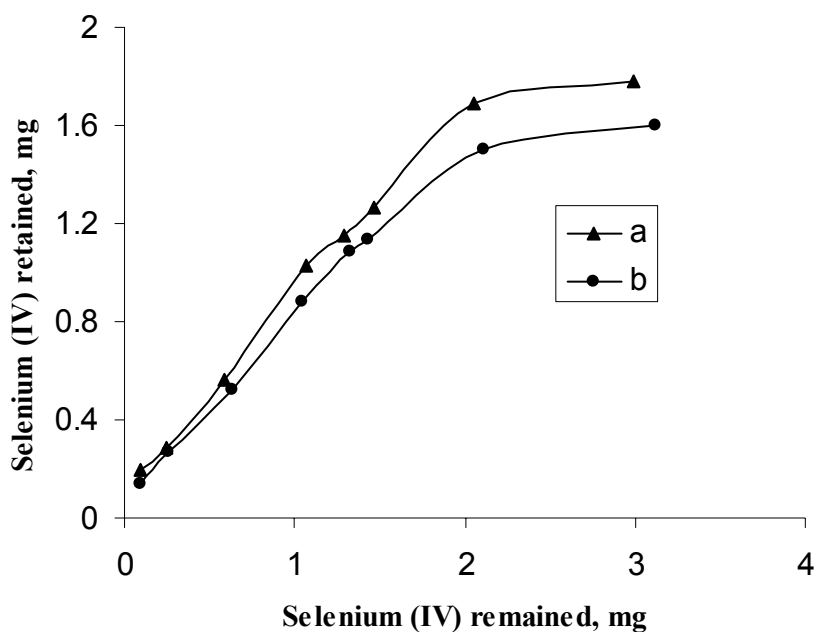


Figure 2. Sorption isotherms of selenium (IV) uptake onto the unloaded (a) and TBP immobilized (b) PUFs from aqueous solutions containing HCl (4.0 M) and KBr (2.0 M) at  $25 \pm 1^\circ\text{C}$

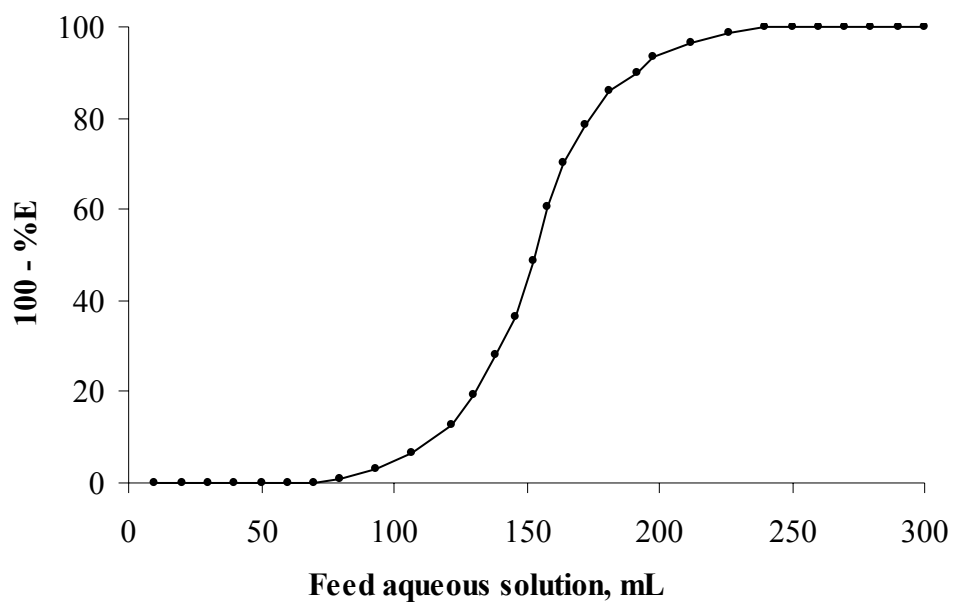


Figure 3. Breakthrough capacity curve of selenium (IV) uptake onto TBP loaded (b) PUFs ( $4.0 \pm 0.01$  g) packed columns at  $5 \text{ ml min}^{-1}$

# One-pot Preparation of $\beta$ -amino Carbonyl Compounds by Mannich Reaction Using MgO/ZrO<sub>2</sub> as Effective and Reusable Catalyst

Nagrik D.M. (Corresponding author)

Department of Chemistry, PLIT and MS

Buldana-443001, M.S., India

Ambhore D.M.

P.G.Department of Chemistry, Jijamata Mahavidyalaya

Buldana-443001, M.S., India

Gawande M.B.

Departamento de Química, Faculdade de Ciências and Tecnologia

Quinta da Torre, 2829-516 Caparica, Portugal

E-mail: dmnnagrik@rediffmail.com

## Abstract

A new one-pot and efficient three-component condensation of aldehyde, ketones, and amines in the presence of MgO/ZrO<sub>2</sub> as an inexpensive and effective catalyst for the synthesis of  $\beta$ -amino carbonyl compounds by Mannich reaction is described. The present methodology offers several advantages, such as good yields, Short reaction times and a recyclable catalyst with a very easy work up.

**Keywords:** Multi-component reaction, MgO/ZrO<sub>2</sub>, Heterogeneous catalyst,  $\beta$ -amino Carbonyl compounds

## 1. Introduction

The synthesis of natural molecules, pharmaceuticals and other nitrogenous biologically active compounds has long been a significant branch of organic synthesis. (B. List, 2002; 2000; R. O. Duthaler, 2003) The Mannich reaction provides one of the most basic and useful methods for the synthesis of such compounds. Multi-component reactions (MCRs) are important for the achievement of high levels of brevity and diversity. They allow more than two simple and flexible building blocks to be combined in practical, time-saving one-pot operations, giving rise to complex structures by simultaneous formation of two or more bonds, according to the domino principle. (Zhu, J., 2005) MCRs contribute to the requirements of an environmentally friendly process by reducing the number of synthetic steps, energy consumption and waste production. Researchers have transformed this powerful technology into one of the most efficient and economic tools for combinatorial and parallel synthesis. (Zhu, J., 2005; Beck, B., 2000) Due to their inherent simple experimental procedures and their one-pot character, they are perfectly suited for automated synthesis.

An amine, two carbonyl compounds and catalysts are used to produce Beta-amino carbonyl compounds (Scheme1)

Beta-amino carbonyl compounds are very useful in pharmaceutical and other biologically related areas of chemistry. One of the many synthetic routes to these compounds is the Mannich reaction which brings together three compounds under appropriate catalytic conditions. These simplified reaction systems fulfill several of the principles of green chemistry including the use of recyclable catalysts and reduced auxiliaries. Mannich reaction is one of the most important C-C bond forming reactions in organic synthesis for the preparation of secondary and tertiary amine derivatives (M. Arend, 1998). These amines are further used for the synthesis of many intermediates, biologically active and natural products such as alkaloids and polyketides. The products of Mannich reaction are mainly  $\beta$ -amino carbonyl compounds and its derivatives that are used for the synthesis of amino alcohols, peptides, and lactams and as precursors to optically active amino acids. The conventional catalysts for classical Mannich reaction of aldehydes, ketones and amines involve mainly organic and mineral acids like proline (B. List, 2002; 2000; R.O. Duthaler, 2003), acetic acid (K. Mogilaiah, 2002),



*p*-dodecylbenzenesulfonic acid (K. Manabe, 2001) and some Lewis acids (S. Kobayashi, 2002; P. Desai, 2000). They often suffer from the drawbacks of long reaction times and harsh reaction conditions, toxicity and difficulty in product separation, which limit its use in the synthesis of complex molecules. Yarahmadi et.al (Hamid Reza Shaterian, 298-313) have synthesized  $\beta$ -amido ketones and esters in four-component condensation reaction using ferric hydrogensulfate as effective and reusable catalyst. Trissa Joseph et.al (Suman Sahoo, 2006) have synthesized  $\beta$ -amino carbonyl compounds by using Bronsted ionic liquids as a solvent and catalyst. Guoying Zhao, Tao Jiang et.al (2004) have carried out Mannich reaction by using ionic liquids as a solvent and catalyst. Gawande M.et.al. (2006) Have synthesized some industrially important and biologically active molecules via MCRs by using MgO/ZrO<sub>2</sub> as catalyst. The use of MgO/ZrO<sub>2</sub> as effective catalyst has not been described for the synthesis of  $\beta$ -amino carbonyl compounds. Therefore we decided to synthesize  $\beta$ -amino carbonyl compounds by using MgO/ZrO<sub>2</sub> as catalyst.

## 2. Experimental

### 2.1 Chemicals

All the aldehydes, ketones, amines, were obtained from S.D. Fine Chemicals, Mumbai, and used without further purification. For Mannich reactions, the aldehydes used were Piperonal (**1a**), *p*-methoxy benzaldehyde (**2a**), 3-chloro-benzaldehyde (**3a**), 3-chloro-benzaldehyde (**4a**) and benzaldehyde (**5a**). The amines included aniline (**1b**), 2-nitroaniline (**2b**) and 4-bromoaniline (**3b**) and the ketones were acetophenone (**1c**) and *p*-hydroxy acetophenone (**2c**).

### 2.2 General procedures for the synthesis of catalyst

In a typical experiment for the preparation of MgO/ZrO<sub>2</sub> with varying mole compositions (0.44:0.56, 0.35:0.65, 0.25:0.75, 0.14:0.86), an appropriate amount of magnesium nitrate[MgO(NO<sub>3</sub>)<sub>2</sub>.6H<sub>2</sub>O] and zirconium oxy chloride[ZrOCl<sub>2</sub>.8H<sub>2</sub>O] were dissolved separately in deionised water and mixed together. Dilute ammonia solution was added dropwise with vigorous stirring until the precipitation was complete (PH=10). The resultant solution was filtered and washed with distilled water till free from chloride ions. The residue was dried for 24 hours at 383K in an oven and further calcined at 873K for 6 hours, in a muffle furnace in air. The % and mole composition of MgO/ZrO<sub>2</sub> are given in following **table 1**

### 2.3 Procedures for Mannich reactions

In a typical experiment, 10 mmol amine, 10 mmol aldehyde, 10 mmol ketone, and 0.35/0.65 Wt. % of catalyst in acetonitrile were loaded into a magnetically stirred glass reactor in a constant temperature water bath at 25 °C. The reaction mixture turned turbid after a certain reaction time and at last became very viscous and close to solid. After reaction, the mixture was washed with distilled water (15 mL) and filtered. The solid product was re-crystallized using ethanol or a mixture of ethanol and benzene and then dried at 50 °C under vacuum until constant weight. The reusability of the catalyst was checked by the reaction of benzaldehyde, aniline and acetophenone in the presence of acetonitrile using 0.35/0.65 Wt.% of MgO/ZrO<sub>2</sub> under reflux condition at 80°C. The results indicate that the catalyst can be used five times without any loss of its activity. (Table: 2)

## 3. Results and discussion

In this article, we wish to report a mild, convenient and efficient protocol for the synthesis of  $\beta$ -amino carbonyl compounds by Mannich reaction using MgO/ZrO<sub>2</sub> as a novel catalyst. First, we optimized the amount of MgO/ZrO<sub>2</sub> as catalyst in the reaction between benzaldehyde, acetophenone, and aniline. The amount of MgO/ZrO<sub>2</sub> was chosen to be 0.35/0.65 Wt. %

(**Table 3**). The most efficient reaction went to completion in 8 hours at 80°C

The Mannich reaction of aldehyde, ketones and amines in presence of MgO/ZrO<sub>2</sub> catalyst is conducted at room temperature and the results are summarized in **Table 4**.

## 4. Conclusions

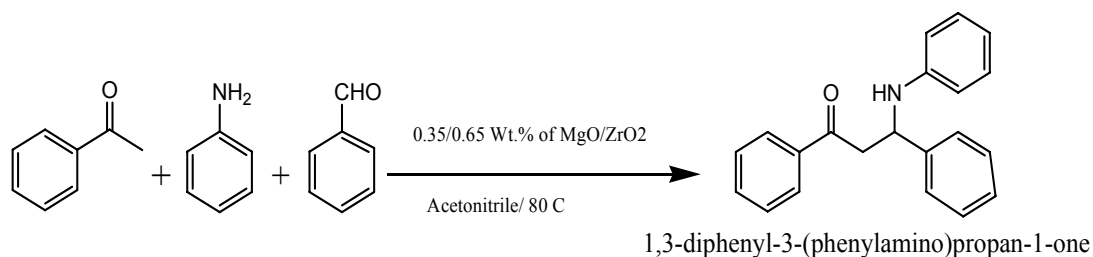
MgO/ZrO<sub>2</sub> has been successfully used as catalyst for Mannich reactions using aldehydes, amines, and ketones. Utilization of this catalyst has several advantages: (1) high yield and high reaction rate can be achieved; (2) the preparation of catalyst is simple; (3) the catalyst can be easily recycled and reused; (4) this protocol provides further examples of the capacity of MgO/ZrO<sub>2</sub> to be fashioned for specific chemical applications. The main contribution of this work is synthesizing MgO/ZrO<sub>2</sub> successfully, which shows a balance between recyclisation and activity for the Mannich reaction.

## Acknowledgements

We are thankful to The Principal, Jijamata Mahavidyalaya, Buldana (M.S.) India, The Head, P.G.Dept. of Chemistry, Jijamata Mahavidyalaya, Buldana (M.S.), India, for providing necessary laboratory facilities. The main author (DMN) is thankful to his mother for her inspiration and moral support.

## References

- B. List, P. Pojarliev, W. T. Biller and H. J. Martin. (2002). *J. Am. Chem. Soc.*, 124, 827.
- B. List. (2000). *J. Am. Chem. Soc.*, 122, 9336.
- Beck, B., Hess, S., Dömling, A. (2000). *Bioorg. Med. Chem. Lett.*, 10, 1701.
- Guoying Zhao, Tao Jiang, Haixiang Gao, Buxing Han, Jun Huang and Donghai Sun. (2004). *Green Chem.*, 6, 75-77.
- Hamid Reza Shaterian, Hossein Yarahmadi, and Majid Ghashang, *ARKIVOC (xvi)* 298-313.
- K. Manabe, Y. Mori, S. Kobayashi. (2001). *Tetrahedron*, 57, 2537.
- K. Mogilaiah, G. Kankaiah. (2002). *Indian J. Heterocycl. Chem.*, 11, 283.
- M. Arend, B. Westermann, N. Risch, *Angew. (1998). Chem., Int. Ed. Engl.*, 37, 1044.
- M.B. Gawande, R.V. Jayaram. (2006). *Catalysis Communications*, 7, 931-935.
- P. Desai, K. Schildknegt, K.A. Agrios, C. Mossman, G.L. Milligan, J. Aube. (2000). *J. Am. Chem. Soc.*, 122, 7226.
- R. O. Duthaler, *Angew. (2003). Chem. Int. Ed.*, 42, 975.
- S. Kobayashi, T. Hamada, K. Manabe. (2002). *J. Am. Chem. Soc.*, 124, 5640.
- Suman Sahoo, Trissa Joseph, S.B. Halligudi. (2006). *Journal of Molecular Catalysis A Chemical*, 244, 179-182.
- Zhu, J., Bienayme, H. (2005). *Multicomponent Reactions*; Wiley.



Scheme 1.

Table 1. Mixed oxides of MgO/ZrO<sub>2</sub>

Entry	Mixed oxides of MgO/ZrO <sub>2</sub>		
	MgO Wt%	ZrO <sub>2</sub> Wt.%	MgO/ZrO <sub>2</sub>
1	5	95	0.14/0.86
2	10	90	0.25/0.75
3	15	85	0.35/0.65
4	20	80	0.44/0.56

Table 2. Recyclability of the catalyst in the reaction of benzaldehyde, aniline and acetophenone in the presence of acetonitrile using 0.35/0.65 Wt.% of MgO/ZrO<sub>2</sub> under reflux condition at 80°C

Run no.	Yield (%)
1	91
2	90
3	89
4	87
5	87

Table 3. Reaction of Benzaldehyde, acetophenone, and aniline using various amounts of MgO/ZrO<sub>2</sub> under reflux condition at 80°C

Entry	MgO/ZrO <sub>2</sub> (Wt.%)	Time/h	Yield%
1	0.14/0.86	12	77
2	0.14/0.86	16	85
3	0.35/0.65	8	91
4	0.44/0.56	12	81
5	0.14/0.86	13	79

Table 4. Three-component Mannich reactions of aldehydes, amines, and ketones in the presence of MgO/ZrO<sub>2</sub> catalyst at 25 °C

Entry	Aldehyde	Ketone	Amine	Time/h	Yield (%)
1	1a	1c	1b	08	91
2	2a	1c	1b	08	66
3	3a	1c	1b	05	62
4	4a	1c	1b	04	31
5	5a	1c	1b	12	89
6	1a	1c	2b	12	67
7	2a	1c	2b	12	54
8	3a	1c	2b	12	87
9	4a	1c	2b	12	81
10	5a	1c	2b	12	83
11	1a	1c	3b	12	0

# The Effect of Gel and Pressure Induced Flow (PIF) Processing Conditions on the Dispersion and Intercalation of MMT Nanoclay in UHMWPE/ Montmorillonite (MMT) Clay Based Nanocomposite Sheets

Musa E. Babiker, Zhang Sen, Tang Yi Fei, Guangcheng Wang & Yu Muhuo (Corresponding author)

State Key Laboratory for Modification of Chemical Fibers & Polymer Materials

College of Material Science & Engineering, Donghua University

Shanghai, P.O. Box 201620, China

Tel: 86-139-0175-9052 E-mail: yumuhuo@dhu.edu.cn

## Abstract

The paper analyzes the effect of gel and pressure induced flow processing on the dispersion and intercalation of MMT nanoparticles. To reach our objective, we conducted various experiments for the preparation of dispersed nanoclay in nanocomposite sheets based on the preparation of UHMWPE gel sheet with MMT through the use of paraffin oil (solvent) and then removed the solvent utilizing PIF and extraction processes. The analysis of the UHMWPE microstructure sheet by X-Ray diffraction (XRD); transmission electron microscopy (TEM); Scanning electron microscope (SEM); and differential scanning calorimetry (DSC) was done as well. Our results highlight that good dispersion, partial exfoliation and full intercalation of MMT nanoparticle effective; that intercalated nanocomposites and the different layers correspond to flexibility chains and the presence of multi-peaks are due to the processing of different materials. The images obtained by SEM present a gel-like layers structure of UHMWPE/MMT sheet is the consequence of the deformation and re-arrangement of the gel sheets during PIF process.

**Keywords:** UHMWPE/MMT clay nanocomposites sheet, Gel process, Pressure-induced flow, Dispersion

## 1. Introduction

Since the last two decades, there has been revolutionary progress in the field of nanocomposite and microscale materials. Clay-Polymer nanocomposites as one of these materials has recently attracted researchers and professionals, attention as they enhance mechanical and thermal properties when compared to conventional materials. Because of their properties, the nanocomposite materials present a wide range of applications depending upon the type of inorganic material that is present in the polymers. The progress of polyolefin-clay nanocomposites is an interesting field of materials that is growing rapidly. These materials have a basic role of enhancing mechanical and physical properties in comparison with the pure polymer Alexandre et al. (2000). When those materials are processed by gel and pressure induced flow processes, better properties are expected.

In the past decade, preparation of dispersed, intercalated and exfoliated MMT clay with HDPE nanocomposites have emphasized experimental studies of their morphology and mechanical properties (Tanniru et al. 2006; Min et al. 2006) to reveal that it has been reported that strengthening of HDPE with MMT clay platelets will improve the morphology and mechanical properties of HDPE compared with the pure PE. Quang et al. (2007) improved a new technique for exfoliating and dispersing nanoclay particles into polypropylene matrices using supercritical carbon dioxide. This method relies on rapid expansion of the clay followed by direct injection into the extruder where the mixture is dispersed into the polymer melt. The nanocomposites showed more effective than conventional composites in reinforcement when the montmorillonite clay modified by using the reactive intercalating agent and the PE/clay nanocomposites were then prepared by melt intercalation method. Zhao et al. (2005)

In general, the most serious factor that governs the final development in the morphology properties of polymer/MMT clay nanocomposites is the level of dispersion, exfoliation and intercalation of the nanoclay in the nanocomposite structure. Hotta et al. (2004) studied the melt compounding of many different organoclays into linear low density polyethylene and established that clay loading resulted in increase in modulus and the clay was largely exfoliated. Homminga et al. (2005) stated that the intercalation and exfoliation of the clay are largely accelerated in the presence of flow. However, a negative effect of the screw speed on exfoliation was also

observed in the specific case of a polybutadiene/organoclay system. Sarashi et al. (2003) acknowledged that the intercalation of MMT clay with styrene and butadiene monomer before polymerization. Only partial achievement has been achieved in compounding organo-MMTs with styrene-butadiene rubber to prepare rubber nanocomposites. Knudson et al., (2002) discovered that flocculation of the aqueous blend of styrene-butadiene latex and MMT clay gives an exfoliated clay-rubber nanocomposite. The approach offers the most convenient and effective method for the preparation of clay-styrene-butadiene rubber nanocomposites. Researchers (see for instance Sadhu et al. 2004) have shown that the styrene-butadiene rubber dissolved into toluene (as a polymer solution) and organically treated and untreated MMT was dispersed into the polymer solution. The organoclays was prepared by the exchange of octadecyl amine. The toluene was removed by evaporation. The untreated clay was intercalated with polymer; the organically treated clay was fully exfoliated. The exfoliated rubber nanocomposite has significantly improved mechanical properties when compared to the intercalated rubber nanocomposite. Both rubber composites had superior mechanical performance when compared to the pure rubber. Mousa et al. (2001) observed that the same organoclays that was utilized in Sadhu et al. (2004) was compounded with styrene-butadiene. The rheology of the polymer nanocomposite highlighted shear rate thinning behavior. This is common with MMT dispersed systems. The mechanical properties were as predicted except the increase in percent elongation to failure as a function of clay loading. The percent elongation to failure increased along with modulus and tensile strength. This is not expected or predicted by standard reinforcing theories. Ganter et al. (2001) argued that the organoclay-styrene-butadiene rubber nanocomposites by dispersing the rubber and organoclay in toluene and evaporating the solvent to prepare the rubber nanocomposite. For Federica et al. (2008) they stated that the exfoliation and dispersion of the clay in polymer nanocomposites depend on several factors such as the nature of the polymer, the nature of the clay, the type, packing density, and the size of the organic modifier on the silicate layers. Yong et al. (2007) affirmed that the influence of nanoclay on properties of HDPE/Wood composites by two steps; melt compounding and then injection molding. Yang et al. (2008) acknowledged that the dispersion polymerization based on stabilization by nano-platelets is achieved without using any other conventional stabilizers.

### *1.1 Pressure Induced Flow (PIF) Process*

PIF gel sheet technique is a simple method to prepare thin, flexible sheets and composite based upon pressure and removal of the solvent. The process is based on subjecting the gel sheet in a swelling state under pressure. However, the re-arrangement of the gel molecules is effective because of the removal of solvent from the gel sheet. The thin and highly tuning gel sheet can be precisely controlled to achieve optimized gel sheet properties. Gonzalez et al. (2003) highlighted different aspects of fabricating plastic materials by PIF process. When this material is placed under pressure, the rigid plastic starts to dissolve into the soft region, creating a mixture that can flow like slurry of ice and water, which enables the material to be molded into an object. When the pressure is released, the plastic re-hardens, which indicated that the pressure was enough to make a polymer designing act like a fluid. Bartczak et al. (1996; 2005) observed the advantages from the plane-strain compression in a channel die for applying such a mode of deformation is that the deformation is homogeneous in the whole range of the strain without necking or local instabilities, and avoids internal cavitations and related artifacts. Besides, the channel die plane-strain compression is kinematically identical to plane-strain tension, which results in one direction flow of the polymer in plane-strain conditions. The use of a deep channel-die is the approach to produce samples by compression in such a die is relatively large, sufficient for other experiments. After compression, the structure and orientation produced by plastic deformation in such large specimens could be investigated.

## **2. Experimental**

### *2.1 Materials*

The UHMWPE used in this study was supplied by Celanese (China) Holding Co. Ltd with ( $M_w = 5 \times 10^6$  kgmol<sup>-1</sup>,  $M_w/M_n = 8$ ) and was used as received. Organo-MMT clay was supplied by Zhejiang Fenghong clay chemicals Co. Ltd, (China), with average lamellar thickness less than 25nm; mean diameter nm 25X1000; content montmorillonite 95-98%, and density 1.8g/cu.cm. Paraffin oil (Shanghai- China), density (20°C) is 0.835-0.855 g/ml, and boiling point at 340°C. Oxidative degradation of the polyethylene was prevented by mixing all solutions with 0.5 wt % (weight of paraffin oil) of antioxidant 2, 6-Di-tert-butyl-p-cresol M. p 69~71°C. And N-hexane with density (20°C) is 0.6583~0.6613 g/ml, and refractive index 1.3741~1.3761.

### *2.2 Sample Preparation*

For the gel-processing, 6 samples were prepared using the materials listed in Table 1. The recipe was dissolved in a beaker (250 ml) with paraffin oil at 120°C followed by hand stir to distribute the material in the solvent and

to prevent generation of bubbles. When the temperature reached 130 – 135 °C, a white solution of UHMWPE gel was formed; the stirred was stopped and the solutions were stored at 150°C for 48 hours and subsequently cooled slowly to room temperature.

Insert Table 1 about here

### 2.3 PIF experiments

PIF was designed as a mini-mold apparatus in this study. The PIF stages were performed using the weighting as a compression tool. Four types of different size and geometry were used in this study. As shown in Fig. 1. The first apparatus (Fig. 1(a)) was a mini-mold with 120 mm width (w2) for the mould, 40 mm wide (w1) as (a long constrained direction, CD), 250 mm long (along flow direction, FD) and 50 mm deep (along loading direction, LD), allowing samples up to 40 mm high (i.e. dimension along LD) to be compressed with that mini-mold. The difference between the two deeps (d1-d2) is equal to the thickness of the sheet, where, the extensions of the material along flow direction and constrain direction show the length and the wide of the sheet. This apparatus allows the sample to flow only along the flow direction (FD). The second apparatus (Fig. 1(b)) was a set of a square mould with 120 width and length. This apparatus enhances the sample to flow in two directions (FD1 and FD2). The third apparatus (Fig. 1(c)) was similar to the first apparatus (Fig. 1(a)) but small in size, weight and dimensions. The fourth apparatus (Fig. 1(d)) was similar to the first apparatus (Fig. 1(b)) but small in size, weight and dimensions.

<Figure 1>

The advantage of a deep mould is that the samples produced by compression in such a mould are relatively large, so that the structure and orientation produced by plastic deformation and the macroscopic recovery behavior could be studied easily. Due to a large lateral surface area of the sample, friction forces between the sample and mould could not be neglected, which resulted in overestimation of the stress. That was the case when the sample placed on the mould was accurately weighted prior to compression. The size of specimens used in apparatus (Fig. 1(a)) was 3.9x50x35 mm<sup>3</sup> (along CD, FD and LD, respectively), while the square apparatus (Fig. 1(b)) was 5x 6x4 mm<sup>3</sup>, the apparatus (Fig. 1(c)) was 12.5x5x17 mm<sup>3</sup> (CD, FD, and LD, respectively), and the apparatus (Fig. 1(d)) was 4x3x3 mm<sup>3</sup>. All PIF experiments were performed as shown in Fig.2 at a constant load and at room temperature for 1 to 25 days. The residual paraffin oil was extracted by N-hexane at room temperature for 1 hour repeated many times until extraction reached equilibrium state.

<Figure 2>

## 3. Characterizations

### 3.1 Calorimetric measurements

The differential scanning calorimetry DSC measurements were carried out using a Perkin-Elmer Diamond DSC Differential Scanning Calorimeter controlled by a Thermal Analyst 2000 system. Typical sample weights used were approximately 4mg and were placed in sealed Aluminum pans. The heating/cooling rate of 10°C/min was applied and upper temperature ranges of 40 – 190°C were selected. Prior to use, the calorimeter was calibrated with Indium standard (Mp 156.5°C). An empty Aluminum pan was used as a reference. The specimens were tested in Nitrogen as an inert gas with flow rate 20.0ml/min.

### 3.2 Transmission Electron Microscopy (TEM)

The transmission electron microscopy of the UHMWPE/MMT gel sheets observations were conducted on a Hitachi H – 800 (Japan) operated at an accelerating voltage of 200 KV. Ultra-thin sections (60–80 nm in thickness) were obtained at room temperature cryogenic environment using a Reichert–Jung Ultracut E microtome with a diamond knife. The Samples for TEM analysis were cut parallel to the LD–FD plane, as depicted in Fig.1. The thin sections were then put on the 100-mesh Formvar/carbon coated copper grids for TEM observation.

### 3.3 Scanning electron microscopy (SEM)

The scanning electron microscopy (SEM) cryogenically fractured surfaces of the UHMWPE/OMMT gel sheets were observed by S-3000N type scanning electron microscopy Hitachi, Japan. The SEM samples were gold sputtered prior to observation.

## 4. Results and Discussion

### 4.1 X-Ray Diffraction

Polymer/clay nanocomposites are formed by the insertion of polymer chains between the clay layers. Practically,

it is difficult to define nanocomposite structures by a single measurement. The most common method to obtain structural information is X-ray diffraction (XRD). XRD can be used to measure the interlayer spacing distance ( $d$ ) between clay layers.

The WXR patterns of samples are given in Fig. 3. The diffraction patterns of UHMWPE/MMT with different MMT contents are the same.

Insert Figure 3 about here

To study their crystal structure, peak-fit analyzing software was used to obtain a series of crystal parameters, namely, interplanar space ( $d$ ), half-width ( $b$ ), apparent crystal size ( $L_{hkl}$ ) to mention a few. The degree of crystallinity ( $X_c$ ) are given by the equation as follows:

$$X_c = 1 - \frac{A_a}{A_c + A_a} \quad (1)$$

Where  $A_a$  and  $A_c$  are the areas of the amorphous and the total crystal peaks.

The interplanar spacing ( $d$ ) and apparent crystal size ( $L_{hkl}$ ) values for the different peaks can be calculated by Bragg's law and Scherrer's formula (1969), respectively.

$$d = \frac{\lambda}{2 \sin \theta} \quad (2)$$

$$L_{hkl} = \frac{k' \times \lambda}{\beta_o \times \cos \theta} \quad (3)$$

$$\beta_o = \sqrt{\beta^2 - b_o^2} \quad (4)$$

<Table 2>

Table 2 shows that most XRD results of the MMT in UHMWPE/MMT have been partially exfoliated in the nanocomposites. As the content of Org-MMT increases, there are also some intercalated structures lying in the composites, which are caused by the weak peaks appearing on the XRD pattern. The partially exfoliated and intercalated of the MMT clay indicate that the MMT was dispersed inside the UHMWPE/MMT nanocomposite.

#### 4.2 DSC results

The degree of crystallinity ( $X_c$ ) was calculated using the following equation:

$$X_c = \frac{H_{mc}}{H_o} \times 100\% \quad (5)$$

Where:  $X_c$  is the degree of crystallinity %

$H_{mc}$  is the melting enthalpy of crystallization of HDPE (J/g)

$H_o$  is the standard melting enthalpy of crystallization of HDPE (J/g)

In practice, the heat of fusion of pure crystalline polyethylene is taken to be in the range of 276.15- 292.88 J/g, with a commonly accepted value of 288.70 J/g Flory (1963). The degree of crystallinity and the peak melting temperature determined from DSC for the first run are summarized in Table 3, Figs. 4 and Figs. 5. The degree of crystallinity decreased slightly for the UHMWPE gel sheet with the increase of MMT clay percent. A small variation is observed for the melting temperature of the samples. The difference in the degree of crystallinity estimated from DSC reflects the differential result of MMT clay content on the crystalline phase, interface, and amorphous phase. Table 3 presents the crystalline percent for UHMWPE 4% - 5% and MMT clay 0%, 10% and 20%. The increase of MMT clay content resulted in a 10.3%, 18.7%, and 27.2% decrease in the crystalline for UHMWPE 4% and 14.5%, 13.1%, and 25.9% for UHMWPE 5% where the increase of UHMWPE from 4% - 5% and 0%, 10%, and 20% MMT clay resulted in a 9.3%, 4.9%, and 10.9% increase in the crystalline respectively.

Insert Table 3, Figure 4 and Figure 5 about here

Fig.4 and Fig.5 present the DSC melting thermograms of pure UHMWPE 4%, 5%, and UHMWPE 4%, 5% with

10%, 20% MMT clay, processed in the same conditions. The thermograms of the UHMWPE 4% and 5% specimen show the melting peak ( $T_m$ ) at 133.6°C and 131.8°C respectively. The temperature of the melting of the component in blends increased slightly compared to the pure UHMWPE. The above changes demonstrate that the presence of MMT clay in the nanocomposite markedly influences the crystallization and the thermal behavior of the UHMWPE component.

#### 4.3 TEM results

TEM results for the UHMWPE/MMT clay nanocomposite sheets are shown in Fig.7 and Fig.8. They provide some direct evidence of MMT clay nanoparticles dispersion in the nanocomposite. The exfoliated and intercalated MMT clay nanoparticles are almost parallel to one another and they are highly aligned along the flow direction and parallel to the part surface as in shown in Fig.6. Some MMT clay nanoparticles started to deviate from being aligned with the flow direction as depicted in Fig.7. The difference in the degree of planar orientation between the surface and the inner layers becomes more noticeable. It is clear that the MMT clay nanoparticles were less aligned orderly along the flow direction in the nanocomposite. This is may be due to the effect of the quench of paraffin oil and extension during PIF and extraction stages.

<Figure 6 and Figure 7>

The TEM images (Fig. 7) of UHMWPE/MMTclay nanocomposite sheets confirmed the presence of the exfoliated structure and the good dispersion of the MMT clay nanoparticles in the nanocomposite. The TEM image of UHMWPE/MMT clay (Fig.8) confirmed the SEM results in term of showing a significant degree of intercalation between the silicate layers in the nanocomposite. Similar results have been obtained by (Filippi et al, 2007; Ali et al, 2007; Asim et al, 2005; Quang et al, 2007; Fang et al, 2007; Periyayya et al, 2005) when using MMT clay to prepare nanocomposite utilizing different materials and processes. At a higher content of MMT clay nanoparticles, a complete and effective entry of monomers into the organically modified silicate layers is very difficult Theng (1979). The TEM can present more direct information on morphology in real space. All the TEM images for the both contents of MMT clay nanoparticles show an intercalated structure.

<Figure 8>

#### 4.4 Scanning Electron Microscopy (SEM) results

Figs (9, 10, and 11) present SEM micrographs of the fracture surface of UHMWPE/MMT clay nanocomposites processed using gel and PIF processes, respectively, for MMT clay content of 10% and 20% and UHMWPE content of 4% and 5%. The differences in scattering densities of MMT clay and UHMWPE facilitate differentiation of MMT clay aggregates, their characteristics and distribution. These micrographs provide important insights concerning MMT clay distribution, intercalation, and exfoliation, and help in better understanding the processing-structure property relationships. The fracture surfaces of pure UHMWPE specimens Fig.9 (a, b) revealed that the UHMWPE chains were high fully aligned along the flow direction, and a river-line markings, which can affect the crystallinity of the UHMWPE gel nanocomposite sheet.

<Figure 9>

Fig.10 shows the micrographs of the fracture surface of UHMWPE/MMT clay nanocomposites for MMT clay content of 10% and UHMWPE content of 4% and 5%, which highlight that the UHMWPE/MMT clay nanocomposite sheets were intercalated, exfoliated and the MMT clay nanoparticles was dispersed as in Fig.6. Also many voids were observed due to the removal of paraffin oil during the PIF and extraction processes.

<Figure 10>

Fig.11 shows the micrographs of the fracture surface of UHMWPE/MMT clay nanocomposites for MMT clay content of 20% and UHMWPE content of 4% and 5%, which exhibited a gel-like layer, and many voids between these layers. Fig.11 confirms that the increase of MMT clay content revealed a structure having large clay aggregates, which perform as stress concentrators hence, increases the amount of the oriented lamellar in the SEM images, decreases the degree of crystallinity and increases the melting temperature in the DSC images. In contrast, the samples containing 20% MMT clay permitted the intercalation, exfoliation and dispersion of MMT clay.

Insert Figure 11 about here

### 5. Conclusion

This study provided evidence that a significant and challenging task in understanding the advantages of the addition of MMT nanoclay into UHMWPE lies in ensuring the uniform dispersion of the high aspect ratio crystal-like platelets in the UHMWPE/MMT clay nanocomposites. XRD and TEM indicate that the MMT



dispersed randomly, intercalated and exfoliated partially UHMWPE/MMT clay nanocomposites were successfully achieved using two methods gel and PIF processes. The rheological properties of UHMWPE/MMT clay nanocomposites were affected by the content and the degree of dispersion of the MMT clay nanoparticles. With the increase of MMT clay nanoparticles content, fully dispersed UHMWPE/MMT clay nanocomposites with good nanoscale intercalation of clay platelets showed remarkable improvements in rheological over their unfilled base material at very small levels of clay (10–20 wt %), when compared with those containing mixtures of aggregated and intercalated clay. The addition of MMT clay nanoparticles decreased the melting temperature and crystallization degree of the UHMWPE/MMT clay nanocomposites.

### Acknowledgements

The research is financed by National Natural Science Foundation of China (Grant No. 50833002).

### References

- Alexander L. E. (1969). X-ray diffraction methods in polymer science, Wiley, New York
- Alexandre M., Dubois P. (2000). Poly layered silicate nanocomposite preparation, properties and uses of a new class of materials. *Mater. Sci. & Eng.*, 28, 1–63.
- Ali D., Maybelle W., Ahmet K., Christopher W. M., Michael T. (2007). Intercalated (LLDPE)/clay nanocomposites prepared with oxidized polyethylene as a new type compatibilizer: Structural, mechanical and barrier properties. *European Polymer Journal*, 43, 3737–3749.
- Asim P., Sadhan C. Jana. (2005). Synthesis of thermoplastic PE nanocomposites of reactive nanoclay by bulk polymerization methods. *Polymer*, 46, 3275–3288.
- Bartczak Z., Krasnikova N. P., & Caleski A. (1996). Morphology and texture of HDPE/PS blends deformed by plane strain compression. *J. of Appl. Polymer Science*, 62, 167–179.
- Bartczak Z., & Lezak E. (2005). Evolution of lamellar orientation and crystalline texture of various polyethylenes and ethylene-based copolymers in plane-strain compression. *Polymer*, 46, 6050–6063
- Fang Z. P., Xu Y. Z., Tong L. F. (2007). Effect of clay on the morphology of binary blends of Polyamide 6 with HDPE and HDPE graft Acrylic Acid. *Polym. Eng. and Sci.*, 551–559.
- Federica B., Andrea T., Andreas L., Doris P., Alberto F., Giuliano T., & Giovanni C. (2008). Intercalation degree in PP/organoclay nanocomposites role of surfactant structure. *Polymers for Advanced Technologies*, 19, 547–555.
- Filippi S., Elena M., Cristina M., & Pierluigi M. (2007). Comparison of solution blending and melt-intercalation for the preparation of poly(ethylene-co-acrylic acid)/organoclay nanocomposites. *European polymer Journal*, 43, 1645–1659.
- Flory P.J., Vrij A. (1963). Melting points of Linear-chain homologs: The normal paraffin hydrocarbons. *Journal of American Chemical Society*, 85, 3548.
- Ganter M., Gronski W., Riechert P., & Mulhaupt R. (2001). Rubber nanocomposites: Morphology and mechanical properties of BR and SBR vulcanizates reinforced by organophilic layered silicates. *Rubber Chemistry and Technology*, 74, (2), 221–235.
- Gonzalez L., J. A., M. H. Acar, S. W. Ryu, Ruzette A. V. G., Mayes A. M. (2003). Low temperature processing of baroplastics by pressure induced flow. *Nature*, 426, 424 - 428.
- Homminga D., Goderis B., Hoffman S., Reynaers H., & Groeninckx G. (2005). Influence of shear flow on the preparation of polymer layered silicate nanocomposites. *Polymer*, 46, 9941.
- Hotta, S., & Paul, D. R. (2004). Nanocomposites formed from linear low density polyethylene and organoclays. *Polymer*, 45, 7639–7654.
- Knudson M. L., Powell C. (2002). P. C. T. Int. Pat. WO: 02/070589 A2.
- Min K.D., Kim M.Y., Choi K. Y., Lee J. H. & Lee S. G. (2006). Maleated and non-maleated PE–MMT layered silicate blown films: creep, dispersion and crystallinity. *Polymer Bulletin*, 57, 101–108.
- Mousa A., Kocsis J.K. (2001). Rheological & thermodynamical behavior of Styrene/Butadiene Rubber Organoclay Nanocomposites. *Macromolecular Material and Engineering*, 286, (4): 260–266.
- Osman M.A., Jörg E.P. R. (2005). Interfacial interactions and properties of PE layered silicate nanocomposites. *Macromolecular Rapid Communications*, 26, 880–884.

- Periyayya U., Yoon B. H., Kee S. N., & Youn S. L. (2005). Exfoliated high- impact PS/MMT nanocomposites prepared using anchored cationic radical initiator MMT hybrid. *European Polymer Journal*, 41: 1582–1588.
- Quang T. N., & Donald G. B. (2007). An improved technique for exfoliating and dispersing nanoclay particles into polymer matrices using supercritical carbon dioxide. *Polymer*, 48, 6923–6933.
- Sarashi H. (2003). *Japan Patent* No. JP: 2003327751.
- Sadhu S., & Bhowmick A. K. (2004). Preparation and properties of nanocomposites based on Acrylonitrile–Butadiene Rubber, Styrene–Butadiene Rubber, and Polybutadiene Rubber. *Journal of Polymer Science Part B: Polymer Physics*, 42, 1573–1585.
- Tanniru M., Yuan Q. & Misra R.D.K. (2006). On significant retention of impact strength in clay reinforced (HDPE) nanocomposites. *Polymer*, 47, 2133–2146.
- Theng B. K. G. (1979). *Formation and Properties of Clay Polymer Complexes*. New York: Elsevier,
- Yang J. X., Tom H., Wang W. X., Jun L., Brown P., Martyn P., Lesterb E., & Steven M. H. (2008). Preparation of hybrid polymer nanocomposite microparticles by a nanoparticle stabilized dispersion polymerization. *Journal of Materials Chemistry*, 18: 998–1001.
- Yong L., Wu Q. L., Craig M. C., Fei Y., Xu Y. J. (2007). Influence of nanoclay on properties of HDPE/Wood Composites. *Journal of Applied Polymer and Science*, 106: 3958–3966.
- Zhao C. G., Qin H. L., Gong F. L., Meng F., Zhang S. M., Yang M. S. (2005). Mechanical, thermal and flammability properties of polyethylene/clay Nanocomposites. *Polymer Degradation and Stability*, 87: 183-189.

Table 1. Materials used in this study

Material Samples	UHMWPE wt%	MMT Clay wt% out of UHMWPE wt %	Paraffin Oil wt%	Anti Oxidant wt%
1	4	0	95.55	0.45
2	4	10	95.025	0.4775
3	4	20	95.525	0.4725
4	5	0	94.50	0.45
5	5	10	94.0275	0.4725
6	5	20	93.53	0.47

Table 2. XRD results of UHMWPE and its nanocomposite samples

Sample	2 $\theta$	d-spacing (nm)	difference	Crystallinity%
OMMT	19.72	3.01	–	–
4Pure%	19.20	4.17	1.16	52.34
5Pure%	19.22	4.21	1.20	55.73
4/10%	19.19	4.54	1.53	54.43
5/10%	19.36	4.52	1.51	58.52
4/20%	19.34	4.60	1.59	56.35
5/20%	19.34	4.62	1.61	58.70

Table 3. DSC crystallinity and melting temperature of UHMWPE and its nanocomposite samples

Samples	4%			5%		
MMT clay %	0	10	20	0	10	20
Crystallinity %	65.8	64.4	52.3	69.2	67.7	58.7
Melting temperature	124.692	133.608	126.323	121.55	131.788	130.844

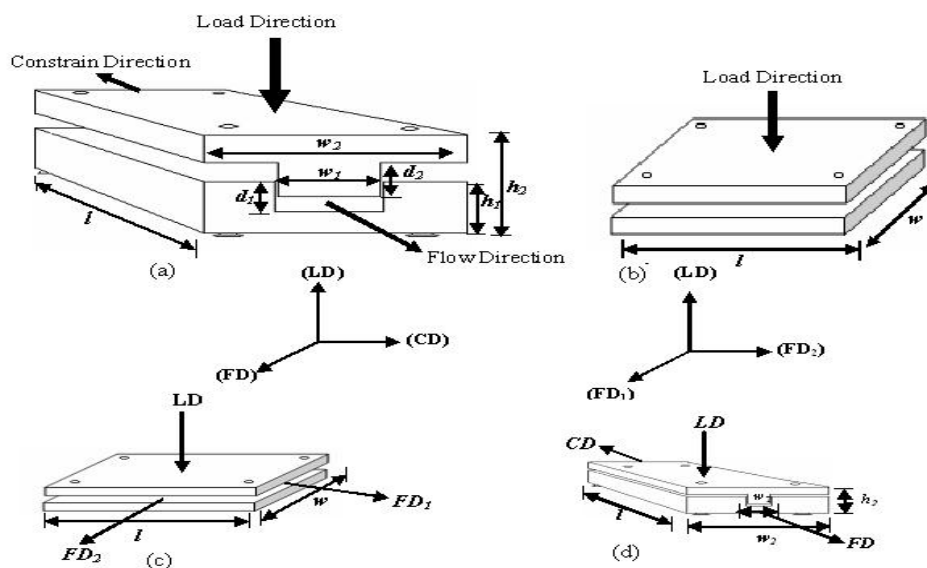


Figure 1. Illustration of the types of a mini-mold apparatus

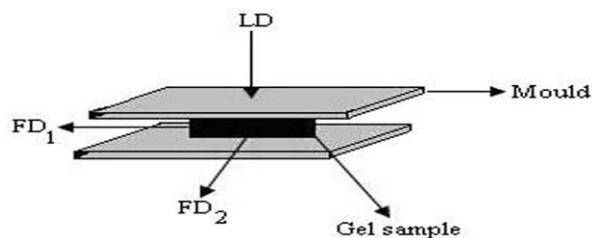


Figure 2. The PIF process of the UHMWPE gel sheet

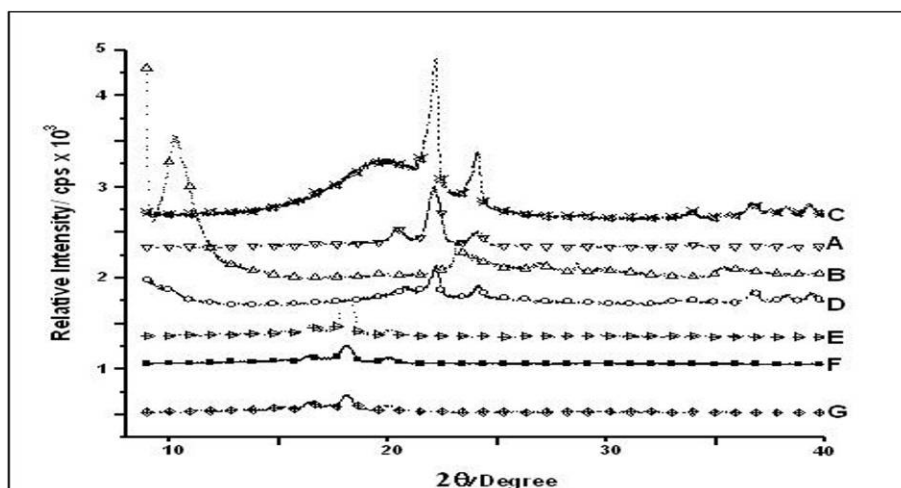


Figure 3. The XRD patterns of UHMWPE and its nanocomposite samples: (A) OMMT (B) 4% Pure (C) 5% Pure (D) 4/10% (E) 5/10% (F) 4/20% and (G) 5/20%

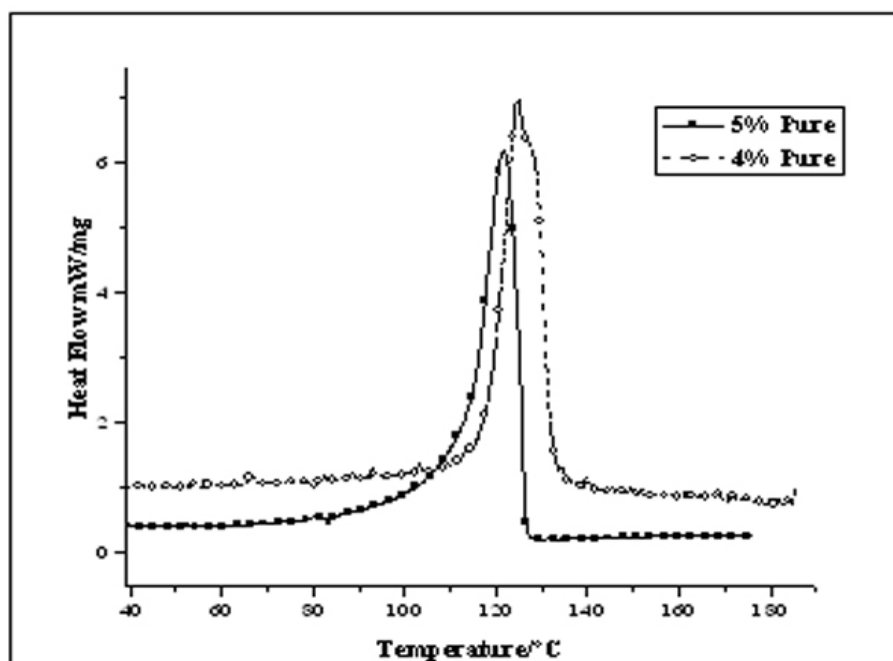


Figure 4. The DSC of 4% and 5% UHMWPE pure

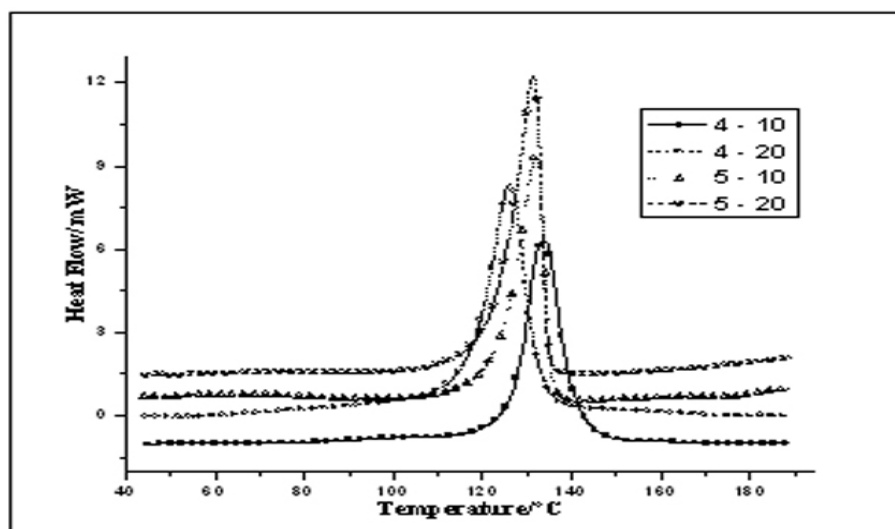


Figure 5. The DSC of 4% and 5% UHMWPE with 10% and 20% MMT clay

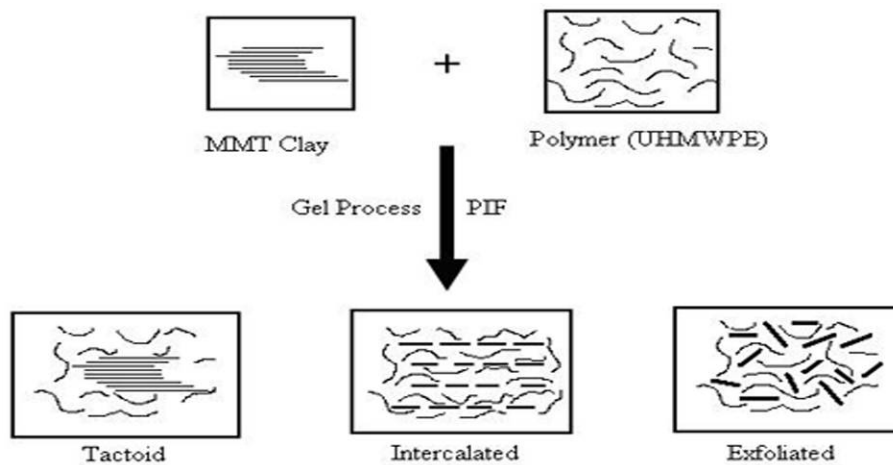


Figure 6. Schematic illustration of Intercalation and Exfoliation of UHMWPE nanocomposite

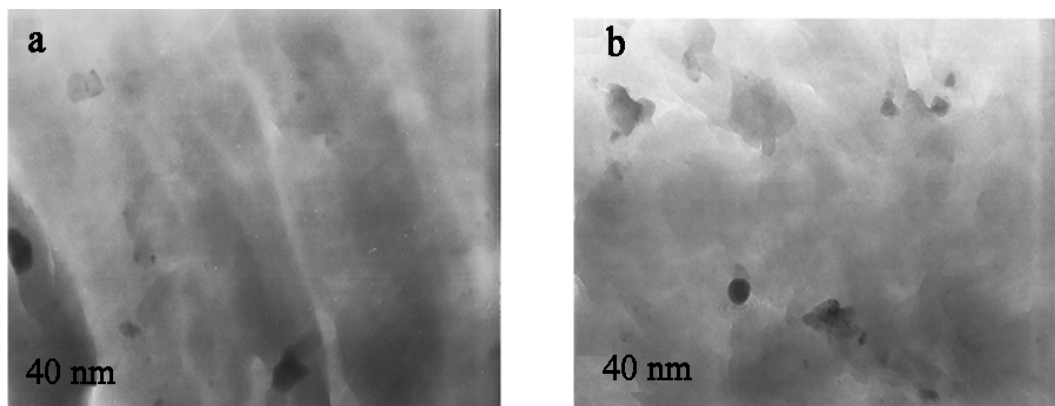


Figure 7. TEM micrographs of UHMWPE /montmorillonite clay nanocomposite with contents of 10% MMT clay and (a) (UHMWPE 4/10 %), (b) (UHMWPE 5/10%)

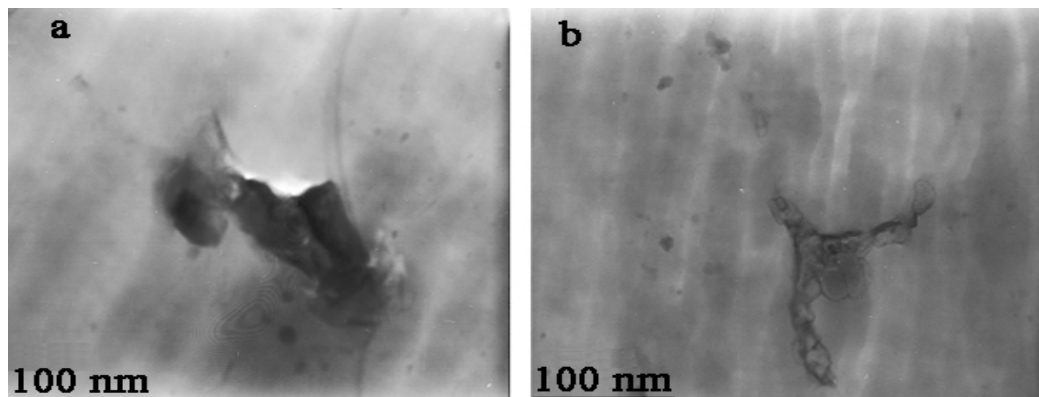
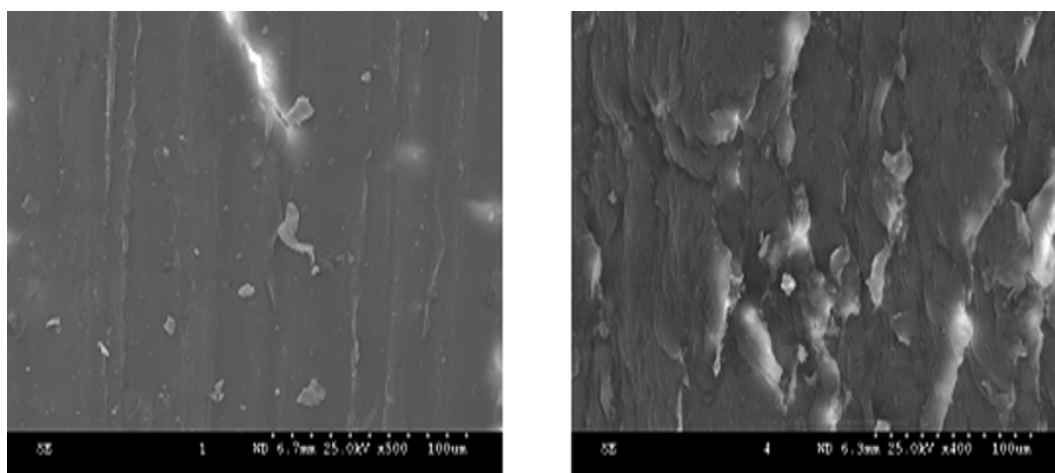


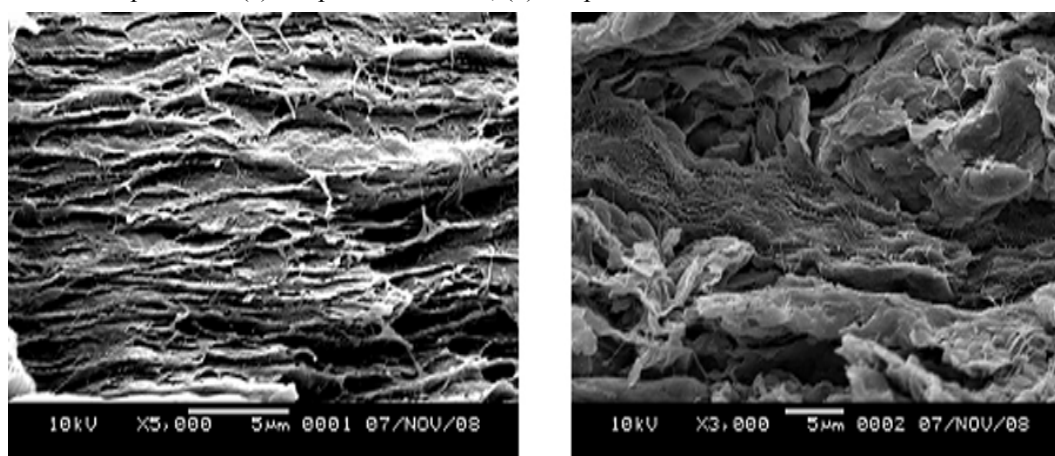
Figure 8. TEM micrographs of UHMWPE/MMT clay nanocomposite with contents of 20% MMT clay and (a) (UHMWPE 4/20 %), (b) (UHMWPE 5/20%)



(a)

(b)

Figure 9. SEM micrographs of fracture surface of pure UHMWPE nanocomposite fabricated by gel and PIF processes (a) 4% pure UHMWPE, (b) 5% pure UHMWPE volume fractions



(a)

(b)

Figure 10. SEM micrographs of fracture surface of UHMWPE/MMT clay nanocomposite: (a) 4% UHMWPE and 10% MMT clay volume fraction, and (b) 5% UHMWPE and 10% MMT clay volume fraction volume fractions

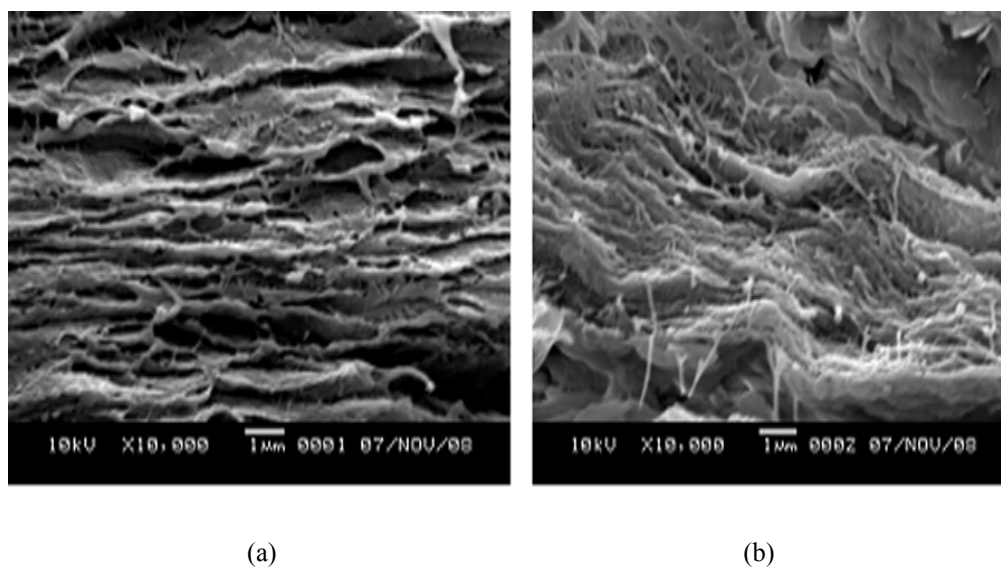


Figure 11. SEM micrographs of fracture surface of UHMWPE/MMT clay nanocomposite (a) 4% UHMWPE and 20% MMT clay volume fraction, and (b) 5% UHMWPE and 20% MMT clay volume fraction volume fractions

# Synthesis, Characterization and Antimicrobial Study of Some New Cyclohexenone Derivatives

Anil N. Mayekar

Department of Studies in Chemistry, University of Mysore  
Manasagangotri 570 006, India

&

SeQuent Scientific Limited, 120 A and B, Industrial Area  
Baikampady, New Mangalore, 575 011, India

Tel: 91-824-240-2306 E-mail: anilmayekar@gmail.com

Hongqi Li

Key Laboratory of Science & Technology of Eco-Textile  
Ministry of Education, College of Chemistry  
Chemical Engineering & Biotechnology, Donghua University  
Shanghai 201620, China

Tel: 86-21-6779-2594 E-mail: hongqili@dhu.edu.cn

H. S. Yathirajan (Corresponding author)

Department of Studies in Chemistry, University of Mysore  
Manasagangotri 570 006, India

Tel: 91-821-241-9656 E-mail: yathirajan@hotmail.com

B. Narayana

Department of Chemistry, Mangalore University  
Mangalagangothri 574 199, India

Tel: 91-824-228-7262 E-mail: nbadiadka@yahoo.co.uk

N. Suchetha Kumari

Department of Biochemistry, Justice K.S. Hegde Medical Academy, Deralakatte  
Mangalore-574 162, India

Tel: 91-824-220-2471 E-mail: suchetha.shetty@rediffmail.com

*This research work is supported by University of Mysore, Mysore, SeQuent Scientific Ltd., Mangalore and Donghua University, People's Republic of China.*

## Abstract

A series of chalcones and its cyclohexenone derivatives derived from 6-methoxy-2-naphthaldehyde are described. The chalcones synthesized through Claisen-Schmidt condensation reaction were treated with ethylacetoacetate in presence of NaOH to get the cyclocondensed product ethyl-4-(aryl)-6-(6-methoxy-2-naphthyl)-2-oxo-cyclohex-3-ene-1-carboxylate. The synthesized compounds were characterized from elemental analysis and spectral data. Ethyl 4-(4-chlorophenyl)-6-(6-methoxy-2-naphthyl)-2-oxo-cyclohex-3-ene-1-carboxylate (**4f**) was studied by single crystal X-ray diffraction. The newly synthesized compounds were screened for their antimicrobial activity.

**Keywords:** Cyclohexenones, 6-Methoxy-2-naphthyl chalcones, Single Crystal XRD, Antimicrobial activity



## 1. Introduction

Chalcones belong to a class of  $\alpha,\beta$ -unsaturated aromatic ketones which occur abundantly in nature, and have drawn much attention because of their benefits to human application (Dhar, 1981; Torigoo *et al.*, 1983; Sukumaran & Kuttan, 1991). These compounds are precursors of flavonoids and isoflavonoids which are abundant in plants. Various biological activities are associated with chalcones, such as anticancer (Modzelewska *et al.*, 2006), antitumor (Kumar *et al.*, 2003), antioxidant (Suksamrarn *et al.*, 2003) and antimalarial (Ferrer *et al.*, 2009). In addition of being used in pharmaceutical industries, chalcones also find wide applications in dyes (Asiri, 2003) and cosmetic compositions (Forestier *et al.*, 1989). Apart from being biologically important compounds, chalcone derivatives show non-linear optical (NLO) properties with excellent blue light transmittance and good crystallizability (Shettigar *et al.*, 2006). The presence of naphthyl ring in chalcones has shown promising antimicrobial and antihyperglycemic activity (Damazio *et al.*, 2010; Rajendraprasad *et al.*, 2006). Michael addition of ethylacetoacetate to chalcone yields 4,6-diaryl-2-oxo-cyclohex-3-ene-1-carboxylate derivatives, which are efficient synthons for fused isoxazoles pyrazoles and quinazolins (Padmavathi *et al.*, 2000; Senguttuvan *et al.*, 2010). Cyclohexenone derivatives are well known lead molecules for the treatment of inflammation and autoimmune diseases (Tanaka *et al.*, 1997). Several reports have pointed out the importance of cyclohexenones for antimicrobial and antitubercular activity (Vyas *et al.*, 2009). Nebumetone, 4-(6-methoxy-2-naphthyl)-2-butanone and Naproxen, 2-(6-methoxy-2-naphthyl) propanoic acid have been shown to possess good nonsteroidal anti-inflammatory (NSAI) activity. Keeping in view of the useful findings of 6-methoxy-2-naphthyl group and in continuation of our work on 4,6-diaryl-2-oxo-cyclohex-3-ene-1-carboxylates (Sreevidya *et al.*, 2009), we have synthesized some new cyclohexenone derivatives. We have already reported the crystal and molecular structure studies of some of the related chalcones and cyclohexenone derivatives (Li *et al.*, 2009, 2009a; Jasinski *et al.*, 2009; Yathirajan, Mayekar, Narayana *et al.*, 2007; Yathirajan, Mayekar, Sarojini *et al.*, 2007; Yathirajan, Sarojini, Bindya *et al.*, 2006; Yathirajan, Narayana, Ashalatha *et al.*, 2006). The present paper reports the synthesis, characterization and antimicrobial activity of some new cyclohexenone derivatives derived from 6-methoxy-2-naphthylaldehyde. One of the newly synthesized compound, viz., ethyl 4-(4-chlorophenyl)-6-(6-methoxy-2-naphthyl)-2-oxocyclohex-3-ene-1-carboxylate (**4f**) is characterized by single crystal studies.

## 2. Experimental

TLC was run on a Merck silica gel 60 F254 coated aluminum plates and melting points were taken in open capillary tubes and are uncorrected. Elemental analysis was carried out using Flash EA 1112 Series, CHNSO Analyzer (Thermo). IR spectra in KBr pellets were recorded on Jasco FT/IR-4100 FTIR spectrophotometer.  $^1\text{H}$ -NMR spectra were recorded in  $\text{CDCl}_3$  and in  $\text{DMSO}-d_6$  on a Bruker (400 MHz) spectrometer using TMS as internal standard and Mass spectra were recorded on LC/MSD Trap XCT spectrometer. Bruker SMART CCD diffractometer was used for crystal structure studies.

### 2.1 General procedure for preparation of 1-(aryl)-3-(6-methoxynaphthalen-2-yl)prop-2-en-1-one (**3a-3l**)

To a thoroughly stirred solution of 6-methoxy-2-naphthaldehyde (1.86 g, 10 mmol) and substituted acetophenones (10 mmol) in 15 ml methanol, 5 ml of 40% KOH solution was added. The reaction mixture was stirred overnight and the solid separated was collected by filtration. The product obtained was recrystallized from methanol.

#### (2E)-1-(2-Hydroxyphenyl)-3-(6-methoxy-2-naphthyl)prop-2-en-1-one (**3b**)

Yellow crystals, Yield 70%, M.p.: 216-218 °C, Anal. Calculated %  $\text{C}_{20}\text{H}_{16}\text{O}_2$ : C-78.93, H-5.29. Found C-78.90, H-5.26. IR (KBr  $\nu_{\text{max}}$   $\text{cm}^{-1}$ ): 1650 (C=O), 1630 (C=C) and 3400 (OH);  $^1\text{H}$  NMR (DMSO,  $\delta$  ppm): 3.88 (s, 3H, -OCH<sub>3</sub>), 6.89 (d, 2H,  $J$  = 8.5 Hz, ArH), 7.20 (d, 1H,  $J$  = 6.7 Hz, ArH), 7.36 (d, 1H,  $J$  = 2.1 Hz, ArH), 7.79 (d, 1H,  $J$  = 15.5 Hz, CH=C), 7.86 (m, 2H, ArH), 7.97 (d, 1H,  $J$  = 15.5 Hz, CH=C), 8.02-8.10 (m, 3H, ArH), 8.22 (s, 1H, ArH), 10.41 (s, 1H, OH). LCMS: 305 (M+1).

#### (2E)-1-(4-chlorophenyl)-3-(6-methoxy-2-naphthyl)prop-2-en-1-one (**3f**)

Yellow crystals, Yield 78%, M.p.: 200-202 °C, Anal. Calculated %  $\text{C}_{20}\text{H}_{15}\text{ClO}_2$ : C-74.42, H-4.68. Found C-74.38, H-4.63. IR (KBr  $\nu_{\text{max}}$   $\text{cm}^{-1}$ ): 1695 (C=O) and 1660 (C=C);  $^1\text{H}$  NMR (DMSO,  $\delta$  ppm): 3.89 (s, 3H, -OCH<sub>3</sub>), 7.19 (d, 1H,  $J$  = 8.5 Hz, ArH), 7.38 (d, 1H,  $J$  = 2.2 Hz, ArH), 7.64 (d, 2H,  $J$  = 8.6 Hz, ArH), 7.84-7.90 (m, 4H, ArH), 8.02 (d, 1H,  $J$  = 15.1 Hz, CH=C), 8.20 (d, 2H,  $J$  = 8.5 Hz, ArH), 8.26 (s, 1H, ArH). LCMS: 323 (M+1).

#### (2E)-3-(6-Methoxy-2-naphthyl)-1-(4-nitrophenyl)prop-2-en-1-one (**3g**)

Yellow crystals, Yield 78%, M.p.: 178-180 °C, Anal. Calculated %  $C_{20}H_{15}NO_4$ : C-70.06, H-4.53, N-4.20. Found C-70.01, H-4.49, N-4.18. IR (KBr  $\nu_{\max}$   $cm^{-1}$ ): 1686 (C=O) and 1643 (C=C);  $^1H$  NMR (DMSO,  $\delta$  ppm): 3.89 (s, 3H, -OCH<sub>3</sub>), 7.23 (d, 1H,  $J$  = 8.9 Hz, ArH), 7.38 (d, 1H,  $J$  = 2.2 Hz, ArH), 7.87 (d, 1H,  $J$  = 15.1 Hz, CH=C), 7.97 (d, 1H,  $J$  = 15.4 Hz, CH=C), 8.06 (d, 2H,  $J$  = 6.9 Hz, ArH), 8.10 (s, 1H, ArH), 8.29 (s, 1H, ArH), 8.38 (m, 4H, ArH). LCMS: 334 (M+1).

*(2E)-3-(6-Methoxy-2-naphthyl)-1-(1-naphthyl)prop-2-en-1-one (3j)*

Yellow crystals, Yield 70%, M.p.: 192-194 °C, Anal. Calculated %  $C_{24}H_{18}O_2$ : C-85.18, H-5.02. Found C-85.15, H-5.06. IR (KBr  $\nu_{\max}$   $cm^{-1}$ ): 1682 (C=O) and 1641 (C=C);  $^1H$  NMR (DMSO,  $\delta$  ppm): 3.90 (s, 3H, -OCH<sub>3</sub>), 7.22 (dd, 1H,  $J$  = 6.7 Hz, ArH), 7.40 (s, 1H, ArH), 7.64-7.69 (m, 2H, ArH), 7.73 (d, 1H,  $J$  = 15.9 Hz, CH=C), 7.89-7.92 (m, 2H, ArH), 7.99 (d, 1H,  $J$  = 15.5 Hz, CH=C), 8.04-8.21 (m, 6H, ArH), 8.29 (s, 1H, ArH), 8.9 (s, 1H, ArH). LCMS: 339 (M+1).

*(2E)-1-(3-Bromophenyl)-3-(6-methoxy-2-naphthyl)prop-2-en-1-one (3k)*

Yellow crystals, Yield 78 %, M.p.: 154-156 °C, Anal. Calculated %  $C_{20}H_{15}BrO_2$ : C-65.41, H-4.11. Found C-65.38, H-4.07. IR (KBr  $\nu_{\max}$   $cm^{-1}$ ): 1670 (C=O) and 1640 (C=C);  $^1H$  NMR (DMSO,  $\delta$  ppm): 3.89 (s, 3H, -OCH<sub>3</sub>), 7.22 (dd, 1H,  $J$  = 6.7 Hz, ArH), 7.31-7.38 (m, 3H, ArH), 7.82 (s, 1H, ArH), 7.86-7.89 (m, 2H, ArH), 7.94 (d, 1H,  $J$  = 14.6 Hz, CH=C), 8.05-8.08 (m, 2H, ArH and CH=C), 8.25 (s, 1H, ArH), 8.35 (s, 1H, ArH). LCMS: 368 (M+1).

*2.1.1 General procedure for preparation of Cyclohexenones (4a-4l)*

1-(Aryl)-3-(6-methoxynaphthalen-2-yl)prop-2-en-1-one (5 mmol) and ethyl acetoacetate (5 mmol) were refluxed for 4-6 hrs in 15 ml ethanol in presence of 0.8 ml of 10% NaOH. The reaction mixture was cooled to room temperature and the reaction mass was filtered. The compound was recrystallized from methanol.

*Ethyl 4-(2-hydroxyphenyl)-6-(6-methoxy-2-naphthyl)-2-oxocyclohex-3-ene-1-carboxylate (4b)*

Off white crystals, IR (KBr  $\gamma_{\max}$   $cm^{-1}$ ): 1632  $cm^{-1}$  (C=O ketone), 1742  $cm^{-1}$  (C=O ester) 3411  $cm^{-1}$  (-OH);  $^1H$  NMR (CDCl<sub>3</sub>, 400MHz,  $\delta$  ppm): 1.00 (t, 3H,  $J$  = 6.8 Hz, CH<sub>2</sub>-CH<sub>3</sub>), 2.97-3.18 (m, 2H, CH<sub>2</sub>, CH<sub>2</sub>-CHAr), 3.86 (s, 1H, CH), 3.90 (s, 1H, CH), 3.93 (s, 3H, OCH<sub>3</sub>), 4.0 (q, 2H,  $J$  = 6.0 Hz, CH<sub>2</sub>-CH<sub>3</sub>), 5.4 (bs, 1H, OH), 6.55 (s, 1H, =CH-CO-), 6.86 (d, 2H,  $J$ =8.7 Hz, ArH), 7.13-7.17 (m, 2H, ArH), 7.42 (d, 1H,  $J$ =8.4 Hz, ArH), 7.49 (d, 2H,  $J$ =8.7 Hz, ArH), 7.69-7.75 (m, 3H, ArH). LCMS: 417 (M+1).

*Ethyl 4-(4-hydroxyphenyl)-6-(6-methoxy-2-naphthyl)-2-oxocyclohex-3-ene-1-carboxylate (4c)*

Off white crystals, IR (KBr  $\gamma_{\max}$   $cm^{-1}$ ): 1609  $cm^{-1}$  (C=O ketone), 1730  $cm^{-1}$  (C=O ester) 3376  $cm^{-1}$  (-OH);  $^1H$  NMR (CDCl<sub>3</sub>, 400MHz,  $\delta$  ppm): 0.99 (t, 3H,  $J$  = 6.8 Hz, CH<sub>2</sub>-CH<sub>3</sub>), 3.11-3.14 (m, 2H, CH<sub>2</sub>, CH<sub>2</sub>-CHAr), 3.91 (s, 3H, OCH<sub>3</sub>), 3.93(s, 1H, CH), 3.94 (s, 1H, CH), 4.0 (q, 2H,  $J$  = 6.0 Hz, CH<sub>2</sub>-CH<sub>3</sub>), 6.76 (s, 1H, =CH-CO-), 6.81 (bs, 1H, OH), 6.90 (d, 2H,  $J$ =6.4 Hz, ArH), 7.10-7.14 (m, 2H, ArH), 7.20-7.27 (m, 2H, ArH), 7.40 (dd, 1H,  $J$ =6.8 Hz, ArH), 7.67 (d, 2H,  $J$ =8.8 Hz, ArH), 7.70 (s, 1H, ArH). LCMS: 417(M+1).

*Ethyl 4-(4-methoxyphenyl)-6-(6-methoxy-2-naphthyl)-2-oxocyclohex-3-ene-1-carboxylate (4d)*

White crystals, IR (KBr  $\gamma_{\max}$   $cm^{-1}$ ): 1666  $cm^{-1}$  (C=O ketone), 1743  $cm^{-1}$  (C=O ester);  $^1H$  NMR (CDCl<sub>3</sub>,  $\delta$  ppm): 0.98 (t, 3H,  $J$  = 7.0 Hz, CH<sub>2</sub>-CH<sub>3</sub>), 3.02-3.19 (m, 2H, CH<sub>2</sub>, CH<sub>2</sub>-CHAr), 3.84 (s, 4H, OCH<sub>3</sub> and CH), 3.88 (s, 1H, CH), 3.97 (s, 3H, OCH<sub>3</sub>), 3.99 (q, 2H,  $J$  = 6.9 Hz, CH<sub>2</sub>-CH<sub>3</sub>), 6.55 (s, 1H, =CH-CO-), 6.92 (d, 2H,  $J$ =8.8 Hz, ArH), 7.12-7.17 (m, 2H, ArH), 7.41 (d, 1H,  $J$  = 7.2 Hz, ArH), 7.53 (d, 2H,  $J$  = 8.7 Hz, ArH), 7.71 (d, 2H,  $J$  = 9.7 Hz, ArH), 7.75 (s, 1H, ArH). LCMS: 431(M+1).

*Ethyl 4-(4-methylphenyl)-6-(6-methoxy-2-naphthyl)-2-oxocyclohex-3-ene-1-carboxylate (4e)*

White crystals, IR (KBr  $\gamma_{\max}$   $cm^{-1}$ ): 1634  $cm^{-1}$  (C=O ketone), 1735  $cm^{-1}$  (C=O ester);  $^1H$  NMR (CDCl<sub>3</sub>, 400MHz,  $\delta$  ppm): 1.00 (t, 3H,  $J$  = 7.0 Hz, CH<sub>2</sub>-CH<sub>3</sub>), 2.39 (s, 3H, CH<sub>3</sub>), 3.06-3.19 (m, 2H, CH<sub>2</sub>, CH<sub>2</sub>-CHAr), 3.87 (s, 1H, CH), 3.91(s, 1H, CH), 3.94 (s, 3H, OCH<sub>3</sub>), 4.0 (q, 2H,  $J$  = 6.9 Hz, CH<sub>2</sub>-CH<sub>3</sub>), 6.59 (s, 1H, =CH-CO-), 7.13-7.26 (m, 4H, ArH), 7.41-7.48 (m, 3H, ArH), 7.72-7.75 (m, 3H, ArH). LCMS: 415(M+1).

*Ethyl 4-(4-chlorophenyl)-6-(6-methoxy-2-naphthyl)-2-oxocyclohex-3-ene-1-carboxylate (4f)*

White crystals, IR (KBr  $\gamma_{\max}$   $cm^{-1}$ ): 1651  $cm^{-1}$  (C=O ketone), 1758  $cm^{-1}$  (C=O ester);  $^1H$  NMR (CDCl<sub>3</sub>,  $\delta$  ppm): 0.98 (t, 3H,  $J$  = 6.8 Hz, CH<sub>2</sub>-CH<sub>3</sub>), 3.05 (m, 2H, CH<sub>2</sub>, CH<sub>2</sub>-CHAr), 3.84 (s, 1H, CH), 3.88 (s, 1H, CH), 3.90 (s, 3H, OCH<sub>3</sub>), 3.99 (q, 2H,  $J$  = 6.9 Hz, CH<sub>2</sub>-CH<sub>3</sub>), 6.54 (s, 1H, =CH-CO-), 7.12-7.16 (m, 3H, ArH), 7.38 (d, 3H,  $J$ =8.0 Hz, ArH), 7.47 (d, 2H,  $J$  = 8.1 Hz, ArH), 7.67-7.74 (m, 2H, ArH). LCMS: 435(M+1), 436(M+2).

*Ethyl 4-(4-nitrophenyl)-6-(6-methoxy-2-naphthyl)-2-oxocyclohex-3-ene-1-carboxylate (4g)*

Yellow crystals, IR (KBr  $\gamma_{\max}$   $\text{cm}^{-1}$ ): 1658  $\text{cm}^{-1}$  (C=O ketone), 1761  $\text{cm}^{-1}$  (C=O ester);  $^1\text{H}$  NMR ( $\text{CDCl}_3$ ,  $\delta$  ppm): 0.98 (t, 3H, J= 6.8 Hz,  $\text{CH}_2\text{-CH}_3$ ), 3.05 (m, 2H,  $\text{CH}_2$ ,  $\text{CH}_2\text{-CHAr}$ ), 3.84-3.99 (m, 5H,  $\text{OCH}_3$  and 2CH), 4.01 (q, 2H, J= 6.9 Hz,  $\text{CH}_2\text{-CH}_3$ ), 6.54 (s, 1H, =CH-CO-), 7.12-7.16(m, 3H, ArH), 7.38 (d, 3H, J=8.0 Hz, ArH), 7.47 (d, 2H, J= 8.1 Hz, ArH), 7.67-7.74 (m, 2H, ArH). LCMS: 446 (M+1).

*Ethyl 4-(pyridin-4-yl)-6-(6-methoxy-2-naphthyl)-2-oxocyclohex-3-ene-1-carboxylate (4h)*

Yellow crystals, IR (KBr  $\gamma_{\max}$   $\text{cm}^{-1}$ ): 1638  $\text{cm}^{-1}$  (C=O ketone), 1742  $\text{cm}^{-1}$  (C=O ester);  $^1\text{H}$  NMR ( $\text{CDCl}_3$ ,  $\delta$  ppm): 0.98 (t, 3H, J= 6.8 Hz,  $\text{CH}_2\text{-CH}_3$ ), 3.11-3.18 (m, 2H,  $\text{CH}_2$ ,  $\text{CH}_2\text{-CHAr}$ ), 3.88 (s, 1H, CH), 3.90 (s, 4H,  $\text{OCH}_3$  and CH), 3.99 (q, 2H, J= 6.9 Hz,  $\text{CH}_2\text{-CH}_3$ ), 6.40 (s, 1H, =CH-CO-), 7.11-7.17 (m, 2H, ArH), 7.37-7.55 (m, 5H, ArH), 7.70-7.73 (m, 3H, ArH). LCMS: 402(M+1).

*Ethyl 4-(1-naphthyl)-6-(6-methoxy-2-naphthyl)-2-oxocyclohex-3-ene-1-carboxylate (4j)*

White powder, IR (KBr  $\gamma_{\max}$   $\text{cm}^{-1}$ ): 1651  $\text{cm}^{-1}$  (C=O ketone), 1758  $\text{cm}^{-1}$  (C=O ester);  $^1\text{H}$  NMR ( $\text{CDCl}_3$ ,  $\delta$  ppm): 1.01 (t, 3H, J= 7.2 Hz,  $\text{CH}_2\text{-CH}_3$ ), 3.29 (m, 2H,  $\text{CH}_2$ ,  $\text{CH}_2\text{-CHAr}$ ), 3.92 (s, 3H,  $\text{OCH}_3$ ), 3.93 (s, 1H, CH), 3.95 (s, 1H, CH), 4.03 (q, 2H, J= 6.9 Hz,  $\text{CH}_2\text{-CH}_3$ ), 6.74 (s, 1H, =CH-CO-), 7.13-7.17(m, 2H, ArH), 7.68 (dd, 1H, J=8.8 Hz, ArH), 7.70 (s, 1H, ArH), 7.72 (d, 3H, J=8.1, ArH) 7.76 (d, 2H, J= 8.4 Hz, ArH), 7.82-7.88 (m, 3H, ArH), 8.02 (s, 1H, ArH). LCMS: 451(M+1).

*Ethyl 4-(3-bromophenyl)-6-(6-methoxy-2-naphthyl)-2-oxocyclohex-3-ene-1-carboxylate (4k)*

Yellow crystals, IR (KBr  $\gamma_{\max}$   $\text{cm}^{-1}$ ): 1661  $\text{cm}^{-1}$  (C=O ketone), 1754  $\text{cm}^{-1}$  (C=O ester);  $^1\text{H}$  NMR ( $\text{CDCl}_3$ , 400MHz,  $\delta$  ppm): 0.99 (t, 3H, J= 7.0 Hz,  $\text{CH}_2\text{-CH}_3$ ), 3.04-3.08 (m, 2H,  $\text{CH}_2$ ,  $\text{CH}_2\text{-CHAr}$ ), 3.89 (s, 1H, CH), 3.90 (s, 1H, CH), 3.91 (s, 3H,  $\text{OCH}_3$ ), 4.01 (q, 2H, J= 6.0 Hz,  $\text{CH}_2\text{-CH}_3$ ), 6.55 (s, 1H, =CH-CO-), 7.12 (d, 1H, J= 2.8 Hz, ArH), 7.15 (d, 1H, J=8.6 Hz, ArH), 7.29 (d, 1H, J=8.0 Hz, ArH), 7.40 (dd, 1H, J=8.4 Hz, ArH), 7.48 (d, 1H, J=8.0Hz, ArH), 7.55 (d, 1H, J=7.6Hz, ArH), 7.66-7.68 (m, 2H, ArH), 7.71 (s, 1H, ArH), 7.72 (s, 1H, ArH), 7.74 (s, 1H, ArH). LCMS: 480(M+1), 481(M+2)

*Ethyl 4-(2,4-dichlorophenyl)-6-(6-methoxy-2-naphthyl)-2-oxocyclohex-3-ene-1-carboxylate (4l)*

Off white crystals, IR (KBr  $\gamma_{\max}$   $\text{cm}^{-1}$ ): 1665  $\text{cm}^{-1}$  (C=O ketone), 1743  $\text{cm}^{-1}$  (C=O ester);  $^1\text{H}$  NMR ( $\text{CDCl}_3$ , 400MHz,  $\delta$  ppm): 1.00 (t, 3H, J= 7.0 Hz,  $\text{CH}_2\text{-CH}_3$ ), 2.95-3.05 (m, 2H,  $\text{CH}_2$ ,  $\text{CH}_2\text{-CHAr}$ ), 3.89 (s, 1H, CH), 3.91 (s, 3H,  $\text{OCH}_3$ ), 3.92 (s, 1H, CH), 4.02 (q, 2H, J= 6.0 Hz,  $\text{CH}_2\text{-CH}_3$ ), 6.21 (s, 1H, =CH-CO-), 7.0 (d, 1H, J= 2.8 Hz, ArH), 7.13-7.17 (m, 2H, ArH), 7.19 (s, 1H, ArH), 7.28-7.30 (m, 2H, ArH), 7.44 (d, 1H, J= 2.0 Hz, ArH), 7.66 (s, 1H, ArH), 7.70 (s, 1H, ArH). LCMS: 470(M+1), 471(M+2).

## 2.2 Pharmacology

### 2.2.1 Antibacterial studies

The newly synthesized compounds were screened for their antibacterial activity against *Escherichia coli* (ATTC-25922), *Staphylococcus aureus* (ATTC-25923), *Pseudomonas aeruginosa* (ATCC-27853) and *Klebsiella pneumoniae* (recultured) bacterial stains by serial plate dilution method (Barry, 1991; James, 1970). Serial dilutions of the drug in Mueller Hinton broth were taken in tubes and their pH was adjusted to 5.0 using phosphate buffer. A standardized suspension of the test bacterium was inoculated and incubated for 16-18 h at 37°C. The minimum inhibitory concentration (MIC) was noted by seeing the lowest concentration of the drug at which there was no visible growth.

A number of antimicrobial discs were placed on the agar for the sole purpose of producing zones of inhibition in the bacterial lawn. Twenty milliliters of agar media was poured into each Petri dish. Excess of suspension was decanted and plates were dried by placing in an incubator at 37°C for an hour. Using a punch, wells were made on these seeded agar plates and minimum inhibitory concentrations of the test compounds in dimethylsulfoxide (DMSO) were added into each labeled well. A control was also prepared for the plates in the same way using solvent DMSO. The Petri dishes were prepared in triplicate and maintained at 37°C for 3-4 days. Antibacterial activity was determined by measuring the diameter of inhibition zone. Activity of each compound was compared with ampicillin as standard. Zone of inhibition was determined for newly synthesized compounds and the results are summarized in **Table 2**.

### 2.2.2 Antifungal studies

Newly prepared compounds were screened for their antifungal activity against *Aspergillus flavus* (NCIM No.524), *Aspergillus fumigates* (NCIM No. 902), *Penicillium marneffe* (recultured) and *Trichophyton mentagrophytes* (recultured) in DMSO by serial plate dilution method (Arthington-skaggs 2000; Verma, 1998). Sabourands agar media was prepared by dissolving peptone (1 g), D-glucose (4 g) and agar (2 g) in distilled water (100 ml) and adjusting the pH to 5.7. Normal saline was used to make a suspension of spore of fungal strains for lawning. A

loopful of particular fungal strain was transferred to 3 ml saline to get a suspension of corresponding species. Twenty milliliters of agar media was poured into each Petri dish. Excess of suspension was decanted and plates were dried by placing in incubator at 37°C for 1 h. Using a punch, wells were made on these seeded agar plates minimum inhibitory concentrations of the test compounds in DMSO were added into each labeled well. A control was also prepared for the plates in the same way using solvent DMSO. The Petri dishes were prepared in triplicate and maintained at 37°C for 3-4 days. Antifungal activity was determined by measuring the diameter of inhibition zone. Activity of each compound was compared with itraconazole as standard. Zones of inhibition were determined and the results are summarized in **Table 3**.

### 3. Results and discussion

Chalcones were synthesized by a base catalyzed Claisen–Schmidt condensation reaction of 6-methoxy-2-naphthaldehyde and substituted acetophenones. The reaction of chalcones with ethyl acetoacetate is known to lead three structurally diverse types of compounds, depending on the experimental conditions employed. Thus in the presence of a base, chalcones (**3a-3l**) and ethyl acetoacetate produce cyclohexenones (**4a-4l**) by means of an intermediate Michael adduct, as given in **Scheme 1**. The cyclocondensation of ethyl acetoacetate with chalcones leads to the generation of two chiral centers in the structure of cyclohexenones and both configuration of chiral carbon atoms are expected in the synthesized cyclohexenones, which would result in a mixture of diastereomers. No attempt has been undertaken to separate the diastereomeric cyclohexenones and have been characterized as such. The newly synthesized compounds were characterized by elemental analysis, IR, <sup>1</sup>H NMR, LCMS and single crystal X-ray analysis. The elemental analysis data of cyclohexenone derivatives are reported in **Table 1**.

The IR spectra of (2*E*)-1-(2-hydroxyphenyl)-3-(6-methoxy-2-naphthyl)prop-2-en-1-one (**3b**) revealed a strong band at 3400 cm<sup>-1</sup> confirming the presence of –OH group and a sharp band at 1650 cm<sup>-1</sup> indicating the presence of C=O. The proton NMR showed a singlet at δ 3.88 ppm representing three protons of methoxy group. The peaks of CH<sub>α</sub> = CH<sub>β</sub> were observed at δ 7.79 ppm as doublet with *J* = 15.48 Hz and at δ 7.97 ppm as doublet with *J* = 15.5 Hz, respectively. The LCMS showed the peak at *m/z* 305 (M+H), confirming the structure of the compound.

The IR spectra of ethyl 4-(2-hydroxyphenyl)-6-(6-methoxy-2-naphthyl)-2-oxocyclohex-3-ene-1-carboxylate (**4b**) revealed a strong sharp band at 1632 cm<sup>-1</sup> representing C=O group of the cyclohexenone ring and the band for C=O of ester was observed at 1742 cm<sup>-1</sup>.

In the <sup>1</sup>H NMR spectra, the CH<sub>3</sub> protons of ester group came into resonance at δ 1.0 as triplet with *J* = 6.8 Hz. The CH<sub>2</sub> protons of cyclohexenone ring were observed as multiplets at δ 2.97-3.18 ppm and two CH proton of cyclohexenone ring resonated at δ 3.86 ppm and at δ 3.90 ppm as singlet. The OCH<sub>3</sub> protons resonated as singlet at δ 3.93 ppm accounting for three protons. The CH<sub>2</sub> protons of ester group resonated as quartet at δ 4.0 ppm with *J* = 6.0 Hz. A broad singlet was observed at δ 5.4 ppm representing OH proton. The signal for =CH-CO- of cyclohexenone ring appeared at δ 6.55 ppm as singlet. The aromatic protons appeared at δ 6.86 ppm a doublet with *J* = 8.7 Hz accounting for two protons. Two protons came into resonance as multiplet at δ 7.13-7.17 ppm. Doublets were observed at δ 7.42 ppm and 7.49 ppm with *J* = 8.4 Hz and *J* = 8.7 Hz respectively representing two aromatic protons. Three aromatic protons resonated as multiplets at δ 7.69-7.75 ppm. The LCMS of this compound showed the M+1 Peak at *m/z* 417.

Compound **4f** was obtained as colourless blocks by recrystallisation from acetonitrile solution and its structure was elucidated by single crystal X-ray diffraction. Molecular structure of ethyl 4-(4-chlorophenyl)-6-(6-methoxy-2-naphthyl)-2-oxocyclohex-3-ene-1-carboxylate (**4f**) is shown in **Fig. 1**. C<sub>26</sub>H<sub>23</sub>ClO<sub>4</sub>, *M<sub>r</sub>* = 434.89, monoclinic, *P*2(1)/*c*, *a* = 18.5546 (8) Å, *b* = 11.4501 (5) Å, *c* = 10.2810 (5) Å, β = 93.454 (1)°, *V* = 2180.25 (17) Å<sup>3</sup>, *Z* = 4, ρ<sub>calc</sub> = 1.325 g cm<sup>-3</sup>, μ = 0.21 mm<sup>-1</sup>, *F*(000) = 912, Bruker SMART CCD diffractometer, Mo Kα radiation, λ = 0.71073 Å, *T* = 296 K, *R*(*F*) = 0.054, *wR*(*F*<sup>2</sup>) = 0.172, *S* = 1.03. Atoms C9 and C10 and their attached H atoms are disordered over two sets of sites on a 0.745 (8):0.255 (8) ratio. The dihedral angle between the naphthalene and benzene rings is 70.75 (7)°. Atom C23 deviates from the naphthalene ring mean plane by a negligible amount [0.011 (6) Å]. Atoms C9 and C10 are disordered over two sites in a 0.745 (8):0.255 (8) ratio. The major orientation corresponds to the *S,S*-enantiomer and the minor orientation to the *R,R*-enantiomer: crystal symmetry generates a racemic mixture. In the crystal, a weak intermolecular C—H⋯O interaction occurs. Similar disorder of the equivalent atoms have been seen in related structures (Li *et al.*, 2009, 2009a). All the H atoms were placed in idealized locations (C—H = 0.93-0.98 Å) and refined as riding with *U*<sub>iso</sub>(H) = 1.2*U*<sub>eq</sub>(C) or 1.5*U*<sub>eq</sub> (methyl C). The methyl groups were allowed to rotate, but not to tip, to best fit the electron density. [X-ray crystallographic files, in CIF format, for the structure

determinations of (I) (CCDC 769575) has been deposited with the Cambridge Crystallographic Data Centre, CCDC: 26091. Copies of this information may be obtained free of charge from the Director, CCDC, 12 Union Road, Cambridge, CB2 1EZ (fax: +44-1223-336033; email: deposit@ccdc.cam.ac.uk or <http://www.ccdc.cam.ac.uk>].

All the newly synthesized compounds were screened for their antimicrobial activity. The investigation of antibacterial and antifungal screening data revealed that some of the compounds (**4a-l**) showed moderate to good inhibition at  $\mu\text{g mL}^{-1}$  in DMSO. The compounds **4k** and **4l** showed comparatively good activity against all the bacterial and fungal strains. The good activity is attributed to the presence of pharmacologically active group attached to the cyclohexenone ring. Introduction of aryl moiety carrying bromo and dichloro group enhanced activity compared to the standard against *Escherichia coli*, *Staphylococcus aureus*, *Pseudomonas aeruginosa*, *Klebsiella pneumoniae*, *Penicillium marneffei*, *T. mentagrophytes*, *A. flavus* and *A. fumigatus*. Results of antibacterial and antifungal screening are discussed in **Table-2** and **Table-3** respectively.

#### 4. Conclusion

The research study reports the successful synthesis of chalcones derived from 6-methoxy-2-naphthaldehyde. These chalcones were converted to cyclohexenone derivatives by treating with ethyl acetoacetate in presence of a base, which are useful intermediates in the synthesis of heterocyclic compounds. The newly synthesized cyclohexenone derivatives were tested for their antibacterial and antifungal activity. Some of these derivatives have shown promising results. Ethyl 4-(4-chlorophenyl)-6-(6-methoxy-2-naphthyl)-2-oxo-cyclohex-3-ene-1-carboxylate (**4f**) was studied by single crystal X-ray diffraction.

#### Acknowledgements

ANM is thankful to University of Mysore for research facilities and SeQuent Scientific Ltd for allowing to undertake research. HSY thanks University of Mysore for sabbatical leave.

#### References

- Arthington-Skaggs, B. A., Motley, M., Warnock, D.W., Morrison, C.J. (2000). Comparative Evaluation of PASCO and National Committee for Clinical laboratory standards M27-A broth micro dilution methods for antifungal drug susceptibility testing of yeasts. *Journal of Clinical Microbiology*, 38:2254-2260.
- Asiri, A.M. (2003). Synthesis and Absorption Spectral Properties of Bis-methine Dyes Exemplified by 2,5-Bis-arylidene-1-dicyanomethylene-cyclopentanes. *Bulletin of the Korean Chemical Society*, 24:426-430.
- Barry, A. L. (1991). Procedure for testing antimicrobial agents in agar media, in: VL Corian (Ed), *Antibiotics in Laboratory Medicine*, Williams and Wilkins, Baltimore, MD, 1-16.
- Damazio, R.G., Zanatta, A.P., Cazarolli, L.H., Chiaradia, L.D., Mascarello, A., Nunes, R.J., Yunes, R.A., Barreto Silva, F.R. (2010). Antihyperglycemic activity of naphthylchalcones. *European Journal of Medicinal Chemistry*, 45:1332-1337.
- Dhar, D.N. (1981). *The Chemistry of Chalcones and Related Compounds*, Wiley, New York, p 213.
- Ferrer, R., Lobo, G., Gamboa, N., Rodrigues, J., Abramjuk, C., Jung, K., Lein, M., Charris, J.E. (2009). Synthesis of [(7-chloroquinolin-4-yl)amino]chalcones: Potential antimalarial and anticancer agents. *Scientia Pharmaceutica*, 77:725-741.
- Forestier, S, Moire, C., Lang, G. (1989). Cosmetic composition containing hydroxylated chalcone derivatives and its use for protecting the skin and the hair against luminous radiations, new hydroxylated chalcone derivatives employed and process for their preparation. US Patent 4,867,964.
- James, D., Lowry, M., Jaqua, M. J., Selepak, S. T. (1970). Detailed Methodology and Implementation of a Semi automated Serial Dilution Micro technique for Antimicrobial Susceptibility Testing. *Applied Microbiology*, 20: 46-53.
- Jasinski, J.P., Butcher, R.J., Mayekar, A.N., Yathirajan, H.S., Narayana, B. (2009). Structures of three chalcones derived from 6-methoxy-2-naphthaldehyde. *Journal of Chemical Crystallography*, 39:157-162.
- Kumar, S.K, Hager, E., Catherine, P., Gurulingappa, H., Davidson, N.E., Khan, S.R. (2003). Synthesis and evaluation of novel boronic-chalcone derivatives as antitumor agents. *Journal of Medicinal Chemistry*, 46:2813-2815.
- Li, H., Mayekar, A.N., Narayana, B., Yathirajan, H.S., Harrison, W.T.A. (2009a). Ethyl 6-(6-methoxy-2-naphthyl)-2-oxo-4-(2-thienyl)cyclohex-3-ene-1-carboxylate. *Acta Crystallographica*, E65:o1533.

- Li, H., Mayekar, A.N., Narayana, B., Yathirajan, H.S., Harrison, W.T.A. (2009). ( $\pm$ )-Ethyl 6-(6-methoxy-2-naphthyl)-4-(4-methylphenyl)-2-oxocyclohex-3-ene-1-carboxylate. *Acta Crystallographica* E65:o1186.
- Modzelewska, A., Pettit, C., Achanta, G., Davidson, N.E., Huang, P., Khan, S.R. (2006). Anticancer activities of novel chalcone and bis-chalcone derivatives. *Bioorganic and Medicinal Chemistry*, 14:3491-3495.
- Padmavathi, V., Reddy, B.J.M., Balaiah, A., Reddy, K.V., Reddy, D.B. (2000). Synthesis of some fused pyrazoles and isoxazoles. *Molecules*, 5:1281-1286.
- Rajendra Prasad, Y., Ravi Kumar, P., Asha Deepti, C.H., Venkata Ramana, M. (2006). Synthesis and antimicrobial activity of some novel chalcones of 2-hydroxy-1-acetonaphthone and 3-acetyl coumarin *E-Journal of Chemistry*, 3:236-241.
- Senguttuvan, S., Nagarajan, S. (2010). Synthesis of 2-Amino-5-aryl-5,6-dihydro-7-(naphthalene-2-yl) Quinazolin-4-ols. *International Journal of Chemistry*, 2: 108-112.
- Shettigar, S., Chandrasekharan, K., Umesh, Sarojini, B.K., Narayana, B. (2006). Studies on nonlinear optical parameters of bis-chalcone derivatives doped polymer. *Polymer*, 47:3565-3567.
- Sreevidya, T.V., Narayana, B., Yathirajan, H.S. (2009). Synthesis and characterization of some chalcones and their cyclohexenone derivatives. *Central European Journal of Chemistry*, 8:174-181.
- Sukumaran, K., Kuttan, R. (1991). Screening of 11 ferns of cytotoxic and antitumor potential with special reference to Pityrogramma calomelanos. *Journal of Ethnopharmacology*, 36:93-96.
- Suksamrarn, A., Poomsing, P., Aroonrerk, N., Punjanon, T., Suksamrarn, S., Kongkun, S. (2003). Antimycobacterial and antioxidant flavones from *Limnophila geoffrayi*. *Archives of Pharmacal Research*, 26:816-820.
- Tanaka, M., Nara, F., Suzuki, K., Hosoya, T., Ogita, T. (1997). Structural elucidation of sciphostatin, an inhibitor of membrane-bound neutral sphingomyelinase. *Journal of the American Chemical Society*, 119: 7871-7872.
- Torigoo, T., Arisawa, M., Iloch, S., Fujiu, M., Mayuyama, H.B. (1983). Anti-mutagenic chalcones: Antagonizing the mutagenicity of benzo(a)pyrene in *Salmonella typhimurium*. *Biophysical Research Communications*, 112:833-842.
- Verma, R. S., Khan, Z. K., Singh, A. P. (1998). (Ed), Antifungal Agents: Past, Present and Future Prospects, National Academy of Chemistry and Biology, Lucknow, India, 55-128.
- Vyas, D.H., Tala, S.D., Akbari, J.D., Dhaduk, M.F., Joshi, H.S. (2009). Synthesis, antimicrobial and antitubercular activity of some cyclohexenone and indazole derivatives. *Indian Journal of Chemistry*, 48B: 1405-1410.
- Yathirajan, H.S., Mayekar, A.N., Narayana, B., Sarojini, B.K., Bolte, M. (2007). (2E)-1-(2,4-Dichlorophenyl)-3-(6-methoxy-2-naphthyl)prop-2-en-1-one. *Acta Crystallographica*, E63:o540.
- Yathirajan, H.S., Mayekar, A.N., Sarojini, B.K., Narayana, B., Bolte, M. (2007). (2E)-3-(6-Methoxy-2-naphthyl)-1-phenylprop-2-en-1-one. *Acta Crystallographica*, E63:o1012.
- Yathirajan, H. S., Sarojini, B.K., Bindya, S., Narayana, B., Bolte, M. (2006). 3-(6-Methoxy-2-naphthyl)-1-(2-naphthyl)prop-2-en-1-one. *Acta Crystallographica*, E62:o4046.
- Yathirajan, H.S., Narayana, B., Ashalatha, B.V., Sarojini, B.K., Bolte, M. (2006). 3-(6-Methoxy-2-naphthyl)-1-(2-thienyl)prop-2-en-1-one. *Acta Crystallographica*, E62:o4440.

Table 1. Characterization data of compounds (4a-4l)

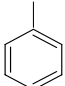
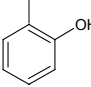
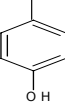
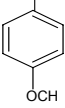
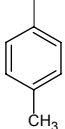
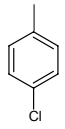
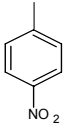
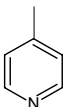
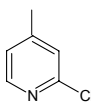
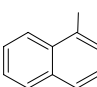
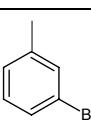
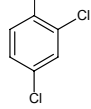
Compd	R	m.p (°C)	Yield %	Elemental analysis		
				% found (calculated)		
				C	H	N
4a		152-154	70	77.94 (77.98)	6.02 (6.04)	-
4b		172-174	56	74.91 (74.98)	5.01 (5.08)	-
4c		182-184	62	74.92 (74.98)	5.04 (5.080)	-
4d		148-150	60	75.30 (75.33)	6.02 (6.08)	-
4e		162-164	68	78.21 (78.24)	6.30 (6.32)	-
4f		150-152	72	71.78 (71.80)	5.30 (5.33)	-
4g		120-122	50	70.11 (70.10)	5.18 (5.20)	3.10 (3.14)
4h		202-204	58	74.76 (74.79)	5.71 (5.72)	3.45 (3.48)
4i		178-180	51	68.84 (68.880)	5.06 (5.08)	3.18 (3.21)
4j		124-126	60	79.95 (79.98)	5.79 (5.81)	
4k		146-148	68	65.12 (65.14)	4.81 (4.83)	-
4l		120-122	51	66.50 (66.53)	4.68 (4.72)	-

Table 2. Antibacterial activity of the compounds. MIC in  $\mu\text{gml}^{-1}$  (Zone of inhibition in mm)

Compounds	<i>E.Coli</i> (ATTC-25922)	<i>Staphylococcus</i> (ATTC-25923)	<i>Klebsiella</i> (Recultured)	<i>Pseudomonas</i> (ATTC-27853)
4a	-	-	-	-
4b	-	-	-	-
4c	-	-	-	-
4d	12.5(15)	12.5(16)	12.5(16)	12.5(16)
4e	12.5(10)	12.5(12)	12.5(12)	12.5(12)
4f	6.25(11)	6.25(11)	6.25(11)	6.25(11)
4g	-	-	-	-
4h	6.25(10)	6.25(11)	6.25(12)	6.25(11)
4i	12.5(16)	12.5(16)	12.5(16)	12.5(16)
4j	-	-	-	-
4k	6.25(18)	6.25(18)	6.25(18)	6.25(18)
4l	6.25(18)	6.25(20)	6.25(18)	6.25(20)
Ampicillin	6.25(30)	6.25(30)	6.25(27)	6.25(28)

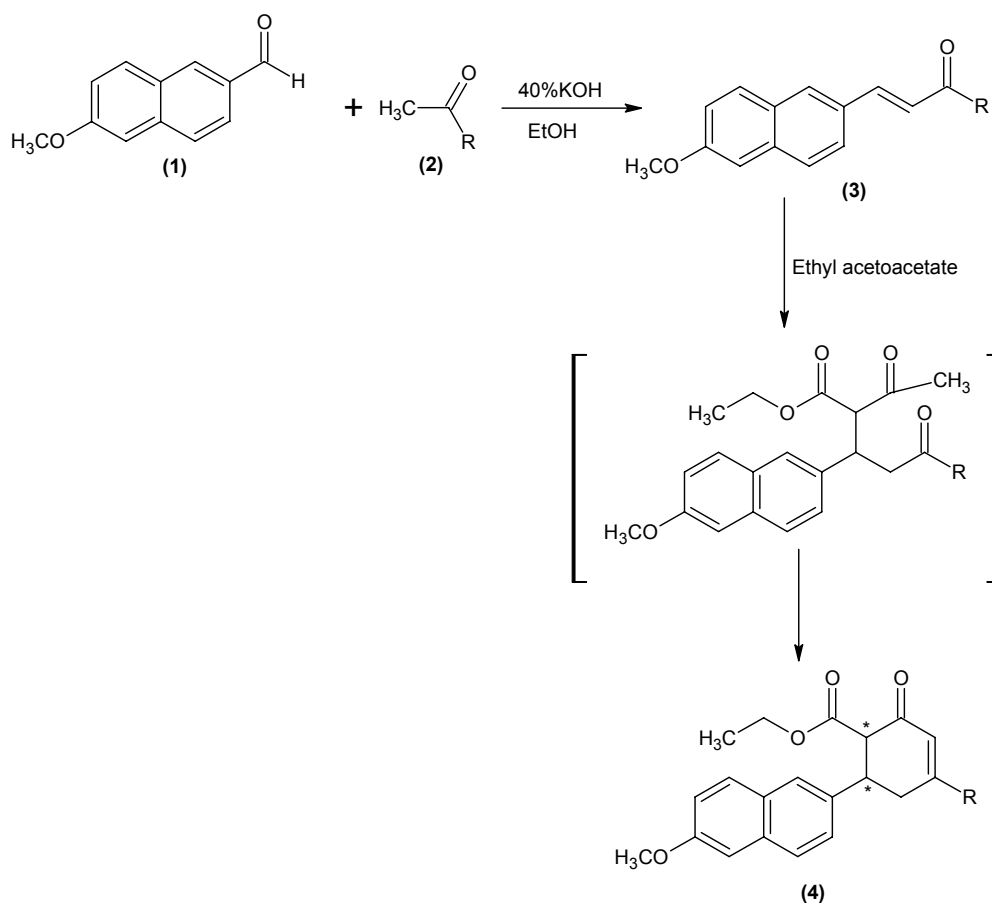
Note: The MIC values were evaluated at concentration range, 1.5-12.5  $\mu\text{g} / \text{ml}$ . The figures in the table show the MIC values in  $\mu\text{g}/\text{ml}$  and the corresponding zone of inhibition in mm.

Table 3. Antifungal activity of the compounds. MIC in  $\mu\text{gml}^{-1}$  (Zone of inhibition in mm)

Compounds	<i>Penicillium</i> <i>Marneffi</i> (Recultured)	<i>Trichophyton</i> <i>Mentagrophytes</i> (Recultured)	<i>AS Flavus</i> (NCIM No.524)	<i>AS fumigatus</i> (NCIM No.902)
4a	-	-	-	-
4b	-	-	-	-
4c	-	-	-	-
4d	12.5(15)	12.5(16)	12.5(14)	12.5(16)
4e	12.5(10)	12.5(12)	12.5(12)	12.5(12)
4f	12.5(11)	12.5 (12)	12.5 (12)	12.5 (11)
4g	-	-	-	-
4h	6.25(10)	6.25(11)	6.25(12)	6.25(11)
4i	12.5(14)	12.5(16)	12.5(14)	12.5(14)
4j	-	-	-	-
4k	6.25(20)	6.25(18)	6.25(18)	6.25(18)
4l	6.25(20)	6.25(18)	6.25(18)	6.25(18)
Itraconazole	6.25(28)	6.25(30)	6.25(28)	6.25(28)

Note: The MIC values were evaluated at concentration range, 1.5-12.5  $\mu\text{g} / \text{ml}$ . The figures in the table show the MIC values in  $\mu\text{g}/\text{ml}$  and the corresponding zone of inhibition in mm.





Scheme 1. Synthesis of ethyl-6-(6-methoxy-2-naphthyl)-2-oxo-4-(aryl)cyclohex-3-ene-1-carboxylate (4a-4l)

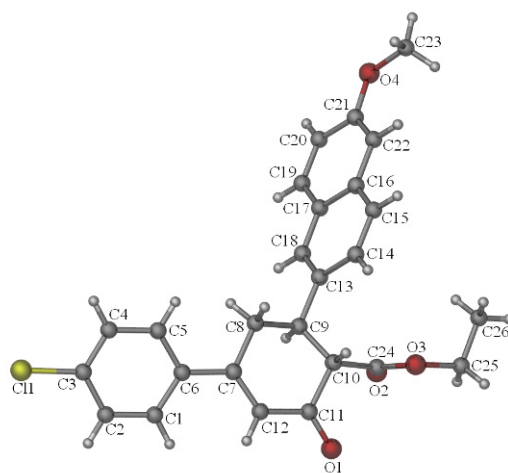


Figure 1. Molecular structure of ethyl 4-(4-chlorophenyl)-6-(6-methoxy-2-naphthyl)-2-oxocyclohex-3-ene-1-carboxylate (4f)

# Analysis of the Characteristics of Nickel-Plating Baths

Ahmet Ozan GEZERMAN (Corresponding author) & Burcu Didem CORBACIOGLU

Chemical and Metallurgical Engineering Faculty, Yildiz Technical University

Istanbul, Turkey

Tel: 90-532-653-8505 E-mail: ahmet\_ozan@yahoo.com

## Abstract

Nickel plating processes, popularly used in Europe since 1950s, have been increasingly employed in Turkey in recent years. As a result, industrial usage has developed rapidly. Nickel plating is the preferred process for this study because of the uniformity of the plating thickness on the plated surface and the ease with which complex components can be plated. It is also resistant to corrosion and has good levels of hardness.

In this experiment, the following parameters were investigated: the effect of varying the amount of nickel, the thickness of the plating, and sheen (whether shiny or dull).

In this study, brightening and carrying agents have been used to determine the best operational parameters for the Kale Kilit Factory. The compositions of the brightening and carrying agents used in the experiment are included in this text. Additionally, investigations were conducted on how the plating color changed when compared to the original bath as a result of using  $\text{Fe}^{2+}$  complex concentration in nickel plating baths, as a brightening agent and for analyzing the color of the plated sample, under a visible region spectrophotometer at 350 nm and 6500 kelvin light power and D65 (Average North Sky Daylight) light. In our research, the most important feature of analysis is that the desired color effect is obtained by using brightening agents containing  $\text{Fe}^{2+}$  complex concentration without any interference from any colorant after nickel plating by electrolysis. In this study where nickel plating bath characteristics are researched, physical tests such as brittle test are applied to the plated materials, which provide us important ideas about the accuracy of the choices made according to standards.

**Keywords:** Nickel plating, Electrolytic plating, Corrosion, Electron microscopy, X-ray unit, Visible region spectrophotometer, Brightening agent, Carrying agent

## 1. Introduction

Various types of plating processes are extensively employed in different industries, both to increase the resistance to corrosion and to impart a more decorative appearance to steel and to metals such as aluminum, zamak, and brass. Second, and the most frequently used plating process is nickel plating (with zinc plating being the most popular). As nickel alone does not provide the desired visual effects, it is plated over with chromium in most cases.

When applied to hard and soft metals, nickel plating does produce a distinct decorative appearance and provide corrosion resistance; however, best results have been obtained with chromium plating over sulfate- based nickel plating.

## 2. Experiments

In this experiment, the following parameters of the nickel plating process were investigated: amount of nickel, thickness of the plating, and sheen (whether shiny or dull).

### 2.1 Experimental Conditions

In the present study, the “Kale Kilit and Kalıp Sanayi A.Ş.” Chemistry Laboratories and their plating facilities were selected as the environment for the experiments. In addition to nickel baths, the Kale Kilit A.Ş. plating facility possesses cyanide copper baths, chromic acid baths, zinc acid baths, brass sulfate baths, and brass cyanide baths, all of 1- ton capacity.

### 2.2 Choice of the Chemicals

Watt- type baths (Saticioglu, 2006, pp. 22-25; Yilmaz, 2006, pp. 36-44) are used in all nickel processes, indicating that the inorganic compositions resemble one another. Therefore, the main composition of the nickel-plating bath in our experiments was as in Table 1, and the analytical composition of the bath was as in Table 2.

### 2.3 Hull Cell

In 1937, the American scientist A. Hull analyzed the link between anode-cathode spacing and the current density on a piece of metal and developed a formula based on his findings. Hull then designed a special container with this information in mind. Today, both the experiment and the container are referred to as Hull Cells (Cetinkaya, 2006, pp.34-36). The Hull Cell container is a miniature plating unit consisting of cathodic plating on a metal plate, designed to test the bath and the plating characteristics. The interpretation of the plated test panel provides data on the brightness, homogeneity, plating quality, distribution power, contamination, and the chemistry of the plating bath. The Hull Cell reflects the actual process that occurs in the plating bath in the context of the proposed operational parameters. The plated specimen and the Hull Ruler are together used to carry out the research. Thus, preventative maintenance, error correction, and quality control functions are tested and rapidly performed without damaging the actual bath. All plating in this study was done using a Hull Cell.

### 2.4 Preliminary Preparation for the Experiment

The plating experiments were performed using Hull Cell (HC) containers. The HC work was done at 50°C, without mixing. In each case, shiny stainless steel plates of 70 cm<sup>2</sup> (10 cm \* 7 cm) surface area were used. A current of 1 A, (0.01 A/cm<sup>2</sup>), was applied to the plates for 10 minutes. However, since the plating was not sufficiently thick, a bath with the same chemical composition was used for a second time, with the current increased to 2 A, (0.02 A/cm<sup>2</sup>), for 10 minutes. The plates were cleaned in an degreasing electrolytic bath prior to plating and were rinsed with tap water. They were then neutralized in a 10% sulfuric acid bath prior to being rinsed once again with tap water. The plates were then subjected to the Hull Cell operation without being dried.

### 2.5 Hull Cell Test

Initial experiments were performed without adding organic chemicals (such as a carrying or a brightening agent) to the electrolyte solution (Figure 1).

#### 2.5.1 The Effect of the Carrying Agent

The composition of the carrying agent is shown in Table 3.

We investigated varying concentrations of the carrying agent: 5 g/L (Figure 2), 10 g/L (Figure 3), and 15 g/L (Figure 4). Anticipating the quantities that would be required in later experiments, as well as, other influences, the 10 g/L amount was chosen and then further increased by 10% to 11 g/L. An 11 g/L concentration of carrying was added to the solution and the test panel was plated by the Hull Cell. The resultant plating had a matte texture. Following X-ray examination, it was determined that plating ranging between 1 and 5 microns in thickness was achieved over the investigated current range. As good results were obtained with the 11 g/L carrying agent concentration, this was selected as the most suitable concentration from a cost perspective.

#### 2.5.2 The Effect of the Brightening Agent

The composition of the brightening agent is shown in Table 4.

The concentrations of the brightening agent used were 0.3 g/L (Figure 5), 0.5 g/L (Figure 6), and 0.7 g/L (Figure 7). From this survey, for the desired color difference, the optimal concentration of brightening agent to be used was defined as 0.5 g/L according to the fragility test results. The repeated addition of 6 g/L Ni<sup>2+</sup> to the bath resulted in reduced brightness. Accordingly, it was decided to maintain the Ni<sup>2+</sup> density at 75 g/L. A high percentage of nickel in the plating caused brittleness of the plating. The quantities of the brightening agent and other compounds were determined in separate instances. To ensure a standard concentration of the various compounds used a large volume of the mixture. Thus, the proportions were kept constant, irrespective of the quantity that was added to the bath.

### 2.6 Results of the X-Ray Examination

The X-ray equipment (Fischer Instruments GmbH, 2002) measures the plating thickness and provides accurate information on the Ni percentages, as well as the average, maximum and minimum values, and the standard deviation.

The plating thickness of the nickel-plated iron, plated in the bath, was measured by a Helmut Fischer brand X-ray coating thickness measurement gauge. The results are given in Table 5, Table 6, Table 7, Table 8, Table 9, Table 10, Table 11, Table 12, Table 13.

The nickel plating thickness standard for the lock components at the Kale Kilit Factory was set in range of 10-20 microns. The nine plated pieces complied with these standards.

### 2.7 Nickel-Plating Bath Analyses

#### Necessary Materials

25% Ammonia solution ( $\text{NH}_3/\text{H}_2\text{O}$ , pH=11.7), 10% Potassium chromate solution, Murexide indicator, Boric acid buffer solution, 0.1 M EDTA, 0.1 N Silver nitrate, 0.2 N Sodium hydroxide.

#### 2.7.1 Metallic Nickel Analysis

Using a pipette, 1 g of sample was transferred from the bath into an Erlenmeyer flask. Next, 100 g of pure water, 10 g of ammonia (25%, pH=11.7), and a small quantity of murexide indicator were added. This was titrated with EDTA until a color change was observed.

Result: Consumption  $\times 5.87 = \dots$ g/L metallic nickel ( $\text{Ni}^{2+}$ )

#### 2.7.2 Chloride Analysis

A 1 g sample was pipetted from the bath and transferred into an Erlenmeyer flask. Next, 100 g of distilled water and four or five drops of potassium chromate were added, and the color changed to crimson-red. It was then titrated with silver nitrate until it became reddish-brown in color.

Result: Consumption  $\times 3.75 = \dots$ g/L chloride ( $\text{Cl}^-$ )

#### 2.7.3 Analysis of Boric Acid

A 1 g sample was pipetted from the bath and transferred into an Erlenmeyer flask. Next, 25 g of boric acid buffer solution was added. This was titrated with sodium hydroxide until a violet color was achieved.

Result: Consumption  $\times 6.2 = \dots$ g/L boric acid ( $\text{H}_3\text{BO}_3$ )

The experimental results are given in Table 14.

### 3. Discussion

Recently, the decorative use of nickel plating baths in the plate industry has caused the industry itself to seek new waves of research. One of those states that instead of applying colorants according to the desired colors after the metal coating for corrosion protection and decorative purposes, simply add brightening agents, simultaneously to the metal plating bath solutions, as colorants. In our studies, the results we obtain from different proportions, according to the desired colorant effect, is measured with electron microscopy, hardness durability, X-ray method (to measure the thickness of plate), and visible spectrophotometry.

When analyzing with the electron microscope, Jeol 6060 Scanning Electron Microscope is used. The working range of this microscope is; high voltage separation power 1~ 30 kV, magnification 10~ 1 000 000, using SEI mode (secondary electron image)~ BEI (backscattered electron image), its resolution is 30 kV (SEI) at 1.2 nm, and 30 kV (BEI) at 3.0 nm. Also the listed parameters of the electron microscope with regard to image definition and working quality are determined as follows: resolution 100 nm, high voltage separation 8.0 kV, using SEI mode, working distance (WD) 8.1 mm, and a magnifying scale of 80 000. To produce images of surfaces, SEI is used as a first choice because in electron microscopes, the electrons sent on to the specimen produce two kinds of images. The first is the secondary electron image (SEI), which is used to produce images of secondary electrons that originate after stimulating specimen atoms, and the second is the backscattered electron image (BEI), which consists of the electrons that are backscattered out of the specimen interaction volume by elastic scattering interactions with specimen atoms. SEI uses a topographical contrast, whereas, BEI creates the contrast according to the atomic numbers. In other words, with SEI it is possible to examine the sample surface with regard to its form and with BEI with regard to the chemical differences. This is why we have used secondary electron images (SEI) in our studies.

In total we have carried out our research with seven bath samples, which consists of one original, three different proportions of nickel baths including carrying agent chemicals, and three different proportions of nickel baths with brightening agent chemicals, thus acquiring seven electron microscope images. As can be seen from the electron microscope images, the concentration of carrying agent chemicals does not have a significant effect on the surface, whereas, the concentration involving brightening agents, with the proportions rising, the color of the nickel plated metal surface transforms into the different tones of red, because the brightening agent has metallic iron (from figure 1 to figure 7).

The impact of the  $\text{Fe}^{2+}$  complex present in the brightening agent on the plating surface is measured with CIE  $L^*a^*b$  color space (Yilmaz, 2002, pp.340-350; Dogan, & Zaimoglu, 2006, pp.107-118). CIE  $L^*a^*b$  color system is the most used space. Measurement of the comparison of color values is more recognizable with this system. This method is used to measure the contrast between a certain specified standard color and a sample color. In the

CIE  $L^*a^*b^*$  color system (Icoglu, 2006, pp.41-43),  $L^*$ ,  $a^*$ ,  $b^*$ ,  $c^*$ , and  $h^0$  values are the main parameters used in defining the colors.

Where

$L^*$ : is the central vertical axis. The values used are  $0^\circ$  for black and  $100^\circ$  for white.  $L$  values range between these two.  $L^*$  value represents lightness.

The chromatic coordinates  $a^*$  and  $b^*$ : in the CIE  $L^*a^*b^*$  color space, represent  $+a^*$  red,  $-a^*$  green,  $+b^*$  yellow, and  $-b^*$  blue.

$c^*$ : Is named as chromaticity. The chromaticity value of the color increases as the value drifts from the center of the color space in a horizontal level. It gives information about the saturation of the color. A color and its tone at the same level is the characteristic defining its distinction level from another color (between black and white). If a color diverges from black, its saturation will increase, if it approaches to gray, its saturation will decrease. Exact gray's saturation is 0. As each color's maximum saturation degree varies, the upper limit cannot be indicated. In the CIE  $L^*a^*b^*$  color space, the  $c^*$  value, is measured by the angle between the measured color's projection in the axis of ordinate and its angle in the axis of ordinate.

$h^0$  (hue): Is the basic color of an object (like red, blue, yellow), it is an angle between  $c^*$  (chromaticity) and the axis of abscissa. Angle  $h^0$  is  $0^\circ$  and  $360^\circ$  along  $+a^*$ ,  $90^\circ$  for  $+b^*$ ,  $180^\circ$  for  $-a^*$ , and  $270^\circ$  for  $-b^*$ . It gives an idea about the size of the color. The  $h^0$  value can be defined as the angle between the axis of the abscissa of measured color and axis of the abscissa of standard color (Figure 8).

The colorant effect of the chemical, which contains the  $Fe^{2+}$  complex added to the nickel plating bath, on the metal plate is examined with the Macbeth CMC-CE-7000-XL0339 which is a visible region spectrophotometer. The device is at 325 nm wavelength and capable of taking measurements in the range of 2000~7500 kelvin light power. D65 daylight used in the spectrophotometer is equal to 6500 kelvin light power, and this light power means light power for the plated material surfaces. These values are decided according to European and Japanese standards. According to the information gathered from the result of this analysis, under D65 daylight measurement, it is observed that brightening agent plates located on the red side of the red~ green axis of the illuminant D65 graphics result in an increase in the red axis when the brightening agent concentration is increased. Similarly, during addition of carrying agent, it is observed that the sample plate in illuminant D65 graphic does not diverge from the standard (original) bath plate axis (from figure 9 to figure 14). It is observed that the  $h^0$  (hue) and  $c^*$  (chromaticity) values of the samples do not change much at the point of saturation and hue value of red color. Similarly, the  $L$  value, which can be expressed as lightness~ darkness, is observed and does not change with addition of brightening agent and carrying agent, and is shown as a 'light~ dark' scale at each graphic axis. At the measurement of the  $L$  value, the distance to the standard rectangle located at the middle of the light~ dark scale is referenced.

When deciding the optimum working conditions for nickel baths which are the main topic of our study, effects of the medium with added chemicals on the bath's physical features are researched. As for this, effects of nickel baths with increasing pH, due to added brightening agent, on the working quality of the baths are researched by brittling tests of the plated materials. Increase of the brightening agent amount added to the bath raises the pH of the bath, as is shown in the X-ray report. Increase of pH in the bath causes more fragility in the plating. The 'Increasing Progressive Power Test Method' (Kiray, 2007, pp.313) is used in brittle tests as the measurement method. In this method, power is applied to a plate that is progressively between two plates. For iron platings, 14.701 N power is applied, which is acceptable by ASTM 8 standards. A bath plating material with 5.5 pH cracked after 15 hours; a plate with 6 pH cracked after 14.9 hours; and a plate with 6.5 pH cracked after 10 hours of the test.

Visible region spectroscopy:

For visible region spectroscopy, two different measurements are taken from each plate surfaces. Therefore, these measurements are figured as 2 in the light axis. The original axis ( $-a, +a$  and  $-b, +b$ ) whose every aperture is figured as 1, means the color measurement of the plate is taken from the visible the region spectroscopy and does not contain any brightening agent or carrying agent. Other axes in the arch form shows color measurements of plated materials with nickel bath to which brightening and carrying agent are added at different proportions for determining  $h^0$  and  $c^*$  parameters. Therefore, the parameters for appointing color for standard (original) bath are calculated as follows (Dogan, & Zaimoglu, 2006, pp.107-118);

$$\Delta L^* = L^*_{\text{sample}} - L^*_{\text{standard}}$$

$$\Delta c^* = c^*_{\text{sample}} - c^*_{\text{standard}}$$

$$\Delta h^0 = h^0_{\text{sample}} - h^0_{\text{standard}}$$

Color measurements and the results of calculations of the color measurements are given in Table 15, Table 16, Table 17, Table 18, Table 19, Table 20, Table 21, Table 22. All measurements given in tables are color measurements which were gathered with the original bath taken as the standard.

#### 4. Conclusion

The effects of the carrying and brightening agents were observed under laboratory conditions. In this study, it was observed that the carrying agent facilitated the deposition of nickel onto the surface and increased cohesion, thus resulting in coating of all surfaces of the component to be plated. This has been confirmed by thickness reports from X-ray equipment and observations by electron microscopy. The brightening agent reduced the productivity of the current. All of these results could have been obtained from thickness reports of the X-ray unit because, according to these reports, plating thickness was decreased. When carrying and brightening agents were added, it was observed the brightening agent increased the pH level of the nickel bath, but the carrying agent did not affect the pH levels. In the bending experiments that were performed on a coated plate, after adding a brightening agent, increased brittleness was observed. On the other hand, the desired decorative appearance was obtained. Current density was as 0.02 A/cm<sup>2</sup> because plating thickness of 10-20 microns, the determined quality standard at the Kale Kilit factory has been obtained at this current density. The conducted experimental work determined the optimum quantities of both organic compounds. It was concluded that the optimum quantity of the carrying agent was 11 g/L, and of the brightening agent, 0.5 g/L.

After the study, the main composition of the nickel bath was determined to be as follows:

260 g/L Nickel sulfate (NiSO<sub>4</sub> .6H<sub>2</sub>O)

67 g/L Nickel chloride (NiCl<sub>2</sub>)

45 g/L Boric acid (H<sub>3</sub>BO<sub>3</sub>)

Chemicals:

11 g/L Carrying agent

0.5 g/L Brightening agent

The optimal working parameters for the factory are as follows:

45°C–55°C Temperature

0.01-0.05 A/cm<sup>2</sup> Current Density

0.44 micron/min. (at 0.02 A/cm<sup>2</sup>) plating speed

#### References

- Cetinkaya, E. (2006). Cinko-Nikel Alasim Kaplamalarının Karakteristiklerinin Incelenmesi. Yüksek Öğretim Kurulu Ulusal Tez Merkezi. (pp.34-36). Tez No: 182745. [Online] Available: <http://tez2.yok.gov.tr/> (2006).
- Dogan, E., Zaimoglu, A. (2006). Comparison of the Colour Stability of Low Fusing Porcelain with Different Thickness Baked on Base Metal Alloy and Metal Free Cores after Aging Process. Ankara: *A.U., Dis Hek. Fak. Derg.* 33(1), 107-118.
- Icoglu, H. (2006). Pamuklu Dokunmuş Kumaşların Reaktif Boyarmaddelerle Boyanması Ve Uygulama Yöntemlerinin Incelenmesi. [Online] Available: <http://library.cu.edu.tr/tezler/5708.pdf> (2006).
- Kiray, S. (2007). Hidrojen Gevrekliği; Sebepleri ve Cozumleri. [Online] Available: [http://www.muhendisim.org/hidrojen\\_gevrekligi\\_sebepleri\\_ve\\_cozumleri-t313.0.html](http://www.muhendisim.org/hidrojen_gevrekligi_sebepleri_ve_cozumleri-t313.0.html) (Mar. 14, 2007).
- Saticioglu, F. (2006). Nikel Kaplama Banyolarında Komponentler ve Çalışma Limitleri., *Yüzey İşlemler Sanayi Katalogu*. (pp. 22-25). Istanbul: E-Publishing Inc.
- Yılmaz, I. (2002). Renk Sistemleri, Renk Uzayları Ve Donusumler, Selcuk Universitesi Jeodezi Ve Fotogrametri Muhendisligi Öğretiminde 30. Yıl sempozyumu. [Online] Available: [http://www.harita.selcuk.edu.tr/arsiv/semp\\_pdf/340\\_350.pdf](http://www.harita.selcuk.edu.tr/arsiv/semp_pdf/340_350.pdf) (October 16-18, 2002).
- Yılmaz, P. (2006). Kaplama Tesisinde Karsilasilabilecek Sorunlar Ve Cozumleri., *Yüzey İşlemler Sanayi Katalogu*. (pp. 36-44). Istanbul: E-Publishing Inc.

Table 1. The main composition of the nickel-plating bath

Material Name	Formulation	Concentration (g/L)
Nickel sulfate	$\text{NiSO}_4 \cdot 6\text{H}_2\text{O}$	260
Nickel chloride	$\text{NiCl}_2 \cdot 6\text{H}_2\text{O}$	67
Boric acid	$\text{H}_3\text{BO}_3$	45

Table 2. The analytical composition of the bath

Material Name	Formulation	Concentration (g/L)
Metallic nickel	$\text{Ni}^{2+}$	75
Chloride	$\text{Cl}^-$	20
Boric acid	$\text{H}_3\text{BO}_3$	45

Table 3. The composition of the carrying agent

Material Name	Formulation	For a 100 kg product
Sodium saccharine	$\text{C}_7\text{H}_4\text{NNaO}_3\text{S} \cdot 2\text{H}_2\text{O}$	25.0 kg
35% Sodium allyl sulfonate	$\text{C}_3\text{H}_5\text{NaO}_3\text{S}$	6.7 kg
Water	$\text{H}_2\text{O}$	68.3 kg

Table 4. The composition of the brightening agent

Material Name	Formulation	For a 100 kg product
Metasulfobenzaldehyde	$\text{HSO}_3\text{C}_6\text{H}_5\text{CHO}$	7.6 kg
Pyridine-3-sulfonic acid	$\text{SO}_2\text{OH}_3\text{C}_5\text{H}_5\text{N}$	3.8 kg
p-vinylbenzenesulfonic acid	$\text{C}_6\text{H}_5\text{CHCH}_2\text{C}_6\text{H}_4\text{O}_3\text{S}$	1.9 kg
o-benzoylsulfonamide	$\text{C}_6\text{H}_5\text{SO}_2\text{NH}_2$	8.6 kg
Sodium saccharine	$\text{C}_7\text{H}_4\text{NNaO}_3\text{S} \cdot 2\text{H}_2\text{O}$	10.0 kg
Iron (II) acetylacetonate	$\text{CH}_3\text{COCH}=\text{C}(\text{O})\text{CH}_3)_2\text{Fe}$	0.3 kg
Water	$\text{H}_2\text{O}$	67.8 kg

Table 5. Product: 1/Ni/Fe Dir.: Fischer Block: 3.7.1

Application: 1/Ni/Fe  $-0.01 \text{ A/cm}^2$  current density

Number of Reading	Nickel Plating Thickness ( $\mu\text{m}$ )			Mean ( $\mu\text{m}$ )	Standart Deviation ( $\mu\text{m}$ )	C.O.V (%)	Range ( $\mu\text{m}$ )	Maximum Reading ( $\mu\text{m}$ )	Minimum Reding ( $\mu\text{m}$ )	Measuring Time (Sec.)
3	6.1	7.2	8.5	7.26	1.513	20.84	2.4	8.5	6.1	10

Table 6. Product: 1/Ni/Fe Dir.: Fischer Block: 3.7.2

Application: 1/Ni/Fe -0.02 A/cm<sup>2</sup> current density

Number of Reading	Nickel Plating Thickness (μm)			Mean (μm)	Standart Deviation (μm)	C.O.V (%)	Range (μm)	Maximum Reading (μm)	Minimum Reding (μm)	Measuring Time (Sec.)
3	10.2	11.4	13.7	11.76	2.206	18.758	3.5	13.7	10.2	10

Table 7. Product: 1/Ni/Fe Dir.: Fischer Block: 3.7.3

Application: 1/Ni/Fe -0.03 A/cm<sup>2</sup> current density

Number of Reading	Nickel Plating Thickness (μm)			Mean (μm)	Standart Deviation (μm)	C.O.V (%)	Range (μm)	Maximum Reading (μm)	Minimum Reding (μm)	Measuring Time (Sec.)
3	18.7	21.4	25.6	21.9	4.350	19.86	6.9	25.6	18.7	10

Table 8. Product: 1/Ni/Fe Dir.: Fischer Block: 3.7.4

Application: 1/Ni/Fe -5 g/L carrying agent, 0.02 A/cm<sup>2</sup> current density

Number of Reading	Nickel Plating Thickness (μm)			Mean (μm)	Standart Deviation (μm)	C.O.V (%)	Range (μm)	Maximum Reading (μm)	Minimum Reding (μm)	Measuring Time (Sec.)
3	11.3	15.1	16.8	14.42	2.837	19.68	5.54	16.8	11.3	10

Table 9. Product: 1/Ni/Fe Dir.: Fischer Block: 3.7.5

Application: 1/Ni/Fe -10 g/L carrying agent, 0.02 A/cm<sup>2</sup> current density

Number of Reading	Nickel Plating Thickness (μm)			Mean (μm)	Standart Deviation (μm)	C.O.V (%)	Range (μm)	Maximum Reading (μm)	Minimum Reding (μm)	Measuring Time (Sec.)
3	11.7	13.2	16.2	13.7	2.453	7.6	2.54	16.2	11.7	10

Table 10. Product: 1/Ni/Fe Dir.: Fischer Block: 3.7.6

Application: 1/Ni/Fe -15 g/L carrying agent, 0.02 A/cm<sup>2</sup> current density

Number of Reading	Nickel Plating Thickness (μm)			Mean (μm)	Standart Deviation (μm)	C.O.V (%)	Range (μm)	Maximum Reading (μm)	Minimum Reding (μm)	Measuring Time (Sec.)
3	15.4	18.9	18.6	17.62	1.939	11.01	3.52	18.6	15.4	10



Table 11. Product: 1/Ni/Fe Dir.: Fischer Block: 3.7.7

Application: 1/Ni/Fe – 0.3 g/L brightening agent, 0.02 A/cm<sup>2</sup> current density

Number of Reading	Nickel Plating Thickness (μm)			Mean (μm)	Standart Deviation (μm)	C.O.V (%)	Range (μm)	Maximum Reading (μm)	Minimum Reding (μm)	Measuring Time (Sec.)
3	16.7	18.2	20.1	18.33	1.85	15.47	3.4	20.1	16.7	10

pH: 5.5

Table 12. Product: 1/Ni/Fe Dir. Fischer Block: 3.7.8

Application: 1/Ni/Fe – 0.5 g/L brightening agent, 0.02 A/cm<sup>2</sup> current density

Number of Reading	Nickel Plating Thickness (μm)			Mean (μm)	Standart Deviation (μm)	C.O.V (%)	Range (μm)	Maximum Reading (μm)	Minimum Reding (μm)	Measuring Time (Sec.)
3	11.4	15.7	16.3	14.42	3.08	21.42	4.9	16.3	11.4	10

pH: 6

Table 13. Product: 1/Ni/Fe Dir. Fischer Block: 3.7.9

Application: 1/Ni/Fe – 0.7 g/L brightening agent, 0.02 A/cm<sup>2</sup> current density

Number of Reading	Nickel Plating Thickness (μm)			Mean (μm)	Standart Deviation (μm)	C.O.V (%)	Range (μm)	Maximum Reading (μm)	Minimum Reding (μm)	Measuring Time (Sec.)
3	8.3	9.5	10.1	9.3	1.13	12.20	1.8	10.1	8.3	10

pH: 6.5

Table 14. The experimental results

Material	Consumption		Material	Consumption		Material	Consumption
Ni <sup>2+</sup> (g/L)	EDTA (g)		Cl <sup>-</sup> (g/L)	AgNO <sub>3</sub> (g)		H <sub>3</sub> BO <sub>3</sub> (g/L)	NaOH (g)
70.44	12		24.85	6.6		37.2	6

Table 15. Color measurement of plated sample (material) with bath which does not contain brightening and carrying agent

Standart	Illuminant	L*	c*	h <sup>0</sup>
Original bath	D65	19.664	22.631	17.213

Table 16. Color measurement of 5 g/L carrying agent added plating bath (Figure 9)

Sample (Material)	Illuminant	L*	c*	h <sup>0</sup>
Trial 1	D65	19.659	22.609	17.200
Trial 2	D65	19.645	22.599	17.188

Table 17. Color measurement of 10 g/L carrying agent added plating bath (Figure 10)

Sample (Material)	Illuminant	L*	c*	h <sup>0</sup>
Trial 1	D65	19.643	22.625	17.205
Trial 2	D65	19.626	22.618	17.206

Table 18. Color measurement of 15 g/L carrying agent added plating bath (Figure 11)

Sample (Material)	Illuminant	L*	c*	h <sup>0</sup>
Trial 1	D65	19.622	22.617	17.198
Trial 2	D65	19.624	22.611	17.166

Table 19. Color measurement of 0.3 g/L brightening agent added plating bath (Figure 12)

Sample (Material)	Illuminant	L*	c*	h <sup>0</sup>
Trial 1	D65	18.342	23.530	19.366
Trial 2	D65	18.205	23.444	19.506

Table 20. Color measurement of 0.5 g/L brightening agent added plating bath (Figure 13)

Sample (Material)	Illuminant	L*	c*	h <sup>0</sup>
Trial 1	D65	18.135	23.410	19.436
Trial 2	D65	18.027	23.261	19.618

Table 21. Color measurement of 0.7 g/L brightening agent added plating bath (Figure 14)

Sample (Material)	Illuminant	L*	c*	h <sup>0</sup>
Trial 1	D65	18.299	23.368	19.320
Trial 2	D65	18.283	23.298	19.584

Table 22. Results of calculations of the color measurements

Sample (Material)	Trial 1			Trial 2		
	$\Delta L^*$	$\Delta c^*$	$\Delta h^0$	$\Delta L^*$	$\Delta c^*$	$\Delta h^0$
5 g/L carrying agent added bath	-0.005	-0.022	-0.013	-0.019	-0.0232	0.025
10 g/L carrying agent added bath	-0.021	-0.006	-0.008	-0.038	-0.013	-0.007
15 g/L carrying agent added bath	-0.042	-0.014	-0.015	-0.04	0.02	-0.047
0.3 g/L brightening agent added bath	-1.322	0.899	2.153	-1.459	0.813	2.293
0.5 g/L brightening agent added bath	-1.529	0.779	2.223	-1.637	0.630	2.405
0.7 g/L brightening agent added bath	-1.365	0.737	2.107	-1.381	0.667	2.371

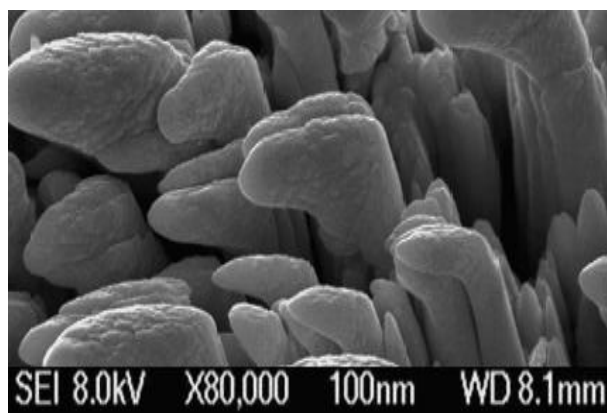


Figure 1. The SEM image of the original form of the nickel plating bath

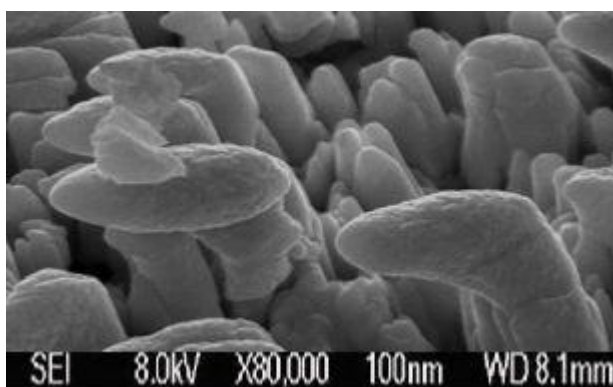


Figure 2. The SEM image of 5 g/L carrying agent added plating bath

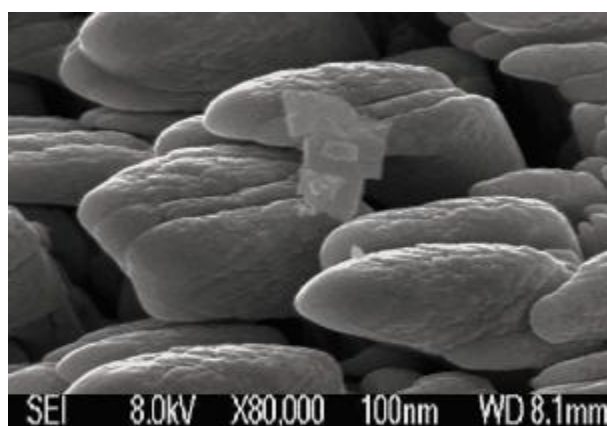


Figure 3. The SEM image of 10 g/L carrying agent added plating bath

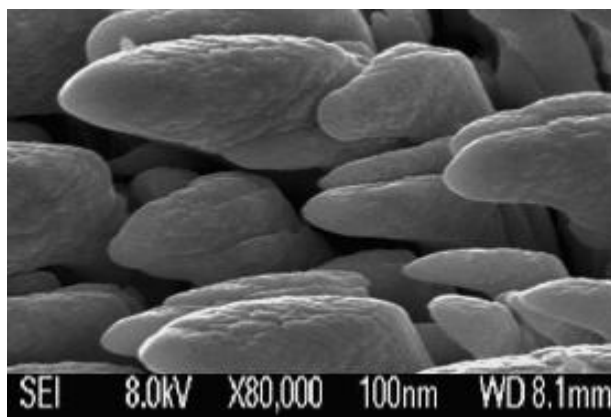


Figure 4. The SEM image of 15 g/L carrying agent added plating bath

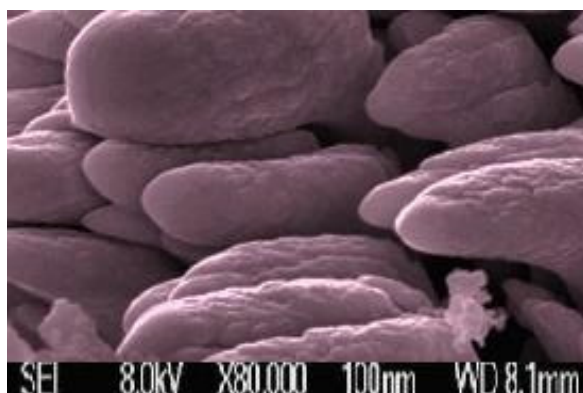


Figure 5. The SEM image of 0.3 g/L brightening agent added plating bath

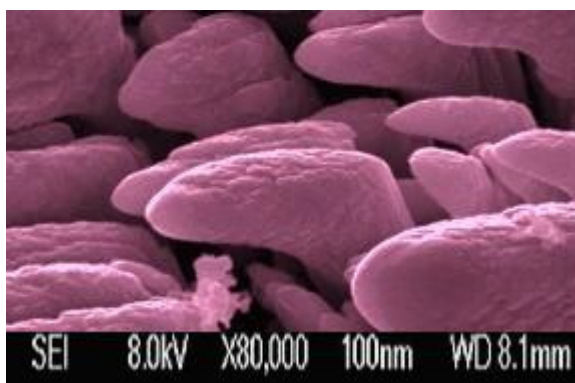


Figure 6. The SEM image of 0.5 g/L brightening agent added plating bath

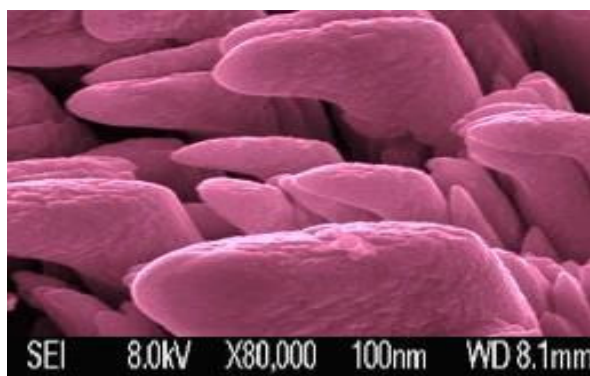


Figure 7. The SEM image of 0.7 g/L brightening agent added plating bath

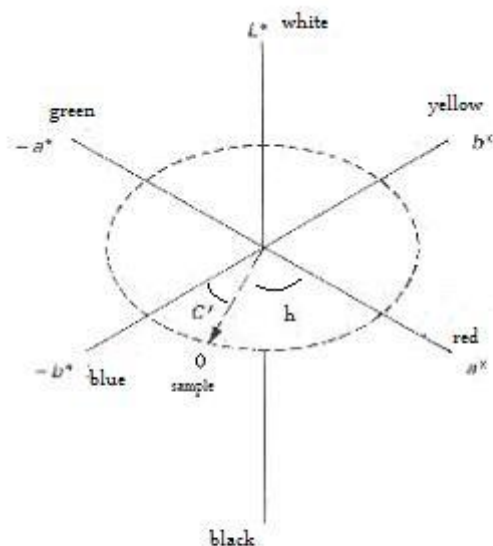


Figure 8. CIE L\*a\*b\* Color Space

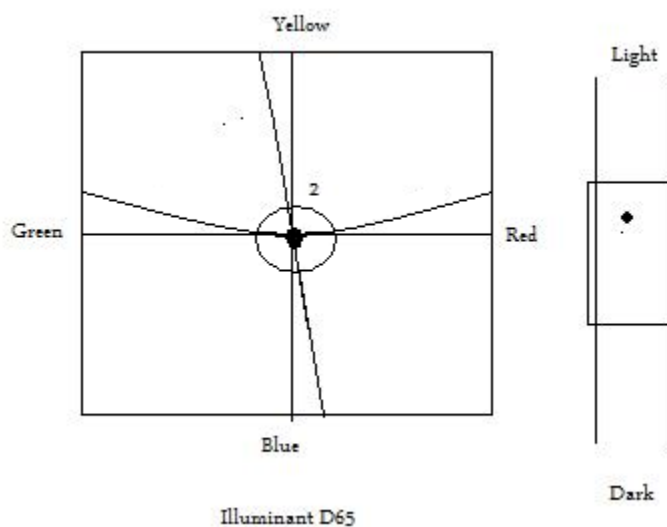


Figure 9. Color measurement of 5 g/L carrying agent added plating bath

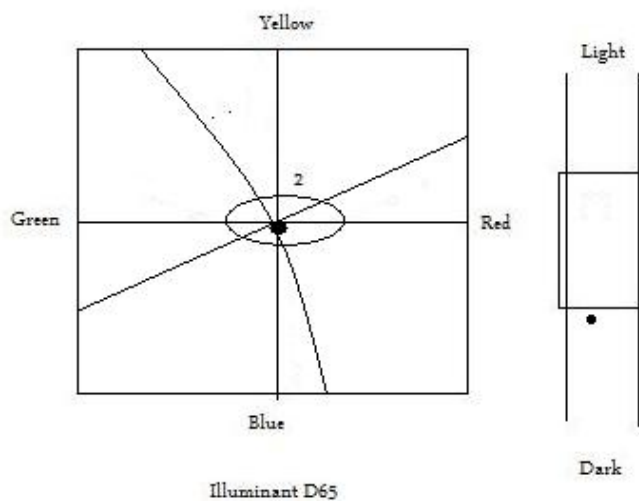


Figure 10. Color measurement of 10 g/L carrying agent added plating bath

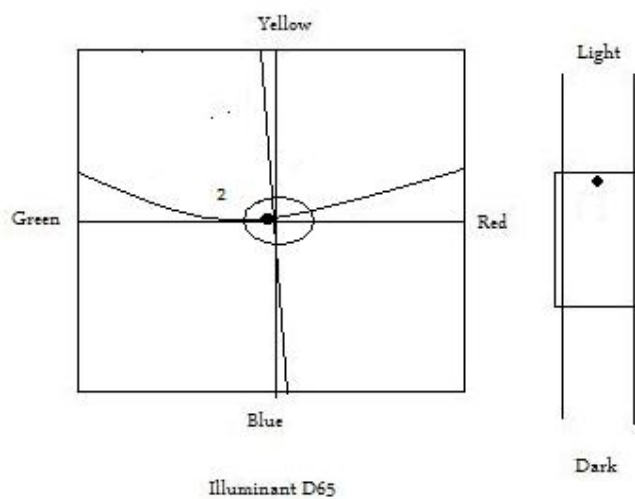


Figure 11. Color measurement of 15 g/L carrying agent added plating bath

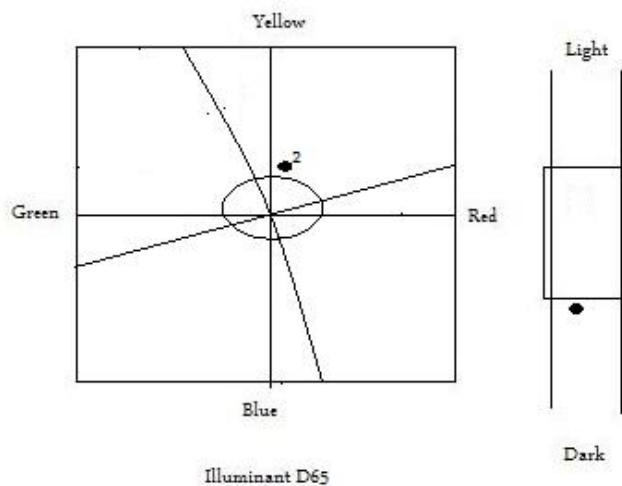


Figure 12. Color measurement of 0.3 g/L brightening agent added plating bath

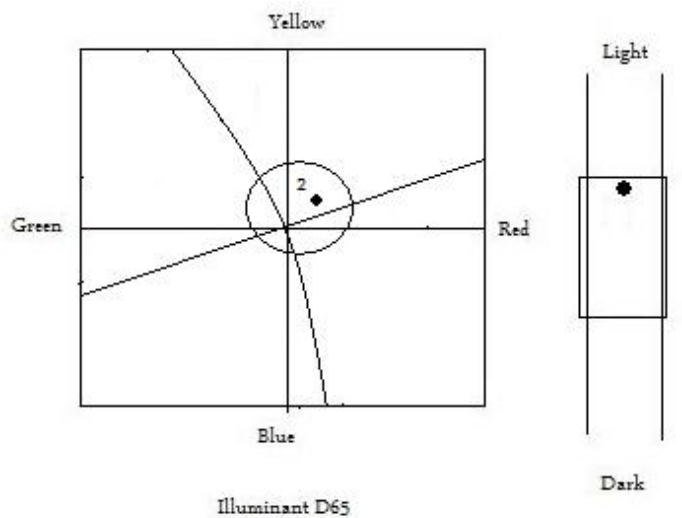


Figure 13. Color measurement of 0.5 g/L brightening agent added plating bath

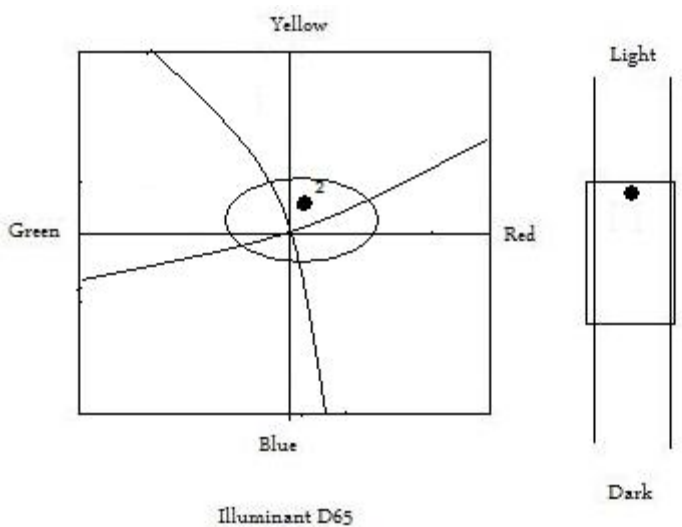


Figure 14. Color measurement of 0.7 g/L brightening agent added plating bath

# Corrosion Inhibition of Carbon Steel in Open Recirculating Cooling Water System of Petroleum Refinery by Thiourea and Imidazole in Presence of Zinc (II) Sulphate

P.K.Gogoi

Department of Chemistry, Dibrugarh University

Dibrugarh-786004, India

Tel: 91-943-513-1158 E-mail: dr\_pradip@yahoo.com

B. Barhai (Corresponding author)

Department of Chemistry, Dibrugarh University

Dibrugarh-786004, India

Tel: 91-943-515-2247 E-mail: bedobratlab@nrl.co.in

## Abstract

The inhibiting action of thiourea and imidazole towards corrosion for carbon steel in open recirculating cooling system (ORCS) of Numaligarh Refinery Limited (NRL), Golaghat, Assam, India has been studied in presence of  $Zn^{2+}$  (as  $ZnSO_4 \cdot 7H_2O$ ) by weight loss and potentiodynamic polarization methods. The values of inhibition efficiency from weight loss method are in good agreement with those obtained from polarization studies. Polarization study indicates that imidazole retards the cathodic corrosion reaction where as thiourea inhibits anodic corrosion reaction in these particular blends of inhibitors. SEM and EDS study confirm the formation of an adsorbed protective film on the carbon steel surface.

**Keywords:** Thiourea, Imidazole,  $Zn^{2+}$ , Weight loss method, Potentiodynamic polarization method, SEM and EDS

## 1. Introduction

In open recirculating cooling water system (ORCS) of a petroleum refinery, carbon steel corrosion is a major problem. The make up water used in ORCS are either from river, sea or underground sources. The presence of large amount of total dissolved solids, total suspended solids, total hardness, microorganism and dissolved gases, such as,  $O_2$  and  $CO_2$  in the makeup water are responsible for scaling, fouling, under deposit and microbiological corrosion in the various equipments of cooling water system. Due to such corrosion the tubes of heat exchanger, an important part of ORCS get damaged easily, which affect the productivity and profitability. To minimize the adverse effect of corrosion, various protective methods have been adopted, one of the frequently used measure is the use of organic compounds containing nitrogen and sulphur atoms (Al-Faiyz YSS *et al.*, 2006, Hossini *et al.*, 2009 and Shetty *et al.*, 2006). These compounds either can form strong co-ordination bond with metal atom or form passive film on the surface (Hassan *et al.*, 2009). There is still a continuous search for better inhibitors or blend of inhibitors to meet the demand of the industry. The selection criteria for various inhibitors include low concentration, stability in recirculation, cost effectiveness and low operational hazard. There are reports of use of several substituted thiourea with increased electron densities at donor sites (Shetty *et al.*, 2006).

We report here the effect of addition of thiourea and another electron donor imidazole in presence of  $Zn^{2+}$  as corrosion inhibitor in ORCS of petroleum refinery and evaluation of their optimum ratio to give the most effective blend for inhibition of corrosion, scale formation and microbiological problems.

## 2. Experimental procedures

Experiments were carried out by weight loss and potentiodynamic polarization methods. For performing these experiments, blends of imidazole (AR, Merck, 25 ppm to 150 ppm) thiourea (AR, Merck, 25 ppm to 150 ppm) and  $Zn^{2+}$  as  $ZnSO_4 \cdot 7H_2O$  (AR, CDH, 50 ppm) of different concentrations were prepared separately. Table-1 gives the details of these blends.



### 2.1 Weight loss method

Carbon steel specimens of C-1010 coupons of known composition (S, 0.05; P, 0.04; Mn, 0.306, C; 0.08-0.13; Al, 0.03; Si, 0.21 and Fe remainder) and size (1.0×1.0×0.15 cm) were used for weight loss study. All these strips were mechanically polished, degreased with acetone and finally dried in an oven at 105°C before and after each experiment. The weight of the test coupons were recorded and tests were carried out in a constant temperature bath of cooling water used in ORCS of NRL, Golaghat, Assam, India in absence and in presence of various blends of inhibitors separately for 15 days at temperature of 30±1°C. The various parameters of cooling water was analyzed by using standard method (Andrew *et al.*, 1995) (Table-2). Strips were then kept in a moisture free desiccator for conditioning. After conditioning, coupons were weighed. From the weight difference the corrosion rate (CR) and percentage of inhibition efficiency (%IE) were calculated by using the equations 1 (AN 116, Corrosion rate calculations from coupons. Rohrbach Cossack Systems 11841 E. Smith Avenue, Santa Fe Springs, CA 90670 USA.) and 2 (Quraishi *et al.*, 2005) respectively.

$$CR = \frac{3,650 \times \text{Weight loss (grams)}}{\text{Metal density (g/cm}^3\text{)} \times \text{Coupon area} \times \text{time (T)}} \quad \text{..... (1)}$$

Where CR is expressed in mm/year, weight loss in grams, corrosion period (T) in days and coupon area in cm<sup>2</sup>.

$$IE\% = R_0 - R \times 100 / R_0 \quad \text{..... (2)}$$

Here  $R_0$  and  $R$  are the corrosion rates in absence and in presence of inhibitors respectively.

### 2.2 Electrochemical studies

For electrochemical studies a carbon steel rod of same composition as those of the coupons used in weight loss studies, embedded in teflon with an exposed area of 0.05 cm<sup>2</sup> was used as a working electrode. A platinum foil was used as a counter electrode and the reference electrode was a silver-silver chloride electrode. In the electrochemical study, tests were carried out in a three electrode cell assembly at room temperature (30°C) using a potentiostat of model 600C of CH instrument. The studies were made in the scan rate of 0.05 v/s. Before starting the polarization scan, a minimum of thirty minutes was given to stabilize the open circuit potential (OCP) within ±10 mv. The plot of E (potential) versus log I was drawn and from this the corrosion kinetic parameters such as corrosion potential ( $E_{\text{corr}}$ ) and corrosion current ( $I_{\text{corr}}$ ) were evaluated (Poongothai N *et al.*, 2007). The percentage of inhibition efficiency (%IE) can be calculated from the equation 3 (Taha K K *et al.*, 2006)

$$\% IE = (i_{\text{corr}} - i_{\text{o corr}}) \times 100 / i_{\text{corr}} \quad \text{..... (3)}$$

Where  $I_{\text{corr}}$  and  $i_{\text{o corr}}$  are corrosion current densities in absence and in presence of inhibitors respectively.

### 3. Scanning electron micrograph

Samples of carbon steel specimen for scanning electron micrographs were prepared by treatment with cooling water used in NRL, Golaghat, Assam, India in absence and in presence of inhibitors (blend of SET-I-100 was taken) for 5 days separately. The SEM and EDS of these samples were recorded at CIF, IIT, Guwahati, Assam, India which are shown in Figure 1, Figure 2 and Figure 3 respectively.

### 4. Results and discussion

From the weight loss study (Table-3) it is found that in case of the inhibitor blends of SET-I (SET-I includes SET-I-25, SET-I-50, SET-I-100, SET-I-150), the percentage of inhibition efficiency increases on increasing the imidazole concentration from 25 ppm to 100 ppm at constant  $Zn^{2+}$  and thiourea concentration ( $Zn^{2+}$ =50 ppm and thiourea =50 ppm), which does not increase on increasing the imidazole concentration beyond 100 ppm. This is also explainable with the help of polarization study. In polarization study the corrosion current density value decreases from the blank value of 10.96  $\mu\text{A/cm}^2$  to 2.04  $\mu\text{A/cm}^2$  (Table-4) on increasing the imidazole concentration from 25 ppm to 100 ppm (the inhibition efficiency increases from 42.42% to 81.38%), after that it increases on increasing the imidazole concentration from 100 to 150 ppm. The  $E_{\text{corr}}$  values shifted from the blank value of -0.1952 mv to -0.2474 mv (Figure 4) on increasing the imidazole concentrations i.e. slightly towards the negative side, which implies that imidazole works as a cathodic inhibitor in these blends of inhibitors (Achary *et al.*, 2007). Similarly in case of the inhibitor blends of SET-II (SET-II includes SET-II-25, SET-II-50, SET-II-100, SET-II-150), the percentage of inhibition efficiency increases on increasing the thiourea concentration from 25 ppm to 100 ppm at constant  $Zn^{2+}$  and imidazole concentration ( $Zn^{2+}$ =50 ppm and imidazole =50 ppm) but beyond 100 ppm of thiourea concentration there is no corresponding increase in corrosion inhibition. In using SET-II inhibitors, the corrosion current density value decreases from the blank value of 13.80  $\mu\text{A/cm}^2$  to 2.75  $\mu\text{A/cm}^2$  on increasing the thiourea concentration from 25 ppm to 100 ppm, implying increase in inhibition efficiency from 38.33% to 80.07 %. The corrosion current density increases on

increasing the thiourea concentration beyond 100 ppm, indicating decrease of inhibition efficiency (Vishnudevan M *et al.*, 2007). The corrosion potential values ( $E_{\text{corr}}$ ) shifted from the blank value - 0.2290mv to -0.1546mv (Figure 5) on increasing the thiourea concentrations, implying the anodic character (Hossini SMA *et al.*, 2009) of thiourea as well as bond formation or physical adsorption.

The SEM micrograph of the test coupon (Figure 2) taken after treatment with inhibitors, shows smooth surface in comparison with the SEM micrograph of untreated coupon (Figure 1), indicating the formation of an adsorbed film of the inhibitors on the metal surface. EDS analysis of the specimen surface (Figure 3) showed presence of carbon, oxygen, nitrogen, zinc, phosphorus, sulphur, and iron after immersion in the solution containing the blended mixture, further corroborates the adsorption of zinc, imidazole and thiourea on the metal surface.

## 5. Conclusion

The present study shows that zinc and imidazole in presence of thiourea in respective ratio of 1.0:2.0:2.0 gives the most effective blend of inhibitors for corrosion, scale formation and microbiological growth of carbon steel in ORCS. The Polarization study indicates that imidazole retards the cathodic corrosion reaction whereas thiourea inhibits anodic corrosion reaction. The inhibition of corrosion is due to formation of an adsorbed passive film on the metal surface as observed from SEM and EDS results.

## Acknowledgements

The authors are grateful to the authorities of Numaligarh Refinery Limited, Golaghat, Assam, India for allowing us to use the cooling water and providing other facilities connected in this study.

## References

- Al-Faiyz Y S S, Ai-Eaid M A and Assubaie F N. (2006). Inhibitive effects of thiourea on BSK46 microalloyed steel. *The Journal of Corrosion Science and Engineering*, 10, 1466.
- Andrew D et al. (1995). *Standard method for the examination of water and wastewater*. American public health association, Water works association and Water environment federation, 19<sup>th</sup> edition 2-36.
- AN 116, Corrosion rate calculations from coupons. Rohrbach Cossack Systems 11841 E. Smith Avenue, Santa Fe Springs, CA 90670 USA.
- Divakara S Shetty and Shetty Prakash. (2008). Inhibition of mild steel corrosion in acid media by benzy l-N'-phenyl thiourea. *Indian Journal of Chemical Technology*, 15, 216.
- Hassan Nazyl and Holze Rudolf. (2009). A Comparative electrochemical study of electrosorbed 2-and 4-mercaptopyridines and their application as corrosion inhibitors at C60 steel. *Journal of Chemical Sciences*, 121, p-693.
- Hossini S M A and Salari M. (2009). Corrosion inhibition of stainless steel 302 by 1-methyl-3-pyridine-2-Y 1-thiourea in acidic media. *Indian Journal of Chemical Technology*, 16, 480.
- Muralidharan S, Madhavan K, Karthikeyan S and Iyer Venkatakrishna. (2002). Influence of anions on corrosion inhibition and hydrogen permeation through mild steel in acidic solutions in the presence of p-tolyl thiourea. *Indian Journal of Chemical Technology*, 9, 68.
- Peterson, Richard A. (1994). Corrosion prevention in boilers using 1,3-imidazole. *United States Patent 5294400*.
- Poongothai N, Natesan M, Palanisamy N, Murugavel SC and Ramachandran T. (2007). Azole, amine, benzoate and nitrate compound mixture as VPI for metals in NaCl and SO<sub>2</sub> environments. *Indian Journal of Chemical Technology*, 14, 481.
- Quraishi M A and Khan S. (2005). Thiadiazoles-A potential class of heterocyclic inhibitors for prevention of mild steel corrosion in hydrochloric acid solution. *Indian Journal of Chemical Technology*, 12, 576.
- Shetty S D, Shetty P and Nayak H V S. (2006). Inhibition of mild steel corrosion in acid media by N-(2 Thiophenyl)-N'-Phenyl Thiourea. *Journal of the Chilean Chemical Society*, 51, 849.
- Shetty S D, Shetty P and Nayak H V S. (2006). The Inhibition action of N-furfuryl -N'-phenyl thiourea on the corrosion of mild steel in acid media. *Journal of Serb. Chemical Society*, 71, 1073.
- Singh Rajesh Kumar, Prakash S Singh S K and Prakash D. (2008). Inhibition of stainless steel by use of thiourea as inhibition in 20% HCl. *Journal of Indian Chemical Society*, 85, 643.
- Taha K K, Sheshadri B S, Ahmed M F and Muralidharan. (2006). Corrosion inhibition of brass by thiocarbamides. *Indian Journal of Chemical Technology*, 13, 128.

Vishnudevan M and Thangavel K. (2007). A comparative study of inorganic versus organic corrosion inhibitors for mitigation of steel in chloride contaminated alkaline solution. *Indian Journal of Chemical Technology*, 14, 22.

Table 1. Composition of various inhibitors

Blends	Zn <sup>2+</sup> (ppm)	Thiourea (ppm)	Imidazole (ppm)
SET-I-25	50	50	25
SET-I-50	50	50	50
SET-I-100	50	50	100
SET-I-150	50	50	150
SET-II-25	50	25	50
SET-II-50	50	50	50
SET-II-100	50	100	50
SET-II-150	50	150	50

Table 2. Parameters of cooling water used

P <sup>H</sup>	Turbidity (NTU)	Conductivity (μs/cm <sup>2</sup> )	TDS (ppm)	Total hardness (ppm)	Ca Hardness (ppm)	SiO <sub>2</sub> (ppm)
7.5	0.37	207.0	136.6	54.0	46.0	2.36

Table 3. Corrosion parameters obtained from weight loss measurements for carbon steel at various concentrations of inhibitors at 30°C

Blends	Weight loss (gm)	Corrosion rate (mmpy)	Inhibition efficiency (%)
BLANK	0.0178	0.2120	-
SET-I-25	0.0082	0.0976	53.96
SET-I-50	0.0072	0.0857	59.57
SET-I-100	0.0059	0.0702	66.88
SET-I-150	0.0062	0.0738	65.18
SET-II-25	0.0075	0.0898	57.64
SET-II-50	0.0068	0.0815	61.56
SET-II-100	0.0052	0.0619	70.80
SET-II-150	0.0057	0.0685	67.69

Table 4. Inhibition efficiency of various blends of inhibitors by potentiodynamic polarization method

Blends	$-E_{\text{corr}}$ (mv)	$I_{\text{corr}}$ ( $\mu\text{A}/\text{cm}^2$ )	IE (%)
BLANK-I	0.1952	10.96	--
SET-I-25	0.2222	6.31	42.42
SET-I-50	0.2581	3.31	69.80
SET-I-100	0.2799	2.04	81.38
SET-I-150	0.2474	2.34	78.64
BLANK-II	0.2290	13.80	-
SET-II-25	0.2173	8.51	38.33
SET-II-50	0.2054	7.94	42.46
SET-II-100	0.1878	2.75	80.07
SET-II-150	0.1546	4.36	68.40

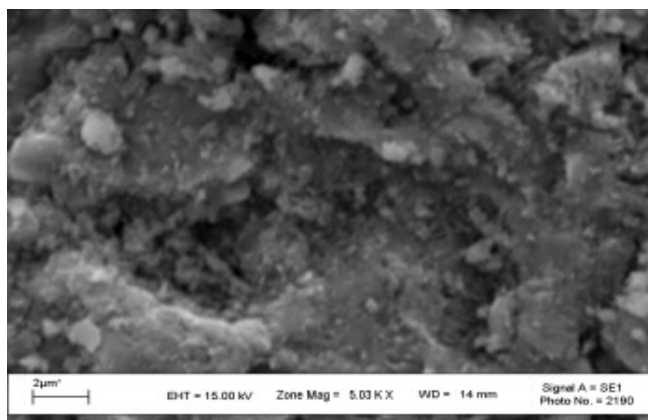


Figure 1. SEM micrograph of carbon steel after 5 days of treatment in absence of inhibitors

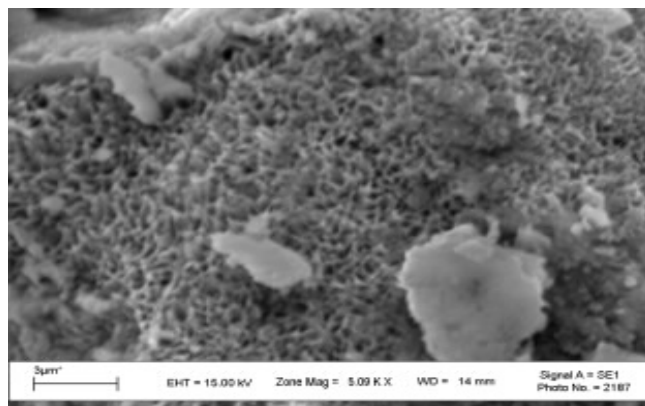


Figure 2. SEM micrograph of carbon steel after 5 days of treatment in presence of inhibitors

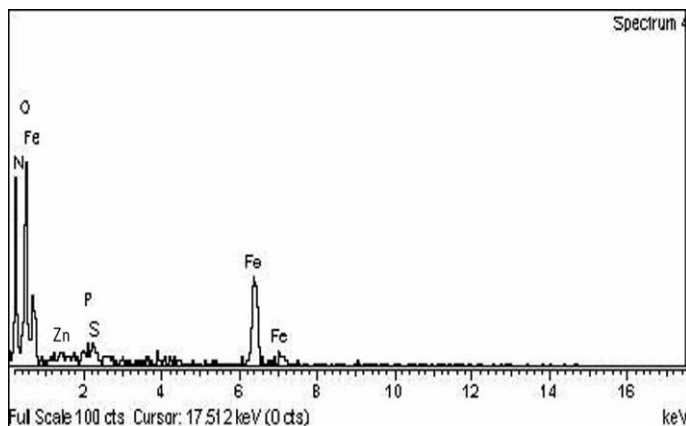


Figure 3. EDS analyses of carbon steel after 5 days of treatment in presence of inhibitors

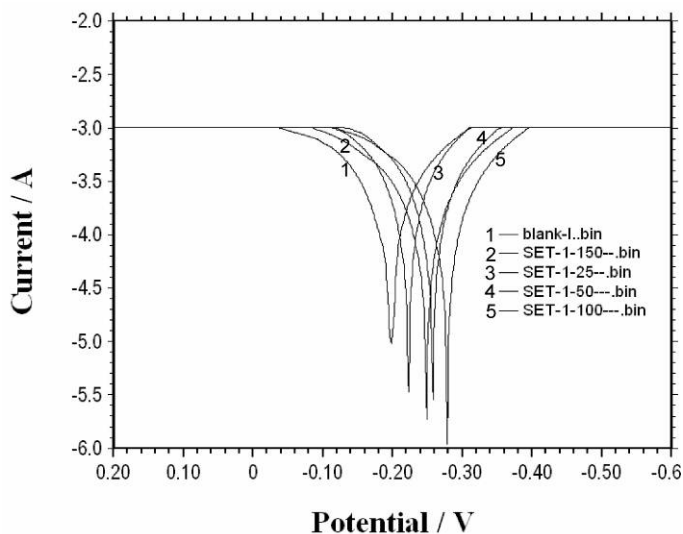


Figure 4. Potentiodynamic polarisation curves for the blends of SET-I

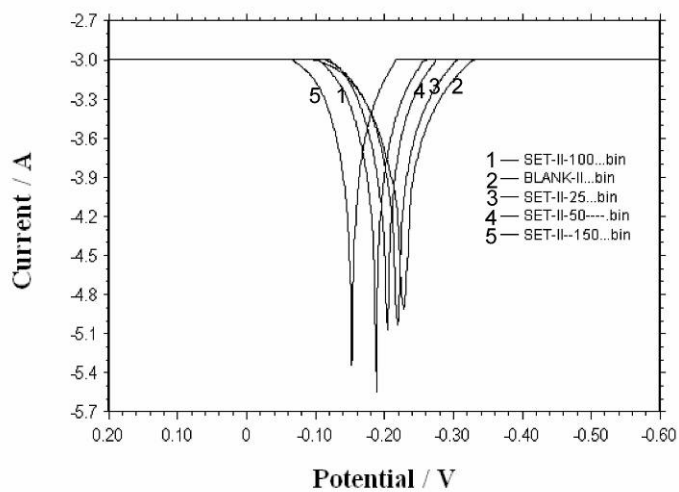


Figure 5. Potentiodynamic polarisation curves for the blends of SET-II

# Preparation and Characterization of Disulfide Functionalized Multi-Walled Carbon Nanotubes for Biomedical Applications

Ke Long Huang (Corresponding author)

Institute of Functional Materials and Chemistry, College of Chemistry and Chemical Engineering

Central South University, Changsha, Hunan 410083, China

Tel: 86-731-887-9850 E-mail: huangkelong@yahoo.com.cn

Ling Hu

Institute of Functional Materials and Chemistry, College of Chemistry and Chemical Engineering

Central South University, Changsha, Hunan 410083, China

E-mail: huling19821216@163.com

Su Qin Liu

Institute of Functional Materials and Chemistry, College of Chemistry and Chemical Engineering

Central South University, Changsha, Hunan 410083, China

## Abstract

To interact with different biologic systems for biomedical applications, chemical modification of carbon nanotubes is always a key step. Disulfide is sensitive to the reductive intracellular environment, and such stimulus-responsive covalent bonds were used to modify carbon nanotubes. After deprotection of N-tert-butoxycarbonyl (Boc) groups of the N-(tert-butyloxycarbonyl) cystamine modified multi-walled carbon nanotubes (MWNTs), positively charged ammonium ( $\text{NH}_3^+$ ) functionalized MWNTs ( $\text{MWNTs-S-S-NH}_3^+$ ) with disulfide linkages were obtained. Their surface functional groups and changes of morphologies were characterized by infrared (IR) spectroscopy and transmission electron microscope (TEM), respectively. The weight percentage of the immobilized disulfide was estimated by thermogravimetric analysis (TGA). And their cytotoxicity in vitro on cultured human nasopharyngeal SUNE1 cells was evaluated. The biocompatibility of MWNTs was improved compared to that of MWNTs without functional groups.

**Keywords:** Multi-walled carbon nanotubes, Disulfide, Functionalization, In vitro cytotoxicity tests

## 1. Introduction

Recently, carbon nanotubes (CNTs) have attracted considerable attention in biomedical applications. CNTs can act as carriers to deliver a variety of biological and bioactive components such as proteins, peptides, DNAs/RNAs, drugs and other biological molecules into cells (Wong *et al.*, 2005, p.6021; Bianco *et al.*, 2005, p.571; Pantarotto *et al.*, 2004, p.5242; Wu *et al.*, 2005, p.6358). To get a kind of well physiologically acceptable material, CNTs should be functionalized firstly. Amines can be further modified with a wide range of biological molecules and therapeutic agents. For example,  $\text{NH}_3^+$ -functionalized CNTs ( $\text{CNTs-NH}_3^+$ ) is such a useful material, which can conjugate biomolecules and deliver them into cells. Georgakilas and Prato (Georgakilas *et al.*, 2002, p.3050; Prato *et al.*, 2008, p.60) have reported that amphotericin B, anticancer agent methotrexate, immunogenic peptides have been carried successfully into cells by  $\text{CNTs-NH}_3^+$ .

Disulfide linkage is stable under extracellular physiological conditions but sensitive to the reductive intracellular environment. Introducing disulfide linkages to CNTs could facilitate releasing the targets from modified CNTs. The concentration of intracellular glutathione is adequate to break the disulfide linkages, while glutathione outside the cells has no such ability due to the relative low concentration (Piest *et al.*, 2008, p.308; Lin *et al.*, 2006, p.130). You (You *et al.*, 2007, p.16161) has decorated MWNTs with small molecules of pyridyl-ended disulfide and conjugated bovine serum albumin (BSA) onto the material through a disulfide-exchange reaction, and the BSA could be smartly released from MWNTs in the presence of glutathione in vitro.

However, there is little information available of functionalizing MWNTs in literature for the purpose of conjugating biomolecules onto CNTs conveniently as well as releasing these molecules smartly. The aim of the work described herein was to functionalize MWNTs, and then to assess the characteristics of toxicity of MWNTs functionalized with disulfide. By this procedure, we can obtain the disulfide functionalities decorated MWNTs with ammonium terminal to endue MWNTs with more convenience for transporting targets and releasing these molecules. The chemical reactions for functionalization of MWNTs are illustrated in Figure 1.

## 2. Experimental

### 2.1 Reagents and Measurements

All solvents and reagents were purchased from commercially available sources and used without further purification unless otherwise stated. The MWNTs (98%, 40-60 nm outside diameters, 5-15  $\mu\text{m}$  lengths ) were purchased from Shenzhen Nanotech Port Co., Ltd.

Fourier transform infrared (FT-IR) spectra were recorded on a Nicolet 6700 IR spectroscopy. Transmission electron microscopy (TEM) images were acquired on a JEOL JEM-1230 electron microscopy at an accelerating voltage of 100 kV. Thermal gravimetric analysis (TGA) was carried out on a Diamond TG-DTA 6300 instrument in flowing Argon at a heating rate of 10  $^{\circ}\text{C}/\text{min}$  from room temperature to 600  $^{\circ}\text{C}$ .

### 2.2 Preparation of functionalized MWNTs

The N-(tert-butyloxycarbonyl) cystamine, containing disulfide linkage, was synthesized via a procedure reported by Niu ( Niu *et al.*, 2008, p.11988).

Oxidized MWNTs (MWNTs-COOH) were obtained by refluxing MWNTs and concentrated nitric acid for 28h. The as-prepared MWNTs-COOH (100mg) were suspended in 15 mL of DMF solution by sonicating the mixture for 30min, then EDC (4.5 mmol) and NHS (4.5 mmol) were added to the above suspension and mixed sufficiently. After stirring the mixture for 24 h, N-(tert-butyloxycarbonyl) cystamine (1.14 g, 4.5 mmol) was added. Then, the reaction was allowed to stir for another 36 h under Ar gas protection, following by centrifuging, sonication and repeated washing. The products of N-(tert-butyloxycarbonyl) cystamine functionalized MWNTs (MWNTs-S-S-NHBoc) were obtained by drying under vacuum. The Boc protecting groups of the MWNTs-S-S-NHBoc are cleaved by treatment with trifluoroacetic acid in dichloromethane for 2 h at the room temperature under Ar gas protection. After centrifuging and washing, the disulfide functionalized MWNTs (MWNTs-S-S-NH<sub>3</sub><sup>+</sup>) were obtained.

### 2.3 Toxicity test in vitro

We studied the toxicity effects of MWNT-S-S-NH<sub>3</sub><sup>+</sup> on human nasopharyngeal SUNE1 cells by MTT assay which was used to determine cell survival in the past few years. SUNE1 cells were incubated with either MWNT-S-S-NH<sub>3</sub><sup>+</sup> or pristine MWNTs. As a control, cells were exposed to physiological saline. The cells were grown in RPMI-1640 cell culture media at 37  $^{\circ}\text{C}$  in 5 % CO<sub>2</sub> humidified incubator and treated for 24 h, 48 h or 72 h with doses of MWNT-S-S-NH<sub>3</sub><sup>+</sup> increasing from 6.25 to 200  $\mu\text{g}/\text{mL}$ . The dose of pristine MWNTs used was 50  $\mu\text{g}/\text{mL}$ .

## 3. Results and discussion

### 3.1 IR spectroscopy

IR spectra of the oxidized MWNTs and positively charged MWNTs are shown in Figure 2. The presence of the added functional groups onto MWNTs is verified. In the spectrum of MWNTs-S-S-NH<sub>3</sub><sup>+</sup> (Figure 2(b)), the characteristic C-H stretching vibration (2923  $\text{cm}^{-1}$ ), as well as amide I band C=O stretching and amide II band N-H bending vibration (1624 and 1540  $\text{cm}^{-1}$ , respectively) are observed. These peaks confirm that disulfide were connected to MWNTs successfully.

### 3.2 TEM analysis

Morphology and nano-structures of pristine MWNTs, MWNTs-S-S-NH<sub>3</sub><sup>+</sup> are observed by TEM which are shown in Figure 3, TEM observations give definitive proof of the presence of MWNTs-S-S-NH<sub>3</sub><sup>+</sup> in the solution. The MWNTs cut by concentrated nitric acid appear in bundles. After functionalization, the MWNTs-S-S-NH<sub>3</sub><sup>+</sup> are shorter and thinner than pristine MWNTs, with diameters of 20-40 nm and lengths of 400-600 nm.

### 3.3 TGA analysis

Thermogravimetric analysis (TGA) measurements of the MWNTs-S-S-NH<sub>3</sub><sup>+</sup> material supplies the quantitative evaluation of the disulfide grafted onto MWNTs (Figure 4). The weight loss of all samples below 200  $^{\circ}\text{C}$  is mainly attributed to release of water molecules and organic molecules adsorbed by samples. Oxidized MWNTs

sample (Figure 4(a)) displays a small quantity of weight loss in the region 200-500 °C. A weight loss, corresponding to 21% for MWNTs-S-S-NH<sub>3</sub><sup>+</sup> sample is observed in the region 200-500 °C (Figure 4(b)), which is attributed to phrolysis of the disulfide connected with the carboxyl groups of MWNTs. The thermal analysis indicate the surface of MWNTs are grafted with a large number of disulfide.

### 3.4 In vitro toxicity

Insoluble and pristine CNTs have induced cell death in vitro (Cui *et al.*, 2005, p.73; Bottini *et al.*, 2006, p.121; Kiura *et al.*, 2005, p.359). To assess the biological properties of the functionallized MWNTs-S-S-NH<sub>3</sub><sup>+</sup>, we study their toxicity effects on SUNE1 cells. The dates were taken for 24, 48 and 72 h time points. As can be seen in Figure 5, the percentages of cell death are all less 25 % when cells were treated with MWNTs-S-S-NH<sub>3</sub><sup>+</sup>, showing no significant loss of cell viability compared to untreated cells. According to the 72 h time point dates, more than 50 % of the cells died in the presence of pristine MWNTs, whereas the vast majority of cells remained alive upon treatment with MWNTs-S-S-NH<sub>3</sub><sup>+</sup>. However, an expected dose-response relationship is observed. At higher concentrations of MWNTs-S-S-NH<sub>3</sub><sup>+</sup>, regardless of 24, 48 or 72 h points dates, MWNTs-S-S-NH<sub>3</sub><sup>+</sup> have continuous reinforcing effects on the cells. The initial studies indicate functionalization of MWNTs reduces toxicity and improves biocompatibility of cells in vitro. These results agree well with previous observations (Sayes *et al.*, 2006, p.135; Lacerda *et al.*, 2006, p.1460).

## 4. Conclusions

We have prepared positively charged MWNTs by attaching disulfide to the nanotubes followed cleavage of the Boc protecting groups. The method is effective for functionalization. Infrared spectroscopy characterization, electron microscope measurements and thermal gravimetric analysis reveal that disulfide linkages are introduced onto the surface of MWNTs via amide bonds. The toxicity studies show MWNTs-S-S-NH<sub>3</sub><sup>+</sup> material has only very limited impact upon cell proliferation and cell viability, indicating that functionalization of nanotubes dramatically improves the toxicity profile of this nanomaterials.

### Acknowledgements

The financial support from National Natural Science Foundation of China (No. 50772133) and Doctor's Scientific Research and Innovation Foundation of Central South University of China (No.134376211) are greatly acknowledged.

## References

- Bianco, A., Kostarelos, K., & Prato, M. (2005). Biomedical applications of functionalised carbon nanotubes. *Chem. Commun.*, 571-577.
- Bottini, M., Bruckner, S., & Mustelin, T. (2006). Multi-walled carbon nanotubes induce Tlymphocyte apoptosis. *Toxicol. Lett.*, 160, 121-126.
- Cui, D. X., Tian, F. R., & Gao, H. J. (2005). Effect of single wall carbon nanotubes on human HEK293 cells. *Toxicol. Lett.*, 155, 73-85.
- dependence of single-walled carbon nanotubes cytotoxicity in vitro. *Toxicol. Lett.*, 161, 135-142.
- Georgakilas, V., Tagmatarchis, N., & Pantarotto, D. (2002). Amido acid functionalisation of water soluble carbon nanotubes. *Chem. Commun.*, 3050-3051.
- Kiura, K., Sato, Y., & Shibata, K. I. (2005). Activation of human monocytes and mouse splenocytes by single-walled carbon nanotubes. *J. Biomed. Nanotechnol.*, 1, 359-364.
- Lacerda, L., Bianco, A., & Kostarelos, K. (2006). Carbon nanotubes as nanomedicines:from toxicology to pharmacology. *Adv. Drug Deliv. Rev.*, 58, 1460-1470.
- Lin, C., Zhong, Z., & Lok, M. C. (2006). linear poly(amido amine)s with secondary and tertiary amino groups and variable amounts of disulfide linkages:Synthesis and in vitro gene transfer properties. *J. Controlled Release*, 116, 130-137.
- Molecular recognition of theophylline derivatives. *Langmuir*, 24, 11988-11994.
- Niu, J., Liu, Z. H., & Zhang, X. (2008). Surface-Imprinted nanostructured layer-by-layer film for
- Pantarotto, D., Singh, R., & McCarthy, D. (2004). Functionalized carbon nanotubes for plasmid DNA gene delivery. *Angew. Chem. Int. Ed.*, 43, 5242-5246.
- Piest, M., Lin, C., & Mateos Timoneda, M. A. (2008). Novel poly(amido amine)s with bioreducible disulfide linkages in their diamino-units:Structure effects and in vitro gene transfer properties. *J. Controlled Release*, 130,



38–45.

Prato, M., Kostarelos, k., & Bianco, A. (2008). Functionlized carbon nanobubes in drug design and discovery. *Acc. Chem. Res.*, 41, 60-68.

Sayes, C. M., Liang, F., Hudson, J. L., Mendez, J., & Colvin, V. L. (2006). Functionalization density

Wong, N., Kam, S., & Dai, H. J. (2005). Carbon nanotubes as intracellular protein transporters:generality and biological functionality. *J. AM. CHEM. SOC.* 127, 6021-6026.

Wu, W., Wieckowski, S., & Bianco, A. (2005). Targeted delivery of amphotericin B to cells by using functionalized carbon nanotubes. *Angew. Chem. Int. Ed.*, 44, 6358-6362.

You, Y. Z., Hong, C. Y., &Pan, C. Y. (2007). Covalently immobilizing a biological molecule onto a carbon nanotube via a stimuli-sensitive bond. *J. Phys. Chem. C*, 111, 16161-16166.

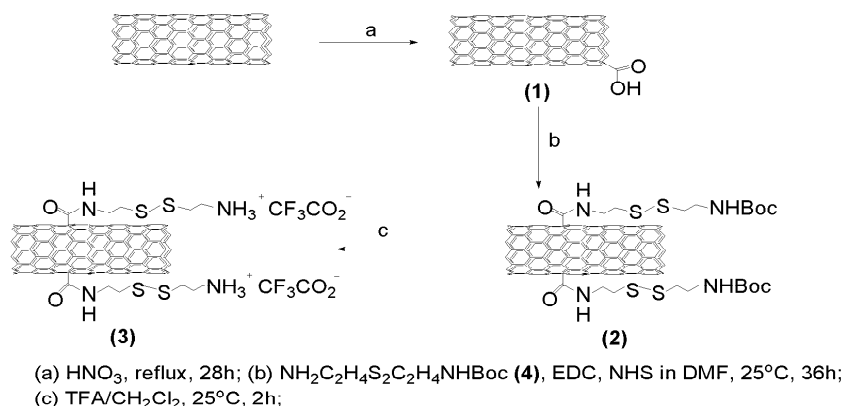


Figure 1. Preparation of disulfide functionalized MWNTs and positively ammonium functionalized MWNTs-S-S- $\text{NH}_3^+$

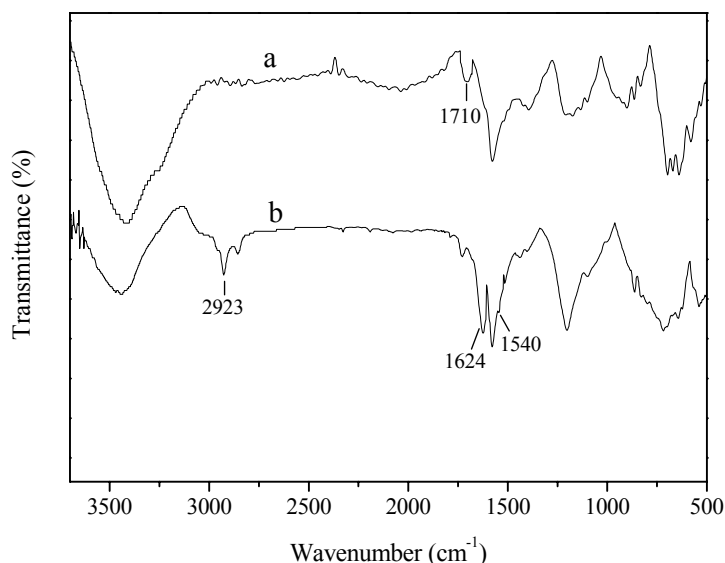


Figure 2. FT-IR spectra of (a) oxidized MWNTs and (b) MWNTs-S-S- $\text{NH}_3^+$

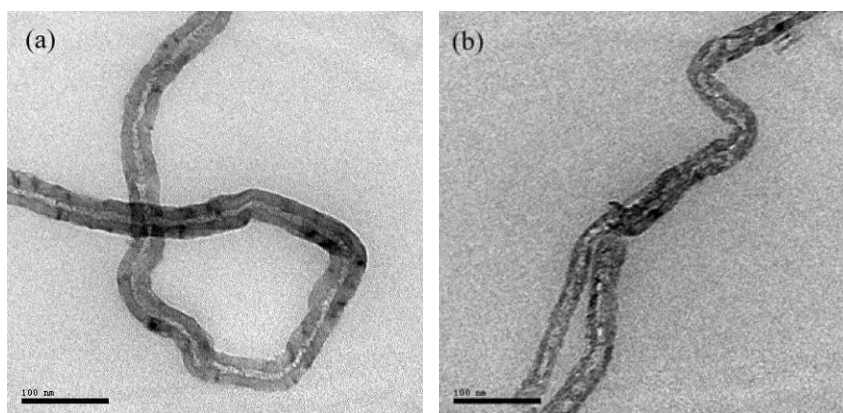


Figure 3. TEM images of (a) pristine MWNTs and (b) MWNTs-S-S-NH<sub>3</sub><sup>+</sup>. The scale toolbars represent 100 nm

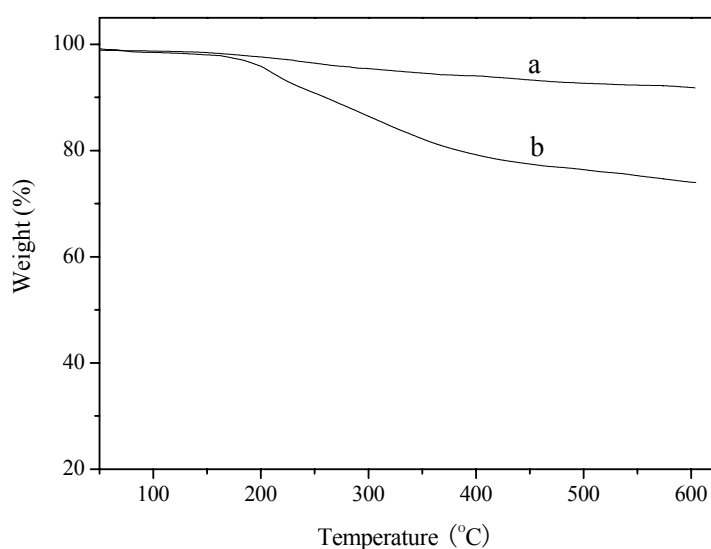


Figure 4. Thermal gravimetric analysis of (a) oxidized MWNTs and (b) MWNT-S-S-NH<sub>3</sub><sup>+</sup>

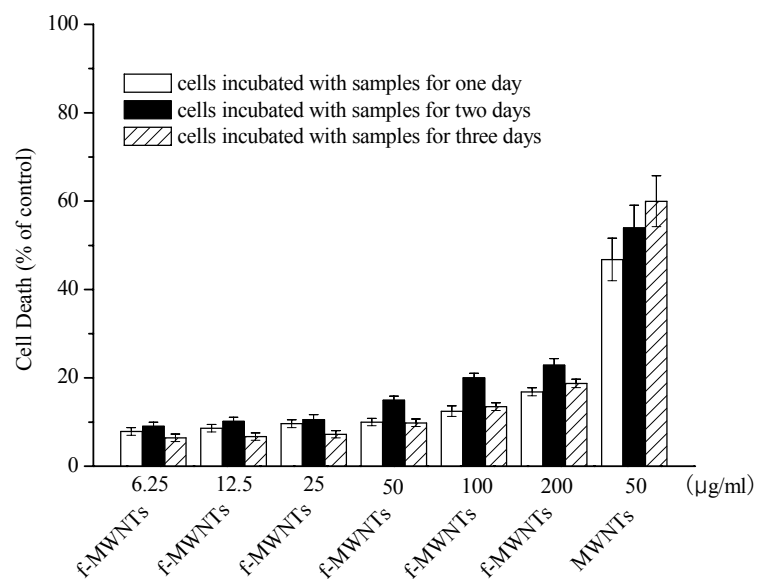


Figure 5. Cell death after treatment with MWNTs-S-S-NH<sub>3</sub><sup>+</sup> (f-MWNTs) and pristine MWNTs for 24 h, 48 h or 72 h, respectively

# Synthesis and Antibacterial Activity of Novel Organoselenium Compounds

P. M. Radhakrishna (Corresponding author)

Provimi India Innovation Centre, Provimi Animal Nutrition India Ltd.  
Bangalore 560 106, India  
Tel: 91-80-2856-2298 E-mail: pmradhakrishna@provimi.in

K. C. Sharadamma

Provimi India Innovation Centre, Provimi Animal Nutrition India Ltd.  
Bangalore 560 106, India  
E-mail: ksharada@provimi.in

H. M. Vagdevi

Department Of Chemistry, Sahyadri Science College (Autonomous)  
Shimoga-577 203, India  
E-mail: vagdevihm@gmail.com

P. M. Abhilekha

Provimi India Innovation Centre, Provimi Animal Nutrition India Ltd.  
Bangalore 560 106, India  
E-mail: abhilekhapmantri@provimi.in

S. Rubeena Mubeen

Provimi India Innovation Centre, Provimi Animal Nutrition India Ltd.  
Bangalore 560 106, India  
E-mail: rdconcept@provimi.in

K. Nischal

Provimi India Innovation Centre, Provimi Animal Nutrition India Ltd.  
Bangalore 560 106, India  
E-mail: knischal@provimi.in

## Abstract

Organoselenium compounds are known to possess antioxidant, anticancer and antibacterial activities. In the present study, 3-[(phenylcarbonyl)selenyl]propanoic acid was synthesized and different ester derivatives of 3-[(phenylcarbonyl)selenyl]propanoic acid and 2-[(phenylcarbonyl)selenyl]acetic acid (benzoylselenoglycolic acid) were synthesized and characterized using IR, <sup>1</sup>HNMR and Mass spectral methods. Minimum Inhibitory Concentration (MIC) of the newly synthesized compounds was determined against gram positive and gram negative bacteria. Some of the compounds showed moderate to significant activity against *Staphylococcus aureus*, *Salmonella typhimurium*, *Escherichia coli* and *Bacillus subtilis*.

**Keywords:** Organoselenium compounds, Antibacterial activity, Esters

## 1. Introduction

Selenium, an essential trace mineral (Rayman, 2002) is a vital component of the selenoproteins specifically glutathione peroxidase mainly required for normal health and reproduction (Rayman, 2000). Selenium was discovered in 1818 by Swedish chemist Berzelius. It was considered as a poison until it was identified as a micronutrient for bacteria, mammals and birds (Schwarz & Foltz, 1957). Selenium is essential for the efficient and effective operation of the immune system in both animals and humans (Arthur *et al.*, 2003). Organoselenium compounds have substantially greater bioavailability than that of inorganic selenium (Cantor *et al.*, 1975). More importantly, organic selenium is usually found to be less toxic than inorganic forms (Bendsleve *et al.*, 1988; Khalil, 1989; Khalil, 1994).

Organoselenium compounds have been tested as antibacterial, antiviral, antifungal, antiparasitic, antihistamine and anticancer agents (Athayde-Filho *et al.* 2004). During the last few years, tremendous effort has been directed towards the synthesis of stable organoselenium compounds that could be used as antioxidants, enzyme modulators, antitumors, antivirals, antimicrobials, antihypertensive agents and cytokine inducers (Mugesh *et al.*, 2001; Garcia, 2004; Carland & Fenner, 2005). Though several organoselenium compounds are known, they are less explored for their antibacterial properties. Some novel organoselenium compounds were synthesized and their antibacterial activity was tested.

One of the reagents adopted to synthesize organoselenium compounds is sodium hydrogen selenide, which can be prepared by the action of sodium borohydride on metallic selenium in protic solvents (Klayman & Griffin, 1973). Aqueous solution of sodium hydrogen selenide has been effectively used to synthesize benzoylselenoglycolic acid (**1**) (Athayde-Filho *et al.*, 2004). In the present work benzoylselenoglycolic acid was synthesized as per the reported method and 3-[(phenylcarbonyl) selenyl]propanoic acid (**2**) was synthesized with slight modification (Scheme 1). Several esters of compound **1** and **2** were also synthesized (Scheme 2).

## 2. Experimental Section

### 2.1 Chemistry material

Sodium borohydride, hexane, ethyl acetate were procured from RFCL India, selenium metal from Sigma Aldrich, benzoyl chloride and 3-chloropropanoic acid from Merck. Reaction was monitored using silica gel 60 F<sub>254</sub> TLC plates from Merck. Melting points were taken in open capillary tubes and are uncorrected. All the compounds were characterized by <sup>1</sup>HNMR, IR, and Mass spectral methods. The IR spectra were recorded on Bruker IR spectrophotometer. <sup>1</sup>HNMR in CDCl<sub>3</sub> was recorded on Bruker 200MHz instrument using TMS as internal standard and mass spectra was recorded using Shimadzu LCMS 2010A system.

### 2.2 Synthesis of 3-[(Phenylcarbonyl)selenyl] propanoic acid (**2**)

Selenium metal (1g, 12.66 mmol) was suspended in 12 mL of water. Sodium borohydride (1g, 26.5 mmoles) was dissolved in 12 mL of water and added slowly to the selenium suspension under nitrogen atmosphere. The reaction was exothermic with vigorous evolution of hydrogen gas. Benzoyl chloride (1.8g, 12.8 mmol) was then added slowly at 30°C. A yellow colored solution was obtained. 3-Chloropropanoic acid (1.4g, 13 mmol) was added slowly to the above reaction mass at 65-70°C and solid precipitated out towards the end of the addition. The solid was filtered and dissolved in 20 mL of dichloromethane and extracted into 5% sodium bicarbonate solution. The pH of the collected sodium bicarbonate layer was adjusted to 4-5 using 5% hydrochloric acid. The product was extracted back into dichloromethane and concentrated under vacuum to obtain white solid. Yield: 80%.

Melting point: 84-88°C. IR ( $\gamma_{\max}$  cm<sup>-1</sup>): 1697(-COOH) 1665(-Se-CO-).

MS: m/z: 257 (base peak) (calculated for C<sub>10</sub>H<sub>10</sub>O<sub>3</sub>Se : 257.14).

<sup>1</sup>H NMR (CDCl<sub>3</sub>):  $\delta$  2.92(t, 2H, -CH<sub>2</sub>-CO-), 3.28(t, 2H, -Se-CH<sub>2</sub>), 7.42–7.91(5H, Ar-H).

### 2.3 General procedure for the preparation of esters (**3a-3d**)

Benzoylselenoglycolic acid (**1**) (2.43g, 10 mmol) was dissolved in corresponding alcoholic solvent. Thionyl chloride (1.78g, 15 mmol) was added slowly at 55- 60°C. Reaction mass was stirred for 30 minutes at 50-55°C. The solvent was distilled out completely and the residue was dissolved in 15 mL of dichloromethane. Dichloromethane layer was washed with 10 mL of 5% sodium bicarbonate solution and then with water. The organic layer was collected and dried over anhydrous sodium sulfate. Solvent was distilled under vacuum and the product was obtained in the form of oil which was further purified using silica gel column. Combination of hexane and ethyl acetate was used as eluant by progressively increasing the polarity. Finally the desired compounds were eluted by hexane: ethyl acetate in the ratio of 85:15.

Similarly ester derivatives of Compound **2** (**3e-3h**) were also prepared using the same method.

### 2.3.1 Yield and Characterization Data

#### **3a**

Yield: 60%

IR ( $\gamma_{\max} \text{ cm}^{-1}$ ): 1720(-COO-), 1678(-Se-CO-).

MS: m/z: 259(base peak,  $[\text{M}+\text{H}]^+$ ) (calculated for  $\text{C}_{10}\text{H}_{10}\text{O}_3\text{Se}$  : 257.14).

$^1\text{H}$  NMR ( $\text{CDCl}_3$ ):  $\delta$  3.74(s, 3H, -OCH<sub>3</sub>), 3.85(s, 2H, -Se-CH<sub>2</sub>), 7.43–7.91(5H, Ar-H).

#### **3b**

Yield: 70%

(IR ( $\gamma_{\max} \text{ cm}^{-1}$ ): 1731(-COO-), 1678(-Se-CO-).

MS: m/z: 273(base peak,  $[\text{M}+\text{H}]^+$ ) (calculated for  $\text{C}_{11}\text{H}_{12}\text{O}_3\text{Se}$  : 271.17).

$^1\text{H}$  NMR ( $\text{CDCl}_3$ ):  $\delta$  1.28(t, 3H, -CH<sub>3</sub>), 3.84(s, 2H, -Se-CH<sub>2</sub>), 4.19(quartet, 2H, -OCH<sub>2</sub>), 7.26–7.92(5H, Ar-H).

#### **3c**

Yield: 70%

IR ( $\gamma_{\max} \text{ cm}^{-1}$ ): 1725(-COO-), 1677(-Se-CO-).

MS: m/z: 287(base peak,  $[\text{M}+\text{H}]^+$ ) (calculated for  $\text{C}_{12}\text{H}_{14}\text{O}_3\text{Se}$  : 285.19).

$^1\text{H}$  NMR ( $\text{CDCl}_3$ ):  $\delta$  1.24(d, 6H, -C(CH<sub>3</sub>)<sub>2</sub>), 3.81(s, 2H, -Se-CH<sub>2</sub>), 5.05 (m, 1H, -OCH), 7.39–8.06( 5H, Ar-H).

#### **3d**

Yield: 75%

IR ( $\gamma_{\max} \text{ cm}^{-1}$ ): 1730(-COO-), 1677(-Se-CO-).

MS: m/z: 301 (base peak,  $[\text{M}+\text{H}]^+$ ) (calculated for  $\text{C}_{13}\text{H}_{16}\text{O}_3\text{Se}$  : 299.22).

$^1\text{H}$  NMR ( $\text{CDCl}_3$ ):  $\delta$  0.92(t, 3H, -CH<sub>3</sub>), 1.44(m, 2H, -CH<sub>2</sub>), 1.56(quintet, 2H, -CH<sub>2</sub>), 3.84(s, 2H, -Se-CH<sub>2</sub>), 4.14(t, 2H, -OCH<sub>2</sub>), 7.43–7.91(5H, Ar-H).

#### **3e**

Yield: 75%

IR ( $\gamma_{\max} \text{ cm}^{-1}$ ): 1735(-COO-), 1668(-Se-CO-).

MS: m/z: 273 (base peak,  $[\text{M}+\text{H}]^+$ ) (calculated for  $\text{C}_{11}\text{H}_{12}\text{O}_3\text{Se}$  : 271.17).

$^1\text{H}$  NMR ( $\text{CDCl}_3$ ):  $\delta$  2.86(t, 2H, -CH<sub>2</sub>-CO), 3.29(t, 2H, -Se-CH<sub>2</sub>), 3.71(s, 3H, -OCH<sub>3</sub>), 7.41–7.90 (5H, Ar-H).

#### **3f**

Yield: 75%

IR ( $\gamma_{\max} \text{ cm}^{-1}$ ): 1731(-COO-), 1669(-Se-CO-).

MS: m/z: 287(base peak,  $[\text{M}+\text{H}]^+$ ) (calculated for  $\text{C}_{12}\text{H}_{14}\text{O}_3\text{Se}$  : 285.19).

$^1\text{H}$  NMR ( $\text{CDCl}_3$ ):  $\delta$  1.27(t, 3H, -CH<sub>3</sub>), 2.84(t, 2H, -CH<sub>2</sub>-CO), 3.29(t, 2H, -Se-CH<sub>2</sub>), 4.15(quartet, 2H, -OCH<sub>2</sub>), 7.41 –7.91(5H, Ar-H).

#### **3g**

Yield: 85%

IR  $\gamma_{\max} \text{ cm}^{-1}$ : 1727(-COO-), 1670(-Se-CO-).

MS: m/z: 301 (base peak,  $[\text{M}+\text{H}]^+$ ) (calculated for  $\text{C}_{13}\text{H}_{16}\text{O}_3\text{Se}$  : 299.22).

$^1\text{H}$  NMR ( $\text{CDCl}_3$ ):  $\delta$  1.26(d, 6H, -C(CH<sub>3</sub>)<sub>2</sub>), 2.85(t, 2H, -CH<sub>2</sub>-CO-), 3.29(t, 2H, -Se-CH<sub>2</sub>), 5.04(m, 1H, -OCH), 7.40–7.90 (5H, Ar-H).

#### **3h**

Yield: 87%

IR ( $\gamma_{\max} \text{ cm}^{-1}$ ): 1735(-COO-), 1673(-Se-CO-).

MS: m/z: 315 (base peak,  $[M+H]^+$ ) (calculated for  $C_{14}H_{18}O_3Se$  : 313.25).

$^1H$  NMR ( $CDCl_3$ ):  $\delta$  0.94(t, 3H,  $-CH_3$ ), 1.39(m, 2H,  $-CH_2$ ), 1.62(quintet, 2H,  $-CH_2$ ), 2.84(t, 2H,  $-CH_2-CO-$ ), 3.29(t, 2H,  $-Se-CH_2$ ), 4.03(t, 2H,  $-OCH_2$ ), 7.41–7.90(5H, Ar-H).

#### 2.4 Antibacterial activity

Benzoylselenoglycolic acid, 3-[(phenylcarbonyl) selenyl] propanoic acid and their esters were assayed *in vitro* for their antibacterial activity against a panel of selected gram positive and gram negative bacteria. They were screened for their antibacterial activity against *Escherichia coli* (ATCC 9637), *Bacillus subtilis* (ATCC 6633), *Staphylococcus aureus* (ATCC 29737) and *Salmonella typhimurium* (ATCC 23564) (recultured) bacterial strains which were obtained from National Chemical Laboratory, Pune, India.

The testing was done according to the reported method (Rose & Miller, 1939). Samples were prepared in methanol and serially diluted to determine the minimum inhibitory concentration that inhibited the growth of the tested microorganisms (MIC). After 24 hours of incubation at  $37^\circ C$ , the zone of inhibition was measured in mm. A control was also prepared using only methanol. Doxycycline hydrochloride which is commonly used as an antibiotic in animal health industry was used as positive control. The results obtained are tabulated in Table 1.

### 3. Results and Discussion

One pot synthesis of organoselenium compounds reported in the literature for synthesizing benzoylselenoglycolic acid was used effectively to synthesize 3-[(phenylcarbonyl) selenyl] propanoic acid with slight modification in the reaction temperature. The structure of newly synthesized compound was established on the basis of spectral (IR,  $^1H$  NMR, and mass) data. The IR spectrum of compound **2** showed a band in the region of  $1697\text{cm}^{-1}$  which is characteristic of carbonyl stretching of  $-COOH$  group and  $1665\text{cm}^{-1}$  corresponding to  $-Se-CO$  stretching. In the  $^1H$  NMR spectrum the  $-Se-CH_2-$  proton came into resonance at  $\delta$  3.28 as triplet,  $-CH_2-CO$  protons appeared at  $\delta$  2.92 as triplet. Aromatic protons resonated between  $\delta$  7.42–7.91. The signal corresponding to  $-COOH$  proton was not visible. However presence of  $-COOH$  group was confirmed through esterification reactions. The mass spectrum of this compound showed molecular ion peak at m/z 257 which is also the base peak.

Esters of compounds **1** and **2** were synthesized by the method described above and the confirmation of the structure was obtained by spectral (IR,  $^1H$  NMR, and mass) methods. IR spectrum of compound **3b** showed a band in the region of  $1731\text{cm}^{-1}$  which is characteristic of carbonyl stretching of  $-COO$  group. In the  $^1H$  NMR spectrum the  $-Se-CH_2-$  protons came into resonance at  $\delta$  3.84 as singlet and  $-OCH_2$  protons resonated at  $\delta$  4.19 as quartet. The  $-CH_3$  protons appeared as triplet at  $\delta$  1.28. Aromatic protons resonated between  $\delta$  7.26–7.92. The mass spectrum of this compound showed  $[M+H]^+$  peak at m/z 273 which is also the base peak. The mass spectra of the compounds (**3b-3h**) showed a common fragment peak at m/z 169. A typical pattern which is characteristic of selenium isotopic abundance (Block *et al*, 1996; Ip *et al*, 2000) was observed in the mass spectra of the compounds.

All the newly synthesized compounds were screened for their antibacterial activity. The investigation of antibacterial screening data revealed that majority of the tested compounds (**1, 2 and 3a-3h**) showed moderate to good inhibition against the tested bacterial species. Among all these compounds **3b** and **3d** showed significant inhibitory activity at lower concentrations (less than 0.1 mg/mL) against both gram positive and gram negative bacteria except *S. typhimurium*. Compounds **3a, 3e and 3g** were effective in the concentration range of 0.1-1 mg/mL against all the bacterial species tested. Compounds **2** and **3h** were effective against *S. typhimurium* at slightly higher concentration of 1-10mg/mL. However compounds **3c** and **3d** were less active against *S. typhimurium*.

### 4. Conclusion

This research study reports the successful synthesis and testing for antimicrobial activity of novel organoselenium compounds (**2** and **3a-3h**). These compounds showed moderate to significant antibacterial activity against selected pathogenic gram positive and gram negative bacteria and these results indicate the probable role of organoselenium compounds (**1-3h**) against the tested pathogenic bacterial species. In conclusion, most of the target compounds exhibited *in vitro* antibacterial activity. Further biological evaluation of these compounds is in progress.

### References

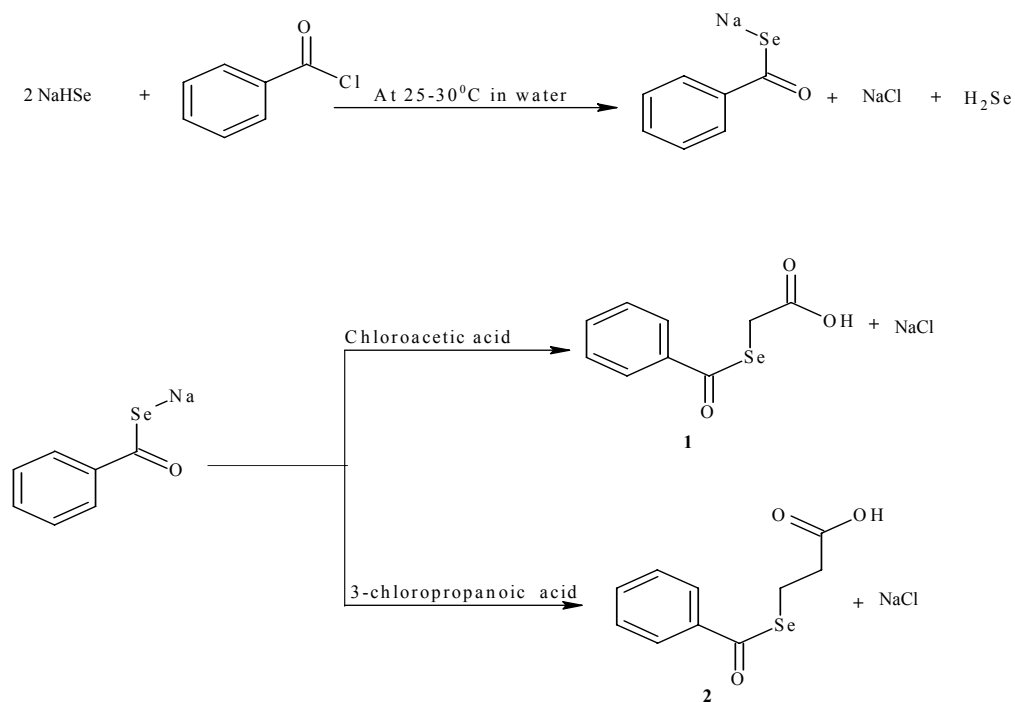
Arenholt-Bendslev, D., Abdulla, M., Jepsen, A., & Pedersen, E. (1988). Effect of organic and inorganic selenium on human keratinocytes. *Trace. Elem. Med.*, 5, 29-34.

- Arthur, J. R., McKenzie, R. C., & Beckett, G. J. (2003). Selenium in the immune system. *J. Nutr*, 133, 1457S-1459S.
- Athayde-Filho, P. F., Souza, A. G., Morais, S. A., Botelho, J. R., Barbosa-Filho, J. M., Miller, J., & Lira, B. F. (2004). Synthesis and characterization of three new organo-selenium compounds. A convenient synthesis of aroylselenoglycolic acids. *ARKIVOC*, vi, 22-26.
- Berzelius, J. J. (1818). *Afhandl. Fys. Kemi Mineralog*, 6, 42.
- Block, E., Cai, X.-J., Uden, P. C., Zhang, X., Quimby, B. D., & Sullivan, J. J. (1996). Allium chemistry: Natural abundance of organoselenium compounds from garlic, onion and related plants and in human garlic breath. *Pure & Appl. Chem.*, 68, 937-944, 1996.
- Ip, C., Birringer, M., Block, E., Kotreba, M., Tyson, J. F., Uden, P. C., & Lisk D. J. (2000). Chemical speciation influences comparative activity of selenium-enriched garlic and yeast in mammary cancer prevention. *J. Agric. Food. Chem*, 48, 2062-2070.
- Cantor, A. H., Langevin, M. L., Noguchi, T., & Scott, M. L. (1975). Efficacy of selenium in selenium compounds and feedstuffs for prevention of pancreatic fibrosis in chicks. *J. Nutr*, 105, 96-105.
- Carland, M., & Fenner, T. (2005). The Use of Selenium-Based Drugs. In M. Gielen, & E. R. T. Tiekink (Eds.), *Medicine in metallotherapeutic drugs and metal-based diagnostic agents*. Wiley, Chichester.
- Khalil, A. M. (1989). The induction of chromosome aberrations in human purified peripheral blood lymphocytes following *in vitro* exposure to selenium. *Mutat. Res*, 224, 503-506.
- Khalil, A. M. (1994). Genotoxicity of two pharmacologically important selenium compounds (selenocystine and selenopuridine) in cultured human blood lymphocytes. *Toxicol. Environ. Chem*, 41, 147-154.
- Klayman, D. L., & Griffin, T. S. (1973). Reaction of selenium with sodium borohydride in protic solvents. A facile method for introduction of selenium into organic molecules. *J. Am. Chem. Soc*, 95, 197-199.
- Mugesh, G., du Mont, W. W., and Sies, H. (2001). Chemistry of biologically important synthetic organoselenium compounds. *Chem. Rev*, 101, 2125-2179.
- Rayman, M. P. (2000). The importance of selenium to human health. *Lancet*, 356, 233-241.
- Rayman, M. P. (2002). The argument for increasing selenium intake. *Proc. Nutr. Soc*, 61, 203-215.
- Rose, S. B., & Miller, R. E. (1939). Studies with the agar cup-plate method. I. A standardized agar cup-plate technique. *J. Bacteriol*, 38, 525-537.
- Schwarz, K., & Foltz, C. M. (1957). Selenium as an integral part of factor 3 against dietary necrotic liver degeneration. *J. Am. Chem. Soc*, 79, 3292-3293.
- Soriano-Garcia, M. (2004). Organoselenium compounds as potential therapeutic and chemopreventive agents: A review. *Curr. Med. Chem*, 11, 1657-1669.

Table 1. Antibacterial activities of compounds **1**, **2**, **3a – 3h**

Compound	<i>S. aureus</i>	<i>E. coli</i>	<i>S. typhimurium</i>	<i>B. subtilis</i>
1	+++++	++++	+++	+++++
2	+++++	+++++	++++	+++++
3a	+++++	+++++	+++++	+++++
3b	+++++	+++++	+++++	+++++
3c	+++++	+++++	++	+++++
3d	+++++	+++++	+	+++++
3e	+++++	+++++	+++++	+++++
3f	++++	++++	+++	++++
3g	+++++	+++++	+++++	+++++
3h	+++++	+++++	++++	+++++
Doxycycline Hydrochloride	+++++	+++++	+++++	+++++

Less than 0.1 mg/mL = ++++++, 0.11- 1 mg/mL = +++++, 1-10mg/mL = +++++, 10.1-50mg/mL = +++, 51-100 mg/mL = ++, above 100mg/mL = +.



Scheme 1. Synthesis of compounds 1 and 2



3a R=CH<sub>3</sub> (n=1), 3b R=C<sub>2</sub>H<sub>5</sub> (n=1), 3c R=CH (CH<sub>3</sub>)<sub>2</sub> (n=1) and 3d R=CH<sub>2</sub>-CH<sub>2</sub>-CH<sub>2</sub>-CH<sub>3</sub> (n=1)  
 3e R=CH<sub>3</sub> (n=2), 3f R=C<sub>2</sub>H<sub>5</sub> (n=2), 3g R=CH (CH<sub>3</sub>)<sub>2</sub> (n=2) and 3h R=CH<sub>2</sub>-CH<sub>2</sub>-CH<sub>2</sub>-CH<sub>3</sub> (n=2)

Scheme 2. Synthesis of esters 3a-3h



# Extraction Equilibrium and Simple Extractive Spectrophotometric Determination of Gold (I& III) in Water Using the Ion - Pairing Amiloride Hydrochloride

A.S. Bashammakh (Corresponding author) & M.S. El-Shahawi

Department of Chemistry, Faculty of Science, King Abdulaziz University

P.O. Box 80203, Jeddah 21589, Saudi Arabia

E-mail: abashammkh@kau.edu.sa

## Abstract

The chemical equilibrium of the ternary complex ion associate of the complex anion  $\text{AuCl}_4^-$  and the ion – pairing reagent 1- (3, 5-diamino-6-chloropyrazinecarboxyl) guanidine hydrochloride monohydrate,  $\text{DPG}^+\text{Cl}^-$  extracted from aqueous solutions of pH 5-6 onto 4-methyl pentan-2-one was demonstrated. The extraction constants ( $K_{\text{ex}}$ ,  $K_D$  and  $\beta$ ) of the chemical equilibrium and the structure of the produced associate were determined. The results have indicated that, the formation of the complex ion associate of the chemical structure  $\text{DPG}^+\text{AuCl}_4^-$  and the extraction mechanism does not involve solvation of the ion associate by the amine and/or water molecules in the organic phase. Beer's law was obeyed in the range 0.01 -2.5  $\mu\text{g mL}^{-1}$  gold (III) in the aqueous solution. The method was applied successfully for the analysis of gold (I) after oxidation to gold (III). The method was also applied for the analysis of gold (I& III) at trace concentrations in industrial wastewater samples. Gold (III) ions at trace level in one liter aqueous solution was concentrated in 10.0 mL by the developed extraction system so an enrichment factor of 100 was achieved. The time taken for the separation and determination of gold ions was in the range of 3-5 min.

**Keywords:** Chemical equilibria, Speciation of gold (I, III), Ion associate, Wastewater

## 1. Introduction

Gold is one of the most important noble metals due to its wide application in industry and economic activity. Gold occur on the Earth in very low natural contents and its concentration in natural water is extremely low, in the range of 0.05 - 0.2  $\text{ng mL}^{-1}$ . It is well known that gold is one of the most interesting micro amount elements due to its significant role on biology and environment. Thus, simple, sensitive and selective methods for determination of trace gold are of great importance.

Several sophisticated techniques, such as laser induced breakdown spectroscopy, inductively coupled plasma mass spectrometry (ICP –MS), inductively coupled plasma atomic emission spectrometry (ICP-AES), electrochemical, neutron activation analysis, total reflection X-ray fluorescence spectrometry have been applied to the determination of gold (Shoursheinin, 2010, PP. 89 -95; Guanghan, 1992, PP. 51-53; Medved, 2004, PP. 60 – 65; Yu, 2003, PP. 225 -231; Navratilova, 2000, PP. 369-372; Itagaki, 2000, PP. 344-349 and Li, 2006, PP. 841-844) in various matrices including wastewater. However, some of these methods are less often applied in gold analysis due to the complexity and cost of the required instrumentation (Guanghan, 1992, PP. 51-53; Medved, 2004, PP. 60 – 65; Yu, 2003, PP. 225 -231; Navratilova, 2000, PP. 369-372). Thus, spectrophotometric methods still have the advantages in respect of simplicity and low operating costs.

Recently (Zuotao, 1999, PP. 237-241; Pyrzynska, 2005, PP. 1316-1322; Hu, 2006, PP. 627-630 and Fazli, 2009, PP. 210-212) a wide variety of spectrophotometric methods for the determination of gold have been reported. The ion pairing reagents had widely been applied for the pre concentration and/or determination of noble metal ions (Filatova, 2004, PP. 243-245; El-Shahawi, 2005, PP. 319-326; Hassan, 2005, PP.673- 678; El-Shahawi, 2008, PP.313 - 319). Charged bulky cations e.g. amidine, rhodamine derivatives, basic dyes, 18- crown-6 (18C6) oxonium cation, tetra alkyl ammonium, phosphonium or arsonium halides and tetrazolium salts are often used to form extractable complex ion associates with charged bulky oxoanions or anionic complex species of gold (I) , gold (III) and other metal ions as their halides, cyanides and thiocyanates (Haddad, 1988, PP. 23 – 36; Burns, 1992, PP. 213-215; Burns, 1992, PP. 131-132; El-Shahawi, 1996, PP. 2037-2043; Biswas, 1996, PP. 804-80; Camagong, 2001, PP. 1725-1728; Farag, 2007, PP. 218-228 and Bashammakh, 2009, PP. 413 – 418). Burns, 1988, PP. 185-187 and Burns, 1996, PP.107-109 and other workers (El-Shahawi, 1997, PP. 85-91; AlDhaheri, 1998, PP. 161-1615 and El-Shahawi, 2007, PP.1494-1499) have used the reagent amiloride mono hydrochloride

extensively as a selective ion-pairing reagent for the determination of some oxoanions e.g. perchlorate, perrhenate, periodate and tetra chloraurate ( $\text{AuCl}_4^-$ ) in different matrices.

Recent literature survey on the title ion – pairing reagent has revealed no study on the chemical equilibrium of the reagent  $\text{DPG}^+\text{Cl}^-$  with  $\text{AuCl}_4^-$ . Hence, the main objectives of the present article was focused on:

- Studying the chemical equilibrium of the reagent  $\text{DPG}^+\text{Cl}^-$  with  $\text{AuCl}_4^-$  in an attempt to develop a precise extractive spectrophotometric method for the determination and chemical speciation of gold (I, III) species in wastewater samples.
- achieving a better association and a better understanding of the extraction mechanism of the produced ion associate of  $\text{DPG}^+\text{Cl}^-$  with  $\text{AuCl}_4^-$  in the organic phase.

## 2. Experimental

### 2.1 Chemicals and reagents

Analytical reagent grade chemicals and solvents (BDH, Poole, UK) were used as received. Potassium aurate [ $\text{KAuCl}_4$ ] and potassium aurocyanide, [ $\text{KAu}(\text{CN})_2$ ] (Fluka AG, USA) were used for the preparation of stock solutions of gold (III) and gold (I) ions, respectively. The reagent,  $\text{DPG}^+\text{Cl}^-$  (Merck, India) was used without purification. A stock solution ( $0.01 \text{ mol L}^{-1}$ , 100 mL) of the reagent  $\text{DPG}^+\text{Cl}^-$  was prepared by dissolving an accurate weight (0.302g) of it in  $\text{H}_2\text{O-HCl}$  (1:1 v/v). Britton - Robinson (B-R) buffer of pH 2.1 - 11 was prepared (Vogel, 1966).

### 2.2 Apparatus

A double beam Perkin-Elmer (model Lambda EZ-210, USA) spectrophotometer (190-1100 nm) with 1 cm (path width) quartz cell was used for recording the electronic spectra and the absorbance of the organic extracts. Infrared (IR) spectra were recorded on a Broker FT-IR (model IFS 66, USA) spectrophotometer. A Perkin-Elmer (Analyst TM 800, USA) flame atomic absorption spectrometer (FAAS) was used for measuring the concentration of gold ions at 242.8 nm at 0.5 nm slit width before and after extraction with the organic solvent. De - ionized water was obtained from Milli-Q Plus system (Millipore, Bedford, MA, USA) and the pH were recorded on a pH meter (Orion EA940, MA, USA) with absolute accuracy limits being defined by NIST.

### 2.3 Recommended extraction procedures

#### 2.3.1 Determination of the extraction equilibrium constants ( $K_D$ , $\beta$ , $K_{ex}$ )

Aliquot aqueous solutions of gold (III) ions (10 mL,  $1\text{-}10 \mu\text{g mL}^{-1}$ ) at pH 5-6 were transferred to separating funnels (50.0 mL). A 2 mL of the reagent  $\text{DPG}^+\text{Cl}^-$  solution ( $8.0 \times 10^{-5} \text{ mol L}^{-1}$ ) was added to each gold solution. The solutions were completed with B-R buffer of pH 5-6 to the mark of measuring flasks (25 mL). Each reaction mixture was mixed well and extracted twice ( $2 \times 2.5 \text{ mL}$ ) with 4-methyl pentan-2-one for 2 min. The two phases were then separated out and the organic extract was collected in a 25 mL beakers containing anhydrous  $\text{Na}_2\text{SO}_4$  (1.0g). The contents were swirled to mix and transferred to volumetric flask (10 mL). The solid residue was then washed with another 5 mL ( $2 \times 2.5$ ) of the solvent and the washings were transferred to the measuring flask. The flask was made up to the mark with the solvent. The absorbance of the organic extract was then measured at 362 nm against blank. The extraction procedures were also carried out in separate experiments at pH 5-6 of the aqueous solutions. After extraction, the gold (III) remained in the aqueous phase ( $C_a$ ) was determined with FAAS. The amount of gold ions of the parallel aqueous solution containing the same amount of gold (III) ions before ( $C_b$ ) extraction was also measured by FAAS. The amount of gold (III) ions extracted in the organic phase was finally calculated by difference ( $C_b - C_a$ ) between the amount of gold (III) ions before and after extraction. The distribution ratio ( $D_{Au}$ ) of the extraction step was calculated as reported (Burns, 1996, PP. 107-109 and El-Shahawi, 1997, PP. 85-91). Following these procedures, the effect of the diverse ions on the accuracy of the developed method for gold (III) was investigated.

#### 2.3.2 Determination of gold (I)

An aliquot portion (10 mL) of the aqueous solutions containing gold (I) at concentration  $< 5 \mu\text{g mL}^{-1}$  was transferred to conical flask (50 mL) and oxidized to gold (III) with bromine water after boiling for 5 min in a closed system (to avoid the evaporation of gold species) and finally cooled to room temperature ( $25 \pm 1^\circ\text{C}$ ). The gold (III) produced was adjusted to pH 5- 6 and completed to the mark with B-R buffer of pH 5-6. The resulting solution was then analyzed following the recommended procedures for gold (III) determination at 365 nm versus the reagent blank with the aid of standard curve.

## 2.4 Analytical application

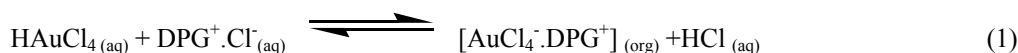
Industrial wastewater samples (100 mL) of fertilizer industry from the boundary side of Jeddah city, Saudi Arabia were collected and filtered through a 0.45  $\mu\text{m}$  membrane filter. The solution pH was then adjusted to pH 5-6 with Britton – Robinson buffer and an accurate amount (0.5 - 10.0  $\mu\text{g}$ ) of gold (III) species was added. To the test solution an accurate amount of the reagent  $\text{DPG}^+\text{Cl}^-$  (2.0 mL,  $8.0 \times 10^{-5} \text{ mol L}^{-1}$ ) was added to the sample solution and the solution mixture was then transferred to 100 mL separating funnel. The organic extract was separated out and the absorbance was measured at 362 nm against reagent blank. The concentration of gold (III) in the organic and aqueous phases was also determined with FAAS.

## 3. Results and discussion

### 3.1 Extraction equilibrium

On mixing the complex anion  $\text{AuCl}_4^-$  with the reagent  $\text{DPG}^+\text{Cl}^-$  in aqueous solutions of pH 5-6 containing sodium chloride (10 % m/v) and shaking with the solvent 4-methyl pentan-2-one for about 2 min, a yellow colored complex ion associate was developed in the organic phase. The electronic spectrum of the organic extract in 4-methyl pentan-2-one showed one well defined peak maximum at 362 nm. Thus, the absorbance of the organic extract of  $\text{AuCl}_4^-$  and  $\text{DPG}^+\text{Cl}^-$  was measured at 362 nm against reagent blank. Assuming no dimerization of the extracted species, the formation of polynuclear complex species is negligible (Alexandrov, 1997, PP. 26-32) and the complex anion  $\text{AuCl}_4^-$  is only predominant at the given pH, the overall reaction between the reagent  $\text{DPG}^+\text{Cl}^-$  and  $\text{HAuCl}_4$  is most likely proceeded as follows (Kamburova, 1992, PP. 997 -1001 and Hiraoka, 1982, PP. 243-245) :

I. Formation of a ternary complex ion associate in the aqueous phase as follows:



The corresponding equilibrium constant,  $\beta$  is given by the equation:

$$\beta = [\text{DPG}^+\text{.AuCl}_4^-]_{(\text{org})} / [\text{AuCl}_4^-]_{(\text{aq})} [\text{DPG}^+]_{(\text{aq})} \quad (2)$$

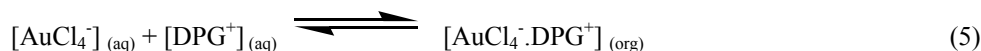
II. Distribution of the complex ion associate between the aqueous and organic phases:



with a distribution constant,  $K_D$  which is given by the equation:

$$K_D = [\text{DPG}^+\text{.AuCl}_4^-]_{(\text{org.})} / [\text{DPG}^+\text{.AuCl}_4^-]_{(\text{aq})} \quad (4)$$

III. Extraction of the complex anion  $\text{AuCl}_4^-$  as follows:



The corresponding extraction constant,  $K_{\text{ex}}$  is then given by the equation:

$$K_{\text{ex}} = [\text{DPG}^+\text{.AuCl}_4^-]_{(\text{org.})} / [\text{DPG}^+]_{(\text{aq.})} [\text{AuCl}_4^-]_{(\text{aq})} = K_D \beta \quad (6)$$

Assuming the complex species  $\text{AuCl}_4^-$  is the only predominant species in the aqueous phase at equilibrium at the given pH, the value of the distribution ratio,  $D_{\text{Au}}$  was then determined at constant concentration of  $\text{AuCl}_4^-$  and various amounts of the reagent  $\text{DPG}^+\text{Cl}^-$  in the aqueous phase employing the equation (Kamburova, 1992, PP. 997 -1001 and Alexandrov, 1997, PP. 26-32):

$$D_{\text{Au}} = [\text{DPG}\text{.AuCl}_4^-]_{(\text{org})} / [\text{AuCl}_4^-]_{(\text{aq})} + [\text{DPG}\text{.AuCl}_4^-]_{(\text{aq})} \quad (7)$$

At low  $\text{DPG}^+\text{Cl}^-$  concentration, the term  $[\text{DPG}^+\text{.AuCl}_4^-]_{(\text{aq})}$  can be neglected and equation (7) takes the form:

$$D_{\text{Au}} = [\text{DPG}^+\text{.AuCl}_4^-]_{(\text{org})} / [\text{AuCl}_4^-]_{(\text{aq})} \quad (8)$$

Substituting equation (8) into equations (2) and (6) and taking the logarithms, equation (9) is obtained:

$$\log D_{\text{Au}} = \log K_D + \log \beta + \log [\text{DPG}^+\text{Cl}^-] \quad (9)$$

The values of  $D_{\text{Au}}$  at the initial concentration of  $\text{AuCl}_4^-$  ( $1 \times 10^{-6} \text{ mol L}^{-1}$ ) in the aqueous phase (pH 5-6) at various concentrations ( $1.0 - 40.0 \times 10^{-5} \text{ M}$ ) of the reagent  $\text{DPG}^+\text{Cl}^-$  were then calculated. The plot of  $\log D_{\text{Au}}$  versus  $\log [\text{DPG}^+\text{Cl}^-]$  was linear (Figure 1) with a slope of 0.91 confirming the formation of 1:1 molar ratio of  $\text{DPG}^+$  and

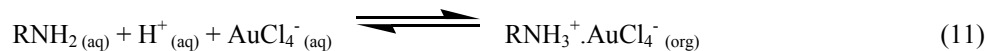
$\text{AuCl}_4^-$  in the formation of ternary complex ion associate  $\text{DPG}^+.\text{AuCl}_4^-$ . The data also have the existence of  $\text{AuCl}_4^-$  species in the organic solvent and the absence of non-specific interaction between the ion associate and the reagent  $\text{DPG}^+.\text{Cl}^-$  and also between the bulky anion  $[\text{AuCl}_4^-]_{(\text{aq})}$  and the organic solvent (Hiraoka, 1982, PP.243-245; Alguacil, 1996, PP. 197-208 and El- Shahawi, 1997 PP85 -91). At high concentration of the reagent  $\text{DPG}^+.\text{Cl}^-$ , the respective term  $[\text{AuCl}_4^-]_{(\text{aq})}$  is negligible and equation (7) takes the following form:

$$D_{\text{Au}} = [\text{DPG}^+.\text{AuCl}_4^-]_{(\text{org})} / [\text{DPG}^+.\text{AuCl}_4^-]_{(\text{aq})} = K_D \quad (10)$$

Thus, at high  $\text{DPG}^+.\text{Cl}^-$  concentration, the plot of the experimental data in the same coordinates of equation (9) has yielded a straight line slightly parallel to the abscissa with negative slope of  $-0.04$  close to zero (Figure 1) confirming, the proposed chemical model, the proposed ternary complex ion associate, the absence of non-specific interaction between the produced complex associate and the reagent and also between the bulky anion  $[\text{AuCl}_4^-]_{(\text{aq})}$  and the organic solvent (Hiraoka, 1982, PP. 243-245 and Alguacil, 1996, PP.197-208). The data have also confirmed the non – specific interaction between the extracted species  $\text{DPG}^+.\text{AuCl}_4^-$  and the solvent (Hiraoka, 1982, PP. 243-245 and Alguacil, 1996, PP.197-208). The values of the equilibrium constants ( $\beta$  and  $K_D$ ) and the extraction constant, ( $K_{\text{ex}} = \beta \times K_D$ ) of the formed ion associate computed from the linear plot (Figure 1) are:  $\beta = 2.07 \pm 0.2 \times 10^4$ ,  $K_D = 11.97 \pm 0.7$ ,  $K_{\text{ex}} = 2.0 \pm 0.3 \times 10^3$ . Using these constants, the theoretical correlation of  $D_{\text{Au}}$  as a function of  $\text{DPG}^+.\text{Cl}^-$  was calculated. The results revealed satisfactory agreement between the experimental and the theoretical data confirming the molar ratio (1:1) of the reagent  $\text{DPG}^+.\text{Cl}^-$  to the complex anion  $\text{AuCl}_4^-$  in the extracted complex ion associate  $\text{DPG}^+.\text{AuCl}_4^-$ . The computed values of the extraction constants  $\beta$ ,  $K_D$  and  $K_{\text{ex}}$  are better than the data reported (Patel, 1986, PP. 1547 -1551) using amidine ion pair. The developed extraction procedures also offered lower reaction time, much less toxic option and low cost for the separation and/or determination of gold (III) species.

### 3.2 Extraction mechanism

Assuming an overall gold (III) extraction in which the reagent amiloride abbreviated by  $\text{RNH}_2$  has the general equilibrium equation:



$$K_{\text{ex}} = [\text{RNH}_3^+.\text{AuCl}_4^-]_{(\text{org})} / [\text{AuCl}_4^-]_{(\text{aq})} [\text{H}^+]_{(\text{aq})} [\text{RNH}_2]_{(\text{aq})} \quad (12)$$

On substituting equation (1) onto equation (10) equation (13) was obtained:

$$K_{\text{ex}} = D_{\text{Au}} / [\text{H}^+]_{(\text{aq})} [\text{RNH}_2]_{(\text{aq})} \quad (13)$$

Taking logarithms and rearranging the equation, the following equation :

$$\log D_{\text{Au}} = \log K_{\text{ext}} - \text{pH} + \log [\text{RNH}_2]_{(\text{aq})} \quad (14)$$

was obtained and the corresponding coefficients for the pH and the amiloride concentration was achieved. The plot of pH *versus*  $\log D_{\text{Au}}$  at constant reagent concentration and the aqueous phase containing  $0.25 \text{ mmol L}^{-1}$  gold (III) using aqueous/organic phase volume ratio of 1/1 and shaking for 3 min was linear with a slope 0.965 close to unity confirming the value for the pH coefficient given in equation (14). Based on the work reported earlier (Alguacil, 1996, PP. 197-208) and by definition, when  $D_{\text{Au}} = 1$  in a solvent extraction system, the pH obtained is known as  $\text{pH}_{50}$ . Thus, on replacing  $\text{pH}_{50}$  in equation (11), the following expression was obtained:

$$\text{pH}_{50} = \log K_{\text{ext}} + \log [\text{RNH}_2]_{(\text{aq})} \quad (15)$$

On plotting  $\log D_{\text{Au}}$  *versus*  $\log [\text{RNH}_2]_{(\text{aq})}$  (Figure 1) a slope of 0.956 was obtained. This value close to unity and corresponds to the value of  $\log [\text{RNH}_2]$  coefficient given in equations (13) and (14). Elemental analysis of the produced ternary complex ion associate in the solid form after solvent evaporation:  $[\text{AuOC}_6\text{H}_9\text{N}_7\text{Cl}_5]$  required: 12.6% C, 1.57% H, 17.2% N, 31.1% Cl and 34.7% Au; Found 12.9% C, 1.7% H, 17.7% N, 31.7 % Cl and 35.6 % Au. The IR spectra of the reagent  $\text{DPG}^+.\text{Cl}^-$  and its solid ion complex associate recorded in KBr disk showed the characteristic frequencies of  $\nu$  (N-H),  $\nu$  (N-N),  $\nu$  (N-H) +(C-N),  $\nu$  (N-C-S) and  $\nu$  (Au-Cl) vibrations at 3456 (br.), 1626 (s), 1516 (s) and  $450 \text{ cm}^{-1}$  (Nakamoto, 1978, PP. 232 -239), respectively confirming the proposed structure. The results also added further conclusive evidence that, the amiloride reagent extracted gold (III) from the aqueous solution containing  $[\text{AuCl}_4^-]_{(\text{aq})}$ , and the absence of non-specific interaction between the ion associate and the reagent  $\text{DPG}^+.\text{Cl}^-$  and also between the bulky anion  $[\text{AuCl}_4^-]_{(\text{aq})}$  and the organic solvent (Hiraoka, 1982, PP.243-245 and Alguacil, 1996, PP. 197-208). Thus, the extraction mechanism of the anion  $\text{AuCl}_4^-$  from the aqueous solution at pH 5- 6 by the reagent  $\text{DPG}^+.\text{Cl}^-$  did not involve solvation of the produced ion associate ( $\text{DPG}^+.\text{AuCl}_4^-$ ) in the organic phase by amine and/or water molecules (Hiraoka, 1982,

PP.243-245 and Alguacil, 1996, PP. 197-208).

### 3.3 Analytical performance

The plot of the absorbance of the developed ion associate  $\text{DPG}^+.\text{AuCl}_4^-_{(\text{org})}$  in the organic phase at 362 nm vs. gold (III) concentration ( $C$ ,  $\mu\text{g mL}^{-1}$ ) was linear confirming Beer's -Lambert law (Marczenko, 1986, PP. 68 – 70 and Miller, 1994, PP.115-125) in the concentration range 0.01 -2.5  $\mu\text{g mL}^{-1}$  gold (III) in the aqueous solution with a correlation coefficient of 0.99. The molar absorptivity calculated from Beer's-Lambert plot and the Sandell's sensitivity index (Marczenko, 1986, PP. 69 -70) of the ion associate were found  $2.05 \times 10^4 \text{ L mol}^{-1} \text{ cm}^{-1}$ ,  $0.069 \mu\text{g cm}^{-2}$ , respectively. The effective concentration range of gold (III) as evaluated by Ringbom's plot (Marczenko, 1986, PP. 69 -70) was found equal 1.5-1.5  $\mu\text{g mL}^{-1}$ . A lower limit of detection (LOD) of  $0.005 \mu\text{g mL}^{-1}$  was achieved using of the formula  $\text{LOD} = 3S_{y/x}/b$  where,  $S_{y/x}$  is the standard deviation of  $y$ - residual and  $b$  is the slope of the calibration plot (Miller, 1994, PP.115-125). The lower limit of quantification ( $\text{LOQ} = 10S_{y/x}/b$ ) under the established conditions for gold (III) was  $0.033 \mu\text{g mL}^{-1}$ . The LOD could be improved to lower value by increasing the sample volume of the aqueous phase containing ultra trace concentration of gold and amiloride at the optimum experimental conditions and shaking with the organic solvent. A relative standard deviation (RSD) of 2.96 % ( $n=5$ ) was obtained for gold (III) at concentration  $0.5 \mu\text{g mL}^{-1}$ . The figure of merits (LOD, linear range, RSD) of the proposed procedure was compared with many of the reported spectrometric methods and in the literature (Pyrzynska, 2005, PP. 1316-1322; Fazli, 2009, PP. 210-212; Zuotao, 1999, PP. 237-241 and El-Shahawi, 2008, PP. 313 -319). The time consuming on the developed method is comparable with some reported methods (Pyrzynska, 2005, PP. 1316-1322 and Fazli, 2009, PP. 210-212) confirming its precision.

### 3.4 Interference studies

The selectivity of the developed method for the determination of gold (III) at  $1.0 \mu\text{g mL}^{-1}$  was tested in the presence of a relatively high excess ( $0.1$ - $1 \text{ mg mL}^{-1}$ ) of some diverse ions which are often accompanying gold in water. The tolerance limit was defined as the concentration of the diverse ion added causing a relative error in the absorbance at 362 nm in the range  $\pm 3\%$ . A recovery percentage of  $100 \pm 2.5\%$  gold (III) and a standard deviation of  $\pm 0.12$  were achieved in the presence of the ions:  $\text{Li}^+$ ,  $\text{Na}^+$ ,  $\text{K}^+$ ,  $\text{Ca}^{2+}$ ,  $\text{NH}_4^+$ ,  $\text{Al}^{3+}$ ,  $\text{Fe}^{2+}$ ,  $\text{Fe}^{3+}$ ,  $\text{Ni}^{2+}$ ,  $\text{Co}^{2+}$ ,  $\text{Pd}^{2+}$ ,  $\text{Pt}^{2+}$ ,  $\text{Cu}^{2+}$ ,  $\text{Zn}^{2+}$  and  $\text{Ag}^+$  at 1:100 tolerable concentration of gold(III) to the diverse ions, respectively. The ions  $\text{Fe}^{3+}$ ,  $\text{MnO}_4^-$ ,  $\text{VO}_3^-$  and  $\text{NO}_3^-$  interfered seriously even at low concentrations. The positive interference of these ions is most likely assigned to the ability of these anions to form relatively stable complex ion associates with the reagent  $\text{DPG}^+.\text{Cl}^-$ . Interference of  $\text{MnO}_4^-$  was eliminated by adding traces of  $\text{NaN}_3$  ( $0.1\% \text{ w/v}$ ) while, the influence of the ions  $\text{Fe}^{3+}$  and  $\text{VO}_3^-$  was minimized successfully by the addition of  $\text{NaF}$  ( $0.1\%$ ) and promotes unambiguous and sensitive determination of gold (III).

### 3.5 Analytical applications

#### 3.5.1 Analysis of gold (I) and / or gold (III)

The values of the extraction constants ( $K_D$ ,  $\beta$  and  $K_{\text{ex}}$ ) in the present study and the molar absorptivity suggested the application of the developed extraction equilibria for extractive spectrophotometric determination of gold (III) at trace concentrations of gold ( $0.05 - 2.0 \mu\text{g mL}^{-1}$ ). Different amounts of gold (III) were spiked onto distilled water ( $100.0 \text{ mL}$ ) and the solutions were subjected to the pre recommended extraction procedures. A satisfactory recovery percentage in the range  $96$ - $98 \pm 3\%$  was obtained between the amount of gold (III) added and measured confirming the accuracy of the developed procedures. The developed procedure was also applied successfully for the determination of gold (I) species at various concentrations ( $0.1$ -  $2.0 \mu\text{g mL}^{-1}$ ) after oxidation to gold (III) with  $\text{Br}_2$  water in the presence of  $\text{HCl}$  as described earlier (El-Shahawi, 2007, PP.1494-1499). A recovery percentage ( $98 \pm 3.4\%$ ,  $n = 5$ ) of gold (I) was also achieved suggesting the use of the method for the analysis of total inorganic gold and chemical speciation of gold (I & III) species and in aqueous media. Thus, the analysis of the binary mixture of gold (I) and (III) at a total amount ( $10$ - $20 \mu\text{g}$ /  $25 \text{ mL}$  aqueous solution) was carried out as follows: an aliquot mixture was first determined according to the described procedure for gold (III). Another aliquot mixture was oxidized to gold (III) with bromine water- $\text{HCl}$  (El-Shahawi, 2007, PP.1494-1499) and determined as described in for gold (I) species. Gold (I) ions in the water samples were then determined by the difference ( $A_2-A_1$ ) between the absorbance of the aliquots before ( $A_1$ ) and after ( $A_2$ ) oxidation. The results are summarized in Table 1. A satisfactory recovery percentage in the range  $96.6$ - $103.2\%$  was obtained with good reproducibility. A relative standard deviation in the range of  $1.9$ - $2.3$  and  $2.1$ - $2.2\%$  for gold (I) and (III) was also obtained, respectively. The proposed method was compared favorably with FAAS and the dithizone spectrophotometric methods (Marczenko, 1986, P. 303) for gold (III) determination. The value of the Student's  $t$ - test ( $t = 2.61$  at  $95\%$ ) was found greater than the theoretical one ( $t = 2.31$ ), so there is no significance differences between the two means.

### 3.5.2 Analysis of gold in wastewater

The extraction procedure was also applied for the separation and subsequent determination of gold (III) by the standard addition of gold (III) species at  $5\text{--}10\ \mu\text{g mL}^{-1}$  onto industrial wastewater samples. A 100.0 mL of water samples was filtered, adjusted to the required pH and extracted as described in the experimental section. The organic extract was analyzed for gold by the developed extractive spectrophotometric method and also by the standard FAAS. The results are given in Table 2. An acceptable recovery percentage of gold (III) in the range of  $98\text{--}103 \pm 2.42\text{--}3.2\%$  was achieved. The decrease in the recovery percentage at  $5.0\ \mu\text{g mL}^{-1}$  gold was improved by increasing the shaking time of the aqueous test solution with the ion pair reagent to 3–4 min. The t- and F-tests at 95% confidence levels did not exceed the tabulated (theoretical) ones and revealed no significant differences (Table 2) between the averages and the variances of the developed and the standard FAAS methods. At 95% confidence, the calculated value of  $t = 2.43$  is greater than the theoretical one ( $t = 2.31$ ) so there is a difference between the two means.

## 4. Conclusion

The reaction of the reagent  $\text{DPG}^+\text{Cl}^-$  with  $\text{AuCl}_4^-$  is rapid (the time taken for the separation and determination of gold ions is at most 3–5 min) and does not involve any stringent conditions. The values of  $K_D$ ,  $\beta$ , and  $K_{\text{ex}}$ , of the produced associate  $\text{DPG}^+\text{AuCl}_4^-$  compete favorably with the most ion pair reagents (El-Shahawi, 1996, PP. 2037–2043 and Patel, 1986 and PP. 1547–1551) and allowed the use of the system for photometric determination of gold (III). Gold (III) ions at trace or ultra trace in one liter aqueous solution was concentrated in 10.0 mL by the developed system so an enrichment factor of 100 was achieved. The extraction system is also suitable for the chemical speciation of gold (I, III) ions.

## References

- AlDhaheri, S.M. (1998). Chemical equilibria of the complex ion associate of periodate and the ion pairing reagent 1- (3, 5-diamino-6-chloropyrazinecarboxyl) guanidine hydrochloride monohydrate. *Talanta*, 46, 161–1615.
- Alexandrov, A., Budevsky, O., Dimitrov, A. (1997). Investigation of the extraction equilibrium of ternary ion – association complex of thallium (III) with iodo-nitro-tetrazolium chloride. *Journal of Radioanalytical Chemistry*, 29, 26–32.
- Alguacil, F.J., Caravaca, C. (1996). Synergistic extraction of gold (I) cyanide with the primary amine primene-Jmt and the phosphine oxide cyanex 921. *Hydrometallurgy*, 42, 197–208.
- Bashammakh, A.S., Bahaffi, S.O., Al-Shareef, F.M., El-Shahawi, M.S. (2009). Development of an analytical method for trace gold in aqueous solution using polyurethane form sorbents: kinetic and thermodynamic characteristic of gold (III) sorption. *Anal Sci, (Japan)*, 25, 413 – 418.
- Biswas, S., Mondal, H.K., Basu, S. (1996). Determination of gold by adogen-464 extraction. *Indian J. Chem.*, 35A, 804–805.
- Burns, D.T., Barakat, S.A., Harriott, M., El-Shahawi, M.S. (1992). Flow injection extraction spectrophotometric determination of manganese (VII) with benzyl tributylammonium permanganate. *Anal. Chim. Acta*, 270, 213–215.
- Burns, D.T., Barakat, S.A., El-Shahawi, M.S., Harriott, M. (1992). Flow-injection extraction spectrophotometric determination of permanganate with triphenylsulphonim cations. *Fresenius J. Anal. Chem.*, 344, 131–132.
- Burns, D.T., El-Shahawi, M.S., Kerrigan, M.J., Smyth, P.M.T. (1996). Spectrophotometric determination of rhenium as perrhenate by extraction with amiloride hydrochloride. *Anal. Chim. Acta*, 322, 107–109.
- Burns, D.T., Hanprasopwattana, P. (1988). Extractive spectrophotometric determination of perchlorate using the ion pair amiloride monohydrochloride. *Anal. Chim. Acta*, 118, 185–187.
- Camagong, C.T., Honjo, T. (2001). Separation of gold (III) as its ion –pair complex with 18-crown-6 from hydrochloric acid media by means of solvent extraction. *Anal. Sci.(Japan)*, 17, 1725–1728.
- El-Shahawi, M.S., Al-Hashimi, F.A. (1996). Spectrophotometric determination of periodate or iodate and ions by liquid-liquid extraction as an ion-pair with tetramethylammonium iodide. *Talanta*, 43, 2037–2043.
- El-Shahawi, M.S., Hassan, S.S.M., Othman, A.M., El-Sonbati, M.A. (2008). Retention profile and subsequent chemical speciation of chromium (III) and (VI) in industrial wastewater samples employing some onium cations loaded polyurethane foams. *Microchemical Journal*, 89, 313 –319.
- El-Shahawi, M.S. (1997). Extraction equilibrium of the ion-associate of periodate with amiloride hydrochloride

and simultaneous spectrophotometric determination of periodate and iodate ions by liquid-liquid extraction. *Anal. Chim. Acta*, 356, 85-91.

El-Shahawi, M.S., Bashammakh, A.S., Bahaffi, S.O. (2007). Chemical speciation and recovery of gold (I & III) from wastewater and silver by liquid-liquid extraction with the ion pair reagent amiloride mono hydrochloride and AAS determination. *Talanta*, 72, 1494-1499.

El-Shahawi, M.S., Hassan, S.S.M., Othman, A.M., Zyada, M.A., El-Sonbati, M.A. (2005). Chemical speciation of chromium (III&VI) employing extractive spectrophotometry and tetraphenylarsonium chloride or tetraphenylphosphonium bromides as an ion-pair reagent. *Anal. Chim. Acta*, 534, 319-326.

Farag, A.B., Soliman, M.H., Abdel-Rasoul, O.S., El-Shahawi M.S. (2007). Sorption characteristics and chromatographic separation of gold (I& III) from silver and base metal ions using polyurethane foams. *Anal. Chim. Acta*, 601, 218-228.

Fazli, Y., Hassan, J., Karbasi, M.H., Sarkouhi M. (2009). A Simple spectrophotometric method for determination of gold (III) in aqueous samples. *Minerals Engineering*, 22, 210-212.

Filatova, D.G., Ryazanova, L.N., Shiryayeva, O.A., Zorov, N.B., Kaprov, Y. (2004). Atomic absorption determination of gold as complex amines. *J. Anal. Chem.*, 59, 243-245.

Guanghan, L., Jinya, X. (1992). Determination of trace amounts of gold in wastewater by graphite furnace atomic-absorption spectrophotometry with preconcentration on trioctylphosphine oxide chemically modified tungsten wire matrix. *Talanta*, 39, 51-53.

Haddad, P.R., Rochester, N.E. (1988). Ion – interaction reversed – phase chromatographic method for the determination of gold (I) cyanide in mine process liquors using automated sample preconcentration, *J. Chromatogr*, 439, 23 – 36.

Hassan, S.S.M., El-Shahawi, M.S., Othman, A.M., Mosaad, M.A. (2005). A potentiometric rhodamine-B based membrane sensor for the selective determination of chromium ions in wastewater. *Anal. Sci. (Japan)*, 21, 673-678.

Hiraoka, M. (1982). Crown compounds, their characteristics and applications, El-Sevier, Tokyo, 243-245.

Hu, Q., Chen, X., Yang, X., Huang, Z., Chen, J., Yang, G. (2006). Solid phase extraction and spectrophotometric determination of Au (III) with 5-(2-hydroxy-5-nitrophenylazo) thiorhodamine. *Anal. Sci. (Japan)*, 22, 627-630.

Itagaki, T., Ashino, T., Takada, K. (2000). Determination of trace amounts of gold and silver in high-purity iron and steel by electrothermal atomic absorption spectrometry after reductive co precipitation. *Fresenius J. Anal. Chem.*, 368, 344-349.

Kamburova, S.M. (1992). A highly sensitive spectrophotometric method for the determination of iodate using leuco xylene cyanol FF. *Talanta*, 39, 997 -1001.

Li, J.F., Bai, L.F., Wang, Y.H., Wang, H.Y. (2006). Rapid determination of gold in geological samples using flow injection solid phase chemiluminescences. *Anal. Sci. (Japan)*, 22: 841-844.

Medved, J., Bujdos, M., Matus, P., Kubova, J. (2004). Determination of trace amounts of gold in acid-attacked environmental samples by atomic absorption spectrometry with electrothermal atomization after preconcentration. *Anal. Bioanal. Chem.*, 379, 60 - 65.

Marczenko, Z. (1986). Spectrophotometric determination of elements, 3<sup>rd</sup> edition, Ellis Horwood Chichester, U.K, PP.68 -70, 203.

Marczenko, Z. (1986). Spectrophotometric determination of elements, 3<sup>rd</sup> edition, Ellis Horwood Chichester, U.K, PP.68 -70, 203.

Miller, J.C., Miller, J.N. (1994). Statistics for analytical chemistry 4<sup>th</sup> edition, Ellis-Horwood, New York, PP.115-125.

Nakamoto, K. (1978). *Infrared and raman spectra of inorganic and coordination compounds*, 3<sup>rd</sup> edition, Wiley: New York.

Navratilova, Z., Kula, P. (2000). Determination of gold using clay modified carbon paste electrode. *Fresenius J. Anal. Chem.*, 367, 369-372.

Patel, K.S., Lieser, K.H. (1986). Extraction and spectrophotometric determination of gold (III) by use of amides and amidines. *Anal. Chem.*, 58 (7), 1547 -1551.

Pyrzynska, K. (2005). Recent development in the determination of gold by atomic spectrometry techniques. *Spectrochim. Acta B*, 60, 1316-1322.

Shoursheinin, F., Sajad, B., Parvin, P. (2010). Determination of gold fineness by laser induced breakdown spectroscopy with the simultaneous use of CW-CO<sub>2</sub> and Q-SW Nd: YAG lasers. *Optics and Lasers in Engineering*, 48, 89 -95.

Vogel, A.I. (1966). *A Text Book of Quantitative Inorganic Analysis* 3<sup>rd</sup> edn., Longmans Group Ltd., England.

Yu, M., Suna, D., Huangb, R., Tian, W., Shen, W., Zhang, H., Xua, N. (2003). Determination of ultra-trace gold in natural water by graphite furnace atomic absorption spectrometry after in situ enrichment with thiol-cotton fiber. *Anal. Chim. Acta*, 479, 225 -231.

Zuotao, Z., Creedy, T.M., Townshend, A. (1999). Flow injection spectrophotometric determination of gold using 5-(4-sulphophenylazo)-8-aminoquinoline, *Anal. Chim. Acta*, 401, 237-241.

Table 1. Analytical data of gold (I) and gold (III) in their binary mixtures in aqueous media (10 mL) by the proposed extractive spectrophotometric method

Gold species,				Recovery, %*	
Taken, µg		Found, µg			
Au <sup>+</sup>	Au <sup>3+</sup>	Au <sup>+</sup>	Au <sup>3+</sup>	Au <sup>+</sup>	Au <sup>3+</sup>
5.0	5.0	4.8	5.1	96.0±2.3	102.0±2.3
10.0	10.0	9.75	10.22	97.5±2.9	102.4 ±2.1
10.0	10.0	9.80	9.90	99.4±2.7	99.0±1.9

\* Average (n=5) ± relative standard déviation.

Table 2. Results of the extractive spectrophotometric determination of gold (III) spiked (0.5 – 10 µg) to industrial wastewater samples (100 mL)

Gold species,		Recovery, %*
Gold (III) added, µg	Gold (III) found, µg	
0.0	0.0	0.0
5.0,	4.9± 0.12	98.± 2.42.
8.0	8.2± 0.22	5.0± 2.7
10.0	10.3± 0.32	103.0±3.2

\*Average (n=5) ± relative standard déviation.



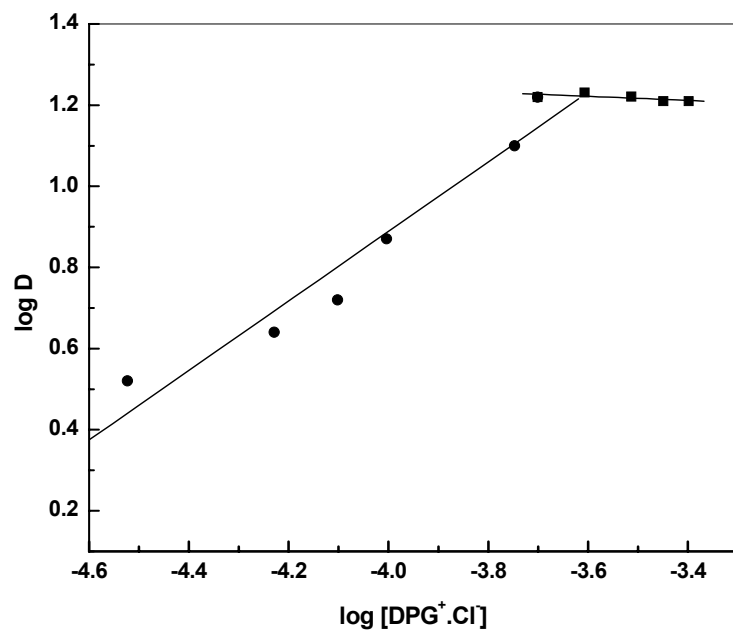


Figure 1. Plot of  $\log [\text{DPG}^+.\text{Cl}^-]$  versus  $\log D_{\text{Au}}$  of the ion associate  $[\text{DPG}^+.\text{AuCl}_4^-]$  Conditions: Aqueous phase (20 mL) at pH 6-7, organic solvent = 5 mL and  $[\text{HAuCl}_4] = 6.2 \times 10^{-6} \text{ mol L}^{-1}$

# Molecular Interactions in Binary Mixture of Polymethylmethacrylate with Acetic Acid

Richa Saxena (Corresponding author) & S.C. Bhatt  
Ultrasonic and Dielectric Laboratory, Department of Physics  
H.N.B. Garhwal University, Srinagar, Garhwal  
Uttarakhand-246174, India  
E-mail: saxena.richa23@gmail.com

## Abstract

Solution is prepared by mixing Polymethylmethacrylate in solid form with acetic acid, which at different concentration were used to measure density, viscosity & ultrasonic velocity in the temperature range 30°C-65°C, using ultrasonic interferometer at 1MHz. Using these measured values of density, viscosity & sound velocity, different parameters like, adiabatic compressibility, acoustic impedance and relaxation time have been measured for solution of polymethylmethacrylate with acetic acid under different conditions of temperature and concentration. Variations of above parameters with respect to temperature and concentration have been discussed in terms of molecular interactions.

**Keywords:** Adiabatic compressibility, Acoustic impedance and relaxation time

## 1. Introduction

Polymers are today one of the most important products which surrounds us in every walk of life. Current applications extend from adhesives, coating, foams and packaging materials to textile and industrial fibers, composites, electronic devices, biomedical devices, optical devices and precursors for many newly developed high-tech ceramics. PMMA is used in Lenses, light covers, glazing, light pipes, meter covers, bathroom fittings, outdoor signs, skylights, baths, and toys. The ultrasonic study of liquid mixtures has been gaining importance in assessing the nature of molecular interaction (Arumugam V, 1998, p. 857). During the last few decades, ultrasonic study of liquid mixtures has gained importance for knowing the molecular interactions and understanding the physio-chemical behaviour of liquid (Palaniappan L, 2008, p.1906). The study of molecular interactions present in the polymer and solvent on one hand polymer-polymer and on the other hand is important as it throws light on the processes involving polymer production and their uses (Seetharaman V, 2005, p.156). Velocity measurements yield useful information on the behavior of the polymer solutions (Rim Bae, J, 2004, p. 559). In general, polymeric mixtures are far less miscible than mixtures of small molecules materials. This effect is a result of the fact that the driving force for mixing is usually entropic, not energetic or miscible materials usually form a material not because their interaction with other is more favorable than their self interaction, but because of an increase in entropy and hence free energy associated with increasing the amount of volume available to each component. This increase in entropy scales with the number of particles (or moles) being mixed. Since polymeric molecules are much larger and generally have much higher specific volumes than small molecules, the numbers of molecules involved in polymer mixtures are far less than number in a small molecules mixture of equal volume. The energetic of mixing, on other hand are comparable on a per volume basis for polymeric and small molecule mixtures.

The studies on ultrasonic parameters have become an emerging field in recent years. The objective of ultrasonic studies is to identify the molecular interaction between solute and solvent and to bring about the structural changes associated with them in terms of acoustic properties like sound velocity, adiabatic compressibility and acoustic impedance etc. Relative variation in the sound velocity in polymethyl methacrylate at intermediate low temperatures has been studied by R. Nava and R. Oentrich (Nava R, 1994, p.337). K. Sudhakar and R.P. Singh (Sudhakar K, 1987, p. 560) have studied the ultrasonic investigation of interpenetrating networks of polymethylmethacrylate and polyurethane. Mechanical and thermal properties of polymethyl methacrylate B.N. Nanotube composites have studied by C.Y. Zhi, et al. (Zhi C Y, 2008, p.1). Kazuhiro kamiguchi et al. (Kamiguchi, Kazuhiro, 2009, p. 231) has studied the structural characterization of inhomogeneous PMMA gels by time dependent diffusion NMR spectroscopy. The purpose of the present study is to clarify the factors

contributing to the compressibility in PMMA-acetic acid system over wide range of temperature and concentration, which will be helpful to enhance the knowledge of this PMMA- acetic acid solution as they have for other system.

## 2. Experimental Details

In the present investigation, of polymethylmethacrylate (of molecular weight  $\approx 15,000$  in solid form) with acetic acid is used. The solutions were prepared by adding known weight of polymethylmethacrylate to fixed volume of acetic acid and stirring under reflux, until a clear solution was obtained. Different acoustic parameters like adiabatic compressibility, acoustic impedance and relaxation time were calculated at different concentration 0.8%, 0.6%, 0.5%, 0.4%, and 0.3% (w/v) at different temperatures 30°C, 35°C, 40°C, 45°C, 50°C, 55°C, 60°C, 65°C at 1MHz frequency by using variable path ultrasonic interferometer (Mittal Enterprises) has reproducibility of  $\pm 0.4\text{m/s}$  at 25°C. The temperature of the solution has been kept constant by circulating water from the thermostatically controlled ( $\pm 0.1^\circ\text{C}$ ) water bath. In this technique, the sample is kept in a cell, which consists of a double walled metallic jacket having inlet and outlet for circulating thermostatic fluid. A quartz crystal is fixed at the bottom of the cell, which when excited by RF source produces longitudinal ultrasonic waves of particular frequency which propagates in the medium. These waves are reflected at the metallic reflector, attached to a sensitive micrometer which can be moved up and down. The incident and reflected waves form standing wave pattern. By moving the micrometer in the sample, maxima and minima are formed which can be observed in the micrometer of interferometer. These maxima are separated by half integral multiple of the wavelength of the ultrasonic wave. The densities at different temperatures were measured using 10ml specific gravity bottle and single pan macro balance. The uncertainty in density measurements was found to be  $0.5\text{kg/m}^3$ . The viscosity of the mixtures was determined by using Ostwald viscometer which was kept inside a double-wall-jacket in which water from thermostat water bath was circulated. The inner cylinder of this double-wall-glass jacket was filled with water of desired temperature so as to establish and maintain the thermal equilibrium. The accuracy in the viscosity measurements is within  $\pm 0.5\%$ . These parameters are calculated by using standard relations (Bhatt S C, 2000, p. 275; Bhatt S C, 2000, p. 293; Marcue Y, 1977).

$$\text{Ultrasonic velocity} \quad v = f \lambda \quad \dots\dots\dots (1)$$

$$\text{Adiabatic compressibility} \quad \beta = 1 / v^2 \rho \quad \dots\dots\dots (2)$$

$$\text{Acoustic impedance} \quad Z = \rho v \quad \dots\dots\dots (3)$$

$$\text{Relaxation time} \quad \tau = 4 \eta / 3 \rho v^2 \quad \dots\dots\dots (4)$$

Where

$\rho$ , is density of the medium.

$v$ , is the ultrasonic velocity in the medium.

$\eta$ , is viscosity of the medium.

$f$ , is frequency.

$\lambda$ , is wavelength

## 3. Results & Discussion

In a dilute solution, the properties of polymer are characterized by the interaction between the solvent and the polymer. In a good solvent, the polymer appears swollen and occupies a large volume. In this scenario, intermolecular forces between the solvent and monomer subunits dominate over intermolecular interactions. When a polymer is added to given solvent, attraction as well as dispersion forces begin acting between its segments, according to their polarity, chemical characteristics and solubility parameters. If the polymer-solvent interactions are higher than the polymer-polymer attraction forces, the chain segment start to absorb solvent molecules, increasing the volume of the polymer matrix and loosening out from their coiled shape.

In the present investigation density, viscosity and ultrasonic velocity are measured at different temperature and concentration of polymethylmethacrylate with acetic acid, which are shown in Table-1, 2, and 3 respectively and the variation with temperature and concentration are shown in Fig.1 & 2, Fig.3 & 4 and Fig.5 & 6 respectively. By using these values for PMMA of (molecular weight  $\approx 15000$ ) adiabatic compressibility, acoustic impedance and relaxation time are calculated using equations (2),(3) & (4) respectively and the results are presented in Table-4, 5 & 6 respectively. The variations of these parameters with temperature and concentration are shown in Fig.7 to Fig.12 respectively.

The variation of density with temperature and concentration is shown in Table-1 and Fig.1 & 2 respectively. It is observed from Table-1 and Fig.1 & 2, that density decreases with increase in temperature and increases with increase in concentration. Measurements of density and for a range of frequencies may lead to a better understanding of the molecular mechanisms responsible for absorption and velocity such as relaxation (Esquivel-Sirvent R, 1993, p.819). Table-2, presents the change in viscosity with temperature and concentration, the variations are shown in Fig.3 and 4 respectively. Table-2 and Fig.3 & 4, reports that viscosity decreases with increasing temperature and it increases with increasing concentration of PMMA in the solution. Similar behaviour has been observed by Surbha and coworkers (Surendra babu N, 2002, p.505). The increasing trend of viscosity with concentration reveals that addition of polymer (PMMA) increases the effective molecular area (Eliel E L, 1985, p. 95). The measurement of viscosity in dilute macromolecular solution has fundamental importance not only in determination of molecular weights, but also in the evaluation of key parameters for the understanding of the conformational characteristics of the polymer solutions. The variations of ultrasonic velocity with temperature and concentration have been shown in Table-3, and Fig.5 & 6, respectively. It is evident from Table-3 and Fig.5 & 6, that ultrasonic velocity decreases with increase in temperature and it increases with increase in concentration. Present values are compared with available values in literature. These are in good agreement with earlier work's (Varada Rajulu A, 1999, p. 379; Selvakumar M, 2008, p. 712) findings. Velocity studies show that as the polymer concentration increases a more rigid molecular structure is formed perhaps by bonding between the large polymer molecules.

Table-4 and Fig.7 & 8, shows the variation of adiabatic compressibility with temperature and concentration respectively. It is observed from Table-4 and Fig.7 & 8, that adiabatic compressibility increases with increasing temperature and decreases with increasing concentration. This can be explained in terms of the electrostatic effect of polymer on the surrounding solvent molecules. It is primarily the compressibility that changes with structure. This leads to change in ultrasonic velocity. The variation of acoustic impedance with temperature and concentration are shown in Table-5 and Fig.9 & 10. It is seen from Table-5 and Fig.9 & 10, that acoustic impedance decreases with increase in temperature and it increases with increase in concentration, which can be attributed to the effective solute-solvent interactions (Syal V K, 2005, p. 61). Table-6 shows the change in relaxation time with change in temperature and concentration. The variation of relaxation time with temperature & concentration are shown in Fig.11 & 12 respectively. It is observed from Table-6 and Fig.11 & 12 that relaxation time decreases with increasing temperature also it decreases with increasing concentration. The above behaviour is obvious as per kinetic theory of fluids. The variation of relaxation time is a cumulative effect of the density, viscosity and ultrasonic velocity.

#### 4. Conclusions

It also shows the nature of polymer in solvent at different concentration and temperature and to study intermolecular interactions. Those in turns are useful for production and uses of polymers in pharmaceuticals and industry.

#### References

- Arumugam, V., Naresh, M.D., Sanjeevi R. (1998). Ultrasonic study of Collagen solutions. *J. Solution chemistry*, 27, 857-864.
- Bhatt, S. C., Semwal, H. K., Lingwal, V., Singh, K., Semwal, B. S. (2000). Acoustical parameters of some molecular liquids. *J. Acous. Soc. India*, 28, 293-296.
- Bhatt, S. C., Semwal, H. K., Lingwal, V., Singh, K., Semwal, B. S. (2000). Relaxation time and ultrasonic attenuation in some binary and ternary liquid systems. *J. Acous. Soc. India*, 28, 275-278.
- Eliel, E.L. (1985). *Stereochemistry of carbon compounds*, 9<sup>th</sup> ed., New Delhi, Tata McGraw Hill, 95-97.
- Esquivel-Sirvent, R., Tan, B., Abdelraziq, I., Yunand, S. S., Stump, F. B. (1993). Absorption and velocity of ultrasound in binary solutions of polyethylene glycol and water. *J. Acous. Soc. Am.*, 93, 819-820.
- Kamiguchi, Kazuhiro, Kuroki, Shigeki., Satoh, M., Ando, Isao. (2009). Structural characterization of inhomogenous polymethylmethacrylate gels by time dependent diffusion NMR spectroscopy. *Macromolecules*, 42, 231-235.
- Marcue Y. (1977). *Introduction to liquid State chemistry*, (New York, Wiley Int.).
- Nava, R., Oentrich R. (1994). Relative variation in the sound velocity in polymethyl methacrylate at intermediate low temperature. *J. Alloys and compounds*, 211/212, 337-339.

- Palaniappan, L., Thiyagarajan, R. (2008). Effect of aniline in methanol + benzene mixture- An ultrasonic study. *Ind. J. Chem.*, 47B, 1906-1909.
- Rim Bae, J. (2004). Ultrasonic velocity and absorption measurements in an aqueous solution of poly(sodium 4-styrenesulfonate). *Macromolecular Research*, 12, 559-563.
- Seetharaman, V., Kalyanasundaram, S., Gopalan A. (2005). Quantitatively study of interaction of vinyl polymers by ultrasonic method. *J. of molecular liquids*, 121, 156-159.
- Selvakumar M., Krishna Bhat D. (2008). Molecular interactions of Polymethyl methacrylate and Polyethyleneglycol solutions in tetrahydrofuran. *Indian Journal of Pure and Applied Physics*, 46, 712-718.
- Sudhakar, K., Singh, R. P. (1987). Ultrasonic investigation of interpenetrating networks of Poly(methyl methacrylate) and polyurethane. *Rheologica Acta*, 26, 560-565.
- Surendra babu, N., Subha, M. C. S. (2002). Effect of polymer and temperature on the critical micellar concentration of aqueous sodium dodecylsulfate. *J. Indian chem. Soc.*, 79, 505-508.
- Syal, V. K., Chauhan, A., Chauhan, S. (2005). Ultrasonic velocity, viscosity and density studies of polyethylene glycols in acetonitrile and water mixtures at 25°C. *J. pure Appl. Ultrason*, 27, 61-69.
- Varada Rajulu, A., Lakshminarayana Reddy, R. (1999). Ultrasonic, refractometric and viscosity studies of polyethylene oxide/polymethylmethacrylate and polyethylene oxide/polystyrene blends in solution. *J. Acous Soc. India*, 27, 379-382.
- Zhi, C. Y., Bando Yoshio, L., Wang W., C., Tang, Chengchun. (2008). Mechanical and thermal properties of PMMA – BN nanotube composites. *J. Nanomaterials*, Article ID 642036, 1-5.

Table 1. Density ( $\times 10^3 \text{kgm}^{-3}$ ) at different temperature and concentration at 1MHz for PMMA

Temperature $\rightarrow$	30°C	35°C	40°C	45°C	50°C	55°C	60°C	65°C
Concentration (w/v)								
0.8%	1.05	1.04	1.03	1.01	.994	0.10	0.96	0.94
0.6%	1.04	1.04	1.03	1.01	1.00	0.99	0.98	0.96
0.5%	1.08	1.06	1.05	1.04	1.02	1.01	0.99	0.98
0.4%	1.04	1.03	1.02	1.01	1.00	0.99	0.98	0.97
0.3%	0.91	0.91	0.90	0.89	0.88	0.87	0.85	0.83

Table 2. Viscosity (Pas) at different temperature and concentration at 1MHz for PMMA

Temperature $\rightarrow$	30°C	35°C	40°C	45°C	50°C	55°C	60°C	65°C
Concentration(w/v)								
0.8%	.0126	.0105	.0089	.0074	.0069	.0063	.0059	.0061
0.6%	.0097	.0087	.0076	.0071	.0069	.0061	.0059	.0053
0.5%	.0101	.0089	.0080	.0075	.007	.0064	.0059	.0058
0.4%	.0098	.0085	.0076	.0072	.0067	.0062	.0058	.007
0.3%	.0085	.0075	.0069	.0065	.0058	.0056	.0052	.0048

Table 3. Ultrasonic velocity ( $\text{ms}^{-1}$ ) at different temperature and concentration at 1MHz for PMMA

Temperature $\rightarrow$ Concentration(w/v)	30°C	35°C	40°C	45°C	50°C	55°C	60°C	65°C
0.8%	1232.4	1229.5	1219.6	1213.7	1204.8	1201.2	1199.8	1194.6
0.6%	1215.2	1215.4	1205.4	1197.4	1192.6	1190.1	1187.0	1182.0
0.5%	1210.7	1196.6	1195.3	1193.5	1181.4	1176.5	1172.7	1170.7
0.4%	1197.4	1182.1	1177.4	1172.3	1168.5	1162.3	1161.4	1158.0
0.3%	1190.2	1182.6	1172.3	1165.7	1163.2	1160.4	1158.3	1154.2

Table 4. Adiabatic compressibility( $\times 10^{-10} \text{kg}^{-1} \text{ms}^2$ ) at different temperature and concentration at 1MHz for PMMA

Temperature $\rightarrow$ Concentration(w/v)	30°C	35°C	40°C	45°C	50°C	55°C	60°C	65°C
0.8%	6.27	6.38	6.56	6.71	6.93	6.96	7.27	7.44
0.6%	6.41	6.52	6.70	6.89	7.01	7.13	7.27	7.47
0.5%	6.33	6.59	6.68	6.78	7.00	7.16	7.34	7.47
0.4%	6.71	6.98	7.08	7.20	7.32	7.48	7.59	7.72
0.3%	7.72	7.89	8.11	8.29	8.44	8.61	8.81	9.07

Table 5. Acoustic impedance ( $10^3 \text{kgm}^2 \text{s}^{-1}$ ) at different temperature and concentration at 1 MHz for PMMA

Temperature $\rightarrow$ Concentration (w/v)	30°C	35°C	40°C	45°C	50°C	55°C	60°C	65°C
0.8%	1294.6	1275.7	1250.7	1227.4	1197.8	1196.0	1146.7	1125.2
0.6%	1276.7	1261.4	1238.8	1212.1	1196.8	1178.4	1158.4	1132.0
0.5%	1305.3	1268.2	1252.2	1235.5	1208.7	1187.6	1162.4	1143.9
0.4%	1243.9	1211.9	1199.1	1185.2	1168.7	1150.8	1135.2	1119.1
0.3%	1087.8	1071.7	1051.6	1034.9	1018.6	1001.0	979.6	955.1

Table 6. Relaxation time( $\times 10^{-12} \text{s}$ ) at different temperature and concentration at 1MHz for PMMA

Temperature $\rightarrow$ Concentration(w/v)	30°C	35°C	40°C	45°C	50°C	55°C	60°C	65°C
0.8%	8.58	8.93	7.78	6.64	6.35	5.8	5.75	6.05
0.6%	8.33	7.57	6.8	6.53	6.45	5.82	5.70	5.31
0.5%	8.20	7.84	7.15	6.78	6.50	6.12	5.73	5.76
0.4%	8.66	7.86	7.18	6.91	6.53	6.18	5.90	5.14
0.3%	8.75	7.89	7.42	7.18	6.53	6.43	6.11	5.81

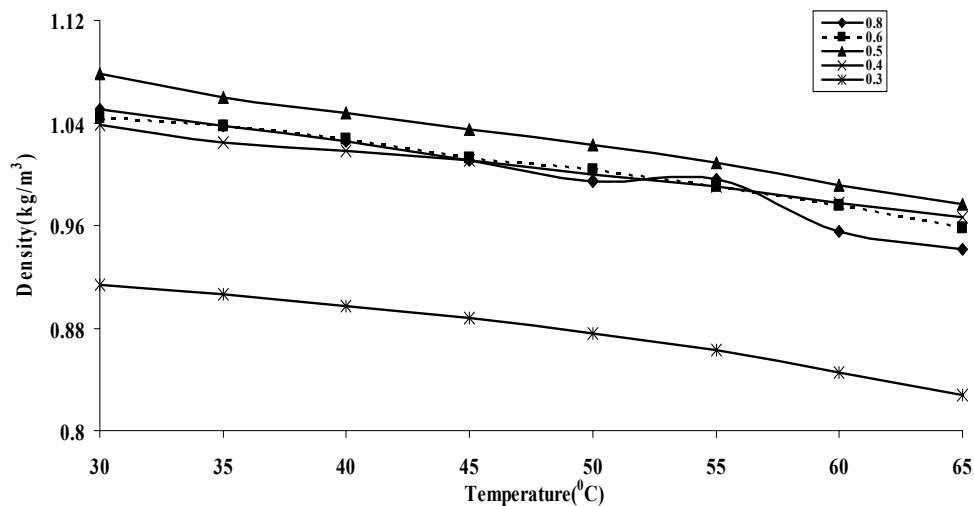


Figure 1. Variation of density with temperature at different concentration of PMMA

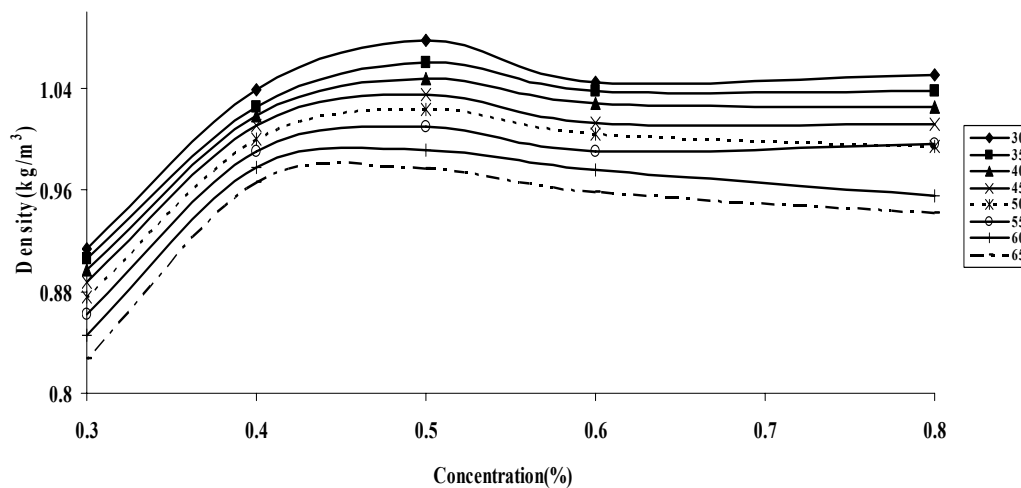


Figure 2. Variation of density with concentration at different temperature of PMMA

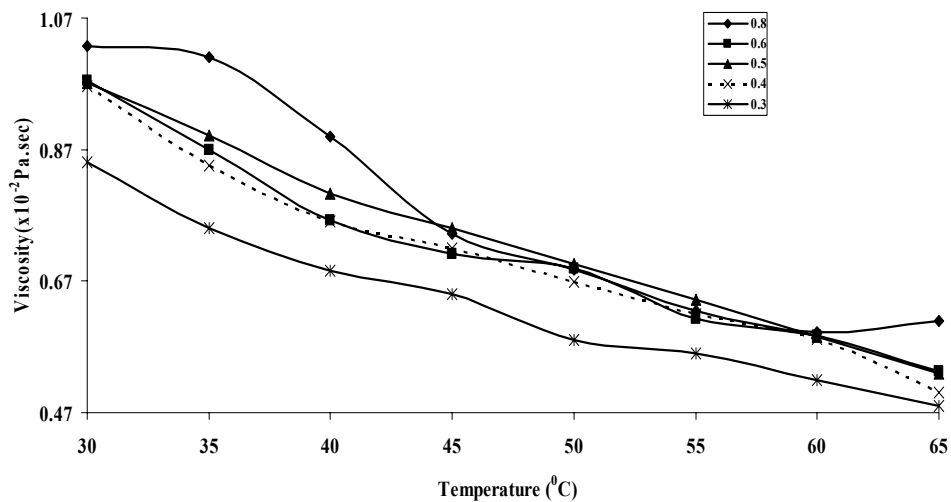


Figure 3. Variation of viscosity with temperature at different concentration of PMMA

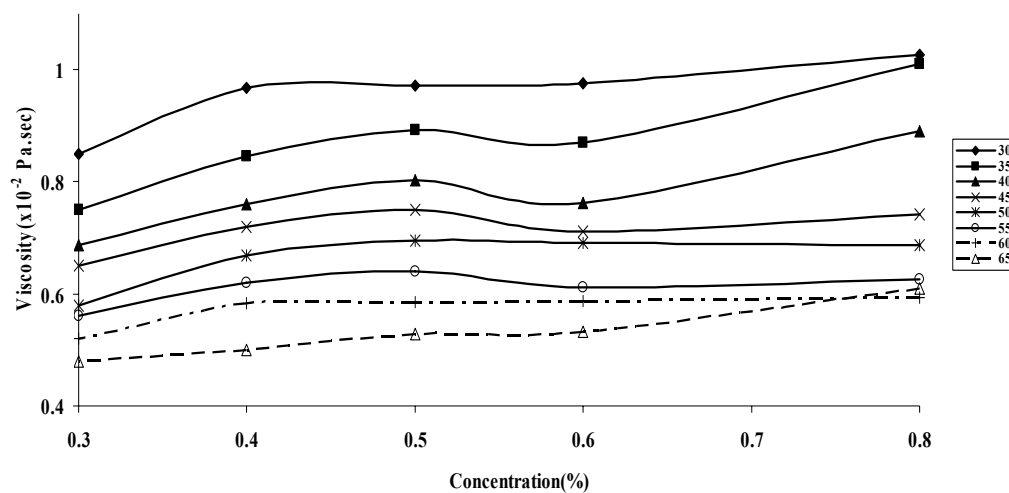


Figure 4. Variation of viscosity with concentration at different temperature of PMMA

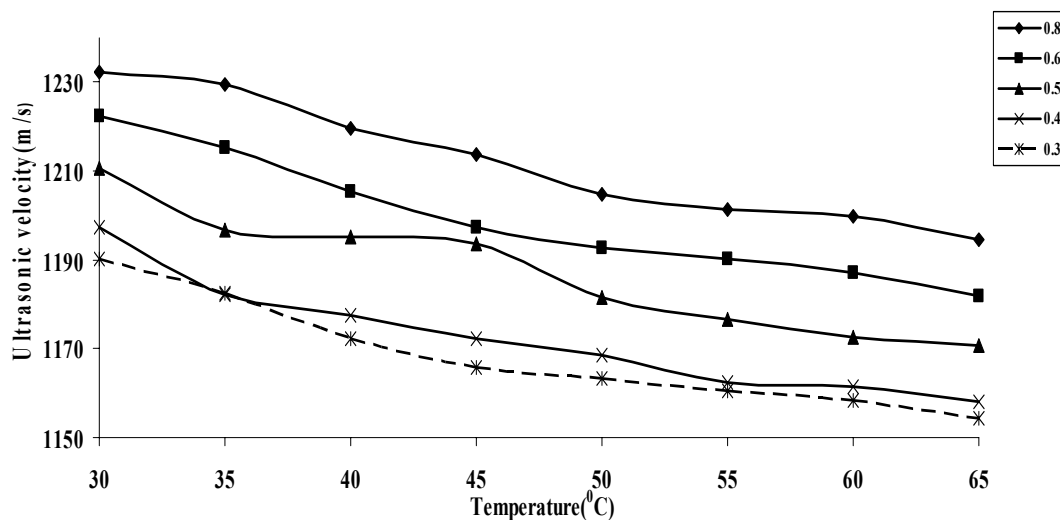


Figure 5. Variation of ultrasonic velocity with temperature at different concentration of PMMA

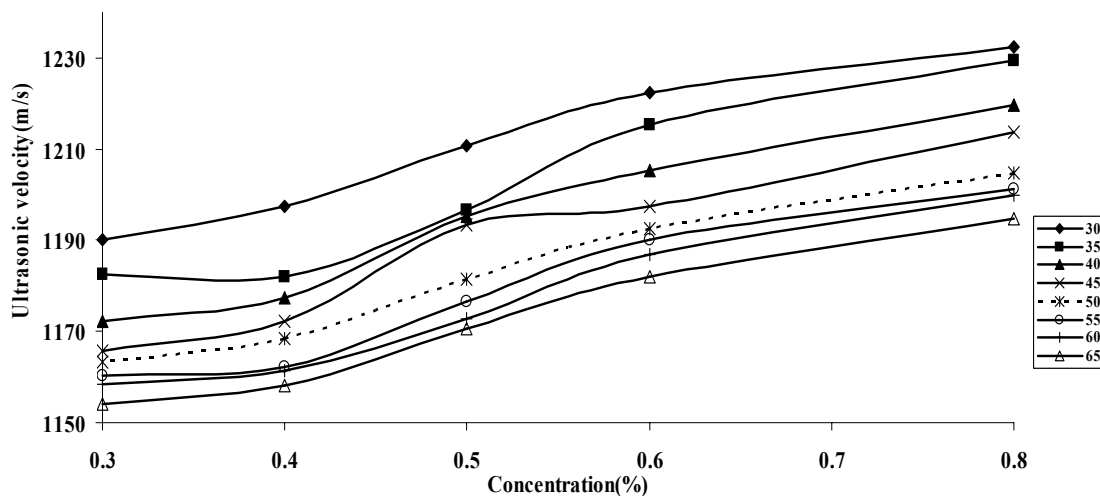


Figure 6. Variation of ultrasonic velocity with concentration at different temperature of PMMA



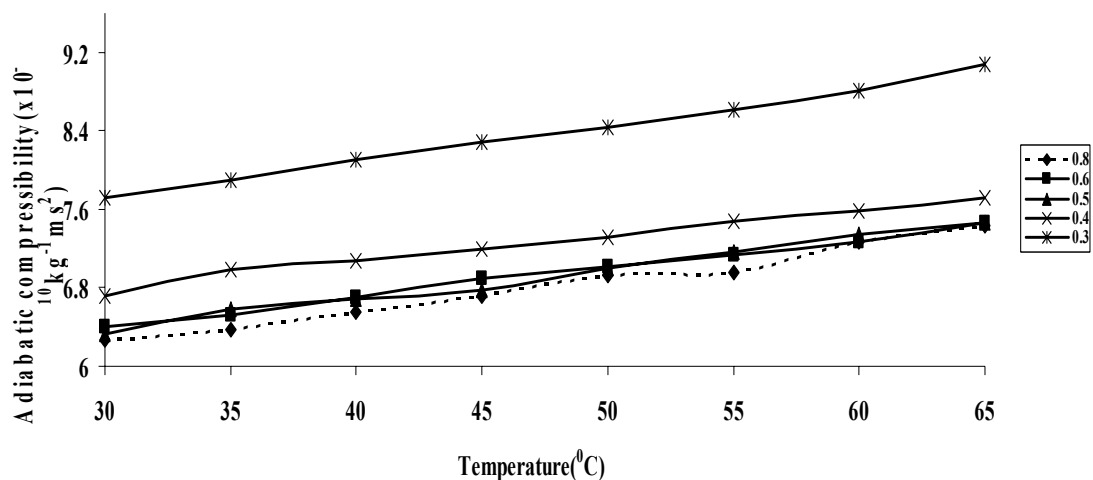


Figure 7. Variation of adiabatic compressibility with temperature at different concentration of PMMA

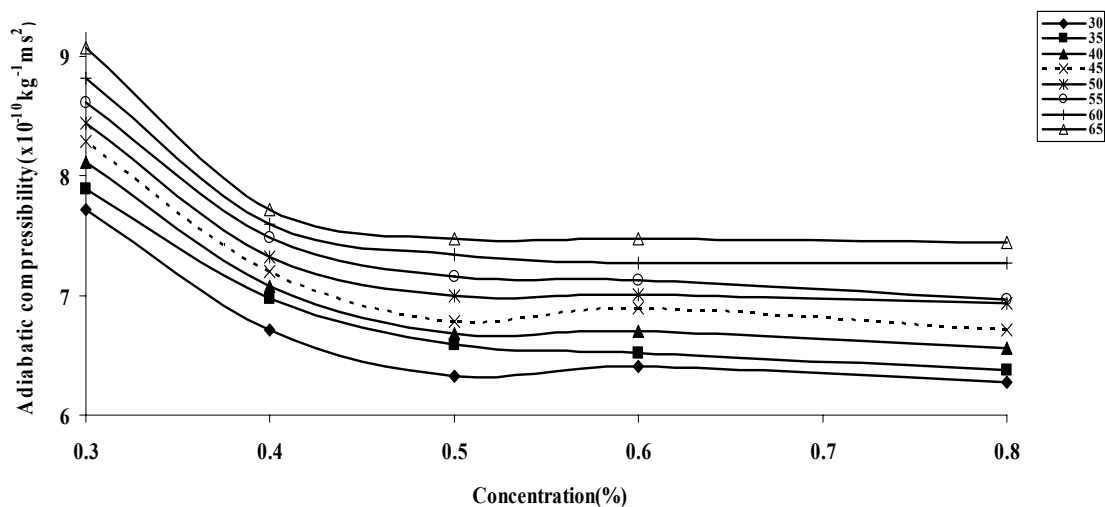


Figure 8. Variation of adiabatic compressibility with concentration at different temperature of PMMA

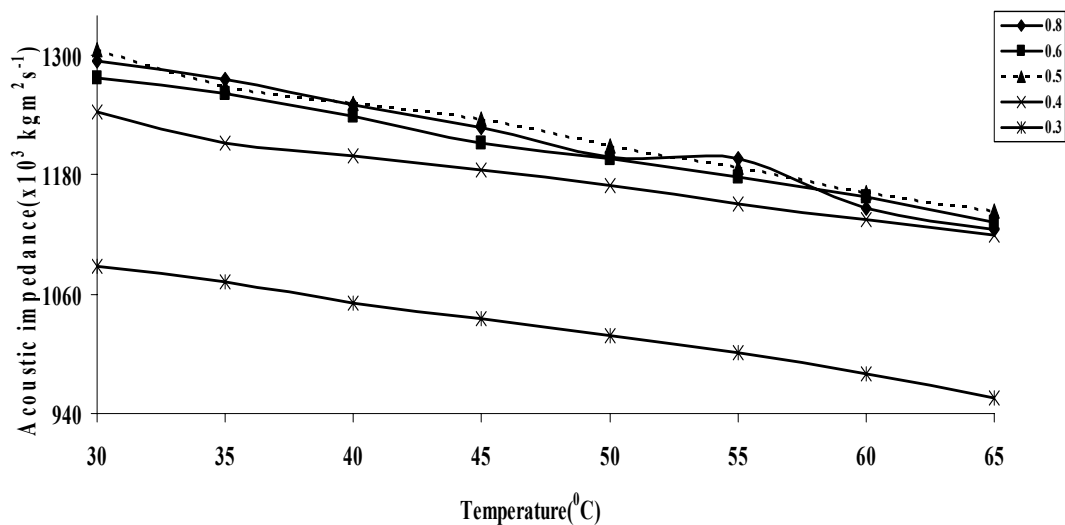


Figure 9. Variation of acoustic impedance with temperature at different concentration of PMMA

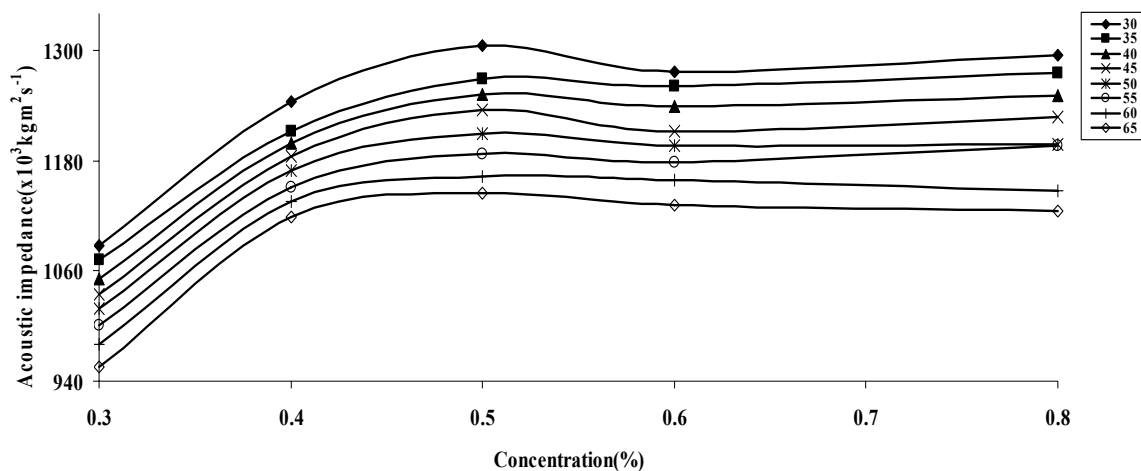


Figure 10. Variation of acoustic impedance with concentration at different temperature of PMMA

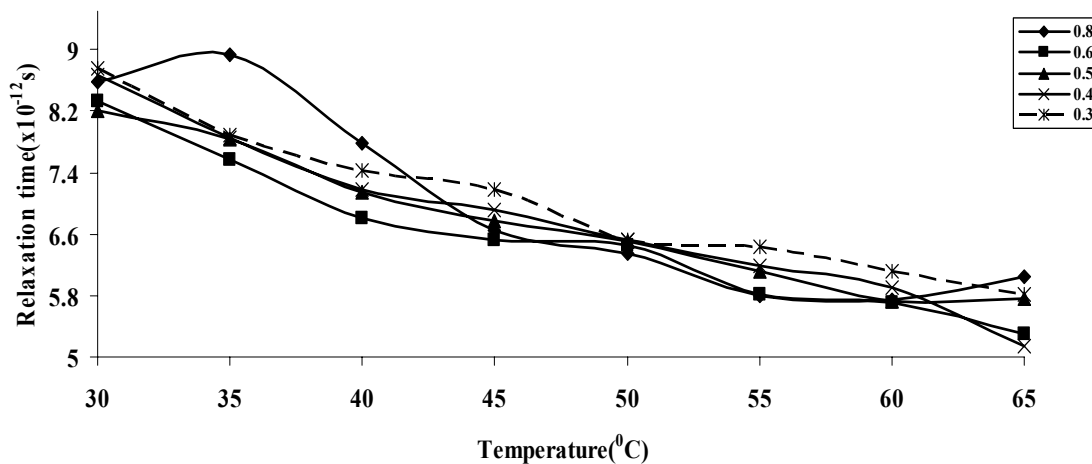


Figure 11. Variation of relaxation time with temperature at different concentration of PMMA

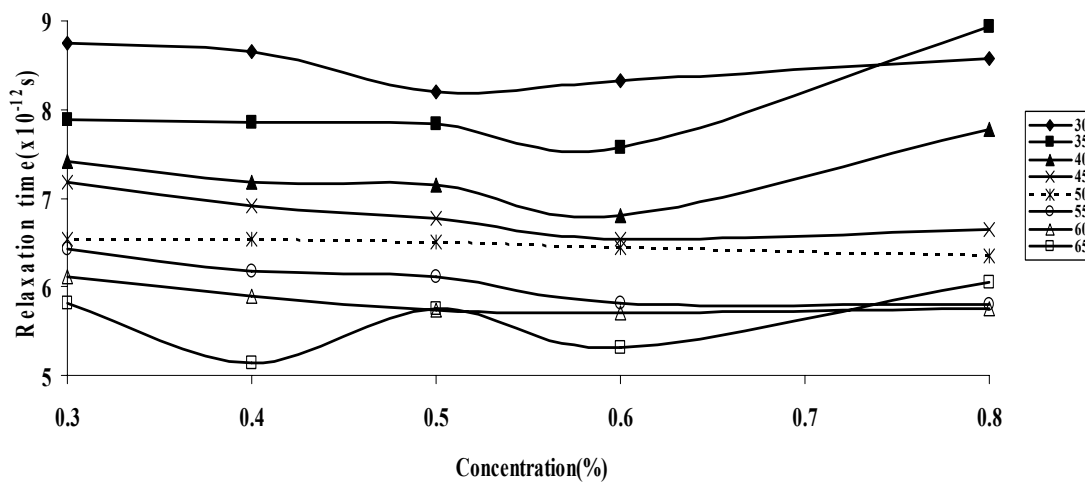


Figure 12. Variation of relaxation time with concentration at different temperature of PMMA

# A Novel Approach for Preparing Red Phosphorus Microcapsule by Hydrothermal Method

Yajuan Zhao (Corresponding author)

College of Chemistry and Materials Engineering, Wenzhou University

Wenzhou, Zhejiang, 325035, China

E-mail: zyj@wzu.edu.cn

Xing Huang

College of Chemistry and Materials Engineering, Wenzhou University

Wenzhou, Zhejiang, 325035, China

E-mail: huangxing27@126.com

Yulei Tai

College of Chemistry and Materials Engineering, Wenzhou University

Wenzhou, Zhejiang, 325035, China

E-mail: taiyulei@163.com

Daofa He

College of Chemistry and Materials Engineering, Wenzhou University

Wenzhou, Zhejiang, 325035, China

E-mail: hedaofa@wzu.edu.cn

*The research is financed by the Science & Technological Project of Zhejiang, China (Grant No.2009C33059) and the Science & Technological Project of Wenzhou, China (Grant No.G20090146 and G20090148)*

## Abstract

A novel and effective protocol for the surface modification of the red phosphorus microcapsule via interfacial polymerization using hydrothermal method is reported. Composite microcapsules consisting of polymer-coated red phosphorous were prepared by interfacial polymerization of isocyanate and ethylenediamine in hydrothermal synthesis vessel. The morphology and magnetic property of microcapsules were characterized by scanning electron microscopy (SEM) and thermogravimetric analysis (TGA). Meanwhile, the water absorption and particle size distribution were examined. The relationship between the content of dispersants and the particle size of microencapsulated red phosphorus was investigated. On the basis of the experimental results, it seemed reasonable to conclude that the smaller the particle size of red phosphorus microcapsule was the better dispersibility in polymer, and then the higher flame retardant capability of polymer.

**Keywords:** Microcapsule, Red phosphorus, Polyurethane

## 1. Introduction

It is well known that red phosphorus (RP) is an inexpensive flame retardant with excellent performance (F. Laoutid *et al.*, 2003; Wang Guo-An *et al.*, 2006; Michael Pecht *et al.*, 2006; Du Longchao *et al.*, 2006; Hatsuhiro Harashina *et al.*, 2006). However, recent reports have acknowledged the shortcoming that the red phosphorus can absorb moisture and release  $\text{PH}_3$  easily, because of its characteristic of inorganic matter. As a result, the application of red phosphorus has been limited. Currently, new challenges are being imposed on surface modification to satisfy the rising demand for safety of red phosphorus by encapsulated red phosphorus that should not only exhibit reinforced properties, but also improve security in multiple applications (Wang Haitao *et al.*, 2008; Tsung-Han Ho *et al.*, 2006; Liu Yuan *et al.*, 2006; Wang Zhengzhou *et al.*, 2002). In

general, some inorganic matters and polymers (such as aluminum hydroxide, melamine resin, phenolic resin etc.) are used as shell to fabricate red phosphorus microcapsules (RPM). Also, hybrid microcapsules have been prepared by synthesis of red phosphorus in the interior of microcapsule, and form single or multiple layers. However, there are still some challenges on using these shell materials. For instance, it is still difficult to disperse red phosphorus in inorganic materials such as aluminum hydroxide. Additionally, formaldehyde may be released from microcapsules used melamine resin and phenolic resin as shell. Therefore, in this work, we describe a novel route to preparing microcapsule for polyurethane resin as shell, which can form compact membrane and possess superior compatibility with other polymers. To date, a number of routes have been developed, but they produce microcapsules that cause the RP particles gathered easily and lead RPM oversize. Such problem would hinder their applications, because of the smaller of particle size of red phosphorus microcapsule, the better of dispersibility in polymer, and then the higher of flame retardant of polymer. Hence, the aim of this work is to develop a new protocol for the surface modification and the decrease of aggregate of RP particles via hydrothermal methods. To our knowledge, this is the first time that, the isocyanate and ethylenediamine are use for the fabrication of the RP microcapsule with polyurethane as shell through interfacial polymerization. In this process, dispersants are frequently utilized in the encapsulation of RP, such as sodium stearate (SS). More specifically, we show the relevance of the kinds of dispersants and the size of RPM particles, and the properties of RPM are measured by DSC-TAG and SEM, and the particle size of RPM is analyzed by laser particle-size analyzer.

## 2. Experimental Section

### 2.1 Materials

Red phosphorus powder was provided by Chemical Reagent Co. Tianjin (China), 200 mesh. 4,4'-diphenyl-methandiisocyanate (MDI) was purchased from Yantai Wanhua Polyurethanes Co. Ltd and ethylenediamine was purchased from Chenbei Fine Chemicals Company. All the other chemicals were of the highest purity available and were used as received.

### 2.2 Instruments

The 50ml of hydrothermal synthesis vessel with pressure gage was used for microencapsulation of RP. The stability was observed by Q600 integrated thermal analyzer, and was purchased from TA Company, U.S.A. The particle sizes were measured with STDY-S digital biological microscope image analyzer, and was provided by Shenzhen Kailida Science and Technology Co., Ltd. The morphology of the microcapsule was obtained on scanning electronic microscope (SEM; JSM-6700F), and was bought in Japan JEOL. The average grain diameter was measured with N4plus laser particle-size analyzer, and was purchased from Beckman Coulter, Inc. U.S.A. The fire resistance of red phosphorus microcapsule was carried out on a XYZ-460 oxygen index determinator, and was purchased from Beijing east Co., Ltd.

### 2.3 Preparation of RP Microcapsules

RP microcapsules were synthesized by interfacial polymerization. Briefly, The 40 mL mixture, consisting of certain amount of pretreated red phosphorus, water, dispersant, ethylenediamine and organic solvent, was added into a 50ml hydrothermal synthesis vessel with pressure gage. The mixture was dried by oven 24h at 423K. After the reaction temperature was slowly cooled to room temperature, MDI was added into hydrothermal synthesis vessel, and maintained at that temperature for 3h with stirring. The mixture was then filtered, washed and desiccated to afford red phosphorus. The preparation of RPM was shown in the following Fig.1.

## 3. Results and Discussion

### 3.1 Effect of different dispersant on size of RPM

First, the different types of dispersants were studied, taking into account the fact that the grain diameter of microencapsulated red phosphorus would change with varying dispersants. A water solution of red phosphorus (0.1M) and dispersant (0.01M) and ethylenediamine (0.05M) was prepared by heating it at 423K for 24h in hydrothermal synthesis vessel with magnetic stirring. Three series dispersants, D<sub>1</sub> (polyvinyl alcohol (PVA) and polyethylene glycol (PEG)), D<sub>2</sub> (OP-10 and span-20 and span-60 and span-80), D<sub>3</sub> (sodium laurylsulfate (SDS) and sodium dodecyl benzene sulfonate (SDBS) and sodium stearate (SS)) were added to hydrothermal synthesis vessel, respectively. Finally, the toluene solution of 4,4'-diphenyl-methandiisocyan-

ate (MDI) (0.05M) was added, and proceed for 3h. Microencapsulated red phosphorus was obtained by filter and the particle size distribution was measured by laser particle size analyzer. The grain diameter of microencapsulated red phosphorus preparing by three series dispersants respectively were shown in Fig. 2. Fig.2. presents the dependence of the grain diameter of microcapsule on the types of dispersants. It is well known that

the polarity of dispersant affect the size distribution. The RP can be dispersed in polymer matrix easily by using  $D_1$  polymer dispersants, which are attributed to cationic characteristics. On the contrary, The RP cannot be dispersed in polymer matrix very well by using nonionic surfactant  $D_2$  and anionic surfactant  $D_3$ . Compared with anionic surfactant  $D_3$ , nonionic surfactant  $D_2$  is good dispersant for RP. But it does not always hold. The sodium stearate (SS) added in dispersant  $D_3$  obviously decrease the grain diameter of RP, which may be attributed to red phosphorus scattered by dispersants to micron scale at higher temperature and pressure. The result shows that the sodium stearate is the best dispersant in the process, due to electro-negativity interactions with surface of red phosphorus as an anionic surfactant. Although, SDBS and SDS are anionic surfactant, the hydrophobic chain is shorter than SS to lower surface activity.

### 3.2 The moisture absorption rate and LOI of RP and RPM

As we all know that the moisture absorption and LOI (limited oxygen index) of microencapsulated RP are directly related with the size of microcapsules, because smaller bare RP is easily coated and scattered in polymer. In Fig.3, we can find that bare RP and coated RP have the larger difference of moisture absorption rate. The content of RPM was achieved to 9%, and the limited oxygen index was 27%.

### 3.3 Appearance on red phosphorus microcapsule

The red phosphorus microcapsule is a kind of lavender and fluid powder in this paper. Content of red phosphorus  $\geq 85\%$ , moisture absorption rate  $\leq 0.3\%$ , ignition point  $\geq 350^\circ\text{C}$ ,  $\text{PH}_3 < 1\text{ppm}$ . The uncoated red phosphorus is shown in Fig.4. The red phosphorus microcapsule is thousand-fold (1,000 times) zoomed-in aggregation, and is displayed in Fig.4 and Fig.5. The image of Fig.4 was measured by Model STDY-S digital biological microscope image analyzer. The red phosphorus microcapsule with small particle diameter is invisibly observed, moisture in the air is absorbed by uncoated red phosphorus and water trail is left around the red phosphorus.

In Fig. 5, the morphology of red phosphorus microcapsule is measured by scanning electronic microscope, showing that the red phosphorus has been coated with polyurethane resin. As lavender and fluid power, red phosphorus does not absorb moisture while being put in the air.

### 3.4 Particle analysis of RPM

The particle size and distribution (frequency analysis) of the red phosphorus microcapsule is presented in Fig.6, which is measured by laser particle size analyzer. The average particle diameter is 1,019 nm, and is clearly showed by abundance curve, which is a example of particle size and distribution of RPM in this paper.

### 3.5 Stability analysis of RPM

As shown in Fig.7, comparing DSC-TGA spectrograms of RP and RPM, we can conclude that the thermo gravimetric curve at around  $230^\circ\text{C}$  has a gradient reduction, because of the decomposition of the polyurethane resin which is on the surface of the red phosphorus.

## 4. Conclusion

Red phosphorus is an innocuous, low-consumption, low-smoke and inexpensive flame retardant with excellent performance, which has extensive potential applications in many fields by surface modification. The microencapsulation of red phosphorus is one of the main modification methods. In this paper, A novel and effective protocol for the surface modification of the red phosphorus microcapsule via interfacial polymerization using hydrothermal method has been reported. polyurethane resin is used as the shell materials to prepare the red phosphorus microcapsules in hydrothermal synthesis vessel. The effects of dispersants on sizes of RPM are investigated. The results elucidate that the sodium stearate is the best dispersant, due to electro-negativity interactions with surface of red phosphorus as an anionic surfactant, the red phosphorus is coated by polyurethane resin successfully, and exhibit reasonable moisture absorption rate. Other surface treatment methods of red phosphorus still require further research.

## References

- Du Longchao, Qu Baojun and Xu Zhenjin. (2006). Flammability characteristics and synergistic effect of hydrotalcite with microencapsulated red phosphorus in halogen-free flame retardant EVA composite. *Polymer Degradation and Stability*, 91,995-1001.
- F., Laoutid, L., Ferry, J.M., Lopez,Cuesta and A., Crespy. (2003). Red phosphorus/aluminium oxide compositions as flame retardants in recycled poly (ethylene terephthalate). *Polymer Degradation and Stability*, 82,357-363.
- Hatsuhiko Harashina, Yoshihisa Tajima and Takahito Itoh. (2006). Synergistic effect of red phosphorus, novolac

and melamine ternary combination on flame retardancy of poly(oxymethylene). *Polymer Degradation and Stability*, 91, 1996-2002.

Liu Yuan and Wang Qi. (2006). Melamine cyanurate-microencapsulated red phosphorus flame retardant unreinforced and glass fiber reinforced polyamide 66. *Polymer Degradation and Stability*, 91, 3103-3109.

Michael Pecht and Yuliang Deng. (2006). Electronic device encapsulation using red phosphorus flame retardants. *Microelectronics Reliability*, 46, 53-62.

Tsung-Han Ho, Tsu-Shang Leu and Yih-Min Sun. (2006). Thermal degradation kinetics and flame retardancy of phosphorus-containing dicyclopentadiene epoxy resins. *Polymer Degradation and Stability*, 91, 2347-2356.

Wang Guo-An, Wang Cheng-Chien and Chen Chun-Yung. (2006). The flame retardant material e 1. Studies on thermal characteristics and flame retardance behavior of phosphorus-containing copolymer of methyl methacrylate with 2-methacryloxyethyl phenyl phosphate. *Polymer Degradation and Stability*, 91, 2683-2690.

Wang Haitao, Meng Xiangfu and Wen Bin. (2008). A simple route for the preparation of red phosphorus microcapsule with fine particle distribution. *Materials Letters*, 62, 3745-3747.

Wang Zhengzhou, Wu Guosheng, Hu Yuan. (2002). Thermal degradation of magnesium hydroxide and red phosphorus flame retarded polyethylene composites. *Polymer Degradation and Stability*, 77, 427-434.

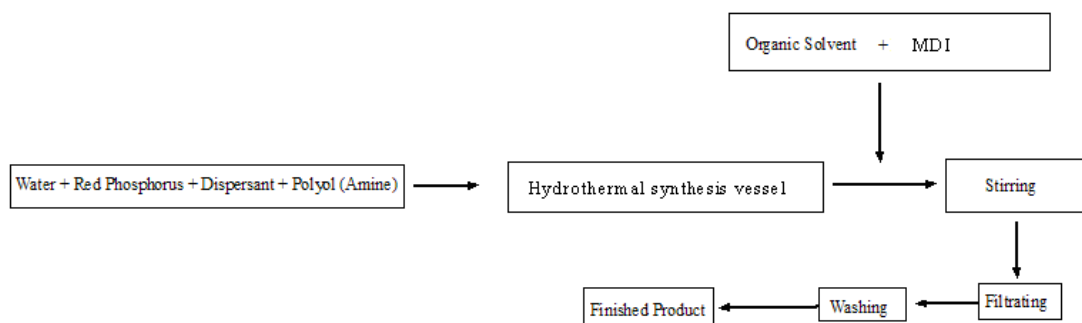


Figure 1. The Schematic of the preparation of RPM

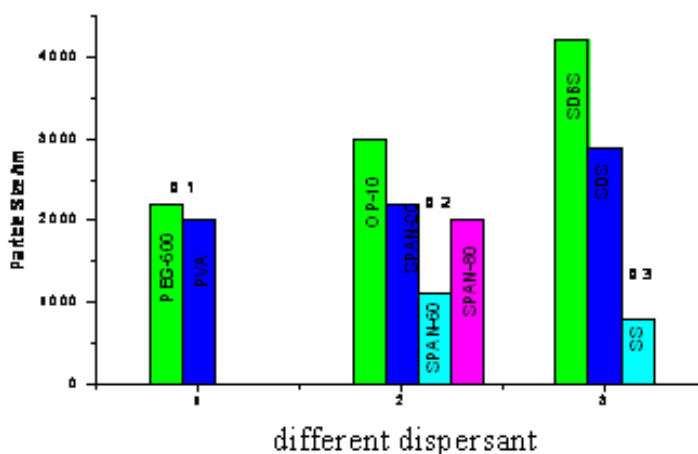


Figure 2. The effect of particle size on different dispersant

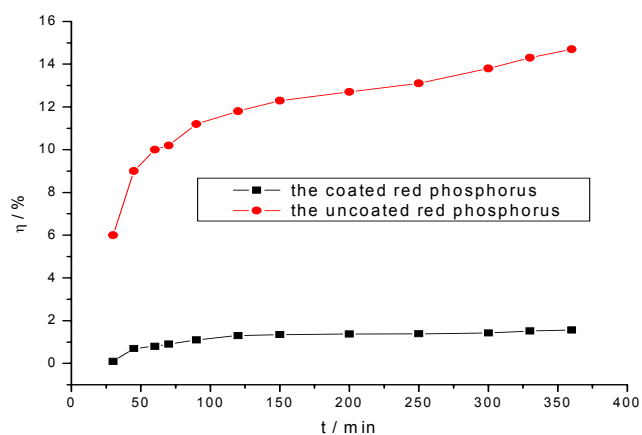


Figure 3. The moisture absorption rate for the uncoated and coated red phosphorus



Figure 4. The figure of uncoated red phosphorus and red phosphorus microcapsule

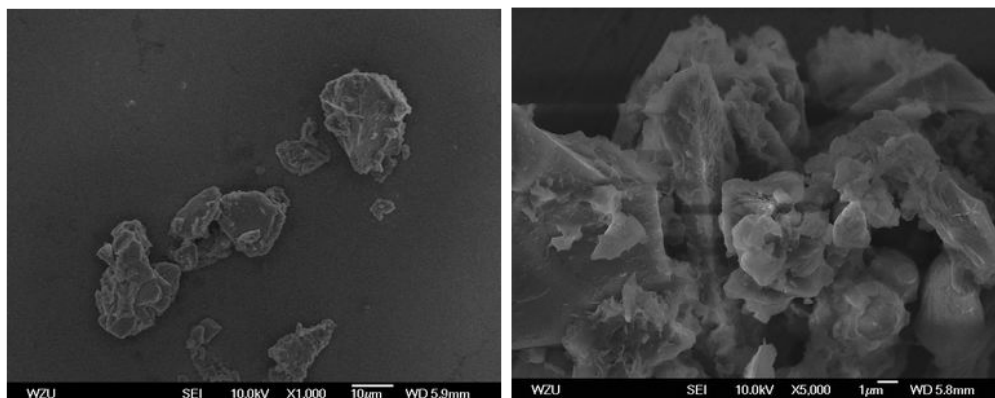


Figure 5. SEM of red phosphorus microcapsule

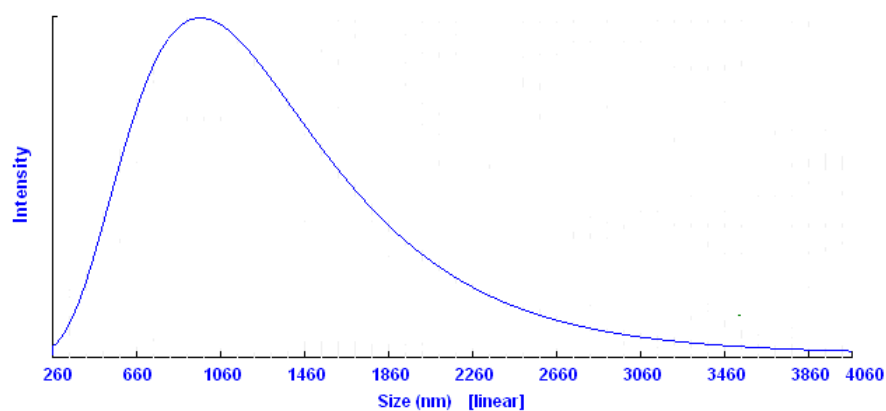


Figure 6. The particle size and distribution curve of RPM

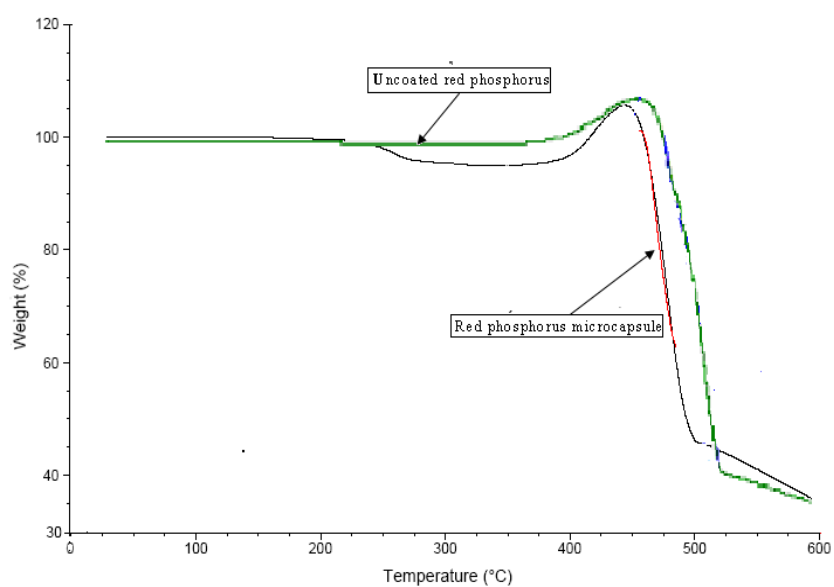


Figure 7. The DSC-TGA curve of RP and RPM



# Application of a New pH-metric Method to the Kinetic Study of Copolymerization of Polysaccharides Fucan N1 with PMMA in Presence of Cerium $Ce^{+4}$

El B. Sakri

Department of chemistry, Faculty of Sciences, University of Annaba

BP: 12, Annaba 23000, ALGERIA

E-mail: sakribahri@yahoo.fr

## Abstract

The copolymerization of a Poly-Acrylic PMMA with polysaccharide, Fucan N1 and Dextran T70, in presence of a ceric salt used as initiator in acidic medium, was carried out under the following conditions: Fucan N1=0,5 g;  $[CAN]=3,6.10^{-3}M$ ,  $[HNO_3]=0,2M$ ; temperature  $=40^{\circ}C$  with a relative ratio between the initiator and the monomer, initiator/monomer =1/10. Besides a pH study of the reaction medium, an infrared spectroscopy (IR) proved the appropriateness of these best conditions of synthesis, and this by showing the presence of a characteristic peak of the carbonyl grouping situated at  $1733cm^{-1}$  for the copolymer Fucan PMMA in respect to the individual PMMA spectra and Fucan N1. In addition, a  $^{13}C$  NMR study has been conducted on the copolymer.

A viscosimetry study of two Fucan fractions was performed in aqueous medium ( $H_2O$ ), and also of the obtained copolymer in DMSO.

An outcome of this work allows for us the suggestion of a plausible reaction mechanism, of which the copolymerization rate  $-Rp-$  is first order dependant to the monomer concentration, and to the square concentration of both the initiator and the polysaccharide.

**Keywords:** Poly-acrylic, Copolymerization, Polysaccharide with ceric initiator

## 1. Introduction

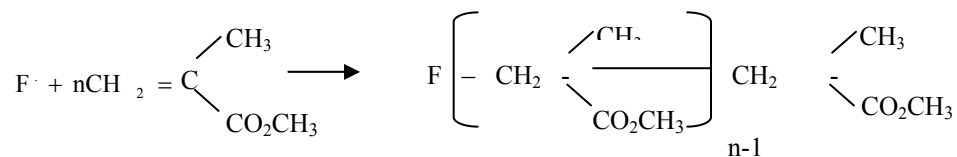
The essential aim of this work is to apply the pH-metric measuring method to the study of the PMMA copolymerization with polysaccharides Fucan N1 and Dextran T70 (Fucan N1 is a sulfated polysaccharide extracted from a brown seaweed of the *Ascopohyllum nodosum* kind), in presence of ceric ions  $ce^{4+}$  in nitric acidic medium  $pH=1$ , at a temperature  $40^{\circ}C$  during 40mn, under argon atmosphere (Chowdhury and Pal, 1999; Dalton *et al.*, 2002; Masci *et al.*, 2004; Fuoss and Cathers, 1949; Costa and Vasconcelos, 2002), with a relative ratio between the initiator and the monomer

$$\frac{\text{initiator}}{\text{monomer}} = \frac{1}{10}.$$

The reaction is conducted in suspension, and initiated by the ions  $ce^{4+}$  (Hexanetratace rate of ammonium)  $(NH_4)_2 [Ce(NO_3)_6]$  "Acros" leading first to the formation of a white- milky complex that disappears immediately, giving a radical (F) of Fucan to a proton ( $H^+$ ) and an ion  $Ce^{3+}$ , as it is shown in the following reaction equation :

## Initiation:



**Propagation:**

The kinetic study of this copolymerization, of which the polymerization rate measure is performed by pH metric measuring method -that we had put in evidence - and with comparison to the method of extraction by soxhelt with acetone.

**2. Experimental Work****2.1 Products**

Dextran of different molecular weights (MW= 10, 40, 70, 80.7, and 264 kg/mol) were purchased from Sigma for molecular weight assessment. Dextran (70 kg/mol) was also used for synthesis. It was dried in a vacuum oven at 60°C for 24h. Methyl methacrylate monomers were obtained from Acros France and were purified by washing with 5% NaOH and 20% NaCl, followed by distilled water. Ammonium cerium (IV) nitrate (Acros France) was dried at 80°C under vacuum for 24h. Solvents were of the highest commercially available purity.

Fucan N1 and Fucan BBP-2, having a mass of 95500g/mol and 46600g /mol respectively, are two fractions of Fucan obtained by HPLC chromatography on a S 5300 HR gel after an acidic extraction followed by an acidic hydrolysis (Hoppe HA, 1979), ( see Figure 1).

The Dextran is, like the Fucan, soluble in water, whereas its copolymer with PMMA is soluble in the water /THF (20/ 80 v/v) mixture and in the dimethylsulfoxide (DMSO).

The polymerization of the methyl methacrylate « MMA »with Fucan N1 and Dextran T-70 depends closely on the concentration of the initiator (Collic, 1993; Mulloy, B, 2002) of the monomer (MMA) and the concentration of the used polysaccharide.

This polymerization is performed by cycle –opening forming active radicals F or D that are likely to be bound by covalent links to the methyl poly-methacrylate (PMMA) forming Fucan copolymer(PMMA) and Dextran (PMMA).

This copolymerization is conducted in a highly acidic medium to avoid a possible formation of the ceric hydroxide, which can take place at a medium in which pH=4 to 5. In such a medium, the IR spectrum shows no anomaly.

The kinetic polymerization is performed by applying the PH- Metric measuring method, as an experimental technique, we know that the variation of the PH in the medium is linked to the initiator concentration at instant "t", with the equation:

$$[M]_t = [M]_0 \left( 1 - \frac{\Delta C_t^H}{\Delta C_\infty^H} \right) \quad (1)$$

where :  $\Delta C_t^H$ , et  $\Delta C_\infty^H$  - variation of the hydrogen concentration during the synthesis .

$$\Delta C_t^H = 10^{-pH_t} - 10^{-pH_0}$$

$$\Delta C_\infty^H = 10^{-pH_\infty} - 10^{-pH_0}$$

So we can write the equation (1) as follows :

$$[M]_t = [M]_0 \left( 1 - \frac{10^{-pH_t} - 10^{-pH_0}}{10^{-pH_\infty} - 10^{-pH_0}} \right) \quad (2)$$

with  $pH_0$ ,  $pH_t$  and  $pH_\infty$  are respectively the variation of the pH at the instant "t=0", at time t (we take t=30mn) and the instant when the whole monomer will be converted into copolymer ( $pH_\infty = pH_{const}$ ).

The equation (2) permits to determine directly the polymerization rate  $-V_p$ ; monitoring the variation of the monomer concentration in function of pH, and time. We have also determined the polymerization rate by applying the extraction by soxhlet with the acetone method. We determined the percentage ( $P_g$  %) of the PMMA grafting, the grafting rate ( $V_g$ ) of the copolymerization, polymerization, the homo-polymerization ( $V_h$ ), and the total rate ( $V_p$ ) of the polymerization that are calculated from the weight of the grafted poly-acrylic of the obtained products (Lepoutre P, 1975).

$$P_g \% = \frac{\text{grafted weight of PMMA} \times 100}{\text{weight of polysaccharide}} \quad (3)$$

$$V_g = \frac{\text{grafted weight of PMMA} \times 1000}{Mw \text{ de MMA} \times \text{reaction time(s)} \times \text{volume (ml) of reaction}} \quad (4)$$

$$V_h = \frac{\text{weight of homo-PMMA} \times 1000}{Mw \text{ de MMA} \times \text{reaction time(s)} \times \text{volume (ml) of reaction}} \quad (5)$$

The total rate of the polymerization is:

$$V_p = V_g + V_h \quad (6)$$

We have determined the polymerization rate- $V_p$ -by applying two methods independent the one from the other (equations 2 and 6) (table III), for a comparison purpose.

## 2.2 Synthesis and Reaction of the copolymerization

In a (250 ml) reactor equipped with three flasks, we take a polysaccharide mass of 0, 5 to 1g (Fucan N1 or Dextran) dissolved in  $HNO_3$  at 0, 2M. after 10minutes of agitation under an atmosphere of Argon (or  $N_2$ ) at a temperature of  $40 \pm 1^\circ C$ , we add at the same time  $3,6.10^{-3} M/L$  of cerium and 0,5M of MMA (of which the relative ratio  $\frac{\text{initiator}}{\text{Monomer}} = \frac{1}{10}$ ), The time variation of the pH is measured at a sampling interval of 5mn. The reaction is considered finished when the pH does not change any more, and this is the case after 30 minutes of reaction ( $pH_\infty = pH_{const}$ ).

The obtained product is poured into 500ml of methanol with the PH adjusted to a volume of 8, and NaOH at 10M. After that we concentrate the solution to a volume of 20/30ml approximately. We decant the solution into a spectra-membrane of a diameter of  $\phi = 20,4mm$  to be cleaned /washed in EDTA solution at 0, 05 M during 72hours, under permanent agitation. Then, the solution is put under lyophilization, and later on in a vacuum dryer till a constant weight.

First of all, we have monitored pH evolution in time of the reaction medium of the copolymerization. This pH variation is generally not higher than the unity, as it is shown on Figure (2) below.

## 2.3 Extraction of Homo-polymer of PMMA

We weight exactly 2,00gr of each raw product- mentioned above – that was extracted with the acetone by soxhlet during 24 h, to eliminate the homo-polymer- poly (Methyl Methacrylate). The pure copolymer is dried at  $50^\circ C$  till a constant weight.

## 3. Characterization

### 3.1 Preparation OF Three- Dimensional Structures

We prepared discs or films by using dried homopolymer PMMA (15 mg) solubilized in THF. Copolymer DM was dissolved in 1 ml of THF/ $H_2O$  (80/20) that was treated in an ultrasonic bath for 1 h. Dextran gave any 3D structures. To obtain discs, solutions were poured in Petri dishes for 24 h at room temperature in a saturated

atmosphere of THF and in the presence of  $\text{CaCl}_2$  to absorb water. Thin films were stripped from the mold and were dried in an oven at  $30^\circ\text{C}$ . A morphological analysis of the cross section of films was carried out by the use of a Leica S-440 scanning electron microscope (SEM). All 3D structures were extensively washed with before any biological assays.

### 3.2 NMR Analysis

$^{13}\text{C}$  NMR spectra of dextran, PMMA and copolymer DM were recorded by the use of a Varian Gemini 200 Mhz spectrometer in deuterated dimethyl sulfoxide- $\text{d}_6$  at ambient temperature. Tetramethylsilane (TMS) was used as an internal standard. Before use, all products were lyophilized twice with deuterium oxide ( $\text{D}_2\text{O}$ ).

### 3.3 Copolymers Analysis by Infrared Spectroscopy

This technique allows us to identify some chemical groupings that may be present in the polymers and the copolymers. Tablets of 150mg of potassium bromide (KBr), with infrared quality (Fluka).

The sample is mixed in the KBr, ground and then vacuum dried at  $45^\circ\text{C}$  during 6 hours, pressed under 10 tons for 2 minutes, and then stored at a  $45^\circ\text{C}$  in a humidity-free environment. These tablets are analyzed by means of a Fourier transform based infrared spectrophotometer (Perkin Elmer, 1600).

Every spectrum is taken to be an average of the cumulus of 16 increments, in order to decrease the effect of background noise. Figure 3 shows the spectra of MMA, and Dextran taken individually, in addition to that of the synthesized Dextran-PMMA copolymer.

Curve (A) presents many strips characteristic of the PMMA: one at about  $2953\text{cm}^{-1}$  which is assigned to the  $(\text{CH}_2)$  group, another strip is situated at  $1732\text{cm}^{-1}$  which represents the carbonyl ( $\text{C}=\text{O}$ ) group and a third band is located at  $1380\text{cm}^{-1}$  assigned to the  $(\text{CH}_3)$  Methyl group.

Curve (B) presents strips that are specific for Dextran T70: the presence of the radical ( $\text{OH}$ ) is attested by the absorption band that appears at about  $3400\text{cm}^{-1}$ , the strip at  $2930\text{cm}^{-1}$  is assigned to the methylene group  $(\text{CH}_2)$ , the strip around  $1650$  corresponds to the grouping  $(\text{OH})$  of the Dextran T70.

Curve (C) illustrates the spectrum of the product obtained by copolymerization of the Dextran and the MMA monomer by Cerium ( $\text{Ce}^{4+}$ ). This spectrum presents strips that are common to both the Dextran and PMMA. We can notice an important intensity at  $1733\text{cm}^{-1}$  that corresponds to the carbonyl grouping ( $\text{C}=\text{O}$ ).

Figure 4 shows that the individual Fucan N1 spectrum in curve (A) is identical to curve (B) with a concentration of cerium  $[\text{Ce}^{4+}] = 1,8 \cdot 10^{-5} \text{ M/L}$ . Yet, when we increase the concentration of this latter 200 times, i.e. at  $[\text{Ce}^{4+}] = 3,6 \cdot 10^{-3} \text{ M/L}$ , by keeping the same concentration of monomer and polysaccharide, we notice the formation of a copolymer Fucan PMMA characterized by a peak located at  $1725\text{cm}^{-1}$  for PMMA with respect to the spectrum of Fucan N1 alone, as shown on curve (C).

### 3.4 Viscosity Measurements

In order to determine the molar mass of the different obtained products, we have measured the viscosity of Fucan N1, BBP-2 solutions as well as the viscosity of copolymer solutions for different cerium ( $\text{Ce}^{4+}$ ) concentrations. In this technique, we use a well adapted viscometer (the Ubbelohde Viscometer) with a capillary diameter of 0,7mm, was used for two different polysaccharides; Fucan N1 and Fucan BBP-2 having a mass 95500 g/mol and 46600 g/mol respectively.

We determine  $\left(\frac{\ln \eta_2}{C}\right) = \left[\frac{\ln(t/t_0)}{C}\right]$  and the specific viscosity  $\frac{\eta_{sp}}{C} = (t - t_0)/t_0 C$  for a set of an increasing

concentration in the percentage of Fucan N1 and BBP-2 dissolved in water, as follows (0%, 0,45%, 0,65%, 0,75%, 1,0%, 1,25%, 1,45%, 1,65%, and 2%).

On the same graph  $\left(\frac{\ln \eta_r}{C}\right)$ , we have simultaneously plotted the specific viscosity  $\left(\frac{\eta_{sp}}{C}\right)$  in function of polysaccharide concentration. The intrinsic viscosity  $[\eta]$  is obtained by extrapolation and intersections of these two curves at a zero-point concentration. On the other hand, this intrinsic viscosity is related to the molar mass through the formula of Mark Houwkin:  $[\eta] = K \cdot M^a$ , where  $a$  and  $K$  are constants.

As for the two fractions of Fucan N1 and BBP-2 with known mass, the values of the constants were deduced from measures of the intrinsic viscosity  $[\eta]$  at a zero-point concentration. For example, as concerns the first fraction  $[\eta_1]=0,252$  and  $[\eta_2]=0,086$ , we find Fucan values as follows:

$$\begin{cases} a = 1,49 \\ K = 8,8 \cdot 10^{-9} \text{ dl} / \text{g} \end{cases}$$

And for the Dextran T70 (with a mass=73 000g/mol), in water and in DMSO, we have found the following values:

$$\begin{cases} a = 0,50 \\ K = 98,8 \cdot 10^{-5} \text{ dl} / \text{g} \end{cases}$$

The difference in values of 'a' for the Dextran T70 and Fucan, is present only in aqueous solutions, the Dextran is manifested therefore, more flexible than the Fucan.

### 3.4.1 Viscosity and mass measurements of the obtained copolymers

The measurement of the molar mass by applying the viscometric method is performed through measuring the intrinsic viscosity by extrapolation of the two curves at  $[\ln \eta_2]/C$  and  $\frac{\eta_{sp}}{C}$  at a zero -point concentration.

This is why we have synthesized tow Fucan PMMA copolymers; one with no monomer ; the other with the presence of 0,4% of monomer MMA, keeping the same concentration values in the initiator and the polysaccharide (0,5 of Fucan ), soluble in the mixture water/ THF (20/80 v/v) at  $T^\circ = 40^\circ\text{C}$ .

We found the intrinsic viscosity equal to 0,16 dl/g for the first copolymer, but equal to 0,244 dl/g, for the second copolymer .The viscometric mass  $M_v$  corresponding to the viscosity could be formulated through the following equation :

$$\ln [\eta] = \ln [8,8 \cdot 10^{-9}] + 1,49 \ln \bar{M} \quad (7)$$

where

$$[\eta] = 0,244; \quad \bar{M} = 98900 \text{ g} / \text{mol}$$

$$[\eta] = 0,16; \quad \bar{M} = 64800 \text{ g} / \text{mol}$$

We notice that the increase of the viscosimetric mass is due to the increase of PMMA formed in shapes of grafted connections on the polysaccharide, on the one hand, and this prove the effective formation of a copolymer between the Fucan and PMMA for Dextran T70, on the other hand. We can use the following formula:

$$\ln [\eta] = \ln [98,8 \cdot 10^{-5}] + 0,50 \ln \bar{M} \quad (8)$$

By the same manner, knowing  $[\eta]$  we can deduce the molar mass  $\bar{M}$ .

### 3.4.2 Determination of the obtained copolymers by HPLC in function of initiator concentration $[\text{CAN}]^{1/2}$

$\bar{M}_v$  determination of the obtained copolymers by HPLC chromatography on a S 5300 HR gel, shows that those ones decrease as the initiator concentration increases, i.e.:

$$\text{For } [\text{CAN}]^{1/2} = 3 \cdot 10^{-2} \text{ M} / \text{L} \text{ we have } \bar{M} = 1,28 \cdot 10^5 \text{ g} / \text{mol}$$

$$\text{And for } [\text{CAN}]^{1/2} = 6 \cdot 10^{-2} \text{ M} / \text{L} \text{ we have } \bar{M} = 0,59 \cdot 10^5 \text{ g} / \text{mol}$$

We can interpret these results on Figure 5.

As for the case of Dextran, the Fucan mass decreases because of an acid hydrolysis of the macromolecular chains during the different stages of synthesis. We can notice clearly that this mass variation could be interpreted in the following formula:

$$\overline{M} = \frac{3,74 \cdot 10^3}{[Ce^{+4}]^{1/2}} \quad (9)$$

$$[CAN]^{1/2} \cdot 10^2 \text{ mol/l} : 0,9 ; 3 ; 3,46 ; 4,59 ; 6,00$$

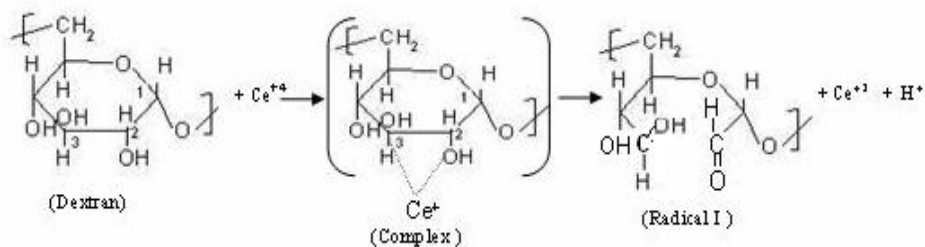
$$\overline{M} : g/mol : 4,0 \cdot 10^5 ; 1,28 \cdot 10^5 ; 1,047 \cdot 10^5 ; 0,87 \cdot 10^5 ; 0,59 \cdot 10^5$$

#### 4. Results and Discussion

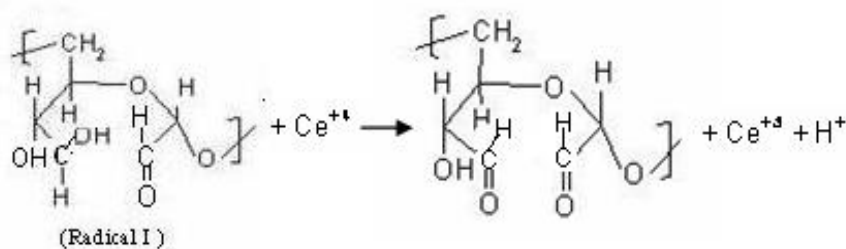
This research consists of applying the pH-metric measuring method in the kinetic study the MMA polymerization of the methacrylate methyl, with the polysaccharides Fucan N1 and Dextran T70, in presence of ceric ions ( $Ce^{4+}$ ) in the best conditions. We must take the quantity of the initiator and the monomer in a reactor we have found equal to 1/10.

The infrared analysis (IR) of the copolymers obtained after radical synthesis, shows that the polymerization depends on the nature of each polysaccharide, and on the concentration of the cerium ( $Ce^{4+}$ ), and the monomer used; the reaction of the polysaccharide / poly acrylic synthesis is performed through several stages, as depicted on the following graph (Mansor A, 2000):

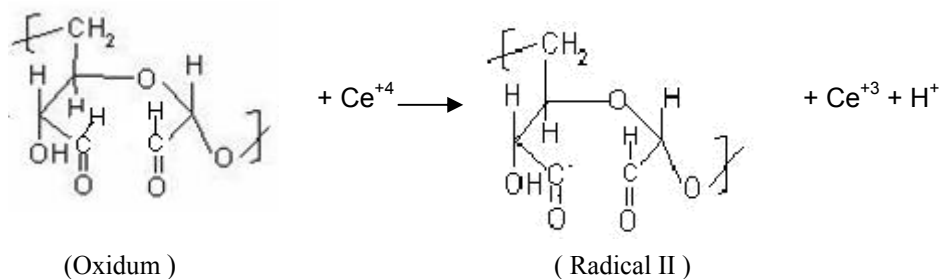
##### Stage 1: Formation of radical I

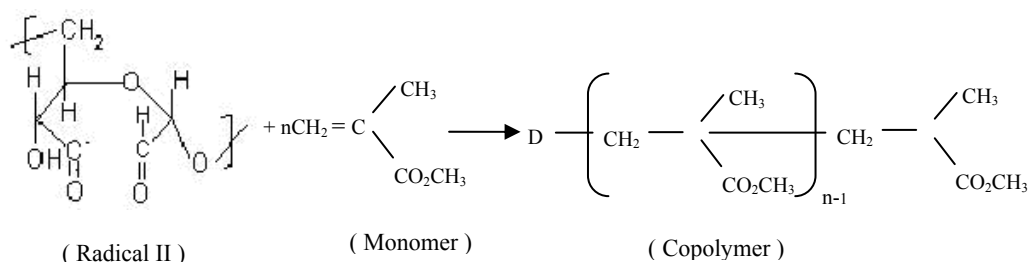


##### Stage 2: Formation of the Oxidum



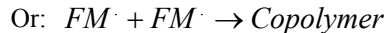
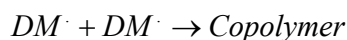
##### Stage 3: Formation of radical II





The radical II is chained to the monomer and engendering copolymers. The first stage consists of forming a complex between the polysaccharide and the cerium ( $Ce^{4+}$ ). This complication is performed between the cerium ( $Ce^{4+}$ ) and hydroxide groups in position 2 and 3 of the Polysaccharide. After a laps of time, it is decomposed giving a Radical I, ion  $Ce^{3+}$  and a proton  $H^+$ . The second stage, however, consists of forming an oxydium from a radical I with the cerium, making the appearance of aldehydic groups in position 2 and 3 of the polysaccharide, an ion  $Ce^{4+}$  and a proton  $H^+$ . As concerns the third stage, it consists of forming a radical II, which is Dextran radical (D or F) responsible for the propagation with the monomer ( $D\cdot + M_n \rightarrow DM_n\cdot$ ) this radical ( $D\cdot$ ) is generated by the reaction between Oxidium and Cerium ( $Ce^{4+}$ ).

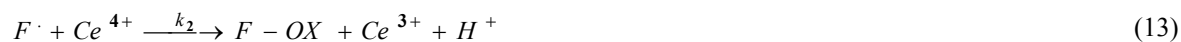
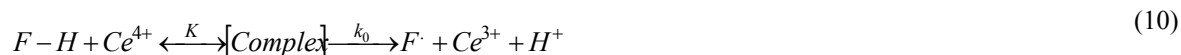
The termination is achieved by classical termination.



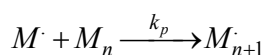
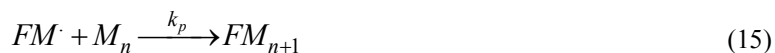
The analysis of  $^{13}C$  NMR spectrum (Fig. 6.) suggests a chemical structure of Dextran-PMMA polymer as indicated in (Chauvière C, 2003).

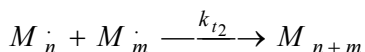
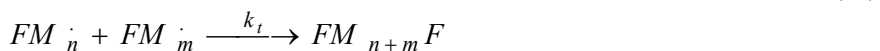
Under the light of the obtained results and the discussion we have led, we may establish that our polymerization follows a reactional mechanism a little complex; the stages of which are governed by the following reaction equation:

#### Initiation:



#### Propagation :



**Termination :**

To put in evidence this polymerization mechanism, we should suppose that the states between the following different initiating species, are quasi-stationary. That is to say:

$$\frac{d[F\cdot]}{dt} = K k_0 [F][Ce^{4+}] + k_3 [Ce][F-OX] - k_a [F\cdot][M] - k_2 [F\cdot][Ce] = 0 \quad (20)$$

$$\frac{d[FM\cdot]}{dt} = k_a [F\cdot][M] - k_k [FM\cdot]^2 - k_{t1} [FM\cdot][M\cdot] = 0 \quad (21)$$

$$\frac{d[M\cdot]}{dt} = k_1 [Ce][M] - k_{t1} [FM\cdot][M\cdot] - k_{t2} [M\cdot]^2 = 0 \quad (22)$$

$$\frac{d[F-OX]}{dt} = k_2 [F\cdot][Ce^{4+}] - k_3 [Ce^{4+}][F-OX] = 0$$

By summing together the equations (20 to 23) and ignoring the equation (22) which is less likely to take place; because we did not notice any considerable attack by the cerium ( $Ce^{4+}$ ) on the monomer. By assuming that the termination constants are equal to the global  $k_t$  ( $k_t = k_{t1} = k_{t2}$ ) (Mansor A, 2000), we obtain that:

$$K k_0 [F][Ce^{4+}] - k_t [FM\cdot]^2 - 2 k_t [FM\cdot][M\cdot] - k_t [M\cdot]^2 = 0 \quad (24)$$

$$K k_0 [F][Ce^{4+}] = k_t ([FM\cdot] + [M\cdot])^2$$

We deduce:

$$[FM\cdot] + [M\cdot] = (K k_0 [F][Ce^{4+}] / k_t)^{1/2} \quad (25)$$

The polymerization rate  $R_p$  of the Fucan N1 or Dextran in presence of a ceric initiator, is expressed in this formula:

$$R_p = k_p [FM\cdot][M] + k_p [M\cdot][M] = k_p ([FM\cdot] + [M\cdot])[M] \quad (26)$$

By substituting the expression of eq. (25) into eq. (26), we obtain:

$$R_p = k_p \left( \frac{K k_0}{k_t} \right)^{1/2} [F]^{1/2} [Ce^{4+}]^{1/2} [M] \quad (27)$$

The expression of the polymerization rate  $R_p$  of the Fucan N1 and Dextran T70 with the MMA in presence of a ceric salt used as initiator, in acidic medium a simple ratio between  $R_p$  and the order equal to the concentration unity of the monomer MMA, and to the square-root of both the polysaccharide and initiator (Figures 7 to 10).

And also, the speed of polymerization is:

$$R_h = R_p / 2 + K [Ce^{4+}]_{\max} \quad (28)$$

The grafting speed is expressed as:

$$R_g = R_p / 2 - K [Ce^{4+}]_{\max} \quad (29)$$

Consequently, the rate of grafting is given by :

$$PG\% = (A R_p^2 + B R_p + C) \cdot 100 \quad (30)$$

where A, B, C and K are constants which can be determined ultimately.

We also know that the speed of polymerization ' $R_p$ ' is proportional to the square-root of initiator concentration  $R_p = K [Ce^{4+}]^{1/2}$ , and the same relationship is found for the quantities  $R_h$ ,  $R_g$  and PG.



The method applied in measuring the polymerization rate ( $R_p$ ) is the PH-metric measuring method, compared to the extraction by soxhlet with the acetone (method of “Le Poutre and Hui (1975) ( see Table III).

### 5. Reliability Control of the PH-Metric Method

In order to control the reliability of the PH-metric method, we compared it to a more exact and precise method; which is the “extraction by soxhlet with the acetone method. By comparing these two methods, we can see that same values of PG,  $V_g$ ,  $V_h$  and the universal constants A, B, C and K are exactly found by both methods. The variation of PG reaches the same maximum for a maximal speed of  $R_p = 3,39 \cdot 10^{-5} \text{ mol.l}^{-1}.\text{s}^{-1}$  and a initiator concentration  $[CAN] = 1,197 \cdot 10^{-3} \text{ M}$  for both methods. The obtained results are given in the following table (see Table III). We notice that the pH-metric method is in good concordance with the extraction by soxhlet with the acetone method, at strong concentration values of the initiator.

$R_p^{(a)}$ ,  $R_h^{(a)}$ ,  $R_g^{(a)}$  and  $PG^{(a)}$  polymerization rate determined by the pH-metric method, that we have worked out.

As Figures (7 -10) show, the quantity  $k_p (k_0/k_t)^{1/2}$  is equal to  $\approx 5,32$ ;  $10,22$  and to  $13,71$  for soluble starch (Mansor and Haron, 2000) ; as concerns Dextran T70 and Fucan N1 respectively. This quality varies increasingly with a rate of nearly 2.5 when going from the soluble starch to the Fucan and this in proportion with the mass of each polysaccharide used, namely :

$M_n = (164,4)_n \text{ g / mol}$  For the soluble starch ;  $73000 \text{ g / mol}$  for the Dextran T70, and finally  $95500 \text{ g / mol}$  for the Fucan N1.

### 6. Conclusion

We can summarize the obtained results in the following points:

Polymerization between polysaccharides and poly-acrylics is generally achieved through opening the polysaccharide cycle. This kinetic polymerization is considered to be a complex one. The pH-metric method used to determine  $R_p$  is found to be very precise and with great concordance with the extraction by the acetone method. The infrared spectroscopy shows that the copolymer can't be formed if the initiator concentration is less than  $[CAN] = 1,8 \cdot 10^{-5} \text{ M / l}$ , but when this latter is increased to 200 times, we notice the formation a copolymer characterized by a peak situated at  $1725 \text{ cm}^{-1}$  for PMMA on the polysaccharide spectrum alone, with an  $[MAM] = 0,4\%$ . The viscometry shows the effective formation of a copolymer between the polysaccharide and the PMMA, due to the intrinsic viscosity increase of  $0,16 \text{ dl/g}$  to  $0,244 \text{ dl/g}$  in absence and presence of  $0,4\%$  of monomer. The polymerization rate  $R_p$  of polysaccharide / poly-acrylic depends on a kinetic complex, first order, equal to the concentration of the monomer and, and to the square-root of the initiator and polysaccharide.

The grafting rate of PMMA (PG%) on the polysaccharide increases with the increase of (CAN) concentration, it reaches a maximum concentration equal to :  $[CAN] = 1,197 \cdot 10^{-3} \text{ Mol/l}$ , and realizes  $196,60\%$  (this maximum value is found to be equal to  $260\%$  at  $0.5 \cdot 10^{-3} \text{ M/l}$  ceric ion).

Regarding difficulties that may face researchers for determining the speed of polymerization  $R_p$ , we propose to use the pH-metric method because it is simple and precise, and also does not require sophisticated means. In addition, it opens doors for great perspectives in this domain of research.

### References

- Chauvière C, Labarre D, Couvreur P, Vauthier C. (2003). Radical Emulsion Polymerization of Alkylcyanoacrylates Initiated by the Redox System Dextran-Cerium(IV) under Acidic Aqueous Conditions. *Macromolecules*, 36: 6018-6027.
- Chowdhury P, Pal CM. (1999). *European Polymer Journal*, 35: 2207-2213.
- Collic- Jouault S. Boisson- Vidal C., Jozefonvitz J. (1993). Low molecular weight fucoidane fraction from *Pelvetia canaliculata*. *Phytochemistry* (under press),.
- Dalton Paul. D, Flynn L, Shoichet M. (2002). *Biomaterials*, 23: 3843-3851.
- Fuoss, RM, Cathers, G.I. (1949). *Journal. Polym. Sci.*, 4: 97.
- Hoppe HA. (1979). Marine algae and their products and constituents in pharmacy: in Hoppe HA, Levring T, Tanak Y, editors. Berlin: Walter de Gruyter, p. 25 –119.
- Lepoutre P, Hui SH. (1975). *Jnl appl. Polym. Sci.*, 19: 1257.

Mansor A, Haron MDJ. (2000). Kinetics and Mechanism of Free Radical Grafting of Methyl Acrylate onto Sago Starch. *Journal of Applied Science*, 77:784-791.

Masci G, Bentempo D, Tiso N, Diociaiuti M, Mannina L, Capitani D, Crescenzi V. (2004). *Macromolecules*, 37: 4461-4473.

Mulloy, B, Mourao PAS., Gray E. (2002). Structure/ function and studies of anticoagulant sulphated polysaccharides using NMR. *Journal of Biotechnology*, 77: 123-135.

O.R Costa R, Vasconcelos W. L. (2002). *Journal of Non-Crystalline Solids*, 304: 84-91.

Okiemen EF, Eghrevba FE. (1992). Graft Copolymerization of Methyl Acrylate on Dextrin. *European Polymer Journal*, 28 (4): 415-417.

Table 1. Measurement of the relative viscosity  $\left(\frac{\ln \eta_r}{C}\right)$  and specific viscosity  $\left(\frac{\eta_{sp}}{C}\right)$  of Fucane N1 in function of its concentration percentage in the solvent H<sub>2</sub>O at a temperature T°=40°C

[Fucan N1]%	0	0,45	0,65	0,75	1,0	1,25	1,45	1,65	2,0
$\frac{\ln \eta_r}{C}$	0,252	0,260	0,265	0,280	0,300	0,305	0,310	0,320	-
$\frac{\eta_{sp}}{C}$	0,252	0,280	0,320	0,340	0,350	0,360	0,380	0,410	-

Table 2. Measurement of the relative viscosity  $\left(\frac{\ln \eta_r}{C}\right)$  and specific viscosity  $\left(\frac{\eta_{sp}}{C}\right)$  BBP-2 in function of its concentration percentage in the solvent H<sub>2</sub>O at a temperature T°=40°C

[BBP-2]%	0	0,45	0,65	0,75	1,0	1,25	1,45	1,65	2,0
$\frac{\ln \eta_r}{C}$	0,086	0,10	0,11	0,12	0,13	0,14	0,15	0,165	-
$\frac{\eta_{sp}}{C}$	0,086	0,11	0,12	0,13	0,14	0,16	0,17	0,185	-

Table 3. Comparative table of the two (Vp) measuring methods: the pH- metric method and the extraction by soxhlet with the acetone method .

$[CAN]^{1/2} \cdot 10^{-2} M / l$	2	3	3,46	4,59	5,99
PG %	145,30	163,05	218,10	201,20	16,220
$R_h \cdot 10^5 mol / l^{-1} s^{-1}$	/	1,476	1,504	2,272	3,084
$R_g \cdot 10^5 mol / l^{-1} s^{-1}$	/	1,004	1,256	1,868	2,436
$R_p = (R_h + R_g) \cdot 10^5 mol.l^{-1} s^{-1}$	/	2,480	2,760	4,140	5,518
$R_p^{(a)} \cdot 10^5 mol.l^{-1} s^{-1}$	2,25	2,660	3,040	4,000	5,520
$PG^{(a)\%} = (-4,084 \cdot 10^9 R_p^2 + 2,774 \cdot 10^5 R_p - 2,698) \cdot 100$ or $= K' [Ce^{+4}] + K'' [Ce^{+4}]^{1/2} + K'''$	147,75	179,31	196,29	186,68	17,58
$R_g^{(a)} = (R_p/2 - 2,71 \cdot 10^{-3} [Ce^{+4}]_{max}) \cdot 10^5 Mol. L^{-1} \cdot s^{-1}$	/	1,006	1,196	1,676	2,436
$R_h^{(a)} = (R_p/2 + 2,71 \cdot 10^{-3} [Ce^{+4}]_{max}) \cdot 10^5 mol.l^{-1} s^{-1}$	/	1,654	1,844	2,324	3,084

seaweed (Thalles)  $\xrightarrow{(1)}$  Parietal material  $\xrightarrow{(2)}$  Raw acidic extract  $\xrightarrow{(3)}$  Fucans.

1- Preprocess, Extraction.

2- Hydrolysis.

3- Deterioration, fractioning.

Figure 1. Simplified flow- chart of Fucans

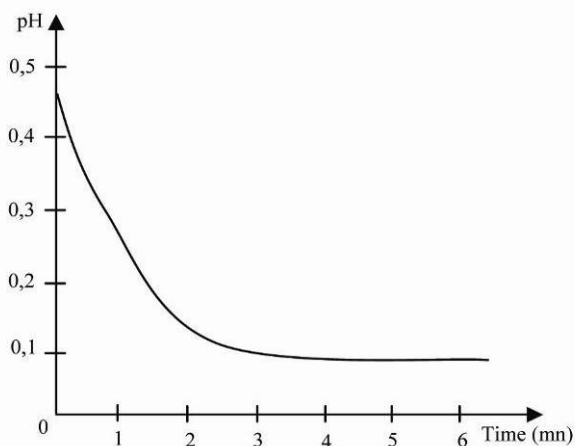


Figure 2. pH evolution during synthesis reaction of the copolymer Fucan PMMA; Temperature :40°C; solvation  $\text{HNO}_3$  at 0,2 M

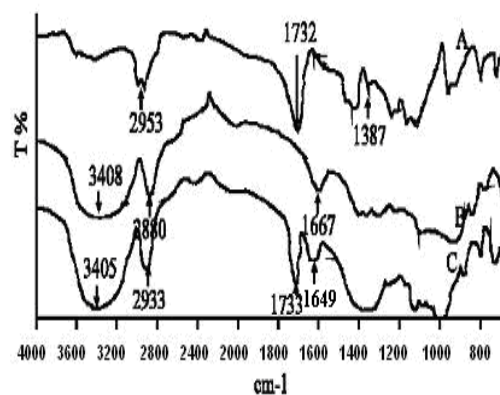


Figure 3. Infrared spectrum of copolymer Dextran-PMMA;  
Curve (A) PMMA alone; Curve (B) Dextran alone;  
Curve (C) copolymer of Dextran ; 0,5g ; MMA 2%;  
Cerium  $3,6 \cdot 10^{-3}$  M.

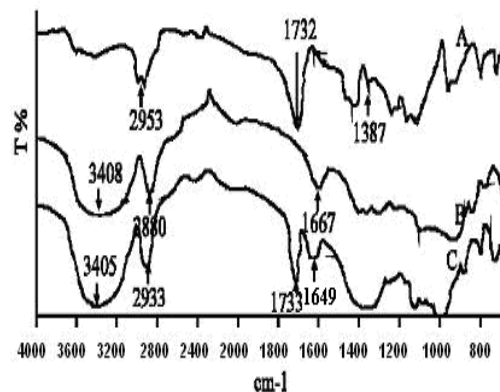


Figure 4. Infrared spectrum of copolymer Fucane-PMMA;  
Curve (A) Fucane alone; Curve (B) 0,5 g of Fucane,  
0, 2% of MAM,  $\text{Ce}^{+4}$   $1,80 \cdot 10^{-5}$  g/mol;  
Curve (C) 0,5g of Fucane, 0,2% of MMA,  $\text{Ce}^{+4}$   $3,6 \cdot 10^{-3}$  g/mol

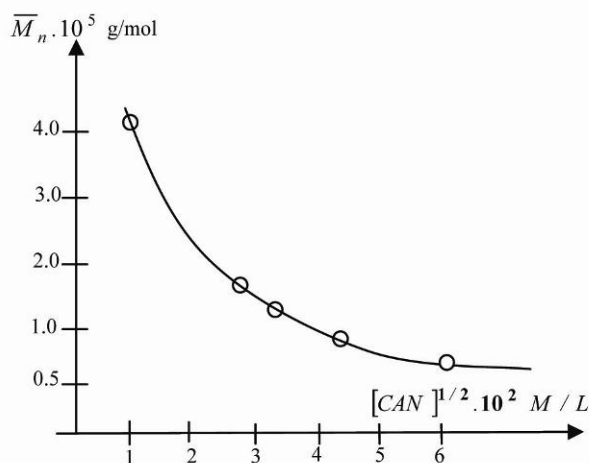


Figure 5. Variation of the copolymer mass obtained by HPLC in function of the monomer concentration  $[CAN] \cdot 10^2 \text{ M/L}$

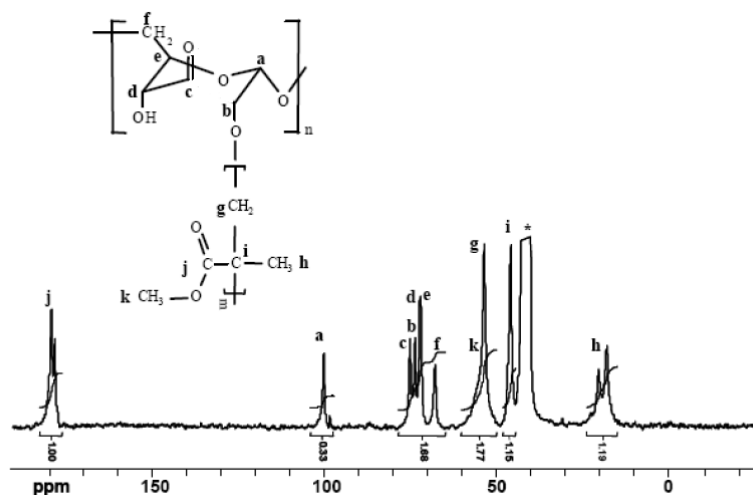


Figure 6. The  $^{13}\text{C}$  NMR spectrum of DEXTRAN-PMMA in deuterated DMSO. Carbon atoms and corresponding peaks are identified by a literal

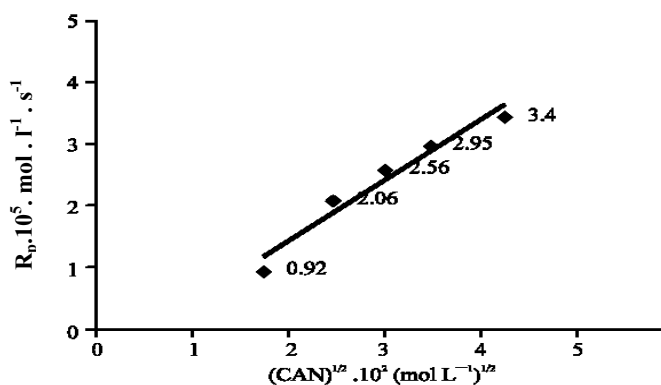


Figure 7. Polymerization rate ( $R_p$ ) of Fucan in function of the square-root of CAN; MMA=0,0742M; (Fu)=00417g; (HNO<sub>3</sub>)= 0,2M ; temperature =40°

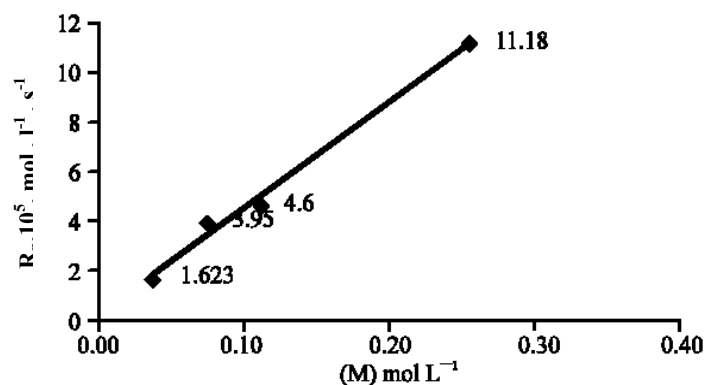


Figure 8. Polymerization rate (Rp) of fucan N1 with MMA in function of monomer;  
(Fu) = 0.0417g ; (CAN) =  $0.503 \cdot 10^{-3}$  M, (HNO<sub>3</sub>) = 0.2M , temperature = 40°C

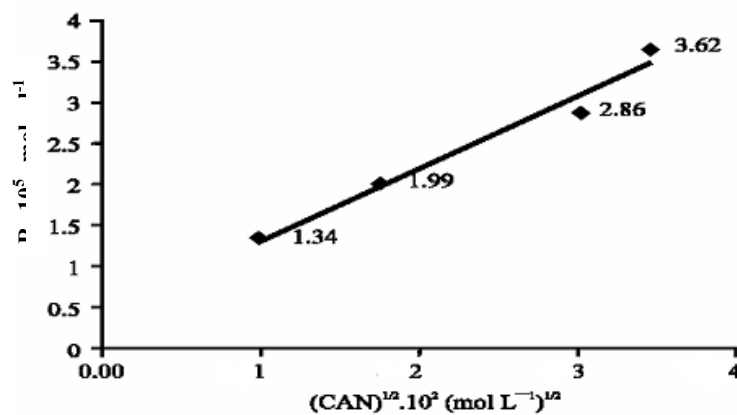


Figure 9. Polymerization rate (Rp) of fucan N1 with MMA in function of the square root of the initiators (CAN),  
Dextran = 0.0318g; (MMA) = 0.0742M (HNO<sub>3</sub>) = 0.2M Température = 40°C

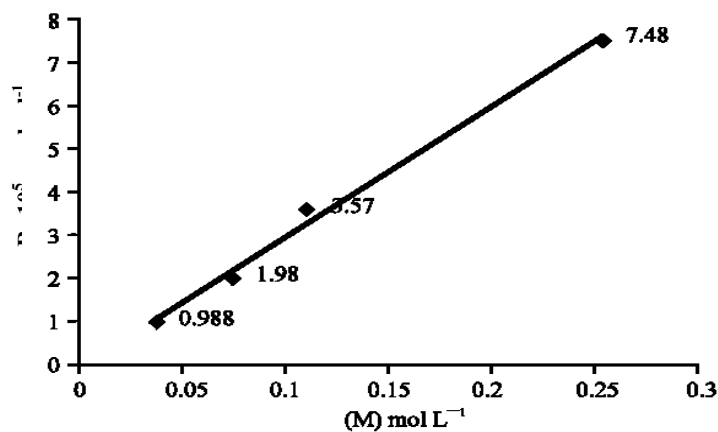


Figure 10. Polymerization rate (Rp) of fucan N1 with MMA in function of monomer concentration (M),  
Dextrane = 0.0318g ; (CAN) =  $0.503 \cdot 10^{-3}$  M, (HNO<sub>3</sub>) = 0.2M Temperature = 40°C

# Kinetics and Mechanism of Oxidation of Nicotine by Permanganate Ion in Acid Perchlorate Solutions

Ishaq A. Zaafarany

Department of Chemistry, Faculty of Applied Sciences  
Umm Al-Qura University, Makkah Al-Mukarramah 1340  
Saudi Arabia Kingdom  
E-mail: ishaq\_zaafarany@hotmail.com

## Abstract

The kinetics of permanganate oxidation of nicotine alkaloid in aqueous perchlorate solutions at a constant ionic strength of  $1.0 \text{ mol dm}^{-3}$  have been investigated spectrophotometrically. The kinetic results showed first-order kinetics in permanganate and fractional-first-order dependence with respect to nicotine concentration. The influence of hydrogen ion concentrations on the reaction rate showed inverse first-order kinetics in  $[\text{H}^+]$  where the oxidation rates were increased with decreasing hydrogen ion concentration. A kinetic evidence for the formation of 1:1 complex has been revealed. The ionization constant of nicotine was calculated from the kinetic data and was found to be  $9.69 \times 10^{-4} \text{ mol dm}^{-3}$  at ionic strength of  $1.0 \text{ mol dm}^{-3}$  and  $25^\circ \text{C}$ . The kinetic parameters have been evaluated and a tentative reaction mechanism consistent with the kinetic results is discussed.

**Keywords:** Nicotine, Permanganate, Oxidation, Kinetics, Mechanism, Ionization constant

## 1. Introduction

Nicotine is a highly lipid soluble alkaloid (Pailer M, 1964, p.15 & Smith L, 1971, p.174) which used effectively on a wide range against aphids, capsids, leaf miners and thrips. It is also used for fumigation of green houses (Larson P, 1964, p.2). Moreover, nicotine is the addictive ingredient in tobacco products that keeps many users hooked (Wang H, 2000, p.1125). However, the great importance of nicotine chemistry which is recognized, the information about the kinetics and mechanistics of nicotine oxidation is scarce. The kinetics of oxidation of many organic (Hassan R, 1991, pp. 2018 & 605), inorganic (Hassan R, 1988, pp. 601 & 538) and macromolecules (Hassan R, 2009, pp. 95 & 184) by permanganate ion as an oxidant has been investigated in more details. However, the oxidation of nicotine by this oxidant was investigated as a tool for spectrophotometric determination of nicotine concentration (Murthy V, 1986, p.78), but no attention was focused to either the kinetics or mechanistics of oxidation.

In view of the above arguments, the present investigation seemed to be of interest in order to shed some light on the mechanistic of oxidation of nicotine with the aim at determining the ionization constant of nicotine, kinetically. Again, some information may be gained on the chemistry of nicotine in aqueous solutions from the results obtained.

## 2. Experimental

### 2.1 Materials and Methods

Potassium permanganate used was of analytical grade (BDH). The preparation and standardization of permanganate solutions were the same as described earlier (Hassan R, 1988, pp. 601 & 605). Optical density versus concentration plots for acidified  $\text{MnO}_4^-$  showed that Beer's law is obeyed at a wavelength of 525 nm where the molar extinction coefficient is  $2250 \pm 25 \text{ dm}^3 \text{ mol}^{-1} \text{ cm}^{-1}$  in good agreement with that reported previously (Hassan R, 1988, pp.601 & 605).

Solutions of nicotine (Fluka Chemical Reagent) were freshly prepared before each experiment. Doubly distilled conductively water was used in all preparations. The temperature was controlled within  $\pm 0.05^\circ \text{C}$ .

All other reagents employed in the present work were of analytical grade and their solutions were prepared by dissolving the requisite amounts of the sample in doubly distilled water.

The ionic strength of the reaction mixtures was maintained constant at  $1.0 \text{ mol dm}^{-3}$  using  $\text{NaClO}_4$  as a non-complexing agent.

All kinetic measurements were performed under pseudo-first-order conditions, where nicotine was present in a large excess over that of  $[\text{MnO}_4^-]$ . The procedure of the kinetic measurements was the same as described earlier (Hassan R, 1988, p.601 & 605). The course of reaction was followed by recording the decrease in absorbance of  $\text{MnO}_4^-$  at its absorption maximum, 525 nm, as a function of time. It was verified that there was no interference from other reagents at this wavelength. The absorption spectra of the reactants and typical traces of the spectral changes are shown in Fig. 1.

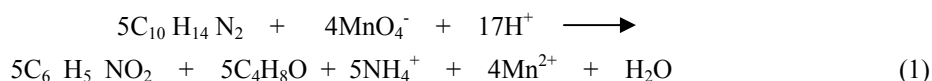
## 2.2 Polymerization test

The possibility of formation of free-radicals was examined by adding acrylonitrile to the partially oxidized reaction mixture. The formation of a white precipitate indicates that the reaction proceeds by free-radical mechanism.

## 3. Results and Discussion

### 3.1 Stoichiometry

Reaction mixtures containing a slightly known excess of permanganate over that of nicotine substrate concentration at  $[\text{H}^+] = 0.5 \text{ mol dm}^{-3}$  were equilibrated at room temperature. The unreacted permanganate was estimated periodically until it reached a constant value, i.e. completion of the reaction. Spectrophotometric estimation of the unreacted oxidant revealed that 1 mol of permanganate consumed  $1.25 \pm 0.1$  mol of nicotine. Product analyses indicated the formation of nicotinic acid as the oxidation product. No detection of  $\text{CO}_2$  or  $\text{NH}_3$  was observed. This result suggest that the stoichiometry of the reaction conforms to the following stoichiometric equation



where  $\text{C}_{10}\text{H}_{14}\text{N}_2$ ,  $\text{C}_6\text{H}_5\text{NO}_2$  and  $\text{C}_4\text{H}_8\text{O}$  represent to nicotine, nicotinic acid and butaldehyde, respectively. The formation of nicotinic acid, aldehyde and ammonium ion, were confirmed by spot test (Feigl F, 1975, p.290) and IR-spectra. The absence of  $\text{CO}_2$  and  $\text{NH}_3$  were confirmed by the tests of pubbling  $\text{N}_2$  gas through a tube containing lime water and Nessler's reagent, respectively (Vogel A, 1978, p.730). The formation of the present products were found to be in good agreement with that reported elsewhere (Murthy V, 1986, p.78). The latter species could not be identified under our experimental conditions owing to the low concentration of the substrate used.

### 3.2 $[\text{MnO}_4^-]$ and $[\text{Nicotine}]$ Dependences

Pseudo-first-order plots of  $\ln(\text{absorbance})$ -time plots were found to be linear for more than three half-lives of reaction completion. This result indicates that the reaction is first-order with respect to  $[\text{MnO}_4^-]$ . The values of pseudo-first-order rate constants,  $k_{\text{obs}}$ , were calculated from the gradients of these plots at a variety of initial  $\text{MnO}_4^-$  and nicotine concentrations. The first-order dependence was confirmed not only by the observed linearity of the pseudo-first-order plots but also by the independence of the obtained rate constants on different initial concentrations of the oxidant ranging between  $(1-6) \times 10^{-4} \text{ mol dm}^{-3}$ .

The non-constancy of the second-order rate constants derived from dividing the observed first-order rate constants by the initial  $[\text{Nicotine}]$  indicates that the rate is of fractional-order in  $[\text{Nicotine}]$ . Again, a plot of  $1/k_{\text{obs}}$  against  $1/[\text{Nicotine}]$  was found to be linear with a positive intercept on the  $1/[\text{Nicotine}]$  axis as shown in Fig. 2. This linearity obeys the Michaelis-Menten kinetics for the formation of 1:1 intermediate complex.

### 3.3 Dependence of reaction rate on $[\text{H}^+]$

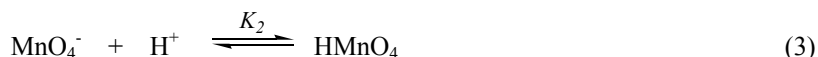
To clarify the influence of the  $[\text{H}^+]$  on the rate of reaction and to elucidate a reaction mechanism, some kinetic measurements were performed at different  $[\text{H}^+]$  and constant ionic strength and temperature. An increase in acid concentration was found to accompany by a decrease in the observed first-order-rate constant. This means that the reaction is acid-inhibitor. The order with respect to  $[\text{H}^+]$  was found to be of inverse non-integral order (obtained from  $\log k_{\text{obs}} - \log [\text{H}^+]$  plots). The results are summarized in Table 1.

In acid solutions, nicotine is usually existed as the protonated form (Peterson E, 2002, p.12662). The inverse-order dependence in  $[\text{H}^+]$  may be explained by the release of protons from nicotine prior to the rate-determining step.

Again, obeying the oxidation reaction to the Michaelis-Menten kinetics (Fig. 2) with the observed fractional-first order in  $[\text{Nicotine}]$  may suggest the formation of 1:1 complex between the reactants prior to the rate-determining step.



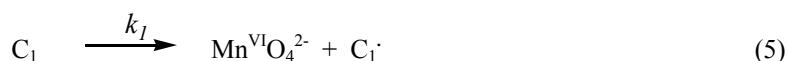
In view of the foregoing interpretations and the experimental observations, the most likely reaction mechanism which may be suggested involves the two following equilibria



where S and  $\text{SH}^+$  denote the nicotine substrate and its protonated form, whereas  $K_1$  and  $K_2$  are the ionization and protonation constants of nicotine [(Peterson E, 2002, p.12662) and permanganate ion (Baes C, 1976, p. 224) respectively. Then, the oxidant attacks nicotine substrate to form an intermediate complex ( $\text{C}_1$ ),



followed by fast decomposition of the intermediate ( $\text{C}_1$ ) in the rate-determining step to give rise to the product via formation of free-radical substrate as expressed by Eq. (5)



where  $K_3$  is the formation constant of the complex and  $k_1$  is the first-order rate constant of the complex decomposition in the rate-determining step.

The change of the rate constant with the change in the hydrogen ion and nicotine concentrations can be expressed by the following rate-law expression

$$\text{Rate} = \frac{-d[\text{MnO}_4^-]}{dt} = \frac{k_1 K_1 K_2 K_3 [\text{H}^+]^{-1} [\text{S}]_T [\text{MnO}_4^-]}{1 + K_1 [\text{H}^+]^{-1} + K_1 K_2 K_3 [\text{MnO}_4^-]} \quad (7)$$

where  $[\text{S}]_T$  represents the analytical total concentration of the substrate. In the presence of a large excess of nicotine over that of permanganate concentration, the rate-law expression is

$$\text{Rate} = \frac{-d[\text{MnO}_4^-]}{dt} = k_{\text{obs}} [\text{MnO}_4^-] \quad (8)$$

Comparing equations (7) and (8) and rearrangement, one concludes that

$$\frac{1}{k_{\text{obs}}} = \left( \frac{1 + K_1 [\text{H}^+]^{-1}}{k_1 K_1 K_2 K_3 [\text{H}^+]^{-1}} \right) \frac{1}{[\text{S}]_T} + K' \quad (9)$$

Equation (9) requires that, at constant  $[\text{H}^+]$  plots of  $1/k_{\text{obs}}$  against  $1/[\text{S}]_T$  to be linear with positive intercepts on  $1/k_{\text{obs}}$  axis. The experimental results were found to satisfy this requirement as shown in the reciprocal Michaelis-Menten plot (Fig. 2). Again, plots of  $1/k_{\text{obs}}$  against  $[\text{H}^+]$  at constant  $[\text{S}]$  gave good straight lines with positive intercepts on  $1/k_{\text{obs}}$  axis. The small intercept observed in Fig. 2 may lead us to simplify Eq. (9) to Eq. (10)

$$\frac{[\text{S}]_T}{k_{\text{obs}}} = \frac{1}{k'} = \left( \frac{[\text{H}^+]}{k_1'} + \frac{1}{k_1''} \right) \quad (10)$$

where  $k_1'$  and  $k_1''$  are the apparent rate constants which equal to  $k_1 K_1 K_2 K_3$  and  $k_1 K_2 K_3$ , respectively and  $k'$  is the second-order rate constant.

According to Eq. (10), plots of  $[S]_T/k_{obs}$  vs.  $[H^+]$  gave good straight lines with positive intercepts on  $[S]_T/k_{obs}$  axis as shown in Fig. 3. The values of  $k_1'$  and  $k_1''$  and the ionization constant of the substrate,  $K_1$ , can be evaluated from the slopes and intercepts of those plots. These values were calculated by the least-square method and listed in Table 2. The ionization constant values obtained for nicotine were found to be in good agreement to that reported elsewhere (Peterson E, 2002, p.12662).

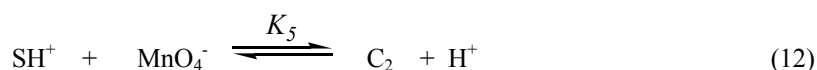
Unfortunately, the values of the rate constants of the elementary reaction,  $k_1$ , could not be calculated because of the non-availability of the formation constants,  $K_3$ . Some attempts have been made to calculate the formation constants from the experimental data, but the results were not encouraged. Therefore, the listed values of rate constants are considered to be composite quantities of the products of the rate constant, the formation constant and the protonation constant, respectively.

The activation parameters of the apparent rate constants and the second-order rate constant were calculated from the temperature-dependence of the rate constants by the method of least-squares using the Arrhenius and Eyring equations. These parameters are summarized along with that of the thermodynamic parameters for ionization constant in Table 3.

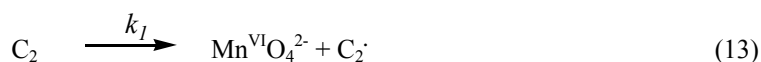
An alternative reaction mechanism could be suggested. It involves the rapid protonation of the substrate,



followed by an attack of the oxidant to the positive protonated- substrate to form an intermediate complex  $C_2$ ,



The formed intermediate ( $C_2$ ) is rapidly decomposed in the rate-determining step to give rise to the product through the formation of a free-radical substrate



In a similar manner, the change of the rate constant with the change in  $[H^+]$  and [Nicotine] will lead to the following relationship

$$\frac{1}{k_{obs}} = \left( \frac{1 + K_4[H^+]}{k_2 K_4 K_5} \right) \frac{1}{[S]_T} + K'' \quad (15)$$

where  $K_4$  is the protonation constant of the substrate. This relationship resembles Eq. (8) in which a plot of  $1/k_{obs}$  against  $1/[S]_T$  at constant  $[H^+]$  gave a good straight line with a positive intercept on  $1/k_{obs}$  axis (Fig. 2). The small intercept shown in Fig. 2 may also lead us to simplify Eq. (15) to Eq. (16)

$$\frac{[S]_T}{k_{obs}} = \left( \frac{1}{k_2'} + \frac{[H^+]}{k_2''} \right) \quad (16)$$

where  $k_2' = k_2 K_4 K_5$  and  $k_2'' = k_2 K_5$ , respectively. According to Eq. (16), plots of the left-hand side against  $[H^+]$  should be linear with positive intercepts on  $[S]_T / k_{obs}$  axis as was experimentally observed. The values of  $k_2'$  and  $k_2''$  as well as the protonation constant,  $K_4$ , can be evaluated from the slopes and intercepts of those plots. These values were found to be quite similar to that evaluated in the former mechanism where  $k_2' = k_1'$ ,  $k_2'' = k_1''$  and  $K_4 = 1/K_1$ , respectively. This fact may be considered a good evidence to support the proposed mechanism.

The smaller activation energies obtained in the present work may support the fact that the reaction takes place between ions of different charges or two neutral molecules. Therefore, the electrostatic attraction between the reactants does not need much energy to bring them together in order to form the activated complex.

Since, permanganate ion is a multi-equivalent oxidant, a variety of mechanistics are possible depending on the nature of both the medium and the reactive species (Stewart R, 1965, p.2). The mechanistic approach of some

reactions involving acidic permanganate as an oxidant has been based on the formation of intermediate complexes (Hassan R, 1991, p.2018) and other results have been interpreted by free-radical mechanisms (Hassan R, 1992, p.661). Again, the mechanism of electron-transfer is sometimes suggested to be of successive one electron-transfer mechanism of outer-sphere type (Moore F, 1975, p.413) or inner-sphere nature (Hicks K, 1971, p.1107). In other redox reactions, a simultaneous two-electron changes in a single step of inner-sphere nature (Hassan R, 1988, p.605) has been suggested. In this context, it should be noticed that there does not appear to be any experimental confirmation of an outer-sphere of two-electron transfer process (Hassan R, 1991, p.3003).

Although the rate-law expression here provides no information about electron transfer process, whether it is of inner- or outer-sphere nature, some information may be expected by examining the magnitudes of the rate constants and the activation parameters (Moore F, 1975, p.413). Unfortunately, no data are available on the formation constants in order to evaluate the rate constants of the principal elementary reactions. Moreover, it noticed that the entropy of activation tends to be more positive for outer-sphere types, whereas the reactions of negative  $\Delta S^\ddagger$  values are mainly proceeded via inner-sphere mechanism (Hassan R, 1992, p.255). The entropy of activation obtained in the present work suggests that the inner-sphere type is the more favorable one for oxidation of nicotine by permanganate ion via free-radical mechanism of one-electron transfer process. A plausible mechanism of oxidation in good consistent with the experimental kinetics may be illustrated by Schemes 1.

#### 4. Conclusion

The oxidation of nicotine by potassium permanganate in acid perchlorate solutions have been investigated, spectrophotometrically. The oxidation process was found to proceed through the formation of 1:1 intermediate complex prior to the rate determining step via free radical mechanism. The reaction was found to be acid-inhibition where the oxidation rates were increased with decreasing the hydrogen ion concentration. The kinetic evaluated value of the ionization constant of nicotine was found to be in good agreement with that reported elsewhere. The oxidation product of nicotine was identified as nicotinic acid. A reaction mechanism in good consistent with the kinetic results was suggested and discussed.

#### References

- Baes C F and Mesmer R E. (1976). *The hydrolysis constants*, Wiley, New york, p.224 & Hogfeld Erlic (1st edn)(1982). *Stability constants of Metal Ion complexes*, Part A Inorganic ligand, Pergamon press, New York, 73.
- Fiegl F and Anger V. (1978). *Spot tests in organic analysis*, Elsevier, Oxford, 290 & 332.
- Hassan R M. (1991). Kinetics of reaction of uranium(IV) of hexachloroiridate(IV) in acid perchlorate solutions. Evidence for a binuclear intermediate, *J Chem Soc*, 3003-3008.
- Hassan R M, Mousa M A and Wahdan M H. (1988). Kinetics and mechanism of oxidation of  $\beta$ -phenylalanine by permanganate ion in aqueous perchloric acid, *J Chem Soc, Dalton Trans*, 605-609 & Hassan R M (1991). Kinetics and mechanism of oxidation of DL-  $\alpha$  - alanine by permanganate ion in acid perchlorate media, *Cand J Chem*, 69, 2018-2023.
- Hassan R M, El-Gaiar S A and El-Summan A M. (1993). Kinetics and mechanism of oxidation of selenium(IV) by permanganate ion in aqueous perchlorate solutions. *Collect Czech Commun*, 58, 538-546.
- Hassan R M, Fawzy A, Ahmed G A, Zaafarany I A, Asghar B H and Khairou K S. (2009). Acid catalyzed oxidation of some sulfated macro-molecules. Kinetics and mechanism of permanganate oxidation of kapp-carrageenan polysaccharides in acid perchlorate solutions. *J Mol Cat*, 309, 95-102 & Hassan R M, Abdel-Kader D A, Ahmed S M, Fawzy A, Zaafarany I A and Takagi H D (2009). Acid catalyzed oxidation of carboxymethyl cellulose. Kinetics and mechanism of permanganate oxidation of carboxymethyl cellulose in acid perchlorate solutions. *Cat commun*, 11, 184-190.
- Hassan R M, Mousa M A and El-Shatoury S A. (1988). Kinetics of oxidation of uranium(IV) by permanganate ion in aqueous perchlorate media. *J Chem Soc, Dalton Trans*, 601-603
- Hassan R M. (1992). Kinetics and mechanism of oxidation of kojic acid by permanganate ion in perchlorate media. *Acta Chem Hungar*, 129, 661-669.
- Hicks K W and Sutter J R. (1971). Kinetic studies of permanganate oxidation reactions. III. Reactions with tris (1,10-phenanthroline iron(II), *J Phys Chem*, 76, 1107-1113.
- Larson P S, Silvette H. (1964). Medical uses of tobacco (past and present). In von Euler, U.S.Ed. Tobacco alkaloid and related compounds. The Macmillan Co., New York, 2-12.

Moore F M and Hicks K W. (1975). Mechanism of permanganate oxidation of vanadium(IV), *Inorg Chem*, 14,413-416.

Murthy V K. (1986). Oxidation of nicotine. Determination of nicotine concentration. *Tobacco Res*, 12, 78-93.

Pailer M. (1964). Tobacco alkaloid and related compounds, van Euler, U.S. Edn., Macmillan Co., New York, 15-36.

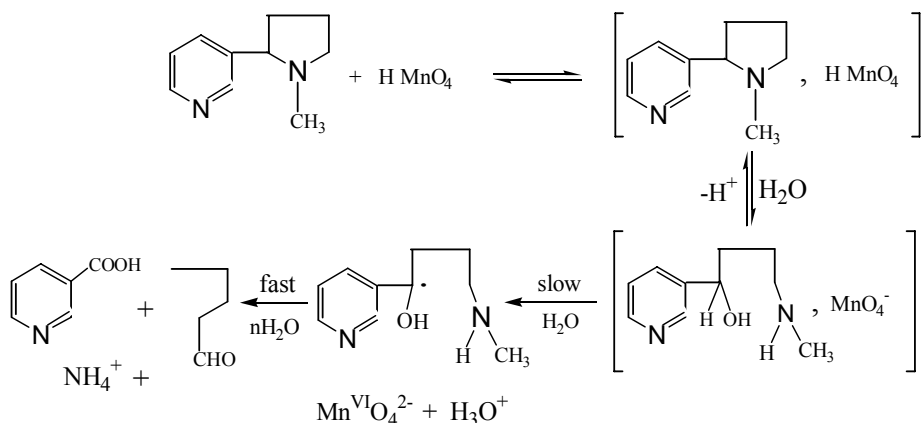
Peterson E J , Choi A, Dahan D S, Lester H A and Dougherty D A. (2002). A Petruded pKa at the binding site of nicotinic acetylcholine acceptor. Implication for nicotine binding. *J Am Chem Soc*, 124, 12662-1266.

Smith L O and Cristol S J (West Edn.). (1971). *Organic Chemistry*, p.174.

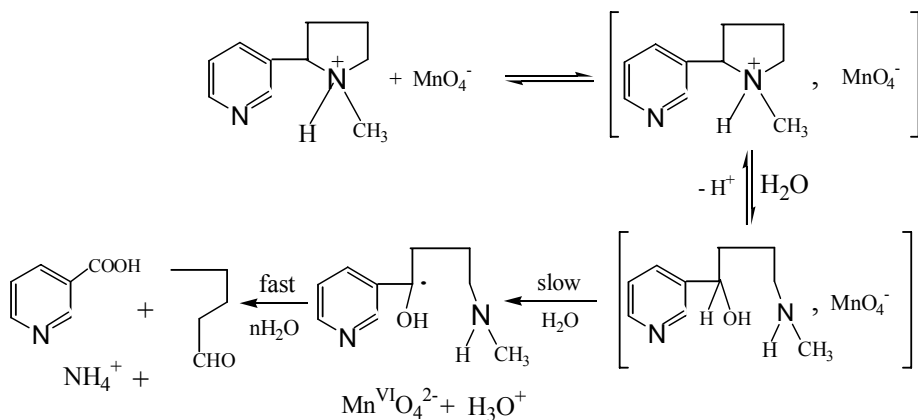
Stewart R. (1965). Oxidation by permanganate in Wiberg K B Editor. *Oxidation in inorganic chemistry*, Academic Press, New York, 2-33.

Vogel A I (4 th Edn). (1978). A text book of quantitative inorganic analysis, EIBS, 730 & Vogel A I. (1962). *Practical organic chemistry*, longman, London, 325.

Wang H, Ma L, Li Y and Cho, Ch. (2000). Exposure to cigarette smoke increases apoptosis in the rat gastric mucosa through a reactive oxygen species-mediated and P-35 independent pathway. *Free Radical Biol Med*, 28, 1125-1131.



Scheme I



Scheme II

Table 1. The observed first-order rate constants in the oxidation of nicotine by permanganate ion in aqueous perchlorate solutions.  $[\text{MnO}_4^-] = 4.0 \times 10^{-4}$ ,  $[\text{Nicotine}] = 1 \times 10^{-2}$  and  $I = 1.0 \text{ mol dm}^{-3}$  at  $25^\circ \text{C}$

$10[\text{H}^+], \text{mol dm}^{-3}$	1.25	2.50	3.75	5.00
$10^3 k_{\text{obs}}, \text{s}^{-1}$	4.05	2.04	1.035	1.02

Table 2. The values of the apparent rate constants ( $k'_1$  and  $k''_1$ ) and the ionization constant ( $K_1$ ) in the oxidation of nicotine by permanganate ion in aqueous perchlorate solutions.  $[\text{MnO}_4^-] = 4 \times 10^{-4}$ ,  $[\text{Nicotine}] = 1 \times 10^{-2}$  and  $I = 1.0 \text{ mol dm}^{-3}$

Constant	Temperature ( $^\circ \text{C}$ )	
	25	45
$10^2 k'_1, \text{dm}^3 \text{mol}^{-1} \text{s}^{-1}$	5.10	8.70
$10^2 k''_1, \text{dm}^6 \text{mol}^{-2} \text{s}^{-1}$	0.53	2.00
$10^4 K_1, \text{mol dm}^{-3}$	9.69	3.48

Experimental error  $\pm 3\%$

Table 3. Activation parameters of the apparent rate constants ( $k'_1$  and  $k''_1$ ) and the second-order rate constant ( $k'$ ) along with that of the thermodynamic parameters of the ionization constant ( $K_1$ ) in the oxidation of nicotine by permanganate ion in aqueous perchlorate solutions.  $[\text{MnO}_4^-] = 4 \times 10^{-4}$ ,  $[\text{Nicotine}] = 1 \times 10^{-2}$  and  $I = 1.0 \text{ mol dm}^{-3}$

Constant	Parameter				
	$\Delta H^\ddagger$ $\text{kJ mol}^{-1}$	$\Delta S^\ddagger$ $\text{J mol}^{-1} \text{K}^{-1}$	$\Delta G^\ddagger$ $\text{kJ mol}^{-1}$	$E_a^\ddagger$ $\text{kJ mol}^{-1}$	A $\text{mol}^{-1} \text{s}^{-1}$
$k'_1$	19.42	-204.65	80.41	22.00	$2.79 \times 10^2$
$k''_1$	58.42	-15.87	63.87	60.96	$2.55 \times 10^{12}$
$*k'$	17.49	-199.54	76.95	21.13	$1.01 \times 10^3$
Temp. ( $^\circ \text{C}$ )	25	35	45	55	
$K \times 10^4$	9.69	5.48	3.48	2.28	
Parameter	$\Delta H^\circ$ $\text{kJ mol}^{-1}$	$\Delta S^\circ_{298}$ $\text{J mol}^{-1} \text{K}^{-1}$	$\Delta G^\circ_{298}$ $\text{kJ mol}^{-1}$		
Value	-39.014	-188.61	17.19		

\* At  $[\text{H}^+] = 0.25 \text{ mol dm}^{-3}$

Experimental error  $\pm 4\%$

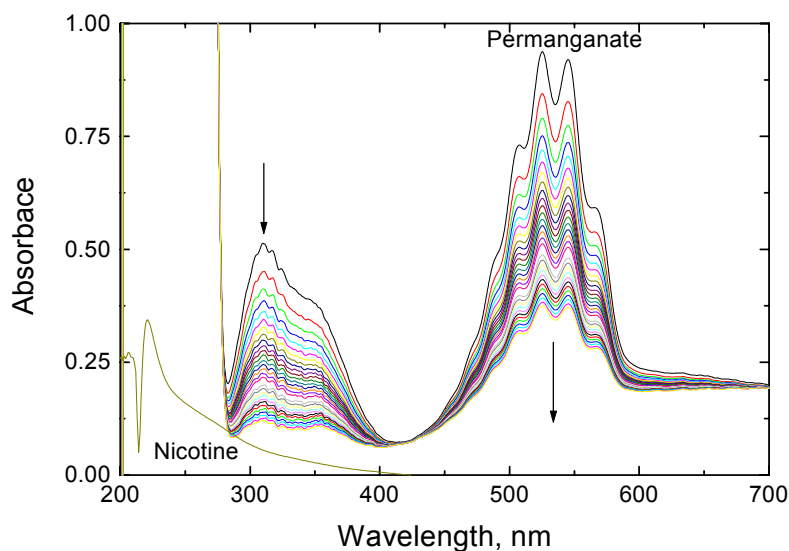


Figure 1. Spectral changes (200 - 600 nm) in the oxidation of nicotine by permanganate ion in aqueous perchlorate solutions.  $[\text{MnO}_4^-] = 4 \times 10^{-4}$ ,  $[\text{Nicotine}] = 1 \times 10^{-2}$  and  $I = 1.0 \text{ mol dm}^{-3}$  at  $25^\circ \text{C}$ . Scanning time intervals 2 min

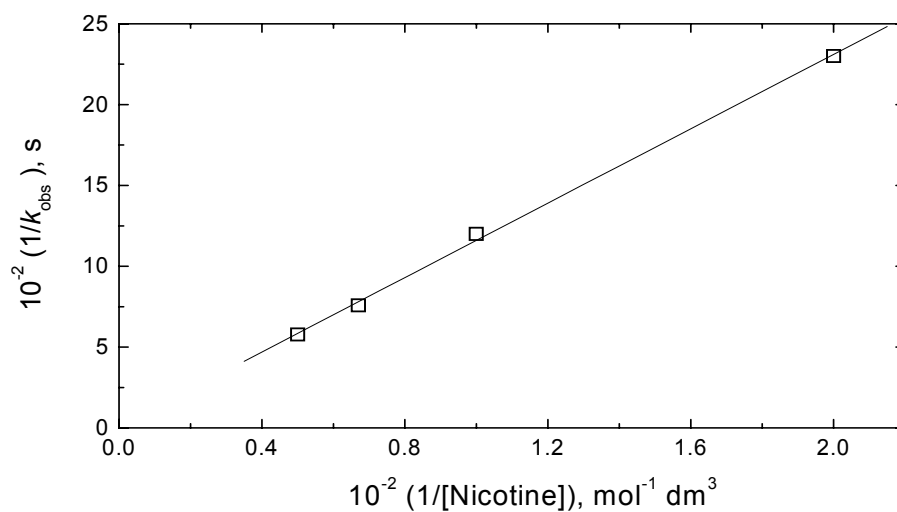


Figure 2. Michaelis-Menten plot in the oxidation of nicotine by permanganate ion in aqueous perchlorate solutions.  $[\text{MnO}_4^-] = 4.0 \times 10^{-4}$ ,  $[\text{Nicotine}] = 1 \times 10^{-2}$  and  $I = 1.0 \text{ mol dm}^{-3}$  at  $25^\circ \text{C}$ .

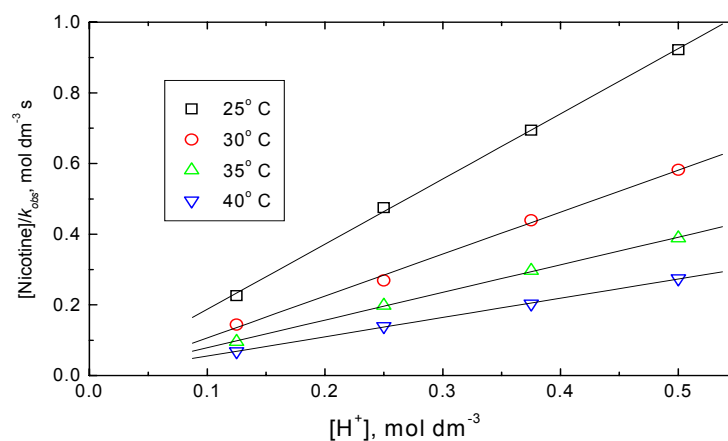


Figure 3. Plots of  $[\text{Nicotine}]/k_{\text{obs}}$  vs.  $[\text{H}^+]$  in the oxidation of nicotine by permanganate ion in aqueous perchlorate solutions.  $[\text{MnO}_4^-] = 4 \times 10^{-4}$ ,  $[\text{Nicotine}] = 1 \times 10^{-2}$  and  $I = 1.0 \text{ mol dm}^{-3}$

## Water Quality in Some Primary Schools in Shala e Bajgorës

Lavdim Zeqiri (Corresponding author)

Faculty of Mining and Metallurgy Department of Chemical Engineering

University of Prishtina, Prishtina, Kosovë

Tel: 86-377-4459-6677 E-mail: lavdimzeqiri@hotmail.com; lavdimzeqiri@gmail.com

Malësore Pllana

Faculty of Mining and Metallurgy Department of Chemical Engineering

University of Prishtina, Prishtina, Kosovë

E-mail: malsore\_p@hotmail.com

Sadije Kadriu

Faculty of Mining and Metallurgy Department of Chemical Engineering

University of Prishtina, Prishtina, Kosovë

E-mail: sadijekadriu@hotmail.com

Kadri Berisha

Faculty of Mining and Metallurgy Department of Chemical Engineering

University of Prishtina, Prishtina, Kosovë

E-mail: kadrushberisha@hotmail.com

Shukri Maxhuni

Ministry of Education, Science and Technology, Kosovë

E-mail: shumax4@hotmail.com

### Abstract

In this scientific report are given some results of drinking water in some primary schools in Shala e Bajgorës. Samples which are analyzed are in region that is near mining Trepça in Mitrovica Municipality that are presented. Taking into consideration all important parameters we found they were within given limits, just temperature that is higher than given limits, so analysis of water samples for thermo tolerant faecal coli forms which are carried out by passing a measured quantity of water through sterile filter told us more than 60 % of samples were contaminated.

Therefore it was necessary to complete the procedure for chlorination of wells using Galisept.

On the base of physical – chemical and bacteriological parameters we may conclude that only after continual procedure of chlorination of wells it will be completed the conditions for drinking water in analyzed samples.

**Keywords:** Water, Physical and chemical properties, Presence of coli form bacteria

### 1. Introduction

Water is solvent of life; human body is about  $\frac{3}{4}$  water by mass. More chemical and biochemical reactions take place in water than in other solvents combined. In absence of water, no known form of life is possible. The total amount of water on earth is estimated to be  $1.4 \times 10^9 \text{ km}^3$  of which 97. 4% is sea water and 2. 6 % is fresh water. Of the fresh water  $\frac{4}{5}$  is located in ice caps and glaciers and about  $\frac{1}{5}$  is relatively inaccessible ground water. Less than 1% of fresh water (0. 014 percent of total) is located in lakes, soils, rivers, biota and the atmosphere.

In Kosova about 70% of inhabitants live in villages (country side) and 60 % of them take drinking water from non hygienic shallow wells where distances WC – well is not adequate.

The supply of population with drinking water propound same request and criterion, starting with quality of water, construction and technology of cleaning, operation of preparing, overseeing supplying of reservoir. Therefore physical chemical and bacteriological parameters are necessity

The presence of same chemicals in drinking water is preferable because they give determined characteristics. Drinking water needs to be clean in bacteriological terms, to be clear, to have a nice taste without odorous and with temperature which gives water refreshment taste.

Refreshment properties and tasteful water is a result of present gaseous dissolved in water ( $O_2$  and  $CO_2$ ) and small amount of  $Ca(HCO_3)_2$ . The concentration of oxygen in water depends on temperature and partial pressure but also in level of pollution of water. The presence of reduction substances as ammonia  $NH_3$ , Fe (II),  $NO_2^-$  and other substances which oxidize very easy throw of this equilibrium by reducing the quantity of dissolvent oxygen this way. Concentration of dissolved oxygen is a parameter of impurity in water.

One of very important parameters about level of purity or impurity of water is chemical consumption of oxygen (oxidization) which presents quantity of reagent for oxidization of organic, inorganic or colloidal substances.

The production of decomposed organic substances, done by influence of special bacterium, gives to water unpleasant taste.

## 2. Experimental work

For investigation of quality of water in several schools in some villages in region Shala e Bajgorës that is near mining Trepça municipality of Mitrovica we take water samples in fields.

Some parameters as: odour, color, turbidity, temperature, pH, Chlorine, faecal coli forms were determined with "Portable Water Testing kit", while other parameters as specific conductivity, dissolved oxygen, oxygen saturation, spending of  $KMnO_4$  dry remain,  $NO_2^-$ , Fe, Mn, etc. were determined in laboratory. The analysis of chlorine and pH has been done in comparator which is part.

The samples of water were taken by non sterile vacuum – cup (part of apparatus). The comparator cells were washed many times with water which is to be analyzed and finally filled with sample, than we droop DPD – 1 into the right – hand cell ( $Cl_2$ ) hand a phenol red tablet into left – hand cell (pH). We replace the led of comparator and push down firmly to seal.

Then we invert the comparator repeatedly until the tablets have dissolved completely. Immediately we read the free chlorine residual and pH concentrations by holding comparator up day light and matching color developed in cell with standard color scale in the central part of the comparator. For testing total chlorine residual we don't discard the liquid in the comparator, but we do remove the lid and add a tablet DPD – 3.

Turbidity was determined in turbidity tubes cover the range 2 -5 TU. The turbidity tubes are graduated in logarithmic scale with the most critical values. The result is the value of the line nearest to the water level. In our cases the values were under level according to standards.

The analysis of water samples for thermo tolerant (faecal) coli forms is carried out by passing a measured quantity of water through a sterile filter. Any bacteria present in the water are caught in filter. The filter is then placed onto a paper pad soaked in liquid growth medium which feeds coli form bacteria, but inhibits any other bacteria caught in filter. To ensure that only thermo tolerant (faecal) coli form bacteria are allowed to grow, the filter is kept at  $44^0$  C in the kit's incubator until the bacteria multiply many times to form colonies of bacteria which can seen with naked eye. Thermo tolerant (faecal) coli forms are recognized by their ability to produce a color (from red to yellow) in the culture medium at  $44^0$  C. Results are expressed as colony forming units per  $100\text{ cm}^3$  of water.

Thermo tolerant (faecal) coli forms are of sanitary significance when present in drinking water supplies. Users should refer to country specific water quality standards or to World Health Organization (WHO).

Determination of electrical conductivity has been done using conduct meter WTN – D 812 Weilheim LBR 40, therefore determination of oxygen has been done by Winkler bottles. Nitrites were determined in a Helligen's comparator. Other parameters have been determined using standard methods.

## 3. Results and discussion

The experimental results of our investigation are present in table 1, 2 and 3. The temperature is very important factor for development of biological processes. Different organisms present in water, will adopt in given thermal



conditions to grow their activity of vital importance. In different water supplies the results of temperature were different. Temperature in more cases was surplus value up  $12^{\circ}\text{C}$  which means that value was higher than standards.

Water which contains some organic substances (material) with plants and animal origin spends a quantity of  $\text{KMnO}_4$  for their oxidation. Inorganic substances as  $\text{NO}_2^-$ ,  $\text{Fe (II)}$ ,  $\text{H}_2\text{S}$ , etc. can oxidize with  $\text{KMnO}_4$ . Therefore spending of  $\text{KMnO}_4$  will be taken into consideration as a measure for all present substances which are capable for oxidation. On the bases of spending  $\text{KMnO}_4$  and taking into consideration standards we may conclude that investigation samples of water can be used as drinking water.

Turbidity of analyzed water every time was under the limits so we can say that this parameter doesn't have the influence on drinking water.

The investigation tells us that in most of analyzed samples there are present thermo tolerant (faecal) coli forms. On the bases of physical – chemical and bacteriological parameters given in tables 1 – 3, we can verify that in contaminated water supplies we need to do the process of chlorination continually to have criteria of drinking water.

### References

- CDF/ASD. (2003). "Manual për promovimin e shëndetit dhe higjienës", Mitrovicë.
- Donald A. Mc. Quarrie and Peter A. Rock. (1991). *General Chemistry*. W. H. Freeman and Company, New York.
- Information sheet prepared by UNHCR, action against hunger, ADRA and IRC. Dt. 28. 07. 99.
- International Standards for drinking Water. (1971). 3<sup>rd</sup> edition. World Health Organization, Geneva, JIAS / UNMIK IA 2/99.
- J. Djukovic, B. Djukic, D. Lazic, M. Marsenic. (2000). *Tehnologija Vode*, Beograd.
- Kosova Academy of Sciences and Arts. (2008). *The Environment of Kosova Resources and Human Factor*, Prishtinë.
- Lavdim Zeqiri. (2004). Diploma Project, Faculty of Mining and Metallurgy, Mitrovicë.
- N. F. Voznaya. *Chemistry of Water and Microbiology*, Mir Oxfam Delagua, Portable Water Testing Kit, Users Manuel.
- Nexhat M. Daci. (1998). *Environmental chemistry*. Industrial Pollution – Prevention, academy of arts and science of Kosova, Prishtinë.
- S. Krasniqi, B. Nushi. (2002). Latifi, konferenca shkencore, Zhvillimi i qëndrueshëm tekniko – teknologjik dhe mjedisi f 203-207, Prishtinë.
- Standard Methods for the Examination of Water and Wastewater. (1985). p, 506-508 A, 16 Edition.

Table 1. Physical, chemical and bacteriological properties of water

<i>Nr</i>	<i>Parameter</i>	<i>Unit</i>	<i>Primary school in Rashan</i>	<i>Primary school in Mazhiq</i>	<i>Primary school in Maxhera</i>	<i>Detection limit</i>
1	Temperature	<sup>0</sup> C	<b>17</b>	<b>14</b>	<b>15</b>	8-12
2	Odour	-		-	-	-
3	Colour	-		-	-	-
4	Turbidity	NTU	0,00	0,00	5,99	1.2-2.4
5	Sp. Conductivity	μcm <sup>-1</sup>	794	564	4,02	Until 1500
6	pH	-	7,6	6,7	7,9	6,00-8,20
7	Spend. KMnO <sub>4</sub>	mg/dm <sup>3</sup>	1,26	2.212	6,11	Until 12
8	Residual Chlorine	mg/dm <sup>3</sup>	-	-	-	0,2-0,5
9	Chloride	mg/dm <sup>3</sup>	38	27	16	Until 200
10	Nitrite	mg/dm <sup>3</sup>	0,011	0, 004	0,022	0.005
11	Nitrate	mg/dm <sup>3</sup>	3,0	1,8	0,11	10
12	Iron	mg/dm <sup>3</sup>	-	-	-	Until 0.30
13	Manganese	mg/dm <sup>3</sup>	-	-	-	Until 0.05
14	Ammonia	mg/dm <sup>3</sup>	0,06	0,04	0,00	0,1
15	Sulfate	mg/dm <sup>3</sup>	39,1	52,86	9,34	200
16	Hardness of H <sub>2</sub> O	<sup>0</sup> dH	12,09	14,33	5,6	30
17	F. C. / 100 cm <sup>3</sup>		<b>20</b>	-	<b>220</b>	-

Table 2. Physical, chemical and bacteriological properties of water

<i>Nr</i>	<i>Parameter</i>	<i>Unit</i>	<i>Public source in Kutllovc</i>	<i>Primary school in Kodër</i>	<i>Primary school in Melenicë</i>	<i>Detection limit</i>
1	Temperature	<sup>0</sup> C	<b>14</b>	<b>16</b>	<b>13</b>	8-12
2	Odour	-	-	-	-	-
3	Colour	-	-	-	-	-
4	Turbidity	NTU	-	0,00	0,00	1.2-2.4
5	Sp. Conductivity	μcm <sup>-1</sup>	637	804	272	Until 1500
6	pH	-	7,5	7,2	7,7	6,00-8,20
7	Spend. KMnO <sub>4</sub>	mg/dm <sup>3</sup>	4,09	3,43	8,47	Until 12
8	Residual Chlorine	mg/dm <sup>3</sup>	-	-	-	0,2-0,5
9	Chloride	mg/dm <sup>3</sup>	15	21,5	20	Until 200
10	Nitrite	mg/dm <sup>3</sup>	0,004	0,015	0,05	0.005
11	Nitrate	mg/dm <sup>3</sup>	0,7	3,7	2,4	10
12	Iron	mg/dm <sup>3</sup>	-	-	0.01	Until 0.30
13	Manganese	mg/dm <sup>3</sup>	-	-	-	Until 0.05
14	Ammonia	mg/dm <sup>3</sup>	0,02	0,032	0,01	0,1
15	Sulfate	mg/dm <sup>3</sup>	16,06	21,50	5,18	200
16	Hardness of H <sub>2</sub> O	<sup>0</sup> dH	15,68	9,63	5,6	30
17	F. C. / 100 cm <sup>3</sup>		<b>10</b>	<b>4</b>	<b>220</b>	-

Table 3. Physical, chemical and bacteriological properties of water

Nr	Parameter	Unit	Public source in Zjaçë	Primary school in Zhazhë	Public source in Boletin	Detection limit
1	Temperature	$^{\circ}\text{C}$	<b>13</b>	6	8	8-12
2	Odour	-	-	-	-	-
3	Colour	-	-	-	-	-
4	Turbidity	NTU	0,00	0,00	0,00	1.2-2.4
5	Sp. Conductivity	$\mu\text{cm}^{-1}$	779	257	224	Until 1500
6	pH	-	7,6	3,9	7,6	6,00-8,20
7	Spend. $\text{KMnO}_4$	$\text{mg}/\text{dm}^3$	3,36	3,76	3,14	Until 12
8	Residual Chlorine	$\text{mg}/\text{dm}^3$	-	-	-	0,2-0,5
9	Chloride	$\text{mg}/\text{dm}^3$	43	250	17	Until 200
10	Nitrite	$\text{mg}/\text{dm}^3$	0,014	0,04	0,05	0.005
11	Nitrate	$\text{mg}/\text{dm}^3$	0,9	20,5	1,8	10
12	Iron	$\text{mg}/\text{dm}^3$	-	-	-	Until 0.30
13	Manganese	$\text{mg}/\text{dm}^3$	-	-	-	Until 0.05
14	Ammonia	$\text{mg}/\text{dm}^3$	0.00	0,01	0,00	0,1
15	Sulfate	$\text{mg}/\text{dm}^3$	26,62	-	-	200
16	Hardness of $\text{H}_2\text{O}$	$^{\circ}\text{dH}$	11,42	2,35	4,48	30
17	F. C. / $100\text{ cm}^3$		<b>7</b>	<b>300</b>	<b>E. coli</b>	-

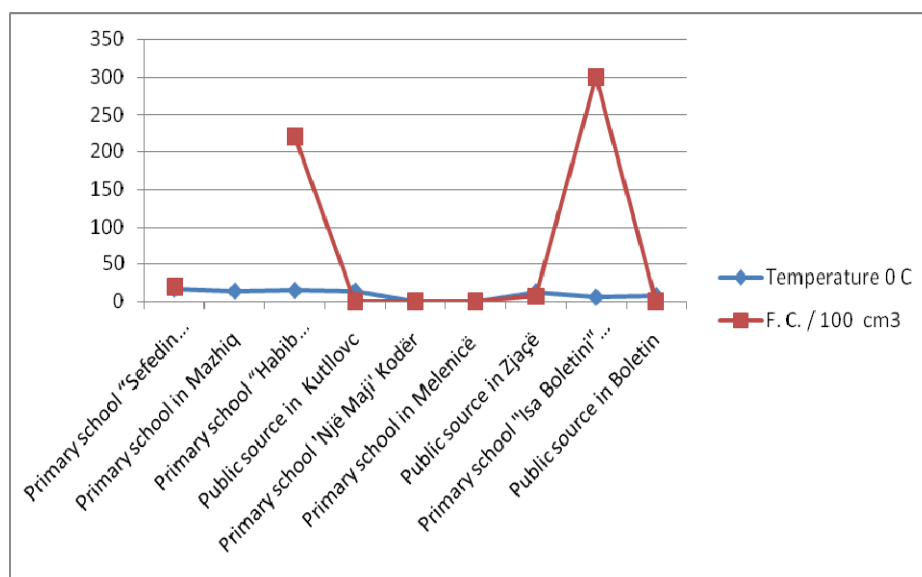


Figure 1. High value of Temperature and presence of Fecal Coli forms bacteria in samples

# Synthesis of Novel Multifluorinated Pyrazolone-5-one Derivatives via Conventional and Non-conventional Methods

Amol Gadakh (Corresponding author)

P. G. Department of Chemistry, New Arts, Science and Commerce  
College, Ahmednagar, University of Pune, Pune- 414003, India  
Tel: 91-2852-1314 E-mail: gadakhamol@yahoo.com

Chetan Pandit

Aurigene Discovery Technologies Ltd, 39-40, KIADB Industrial area  
Electronic city, Phase-2, Hosur Road, Bangalore-560100  
Tel: 91-2852-1314 E-mail: Chetan\_p@aurigene.com

Sahebrao S. Rindhe

P. G. Department of Chemistry, New Arts, Science and Commerce  
College, Ahmednagar, University of Pune, Pune- 414003, India  
Tel: 91-241-243-1895 E-mail: rindhe\_ss@yahoo.com

Bhausahab Karale

Department of Chemistry Radhabai Kale mahila Mahavidyalaya  
Ahmednagar, University of Pune, Pune-411003  
E-mail: bkkarale@yahoo.com

## Abstract

An efficient synthesis of 3-trifluoromethyl-1-(3,4-difluorophenyl)-1*H*-pyrazol-5(4*H*)-one (**3**) and their Knoevenagel condensation reaction with 1,4-diphenyl -1*H*-pyrazole-3-carbaldehydes **4**, 4-oxo-4*H*-chromene-3-carbaldehydes **6** and 2-chloroquinoline-3-carbaldehydes **8** have been described by using conventional and non-conventional techniques. Comparison of conventional and non-conventional techniques like Microwave, Ultrasonic assisted reactions showed that, the later procedure require shorter reaction time, good yield and was applicable for larger set of substrates emphasizing the importance of eco-friendly conditions.

**Keywords:** Pyrazol-5(4*H*)-one, Pyrazoles, Chromones, Quinolines, Knoevenagel condensations

## 1. Introduction

Pyrazolone are very important class of heterocycles due to their wide applications in pharmacological and biological activities (Arnost *et al.* 2010; Gursoy *et al.* 2000; Venkat Ragavan *et al.* 2009). Large numbers of 2-pyrazolin-5-ones have been used as therapeutics agents such as analgesics and antipyretics, (Himly *et al.* 2003). It is also well known that they exhibit varied biological activities like antiinflammatory, antibacterial, antifungal, etc. (Karale *et al.* 2000; Rena *et al.* 2005).

The chemistry of chromones and its derivatives received considerable attention as it was found readily in natural products, which exhibit antimicrobial activities (Deng *et al.* 2000; Khan *et al.* 2000). Also, quinoline moiety is of great importance to the chemists as well as biologists as it is found in a large variety of naturally occurring compounds and also chemically useful molecules having diverse biological activities (Nasveld *et al.* 2005; Denny *et al.* 2006; Mohamoud *et al.* 2006; Muruganantham *et al.* 2004). In the view of various therapeutic aspects of introduction of fluorine in various drugs and biologically active heterocycles, we have decided to incorporate the CF<sub>3</sub> and fluorine group in various positions of pyrazolinones to enhance their reactivity.

In recent years due to increasing environmental awareness in chemical and industrial research, the challenge for a clean environment calls for best procedures like reducing pollution, hazardous byproduct formations.

Keeping a perception on above problems, Microwave and Ultrasound assisted techniques are found to be more effective from environmental as well as from shorter reaction time, high yields, ease of work-up and isolation of products (Maruthikumar *et al.* 2005; Dalvi *et al.* 2004; Chornous *et al.* 2004; Breeuwer *et al.* 2003; Mojtahedi *et al.* 2008). Compared with traditional methods, the organic reaction can be easily controlled, more convenient, with higher yield, shorter reaction time or milder conditions under ultrasound irradiation.

Keeping in view of demerits of conventional techniques, we report the synthesis of fluorinated pyrazol-5-one **3** and their Knoevenagel condensations reaction with 1, 4-diphenyl-1H-pyrazole-3-carbaldehyde **4**, 4-oxo-4H-chromene-3-carbaldehydes **6** and 2-chloroquinoline-3-carbaldehydes **8** using microwave and Ultrasonic techniques.

## 2. Result and Discussion

In the present work we have synthesized 3-trifluoromethyl-1-(3, 4-difluorophenyl)-1H-pyrazol-5(4H)-one **3** by reacting 3, 4-difluorophenyl hydrazine **1** and ethyl 4, 4, 4-trifluoro-3-oxobutanoate **2** at 130- 135°C for 3h with constant stirring (**Scheme-1**). Knoevenagel condensation of 3-trifluoromethyl-1-(3, 4-difluorophenyl)-1H-pyrazol-5(4H)-one **3** with various Substituted Carbaldehydes like 1,4-diphenyl-1H-pyrazole-3-carbaldehydes **4**, 4-oxo-4H-chromene-3-carbaldehydes **6** and 2-chloroquinoline-3-carbaldehydes **8** resulted in the formation of 3-(trifluoromethyl)-1-(3,4-difluorophenyl)-4-((1,4-diphenyl-1H-pyrazol-3-yl)methylene)-1H-pyrazol-5(4H)-one **5**, 3-(trifluoromethyl)-1-(3, 4-difluorophenyl)-4-((4-oxo-4H-chromen-3-yl)methylene)-1H-pyrazol-5(4H)-one **7** and 4-((2-chloroquinolin-3-yl)methylene)-3-(trifluoromethyl)-1-(3,4-difluorophenyl)-1H-pyrazol-5(4H)-one **9** with a yield of 68-79% using conventional and 82-92% of yields using nonconventional methods (**Scheme-2**). The exact regioisomerism we could not interpreted for all the obtained products due to multiple fluorine couplings and the complexity pattern in the <sup>1</sup>H-NMR.

The characterization data of the newly synthesized compounds were given in (**Table-1**). The reaction reported here by using ultrasonication and microwave techniques are superior in terms of higher yields and rapid, environmental friendly, compared to conventional techniques.

## 3. Experimental

### 3.1 General

All the recorded melting points were determined on electro thermal melting point apparatus and are uncorrected. IR spectra were recorded on Shimadzu-470 infrared spectrophotometer. The <sup>1</sup>H-NMR spectra were recorded on Bruker- AMX 300 MHz instrument in (CD<sub>3</sub>)<sub>2</sub>SO and TMS as an internal standard. <sup>13</sup>C NMR spectra were recorded on 75MHz with TMS as an internal standard. <sup>19</sup>F NMR were recorded on 282 MHz. Microwave Initiator-02 Biotage (700Watt) was used to carry out the reactions. The ultrasonic cleaner from Madhu Lab Tech (Tensil India) 230V, 50 Hz 10006H used to carry out sonication reactions. The purity of compounds was confirmed by thin layer chromatography using Merck silica gel 60 F<sub>254</sub> coated aluminium plates.

### 3.2 Synthesis of 3-trifluoromethyl-1-(3,4-difluorophenyl)-1H-pyrazol-5(4H)-one (**3**)

3, 4-Difluorophenyl hydrazine **1** (10g, 69 mmol) and ethyl 4, 4, 4-trifluoro-3-oxobutanoate **2** (12.77g, 69 mmol) were mixed in a round bottom flask and heated to 130-135°C for 3h with constant stirring. After completion of reaction, cooled the reaction mass and triturated with diethyl ether (25ml). The solid residue was stirred for 5-10min and then filtered and dried to obtain 3-trifluoromethyl-1-(3, 4-difluorophenyl)-1H-pyrazol-5(4H)-one as an off white solid powder (16.48g, 90% yield, mp 186°C).

<sup>1</sup>H-NMR (300MHz, (CD<sub>3</sub>)<sub>2</sub>SO); δ 6.0 (s, 1H, CH), 7.6 (m, 2H, Ar-H), 7.8 (m, 1H, Ar-H), 13.0 (brs, 1H, enol OH).

<sup>19</sup>F NMR (282MHz, (CD<sub>3</sub>)<sub>2</sub>SO); δ -57.98, -131.99, -135.74

<sup>13</sup>C NMR (75MHz, (CD<sub>3</sub>)<sub>2</sub>SO); δ 85.82(C<sub>H</sub>), 111.67(CF<sub>3</sub>), 118.62(Ar-C<sub>H</sub>), 123.08(Ar-C<sub>H</sub>), 134.60(Ar-C<sub>H</sub>), 141.37(Ar-C<sub>H</sub>), 146.70(Ar-C<sub>H</sub>), 147.75(Ar-C<sub>H</sub>), 149.96(Ar-C<sub>H</sub>), 151.01(C<sub>H</sub>-OH)

Mass m/z: 265 (M<sup>+</sup>)

IR (KBr, cm<sup>-1</sup>); 3010 (=C-H aromatic stretch), 1619 (C=O cyclic lactum), 1599 (C=N stretch).

3.3 General methods of synthesis of 3-(trifluoromethyl)-1-(3, 4-difluorophenyl)-4-((1, 4-diphenyl-1H-pyrazol-3-yl)methylene)-1H-pyrazol-5(4H)-one derivatives **5a-d**, 3-(trifluoromethyl)-1-(3,4-

*difluorophenyl)-4-((4-oxo-4H-chromen-3-yl)methylene)-1H-pyrazol-5(4H)-one derivatives 7a-e and 4-((2-chloroquinolin-3-yl)methylene)-3-(trifluoromethyl)-1-(3,4-difluorophenyl)-1H-pyrazol-5(4H)-one derivatives 9a-e using conventional and non-conventional methods*

### 3.3.1 Conventional method (A)

Pyrazolone **3** (1 mmol) and respective carbaldehydes **4**, **6**, and **8** (1 mmol) were taken in ethanol (20-25ml) along with catalytic amount of acetic acid (0.1 mmol) and heated the reaction mass to reflux for about 14-26min as mentioned in (Table 1) to obtain respective products. After completion of reaction (monitored by TLC), the reaction mass was allowed to cool to room temperature. The precipitated solid was filtered and dried. Most of the compounds obtained in pure form without recrystallization.

### 3.3.2 Microwave method (B)

Starting material **3** and respective carbaldehyde analogues **4**, **6**, and **8** were taken in equimolar quantities along with catalytic amount of acetic acid in ethanol (1-2ml) in sealed tube and irradiated for 5 min at temperature 100-125°C in Biotage microwave. The progress of reaction was monitored by TLC. After completion of reaction, the reaction mass was allowed to cool to room temperature. The sealed tube was opened and the precipitated solid was filtered out and suck dried. Most of the compounds obtained in pure form without further recrystallization.

### 3.3.3 Ultrasounds method (C)

Both **3** and the respective starting carbaldehyde analogues **4**, **6** and **8** were taken in equimolar quantities along with catalytic amount of acetic acid in ethanol (5ml) in R.B. flask and reaction mass was subjected to ultrasonication for 10 min. The reaction temperature was monitored. After completion of reaction, precipitated solid was filtered and dried. Most of the compounds obtained in pure form without recrystallization. Some of the product which was not pure recrystallized from acetic acid as a solvent.

In conclusion, we have designed and synthesized a new series of novel multifluorinated pyrazolone-5-one derivatives using ultrasonicated and microwave assisted techniques and are more convenient, environmentally safe as they require less volume of solvent, short reaction span and better yields as compared to conventional techniques.

*The physical and spectral data of all the synthesized compounds 3-(trifluoromethyl)-1-(3,4-difluorophenyl)-4-((1,4-diphenyl-1H-pyrazol-3-yl)methylene)-1H-pyrazol-5(4H)-one derivatives 5a-d, 3-(trifluoromethyl)-1-(3,4-difluorophenyl)-4-((4-oxo-4H-chromen-3-yl)methylene)-1H-pyrazol-5(4H)-one derivatives 7a-e and 4-((2-chloroquinolin-3-yl)methylene)-3-(trifluoromethyl)-1-(3,4-difluorophenyl)-1H-pyrazol-5(4H)-one derivatives 9a-e are as follows.*

4-((4-(2,4-Dichloro-5-fluorophenyl)-1-phenyl-1H-pyrazol-3-yl)methylene)-3-(trifluoromethyl)-1-(3,4-difluorophenyl)-1H-pyrazol-5 (4H)-one (**5a**) :

Orange solid, mp 223-224°C. <sup>1</sup>H-NMR (300MHz, (CD<sub>3</sub>)<sub>2</sub>SO) δ 7.4 (s, 1H, CH), 7.5 (m, 1H, Ar-H), 7.6-7.7 (m, 4H, Ar-H), 7.9 (d, *J* = 3Hz, 1H, Ar-H), 8.0 (m, 3H, Ar-H), 8.2 (d, *J* = 6Hz, Ar-H), 10.2 (s, 1H, pyrazole ring), IR (KBr) ν cm<sup>-1</sup> 3001 (=C-H aromatic stretch), 1624 (C=O cyclic lactum), 1576 (C=N stretch).

4-((4-(4-Ethylphenyl)-1-phenyl-1H-pyrazol-3-yl)methylene)-3-(trifluoromethyl)-1-(3,4-difluorophenyl)-1H-pyrazol-5 (4H)-one (**5b**):

Orange solid, mp 197-199°C. <sup>1</sup>H-NMR (300MHz, (CD<sub>3</sub>)<sub>2</sub>SO) δ 1.28 (t, *J* = 7.7Hz, 3H, CH<sub>3</sub>), 2.8 (q, 2H, *J* = 7.3Hz, CH<sub>2</sub>), 7.4-7.5 (m, 3H, Ar-H), 7.5-7.6 (m, 5H, Ar-H), 7.7 (m, 2H, Ar-H), 8.0 (m, 3H, Ar-H), 10.1 (s, 1H, pyrazole ring), IR (KBr) ν cm<sup>-1</sup> 3010 (=C-H aromatic stretch), 1619 (C=O cyclic lactum), 1598 (C=N stretch).

3-(Trifluoromethyl)-1-(3,4-difluorophenyl)-4-((1,4-diphenyl-1H-pyrazol-3-yl)methylene)-1H-pyrazol-5(4H)-one (**5c**):

Orange solid, mp 208-209 °C. <sup>1</sup>H-NMR (300MHz, (CD<sub>3</sub>)<sub>2</sub>SO) δ 7.5 (m, 1H, Ar-H), 7.6-7.8 (m, 10H, Ar-H), 7.9-8.0 (m, 3H, Ar-H), 10.2 (s, 1H, pyrazole ring), IR (KBr) ν cm<sup>-1</sup> 3011 (=C-H aromatic stretch), 1688 (C=O cyclic lactum), 1595 (C=N stretch).

4-((4-(4-Chlorophenyl)-1-phenyl-1H-pyrazol-3-yl)methylene)-3-(trifluoromethyl)-1-(3,4-difluorophenyl)-1H-pyrazol-5 (4H)-one (**5d**) :

Orange solid, mp 235-237°C. <sup>1</sup>H-NMR (300MHz, (CD<sub>3</sub>)<sub>2</sub>SO) δ 7.4-7.5 (m, 2H, Ar-H), 7.6 (m, 1H, Ar-H), 7.6-7.7 (m, 6H, Ar-H), 7.9-8.0 (m, 3H, Ar-H), 10.0 (s, 1H, pyrazole ring), IR (KBr) ν cm<sup>-1</sup> 3100 (=C-H aromatic stretch),

1638 (C=O cyclic lactum), 1590 (C=N stretch).

4-((5, 7-Dichloro-4-oxo-4H-chromen-3-yl)-methylene)-3-(trifluoromethyl)-1-(3, 4-difluorophenyl)-1H-

Pyrazol-5 (4H)-one (**7a**):

Red solid, mp 248-251 °C. <sup>1</sup>H-NMR (300MHz, CDCl<sub>3</sub>) δ 7.2 (m, 1H, Ar-H), 7.7 (m, 1H), 7.8 (m, 2H, Ar-H), 8.2 (d, *J*=2.3Hz, 1H, Ar-H), 8.4 (s, 1H, =CH), 10.8 (s, 1H, CH-chromone ring), IR (KBr) v cm<sup>-1</sup> 3062 (=C-H aromatic stretch), 1670 (C=O cyclic lactum), 1639 (C=O), 1546(C=N stretch),

4-((6-Chloro-7-methyl-4-oxo-4H-chromen-3-yl)-methylene)-3-(trifluoromethyl)-1-(3,4-difluorophenyl)-1H-pyrazol-5 (4H)-one (**7b**):

Black solid, mp 239-241 °C. <sup>1</sup>H-NMR (300MHz, (CD<sub>3</sub>)<sub>2</sub>SO) δ 2.4 (s, 3H, CH<sub>3</sub>), 7.0 (d, *J*=8.8Hz, 1H, Ar-H), 7.8 (m, 1H, Ar-H), 7.9 (m, 1H, Ar-H), 8.1 (m, 1H, Ar-H), 8.4 (m, 1H, Ar-H), 9.1 (s, 1H, =CH), 12.0 (s, 1H, CH-chromone ring), IR (KBr) v cm<sup>-1</sup> 3004 (=C-H aromatic stretch), 1656 (C=O cyclic lactum), 1627 (C=O), 1569 (C=N stretch).

4-((6-Chloro-4-oxo-4H-chromen-3-yl)-methylene)-3-(trifluoromethyl)-1-(3,4-difluorophenyl)-1H-pyrazol-5 (4H)-one (**7c**):

Green solid, mp 256-257 °C. <sup>1</sup>H-NMR (300MHz, (CD<sub>3</sub>)<sub>2</sub>SO) δ 7.0 (d, *J* = 8.8Hz, 1H, Ar-H), 7.5 (m, 1H, Ar-H), 7.6 - 7.7 (m, 2H, Ar-H), 7.8-7.9 (m, 2H, Ar-H), 8.1 (m, 1H, Ar-H), 10.4 (s, 1H, CH-chromone ring), IR (KBr) v cm<sup>-1</sup> 3074 (=C-H aromatic stretch), 1688 (C=O cyclic lactum), 1668 (C=O), 1645 (C=N stretch).

3-(Trifluoromethyl)-1-(3, 4-difluorophenyl)-4-((6, 8-dimethyl-4-oxo-4H-chromen-3-yl)-methylene)-1H

-Pyrazol-5 (4H)-one (**7d**):

Red solid, mp 264-265 °C. <sup>1</sup>H-NMR (300MHz, CDCl<sub>3</sub>) δ 2.4 (s, 3H, CH<sub>3</sub>), 2.5 (s, 3H, CH<sub>3</sub>), 7.2 (s, 1H, Ar-H), 7.4 (s, 1H, Ar-H), 7.7 (m, 1H, Ar-H), 7.9 (m, 2H, Ar-H), 8.4 (s, 1H, =CH), 10.8 (s, 1H, CH-chromone ring), IR (KBr) v cm<sup>-1</sup> 3049 (=C-H aromatic stretch), 1694 (C=O cyclic lactum), 1655 (C=O), 1612 (C=N stretch).

3-(Trifluoromethyl)-1-(3,4-difluorophenyl)-4-((7-methyl-4-oxo-4H-chromen-3-yl)-methylene)-1H-pyrazol-5 (4H)-one (**7e**):

Red solid, mp 243-244 °C. <sup>1</sup>H-NMR (300MHz, (CD<sub>3</sub>)<sub>2</sub>SO) δ 2.5 (s, 3H, CH<sub>3</sub>), 7.2 (m, 1H, Ar-H), 7.4 (m, 1H, Ar-H), 7.5 (m, 1H, Ar-H), 7.6 (m, 1H, Ar-H), 7.8 (m, 1H, Ar-H), 8.1 (s, 1H, =CH), 8.2 (d, *J* = 7.9Hz, 1H), 10.8 (s, 1H, CH-chromone ring), IR (KBr) v cm<sup>-1</sup> 3008 (=C-H aromatic stretch), 1678 (C=O cyclic lactum), 1635 (C=O), 1600 (C=N stretch).

4-((2-Chloro-6-methoxyquinolin-3-yl)-methylene)-3-(trifluoromethyl)-1-(3,4-difluorophenyl)-1H-pyrazol-5(4H)-one (**9a**):

Black solid, mp 278-279 °C. <sup>1</sup>H-NMR (300MHz, (CD<sub>3</sub>)<sub>2</sub>SO) δ 4.0 (s, 3H, OCH<sub>3</sub>), 6.0 (s, 1H, =CH), 7.2 (dd, *J* = 9.0 & 2.0Hz, 1H, Ar-H), 7.4 (d, *J* = 2Hz, 1H, Ar-H), 7.6 (m, 2H, Ar-H), 7.8 (m, 2H, Ar-H), 8.2 (s, 1H, Ar-H), IR (KBr) v cm<sup>-1</sup> 3014 (=C-H aromatic stretch), 1695 (C=O cyclic lactum), 1661 (C=N stretch),

4-((2-Chloro-6-methylquinolin-3-yl)-methylene)-3-(trifluoromethyl)-1-(3, 4-difluorophenyl)-1H-pyrazol-5(4H)-one (**9b**):

Orange solid, mp 268-269 °C. <sup>1</sup>H-NMR (300MHz, (CD<sub>3</sub>)<sub>2</sub>SO) δ 2.4 (s, 3H, CH<sub>3</sub>), 6.0 (s, 1H, =CH), 7.15 (s, 1H, Ar-H), 7.4 (d, *J* = 6Hz, 1H, Ar-H), 7.6 - 7.7 (m, 2H, Ar-H), 7.8 - 8.0 (m, 2H, Ar-H), 8.3 (s, 1H, Ar-H), IR (KBr) v cm<sup>-1</sup> 3089 (=C-H aromatic stretch), 1687 (C=O cyclic lactum), 1651 (C=N stretch).

4-((2-Chloro-8-methylquinolin-3-yl)-methylene)-3-(trifluoromethyl)-1-(3, 4-difluorophenyl)-1H-pyrazol-5(4H)-one (**9c**):

Orange solid, mp 269-272 °C. <sup>1</sup>H-NMR (300MHz, (CD<sub>3</sub>)<sub>2</sub>SO) δ 2.4 (s, 3H, CH<sub>3</sub>), 6.0 (s, 1H, =CH), 7.2 (m, 1H, Ar-H), 7.5 (m, 1H, Ar-H), 7.6 (m, 2H, Ar-H), 7.7 - 8.0 (m, 2H, Ar-H), 8.3 (s, 1H, Ar-H), IR (KBr) v cm<sup>-1</sup> 3092 (=C-H aromatic stretch), 1678 (C=O cyclic lactum), 1650 (C=N stretch).

4-((2-Chloro-7-methylquinolin-3-yl)-methylene)-3-(trifluoromethyl)-1-(3, 4-difluorophenyl)-1H-pyrazol-5(4H)-one (**9d**):

Red solid, mp 264-265 °C. <sup>1</sup>H-NMR (300MHz, (CD<sub>3</sub>)<sub>2</sub>SO) δ 2.4 (s, 3H, CH<sub>3</sub>), 6.0 (s, 1H, =CH), 7.6 (m, 2H, Ar-H), 7.8 (m, 3H, Ar-H), 8.0 (m, 1H, Ar-H), 8.2 (s, 1H, Ar-H), IR (KBr) v cm<sup>-1</sup> 3034 (=C-H aromatic stretch), 1698 (C=O cyclic lactum), 1646 (C=N stretch).

Published by Canadian Center of Science and Education

4-((2-Chloroquinolin-3-yl)-methylene)-3-(trifluoromethyl)-1-(3,4-difluorophenyl)-1H-pyrazol-5(4H)-one (**9e**):

Red solid, mp 263-265°C. <sup>1</sup>H-NMR (300MHz, (CD<sub>3</sub>)<sub>2</sub>SO) δ 7.2 (m, 1H, Ar-H), 7.4(m, 1H, Ar-H), 7.6 -7.7 (m, 3H, Ar-H), 7.8 (m, 1H, Ar-H), 7.9 (m, 1H, Ar-H), 8.3 (s, 1H, Ar-H) , 10.0 (s, 1H, Ar-H), IR (KBr) v cm<sup>-1</sup> 3045 (=C-H aromatic stretch), 1678(C=O cyclic lactum), 1650 (C=N stretch).

### Acknowledgements

We greatly acknowledge to the C.E.O. Mr. C. S. N. Murthy of Aurigene Discovery Technologies Ltd. for constant encouragement and providing necessary facilities.

### References

63, 1082-1089.

Arnost, M., Pierce, A., Haar, E., Lauffer, D., Madden, J., Tanner, K., Green, J. (2010). 3-Aryl-4-(aryl hydrazano)-1H-pyrazol-5-ones: Highly ligand efficient and potent inhibitors of GSK3β. *Biorg. Med. Chem. Lett.*, 20, 1661-1664.

Breeuwer, R., Blacquière, G. (2003). Modeling, monitoring and control of continuous wave ultrasonic systems. *Ultrason. Sonochem.*, 10, 197-201.

Chloro chromones and 2-(1, 3-Diphenyl-1H-pyrazol-4-yl)-4-(2-hydroxyphenyl)-2, 3-dihydro-1, 5 benzothiazepines. *Korean J. Med. Chem.*, 10 (2) 84-96.

Chornous, V. O., Bratenko, M. K. & Vovk, M. V. (2004). Microwave-Assisted Synthesis of 3-(4-Pyrazolyl) propenoic Acids. *Synth Commun.*, 34(1) 79-83.

Dalvi, N. R., Karale, B. K., Gill, C. H. (2004). Environmentally benign synthesis of fluorinated pyrazolone derivatives and their antimicrobial activity. *Indian J. chem.* 1(8) 582-583.

Deng, Y., Lee, J. P., Ramamonjy, M. T., Snyder, J. K., Des Etages, S. A. , Kanada, D., Snyder, M.P., Turner, C. J. (2000). New Antimicrobial flavanones from *Physena madagascariensis*. *J. Nat. Product*,

Denny, W. A., Wilson, W. R., Ware, D. C., Atwell, G. J., Milbank, J. B., Stevenson, R. J. (2006). U.S. Patent , 7064117.

Gursoy, A., Demirayak, S., Capan, G., Erol, K., Vural, K. (2000). Synthesis and preliminary evaluation of new 5-pyrazolinone derivatives as analgesic agents. *Eur. J. Med. Chem.*, 35, 359-364.

Himly, M., Jahn-Schmid, B., Pittertschatscher, K., Bohle, B., Grubmayr, K., Ferreira, F., Ebner, H., Ebner, C. (2003). IgE-mediated immediate-type hypersensitivity to the pyrazolone drug Propyphenazone. *J. Allergy Clin. Immunol.*, 111, 882-888.

Karale, B. K., Chavan, V. P., Mane, A. S., Hangarge, R. V., Gill, C. H. & Shingare, M. S. (2000). Synthesis, Characterization and Antimicrobial Activities of some 2-(1, 3-Diphenyl-1H-pyrazol-4-yl)-3-

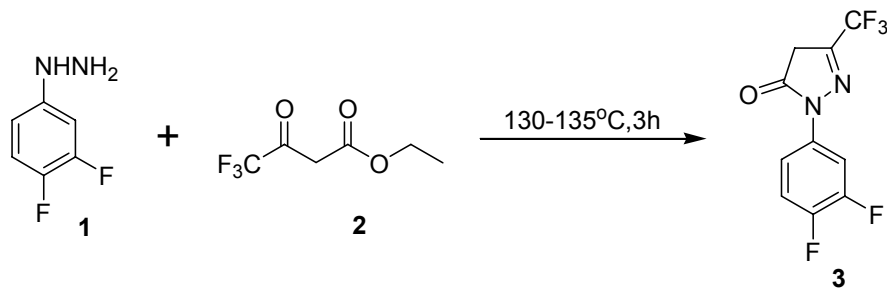
Khan, I. A., Avery, M. A., Burandt, C. L., Goins, D. K., Mikell, J. R., Nash, T. E., Azadegan, A., Walker, L. A. (2000). Anti-giardial Activity of Isoflavones from *Dalbergia frutescens* Bark. *J. Nat. Product*, 63, 1414-1416.

Maruthikumar, T. V., Reddy, V. P. & Rao, P. H. (2005). Microwave induced solvent – free synthesis of 1-aryl-2-(1E)-arylviny-4-arylmethylene-2-imidazolin-5-one. *Indian J. chem.* 44B, 1931.

Mohamoud, A., Chevalier, J., Davin-Regli, A., Barbe, J., Jean-Marie. (2006). Quinoline Derivatives as Promising Inhibitors of Antibiotic Efflux Pump in Multidrug Resistant Enterobacter Aerogenes Isolates. *Current Drug Targets*, 7, 843-847.

Mojtahedi, M., Javadpour, M., Abaee, M.S. (2008). Convenient ultrasound mediated synthesis of substituted pyrazolones under solvent- free condition. *Ultrason. Sonochem.*, 15, 828-832.

Muruganantham, N., Sivakumar, R., Anbalagan, N., Ginasekaran., Leonard, J. T. (2004). Synthesis,





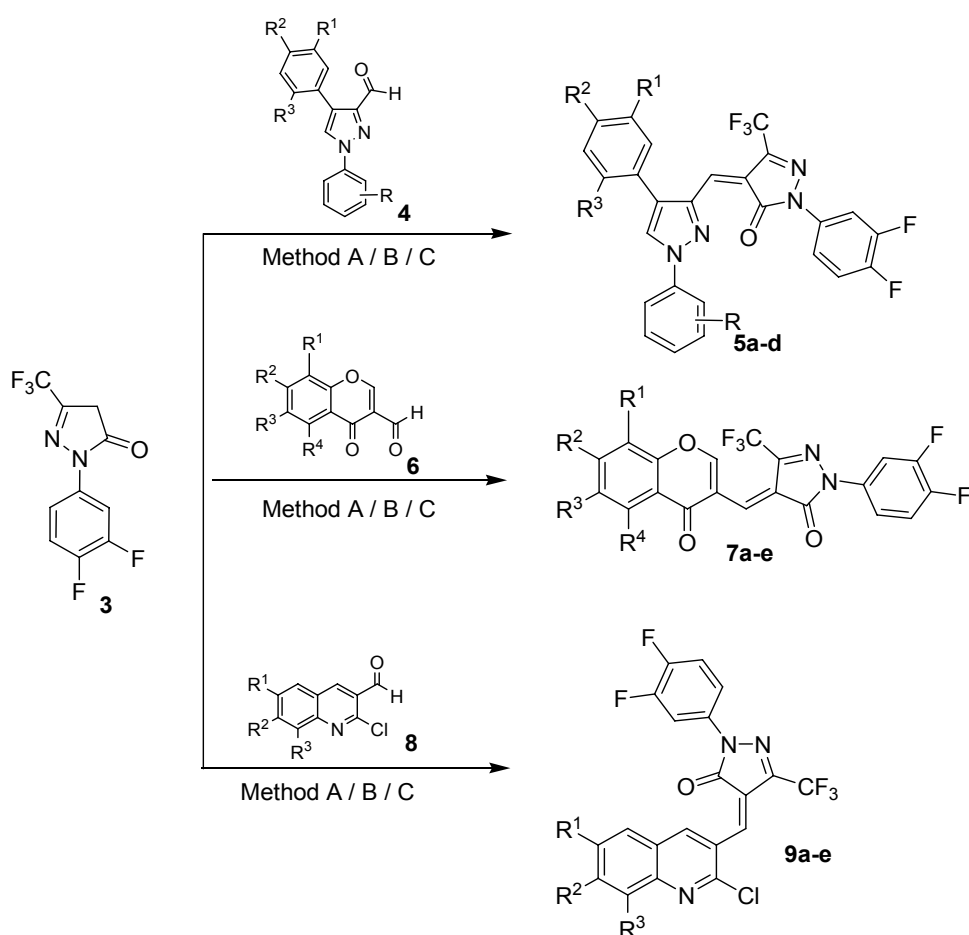
Anticonvulsant and Antihypertensive Activities of 8-Substituted Quinoline Derivatives. *Biol. Pharm. Bull.*, 27, 1683-1687.

Nasveld, P., Kitchener, S. (2005). Treatment of acute vivax malaria with tafenoquine. *Transactions of the Royal Society of Tropical Medicine and Hygiene*, 99, 2-5. Leatham, P. A., Bird, H. A., Wright, V., Seymour, D., Gordon, A., (1983). A double blind study of antrafenine, naproxen and placebo in osteoarthritis. *Eur. J. Rheumatol. Inflamm.*, 6, 209-211.

Rena, X. L., Hua, B., Yang, H. Z. (2005). Synthesis of small library containing substituted pyrazoles. *ARKIVOC*, 15, 59-67.

Venkat Ragavan, R., Vijaykumar, V., Suchetha Kumari, N. (2009). Synthesis of some novel bioactive 4 oxy/thio substituted-1H- pyrazol-5(4H)-ones via efficient cross-Claisen condensation. *Eur. J. Med. Chem.*, 44, 3852-3857.

Scheme 1



Scheme 2. Method A: EtOH, Cat. AcOH, reflux; Method B: EtOH, Cat. AcOH, Microwave; Method C: EtOH, Cat. AcOH, Sonication

Table 1. Time and yield data of newly synthesized compounds **5a-d**, **7a-e** and **9a-e** using conventional, non conventional techniques

Compound no.	R <sup>1</sup>	R <sup>2</sup>	R <sup>3</sup>	R <sup>4</sup>	Conventional		MW (t=5min)	US (t=10min)
					t (min)	% yield	% yield	% yield
<b>5a</b>	F	Cl	Cl	--	15	60	92	77
<b>5b</b>	H	Et	H	--	18	68	95	80
<b>5c</b>	H	H	H	--	14	67	93	77
<b>5d</b>	H	Cl	H	--	20	69	88	80
<b>7a</b>	H	Cl	H	Cl	21	71	88	80
<b>7b</b>	H	CH <sub>3</sub>	Cl	H	23	65	88	82
<b>7c</b>	H	H	Cl	H	24	68	93	78
<b>7d</b>	CH <sub>3</sub>	H	CH <sub>3</sub>	H	26	69	89	76
<b>7e</b>	H	CH <sub>3</sub>	H	H	23	71	93	78
<b>9a</b>	OMe	H	H	--	25	66	92	79
<b>9b</b>	CH <sub>3</sub>	H	H	--	24	59	89	84
<b>9c</b>	H	H	CH <sub>3</sub>	--	23	71	90	82
<b>9d</b>	H	CH <sub>3</sub>	H	--	25	70	92	88
<b>9e</b>	H	H	H	--	23	71	92	83

5a-c R = H; 5d, R = 4-Fluoro; MW = Microwave, US = Ultrasound sonication, t = time

# Quaternized Chitosan as an Efficient Catalyst for Synthesis of N-alkylthio-phthalimides

Zhang Hu (Corresponding author)

College of Science, Guangdong Ocean University

Zhanjiang 524088, Guangdong, China

E-mail: huzhangqyx@126.com

Sidong Li

College of Science, Guangdong Ocean University

Zhanjiang 524088, Guangdong, China

*Zhang Hu is grateful for financial support by the Program for Excellent Talents in Guangdong Ocean University (No. 0912118) and by the Natural Science Foundation of Guangdong Ocean University (No. 1012140).*

## Abstract

A practical and efficient synthesis of N-alkylthio-phthalimides by the reaction of N-chlorophthalimide with thiols catalyzed by quaternized chitosan was described. The reactions were carried out in relatively mild conditions, and a variety of N-alkylthio-phthalimides were efficiently prepared with moderate to good yields.

**Keywords:** Quaternized chitosan, Catalyst, N-Alkylthio-phthalimides

## 1. Introduction

The development of the N-alkylthio-phthalimides is of considerable interest because of the occurrence of many sulfur-containing compounds in many biologically important compounds (Tudge et al. 2006). Stable N-alkylthio-phthalimides have been used to prepare various N-(thioalkyl)amides (Ito et al. 2002; Ito et al. 2003),  $\alpha$ -phenylthio-ketones (Wang et al. 2004), disulfides (Wang et al. 2003; Vigushin et al. 2003).

Different methods for preparation of N-alkylthio-phthalimides have been introduced. The synthesis of alkyl and aryl sulfenimides by the reaction of sulfenyl chlorides with imides in the presence of a tertiary amine was reported by Behforouz (Behforouz & Kerwood, 1969). Klose synthesized some N-alkylthio-phthalimides by the reactions of thiols or disulfides with phthalimides in the presence of bromine in pyridine-acetonitrile solution (Klose et al. 1997).

Chitosan (CS) is a very abundant biopolymer obtained by the alkaline deacetylation of chitin that is present in the exoskeletons of crustaceans, the cuticles of insects and the cell walls of most fungi. Chitosan has been not only extensively used as a support for the preparation of heterogeneous catalysts, but also itself has been used as a catalyst for some reactions. Owing to its biodegradability and non-toxicity, chitosan is considered as an environmentally friendly catalyst (Guibal, 2005). Recently, quaternary ammonium salts covalently bound to chitosan was used as a heterogeneous catalyst for the synthesis of dimethyl carbonate (Zhao et al. 2007; Zhao et al. 2008). We report here that the quaternized chitosan (QCS) can catalyze the reaction of N-chlorophthalimide with thiols under relatively mild conditions yielding N-alkylthio-phthalimides.

## 2. Results and discussion

The QCS catalyst was prepared as shown in Scheme 1. Reaction of CS with glycidyl trimethyl ammonium chloride at 85 °C for 10 h in water afforded QCS with the degree of substitution (DS) of 47%. The IR spectra of CS and QCS were shown in Figure 1. Because chitosan with degree of deacetylation of 90% was used as the starting materials for the quaternization reactions, both spectra of CS and QCS appeared the amide carbonyl signal at 1645  $\text{cm}^{-1}$ . In the spectrum of QCS, the  $\text{NH}_2$ -associated peak at 1595  $\text{cm}^{-1}$  was weakened and a new peak at 1485  $\text{cm}^{-1}$  (attributes to the methyl groups in the ammonium) appeared. The characteristic peaks of primary alcohol and secondary alcohol between 1083 and 1150  $\text{cm}^{-1}$  did not change in QCS comparing with CS that showed the introduction of quaternary amino groups at  $\text{NH}_2$  sites on chitosan chains.

The coupling of N-chlorophthalimide with benzyl mercaptan was studied to identify a suitable catalytic system.

Catalysts pyridine, **CS** and **QCS** were employed to search for the suitable catalyst (as shown in Table 1). It was found that **QCS** was effective (entry 3). It is noteworthy that **QCS** demonstrated a comparable activity to that of the homogeneous catalyst pyridine under the same reaction conditions (entries 1 and 3). However, there was only a trace amount of the corresponding products obtained in the presence of **CS** (entry 2).

The catalytic efficacy of **QCS** for general N-S bond formation between thiols and N-chlorophthalimide was further evaluated. As summarized in Table 2, the coupling reactions were performed under the condition of 10 mol% **QCS** in acetonitrile, the corresponding N-alkylthio-phthalimides **4** were obtained in moderate to good yields. These results demonstrated that **QCS** could be used as a good promoter for the coupling reactions between thiols and N-chlorophthalimide.

In summary, we have demonstrated that the quaternized chitosan can be used as an efficient and general catalyst for the coupling reactions between N-chlorophthalimide and thiols at relatively mild conditions, and a variety of N-alkylthio-phthalimides were prepared with moderate to good yields.

### 3. Experimental

Melting points were obtained on a B-540 Büchi melting-point apparatus and are uncorrected. FT-IR spectra were recorded on a PerkinElmer Spectrum 100 spectrometer from KBr pellets.  $^1\text{H}$  NMR was measured with a Bruker 400 MHz spectrometer with tetramethylsilane (TMS) as an internal standard. LC-MS (ESI) spectra were recorded on a Finnigan Mat LCQ mass Spectrophotometer 214 nm using a Betasil  $\text{C}_{18}$  (3  $\mu\text{m}$ , 100  $\text{\AA}$ , 3 $\times$ 50 mm) column. Chitosan with a degree of deacetylation of 90% was purchased from Shanghai Guoyao Biochemical Co. Ltd (China). Glycidyl trimethyl ammonium chloride was purchased from Dongying Guofeng Chemical Co. Ltd (China). N-chlorophthalimide was prepared according to the reported methods (Mintz & Walling, 1969; Zimmer & Audrieth, 1954). The thiols were purchased from Jiande Xingfeng Chemical Co., Ltd (China). Unless otherwise stated, all other chemicals and reagents used in this study were reagent grade.

#### Preparation of the quaternized chitosan (**QCS**)

Chitosan (2.0 g, 12.1 mmol) was dispersed in isopropyl alcohol (20 mL). Glycidyl trimethyl ammonium chloride (7.34 g, 48.4 mmol) was dissolved in water (5 mL) and added to the chitosan suspension. The mixture was stirred at 85  $^{\circ}\text{C}$  for 10 h. The resulting polymer was precipitated by acetone, dialyzed, and finally freeze-dried to obtain **QCS**. IR ( $\text{cm}^{-1}$ ):  $\nu$  3433 (O-H), 2870 (C-H), 1645 (amide I), 1595 (amide II), 1485 (C- $\text{CH}_3$ ), 1150 ( $\text{C}^2\text{-OH}$ ), 1083 ( $\text{C}^1\text{-OH}$ ).

General procedure for the coupling reaction of N-chlorophthalimide with benzyl mercaptan catalyzed by different catalysts

N-chlorophthalimide (0.5 g, 2.75 mmol) was dissolved in acetonitrile (10 mL). The catalyst (0.25 mmol) was added under an argon atmosphere and the solution was stirred and heated to 80  $^{\circ}\text{C}$ . Benzyl mercaptan (2.5 mmol) in acetonitrile (5 mL) was added dropwise under an argon atmosphere. The mixture was kept at 80  $^{\circ}\text{C}$  for one hour. Then the reaction mixture was allowed to cool to room temperature. The resulting mixture was filtered and the residue was washed with acetonitrile. The filtrate was evaporated under reduced pressure and the residue was purified by flash column chromatography on silica gel.

General procedure for the coupling reaction of N-chlorophthalimide with thiols catalyzed by **QCS**

N-chlorophthalimide (0.5 g, 2.75 mmol) was dissolved in acetonitrile (10 mL). The **QCS** catalyst (0.055 g, 0.25 mmol) was added under an argon atmosphere and the solution was stirred and heated to 80  $^{\circ}\text{C}$ . Thiol (2.5 mmol) in acetonitrile (5 mL) was added dropwise under an argon atmosphere. The mixture was kept at 80  $^{\circ}\text{C}$  for one hour. Then the reaction mixture was allowed to cool to room temperature. The resulting mixture was filtered and the residue was washed with acetonitrile. The filtrate was evaporated under reduced pressure and the residue was purified by flash column chromatography on silica gel. Compounds **4** were characterized by electrospray LC-MS and  $^1\text{H}$  NMR.

N-(Phenylthio)phthalimide (**4a**): White solid;  $^1\text{H}$  NMR (400MHz,  $\text{DMSO-}d_6$ )  $\delta$ : 7.91-7.93 (2H, m), 7.81-7.85 (2H, m), 7.32-7.41 (4H, m), 7.33-7.35 (1H, m). LC-MS (ESI) calcd. for  $\text{C}_{14}\text{H}_9\text{NO}_2\text{S}$   $[\text{M}]^+$  255.3, found 255.6.

N-(4-Chlorophenylthio)phthalimide (**4b**): White solid;  $^1\text{H}$  NMR (400MHz,  $\text{DMSO-}d_6$ )  $\delta$ : 7.91-7.92 (2H, m), 7.82-7.84 (2H, m), 7.43-7.46 (4H, m). LC-MS (ESI) calcd. for  $\text{C}_{14}\text{H}_8\text{ClNO}_2\text{S}$   $[\text{M}]^+$  289.7, found 289.5.

N-(*p*-Tolylthio)phthalimide (**4c**): White solid;  $^1\text{H}$  NMR (400MHz,  $\text{DMSO-}d_6$ )  $\delta$ : 7.90-7.92 (2H, m), 7.81-7.83 (2H, m), 7.29-7.34 (4H, m), 2.26 (3H, s). LC-MS (ESI) calcd. for  $\text{C}_{15}\text{H}_{11}\text{NO}_2\text{S}$   $[\text{M}]^+$  269.3, found 269.5.

N-(Benzylthio)phthalimide (**4d**): White solid;  $^1\text{H}$  NMR (400MHz,  $\text{DMSO-}d_6$ )  $\delta$ : 7.88-7.91 (2H, m), 7.76-7.82 (2H, m), 7.37-7.43 (5H, m), 4.11 (2H, s). LC-MS (ESI) calcd. for  $\text{C}_{15}\text{H}_{11}\text{NO}_2\text{S}$   $[\text{M}]^+$  269.3, found 269.5.

N-(Cyclohexylthio)phthalimide (**4e**): White solid;  $^1\text{H}$  NMR (400MHz, DMSO- $\text{d}_6$ )  $\delta$ : 7.86-7.90 (2H, m), 7.76-7.81 (2H, m), 2.89 (1H, m), 1.31-1.93 (10H, m). LC-MS (ESI) calcd. for  $\text{C}_{14}\text{H}_{15}\text{NO}_2\text{S}$   $[\text{M}]^+$  261.3, found 261.6.

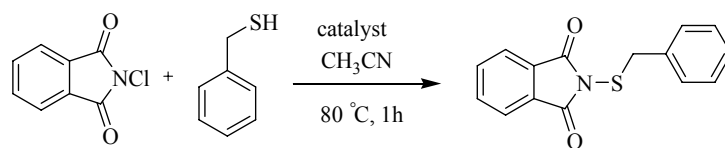
N-(n-Hexylthio)phthalimide (**4f**): White solid;  $^1\text{H}$  NMR (400MHz, DMSO- $\text{d}_6$ )  $\delta$ : 7.86-7.91 (2H, m), 7.76-7.81 (2H, m), 2.91-2.93 (2H, t,  $J = 12.0$  Hz), 1.31-1.61 (8H, m), 0.91-0.92 (3H, t,  $J = 10.0$  Hz). LC-MS (ESI) calcd. for  $\text{C}_{14}\text{H}_{17}\text{NO}_2\text{S}$   $[\text{M}]^+$  263.4, found 263.7.

N-(n-Butylthio)phthalimide (**4g**): White solid;  $^1\text{H}$  NMR (400MHz, DMSO- $\text{d}_6$ )  $\delta$ : 7.86-7.91 (2H, m), 7.77-7.81 (2H, m), 2.90-2.93 (2H, t,  $J = 12.0$  Hz), 1.54-1.61 (2H, m), 1.33-1.40 (2H, m), 0.91-0.93 (3H, t,  $J = 8.0$  Hz). LC-MS (ESI) calcd. for  $\text{C}_{12}\text{H}_{13}\text{NO}_2\text{S}$   $[\text{M}]^+$  235.3, found 235.5.

N-(n-Propylthio)phthalimide (**4h**): White solid;  $^1\text{H}$  NMR (400MHz, DMSO- $\text{d}_6$ )  $\delta$ : 7.86-7.91 (2H, m), 7.78-7.81 (2H, m), 2.91-2.93 (2H, t,  $J = 12.0$  Hz), 1.56-1.63 (2H, m), 0.92-0.94 (3H, t,  $J = 12.0$  Hz). LC-MS (ESI) calcd. for  $\text{C}_{11}\text{H}_{11}\text{NO}_2\text{S}$   $[\text{M}]^+$  221.3, found 221.6.

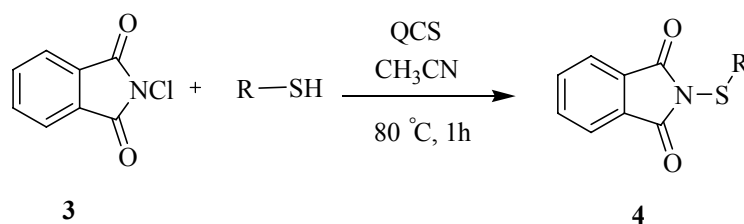
## References

- Behforouz, M. & Kerwood, J. E. (1969). Alkyl and aryl sulfenimides. *J. Org. Chem.*, 34, 51-55.
- Guibal, E. (2005). Heterogeneous catalysis on chitosan-based materials: a review. *Prog. Polym. Sci.*, 30, 71-109.
- Ito, M., Okui, H., Nakagawa, H., et al. (2002). Efficient N-sulfonylation of dihydropyrrole derivatives using N-sulfonylphthalimides. *Heterocycles*, 57, 909-914.
- Ito, M., Okui, H., Nakagawa, H., et al. (2003). Synthesis and insecticidal activity of novel dihydropyrrole derivatives with N-sulfanyl, sulfanyl, and sulfonyl moieties. *Bioorg. Med. Chem.*, 11, 489-494.
- Klose, J., Reese, C. B., Song, Q. (1997). Preparation of 2-(2-cyanoethyl)sulfanyl-1H-indole-1,3-(2H)-dione and related sulfur-transfer agents. *Tetrahedron*, 53, 14411-14416.
- Mintz, M. J. & Walling, C. (1969). *t*-Butyl hypochlorite. *Org. Syn.*, 49, 9-11.
- Tudge, M., Tamiya, M., Savarin, C., et al. (2006). Development of a novel, highly efficient halide-catalyzed sulfonylation of indoles. *Org. Lett.*, 8, 565-568.
- Vigushin, D. M., Brooke, G., Willows, D., et al. (2003). Pyrazino[1,2- $\alpha$ ]indole-1,4-diones, simple analogues of gliotoxin, as selective inhibitors of geranylgeranyltransferase I. *Bioorg. Med. Chem. Lett.*, 13, 3661-3663.
- Wang, W., Li, H., Wang, J., et al. (2004). Direct, organocatalytic  $\alpha$ -sulfonylation of aldehydes and ketones. *Tetrahedron Lett.*, 45, 8229-8231.
- Wang, X., Hu, W., Ramasubramaniam, R., et al. (2003). Formation, characterization, and Sub-50-nm patterning of organosilane monolayers with embedded disulfide bonds: An engineered self-assembled monolayer resist for electron-beam lithography. *Langmuir*, 19, 9748-9758.
- Zimmer, H. & Audrieth, L. F. (1954). Tertiary butyl hypochlorite as an N-chlorinating agent. *J. Am. Chem. Soc.*, 76, 3856-3857.
- Zhao, Y., He, L. N., Zhuang, Y. Y., et al. (2008). Dimethyl carbonate synthesis via transesterification catalyzed by quaternary ammonium salt functionalized chitosan. *Chin. Chem. Lett.*, 19, 286-290.
- Zhao, Y., Tian, J. S., Qi, X. H., et al. (2007). Quaternary ammonium salt-functionalized chitosan: An easily recyclable catalyst for efficient synthesis of cyclic carbonates from epoxides and carbon dioxide. *J. Mol. Catal. A: Chem.*, 271, 284-289.

Table 1. The coupling reaction of N-chlorophthalimide with benzyl mercaptan in the presence of the catalysts <sup>a</sup>

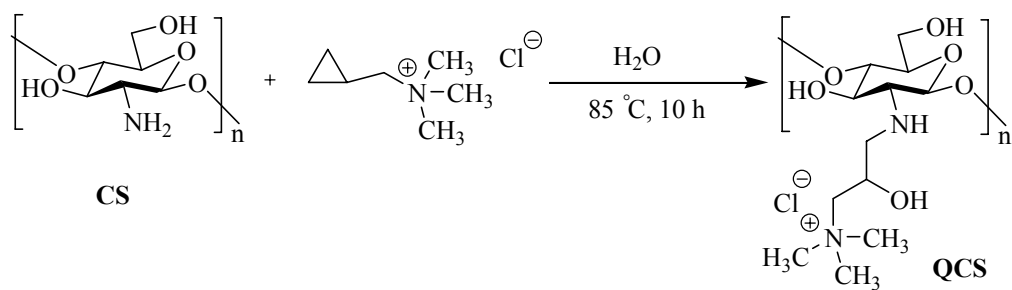
Entry	Catalyst	Yield (%) <sup>b</sup>
1	pyridine	35
2	<b>CS</b>	4
3	<b>QCS</b>	68

<sup>a</sup>Reaction conditions: benzyl mercaptan (1.0 equiv), N-chlorophthalimide (1.1 equiv), catalyst (10 mol%), in acetonitrile under N<sub>2</sub> atmosphere at 80 °C for 1 h. <sup>b</sup>Isolated yield.

Table 2. N-alkylthio-phthalimids prepared from N-chlorophthalimide and thiols catalyzed by **QCS** <sup>a</sup>

Entry	Product	R	Yield (%) <sup>b</sup>	MW (found)	mp (°C)
1	<b>4a</b>		76	255.6 (M <sup>+</sup> )	157-159
2	<b>4b</b>		75	289.5 (M <sup>+</sup> )	177-179
3	<b>4c</b>		71	269.5 (M <sup>+</sup> )	192-194
4	<b>4d</b>		68	269.5 (M <sup>+</sup> )	165-167
5	<b>4e</b>		66	261.6 (M <sup>+</sup> )	91-92
6	<b>4f</b>		75	263.7 (M <sup>+</sup> )	63-65
7	<b>4g</b>		64	235.5 (M <sup>+</sup> )	68-70
8	<b>4h</b>		57 <sup>c</sup>	221.6 (M <sup>+</sup> )	74-76

<sup>a</sup>Reaction conditions: thiol (1.0 equiv), N-chlorophthalimide (1.1 equiv) and catalyst **QCS** (10 mol%), in acetonitrile under N<sub>2</sub> atmosphere at 80 °C for 1 h. <sup>b</sup>Isolated yield. <sup>c</sup>welded ampoule was used to avoid the less yield due to the low boiling point of n-propanethiol.



Scheme 1

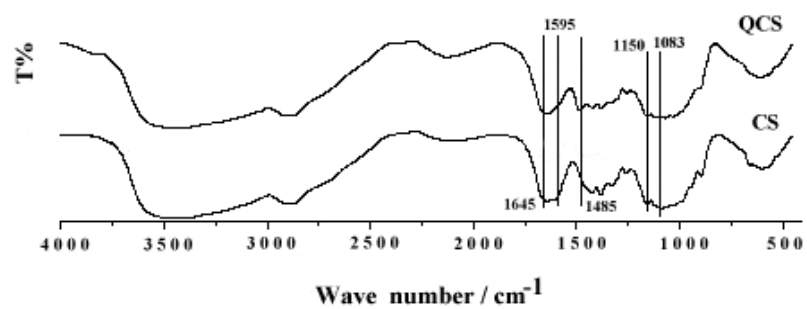


Figure 1. FT-IR spectra for chitosan (CS) and the quaternized chitosan (QCS)

# Dimensional Stability, Thermal Degradation and Termite Resistant Studies of Chemically Treated Wood

Juthika Sonowal (Corresponding author)

Department of Chemistry, Dibrugarh University

Dibrugarh- 786004, Assam, India

Tel: 91-995-443-5710 E-mail: swjuthika@yahoo.co.in

P.K. Gogoi

Department of Chemistry, Dibrugarh University

Dibrugarh- 786004, Assam, India

Tel: 91-943-513-1158 E-mail: dr\_pradip@yahoo.com

## Abstract

The efficacy of the preservative chemicals for the treatment of wood samples was evaluated in ground contact against termite and fungus. The wood samples treated with boric acid followed by maleic anhydride, copper acetate, sodium salt of diethyldithiocarbamate and kerosene showed higher dimensional stability efficiency in terms of anti-shrink efficiency (ASE), bulk co-efficient (BC) and weight percent gain (WPG). The treated wood samples showed higher strength properties such as modulus of rupture (MOR) and modulus of elasticity (MOE) than the untreated sample. The treated samples could resist from termite and fungal attack and also extend the service life.

**Keywords:** Dimensional stability, Anti-shrink efficiency, Modulus of rupture, Modulus of elasticity, Termite resistance

## 1. Introduction

Wood is one of the most important renewable bioresources used by mankind since prehistoric days. It was used for making weapons, in constructing shelters and as fuel. Compared to other lignocellulosic materials, it has better mechanical strength and materials made of wood are of better aesthetic look. Even in this age of novel composite materials, wood is still a prized material in making furniture and used extensively in building construction. Wood contains mainly cellulose, hemicelluloses and lignin, the amount varies from species to species. However, like other lignocellulosic materials, wood is prone to degradation and dimensional variation on exposure to moisture, heat and biological agents like fungi, termite and wood boring insects which make it unfit for further use. In tropical and temperate region, termite pose the serious threat to untreated timber and other lignocellulosic materials used in various constructions. To protect wood from degradation and enhance its working life, various methods have been employed (Connell, M., 1991) during last hundred years, e.g. treating with mineral oil, coal tar, heating in hydrocarbon oil and treatment with CCA (copper-chrom-arsenic). Use of newly developed organochlorins, which are quite cheap and easy to produce, like aldrin, dieldrin, chlordane and sodium pentachlorophenoxide (Logan, J.W.M. & Buckley, D.S., 1991) can control termite upto 30 years. Rowell reported (Rowell, R. M., 1991) various methods of treatment of wood to protect it from dimensional change and attack by insects. Because of their undesirable side effects and long persistence in soil, of late many of these organochlorine formulations have been removed from market. However, if some new formulations are devised, which may be cost effective, easy to prepare and apply, having low mobility in soil and relatively harmless in low concentration and adequately fixed in wood followed by sealing with hydrophobic agents to prevent leaching in contact with ground, it would be an ideal inhibitor. Further, to make it having a wide spectrum of activity some other chemicals in optimum concentration may be used in certain sequence.

Termite, fungi and other insects can degrade lignocellulosic materials as they contain the enzyme *cellulase*, which can decompose cellulose to glucose, a source of biochemical energy. If wood can be made resistant to degradation by heat and moisture and application of some active principle to inhibit the activity of *cellulase* enzyme, wood can be protected with enhanced working life. In this paper, we report the effect of treatment of wood with less toxic chemicals, in low concentrations, like boric acid, maleic anhydride, copper acetate, sodium



salt of diethyldithiocarbamate and kerosene in arresting dimensional change and biodegradation. We also report a protocol for optimum use of chemicals in a particular sequence to get better results.

## 2. Experimental

### 2.1 Raw material

The second class wood samples for the experiments were collected from the wood mart at Dibrugarh, Assam. The wood samples were prepared for the treatment approximately of size 10.5 x 3.0 x 1.5 cm (length x breadth x thickness).

The chemicals used for the treatment were:

- (a) Boric acid (BA, Rankem, 5% w/v in water)
- (b) Copper acetate (CA, Rankem, 5% w/v in water)
- (c) Maleic anhydride (MA, Merk, 5% w/v in 1:1 DMF and MeOH)
- (d) Diethyldithiocarbamate, Na-salt (DEDTC, BDH, 5% w/v in water)
- (e) Kerosene (250ml)

### 2.2 Chemical treatment

For chemical treatment the samples were extracted separately with water followed by methanol and dichloromethane for 3 hrs and then oven dried at  $100 \pm 5^\circ\text{C}$  so that at least 20% moisture remains inside the sample. Unlike other materials, wood is hygroscopic and exchange moisture with the surroundings as water can remain in the cell capillary and cell walls (Beauford, W., 1991). Microbial degradation can occur if moisture is more than 20% of the dry weight. The remaining 20% moisture is essential for diffusion of water soluble inhibitor. The chemical treatment of the wood samples were carried out as follows:

- (a) For maleic anhydride treatment, the wood samples were dipped in maleic anhydride solution (in 1:1 DMF and MeOH) for seven days and then air-dried followed by oven drying at  $100 \pm 5^\circ\text{C}$  for two hours.
- (b) Other wood samples were first treated with the solution of boric acid for seven days and then air-dried followed by oven drying at  $100 \pm 5^\circ\text{C}$  for two hours and then again treated with copper acetate solution for seven days and then oven dried. After the treatment of boric acid and copper acetate, the samples were again treated with sodium salt of diethyldithiocarbamate solution for seven days.
- (c) Another sample was treated with boric acid followed by maleic anhydride, copper acetate and sodium salt of diethyldithiocarbamate in a manner as described in (b) above.

After the completion of chemical treatment, all the samples were treated with kerosene for one day and air-dried.

### 2.3 Evaluation of properties of treated and untreated samples

The dimensional parameters such as volumetric swelling, anti-shrink efficiency (ASE), bulk co-efficient (BC) were calculated by reported method (Schneider, M.H. & Brebner, K.I. 1985).

The weight percent gain (WPG) were determined by using the following relation:

$$\text{WPG} = (W_t - W_u) \times 100/W_u$$

Where,  $W_t$  and  $W_u$  were the oven dried weight of treated and untreated samples in gram.

The volumetric swelling coefficient (S) and anti shrink efficiency (ASE) were calculated by the following relations:

$$S_{u,t} = (V_w - V_{u,t}) \times 100/V_{u,t}$$

Where,

$V_w$  = swollen volume of wood sample after treatment in  $\text{cm}^3$

$V_{u,t}$  = oven-dried volume of either treated and untreated samples in  $\text{cm}^3$

$$\text{ASE} = (S_u - S_t) \times 100/S_u$$

Where  $S_u$  and  $S_t$  were the volumetric swelling co-efficiency based on the oven dried volume of the untreated and treated sample in percentage.

Bulk- coefficient (BC) were determined from the following relation:

$$\text{BC} = (V_t - V_u) \times 100/V_u$$

Where  $V_t$  and  $V_u$  were oven-dried volume of treated and untreated samples in  $\text{cm}^3$

Modulus of rupture (MOR) and modulus of elasticity (MOE) were determined according to IS: 2380 (1977).

$$\text{MOR} = 3PL / 2bd^2$$

Where P is the maximum load in kg, L is the length of span in cm, b is the width of the specimen in cm and d is the depth of the specimen in cm.

$$\text{MOE} = P_1 L^3 / 4bd^3 Y$$

Where  $P_1$  is the load in kg at the proportionality limit, Y is the central deflection at limit of proportionality load in cm.

#### Cellulase inhibition test

In each of five 250ml beakers (marked 1 to 5), 60ml of phosphate buffer ( $\text{pH} 6.47$ ) were taken, to each of which 1g. of wood powder (WP) were added. 5% (w/v) of each of boric acid (BA), copper acetate (CA), sodium salt of diethyldithiocarbamate (DEDTC) and a mixture of 5% (w/v) each of BA, CA and DEDTC were added in the beaker no.2, 3, 4 and 5 respectively (table 2). To each beaker 6ml (300 units) of *cellulase* enzyme (Aldrich) were added. After adding chemicals and *cellulase* enzyme, the beakers were covered for 24 hours at room temperature, after which they were heated at  $60^\circ\text{C}$  for 1 hr in water bath to stop the *cellulase* activity. After cooling to room temperature, the solutions were filtered and made up the volume to 100ml and glucose was estimated by Fehling solution using methylene blue indicator relative to a standard glucose solution.

#### Thermal studies

Simultaneous thermogravimetry and differential thermal analysis of treated and untreated wood samples were carried out using Perkin Elmer Pyris Dimond TG/DTA instrument at a heating rate of  $20^\circ\text{C} / \text{min}$  and the temperature range from  $40 - 500^\circ\text{C}$  in static atmosphere. The weight of the samples were taken in the range of 5.0 – 10.34 mg and  $\alpha$ - alumina was used as a reference material.

#### SEM studies

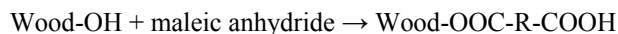
To study the penetration of chemicals into wood structure, the SEMs of treated and untreated samples were recorded at Indian Institute of Technology, Guwahati, on a LEO 1430VP Scanning Electron Microscope.

#### Graveyard test

The evaluation of termite resistance capacity was carried out as per reported method (Kumar *et.al.* 1998). The treated and untreated samples were buried in ground under normal condition. After one year burial test, they were exhumed and examined visually.

### 3. Results and discussion

Table 1 shows the dimensional variations of wood samples treated with different chemicals and their combinations in terms of antishrink efficiency (ASE) along with bulk coefficient (BC) and weight percent gain (WPG). The sample treated with only maleic anhydride gave good bulk coefficient and weight percent gain because of reaction of the dicarboxylic acid anhydride and OH group of the cellulose to give esterified wood with carbonyl group resulting enhanced dimensional stability as follows (Matsuda, H., 1996)



However, the maximum ASE (58.14%) at the level of 27.82% WPG was shown by the sample treated with boric acid followed by maleic anhydride, copper acetate, sodium salt of DEDTC and kerosene. The sample so treated also showed total protection from termite compared to only maleic anhydride and kerosene treated sample. Similarly the sample treated with boric acid, copper acetate and DEDTC showed good biodegradation inhibition but the dimensional stability was not optimum. Lignocellulosic materials are degraded by termites and fungus which contain *cellulase* enzyme. In the mechanism (White, A.R., 1982) of the *cellulase* action, it is found that the *Tricoderma cellulase* consists of three enzyme systems, (a) endoglucanase (EG), (b) cellulohydrolase (CBH) and (c)  $\beta$ -glucosidase ( $\beta$ -G). EG first attack the cellulose fiber and breaks the glucosyl bond of the glucan chain and expose the reducing and non-reducing end. CBH then attack the free non-reducing chain end and cellobiose is released where it is converted to glucose by  $\beta$ -G and the synergistic degradation of cellulose is completed. The inhibition of *cellulase* activity and dimensional stabilization may be concurrently considered from two angles: (i) application of *cellulase* activity inhibitor and (ii) chemical modification of the -OH group of the non-reducing chain end, the site of CBH attack; the -OH groups are not only enzyme attack sites but also water absorption sites through hydrogen bonding, which facilitate swelling. In the *cellulase* activity experiment (table 2) it was observed that in presence of boric acid and copper acetate the *cellulase* activity is slightly reduced. It was

reported earlier that (Vyas *et.al.*, 2005) in alkaline media *cellulase* activity is enhanced compared to acidic media. Hence presence of boric acid and copper acetate – which may hydrolyse to give slightly acidic medium due to presence of acetic acid, inhibit the *cellulase* activity. But in presence of boric acid and copper dithiocarbamate, there is substantial decrease of *cellulase* activity as seen from the amount of glucose released.

From the thermal analysis data (table 3), it was seen that compared to untreated sample, there is substantial decrease in both major decomposition temperature range and percent weight loss for the treated samples. The active decomposition temperature was highest for maleic anhydride treated sample indicating increased bulking and OH group modification to give good dimensional stability. In other treated samples the active decomposition temperature is similar to untreated one, which could be due to easy decomposition of DEDTC during respective major decomposition temperature ranges. Although only maleic anhydride treated sample gave good dimensional stability in terms of ASE, BC, MOR and MOE (table 4) it failed to give total termite protection.

From the measurement of strength (MOR) and stiffness (MOE) of both untreated and treated samples, it was observed that there is increase in the modulus of rupture and modulus of elasticity of the treated samples. It could be due to chemical modification of cellulose by maleic anhydride and physical bulking by copper acetate, boric acid and DEDTC. There is good correlation of dimensional characteristics, *cellulase* inhibition activity, thermal property and mechanical properties of chemically treated wood.

Scanning electron micrographs showed the penetration of chemicals inside the wood that resulted in bulking of the cell wall to give dimensionally stabilized wood. Changes in internal structure of the cell wall due to the presence of chemicals were observed by SEM studies. The white patches which were seen in the micrograph were the chemicals observed on the cell walls of the wood (Fig.6)

After the one year of graveyard test, it was observed that (Fig.7) compared to untreated sample the sample treated only with MA was slightly damaged by termite followed by BA, CA and DEDTC and the sample treated with BA, MA, CA and DEDTC was not at all damaged. Boric acid, copper salts and dithiocarbamate all have antibacterial and antifungal activity. Because of antifungal, bacteriocidal and insecticidal activity, dimethyl dithiocarbamate of copper has been patented (Battershell *et al.*, 1998) in U.S. as wood preservative. Boric acid has been reported as stomach poison for insects (Yamaguchi, H., 2003). Similarly, transition metal compounds of dithiocarbamates and dithiophosphinates are known antifungal and antibacterial agents (Kalita, *et.al.* 2002) and the mode of action being inhibition of certain vital enzymes by the sulphur donors, the  $\text{Cu}^{2+}$  also can inhibit action of several biomolecules. Dithiocompounds also inhibit the enzyme *actylcholinesterase* (Gruzdyev *et al.*, 1980). As these chemicals are easily leached in contact with water, kerosene is used to create hydrophobic environment inside and on the surface of the samples to prevent leaching of preservatives and stop penetration of moisture, which also help to retain dimensional stability. Further, petroleum oils like kerosene have low toxicity to warm blooded animals but prevents metabolism in egg or insect body. The oil can easily penetrate through the wax scale and cuticles, can cause coagulation of the cytoplasm and inhibit the course of enzyme process (Gruzdyev *et.al.*, 1980). Compared to other chemical methods of treatment of wood, the present method appears to be better in the sense that the chemicals are cost effective, can be handled and applied easily and less toxic at low concentration but at the same time give very good results.

#### 4. Conclusion

Dimensional stability and resistance of biodegradation by chemical treatment of lignocellulosic materials depends upon the type of chemicals and their penetration and how much hydroxyl groups are modified to give adequate cross-linking and bulkiness. From the present studies, it may be concluded that wood samples treated with boric acid followed by maleic anhydride, copper acetate, diethyldithiocarbamate and kerosene were more dimensional stability and can resist termite and fungal attack better where kerosene creates hydrophobic environment inside and surface of the samples.

#### References

- Battershell, R. D., Jacobson, B. M., Abraham, A. C., Pereira, B. M. & Kempf, J. V. (1998). *United States Patent No.5731036*. March 24.
- Beauford, W. (1991). In-situ and supplementary treatments using solid water diffusible preservatives. In R. Thompson (Ed.), *The chemistry of wood preservation* (pp.53-68). The Royal Society of Chemistry, Cambridge.
- Bureau of Indian Standards. (1977). Method of test for wood particle boards and boards from lignocellulosic materials. *Indian Standard Institution. IS : 2380*. New Delhi.

- Connell, M. (1991). Industrial wood preservatives- The history, development, use, advantages and future trends. In R. Thompson (Ed.), *The chemistry of wood preservation* (pp.16-33). The Royal Society of Chemistry, Cambridge.
- Gruzdyev, G.S., Zinchenko, V.A., Kalinin, V.A., & Slovtsov, R.I. (1980). Means for controlling plant pests. In G. S. Gruzdyev (Ed), *The chemical protection of plants*, (pp. 236-239). Mir Publishers, Moscow.
- Gruzdyev, G.S., Zinchenko, V.A., Kalinin, V.A., & Slovtsov, R.I. (1980). Fungicides. In G. S. Gruzdyev (Ed), *The chemical protection of plants* (pp. 280-288). Mir Publishers, Moscow.
- Kalita, D. K., Das, D. K. & Gogoi P. K. (2002). Synthesis, characterization and antibacterial activity of 2-methylpiperazine dithiocarbamates of Ru(III), Rh(III), Pd(II), Os(III) and Pt(II). *Proceedings of National Academy of Sciences, India*. 72(A), 7-13.
- Kumar, S., Kainth, P. S. & Chauhan, K. S. (1998). Natural durability and graveyard performance of preservative treated bamboos. *Journal of Timber Development Association (India)*. 44(3), 17-24.
- Logan, J. W. M. & Buckley, D. S. (1991). Subterranean termite control in buildings. In R. Thompson (Ed.). *The chemistry of wood preservation*, (pp. 294-305). The Royal Society of Chemistry, Cambridge.
- Matsuda, H. (1996). Chemical modification of solid wood. In David N. -S. (Ed.). *Chemical modification of lignocellulosic material*, (pp.169). Marcel Dekker, New York.
- Rowell, R. M. (1991). Chemical modification of wood. In David N. -S. Hon & N. Shiraishi (Eds). *Wood and cellulosic chemistry* (pp. 703- 756). Marcel Dekker, Inc., New York.
- Schneider, M. H. & Brebner, K. I. (1985). Wood and polymer combination: The chemical modification of wood by alkoxysilane coupling agents. *Wood Science and Technology*, 19, 67-73.
- Vyas, A., Jain, A., Vyas, D. & Vyas, K. M. (2005). Production and partial characterization of cellulases by two *Aspergillus* spp on pretreated low value lignocelluloses. *Proceedings of National Academy of Sciences, India*. 75(B), 1, 51-57.
- White, A. R. (1982). Visualization of cellulases and cellulose degradation. In R.D. Brown Jr. (Ed.), *Cellulose and other natural polymer system: Biogenesis, structure and degradation* (pp. 489-506). Plenum Press, New York.
- Yamaguchi, H. (2003). Silicic acid: boric acid complexes as wood preservatives. *Wood Science and Technology*, 37, 287-297.

Table 1. Dimensional characteristics

Chemicals used	ASE (%)	BC (%)	WPG (%)
MA, Kerosene	52.95	5.14	23.77
BA, CA, DEDTC, Kerosene	54.31	5.47	25.01
BA, MA, CA, DEDTC, Kerosene	58.14	6.08	27.82

Table 2. Cellulase activity data

Sl.No.	Chemicals used	Amount of glucose (gm/100ml)
1	WP+ Cellulase	0.358
2	WP+BA+ Cellulase	0.297
3	WP+CA+ Cellulase	0.296
4	WP+DEDTC+ Cellulase	0.223
5	WP+BA+CA+DEDTC+ Cellulase	0.190

Table 3. Thermal analysis data

Chemicals used	Major decomp. temperature	Wt. loss	Active decomp. temperature
	( $^{\circ}\text{C}$ )	(%)	( $^{\circ}\text{C}$ )
untreated	241.85-489.25	85.14	335.29
MA, Kerosene	236.59-405.25	63.04	351.66
BA, CA, DEDTC, Kerosene	200.52-381.97	61.78	337.67
BA, MA, CA, DEDTC, Kerosene	209.74-393.08	60.35	346.59

Table 4. Effect of chemical treatment on strength (MOR) and stiffness (MOE) of wood

Chemicals used	MOR(N/mm <sup>2</sup> )	MOE(N/mm <sup>2</sup> )
Untreated	50.44	6616.26
MA, Kerosene	61.06	7867.49
BA, CA, DEDTC, Kerosene	62.20	8281.57
BA, MA, CA, DEDTC, Kerosene	65.87	9510.87

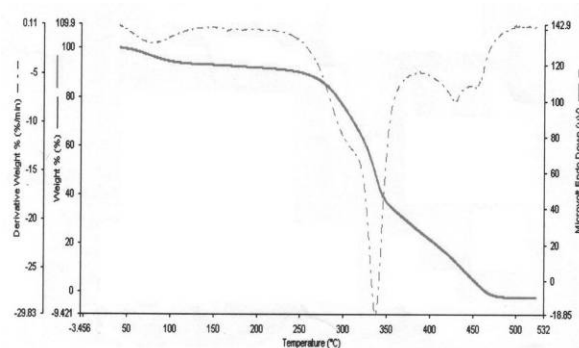


Figure 1. Thermogram of untreated wood sample

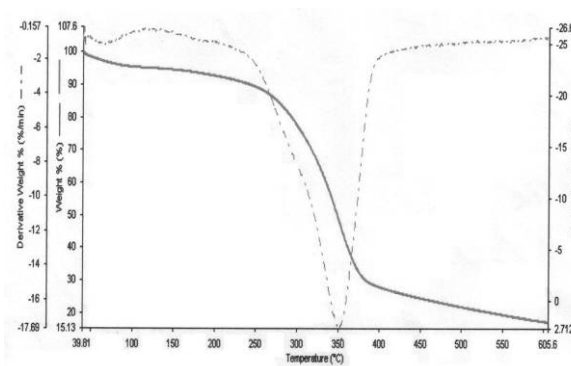


Figure 2. Thermogram of MA and kerosene treated wood sample

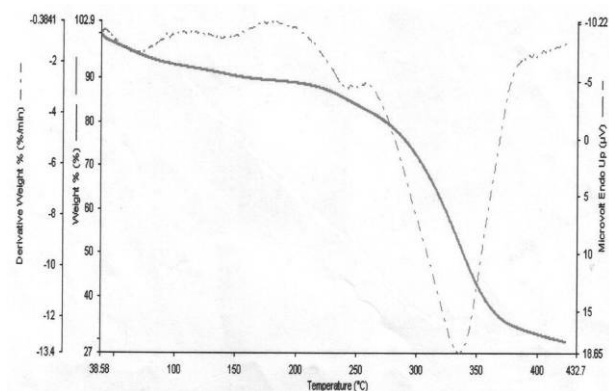


Figure 3. Thermogram of BA, CA, DEDTC and kerosene treated sample

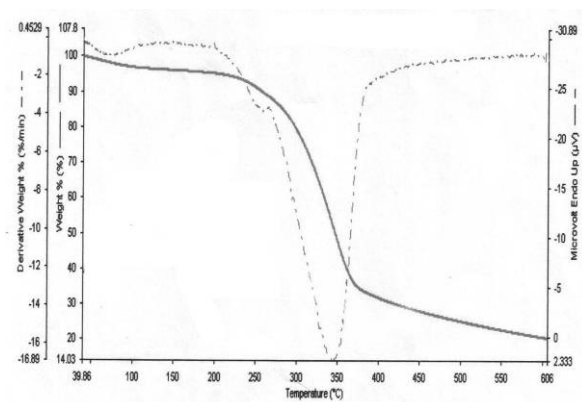


Figure 4. Thermogram of BA, MA, CA, DEDTC and kerosene treated wood sample

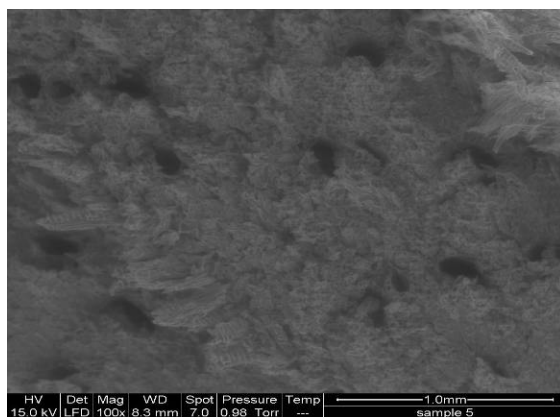


Figure 5. SEM pattern of untreated wood

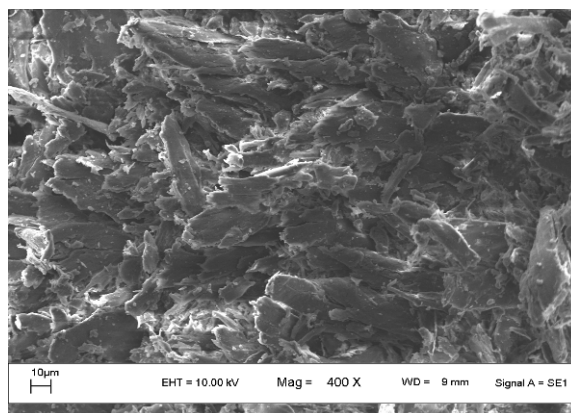


Figure 6. SEM pattern of BA, MA, CA, DEDTC and kerosene treated wood



Figure 7. Wood samples after one year of graveyard test

1. Untreated
2. MA and Kerosene treated
3. BA, CA, DEDTC and Kerosene treated
4. BA, MA, BA, CA, DEDTC and Kerosene treated

# Kinetics and Mechanism of Oxidation of 2-amino-1-Butanol and 3-Amino-1-propanol by Potassium Ferrate

Jinhuan Shan

College of Chemistry and Environmental Science, Hebei University

Baoding 071002, China

E-mail: shanjinhuaner@yahoo.com.cn

Jiying Zhang

College of Chemistry and Environmental Science, Hebei University

Baoding 071002, China

Haixia Shen

College of Chemistry and Environmental Science, Hebei University

Baoding 071002, China

Xiaoqian Wang

College of Chemistry and Environmental Science, Hebei University

Baoding 071002, China

## Abstract

The kinetics of oxidation of 2-amino-1-Butanol and 3-Amino-1-propanol by potassium ferrate(VI) in alkaline liquids at a constant ionic strength has been studied spectrophotometrically in the temperature range of 293.2 K-313.2 K. The reaction shows first order dependence on potassium ferrate(VI), first order dependence on each reductant. The observed rate constant ( $k_{\text{obs}}$ ) decreases with the increase in  $[\text{OH}^-]$ , the reaction is negative fraction order with respect to  $[\text{OH}^-]$ . A plausible mechanism is proposed and the rate equations derived from the mechanism can explain all the experimental results. The rate constants of the rate-determining step and the activation parameters are calculated.

**Keywords:** 2-amino-1-Butanol, 3-Amino-1-propanol, Oxidation, Kinetics and mechanism, Potassium ferrate

## 1. Introduction

As early as 1702, ferrate was found by Starl, then in 1841, Fremy first synthesized out potassium ferrate. Ever since a long time ago, people know little about potassium ferrate because it is unstable in water and humid air. In 1948, high purity potassium ferrate crystal was prepared by oxidizing trivalent iron salt in presence of sodium hypochlorite by Schreye and Thompson (Thompson, G. W., Ockerman, L. T., & Schreye, J. M. 1951). After that, with further research on potassium ferrate, its properties and applications are arousing more and more attention.

Potassium ferrate is a powerful oxidizing agent in the whole pH range; it is widely used as a water treatment agent (Duan, Y. F., Ding, Y., & Zhang, Y. Q. 1998; Wu, L. P. 1994; Zhang, J., Shi, Q. L., & Yang, G. M. 2000) in 1970s. It can remove the phenolic, sulfide and other organic pollutants (Michael, E., Duane, R. C. 1994) which are residual in wastewater, and also can oxidize the cyanide (Waite, T. D., Gray, K. A. 1984) into  $\text{NO}_2^-$ ,  $\text{NO}_3^-$  and  $\text{HCO}_3^-$  which are harmless to environment. Ferrate as a very effective, selective oxidant which can remove effectively  $\text{H}_2\text{S}$ ,  $\text{CH}_3\text{SH}_2$ , and  $\text{NH}_3$  etc (Virender, K. S., John, T. B., & Vishwas, N. J. 1998) odor substances in biological sludge. The treated sludge can be used as chemical fertilizer and soil conditioner, it is propitious to waste resource utilization.

Applied prospects of ferrate oxidation are becoming hotspot of research (Stuart, L., Wang, B. H., & Susanta, G. 1999). Oxidability of ferrate is stronger than potassium permanganate, ozone and chlorine. As a new water



treatment agent, it has a trend to replace chlorine-atom. In recent years, James Carr etc used potassium ferrate as water treatment agent, while they studied self-decomposition of potassium ferrate in a wide pH range (pH=2.53-9.31) (James, Carr. 1985) and the reaction of oxidizing a variety of organic matters (James, 1986). They had proposed rate equation which is applicable to the majority systems. The rate equation includes self-decomposition of potassium ferrate and the reaction of potassium ferrate with the substrate. They also established new methods to deal with kinetic data of such reaction systems (Thompson, G. W., Ockerman, L. T., & Schreyer, J. M. 1951). However, all studies were not put forward the reaction mechanism to explain the experimental facts.

2-amino-1-Butanol is a mixture of optical isomers which is a colorless liquid with ammonia odor. It is mainly used for preparing emulsifiers, surfactants, resinifying agent, polishing agent, vulcanization accelerator and pharmaceutical raw materials. It is also absorbance of acid gas for removing sulfured hydrogen and carbon dioxide. D-structure of this product is also used as raw materials of antimicrobial agents and uterine contraction hemostat. 3-Amino-1-propanol is colorless liquid with hygroscopicity and causticity. It can mixed dissolve with water, ethanol, acetone and chloroform. It is an important organic synthesis intermediates. It can synthesize DL-Panthenol and drugs such as cyclophosphamide and segontin.

In this paper, the kinetics and mechanism of oxidation of 2-amino-1-Butanol and 3-Amino-1-propanol by potassium ferrate were studied in detail.

## 2. Experimental

### 2.1 Materials and apparatus

All the reagents used were of A.R. grade. All solutions were prepared with doubly distilled water. Potassium ferrate ( $K_2FeO_4$ ) was prepared by the method of Thompson et al (Thompson, G. W., Ockerman, L. T., & Schreyer, J. M. 1951). The concentration of  $K_2FeO_4$  was derived from its absorption at 507 nm ( $\epsilon = 1.15 \times 10^3 \text{ L} \cdot \text{mol}^{-1} \cdot \text{cm}^{-1}$ ). The solution of  $K_2FeO_4$  was always freshly prepared before use.  $KNO_3$  and the  $Na_2HPO_4$  buffer solution were used to maintain ionic strength and acidity of the reaction, respectively. Measurements of the kinetics were performed using a TU-1900 spectrophotometer (Beijing, China) fitted with a DC-2010 thermostat ( $\pm 0.1 \text{ K}$ , Baoding, China).

### 2.2 Kinetics measurements

All kinetics measurements were carried out under pseudo-first order conditions. The oxidant and reductant were both dissolve in buffer solution which contained required concentration of  $KNO_3$  and  $Na_2HPO_4$ . The reaction was initiated by mixing the Fe(VI) to reductant solution. The reaction process was monitored automatically by recording the concentration decrease of all the Fe(VI) species with time ( $t$ ) at 507 nm with a TU-1900 spectrophotometer. All other species did not absorb significantly at this wavelength.

### 2.3 Product analysis

After completion of the reaction, adding  $K_3Fe(CN)_6$  to the solution have non-experimental phenomena, while adding  $K_4Fe(CN)_6$  is generated Prussian blue precipitate; by adding 2,2-bipyridyl methanol solution have non-experimental phenomena also. It is prove that the final reduction product of Fe(VI) is Fe(III) (Dong, X. W. 1984). After completion of the reaction, the oxidation product was identified as aldehyde alcohols which was precipitated as 2, 4-dinitrophenylhydrazone derivative.

### 2.4 Reaction intermediate

Added 1,10-phenanthroline to reductant solution, then mixed with the  $K_2FeO_4$  solution, purple disappeared at the same time orange appeared, indicating that  $Fe(phen)_3^{2+}$  have generated in the process of reaction (Dong, X. W. 1984). It is prove that Fe(II) stage have once appeared in the process of Fe(VI) reduction to Fe(III).

## 3. Results and discussion

### 3.1 Evaluation of pseudo-first order rate constants

Under the conditions of  $[reductant]_0 \gg [Fe(VI)]_0$ , the plots of  $\ln(A_t - A_\infty)$  versus time  $t$  were straight line, indicating the reaction is first order with respect to the Fe(VI) complex, where  $A_t$  and  $A_\infty$  are the absorbance at time  $t$  and at infinite time, respectively. The pseudo-first-order rate constants  $k_{obs}$  were calculated by the method of least squares ( $r \geq 0.997$ ). Generally, to calculate  $k_{obs}$  8-10  $A_t$  values within there times of the half-lives were used. The  $k_{obs}$  values were the average values of at least there independent experiments, and reproducibility is within  $\pm 5\%$  (Shan, J. H., Qian, J., & Gao, M. Z. 2004).

### 3.2 Rate dependence on [reductant]

At fixed [Fe(VI)], [OH<sup>-</sup>], ionic strength *I*, the values of *k*<sub>obs</sub> were determined at different temperatures. The *k*<sub>obs</sub> were found to be increased with the increase of reactant concentration. The plots of *k*<sub>obs</sub> versus [reductant] were linear. For the plots passed through the grid origin (**Figure 1 and Figure 2**), the reaction was first order with reductant.

### 3.3 Rate dependence on [OH<sup>-</sup>]

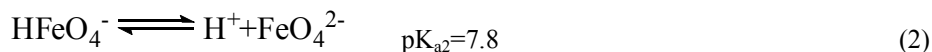
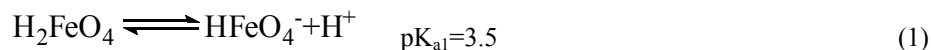
Under fixed [Fe(VI)], [reductant], ionic strength *I* and temperature, *k*<sub>obs</sub> values were decreased with an increase of [OH<sup>-</sup>]. The order with respect to OH<sup>-</sup> was found to be negative fractional. The liners of 1/*k*<sub>obs</sub> versus [OH<sup>-</sup>] were done (**Figure 3 and Figure 4**).

## 4. Reaction mechanism

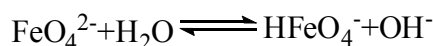
James Carr (James, Carr. 1986) has given the rate equation as follows: rate = *k*<sub>1</sub> [FeO<sub>4</sub><sup>2-</sup>] + *k*<sub>2</sub> [FeO<sub>4</sub><sup>2-</sup>]<sup>2</sup> + *k* [FeO<sub>4</sub><sup>2-</sup>][S]

where [S] represents substrate concentration. James Carr thinks: the first two terms is contribution of K<sub>2</sub>FeO<sub>4</sub> self-decomposition rate to the reaction system when there is no substrate. In this article, under the experimental conditions, the self-decomposition rate of K<sub>2</sub>FeO<sub>4</sub> is far less than oxidation rate of reductant reaction, so we get the rate equation: rate = *k*[FeO<sub>4</sub><sup>2-</sup>][R]. In essence, the results were consistent with James Carr.

Ferrate(VI) is a dicarboxylic acid (James, Carr. 1985), where:



Under the experimental conditions of this paper, FeO<sub>4</sub><sup>2-</sup> will be partial hydrolysis:



Hence:

$$K_h = \frac{[\text{HFeO}_4^-][\text{OH}^-]}{[\text{FeO}_4^{2-}]} = \frac{K_w}{K_{a2}} = 6.31 \times 10^{-7}$$

This experiment is performed at pH = 10.10 and 10.42, then there is

$$\frac{[\text{HFeO}_4^-]}{[\text{FeO}_4^{2-}]} = \frac{K_h}{[\text{OH}^-]} = 5.01 \times 10^{-3} \text{ and } \frac{[\text{HFeO}_4^-]}{[\text{FeO}_4^{2-}]} = \frac{K_h}{[\text{OH}^-]} = 2.40 \times 10^{-3}$$

Obviously, HFeO<sub>4</sub><sup>-</sup> both have a small percentage in the system. The concentration of HFeO<sub>4</sub><sup>-</sup> is small, but it is very easy to form complex with reductant in the presence of hydrogen atom, and the complex has higher activity. Under the attack of hydroxyl, the complex dissociates into Fe(IV) and product, then Fe(IV) with another molecule of reductant further react to generate Fe(II) and product. Therefore, reaction is mainly through HFeO<sub>4</sub><sup>-</sup> to realize.

According to discussion, the following reaction mechanism is proposed:





Reaction (4) is the rate-determining step, where R stands for reductant. As the rate of the disappearance of  $[FeO_4^{2-}]$  was monitored, the rate of the reaction can be derived as:

$$\begin{aligned} -\frac{d[FeO_4^{2-}]}{dt} &= k_2[HFeO_4^-][R] - k_{-2}[X] \\ &= \frac{k_2 k_3 [HFeO_4^-][R][OH^-]}{k_{-2} + k_3 [OH^-]} \end{aligned} \quad (8)$$

Equation (9) can be obtained from (3):

$$[HFeO_4^-] = \frac{K_h [FeO_4^{2-}]}{[OH^-]} \quad (9)$$

Substituting equation (9) into (8), we can get the following equation (10):

$$-\frac{d[FeO_4^{2-}]}{dt} = \frac{k_2 k_3 K_h [FeO_4^{2-}][R]}{k_{-2} + k_3 [OH^-]} = \frac{k_2 k_3 K_h [R]}{k_{-2} + k_3 [OH^-]} [FeO_4^{2-}] \quad (10)$$

$$k_{\text{obs}} = \frac{k_2 k_3 K_h [R]}{k_{-2} + k_3 [OH^-]} = \frac{k_2 k' K_h [R]}{1 + k' [OH^-]} \quad (11)$$

in the equation  $k' = k_3/k_{-2}$

$$\frac{1}{k_{\text{obs}}} = \frac{1 + k' [OH^-]}{k_2 k' K_h [R]} = \frac{1}{k_2 k' K_h [R]} + \frac{[OH^-]}{k_2 K_h [R]} \quad (12)$$

Equation (10) suggests that the reaction should be first order with respect to  $Fe(VI)$ ; equation (11) suggests that the order with respect to R is unity. The plot of  $1/k_{\text{obs}}$  versus  $[OH^-]$  derived from equation (12) at constant [R] is linear with positive intercept. These are consistent with the experimental phenomena.

Meanwhile, the plots of  $1/k_{\text{obs}}$  versus  $[OH^-]$  were liner at different temperatures. From their slopes and equation (12), the rate-determining step constants ( $k_2$ ) were evaluated, and the activation parameters date were obtained (Table 1) (Shan, J. H., Liu, T. Y. 1994).

It is noteworthy that according to equation (12) and Figure (3, 4), we can get the values of  $k'$  under corresponding temperature. And then, substituting the  $k'$ ,  $k_2$  and  $[OH^-]$  into equation (11), we can calculate the rate constants in corresponding [R], we found that the calculated value is very close to the experimental value (Table 2 and Table 3). This also illustrates the equation (12) is correct and the reaction mechanism we supposed is reasonable.

## 5. Conclusion

Based on the above discussion and results, we can know that the reaction of potassium ferrate with 2-amino-1-Butanol and 3-Amino-1-propanol both are completed by double-electron transfer and we also observed the rate of the rate-determining step of 3-Amino-1-propanol is quicker than that of 2-amino-1-Butanol, the rate constants of the rate determining step for 3-Amino-1-propanol are larger than those for 2-amino-1-Butanol. The effect of  $[OH^-]$  and the activation parameters are all in support of the mechanism and consistent with experimental phenomena.

In the reaction system, we also observe that the activation energy of experiment is very small, but the entropy of

activation has a big negative value. So according to the literature (Fu, X. C., Shen, W. X., & Yao, T. Y. 1990), it is reasonable that the reaction rate is not too fast.

## References

- Dong, X. W. (1984). Detection of all kinds of Ions in the Chemical Method, Bei Jing: Beijing Normal University Press, 94.
- Duan, Y. F., Ding, Y., & Zhang, Y. Q. (1998). Preparation of potassium ferrate(VI) and Application in water. *Modern Chemical Industry*, 3, 17.
- Fu, X. C., Shen, W. X., & Yao, T. Y. (1990). *Physical Chemistry*, Beijing: Higher Education Press, 812.
- James, Carr. (1985). Proceedings of the Conference on Water Chlorination and Chem Environ. *Impact Health Eff*, 1285.
- James, Carr. (1986). The kinetics of Oxidation of Simple Aliphatic Sulphur Compounds by Potassium Ferrate. *Transition Met. Chem*, 11, 116.
- Michael, E., Duane, R. C. (1994). Removal of radionuclide in waste water utilizing potassium ferrate(VI). *Water Environment Research*, 66(2), 107.
- Shan, J. H., Liu, T. Y. (1994). Kinetics and mechanism of substitution reactions of bis(N,N-diethyldithiocarbamate)alkylxanthocobalt(III) with dipropylamine and di-n-butylamine in methanol. *Acta Chim. Sinica*, 52, 1140.
- Shan, J. H., Qian, J., & Gao, M. Z. (2004). Kinetics and Mechanism of Oxidation of n-Propanolamine by Dihydroxydiperiodatonickelate(VI) in Alkaline Medium. *Turk J Chem*, 28, 9–15.
- Stuart, L., Wang, B. H., & Susanta, G. (1999). Energetic Iron(VI) Chemistry: The Super-Iron Battery. *Science*, 285(3), 1039-1042.
- Thompson, G. W., Ockerman, L. T., & Schreye, J. M. (1951). Preparation and purification of potassium ferrate(VI). *J AM Chem Soc*, 73, 1379.
- Thompson, G. W., Ockerman, L. T., & Schreyer, J. M. (1951). Preparation and Purification of Potassium Ferrate(VI). *J Am Chem Soc*, 73, 1379-1381.
- Virender, K. S., John, T. B., & Vishwas, N. J. (1998). Oxidation of ammonia by ferrate(VI). *Environ Sci*, 33(4), 635.
- Waite, T. D., Gray, K. A. (1984). Utilizing ferrate(VI) iron oxidation and coagulation of waste water effluent study. *Environ Sci*, 23, 407.
- Wu, L. P. (1994). A new efficient Water Treatment- Potassium Ferrate(VI). *Henan Chemical Industry*, 2, 22.
- Zhang, J., Shi, Q. L., & Yang, G. M. (2000). Synthesis of potassium ferrate(VI) and Application in water. *Environmental Protection of Chemical Industry*, 20(1), 44.

Table 1. Rate constants ( $k_2$ ) and Thermodynamic activation parameters of the rate-determining step

T(K)		293.2	298.2	303.2	308.2	313.2
$k_2/\text{mol}^{-1}\cdot\text{L}\cdot\text{s}^{-1}$	2-amino-1-Butanol	47.60	64.12	85.95	111.64	
	3-Amino-1-propanol		308.52	351.47	410.06	463.33
Thermodynamic activation parameters	2-amino-1-Butanol	$E_a = 42.98 \text{ kJ}\cdot\text{mol}^{-1}$ , $\Delta H^\ddagger = 40.50 \text{ kJ}\cdot\text{mol}^{-1}$ , $\Delta S^\ddagger = -74.54 \text{ J}\cdot\text{K}^{-1}\cdot\text{mol}^{-1}$				
	3-Amino-1-propanol	$E_a = 21.33 \text{ kJ}\cdot\text{mol}^{-1}$ , $\Delta H^\ddagger = 18.85 \text{ kJ}\cdot\text{mol}^{-1}$ , $\Delta S^\ddagger = -134.02 \text{ J}\cdot\text{K}^{-1}\cdot\text{mol}^{-1}$				

The plots of  $\ln k$  vs.  $1/T$  have following intercept (a) slope (b) and relative coefficient (r). 2-amino-1-Butanol: a = 21.44 b = -5152.72 r = 0.9999, 3-Amino-1-propanol: a = 14.34 b = -2566.86 r = 0.9992

Table 2. The values of  $k_{\text{obs}}$  experimental and calculated at different temperatures

([OH <sup>-</sup> ] = $1.26 \times 10^{-4}$ mol·L <sup>-1</sup> R=2-amino-1-Butanol)										
c/mol·L <sup>-1</sup>	0.20		0.40		0.60		0.80		1.00	
T/K	EXP	CAL	EXP	CAL	EXP	CAL	EXP	CAL	EXP	CAL
293.2	0.0119	0.0129	0.0235	0.0258	0.0357	0.0386	0.0504	0.0515	0.0634	0.0644
298.2	0.0173	0.0181	0.0346	0.0362	0.0523	0.0543	0.0715	0.0724	0.0911	0.0905
303.2	0.0245	0.0248	0.0491	0.0496	0.0743	0.0744	0.0991	0.0992	0.124	0.124
308.2	0.0365	0.0358	0.0715	0.0716	0.112	0.107	0.142	0.143	0.183	0.179

Table 3. The values of  $k_{\text{obs}}$  experimental and calculated at different temperatures

([OH <sup>-</sup> ] = $2.63 \times 10^{-4}$ mol·L <sup>-1</sup> R=3-Amino-1-propanol)										
c/mol·L <sup>-1</sup>	0.04		0.08		0.12		0.16		0.20	
T/K	EXP	CAL	EXP	CAL	EXP	CAL	EXP	CAL	EXP	CAL
298.2	0.0108	0.0110	0.0208	0.0221	0.0312	0.0331	0.0427	0.0442	0.0526	0.0552
303.2	0.0152	0.0139	0.0279	0.0278	0.0405	0.0418	0.0554	0.0557	0.0699	0.0696
308.2	0.0183	0.0168	0.0324	0.0335	0.0498	0.0503	0.0656	0.0670	0.0837	0.0838
313.2	0.0225	0.0197	0.0412	0.0394	0.0610	0.0590	0.0798	0.0787	0.105	0.0984

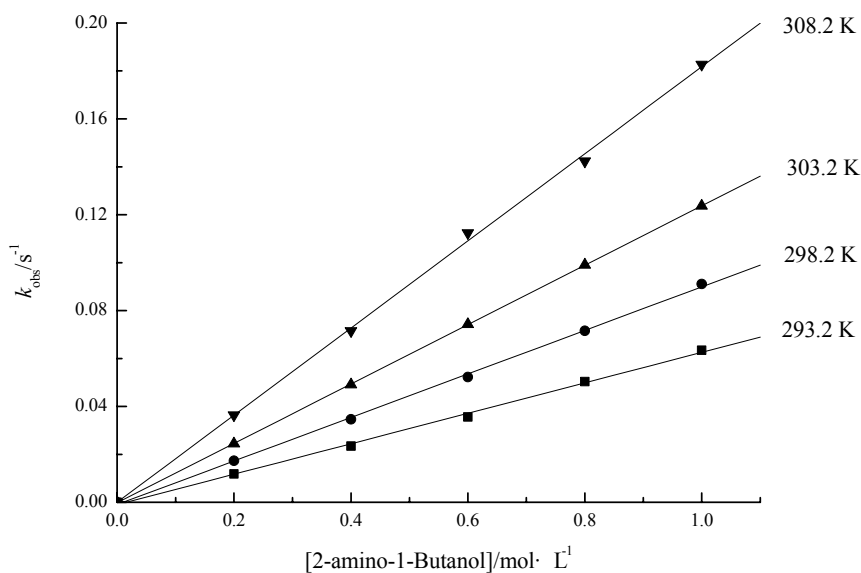


Figure 1. Plots of  $k_{\text{obs}}$  versus [2-amino-1-Butanol] at different temperatures ( $r \geq 0.999$ )  
 $[\text{Fe(VI)}] = 1.83 \times 10^{-4}$  mol·L<sup>-1</sup>,  $[\text{OH}^-] = 1.26 \times 10^{-4}$  mol·L<sup>-1</sup>,  $I = 1.00$  mol·L<sup>-1</sup>

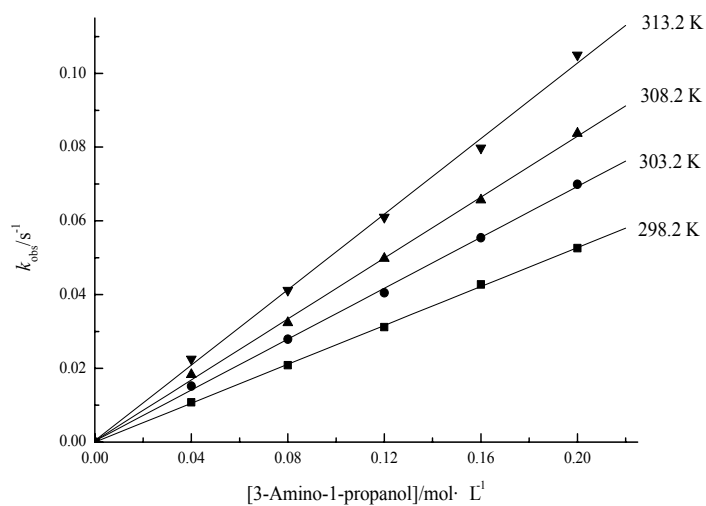


Figure 2. Plots of  $k_{\text{obs}}$  versus [3-Amino-1-propanol] at different temperatures ( $r \geq 0.999$ )

$[\text{Fe(VI)}] = 1.74 \times 10^{-4} \text{ mol}\cdot\text{L}^{-1}$ ,  $[\text{OH}^-] = 2.63 \times 10^{-4} \text{ mol}\cdot\text{L}^{-1}$ ,  $I = 1.00 \text{ mol}\cdot\text{L}^{-1}$

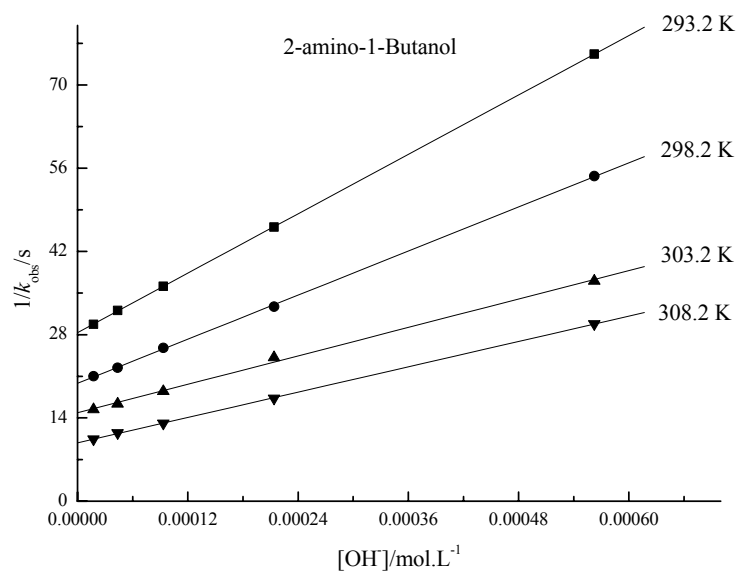


Figure 3. Plots of  $1/k_{\text{obs}}$  versus  $[\text{OH}^-]$  at different temperatures ( $r \geq 0.999$ )

$[\text{Fe(VI)}] = 1.57 \times 10^{-4} \text{ mol}\cdot\text{L}^{-1}$ ,  $[\text{2-amino-1-Butanol}] = 0.40 \text{ mol}\cdot\text{L}^{-1}$ ,  $I = 1.00 \text{ mol}\cdot\text{L}^{-1}$

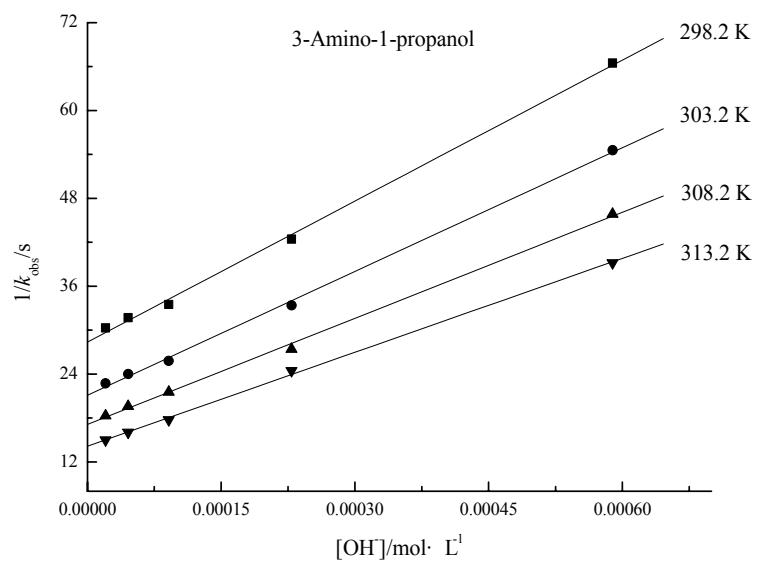


Figure 4. Plots of  $1/k_{\text{obs}}$  versus  $[\text{OH}^-]$  at different temperatures ( $r \geq 0.999$ )  
 $[\text{Fe(VI)}] = 1.74 \times 10^{-4} \text{ mol} \cdot \text{L}^{-1}$ ,  $[\text{3-Amino-1-propanol}] = 0.08 \text{ mol} \cdot \text{L}^{-1}$ ,  $I = 1.00 \text{ mol} \cdot \text{L}^{-1}$

# Instrumental Neutron Activation Analysis of Total Halogen and Extractable Organohalogen in Fish Samples from the Densu Basin

Alfred Kwablah Anim (Corresponding author)

National Nuclear Research Institute, Ghana Atomic Energy Commission

P. O. Box LG. 80, Legon, Accra, Ghana

Tel: 233-208-533-816 E-mail: sekemont@yahoo.com

Samuel Afful

National Nuclear Research Institute, Ghana Atomic Energy Commission

P. O. Box LG. 80, Legon, Accra, Ghana

Tel: 233-275-809-933 E-mail: samuelaffu@yahoo.com

Yaw Serfor-Armah

National Nuclear Research Institute, Ghana Atomic Energy Commission

P. O. Box LG. 80, Legon, Accra

&

Department of Nuclear Sciences and Applications, Graduate School of Nuclear and Allied Sciences

University of Ghana, P. O. Box AE1, Atomic Campus, Accra, Ghana

Tel: 233-543-426-365 E-mail: yawserfor@yahoo.com

## Abstract

Instrumental Neutron Activation Analysis (INAA) has been validated and the method applied to determine total halogen and extractable organohalogen in six fish species namely *Heterotis niloticus*, *Channa obscura*, *Hepsetus odoe*, *Tilapia zilli*, *Clarias gariepinus*, and *Chrysichthys nigrodigitatus*. The samples were collected directly from the fishermen at their landing sites from the two sampling towns, Weija and Nsawam along the Densu river basin in the Greater Accra Region of Ghana. The concentrations of total chlorine, bromine, and iodine analysed by INAA were between 770.70 - 1123.50 mg/kg, 8.00 - 25.00 mg/kg and 0.70 - 4.20 mg/kg respectively. For the extractable organohalogens concentrations ranged from 0.30 - 350.40 mg/kg. The highest concentration of 350.40 mg/kg was obtained for extractable organochlorine (EOCl) in *Hepsetus odoe* sampled from Nsawam, while the lowest concentration was obtained for extractable organoiodine. The content of extractable organohalogen were in the order of EOCl >> EOBr > EOI.

**Keywords:** Neutron activation, Organohalogen, Fish species, Densu basin, Extractable

## 1. Introduction

Environmental chemists, for the past few years, have increased their efforts for the detection of chemicals which are polluting the environment. However, in spite of these efforts, only a limited proportion of the chemicals in the environment have been detected and listed as pollutants. Organohalogens are environmental pollutants, considered as one of the most toxic pollutants of concern. This is because of their persistence in the environment, biota and their adverse effects on organisms [Kawano M, 2004]. Organohalogens have been implicated in a broad range of adverse human health effects including reproductive failures and birth defects, immune system malfunction, endocrine disruptions, and cancers [Garabrant D. H, 1992, p764-771]. Organohalogens, especially organochlorine compounds (OCs), have long been recognized as a potential threat to human health and, therefore these compounds have been widely investigated in foods, vegetation and the atmosphere [Diandu X, 2004, p101-106]. Infants and children are particularly prone to absorbing brominated flame retardants (BFRs) and chlorinated flame retardants (CFRs) through direct physical or oral contact with these compounds in furniture, inhalation of furniture dust containing BFRs and CFRs, and via ingestion of these substances from their mother's milk and from their



diets [Wu ming, 2007]. Common uses of organohalogens include solvents, pesticides, flame retardants, refrigerants, and ingredients of elastomers, adhesives, electrical insulating coatings, plasticizers, and plastics. It is therefore obvious that they are widely used by man.

As a result of the toxicity associated with organohalogens, determination of levels of organohalogens in the environment, particularly in food and water samples are becoming increasingly important. Interest in using extractable organohalogens (EOX) as parameters for the quantification of total organohalogen content in sediment [Gustavson K, 1999, p723-736], biota [Haynes D, 1995, p 463-469], and water [Martinsen K, 1988, p13-24] has dramatically increased. Instrumental neutron activation (INAA) has become one of the most important and most suitable techniques for the determination of organohalogen compounds in environmental samples due to its capability to analyze individual halogens. It is a very reliable analytical tool for simultaneously determining extractable organochlorine (EOCl), extractable organobromine (EOBr), and extractable organiodine (EOI) [Lunde G, 1976, p180-183]. Recently, INAA was conducted for the analysis of EOX in the blubber samples of harbor porpoise and whole body samples of Atlantic herring from the Baltic sea [Kawano M, 2008, p263-266]. Diando Xu et al (2004) analyzed pine needles and foodstuffs collected from Beijing, China, by instrumental neutron activation analysis (INAA) combined with organic solvent extraction for total halogens, extractable organohalogens (EOX) and extractable persistent organohalogen (EPOX).

In this study, INAA has been validated using three reference standard materials, and the validated method has been applied for the determination of total organohalogens and extractable organohalogens (EOX) in fish species sampled from the Densu basin. The Densu basin was selected, to help in establishing the level of organohalogen contamination in the basin and the matrix fish was used for the study as fish can readily accumulate organohalogens through inhalation, dermal absorption and ingestion and therefore, can serve as a biomonitor to indicate the levels of environmental contamination of organohalogen compounds.

## 2. Materials and methods

### 2.1 Study area

The Densu River system is one of the coastal drainage basins of Ghana. The river lies between latitudes 5°30'N to 6°20'N and longitudes 0°10'W to 0°35'W. The basin area is about 2488.41 km<sup>2</sup> with an average length of 225.6 km [Akpabli CK, 2001, p85-86]. Its main tributaries are the Kuia, Adaiso, Nsaki and Aprapon. The basin plays a critical role in the socio-economic development of the many towns and satellite villages dotted within it. Other small settlements also depend on untreated water from the Densu River and its tributaries. The Densu Basin is also intensively used for the cultivation of both cash and food crops. Principal food crops cultivated within the basin are cassava, maize, yam, plantain, banana and cocoyam. Cash crops include cocoa, oil palm, papaya, pineapple, mangoes and citrus. Farmers here use fertilizers and other agrochemicals extensively. Sulphate, phosphate, nitrate and chloride based fertilisers and other agrochemicals, including calcium cabide and kerosene, are used in the farms, which are washed into the river through run-off. In the Adaiso township, car washing, an important economic activity can be identified along the river. Other land use activities include housing, sand winning, animal rearing, salt mining etc. Another economic activity in the Densu basin is fishing. Most of the towns and villages including city dwellers in Accra get their fish supply from the Densu basin. Commercial fishing sites in the basin include Nsawam and Weija. Major large scale commercial pineapple farms, such as, Oyoko farms (New Doblo), Greenlex Farms Ltd. (Dobro), John Laurence Farm Limited is located along the course of river Densu. The Densu finally flows southwards into the Weija reservoir and enters the Gulf of Guinea through the Sakumono Lagoon at Botiano, a fishing village about 16km of west Accra. Fig.1 shows a map of the sampling area.

### 2.2 Sample Collection

Six fish species were collected from Weija and Nsawam portions of the Densu basin for the study. Fish samples were bought directly from commercial fishermen at the landing sites at Weija and Nsawam. The fish samples were packed in ice thermo insulator box and transported to the laboratory. At the laboratory, the fish samples were washed several times with deionized water. The fish species used for the investigation were: *Tilapia Zilli*, *Chrysichthys Nigrodigitatus*, *Heterotis Niloticus*, *Channa Obscura*, *Hepsetus Odoo* and *Clarias Gariepinus*. The fish samples were identified and unique identification codes were given.

### 2.3 Sample preparation

#### 2.3.1 Preparation of powdered fish samples

Fish samples were removed from the freezer and rinsed several times with deionised water. Prior to preparation, each sample was weighed and its lengths were measured. Each fish sample was gutted to remove the intestines.

The scales, head, tails, fins and bones were also removed using a stainless steel knife. One pooled (composite) sample was prepared for each different species from five individual fish species. The muscle tissues of the five individual fish were ground in a waring stainless steel blender to obtain a homogenous fish sample. 100 g of each homogenized sample were freeze dried for 72 hrs. The dried samples were ground using mortar and pestle to obtain powdered sample.

### 2.3.2 Soxhlet extraction

A mass of 10 g of dried powdered fish samples were weighed and wrapped in a filter paper. The wrapped fish samples were placed in a cellulose extraction thimble and extracted with 160 ml of hexane: acetone mixture in the ratio 3:1 for five hours using soxhlet extraction procedure. The extracts were concentrated to dryness on a rotary evaporator fitted to a vacuum pump in a fume chamber. The extracts were recovered by re-dissolving the residues in 10 ml of hexane. A sample blank was also prepared.

### 2.3.3 Preparation of samples for irradiation

200 mg of dried homogenized sample were weighed onto clean polyethylene sheets, wrapped and heat sealed. The sealed samples were then packed into 7 ml polyethylene vials and the vials were heat sealed for irradiation for determination of total Cl, Br and I content by INAA. Three reference materials namely NIST-SRM 1566b (Oyster tissue), CRM-DORM-2 (Dogfish muscle) and NIST-SRM 1547 (Peach leaves) were prepared and packaged in a similar manner. To determine the extractable organohalogen, 200 mg of the concentrated extract were weighed into 1.5ml polyethylene vial, plugged with cotton wool and heat sealed. The 1.5 ml vials were then packed into a 7 ml polyethylene vial, plugged with cotton wool and heat sealed for irradiation to determine the concentration of EOCl, EOBr and EOI in the fish samples.

### 2.3.4 Preparation of elemental comparator standards for analysis of EOX

The potassium halide salts were dried in an oven for at least 24 h at  $110^{\circ}\text{C}$ , then transferred to and stored in a desiccator. These salts were used to produce the aqueous comparator standards used for the study. Standard solutions were made for each of the halogens studied, i.e. chlorine, bromine and iodine. The final standard solution for irradiation contained the following concentrations: 10.0 ppm chlorine, 0.439 ppm bromine, and 0.227 ppm iodine. Vials containing these aqueous standards were prepared as per section 2.3.3.

### 2.3.5 Instrumental neutron activation analysis (INAA) of fish samples

INAA was validated to analyse total Cl, Br, I, and EOCl, EOBr, EOI in the fish samples. Irradiations were performed using the Ghana Research Reactor-1 (GHARR-1) of Ghana Atomic Energy Commission at Kwabenya. The samples, comparator standards and reference materials were all irradiated using thermal irradiation. The reference materials were: NIST-SRM 1566b (Oyster tissue), CRM-DORM-2 (Dogfish muscle) and NIST-SRM 1547 (Peach leaves). GHARR-1 is a 30KW tank-in-pool reactor using light water as moderator and coolant. The fuel source is highly enriched Uranium (90.2%-Al alloy) with metal beryllium as reflectors. The reactor is cooled by natural convection. Samples were sent to the irradiation sites by means of a pneumatic transfer system. The samples were irradiated with a thermal flux of  $5 \times 10^{11} \text{ ncm}^{-2}\text{s}^{-1}$  with the reactor operating at 15KW. The elements of interest were assayed using different timing parameters. Cl, EOCl, I and EOI were typically determined in the samples after 2min irradiation, 1-10 min decay and 10 min counting period (ti: td: tc = 2: 1-10: 10min). For Br and EOBr the samples were irradiated for 1 hr and allowed to decay for 24 hrs and counted for 10 min. Nuclear data [IAEA-TECDOC-564, 1990] for these nuclides are provided in Table 1.

### 2.3.6 Counting of irradiated samples

The irradiated samples were counted by using a computer based gamma-ray spectroscopy system, consisting of an N-type high purity Germanium (HPGe) detector model GR2518 mounted on liquid nitrogen as a coolant, high voltage power supply model 3103, Spectroscopy amplifier model 2020, ACCUSPEC multi-channel analyzer emulation software card (all manufactured by Canberra industries inc.), and a micro computer for data acquisition, evaluation and analysis. The qualitative and quantitative analyses of the nuclides were achieved using the MAESTRO 32 software. The quantitative analysis was done by converting the counts as area under the photo peak of the radionuclide by the comparator method

## 3. Results and discussion

### 3.1 Validation of NAA method

Results obtained when the INAA method was validated using three reference standard materials are presented in Tables 2, 3, and 4. The elemental levels obtained for the standard reference in the present study are compared with reported values. The two sets of data agree favorably within the limits of experimental error, suggesting the

accuracy and reliability of elemental measurement by non-destructive INAA. The results of the present study were in most cases within 0.5 - 5 % deviation of reported values.

### 3.2 Total and extractable organohalogens

The mean concentrations of total halogens and extractable organohalogens (EOX) are presented in Table 5. Margins of errors are standard deviation based on triplicate determination. Results show higher levels of total chlorine and lower levels of total iodine in all the samples. The total halogen content in all the samples were of the order total Cl > total Br > total I. Over all, the highest concentration,  $1123.50 \pm 29.10$  mg/kg in *Channa obscura* (CON) was obtained for total Cl while the lowest concentration,  $0.70 \pm 0.01$  mg/kg was obtained for total I in *Heterotis niloticus* (HNN).

Results show the presence of extractable organohalogen (EOX) in all the samples. The levels of EOX also followed the same trend as levels of total halogen. Thus the highest extractable organohalogen was extractable organochlorine with a mean concentration of  $350.40 \pm 9.10$  mg/kg extracted from *Hepsetus odoe* (HON), while the lowest extractable organohalogen was organoiodine with mean concentration of  $0.30 \pm 0.01$  mg/kg extracted from *Channa obscura* (CON). The reasons for the high content of EOCl may be attributed to the nature of organochlorines being more difficult to be transformed and degraded compared to brominated and iodinated compounds in the environment [Laniewski K, 1999, p 393-409]. Another likely factor is the huge amount of organochlorinated compounds which are continuously being released into the environment through the extensive use of organochlorinated agrochemicals for agriculture purposes. It is also known that most organohalogenated pollutants in the atmosphere are present as organochlorines and these can deposit in river bodies when it rains. Laniewski *et al* had established that most absorbable organohalogens in rain and snow were organochlorines. Further evidence provided suggests that chlorinated methane which originates from both natural and anthropogenic sources was the most abundant organohalogen in the atmosphere [Yokouchi Y, 2000, p295-298].

The high concentrations of the extractable organochlorines were however not comparable to the respective concentrations of the total chlorine. On the other hand, the concentrations of extractable bromine and iodine were comparable to their corresponding total bromine and total iodine. For instance, the total chlorine content in CGW was  $951.60 \pm 36.30$  mg/kg, while the corresponding extractable organochlorine was  $216.00 \pm 8.90$  mg/kg. For the same sample, the total bromine and total iodine content were  $10.70 \pm 0.20$  and  $1.40 \pm 0.02$  mg/kg respectively and their corresponding extractable bromine and iodine were respectively  $8.20 \pm 0.10$  and  $1.35 \pm 0.02$  mg/kg. This results show that most of the total chlorine in the samples are likely to be inorganic as much was not extractable. However, the content of total bromine and total iodine in the samples are predominantly organic in nature as greater percentage was extractable. Thus, as presented in Fig 2, in terms of percentage compositions of extractable organohalogens in relation to their corresponding total halogen, percentage extractable organochlorine was the lowest. It must however, be noted that the content of extractable organohalogen were in the order of  $EOCl \gg EOBr > EOI$ . The same order of the concentration for EOX in harbor porpoise and whole body samples of Atlantic herring from the Baltic sea were reported [Kawano M, 2008, p263-266]. *Heterotis niloticus* (HNN) however recorded exceptionally high EOBr mean concentration of 13.00 mg/kg. This sharp difference may be due to differences in the characteristics of *Heterotis niloticus* which consume small invertebrates, phytoplankton seeds and also eats more frequently over a long period.

Fig. 3 compares the distribution of EOCl in the fish samples from various sample points. The concentrations of EOCl range between 327.50 to 150.00 mg/kg. Lower concentrations between 17.7 and 43.35 mg/kg of EOCl were reported in freshwater mussel tissues [Kawano M, 2001, p233-242]. Results show general higher concentrations of EOCl in samples from Nsawam and lower concentrations in samples from Weija. The level of organohalogens in biota can be contributed by both natural and artificial sources [Gribble G.W, 2003, p289-297]. Nsawam is located upstream where there is a lot of farming activities whilst Weija which is located downstream experiences less agricultural activities. Considering the description of the sampling sites, samples from Nsawam are likely to be more exposed to pesticide residues from agricultural run-off compared to samples from Weija.

Unlike the distribution of EOCl [Fig. 3], levels of EOBr and EOI were however higher in samples from Weija compared to samples from Nsawam [Fig. 4]. Weija is located closer to the sea and also exposed more to automobile emissions due to its closeness to the motor traffic hub. This may contaminate the Weija site with Br from likely emissions of Br containing compounds from vehicle exhaust fumes. Leachate from landfills and direct domestic waste disposal into the Densu basin may also be some of the EOBr contamination pathways into the Densu river basin. The Weija site is closer to the Oblogo landfill site and may therefore be the source of high levels of EOBr compared to levels in Nsawam. Another likely source of bromine contamination is the incineration processes which may release brominated flame retardants (BFRs) from furniture, mattresses. Brominated dioxins

and furans may originate under conditions of incineration [De Wit C.A., 2002, p583-624]. *Heterotis niloticus* (HNN) however recorded exceptionally high EOBr mean concentration of 13.00 mg/kg. This sharp difference may be due to differences in the feeding characteristics of *Heterotis niloticus*.

High levels of EOI were obtained for samples from Weiya compared to samples from Nsawam. The levels of iodine in aquatic organisms depend on the aquatic resource and the specie [Larsen E.H., 1997, p435-439]. The sea is the major source of iodine. Thus much of the iodine in the basin may be contributed by deposition (spray) and intrusion from the sea. Weiya is closer to the sea than Nsawam.

#### 4. Conclusion

The results of this work indicated that organohalogens are present in the Densu basin. The incidence of EOCl, EOBr and EOI were 100 %. The percentage EOCl of the total chlorine in the fish samples ranged from 13.3 to 42.5%. This is an indication that the chlorine content in the fish samples are more of inorganic origin. The EOBr and EOI accounted for 46.0 - 95.6% and 51.8-96.4% of the total bromine and iodine respectively in the fish samples. This result suggests that the bromine and iodine content in the Densu basin are more of organic origin and highly extractable. Notwithstanding the high percentage of EOBr and EOI relative to their corresponding total halogen, the levels of EOX in the fish samples were in the order of EOCl >> EOBr > EOI. The low levels of EOBr compared to EOCl suggests atmospheric deposition and leachate from other bromine containing compounds rather than brominated agrochemicals as the major contamination pathways. The higher levels of EOBr in samples from Weiya compared to Nsawam therefore suggest the leaching of organobromines from the Oblogo landfill site which is sited in Weiya and the atmospheric deposition of brominated flame retardants (BFR) which may be released during incineration of waste. The levels of EOI in the fish samples were exceptionally low. This may be attributed to the fact that organoiodines are easily transformed and degraded in the environment particularly in the tropics. The INAA methodology presented is efficient and reliable and can be used for routine determination of total and extractable organohalogens in environmental samples.

#### References

- Akpabli C K, Drah G K. (2001). Water Quality of The Main Tributaries of the Densu River. *J. of the Ghana Sci. Asso.*, 3 (2): 85-86.
- De Wit C A. (2002). An overview of brominated flame retardants in the environment. *Chemosphere*, 46: 583-624.
- Diandou X, Zhifang C, Hong Z, Xue ying M, Hong O. (2004). Study of Organohalogens in foodstuffs and environmental samples by neutron activation analysis and related techniques, *Nucleonika*, 49(3):101-106.
- Garabrant D. H., J Held., B Langholz., J.M Peter, T.M Mark. (1992). DDT and Related Compounds and Risk of Pancreatic Cancer. *J. Natl. Cancer Inst.*, 84 (10):764-771.
- Gribble G.W. (2003). The Diversity Of Naturally Occuring Organohalogen Compounds. *Chemosphere*, 52:289-297.
- Gustavson K, Jonsson P. (1999). Some halogenated organic compounds in sediments and blue mussel (*Mytilus edulis*) in Nordic Seas. *Mar Pollut Bull*, 38:723-736.
- Haynes D, Mosse P, Levay G. (1995). The use of transplanted cultured mussels (*Mytilus edulis*) to monitor pollutants along the Ninety Mile Beach, Victoria, Australia. *Mar Pollut Bull*, 30:463-469.
- IAEA-TECDOC-564. (1990). Practical aspects of operating NAA laboratory. Vienna. p.197-237.
- Kawano M. (2004). Persistent organohalogens in environmental materials. *Analytical Applications of Nuclear Techniques*, IAEA.
- Kawano M, Falandysz J, Morita M. (2008). Instrumental neutron activation analysis of extractable organohalogens in marine mammal, harbor porpoise (*phocoena phocoena*) and its feed, Atlantic herring (*clupea harengus*), from the Baltic sea. *J. of Radioanalytical and Nuclear Chemistry*, 278(2):263-266.
- Kawano M, Sajwan K.S, Owen D.A. (2001). Extractable organohalogens (EOX) in sediment and mussel tissues from the Kentucky lake and Kentucky Dam tailwater, USA. *Tox. And Environ. Chem.*, 79(3):233-242.
- Laniewski K, Boren H, Grimwall A. (1999). Fraction of Halogenated Organic Matter Present in rain and Snow. *Chemosphere*, 38: 393-409.
- Larsen E. H., M. B. Ludwigsen. (1997). Determination of Iodine in food related certified reference materials using wet ashing and detection by inductively coupled plasma mass spectrometry. *J. Anal. Atomic Spectrometry*, 12(1) :435-439.

Lunde G, J Gether. (1976). Determination of volatility and chemical persistence of lipid-soluble halogenated organic substances in marine organisms. *AMBIO*, 5:180–183.

Martinsen K, Kringstad A, Carlberg G E. (1988). Methods for determination of some parameters and characterization of organochlorine compounds in spent bleach liquors from pulp mills and water, sediment and biological samples from receiving waters. *Water Sci Technol*, 20:13–24.

Wu ming. (2007). Californians for fire safety: chemical companies get cute with voters. [Online] Available: [www.unbossed.com](http://www.unbossed.com), accessed, 20<sup>th</sup> Sept., 2008.

Yokouchi Y, Noijiri Y, Barrie L A. (2000). A Strong Source of Methyl Chloride to the atmosphere from tropical coastal land. *Nature*, 403: 295-298.

Table 1. Nuclear data for the elements

Elements (Kev)	Isotope (% abund)	Nuclide	Cross-section (b)	T <sub>1/2</sub>	t <sub>i</sub>	t <sub>d</sub>	t <sub>c</sub>	Energy
Cl	<sup>37</sup> Cl(24.23)	<sup>38</sup> Cl	0.428±0.005	37min	2min	1-10min	10min	1642.4 2167.5
Br	<sup>81</sup> Br(49.31)	<sup>82</sup> Br	2.69±0.09	35.2hrs	1hr	24hrs	10min	554.3 776.5
I	<sup>127</sup> I(100.00)	<sup>128</sup> I	6.2±0.2	24.99 min	2 min	1-10min	10 min	442.3

Table 2. Comparison of elemental concentrations of NIST-SRM 1566<sup>b</sup> (Oyster tissue), reported values and local laboratory values (mg/kg)

Element	Present study	Reported value
Al	196.4±7.1	197.2±6.0
Ca	0.0796±0.0040	0.0838±0.0020
Cl	0.492±0.03	0.514±0.01
Co	0.331±0.021	0.371±0.009
Cu	69.04±2.0	71.6±1.6
K	0.549±0.011	0.652±0.009
Mg	0.1990±0.0120	0.1085±0.0023
Mn	18.01±0.4	18.5±0.2

Table 3. Comparison of elemental concentrations of CRM-DORM-2 (Dogfish muscle), reported values and local laboratory values (mg/kg)

Element	Present work	Reported value
Al	10.41±1.2	10.9±1.7
As	19±0.9	18±1.1
Cd	0.051±0.006	0.043±0.008
Co	0.212±0.011	0.182±0.031
Cr	35.1±4.8	34.7±5.5
Cu	2.22±0.21	2.34±0.16
Fe	143±8	142±
Ni	19.7±2.8	19.4±3.1
Zn	24.8±1.9	25.6±2.3

Table 4. Comparison of elemental concentrations of NIST-SRM 1547 (Peach leaves), reported values and local laboratory values (mg/kg)

Element	Present study	Reported value
Al	242±4.7	249±8
Br	12±0.28	(11)*
Ca(%)	1.60±0.06	1.56±0.02
Cl	358±16	360±19
Cu	3.9±0.3	3.7±0.4
I	0.4±0.02	(0.3)*
K(%)	2.51±0.02	2.43±0.03
Mg(%)	0.419±0.004	0.432±0.008
Na	22±0.18	24±0.20
Zn	17.2±0.3	17.9±0.4

\*Non Certified/Recommended value

Table 5. Mean concentration of total and extractable organohalogens (EOX) in the fish samples (mg/kg)

Sample	Cl(Total)	EOCl	Br(Total)	EOBr	I(Total)	EOI
CGW	951.60±36.30	216.00±8.90	10.70±0.20	8.20±0.10	1.40±0.02	1.35±0.02
CNW	1066.91±32.60	227.50±6.80	12.30±0.30	8.40±0.10	4.20±0.20	1.70±0.03
TZW	877.60±34.90	189.10±4.00	14.60±0.40	11.00±0.10	1.20±0.03	0.70±0.01
HNN	770.70±29.00	327.50±14.50	25.00±0.40	13.00±0.10	0.70±0.01	0.50±0.01
CON	1123.50±29.10	150.00±5.20	7.80±0.20	7.40±0.10	1.00±0.02	0.30±0.01
HON	831.10±25.20	350.40±9.10	10.30±0.30	8.00±0.10	1.50±0.03	0.90±0.01
TZN	931.00±27.60	303.20±5.50	14.60±0.20	6.70±0.10	0.80±0.02	0.60±0.01
CGN	846.50±29.70	221.60±6.90	8.50±0.10	6.50±0.10	0.72±0.01	0.50±0.01

CGW=*Clarias gariepinus* (Weija), CNW= *Chrysichthys nogroditatus* (Weija), TZW= *Tilapia zilli* (Weija)  
HNN= *Heterotis niloticus* (Nsawam), CON= *Channa obscura* (Nsawam), HON= *Hepsetus odoe* (Nsawam),  
TZN= *Tilapia zilli* (Nsawam), CGN= *Clarias gariepinus* (Nsawam)

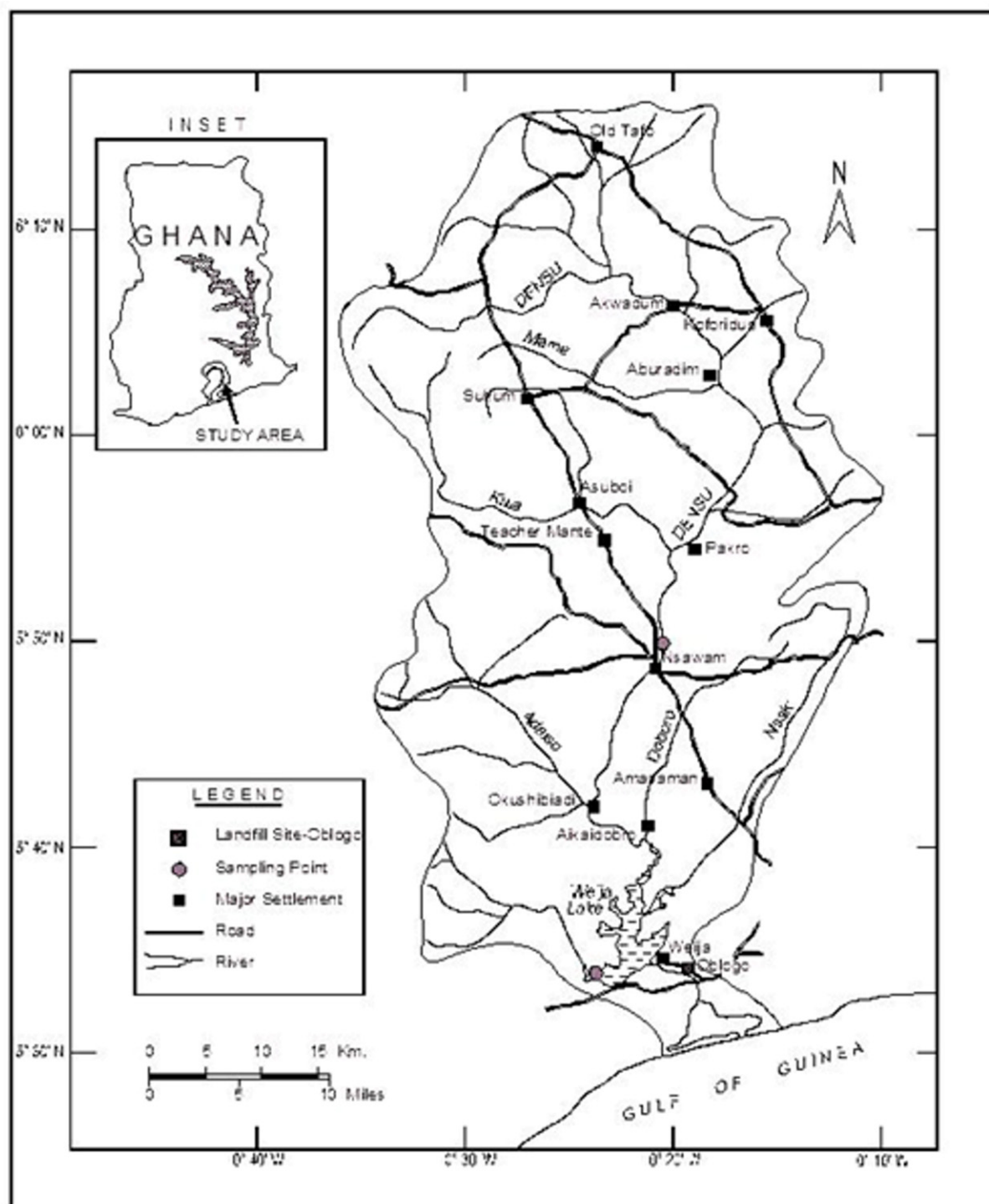


Figure 1. Map of Densu basin showing the sampling points

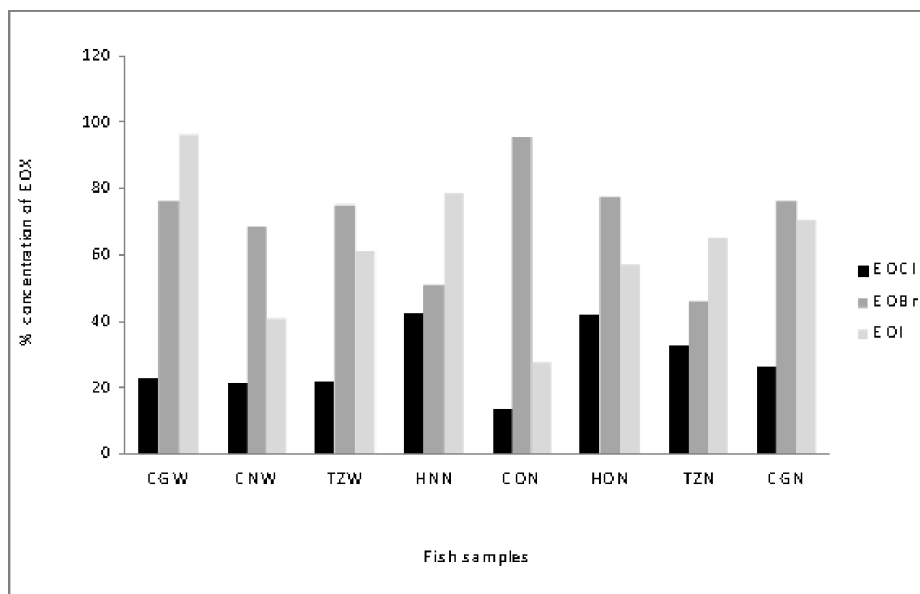


Figure 2. Percentage composition of extractable organohalogen in total halogen

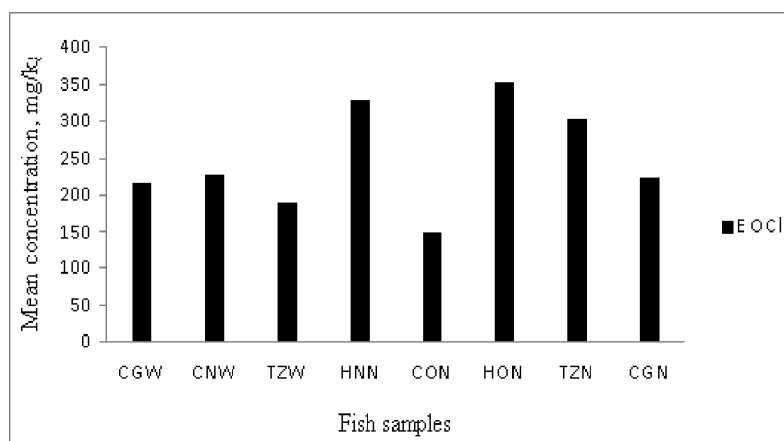


Figure 3. Distribution of EOCI in the fish samples

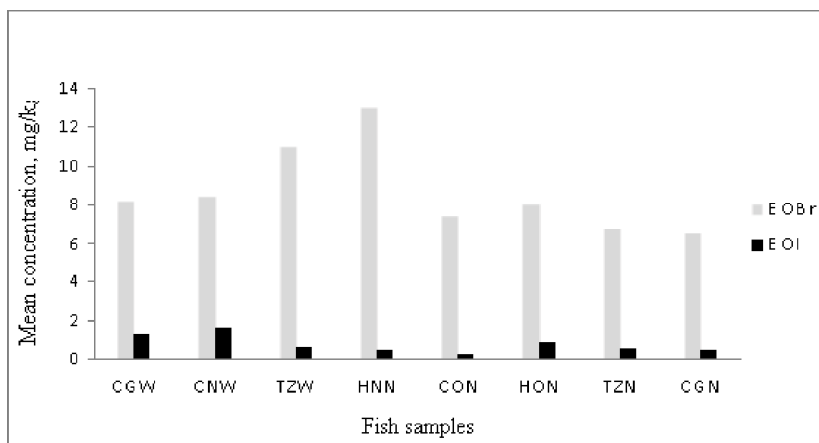


Figure 4. Mean concentrations of EOBr and EOI in the fish samples



# Performance Characteristics of Cells Containing Two Potentiometric Sensors: Application to a Cell Containing Hydralazinium and Chloride Electrodes

Laila A. Al-Shatti

The Public Authority for Applied Education and Training  
College of Nursing, P. O. Box 64923 Shuwaikh, Postal code 70466, Kuwait  
Tel: 965-9978-8632 E-mail: fetoon3@hotmail.com

Hayat Marafie (Corresponding author)

Chemistry Department, Faculty of Science, Kuwait University  
P.O. Box 5969 Safat, Postal Code 13060, Kuwait  
Tel: 965-9970-1877 E-mail: hayat.marafie@ku.edu.kw

Adel F. Shoukry

Chemistry Department, Faculty of Science, Kuwait University  
P.O. Box 5969 Safat, Postal Code 13060, Kuwait  
Tel: 965-9792-0693 E-mail: a.shoukry@ku.edu.kw

## Abstract

Conventional plastic membrane electrode, selective to hydralazinium cation (Hz) was constructed by incorporation of Hz-phosphotungstate ion associate in a poly(vinyl chloride) membrane. The influence of membrane composition, pH of the test solution and foreign ions on the cell performance was investigated. This was compared to the corresponding influence on a cell constructed by replacing the reference electrode in the conventional cell with Cl-selective electrode. The results indicated that the first cell showed Nernstian behavior, while the latter exhibited super Nernstian response. The selectivity for both cases was high. However the working pH range was narrower in case of the cell with two sensors.

**Keywords:** Hydralazinium-electrode, Phosphotungstate, Super Nernstian slope, Hydralazine hydrochloride, Plastic membranes

## 1. Introduction

Hydralazine hydrochloride (hydralazinium chloride, HzCl) is an important pharmaceutical compound used as a vasodilator in the treatment of hypertension (Ellershaw and Gurney 2001; Li et al., 2010). In a previous work a Hz-selective membrane electrode was prepared by incorporation of Hz-tetraphenylborate ion-pair into a poly(vinyl chloride) (PVC) matrix (Badawy et al., 1988). Although the electrode exhibited good performance characteristics, its life span was only about 2 hours. This created the demand to investigate the use of other ion-associates that are more lipophilic than Hz-tetraphenylborate, as ion-exchanger for the construction of plastic membrane Hz-electrodes of longer life times. This was done by introducing hydralazinium phosphotungstate (Hz<sub>3</sub>PT) ion associate as the ion-exchanger (Shoukry et al. 2006). The electrode showed Nernstian behavior over a life span of 17 days.

It was reported that one of the main disadvantages of direct potentiometry is the relatively high percent of error associated with slight indeterminate deviation of the reading (Christian 2004). Thus, for electrodes responsive to mono-, di-, and tri-valent ions; only 1.0 mV deviation results in a 12.0, 8.0 and 4.0 % error in the final determination, respectively. These error percentages were calculated assuming Nernstian behavior of the electrode. This drawback restricted the application of the traditional potentiometric technique using ion-selective electrodes especially for ions with high valency. However, the error can be, significantly decreased if the signal to noise ratio increased by increasing the graph slope.

In the present paper, a new technique has been applied successfully by which calibration graph of multiple Nernstian slope, and consequently higher signal to noise ratio, is obtained. The new technique depends on employing cells containing two ion selective electrodes, one for Hz<sup>-</sup> and the other, in place of the reference, for the counter ion, Cl<sup>-</sup>. The latter was a polycrystalline silver chloride-based electrode (Hodrejarve 1985). The cell potential in this case is given by:

$$E_{\text{cell}} = E_{\text{Hz}} - E_{\text{Cl}} \quad (1)$$

$$E_{\text{cell}} = [E^{\circ}_{\text{Hz}} + 2.303 \text{ RT/F} (\log a_{\text{Hz}})] - [E^{\circ}_{\text{Cl}} - 2.303 \text{ RT/F} (\log a_{\text{Cl}})] \quad (2)$$

where  $E^{\circ}$ , R, T, F and (a) have their familiar meanings.

For a dilute solution of HzCl,  $a_{\text{Hz}} = a_{\text{Cl}}$ ,

$$E_{\text{cell}} = (E^{\circ}_{\text{Hz}} - E^{\circ}_{\text{Cl}}) + 2.303 \text{ RT/F} (\log a_{\text{Hz}}) + 2.303 \text{ RT/F} (\log a_{\text{Cl}}) \quad (3)$$

$$E_{\text{cell}} = E^{\circ}_{\text{cell}} + 2 (2.303 \text{ RT/F}) (\log a_{\text{Hz}}) \quad (4)$$

Equation (4) shows that on plotting  $E_{\text{cell}}$  versus  $\log a_{\text{Hz}}$ , a straight line of double Nernstian slope is obtained, providing that the two sensors are functioning in a thermodynamic manner.

In a previous study (Shoukry, 1988) a cell containing two indicator electrodes was used for potentiometric titration of hexadecylpyridinium bromide with standard solution of sodium tetraphenylborate. Titration curves with sharp peaks or troughs, at the equivalence points, were obtained. Nevertheless, the study didn't include characterization of the cell's performance.

In the present work, the performance characteristics of cells containing two indicator electrodes are studied. Calibration graph's slope, stability and life span of the constructed cells as well as their responses towards changes of pH and presence of foreign ions have been investigated.

## 2. Experimental

### 2.1 Reagents and Materials

All chemicals used were of analytical grade. Bi-distilled water was used throughout all experiments. The Hz-PT ion-associate was prepared by a method similar to that described before by Shoukry et al. (1988). The composition of the produced ion-associate was determined by elemental analysis using Elementar Microcube. The agreement between calculated and found values was confirming the stoichiometry of (3:1) (Hz:PT).

### 2.2 Construction of Electrodes

#### 2.2.1 The chloride-selective electrode

A silver rod of 10.0 cm length and 5.00 mm diameter was tightly insulated by polyethylene tube leaving 1.0 cm at one end for coating and 0.5 cm at the other end for connection. The 1.0 cm terminal was electrolytically coated with AgCl. The coating was carried out in an 0.1 M NaCl solution with the silver rod as the anode and a platinum electrode of 1.0 cm<sup>2</sup> surface area as the cathode. The coating time was 10 minutes with current density of about 10 mA/cm<sup>2</sup>. The prepared electrode was preconditioned before use by soaking in a 10<sup>-2</sup> M NaCl solution for 30 minutes.

#### 2.2.2 The plastic membrane Hz-selective electrode

In about 5 mL tetrahydrofuran, 5.0, 10.0 or 15.5 mg of the ion-exchanger (Hz-PT) were dissolved and as well as 120 mg of each of PVC and dioctylphthalate (DOP), as plasticizer and solvent mediator. The produced solution mixture was poured into a 7.5 cm diameter Petri dish and left to dry in air. The obtained membrane was used to prepare the electrodes as previously described by Issa et al. (1999); the internal solution of the electrode was 10<sup>-3</sup> M in HzCl and 10<sup>-1</sup> M in NaCl.

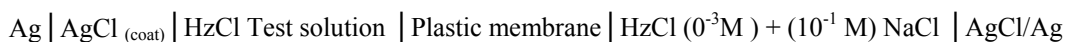
### 2.3 Potentiometric Studies and Electrochemical Systems

Potentiometric measurements were carried out with an Orion, Model 420A pH/mV meter. A Caron circulator thermostat was used to control the temperature of the test solution. The following electrochemical systems were employed:

#### 2.3.1 System containing one ion-selective electrode

Ag | AgCl<sub>(ref)</sub> | HzCl Test solution | Plastic membrane | (10<sup>-3</sup>M) HzCl, (10<sup>-1</sup> M) NaCl | AgCl | Ag

### 2.3.2 System containing two ion-selective electrodes



### 2.4 Construction of the Calibration Graphs

Suitable increments of standard HzCl solution were added to 50 mL of  $10^{-6}$  M HzCl solution to cover the concentration range of  $10^{-6}$  M to  $1.7 \times 10^{-2}$  M. In this solution the sensor and the reference electrode or the two sensors were immersed and the emf was recorded after 10 s, at  $25^{\circ}\text{C}$ , for each addition.

### 2.5 Selectivity

The selectivity coefficients of the Hz- selective electrode, ( $K^{\text{pot}}_{\text{Hz,j}}$ ) or that of the cell containing Hz- and Cl- electrodes, ( $K^{\text{pot}}_{\text{Hz,j}} k^{\text{pot}}_{\text{Cl,x}}$ ) towards different cationic species  $j^{z+}$  and different salts  $j_n^{z+} x_m^{y-}$  ( $nz = my$ ), respectively, were determined by the separate solution method (SSM) (Cosofret and Buck 1984) and matched potential method (MPM) (Ganjali et al. 2010).

## 3. Results and Discussion

### 3.1 Composition of membrane

Three membrane compositions were tried, in a previous work (Shoukry et al., 2006), as given in Table 1. The best responses over a relatively wide range of HzCl concentration are exhibited by electrodes made by using membranes containing 2.1 % ion associate. The response time was always  $< 10$  s. However, membranes containing 4.0% ion-pair exhibited more stable readings, for this reason, electrodes made by using membranes of this composition (4%) were selected for carrying out all consequent studies.

### 3.2 Response characteristics of cell containing Hz- and reference electrodes

The performance characteristics of Hz-selective electrodes were investigated as a function of soaking time. For this purpose the electrode was soaked in  $10^{-3}$  M solution of HzCl and the calibration graphs (pHz vs E, mV) were plotted after different time intervals in a period of 17 days. The electrode proved reasonable activity throughout this period. The conditioning time required for activating the phase boundary exchange process at the surfaces of the membranes was 30 minutes with concentration range of  $1.58 \times 10^{-5} - 1.7 \times 10^{-2}$  M HzCl (Fig. 1a). On soaking the electrode for longer than 17 days, the calibration graph slope decreased gradually. This decrease in the response of the electrode is most probably due to leaching of the active ingredients from the gel layer at the membrane surface to the bathing solution and/or to appearance of asymmetry potential arises as a result of surface deformation. The results also reveal that the origin of plastic membrane electrode potential is phase-equilibrium at the interfacial junction separating the hydrated gel layer from the test solution (Pungor 2001) rather than an equilibrium associated with ionic transport through the membrane body (Morf 2001).

### 3.3 Response characteristics of cell containing two ion selective electrodes

The cell produced calibration graphs of slopes of almost double Nernstian value. The cell attained stable potential within less than 10 seconds when the concentration of HzCl changed. The graphs were obtained at different intervals of soaking the electrodes in  $10^{-3}$  M HzCl (Figure 1b). From this figure, it is evident that only 30 minutes of soaking is sufficient, as conditioning time, for the activation of the cell where a calibration graph of average slope of 107.16 mV/ concentration decade was obtained. The cell retained this slope over fourteen days of continuous soaking, after which a gradual decrease in the slope value was observed. Therefore, it is recommended to store the electrodes in a closed vessel in a refrigerator while not in use.

### 3.4 Effect of pH

The effect of pH of the HzCl test solution on the potential reading is graphically represented in Figure 2. The pH of the initial solution is altered by the addition of small volumes of HCl and /or NaOH (0.1 – 1.0 M each). For cell containing Hz-selective electrode and reference electrode (Fig. 2 a), the pH has negligible effect within a wide range of pH-values extending from 3.2 – 9.4. In this range the electrode can be safely used for Hz determination without interference of Hydronium or hydroxyl ions. On the other hand, for cell containing Hz and Cl-sensors (Fig. 2 b), the working pH range of the cell was much narrower (4.2 – 6.0). This may be attributed to the fact that the pH-change affects two working electrodes surfaces instead of one as in case of the traditional cell. From Fig. 2b, it is clear that at pH-values higher than 6.0, the cell potential increases gradually. This may be attributed to interference of the hydroxyl ions with chloride ions at the surface of the AgCl-indicator electrode. This is confirmed by the fact that the cell potential change within this pH-range was found to be reversible. This excludes the possibility of passivation of the AgCl-electrode surface as a result of irreversible surface adsorption.

### 3.5 Selectivity

#### 3.5.1 Cell containing Hz- and reference electrodes

The selectivity of the Hz-responsive electrodes was studied by applying the separate solution (Cosofret and Buck, 1984) and the matched potential (Ganjali et al., 2010) methods as previously described. The selectivity coefficients towards  $\text{Na}^+$ ,  $\text{K}^+$ ,  $\text{Mg}^{2+}$  and  $\text{Cd}^{2+}$ , as obtained by the separate solution method were  $4.2 \times 10^{-3}$ ,  $5.8 \times 10^{-3}$ ,  $1.7 \times 10^{-3}$  and  $9.20 \times 10^{-3}$ , respectively. In case of applying the matched potential method, the corresponding values were  $5.00 \times 10^{-2}$ ,  $5.3 \times 10^{-2}$ ,  $2.4 \times 10^{-2}$  and  $3.30 \times 10^{-2}$ , respectively. It is noticeable that the values obtained by the matched potential method are, in general higher than those obtained by the separate solution method, this may be attributed to the non-Nernstian behavior of the interfering ion in case of the separate solution method. However, the results, as obtained by the two methods, revealed high selectivity of the electrodes for Hz towards different cationic species.

#### 3.5.2 Cell containing Hz- and Cl- selective electrodes

##### 3.5.2.1 Application of the separate solution method

The cell potential is measured for two separate solutions, one containing HzCl of activity  $a_{\text{Hz}} = a_{\text{Cl}} = 10^{-3} \text{ M}$ ,  $E_1$ , and the other containing the interferent salt  $\text{J}_m^{z+} \text{X}_n^{y-}$ , where  $mz = ny$ , and the activity  $a_j = (m/n) a_x$ ,  $E_2$ .

$$E_1 = [E^\circ_{\text{Hz}} + (2.3RT/F) \log a_{\text{Hz}}] - [E^\circ_{\text{Cl}} - (2.3RT/F) \log a_{\text{Cl}}] \quad (5)$$

where  $E^\circ$ ,  $R$ ,  $T$ ,  $F$  and  $(a)$  have their familiar meaning.

$$E_1 = K + (2.3RT/F) \log a_{\text{Hz}} a_{\text{Cl}} \quad (6)$$

where  $K = E^\circ_{\text{Hz}} - E^\circ_{\text{Cl}}$

$E_2$  is given by Nicolsky (1937) equation,

$$E_2 = [E^\circ_{\text{Hz}} + (2.3RT/F) \log k^{\text{pot}}_{\text{Hz,J}} (a_j)^{m/z}] - [E^\circ_{\text{Cl}} - (2.3RT/F) \log k^{\text{pot}}_{\text{Cl,X}} (a_x)^{n/y}] \quad (7)$$

$$E_2 = K + (2.3RT/F) \log k^{\text{pot}}_{\text{Hz,J}} + (2.3RT/F) \log (a_j)^{m/z} + (2.3RT/F) \log k^{\text{pot}}_{\text{Cl,X}} + (2.3RT/F) \log (a_x)^{n/y} \quad (8)$$

$$E_2 = K + (2.3RT/F) \log k^{\text{pot}}_{\text{Hz,J}} k^{\text{pot}}_{\text{Cl,X}} + (2.3RT/F) \log (a_j)^{m/z} (a_x)^{n/y} \quad (9)$$

From (6) and (9),

$$(2.3RT/F) \log k^{\text{pot}}_{\text{Hz,J}} k^{\text{pot}}_{\text{Cl,X}} = (E_2 - E_1) + (2.3RT/F) \log a_{\text{Hz}} a_{\text{Cl}} - (2.3RT/F) \log (a_j)^{m/z} (a_x)^{n/y} \quad (10)$$

$$\log k^{\text{pot}}_{\text{cell}} = (E_2 - E_1) / (2.3RT/F) + \log a_{\text{Hz}} a_{\text{Cl}} - \log (a_j)^{m/z} (a_x)^{n/y} \quad (11)$$

$k^{\text{pot}}_{\text{cell}}$  is the selectivity coefficient of the cell ( $k^{\text{pot}}_{\text{Hz,J}} k^{\text{pot}}_{\text{Cl,X}}$ ).

It is noticeable that equation (11) is corresponding to the following equation which is applied for a cell containing one sensor electrode (Issa et al., 1999)

$$\log k^{\text{pot}}_{\text{Hz,J}} = (E_2 - E_1) / (2.3RT/F) + \log a_{\text{Hz}} - \log a_j^{z+} \quad (12)$$

The obtained  $\log k^{\text{pot}}_{\text{cell}}$  values are given in Table (3). The results revealed high selectivity of the cell containing two sensors for HzCl towards different inorganic salts.

##### 3.5.2.2 Application of the matched potential method.

The selectivity of the cell was measured by determining the concentration ratio of HzCl and the interfering salt  $\text{J}_m^{z+} \text{X}_n^{y-}$  that causes the same potential change when added to a reference HzCl solution. Thus, the change in potential was measured upon changing HzCl concentration, then the interfering salt was added to an identical reference solution until the same potential change was obtained. The method (Ganjali, 2010) is recommended by IUPAC. It

has the advantage that it gets rid of the limitations of the other methods based on the Nicolsky-Eisenman equation (Girault, 2004, and Koryta, 1986). The main limitation is the non-Nernstian behavior of the interfering ions. According to this method, the selectivity coefficient is calculated as the selectivity ratio of the primary molecule (HzCl) and the interfering salt  $J_m^{z+} X_n^{y-}$  that gives the same potential change in a reference solution,

$$k_{\text{cell}}^{\text{pot}} = \Delta C_{\text{HzCl}} / C_{J_m X_n} \quad (13)$$

where  $\Delta C_{\text{HzCl}}$  and  $C_{J_m X_n}$  are the change in HzCl concentration and the concentration of the interfering salt that cause the same potential change in a reference solution of HzCl.

Collective results of  $k_{\text{cell}}^{\text{pot}}$  obtained for the investigated cells towards NaCl, KCl,  $\text{NaNO}_3$ ,  $\text{KNO}_3$ ,  $\text{CH}_3\text{COONa}$ ,  $\text{MgCl}_2$ ,  $\text{Na}_2\text{SO}_4$ ,  $\text{Cd}(\text{NO}_3)_2$ ,  $\text{Mg}(\text{NO}_3)_2$  and  $\text{MgSO}_4$  as obtained by the separate solution and matched potential methods are given in Table (3). The results revealed that the proposed cells showed comparable selectivity coefficients by applying the two methods although the values obtained by the MPM were, in general, slightly lower than those by the SSM. It is also noteworthy that the values of  $k_{\text{cell}}^{\text{pot}}$  for monovalent salts are higher than those for salts containing divalent ions, this can be explained on the base that electrostatic nature of monovalent salts in its hydrated forms is more relevant to those of a hydralazinium chloride than divalent ions-containing salts.

#### 4. Conclusion

Potentiometric cells, containing two ion selective electrodes, one for Hz- and the second for Cl-, exhibit comparable performance characteristics to those of cells containing Hz and a reference electrode. However, these cells exhibit calibration graphs ( $E_{\text{cell}}$  versus pH<sub>Hz</sub>) with slopes of about double Nernstian values.

#### Acknowledgement

The authors would like to acknowledge Kuwait University support for providing the facilities of ANALAB (grant no. GS01L01) and SAF (grant no. GS03/01).

#### References

- Badawy, S.S. , Shoukry, A. F., Rizk, M.S., and Omar M.M. (1988). Hydralazine-selective PVC membrane electrode based on hydralazinium tetraphenylborate. *Talanta*, **35**(6), 487-489.
- Christian, G. D. (2004). *Analytical Chemistry*, John Wiley & Sons, Inc. 6<sup>th</sup> Edn., p. 383.
- Cosofret, V. V. and Buck, R. P. (1984). Phenothiazine drug poly (vinyl chloride) matrix membrane electrodes and their use in pharmaceutical analysis. *Analyst*, 109, 1321-1325.
- Ellershaw, D. C. & Gurney, A. M. (2001). Mechanisms of hydralazine induced vasodilation in rabbit aorta and pulmonary artery. *British Journal of Pharmacology*, 134, 621-631.
- Ganjali, M. R., Faridbod, F., Larijani, B., Riahi, S., Hosseini, M., Esfahani, E. N. & Norouzi, P. (2010). Terazosin potentiometric sensor for quantitative analysis of terazosin hydrochloride in pharmaceutical formulation based on computational study. *Int. J. Electrochem. Sci.*, 5, 200-214.
- Girault, H. H. (2004). *Analytical and physical electrochemistry*, EPFL Press, Marcel Dekker, Inc., NY 10016, USA.
- Hodrejarv, H. (1985). *Ion-selective Electrodes 4*, Ed. E. Pungor, Elsevier Science Publishers, The Netherland, p. 449.
- Issa, Y.M., Abdel-Ghani, N. T., Shoukry, A.F. and Ahmed, H. M. (1999). Amineptine plastic membrane electrode based on its ion-associate with tetraphenylborate and phosphomolybdic acid. *Mikrochimica Acta*, 132, 83-88.
- Koryta, J. (1986). Ion-selective electrodes. *Annual Review of Materials Science*. 16, 13-27.
- Li, Y., Saito, Y., Kuwahara, K., Rong, X., Kishimoto, I., Harada, M., Horiuchi, M., Murray, M. & Nakao, K. (2010). Vasodilator therapy with hydralazine induces angiotensin AT2 receptor-mediated cardiomyocyte growth in mice lacking guanylyl cyclase-A. *British Journal of Pharmacology*, 159, 1133-1142.
- Morf W. E. (1981). *The Principles of Ion-selective Electrodes and of Membrane Transport*, Akademiai Kiado, Budapest, p.115.
- Pungor, E. (2001). The new theory of ion-selective electrodes. *Sensors*, 1, 1-12.
- Shoukry, A. F. (1988). Use of two ion-selective electrode-containing cells for potentiometric titration of hexadecylpyridinium bromide. *Analyst*, 113, 1305-1308.

Shoukry, A.F., Badawy, S.S. and Farghali, R. (1988). Hexadecylpyridinium-phosphotungstate ion association in construction of a hexadecylpyridinium cation selective electrode. *Anal. Chem.*, 60, 2399-2402.

Shoukry, A.F., Marafie, H. M., El-Shatti, L. A. (2006). X-ray photoelectron spectroscopy and electron microscopy of hydralazinium ion-selective electrode membrane's surface. *Electroanalysis*, 8, 779-785.

Table 1. Effect of membrane composition on Hz-electrode performance (30 minutes soaking)

Ion pair % (mg)	DOP % (mg)	PVC % (mg)	Range M	Slope*	Response Time, sec
2.0 (5.0)	48.98 (120)	48.98 (120)	$2.74 \times 10^{-6}$ - $1.70 \times 10^{-2}$	56.67	< 10
4.0 (10.0)	48.00 (120)	48.00 (120)	$1.58 \times 10^{-5}$ - $1.70 \times 10^{-2}$	53.80	<10
6.1 (15.5)	46.97 (120)	46.98 (120)	$9.33 \times 10^{-6}$ - $1.70 \times 10^{-2}$	49.67	<10

\* mV/Hz concentration decade

Table 2. Effect of soaking on Hz-electrode performance

Soaking time	Slope	Concentration range (M)
0.5hour	53.80	$1.58 \times 10^{-5} - 1.7 \times 10^{-2}$
1 hour	55.490	$3.16 \times 10^{-6} - 1.7 \times 10^{-2}$
2 hours	55.000	$6.31 \times 10^{-6} - 1.7 \times 10^{-2}$
24 hours	54.030	$4.00 \times 10^{-6} - 1.7 \times 10^{-2}$
48 hours	57.640	$1.26 \times 10^{-6} - 1.7 \times 10^{-2}$
72 hours	60.030	$6.31 \times 10^{-6} - 1.7 \times 10^{-2}$
8 days	63.011	$1.00 \times 10^{-6} - 1.7 \times 10^{-2}$
10 days	59.990	$6.31 \times 10^{-6} - 1.7 \times 10^{-2}$
17 days	54.980	$6.31 \times 10^{-6} - 1.7 \times 10^{-2}$

\* mV/Hz concentration decade

Table 3. Selectivity coefficients,  $K_{Hz,j} K_{Cl,x}$ , of a cell containing Hz and Cl<sup>-</sup> selective electrodes, for HzCl towards inorganic salts, at 25°C

Interferent	SSM*	MPM**
NaCl	$1.90 \times 10^{-1}$	$8.30 \times 10^{-3}$
KCl	$2.40 \times 10^{-1}$	$9.79 \times 10^{-3}$
NaNO <sub>3</sub>	$1.20 \times 10^{-2}$	$2.08 \times 10^{-3}$
KNO <sub>3</sub>	$1.23 \times 10^{-2}$	$4.59 \times 10^{-3}$
CH <sub>3</sub> COONa	$1.10 \times 10^{-2}$	$3.95 \times 10^{-3}$
Na <sub>2</sub> SO <sub>4</sub>	$5.86 \times 10^{-3}$	$3.48 \times 10^{-3}$
MgCl <sub>2</sub>	$1.27 \times 10^{-1}$	$8.40 \times 10^{-3}$
MgSO <sub>4</sub>	$0.37 \times 10^{-2}$	$1.31 \times 10^{-3}$
Mg(NO <sub>3</sub> ) <sub>2</sub>	$7.46 \times 10^{-3}$	$2.38 \times 10^{-3}$
Cd(NO <sub>3</sub> ) <sub>2</sub>	$2.23 \times 10^{-3}$	$1.14 \times 10^{-3}$

\*Separate solution method.

\*\*Matched potential method

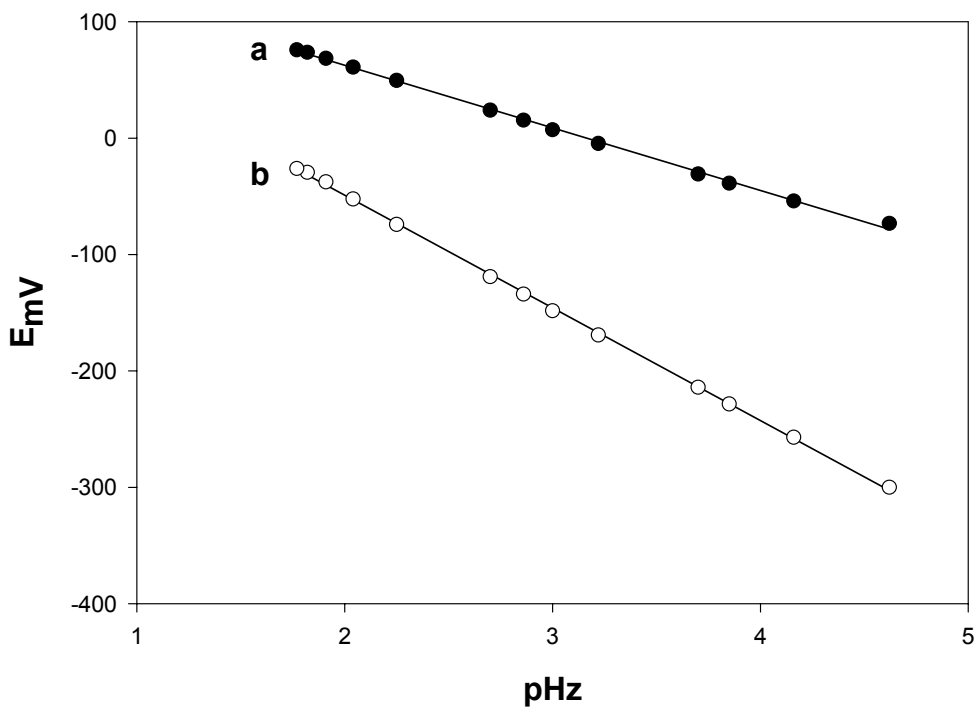


Figure 1. Calibration graphs obtained after 30 minutes conditioning time for (a) cell containing Hz- and reference electrode and (b) cell containing Hz- and Cl- selective electrodes

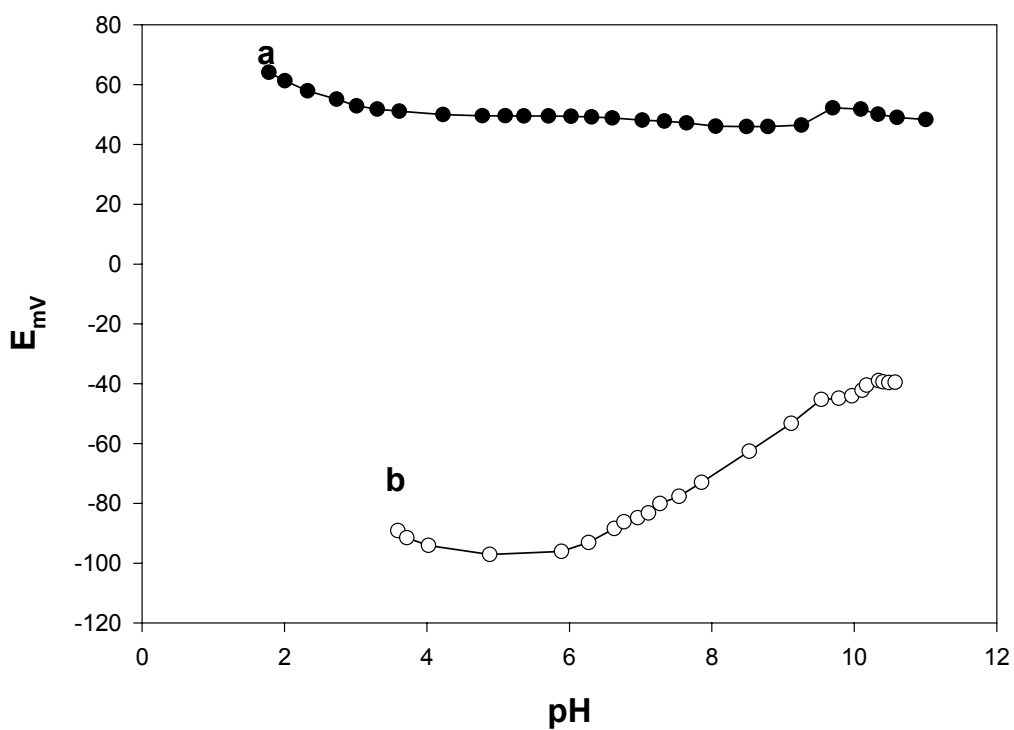


Figure 2. Effect of pH of the test solution on the potential of (a) cell containing Hz- and reference electrodes and (b) cell containing Hz- and Cl- responsive electrodes

# Densities, Viscosities and Refractive Indices of n- Butanol + Allyl Chloride Mixture at 298K

Aruna P. Maharolkar, Y. Sudke, S. Kamble & A Tidar

Microwave Research Lab, Department of Physics

Dr Babasaheb Ambedkar Marathwada University

Aurangabad-431004 MS, INDIA

Tel: 91-932-622-2790 E-mail: aruna\_physics@rediffmail.com

A. G. Murugkar, S.S. Patil & P. W. Khirade (Corresponding author)

Department of Physics, Dr. Babasaheb Ambedkar Marathwada University

Aurangabad-431004 MS, INDIA

E-mail: pwk004@yahoo.com

S. C. Mehrotra

Department of Computer Science & Information Technology

Dr. Babasaheb Ambedkar Marathwada University

Aurangabad-431004, INDIA

## Abstract

The density  $\rho$ , viscosity  $\eta$ , refractive index  $n$  and dielectric constant  $\epsilon_s$  of binary mixture of Allyl Chloride (AC) with n-Butanol including those of the pure liquids, were measured over the complete composition range at 298K. The experimental data is used to calculate excess molar volumes ( $v^E$ ), excess permittivity ( $\epsilon_s^E$ ), excess viscosity ( $\eta^E$ ), excess refractive index, molar refraction, excess molar polarization and Dunstan's constant. The variations of these parameters with composition and the effect of bonding in the binary mixture are discussed from the point of view of intermolecular interactions in these mixtures. The positive value of excess molar volume ( $v^E$ ) is attributed to the breaking of H-bonded associated species formed between unlike molecule at 298K.

**Keywords:** Excess density, Intermolecular interactions, Excess viscosity

## 1. Introduction

The particular manner whereby solute and solvent molecules are associated with one another in a liquid mixture brings about a distinct effect on the properties of the resulting system. Although physical properties of pure liquids abound in the literature, such properties measured for binary systems have been rather scarcely investigated up to now. Previously we described the intermolecular interactions between the components of Alcohols with other groups of liquids. In this work we extend the study by investigating properties like density, refractive index & viscosity. Ordinary liquids are made up of large molecules bound by weakly directional van der Waals forces; n-Butanol on the contrary, is made up of small molecules strongly bound by hydrogen bonds, in order of magnitude greater than van der Waals forces.

Hydrogen bonds in butanol are responsible for the striking behavior, and in some instances provide evidence for the role of butanol in the sequence of chemical reactions. Hydrogen bonding in butanol is believed to be highly cooperative, i.e., interaction of butanol molecule with a cluster of hydrogen bonded molecules is more likely than interaction with a single molecule to give a dimmer. Binary & ternary representations and prediction of intermolecular interactions with liquid dynamics by using reliable models intermolecular interactions is an essential task of considerable importance to gain some insights into the interactions among the groups of molecules or in important technological applications such as mass transfer, fluid flow heat transfer, design calculation or separation processes. To predict nature of interactions within the binary system excess properties were used.



In AC ( $\text{CH}_2=\text{CHCH}_2\text{Cl}$ ) molecules strong dipole - dipole interaction exists. Strong hydrogen bonding is present in n-Butanol ( $\text{C}_4\text{H}_9\text{OH}$ ) molecules. Because of presence of different type of association in both molecules, it is interesting to study the nature of intermolecular interactions between n-Butanol + Allyl Chloride. Allyl chloride is a common alkylating agent, useful in the manufacture of pharmaceuticals and pesticides. n-Butanol is used in the manufacture of pharmaceuticals. n-Butanol is also used as an extractant in the manufacture of antibiotics, hormones, and vitamins (Mellan, I., 1950; Doolittle, 1954); industrial uses of n-Butanol are as polymers, pyroxylin plastics, herbicide esters; n-Butanol is used as an ingredient in perfumes and as solvents for the extraction of essential oils (Doolittle, 1954), a solvent for paints, coatings, natural resins, gums, synthetic resins, dyes, alkaloids, and camphor. Alcohols play an important role in many chemical reactions due to its ability to undergo self-association with manifold internal structures and are in wide use in industries and science as reagents, solvents and fuels (Jui, 2005).

## 2. Experimental

### 2.1 Chemicals

The chemicals used in the present paper (n-Butanol & AC) are of spectroscopic grade and were used without further purification. The solutions were prepared at eleven different volume percentage of AC 0% to 100% in steps of 10% within 0.02% error limit.

### 2.2 Measurements

Viscosities were measured using Brookfield Viscometer with an accuracy of  $\pm 1\%$  for small sample size of 1 ml. Refractive indices (at Sodium D line) were measured by using Abbe Refractometer thermostated with constant water bath with precision of  $\pm 0.001$  and the values presented here are the mean values from five independent readings for each sample.

Density is measured using specific gravity bottle having an internal volume 3 ml and was calibrated with distilled water at 298K. Three specific gravity bottles were immersed in a thermostatic bath which was controlled at 298 K. A precision digital thermometer with a thermister probe was used to read the temperature with an accuracy of  $\pm 0.10$  K. The mixture densities were obtained by averaging the results from these three specific gravity bottles.

Dielectric constant is measured by using self developed setup in our laboratory.

## 3. Result & Discussion

The measured and estimated values of refractive index, density, viscosity and dielectric constant at 298 K are given in table 1. The density of the binary mixture of AC and n-Butanol is increasing as a mole fraction of AC in the mixture is increasing. This is expected because density of pure AC is more than that of pure n-Butanol. This variation of density is shown in table 1. From table 1 it can also be seen that the refractive index (n) is increasing with increase in mole fraction of AC in the mixture. This increase in n is further supported by the increase in density of the mixture with increase in mole fraction of AC.

Viscosity decreases as the mole fraction of AC in the binary mixture increases, as shown in table 1. Decrease in viscosity of the binary mixture can be attributed to decrease in the effect of hydrogen bonding with increase in mole fraction of allyl chloride. This is because n-Butanol is more viscous than AC. It is due to presence of strong hydrogen bonding in n-Butanol and more number of carbon atom and long straight chain compound. Figure 1 shows that the excess viscosity is positive.

The values of dielectric constant decrease with increase in mole fraction of AC in the mixture, as can be seen from the fifth column of table 1. This can be attributed to the decrease in hydrogen bonding in the mixture. This is because there is dipole – dipole interaction in pure AC and strong hydrogen bonding as in pure n-Butanol.

From figure 2 and 3, we see that the excess refractive index and excess density are negative, indicating the existence of intermolecular interaction and that these two excess parameters are supporting each other.

The Excess molar volumes  $v_m^E$  were calculated by using the following relation (El Hefnawy M, 2005; Yaw, 2005)

$$v_m^E = x_1 M_1 \left( \frac{1}{\rho} - \frac{1}{\rho_1} \right) + x_2 M_2 \left( \frac{1}{\rho} - \frac{1}{\rho_2} \right) \quad (1)$$

where  $M$  is the molecular mass; subscripts 1 and 2 stand for the pure components, AC and n-Butanol respectively.

The variation of  $v_m$  as mole fraction of AC is shown in figure 4. In pure n-Butanol, molecules are hydrogen bonded. On adding AC, these molecules get in between the n-Butanol molecules breaking the hydrogen bonds of n-Butanol molecules, thus leading to multimer formation. This changes the intermolecular interaction pattern and becomes the cause for decrease in molar volume of the mixture with increase in mole fraction of AC in the mixture as shown in figure 4. The excess molar volume is positive, as shown in figure 5. This fact is further supported by the negative excess density, shown in figure 3.

Excess permittivity is given by (25-26)

$$\epsilon_s^E = (\epsilon_s)_m - [(\epsilon_s)_A x_A + (\epsilon_s)_B x_B] \quad (2)$$

The variation of  $\epsilon_s^E$  for increase in mole fraction of AC in the binary mixture is shown in figure 6. The positive values of  $\epsilon_s^E$  indicate that the solute and solvent interact in such a way that the effective dipole moment increases. There is formation of monomers and dimers.

Molar refraction is given by the formula

$$R = v_m[(n^2-1)/(n^2+2)] \quad (3)$$

Figure 7 shows that the molar refraction decreases with increase in mole fraction of AC in the mixture. As molar refraction is a measure of total polarizability of a mole of a substance and is dependent on index of refraction and temperature, decrease in molar refraction indicates the decrease in molar polarization and decrease in dielectric constant with increase in the mole fraction of AC increases in the mixture.

Molar polarization is given by

$$P_m = [(\epsilon - 1) / (\epsilon + 2)] \cdot (M / \rho) \quad (4)$$

The estimated  $P_m$  is shown in figure 8. Decrease in  $P_m$  with increase in mole fraction of AC in the mixture also indicates the decrease in the effect of hydrogen bonding in the mixture. Figure 9 shows the positive excess molar polarization for different mole fraction of AC in the mixture.

Dunstan's constant is given by

$$(\rho/M) \eta \cdot 10^6.$$

The calculated values of Dunstan's constant are shown in figure 10.

Dunstan (1909) showed that for 'associated liquids' the value of this constant is much higher. From figure 10, it can be seen that higher values of Dunstan's constant are in the range of 30590 – 3000 indicating the association of the two liquids. The value decreases as the concentration of AC increases. This suggests breaking of hydrogen bonded associated species formed by unlike molecules at same temperature.

The excess properties follow a Redlich –Kister type polynomial equation (23-24)

$$f(x_1) = x_1 \cdot (1 - x_1) \cdot \sum_j B_j \cdot (1 - 2 \cdot x_1)^j$$

This equation is fitted by using method of least squares to all the excess properties. The estimated  $B_j$  coefficients are given in table 2. The standard error ( $\sigma$ ) between the data and the Redlich Kister model for the excess properties is given in the last column of the table.  $\sigma$  is calculated by using the relation

$$\sigma = (\Sigma \text{square of error between data and model} / (n-1)) \quad (5)$$

where  $n$  is the number of experimental data points. The graphs of excess properties and the corresponding Redlich-Kister model are shown the figures.

The standard errors in the  $B_j$  coefficients of the Redlich-Kister model along with the 95% confidence intervals for all excess properties are given in table 3. Comparison of estimated values refractive index, density, viscosity and dielectric constants for pure liquids (i.e. allyl chloride and n-Butanol) at 298K with the literature values is given in table 4.

#### 4. Conclusions

The summary of conclusions of intermolecular interaction between allyl chloride and n-Butanol is as follows:

- The values of refractive index and density are increasing with increase in mole fraction of allyl chloride. These two parameters are supporting each other.
- Decrease in viscosity of the binary mixture with increase in mole fraction of allyl chloride indicates that effect of hydrogen bonding decreases as mole fraction of allyl chloride increases
- The values of  $\epsilon_s$  decrease with the addition of allyl chloride in n-Butanol. This is due to decrease in effect of hydrogen bonding.
- Variations in refractive index, density, viscosity and dielectric constant with mole fraction of AC in the binary mixture of AC + n-Butanol indicate the existence of intermolecular interaction between n-Butanol and allyl chloride.
- There is monomer and dimer formation in the mixture which is supported by positive excess viscosity, positive excess molar volume, positive excess permittivity, decrease in molar refraction, decrease in molar polarization and decrease in dielectric constant.
- The estimated values of refractive index, density, viscosity for pure liquids at 298 K, are in good agreement with those reported in the literature.

## References

- [Online] Available: <http://chemicalland21.com/industrialchem/solalc/ALLYL%20ALCOHOL.htm>.
- [Online] Available: [http://clippercontrols.com/info/dielectric\\_constants.html](http://clippercontrols.com/info/dielectric_constants.html).
- [Online] Available: <http://suppliers.jimtrade.com/3/2913/120934.htm>.
- [Online] Available: <http://www.chemicalland21.com/petrochemical/N-BUTANOL.htm>.
- [Online] Available: [http://www.engineersedge.com/fluid\\_flow/fluid\\_data.htm](http://www.engineersedge.com/fluid_flow/fluid_data.htm).
- [Online] Available: <http://www.proximitycontrols.com/servicemanuals/rfandcrf.pdf>.
- [Online] Available: [http://www.sigmaaldrich.com/catalog/ProductDetail.do?N4=A30702%7CAldrich&N5=Product%20No.%7CBRAND\\_KEY&F=SPEC](http://www.sigmaaldrich.com/catalog/ProductDetail.do?N4=A30702%7CAldrich&N5=Product%20No.%7CBRAND_KEY&F=SPEC).
- [Online] Available: <http://www.solvaychemicals.us/static/wma/pdf/5/0/3/2/CAL.pdf>.
- A munsden J., Goodwin R. J. & Wetzel W. H. (1979). "Water-soluble pentachlorophenol and tetrachlorophenol wood-treating systems", ZA 7801031, published 28 Feb.
- Anil Kumar. (2007). Nain Densities and Volumetric Properties of Binary Mixtures of Formamide with 1-Butanol, 2- Butanol, 1,3-Butanediol and 1,4-Butanediol at Temperatures between 293.15 and 318.15 K. *J Solution Chem*, 36:497–516.
- Aurizio Fermeglia and Romano Lapasin. (1988). Excess Volumes and Viscosities of Binary Mixtures of Organics *J. Chem. Eng. Data*, 33, 415-417
- B. E. de Cominges, M. M. Piñeiro, E. Mascato, L. Mosteiro, T. P. Iglesias and J. L. Legido. (2003). RELATIVE PERMITTIVITIES OF BINARY MIXTURES OF 1-BUTANOL + *n*-ALKANE AT 298.15 K. *Journal of Thermal Analysis and Calorimetry*, Vol. 72 129.133.
- B. E. de Cominges, M. M. Piñeiro, E. Mascato, L. Mosteiro, T. P. Iglesias and J. L. Legido. (2003). RELATIVE PERMITTIVITIES OF BINARY MIXTURES OF 1-BUTANOL + *n*-ALKANE AT 298.15 K. *Journal of Thermal Analysis and Calorimetry*, Vol. 72 129. 133.
- Bonte, W. (1979). "Congener substances in German and foreign beers", Blutalkohol 16: 108–24, cited in *Butanols: four isomers*, Environmental Health Criteria monograph No. 65, Geneva: World Health Organization, 1987, ISBN 92-4-154265-9, [Online] Available: <http://www.inchem.org/documents/ehc/ehc/ehc65.htm>.
- C R C Handbook of Chemistry and Physics 64 th Edition 1983-1984 Editor Robert C Weast.
- Chan R. K. and Liao S.C. (1970). *Canadian Journal of Chemistry*, 48, 2988.
- Chaudhary A., Mehrotra S. C. (2002). *Mol. Phys.*, 100, 3907.
- Dharmalingam K., Ramachandran K., Sivagurunathan, Undre P. B., Khirade P. W., Mehrotra S. C. (2006). Dielectric studies of alkyl acrylates with primary alcohols using time domain reflectometry. *Molecular physics*, (Taylor & Francis). 104(18), 2835-2840.

- Doolittle A. K. (1954). *The Technology of Solvents and Plasticizers*, New York: Wiley, pp.644–45, cited in *Butanols: four isomers*, Environmental Health Criteria monograph No.65, Geneva: World Health Organization, 1987, ISBN 92-4-154265-9.
- Doolittle, A. K. (1954). *The Technology of Solvents and Plasticizers*, New York: Wiley, pp. 644–45, cited in *Butanols: four isomers*, Environmental Health Criteria monograph No. 65, Geneva: World Health Organization, 1987, ISBN 92-4-154265-9, [Online] Available: <http://www.inchem.org/documents/ehc/ehc/ehc65.htm>.
- El Hefnawy M and Tanaka R. (2005). Density and Relative Permittivity for 1-Alkanols + Dodecane at 298.15K. *J. Chem. Eng. Data*, 50, 1651-1656.
- Gabriel C., Gabriel S., Grant E. H., Hasted B. S. J. and Mingos D. M. P. (1998). Dielectric parameters relevant to microwave dielectric heating. *Chem. Soc. Rev.*, 27,213.
- Garcia, B., Herrera, C., Leal, J.M. (1991). Shear viscosities of binary liquid mixtures: 2-pyrrolidinone with 1-alkanols. *J. Chem. Eng. Data*, 36, 269–274.
- Giner, B. Artigas, H., Carrion, A., Lafuente, C., Royo, F.M. (2003). Excess thermodynamic properties of isomeric butanols with 2-methyl-tetrahydrofuran. *J. Mol. Liq.*, 108, 303–311.
- Hall R. L. Oser, B. L. (1965). "Recent progress in the consideration of flavouring ingredients under the food additives amendment. III. Gras substances", *Food Technol.*: 151, cited in *Butanols: four isomers*, Environmental Health Criteria monograph No. 65, Geneva: World Health Organization, 1987, ISBN 92-4-154265-9, [Online] Available: <http://www.inchem.org/documents/ehc/ehc/ehc65.htm>.
- J. A. Riddick, W. B. Bunger, and T. K. Sakano. (1986). *Organic Solvents, Physical Properties and Methods of Purification* (Wiley-Interscience, New York).
- J. Peyrelase, C. Boned and J. P. Le Petit. (1981). *J. Phys. E. Sci. Instrum.*, 14, 1002.
- Jimenez, E., Cabanas, M., Segade, L., Garcia-Garabal, S. Casas, H. (2001). Excess volumes, changes in refractive index and surface tension of binary 1,2-ethanediol + 1-propanol or 1-butanol mixtures at several temperatures. *Fluid Phase Equilib*, 180, 151–164.
- Jui Tang Chem and Wong Chao Chang. (2005). Densities Viscosities of Binary Mixtures of Propylene Glycol Monomethyl Ether Acetate with Methacrylic Acid, Benzyl Methacrylate and 2-Hydroxyethyl Methacrylate between 298.15K and 318.15K. *J Chem. Eng. Data*, 50, 1753-1756.
- Khirade P.W., Chaudhary A., Shinde J. B., Helambe S. N., Mehrotra S. C. (1999). Static Dielectric Constant and Relaxation Time Measurements on Binary Mixtures of Dimethyl Sulfoxide with Ethanol, 2-Ethoxyethanol, and Propanol at 293, 303, 313, 323K. *J. Chem. Engg. Data*, 44, 879.
- Khirade P.W., Chaudhary A., Shinde J. B., Helambe S. N., Mehrotra S. C. (1999). Temperature dependent Dielectric Relaxation of 2-Ethoxyethanol, Ethanol, and 1-Propanol in Dimethylformamide Solution Using Time Domain Technique. *J. Sol. Chem.*, vol, 28, 1031-1043.
- Kuang C. and Nelson S. O. (1997). *J. Micro. Pow. And E M Energy*, 32,114.
- M. Iglesias, B. Orge and J. Tojo. (1996). *Fluid Phase Equilibria*, 126, 203.
- Mellan, I. (1950). *Industrial Solvents*, New York: Van Nostrand Reinhold, pp. 482–88, cited in *Butanols: four isomers*, Environmental Health Criteria monograph No. 65, Geneva: World Health Organization, 1987, ISBN 92-4-154265-9, [Online] Available: <http://www.inchem.org/documents/ehc/ehc/ehc65.htm>.
- Mellan, I. (1950). *Industrial Solvents*, New York: Van Nostrand Reinhold, pp.482–88, cited in *Butanols: four isomers*, Environmental Health Criteria monograph No. 65, Geneva: World Health Organization, 1987, ISBN 92-4-154265-9, [Online] Available: <http://www.inchem.org/documents/ehc/ehc/ehc65.htm>.
- Monich, J. A. (1968). *Alcohols: Their Chemistry, Properties, and Manufacture*, New York: Chapman and Reinhold, cited in *Butanols: four isomers*, Environmental Health Criteria monograph No. 65, Geneva: World Health Organization, 1987, ISBN 92-4-154265-9, [Online] Available: <http://www.inchem.org/documents/ehc/ehc/ehc65.htm>.
- Prabhakar Undre, Helambe S. N., Jagdale S. B., Khirade P. W and Mehrotra S. C. (2007). Microwave dielectric characterization of binary mixture of formamide with N,N-dimethylamionethanol. *Pramana, J. of Phy*, 68, 5, 851-861.

R. L. Gardas S.L. (2008). Oswal Volumetric and Transport Properties of Ternary Mixtures Containing 1-Butanol or 1-Pentanol, Triethylamine and Cyclohexane at 303.15 K: Experimental Data, Correlation and Prediction by the ERAS Model *J Solution Chem*, 37: 1449–1470.

Rana V. A., Vyas A.D. and Mehrotra S. C. (2002). Dielectric relaxation study of mixtures of 1-propanol with aniline, 2-chloroaniline and 3-chloroaniline at different temperatures using time domain reflectometry. *J. Mol. Liq.*, 102, 379.

Rdlich O. Kister A. T. (1948). Algebraic Representation of thermodynamic properties and classification of solutions. *Ind. Eng Chem*, 40 345-348

Schreier Peter, Drawert, Friedrich; Winkler, Friedrich. (1979). Composition of neutral volatile constituents in grape brandies. *J. Agric. Food Chem.*, 27 (2): 365–72, doi:10.1021/jf60222a031.

Shannon E. (1949). *proc. IRE*, 37, 10.

Shirke R. M., Chaudhary A., More N. M., Patil P. B. (2001). *J. Mol. Liq.*, 27, 94.

Sivagurunathan P., Dharmalingam K., Ramachandran K., Undre P. B., Khirade P. W., Mehrotra S.C. (2007). Dielectric study of butyl methacrylate-alcohol mixtures by time-domain reflectometry. *PHYSICA B*, 387-203.

Sivagurunathan P., Dharmalingam K., Ramachandran K., Undre P. B., Khirade P. W., Mehrotra S. C. (2006). Dielectric relaxation study of mixtures of alkyl methacrylates and 1-alcohols using time domain reflectometry. *Philosophical Magazine letters*, (Taylor & Francis), 86(5), 291-300.

Sivagurunathan P., Dharmalingam K., Ramachandran K., Undre P. B., Khirade P. W., Mehrotra S.C. (2007). Dielectric studies on binary mixtures of ester with alcohol using time domain reflectometry. *J. Molecular Liquids*, 133-139.

Viscosity of liquids: theory, estimation, experiment, and data 0.34 By Dabir S. Viswanath ISBN 10-1-4020-5481-5(HB) Springer Dordrecht. Netherlands.

Yaw Wen Sheu and Chein Hsiun Tu. (2005). Densities Viscosities, Refractive indices and Surface Tensions for 12 flavor Esters from T= 288.15K to T=358.15K. *J Chem. Eng. Data*, 50, 1706-1710.

Table 1. Refractive index, density, viscosity and dielectric constant of allyl chloride + n-Butanol mixture at 298K

Mole fraction of AC	Refractive index	Density of AC + n-Butanol	Viscosity	Dielectric constant
0	1.397	0.8055	2.578	15.40
0.111	1.398	0.8155	2.350	14.58
0.220	1.400	0.8255	2.122	13.77
0.326	1.401	0.8365	1.894	12.96
0.429	1.403	0.8485	1.666	12.13
0.530	1.403	0.8606	1.439	11.32
0.629	1.404	0.8732	1.210	10.49
0.725	1.405	0.8851	0.984	9.68
0.819	1.407	0.9002	0.756	8.85
0.910	1.409	0.9119	0.528	8.06
1	1.412	0.9390	0.301	7.27

Table 2.  $B_j$  coefficients and standard error for excess density, excess viscosity, excess refractive index, and excess molar volume

Excess property ↓	$B_j$ coefficients				Standard Error
	$B_0$	$B_1$	$B_2$	$B_3$	
Excess density	-3.633E-02	-0.0331	1.349E-02	0.044403455	1.5223E-03
Excess viscosity	1.921E+00	6.824E-01	-3.464E-01	-2.140E+00	4.053E-02
Excess refractive index	-2.031E-02	-8.026E-03	7.014E-03	-6.525E-03	3.524E-04
Excess molar volume	2.095E+00	3.724E+00	-1.495E+00	-5.355E+00	1.458E-01

Table 3. Standard errors and 95% confidence intervals of the estimated  $B_j$  coefficients for excess density, excess viscosity, excess refractive index and excess molar volume

Excess property ↓		$B_j$ coefficients			
		$B_0$	$B_1$	$B_2$	$B_3$
Excess Density	standard error of parameter	0.0029	0.0115	0.0135	0.0299
	95 % confidence interval	0.0069	0.0271	0.0318	0.0707
Excess Viscosity	standard error of parameter	0.0004	0.0017	0.0020	0.0045
	95 % confidence interval	0.0010	0.0041	0.0048	0.0107
Excess Refractive Index	standard error of parameter	0.0007	0.0026	0.0031	0.0069
	95 % confidence interval	0.0016	0.0062	0.0073	0.0163
Excess Molar Volume	standard error of parameter	0.2598	1.0201	1.1975	2.6600
	95 % confidence interval	0.6143	2.4121	2.8315	6.2898
Excess permittivity	standard error of parameter	0.0117	0.0460	0.0540	0.1199
	95 % confidence interval	0.0277	0.1087	0.1276	0.2835
Excess molar polarization	standard error of parameter	0.1946	0.7641	0.8969	1.9924
	95 % confidence interval	0.4601	1.8068	2.1209	4.7113

Table 4. Comparison of estimated values refractive index, density, viscosity and dielectric constants for pure liquids(i.e. allyl chloride and n-Butanol) at 298K with the literature values

Property ↓	Liquid →	n-Butanol				Allyl chloride			
Refractive index	This work	1.397				1.412			
	Literature value (temperature)	1.3993 (20)	1.39741 (25)	1.39716 (25)	1.39719 (25)	1.4157(20)	1.413 ( )	1.4157 (20 )	1.414 (20 )
	Ref. No.	[28]	[35]	[39]	[40]	[28]	[18]	[17]	[19]
Density	This work	0.80554				0.939			
	Literature value (temperature)	0.8098 (20)	0.80556 (25)	0.80567 (25)	0.80554 (25)	0.81	0.9376 (20)	0.9392 (20 )	0.939 (25 )
	Ref. No.	[28]	[29]	[30]	[31]	[36]	[28]	[43]	[45]
Viscosity	This work	2.578				0.301			
	Literature value (temperature)	2.948 (20)	2.578 (25)	2.2601 (30)	2.2601 (30)	0.347 (15)	0.354 (20)	0.32 (22)	0.34 (20)
	Ref. No.	[28]	[32]	[33]	[34]	[28]	[46]	[47]	[48]
Dielectric constant	This work	15.4				7.27			
	Literature value (temperature)	17.8 (20)	17.5 (20)	17.15 (25)	17.5 (25)	8.2 (20)	8.2 (20)	8.2 ( )	
	Ref. No.	[28]	[35]	[37]	[38]	[44]	[41]	[42]	

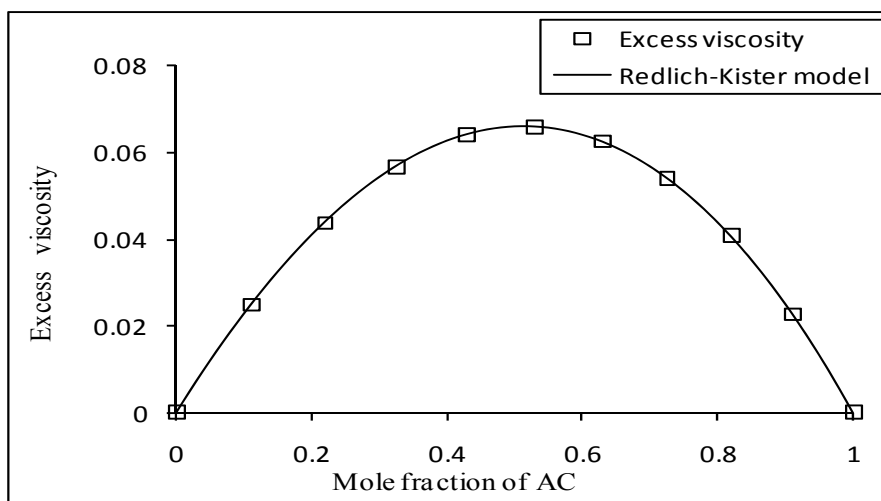


Figure 1. Variation of excess viscosity of AC + n-Butanol at 298

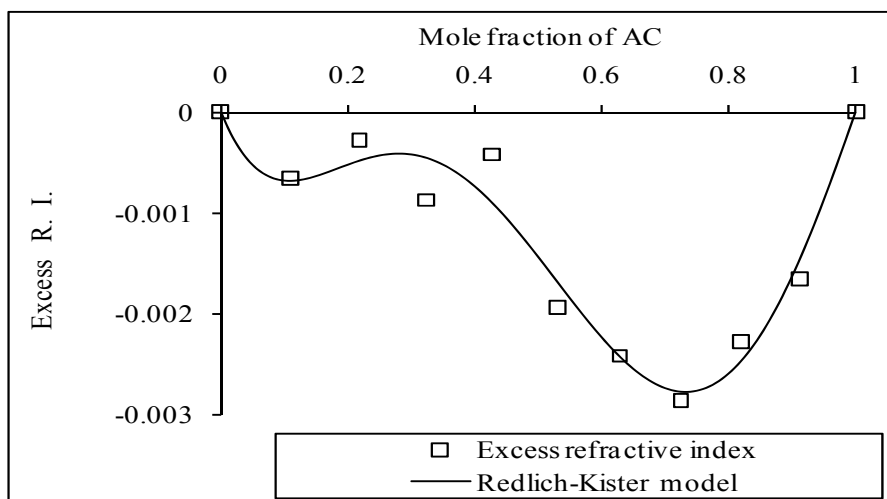


Figure 2. Variation of excess refractive index of AC + n-Butanol at 298 K

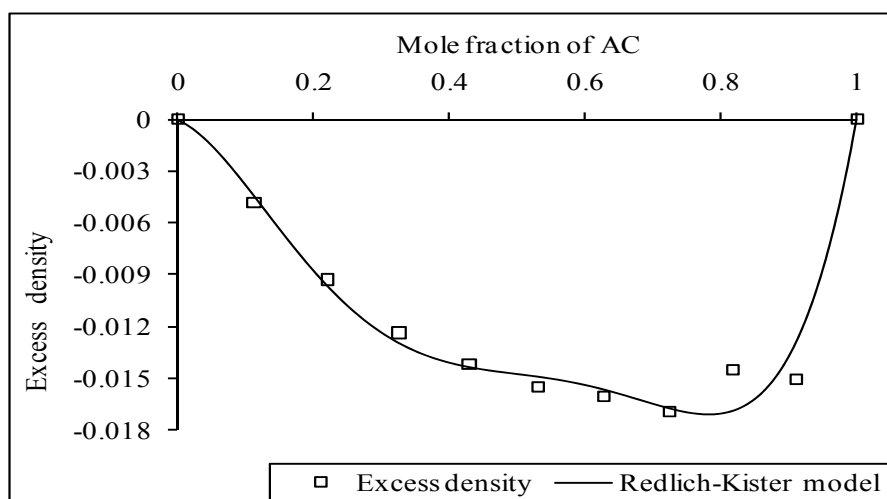


Figure 3. Variation of excess density of AC + n-Butanol at 298 K

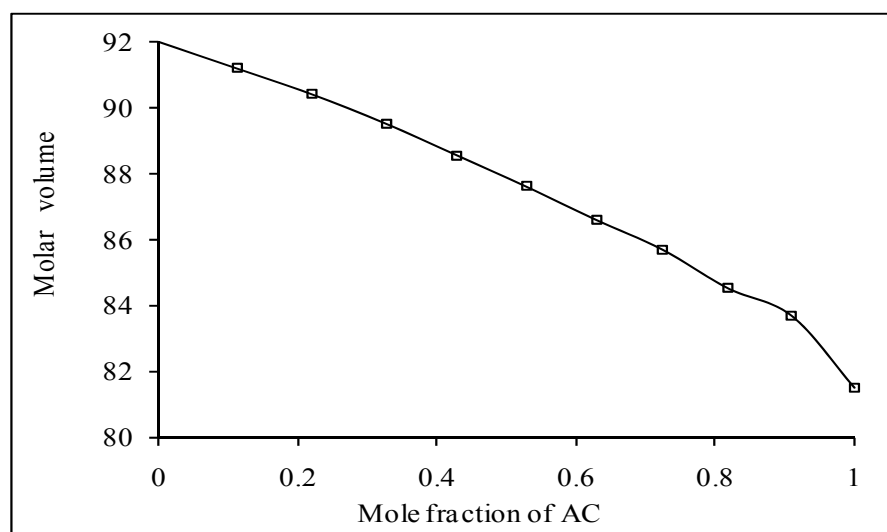


Figure 4. Variation of molar volume of AC + n-Butanol at 298 K



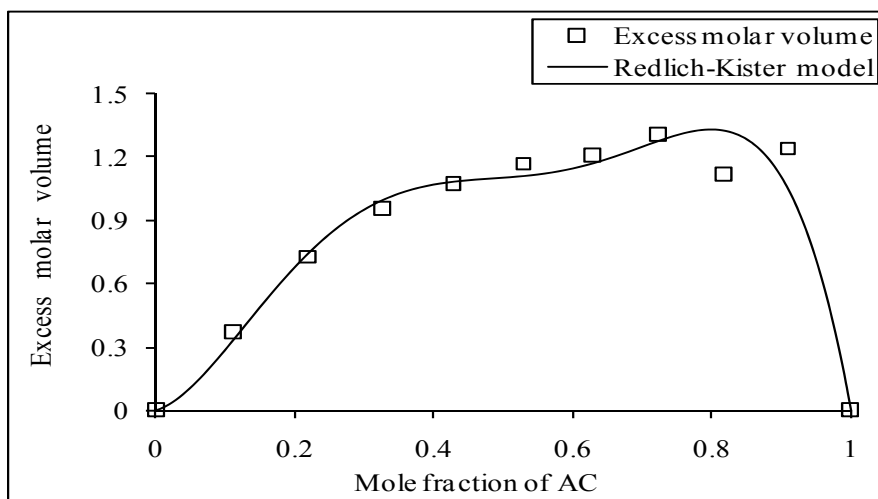


Figure 5. Variation of excess molar volume of AC + n-Butanol at 298 K

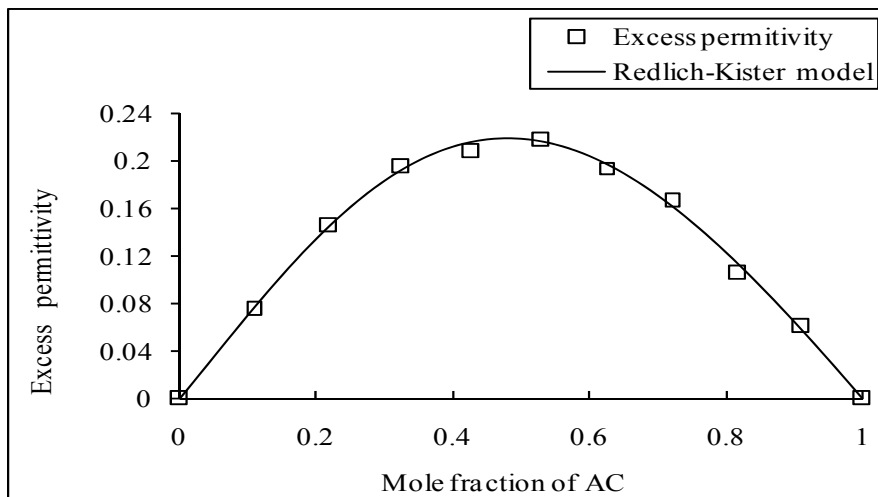


Figure 6. Variation of excess permittivity of AC + n-Butanol at 298 K

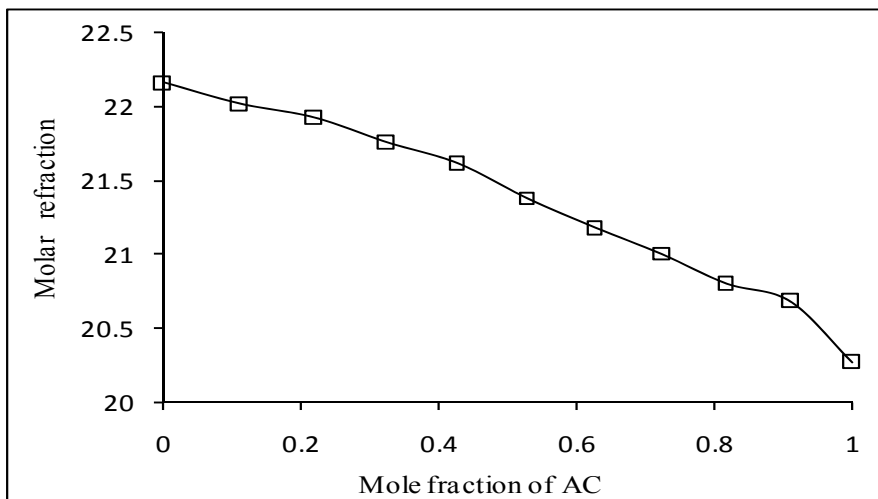


Figure 7. Variation of molar refraction of AC + n-Butanol at 298 K

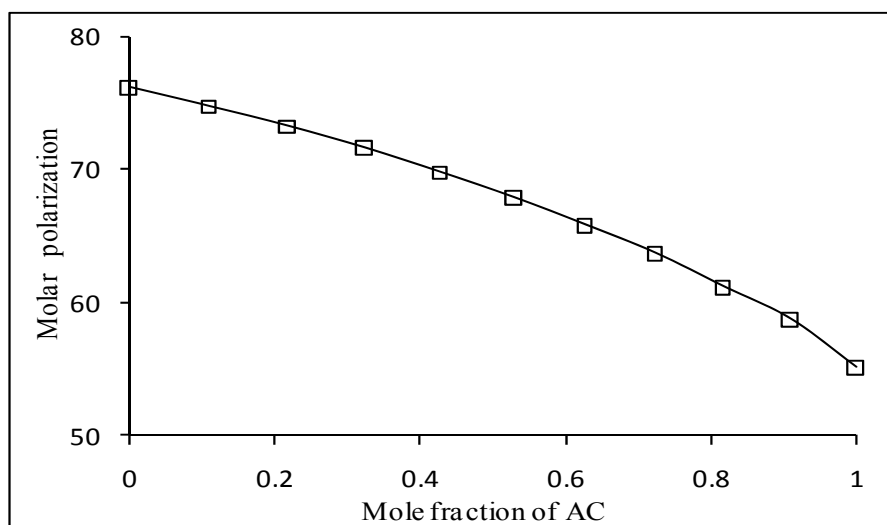


Figure 8. Variation of molar polarization of AC + n-Butanol at 298 K

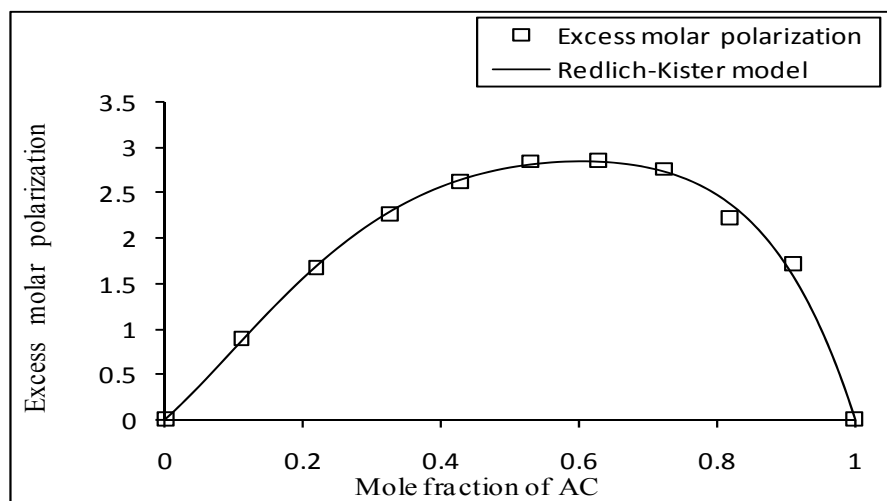


Figure 9. Variation of excess molar polarization of AC + n-Butanol at 298 K

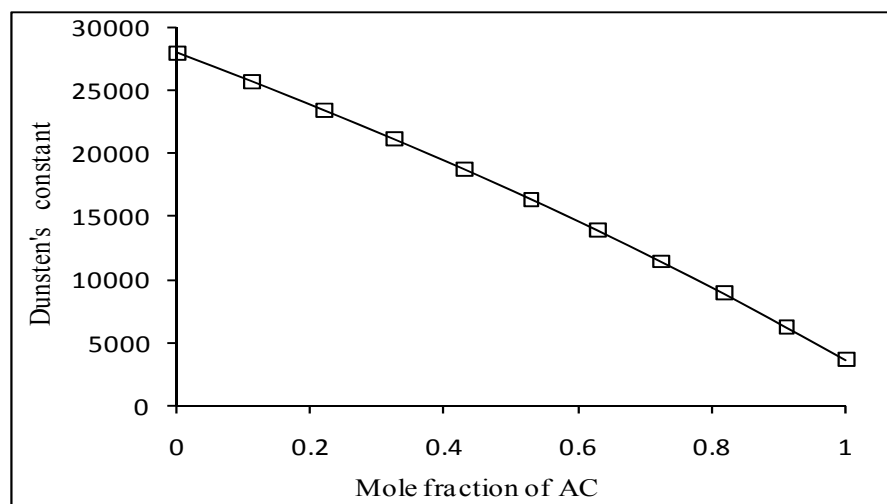


Figure 10. Variation of Dunstan's constant of AC + n-Butanol at 298 K

# DNA Chemical Damage and Its Detected

Shao Jun

Department of Basic Courses, Heze Medical College

Heze 274030, China

E-mail: linxianjie@sina.com

## Abstract

The DNA chemical damage is a very important researching project in chemistry, life science and related fields. In this paper, the biological function of DNA damage, the reason causing damage and the detecting technology of DNA damage are summarized and discussed.

**Keywords:** Living body, DNA damage, Detect

DNA is the main genetic material in living organism. Apart from few viruses using RNA as genetic material, all other organism's genetic material are DNA, which contains all of the genetic information needed for the growth, development and reproduction of organism. As a kind of macromolecule compound, DNA is consist of deoxyribonucleoside monophosphate which are connected each other by phosphodiester bond. DNA has two pieces of polynucleotide chains, which is double helix structure with hydrogen bonds that formed between the base pairs. The DNA damage and its effect to living organism are significant research projects in life science, medicine, chemistry and some other areas, and are also the research hot spots. In this paper, the biological function of DNA damage, the reason causing damage and the detecting technology of DNA damage are summarized and discussed.

## 1. DNA damage and its biological significance

In living organism, DNA is very stable or conservative, and its primary structure is hardly changed in vital processes. This is the fundamental guarantee for the cells, even for the whole living body maintaining and passing down of the vital characters. But the stability of the DNA molecule structure is not absolute, many factors that from the living organism or the environment could cause some abnormal change of the DNA structure, which is known as DNA damage. Because DNA damages are the changes of molecular structure, which almost all of them accompanied with bonds' breakage or formation, it is essentially one kind of chemical damages. Most of the DNA damage could be restored by the repair system in organism, and the unrepaired DNA damage is very little. But just the very a little unrepaired DNA damage maybe has a magically significant influence on the organism (Liu Dianfeng, 2006, p. 3-12; Hoeijmakers, 2001, p.366-374). If this damage occurs in the double-strand of the normal DNA, the structure of the DNA and its function maybe changed. If the damage occurs in the replication process of the DNA, it will lead to base mismatched, absent, and some other damages. And it will generate erroneous encoded RNA and consequently affect the DNA translation, if the damage occurs in the process of transcription. Gene mutation caused by DNA damage may lead to aging of the organism, cancer or some other diseases related to gene. However, not all the gene mutation is harmful to organism. Some of the gene mutation which is beneficial to organism maybe retained, and eventually maybe lead to the biological evolution. From this significance, we can say that DNA damage is one of the important factors for biological evolution. Artificial DNA damage or artificial induced mutation is an important method for the treatment of cancer or genetic diseases, With the development of the genetic engineering, artificial induced mutation have increasingly being used to improve or even create species(Wang, 2003, p. 557-558).

## 2. Causes of DNA damage

Causes of DNA damage are varied. They can be generally divided into physical and chemical factors, the latter is the major cause.

### 2.1 DNA damage caused by physical factors

DNA damage can be caused by some physical factors, such as high temperature, ultraviolet rays and other ionizing radiation. For example, Ultraviolet rays can cause thymine dimerization to yield thymine dimmers. The formation of thymine dimmers can cause a deformation of the DNA's double helix structure, and consequently affects DNA unwinding and other processes, and even lead to the cessation of DNA replication and transcription.

In addition, the ultraviolet rays can also cause the cross-linking of DNA double strand and DNA with protein. Most of DNA damage caused by ionizing radiation is not direct damage, but firstly inducing a large number of free radicals in organism, and then the free radicals will lead to various types of DNA damage. Additional, due to the rupture of phosphodiester bond caused by ionizing radiation, DNA double-strand breaks will be induced, (Miyakoshi, 2000, p.293-302). For example, the mechanism ultraviolet sterilization is just to damage the DNA of bacteria, disturbing the replication process of DNA. The radiation therapy of cancer is also using ionizing radiation to damage the DNA of cancer cells, to stop its division or even make it to death (Charles, 1995, p.115-121).

## 2.2 DNA damage caused by chemical factors

There are a lot of chemical factors that can lead to DNA damage, such as the base molecular isomerization,  $O_2$ ,  $H_2O_2$  and other chemicals yielded by biological metabolism, various types of free radical generated spontaneously or induced in organism. In addition, something, including heavy metal ions, medicine, pesticide and their metabolites, entered the body through various ways can also lead to DNA damage. Some of the heavy metal ions have no direct damage to DNA, but they play a important medium role in the oxidative damage of DNA (Xi, 2003, p.662-667; Lloyd, 1999, p.23-36).

Base molecular isomerization can lead to DNA damage. Isomerization can occur on cytosine (C), thymine (T), adenine (A) and guanine (G), namely all of the DNA bases. The isomerization will enable the position of hydrogen bonds between base pairs changed, then result in the bases-mismatched in the replication process, and bring about DNA damage, such as adenine pairing with cytosine, thymine pairing with guanine and so on (Sun, 2005, 18(3): 325-330). Among the four bases of DNA molecule, cytosine, adenine and guanine bases have exocyclic-amino ( $-NH_2$ ). The exocyclic-amino can be removed under the influence of water, oxidants and free radicals and some other substances, turning the cytosine into uracil, adenine into hypoxanthine and guanine into xanthine. The deamination damage of DNA bases can lead to erroneous encoding in the replication process due to bases-mismatched, and then lead to gene mutation. Among the deamination of DNA bases, the deamination of cytosine changing into uracil has an important biological significance, because it can kill cells by inhabiting the synthesis of RNA and DNA. Nitrite induce the deamination of adenine to form hypoxanthine, and the latter can be paired with cytosine in the DNA replication process, resulting in  $A \cdot T \rightarrow G \cdot C$  conversion. Guanine can turn into xanthine through deamination. Xanthine cannot be matched with other bases, and this will lead to base deletion, erroneous encoding or the termination of DNA replication process (Wink, 1991, p.1001-1003).

Alkylating agent can also cause serious DNA damage because of the alkylation of bases (Ito, 1994, p.273-285). There are many different kinds of Alkylating agent, such as the mustard gas which had been used as a chemical weapon, alkyl sulfate-ester and sulfonic-esters which are widely used in industry, N-nitroso-compound, imine, active halogenated hydrocarbon, epoxides and so on. All of the alkylating agents are electrophilic compounds, which can transfer active alkyl to nucleophilic position of the DNA bases. Some of the alkylating agent have two alkylate functional group, and they can react with two positions of DNA, resulting in the cross-linking of strand within DNA or with another DNA strand or with protein, such as nitrogen mustard, sulfur mustard, carcinogen diethylnitrosamine, anticancer medicine cyclophosphamide, cisplatin, mitomycin and so on. Cross-linking of DNA is a kind of serious DNA damage which can stop the unwinding, the replication and transcription process of DNA or even lead to the death of cells. In fact, for the therapeutic purposes, some anticancer drugs are just making use of their cross-link reaction with DNA to inhabit the growth, division of cancer cells and thereby kill them (Li, 2004, p.262-271).

Purine base or pyrimidine base can be removed by hydrolysis, and base alkylation can also help to the shedding of bases. Several reasons, such as the action of active free radical, fluoride, peroxide and some metal ions, can break DNA strand. DNA double-strand break means death to the monoploid cells of bacteria. Some compounds with a similar structure to DNA base, such as 5-bromouracil, 5-fluorouracil and 2-aminopurine, can bond to DNA in the replication process instead of normal DNA base. When DNA base analogues get into DNA molecular, they can lead to the base mismatch, causing the gene mutation. For example, the incorporation of 5-bromouracil in DNA will lead to the  $G \cdot C \rightarrow A \cdot T$  transition. The base analogues have been used as a mutagen of gene mutation in genetic engineering (Ma, 1998, p. 48-50). Intercalated agent can cause DNA damage through inserting into DNA double-strand. Peroxide and free radical can open the ring of DNA base and some other compounds can modify directly the bases or other position of DNA strand. Dozens of studies have shown that hydroxyl radicals and superoxide free radicals produced by automobile exhaust, cooking smoke or cigarette smoke can react with guanine, generating 8-hydroxy-deoxyguanosine. Nowadays, 8-hydroxy-deoxyguanosine has become a recognized biomarker compound of the oxidative damage of DNA (Xi, 2003, p. 259-262).

### 3. Detection of DNA Damage

Determining the injury site and style is an important component of DNA damage study. In principle, any detecting methods of molecular structure can be used for DNA damage detection. Because the experimental condition is under controlled and the initial chemical composition, chemical structure and spatial structure are known, it is relatively easy for the detection of damage outside the living organism. However, for DNA damage within the living organism, the detection of it is much more hard and complicated due to the extremely complex biochemical environment, so there is very few methods can be used directly to detect the DNA damage within the living organism. By means of study of the cell survival, division and aberrance, we can determine whether there had been DNA damage and the extent of the damage. In recent years, with the development of detecting technology, the study of DNA damage at molecular level has attracted considerable attention, and has also made certain progress. The site and style of DNA damage caused by some physical or chemical factors have been affirmed.

#### 3.1 Electrophoresis technologies

The changing of electrophoresis properties can be used to detect DNA damage. Single cell electrophoresis technique (SCGE) which is also named comet assay, is a rapid, sensitive and simple method for DNA damage detection, and has been widely used in the detection of DNA strand break damage, DNA crosslinking damage or other single-cell DNA damage (Merk, 1999, p. 167-172). If using pulsed electric field, it is called pulsed field gel electrophoresis (PFGE). This technology can be used for the detection of DNA double-strand breaks, and as the resolution and sensitivity having been greatly improved, the minimum amount of radiation inducing DNA strand breaks can be as low as 2Gy (Rojas, 1999, p.225-254). Denaturing gradient gel electrophoresis (DGGE) is primarily used to detect the point mutation in DNA fragments, and latter for the research of the microbial community structure. The developed temperature gradient gel electrophoresis (TGGE) is widely used in microbial molecular ecology, and nowadays, it plays an important role for the study of microbial community structure. One of the commonly used methods in detecting gene mutation is PCR-single strand conformation polymorphism analysis (PCR-SSCP). It is much more simple and sensitive, and can detect 70% -95% of the mutations. However, the technology cannot identify the site and property of the mutation (Wei, p.22-25).

#### 3.2 Spectroscopic methods

Another kind of technology for DNA damage detection is making use of the spectrum property changes after being damaged. Fluorescent spectrophotometry (FP) is depend on the intrinsic fluorescence of some compounds, to detect the DNA adducts, such as polycyclic aromatic hydrocarbons. The developed method in present is respectively synchronous fluorimetric spectrophotometry, fluorescence emission spectrophotometry and cryogenic laser methods. Fluorescent spectrophotometry is of extremely high sensitive, and its detection limit is  $10^6 \sim 10^8$ . Synchronous fluorimetric determination is one of the most frequently used method, but it is not suitable for determination DNA damage induced by non-fluorescent intercalated agent (Vahakangas1985,p.1109-1115).Chromatography, such as denaturing high performance liquid chromatography (HPLC), take the changes of the DNA structure into account to detect the single nucleotide polymorphisms and heritable mutations (Hu, 2005, p.308-309; Wang, 2005, p.34-37 ). Under partially denaturation conditions, high performance liquid chromatography can effectively distinguish the heteroduplex DNA formed by mutated base and normal base with the normal double-strand DNA. Because the resolution of denaturing high performance liquid chromatography can be achieved 1bp /1kb, and the whole operating process can be programmed, scaled and automated, so the test time have been greatly reduced, and the experimental accuracy rate have been increased. To be a powerful tool for the screening gene mutation, it has a pretty good application prospect.

#### 3.3 Biological methods

Making use of the biological response within the organism, such as immunoreaction, DNA damage can also be detected. The elementary principles of immunoassay is based on the response between antigen and antibody, using the antibody of DNA adducts to detect the corresponding DNA adducts in the injured tissue. The commonly used methods are competitive immunoassay, solid-phase competition or non-competitive enzyme-linked immunosorbent assay methods, ultra-sensitive enzymatic radioimmunoassay and so on (Ding, 2007, p. 4753-4760). Immunoassay sensitivity of DNA adducts detection is one adduct each  $10^7$  nucleotides, and it is very easy to be done in the cultured cells in vitro, such as lymphocytes. The advantage of it is simple, low cost and no need to enzomolysis DNA strand. However, it is not suitable for the detection of non-antigenic adducts or unknown antigen adducts, and need a large amount of DNA, further more there is antigen-antibody cross-reactivity. Many mutagenic agents can induce sister chromatid exchange within the cultured mammalian cells and the body of mammals, and the occurrence frequency have a quantitative relationship with DNA

breakage and repair. Therefore, the use of sister chromatid exchange analysis can determine whether DNA damage occurs (Yager, 1985, p. 135-139). Cleaving enzyme fragment length polymorphism analysis is a new type of gene mutation detection methods, which can detect the gene mutation on the DNA fragments more than 1 kb in length. Moreover, as the sites of gene mutation can be accurately determined, and the simple operation, good reproducibility, it shows a great superiority. Compared with the other enzymatic detection methods, it does not need a mismatch heteroduplex to provide enzyme cleavage site, thus eliminating the process of the formation of heteroduplexes (Jenkins1999, p. 37-43). Allele specific amplify method, which is based on PCR technology, is a kind of single nucleotide mutation detection method and can conventionally analyze the replacement of known bases or small fragments absence mutation and insertion mutation. As the rapidity, good reproducibility, low-cost, no isotopic pollution and high efficiency, it is a promising method for large-scale mutation screening (Seki, 2000 p. 299-302).

### 3.4 DNA chip and molecular probe Technologies

DNA chip and molecular probes developed in recent years are new methods for detecting DNA damage. In the rapidly and efficiently detection of genome sequence variation and mutation, gene expression spectrum analysis, disease diagnosis, drug screening, pathogen detection, disease-related genome sequence, copy number changes and the detection of nucleotide sequence polymorphism, DNA chip has a broad perspectives in application (Shaon, 1996, p. 639-643). Synthetic oligonucleotide molecular probe can find out the mutation and its properties through the analysis of hybridization signal, and it is expected to open up a series study methods of DNA chemical modification and DNA damage detection (Gong, 2007, p. 4882-4883).

### 3.5 Other methods

<sup>32</sup>P-postlabeling method can detect the DNA adducts, even if the structure of adducts is unknown. The highest sensitivity make it can detect out one adduct from each  $10^8 \sim 10^{10}$  nucleotides, in other words, it can be detected as long as there is only one adduct in one cell. If combine the <sup>32</sup>P-postlabeling method with high performance liquid chromatography, its sensitivity and specificity can be greatly enhanced (Zhao, 1998, p. 102-103). The detecting method of DNA damage based on the changes of mechanical properties of DNA after being damaged has also been reported (Marszalek, 2007, p. 809-813).

## 4. Peroration

The study of DNA damage and repair is one of the important topics in life sciences and related fields, which is of great theoretical and practical significance. In recent years, with the adventure and development of the new DNA damage detecting technology, a remarkable progress has been made in the study of DNA damage and repair. Through direct or indirect determination of the biological marker of DNA damage and the changes of physical and chemical properties caused by DNA damage, many sites, styles and consequence of DNA damage have been identified. However, because of the specialty and complexity of molecular structure, physiological environment, the damage processes of DNA, most of the damage mechanism of DNA are, more or less, speculation. Many research works are making use of DNA fragments, simulated physiological conditions. So far, it is still very difficult to study the mechanism of DNA damage within living body, and further improvement is awaited the adventure and development of advanced technology.

## References

- Charles J., Robbins J H, Bohr V. A. (1995). Gene specific DNA repair of damage induced in familial Alzheimer disease cells by ultraviolet irradiation or by nitrogen mustard. *Mutat. Res.*, 336, 115-121.
- Ding Guoxiang; Wang Zhi; Wang Li; et al. (2007). Comparative analysis of the result of hepatitis B virus detected by MEIA with preS1Ag and DNA. *Modern Preventive Medicine*, 24, 4753-4760.
- Gong J., Sturla S. J. (2007). A synthetic nucleoside probe that discerns a DNA adduct from unmodified DNA. *J. Am. Chem. Soc.*, 129(16), 4882-4883.
- Hoeijmakers J. H. (2001). Genome maintenance mechanisms for preventing cancer. *Nature*, 411, 366-374.
- Hu Jun, Shi Guixin, Li Lushi. (2005). The detection of single nucleotide polymorphisms, by denaturing high-performance liquid chromatography. *Journal of Clinical Laboratory Science*, 4, 308-309.
- Ito T., Nakamura T. (1994). Roles of transcription and repair in alkylating mutagenesis. *Mutat. Res.*, 314, 273-285.
- Jenkins G. J. S., Takahashi N., Parry J. M. (1999). Inverse restriction site mutation (iRSM) analysis. Mutation detection involving the formation of restriction enzyme sites in target genes. *Mutagenesis*, 14(1), 37-43.

- Li Rui, Lu Zhisong, Qiao an, et al. (2004). Study on the formaldehyde-induced DNA damage with comet assay. *Acta Biologiae Experimentalis Sinica*, 37(4), 262-271.
- Liu Dianfeng, Yu Sansan, et al. (2006). DNA damage checkpoint, damage repair, and genome stability. *J. Genetics and genomics*, 5, 3-12.
- Lloyd D. R., Phillips D. H. (1999). Oxidative DNA damage mediated by copper, iron and nickel fenton reactions: evidence for site-specific mechanisms in the formation of double-strand breaks, 8-hydroxydeoxyguanosine and putative intrastrand cross-links. *Mutat. Res.* 424, 23-36.
- Ma Huiping, Zhao Yongliang and Yang Guangyu. (1998). Application of Induced Mutation Technology for Crop Breeding, *Hereditas*, 4, 48-50.
- Marszalek P. E. (2007). Nanomechanical Fingerprints of UV Damage To DNA. *Small*, 3(5), 809-813.
- Merk O., Speit G. (1999). Detection of crosslinks with the Comet assay in relationship to genotoxicity and cytotoxicity. *Environ. Mol. Mutagen*, 33, 167-172.
- Miyakoshi J., Yoshuda M., et al. (2000). Exposure to strong magnetic field at power frequency potentiates X-ray-induced DNA strand breaks. *J. Radiat. Res.*, 41, 293-302.
- Rojas E. (1999). Single cell gel electrophoresis assay: methodology and applications. *J. Chromatogr. B*, 722, 225-254.
- Seki T., Tanaka T., Nakamura Y. (2000). Genomic structure and multiple single-nucleotide polymorphisms of the thiopurine S-methyltransferase gene. *J. Hum. Genet.*, 45, 299-302.
- Shaon D., Smith J. S., Brown P. O. (1996). A DNA microarray system for analyzing complex DNA samples using 2-color fluorescent-probe hybridization. *Genome Res.*, 6, 639-643.
- Sun Julong, Yang Guanghui, He Guozhong, et al. (2005). DFT study on tautomerism of gaseous cytosine. *Chinese Journal of Chemical Physics*, 18(3), 325-330.
- Vahakangas K., Haugen A., Harris C. C. (1985). An applied synchronous fluorescence spectro- photometric assay to study benzo[a] pyrene-diolepoxide-DNA adducts. *Carcinogenesis*, (8), 1109-1115.
- Wang Gongyao, Huang Daixin. (2005). Denaturing high-performance liquid chromatography and its application in forensic DNA analysis, *Forensic Science and Technology*, 3, 34-37.
- Wang Y., Li J., Lin Z. (2003). Studies on the application of Cre/LoxP site-specific recombination system on plant male sterility and hybrid heterosis. *Molecular plant breeding*, 1(4), 557-558.
- Wei Taiyun, Lin Hanxin and Xie Lianhui. (2002). Optimization of the conditions affecting PCR-SSCP analysis. *Journal of Fujian Agricultural University (Natural Science)*, 01, 22-25.
- Wink D. A., Kasprzak K. S., Maragos C. M., et al. (1991). DNA deaminating ability and genotoxicity of nitric oxide and its progenitors. *Science*, 254, 1001-1003.
- Xi Zhuge, Cao Fuhuan and SunYongmei; et al. (2003). Study on the mechanism of oxidative damage of DNA induced by reactive oxygen species due to metal ions. *Acta Scientiae Circumstantiae*, 23(5), 662-667.
- Xi Zhuge, Li Guanxian, Sun Yongmei, Cao Fuhuan. (2003). Oxidative Damage of DNA and Formation of Its Biomarker 8-Hydroxydeoxyguanosine Induced by Heated Cooking Oil Vapors. *Journal of Environment and Health*, 20(5), 259-262.
- Yager J. W., Cohn K. L., Spear R. C., et al. (1985). Sister-chromatid exchanges in lymphocytes of anatomy students exposed to formaldehyde embalming solution. *Mutat. Res.*, 174, 135-139.
- Zhao C., Koskinen M., Hemminki K. (1998). <sup>32</sup>P-postlabelling of N6-adenine adducts of epoxybutanediol in vivo after 1,3-butadiene exposure. *Toxicol. Lett.*, 12, 102-103.

# Call for Manuscripts

*International Journal of Chemistry* is a peer-reviewed journal, published by Canadian Center of Science and Education. The journal publishes research papers in the fields of applied chemistry, inorganic chemistry, analytical chemistry, organic chemistry, physical chemistry, structural chemistry, polymer chemistry, nuclear chemistry, chemical engineering and environmental chemistry. The journal is published in both printed and online versions, and the online version is free access and download.

We are seeking submissions for forthcoming issues. The paper should be written in professional English. The length of 3000-8000 words is preferred. All manuscripts should be prepared in MS-Word format, and submitted online, or sent to: [ijc@ccsenet.org](mailto:ijc@ccsenet.org)

## **Paper Selection and Publication Process**

- a). Upon receipt of paper submission, the Editor sends an E-mail of confirmation to the corresponding author within 1-3 working days. If you fail to receive this confirmation, your submission/e-mail may be missed. Please contact the Editor in time for that.
- b). Peer review. We use single-blind system for peer-review; the reviewers' identities remain anonymous to authors. The paper will be peer-reviewed by three experts; one is an editorial staff and the other two are external reviewers. The review process may take 2-3 weeks.
- c). Notification of the result of review by E-mail.
- d). The authors revise paper and pay publication fee.
- e). After publication, the corresponding author will receive two copies of printed journals, free of charge.
- f). E-journal in PDF is available on the journal's webpage, free of charge for download.

## **Requirements and Copyrights**

Submission of an article implies that the work described has not been published previously (except in the form of an abstract or as part of a published lecture or academic thesis), that it is not under consideration for publication elsewhere, that its publication is approved by all authors and tacitly or explicitly by the responsible authorities where the work was carried out, and that, if accepted, it will not be published elsewhere in the same form, in English or in any other languages, without the written consent of the Publisher. The Editors reserve the right to edit or otherwise alter all contributions, but authors will receive proofs for approval before publication.

Copyrights for articles published in CCSE journals are retained by the authors, with first publication rights granted to the journal. The journal/publisher is not responsible for subsequent uses of the work. It is the author's responsibility to bring an infringement action if so desired by the author.

## **More Information**

E-mail: [ijc@ccsenet.org](mailto:ijc@ccsenet.org)

Website: [www.ccsenet.org/ijc](http://www.ccsenet.org/ijc)

Paper Submission Guide: [www.ccsenet.org/submission](http://www.ccsenet.org/submission)

Recruitment for Reviewers: [www.ccsenet.org/reviewer.html](http://www.ccsenet.org/reviewer.html)



**The journal is peer-reviewed**

**The journal is open-access to the full text**

**The journal is included in:**

AMICUS

Canadiana

DOAJ

EBSCOhost

Google Scholar

Library and Archives Canada

Open J-Gate

PKP Open Archives Harvester

Socolar

Standard Periodical Directory

Ulrich's

Universe Digital Library

Wanfang Data

# International Journal of Chemistry

Semiannual

Publisher Canadian Center of Science and Education

Address 4915 Bathurst St. Unit 209-309, Toronto, ON. M2R 1X9

Telephone 1-416-642-2606

Fax 1-416-642-2608

E-mail [ijc@ccsenet.org](mailto:ijc@ccsenet.org)

Website [www.ccsenet.org](http://www.ccsenet.org)

Printer Paintsky Printing Inc.

Price CAD.\$ 20.00

